THE
PHYSICAL REVIEW

A journal of experimental and theoretical physics established by E. L. Nichols in 1893

SECOND SERIES, VOL. 78, No. 5 JUNE 1, 1950

The Spallation Products of Antimony Irradiated with High Energy Particles*

M. LINDNER** AND I. PERLMAN
Radiation Laboratory and Department of Chemistry, University of California, Berkeley, California
(Received February 11, 1950)

The distribution and yields have been determined for a considerable number of spallation products resulting from the irradiation of antimony with particles in the 100-Mev range. The highest yields were found for nuclei about five mass numbers removed from the target material showing that compound nucleus formation is not an important mechanism in such high energy reactions. Products in lower yields were found which probably resulted from nuclei which had been excited to the full energy of the projectile. A more detailed discussion of the types of reactions responsible for the observed products is given.

1. INTRODUCTION

THE acceleration of charged particles into the hundred million volt range by the Berkeley 184-inch cyclotron has made it possible to extend investigations of induced nuclear transformations into a new energy region. Preliminary results already reported[1–3] indicated that one of the predominant characteristics is the multiplicity of reactions. Reaction products covering a range from the region of the target nucleus down to nuclei about 20 mass units lighter were readily identified and good evidence was obtained for products even considerably further removed. To indicate these reactions in which excited nuclei are degraded by losing one or more nucleons, the term *spallation* has been suggested.

The present study consists of the determination of the radioactive products which result from the irradiation of antimony with 380-Mev helium ions and with deuterons of 190 Mev and lower. Particular attention was paid to the measurement of the yields of the many product nuclei as a function of projectile energy. Early in the course of these investigations a number of activities were encountered that had not been previously reported. It was necessary to characterize these nuclei and some of the results have been published separately.[4,5]

The distribution of reaction products to be discussed below is in keeping with the general features of a description by Serber[6] of the encounter between high energy particles and nuclei. In this high energy range it is no longer possible to assume compound nucleus formation at each nuclear encounter. Instead, the instantaneous reaction is considered to proceed through individual collisions between target and projectile nucleons, the incidence of which may be described in terms of the geometry of the encounter and the mean free path between collisions within the nucleus. As an example of one type of encounter, a deuteron of high energy may graze a nucleus in such a way that the neutron is sheared off by a single collision with a nucleon while the proton does not react with the nucleus. Even the neutron may leave the nucleus again giving up only part of its kinetic energy. In this type of reaction a relatively small amount of the kinetic energy of the deuteron is transferred as excitation energy to the nucleus and the product of the reaction will be within a few mass units of the target nucleus. On the other hand, it is also possible for the high energy deuteron to give up all of its energy to the nucleus. According to Serber, the mean free path of a nucleon of 100-Mev energy in nuclear matter is 4×10^{-13} cm. It gives up about 25 Mev in its first collision, and as its energy becomes degraded its mean free path decreases. As a result, with a moderately large nucleus such as antimony one might expect a measurable yield of reactions in which a 200-Mev deuteron gives up essentially all of its energy

* This work was performed under the auspices of the AEC.
** Now at the Department of Chemistry, State College of Washington, Pullman, Washington.
[1] G. T. Seaborg *et al.*, Phys. Rev. **72**, 739, 740 (1947).
[2] H. H. Hopkins, Jr. and B. B. Cunningham, Phys. Rev. **73**, 1406 (1948).
[3] Miller, Thompson, and Cunningham, Phys. Rev. **74**, 347 (1948).
[4] M. Lindner and I. Perlman, Phys. Rev. **73**, 1124 (1948).
[5] M. Lindner and I. Perlman, Phys. Rev. **73**, 1202 (1948).
[6] R. Serber, Phys. Rev. **72**, 1114 (1947).

UNIVERSITY OF MICHIGAN LIBRARIES

resulting in a highly excited nucleus which then boils off a large number of nucleons in dissipating its energy.

In the present study reactions illustrative of the extremes cited were noted as well as intermediate types. It was the purpose of these investigations to obtain a survey of the yields of a wide range of reaction products and to determine how these yields vary with projectile energy.

2. PROCEDURE

Irradiations

The antimony targets consisted of strips of pure antimony metal 1 mm in thickness. When the strip is fastened to the end of a movable probe in the cyclotron tank normal to the direction of the deuteron beam, the deuterons strike a thin segment (1 to 2 mm) along the leading edge. The adjustment of the radial position of the probe allows a variation of particle energy to be obtained. Because deuterons in the energy range studied are not degraded in energy readily, antimony targets 1 millimeter thick could be considered as thin targets.

Radiation Counting Methods

After irradiation the targets were separated into chemical fractions by the procedures to be described. Along with half-life determination, the radioactive species present were identified principally by absorption methods using cylindrical end-window Geiger counter tubes with mica windows of approximately 3 mg/cm^2 thickness.

It is characteristic of irradiations with high energy particles that many neutron-deficient isotopes are formed and, in the region of the periodic table under investigation, many of these decay by orbital electron capture. As a result all chemical fractions contained considerable x-ray activity. In order to aid in identifying beta-particles and electrons in the presence of the many x-rays, beryllium rather than aluminum was used for determining the absorption end-points. Using sufficient beryllium to filter out electrons, the x-rays were usually characterized with the use of aluminum absorbers. Gamma-ray energies beyond the x-ray energy region were determined with lead absorbers.

A crude beta-ray spectrometer was used in distinguishing particles of different sign, and was found particularly useful in the cases in which one type was a minor component of the total activity. Used as a spectrometer, lines of electrons could usually be distinguished from continuous beta-spectra and approximate values for the energies were obtainable.

Chemical Separations

The procedure followed in separating the irradiated target into the several chemical fractions was in general the same for the different bombardments. The fractions separated and examined covered the range from tellurium, atomic number 53, to yttrium, atomic number 39. It was not possible to separate all elements in sufficient degree of purity by rapid methods which would at the same time give good yields. However, pure fractions were obtained for tellurium, antimony, tin, indium, cadmium, silver, palladium, ruthenium, molybdenum, and yttrium. In order to determine the chemical yield of each fraction, a known amount of carrier for each element was added before separation and the final step in each purification was the precipitation of a compound suitable for weighing.

The following outline of the methods of separation indicates the reactions used but is not complete in that, in general, the procedures were repeated one or more times to insure adequate purity.

The irradiated antimony metal was dissolved by covering with concentrated hydrofluoric acid and the dropwise addition of concentrated nitric acid. The solution was diluted, carriers for the elements to be separated were added, and the solution was made 0.1*M* in HCl. The yttrium and silver were separated as yttrium fluoride and silver chloride. The silver was dissolved from the precipitate by treatment with ammonium hydroxide. The yttrium fluoride was dissolved in nitric and boric acids, removed as yttrium hydroxide upon addition of sodium hydroxide, and then dissolved in hydrochloric acid. The solution was buffered with sodium acetate and sulfide-insoluble activities removed by addition of indium and precipitation of indium sulfide with hydrogen sulfide. The hydrogen sulfide was expelled from the solution and yttrium fluoride precipitated by the addition of hydrofluoric acid after adding inactive elements to stabilize the activities from which the yttrium was to be separated.

The silver was purified by a series of precipitations of silver chloride from nitric acid solutions interspersed with scavenging precipitations of ferric hydroxide from ammoniacal solutions

The supernatant solution remaining from the precipitation of silver and yttrium was divided into two equal portions. From one of these, palladium was precipitated with dimethylglyoxime, after which addition of alpha-benzoinoxime precipitated molybdenum. The solution remaining from these precipitations was fumed with sulfuric acid in order to destroy the organic reagents. Perchloric acid was added and upon boiling, the ruthenium was distilled and trapped in dilute sodium hydroxide solution from which it was precipitated by the addition of alcohol and warming.

The second portion of the solution from the silver and yttrium removal was evaporated almost to dryness and taken up in 2*M* HCl. Tellurium was reduced to the elemental state by treatment of the hot solution with sulfur dioxide. The excess sulfur dioxide was expelled by heating the supernatant solution and the antimony precipitated with hydrogen sulfide while the solution was maintained near boiling. The hydrogen sulfide was driven off by heating, and the solution was made alkaline by addition of sodium hydroxide. This pre-

cipitated the cadmium and indium, and left the tin in solution. The indium and cadmium were separated by dissolution of the hydroxides in dilute acid and precipitation of the indium with ammonium hydroxide. The cadmium was then recovered by precipitation with hydrogen sulfide. The sodium hydroxide solution containing the tin was made 0.3*M* HCl and the tin removed by hydrogen sulfide treatment.

3. RADIOACTIVE NUCLIDES IDENTIFIED

The isotopic composition of each chemical fraction was determined by combinations of absorption and decay measurements, and in a number of cases through parent-daughter relationships. A brief description of the activities encountered in each fraction follows, with some remarks on the methods used in the resolution. Because of the large number of activities found, references are given only for those which have appeared in the literature recently. Most of the others will be found in the 1948 edition of "Table of Isotopes" by Seaborg and Perlman.[7]

Tellurium Fraction: 143-day Te^{121m}

This isotope appeared as the longest-lived component of the tellurium fraction when counted either without absorbers or through beryllium (electromagnetic radiation) and was followed in all cases through at least one half-life. Identification was made certain by complete absorption curves. The 17-day ground state,[8] Te^{121}, was undoubtedly formed independently, but it could not be resolved readily because of the concomitant presence in good yield of 4.5-day and 6.0-day tellurium periods as well as complications caused by the growth of Te^{121} from Te^{121m}.

4.5-day Te^{119} and 6.0-day Te^{118}

The characteristics and mass number assignments of these activities have been reported previously.[4] The 4.5-day period decays by orbital electron capture; it is characterized by conversion electrons and a hard gamma-ray of 1.6 Mev and is the parent of a 39-hour antimony activity which also decays by orbital electron capture. The 6.0-day tellurium assigned to Te^{118} decays by orbital electron capture and probably shows only x-rays in its decay. It is the parent of Sb^{118}, a 3.5-min. positron-emitter.

When this mixture of isotopes is produced with 190-Mev deuterons on antimony, the activity measured without absorbers is largely that of the 3.5-min. Sb^{118} which serves as an index of the amount of Te^{118} present. When counted through sufficient thickness of beryllium ($\sim$2 g/cm^2) to stop all particles, the electromagnetic radiation is approximately equally divided between the 4.5-day and 6.0-day periods. The yield of Te^{119} is more precisely determined by separating and measuring the amount of 39-hr. Sb^{119} which appears at equilibrium. For elements in this region the *K* x-rays are assumed to be counted with 1 percent efficiency under the conditions employed.

2.5-hr. Te

This activity reported previously[4] is a positron-emitter which has not been otherwise characterized. It probably has a mass number of 117 or less since it appears in measurable yield only when antimony is irradiated with deuterons of energy 75 Mev or higher.

Antimony Fraction: Short-lived Antimony

Activity variously resolved in the range 3 to 5 hours appeared in the antimony fraction following all irradiations using deuterons of 75 Mev or greater. This activity is probably a mixture of 5.2-hr. and 2.8-hr. periods reported by Coleman and Pool[9] and assigned by them to Sb^{118} and Sb^{117}, respectively. The present work demands that the mass numbers be in this region, but Sb^{118} has been assigned to a 3.5-min. activity (see 6.0-day Te^{118} above).

39-hr. Sb^{119}

This isotope, exhibiting only x-rays in its decay,[9] was also identified as the daughter of 4.5-day tellurium[4] as part of the present studies. Since this activity possesses no particles or gamma-rays, it could best be seen in decay curves taken through beryllium. Under these conditions the activity was prominent, and with deuteron energies in excess of 100 Mev, it was formed in much higher yield than its tellurium parent. When counted without absorber, the 2.8-day Sb^{122} negatrons completely overshadowed the less efficiently detected x-rays of Sb^{119} since both were formed in somewhat comparable yields.

5.7-day Sb^{120}

The electromagnetic radiation of the antimony fraction when followed either through beryllium ($\sim$2 g/cm^2) or through beryllium plus lead (130 mg/cm^2) showed a prominent 5.7-day period in all irradiations of antimony with deuterons in the energy range 50–190 Mev. It was assigned as an isomer of the 17-min. Sb^{120} positron-emitter on the basis of irradiations of separated Sn^{120} with deuterons of 19-Mev energy and from other considerations.[4] It was shown to undergo orbital electron-capture decay by critical absorption measurements of the x-rays and to have gamma-rays and conversion electrons.

2.8-day Sb^{122}

This negatron-emitter appeared as the most prominent activity a few days after irradiation when the

[7] G. T. Seaborg and I. Perlman, Rev. Mod. Phys. **20**, 585 (1948).
[8] J. E. Edwards and M. L. Pool, Phys. Rev. **69**, 140 (1946).
[9] K. D. Coleman and M. L. Pool, Phys. Rev. **55**, 1070 (1947).

antimony fraction was counted without absorber. When only electromagnetic radiation was followed, the 2.8-day period of Sb^{122} was not in evidence because of the preponderance of 39-hr. Sb^{119} and 5.7-day Sb^{120} radiation. The identity of the Sb^{122} was confirmed by a beta-ray absorption curve.

60-day Sb^{124}

All antimony decay curves tailed out into this period which could be followed through several half-lives. The beta-ray absorption curve served further to identify the isotope.

Tin Fraction: 4.5-hr. $Sn^{108(?)}$

In the irradiation of antimony with highest energy particles (190-Mev deuterons and 380-Mev helium ions), a 4.5-hr. period was found in the tin fraction. This activity could not be detected following the irradiation of antimony with deuterons of 100 Mev or less. The 4.5-hr. tin decays by orbital electron capture and is the parent of a 70-min. indium positron-emitter of 2.2-Mev energy as determined by a beryllium absorption curve. It was not possible to make a mass assignment on the basis of this work. Recently Mallary and Pool[10] have produced this pair by bombardment of enriched Cd^{106} with 20-Mev alpha-particles and assigned the mass number 108 to it.

The high energy necessary to produce the 4.5-hr. Sn from antimony is consistent with its assignment to an isotope of low mass number, as is its mode of decay.

28-hr. Sn^{121}

This activity which appeared in all irradiations has been described previously.[4] The isotopic assignment was made by the irradiation of separated Sn^{120} with 19-Mev deuterons. Since there is no gamma-ray associated with this isotope, it could only be followed in decay curves taken without absorber.

14-day Sn^{117m}

This period was previously reported by Livingood and Seaborg[11] from the irradiation of cadmium with helium ions, setting the maximum mass number at 119. In the present study critical absorption measurements of the x-rays showed the decay process to be an isomeric transition; from yield considerations of deuterons of different energies on antimony to be discussed below, it seemed probable that the mass number lay in the range 118–122. Of the two possible assignments from these studies, 119 was chosen as the most probable. However, it has recently been shown[12,13] that the mass number more likely is 117.

The radiations from Sn^{117m} are K x-rays in high abundance, an electron of about 0.15 Mev as determined by absorption in beryllium and in a beta-ray spectrometer, and the corresponding gamma-ray of 0.175 Mev determined by absorption in lead.

The 14-day period for Sn^{117m} was resolved readily from the decay curves of the tin fraction from antimony irradiations when the electromagnetic radiation was followed through beryllium.

110-day Sn^{113}

This period could be followed after decay of the 14-day Sn^{117m} and could be determined earlier by removal of its 110-min. In^{113m} daughter.

Indium Fraction: Short-lived Isotopes

The indium fraction, like that of antimony, always contained a complex mixture of activities ranging in half-life from less than an hour to about five hours. Resolution and identification of the different components were unsatisfactory, so no yield data are presented. By following the positrons in the beta-ray spectrograph, the 20-min. period and the 65–70 min. period were found. However, it is fairly certain that 105-min. In^{113m}, 4.5-hr. In^{115m}, 54-min. In^{116}, and 117-min. In^{117} were also present, making quantitative determination of all isotopes difficult.

2.7-day In^{111}

In the irradiation of antimony with 100-Mev deuterons, this activity could barely be detected but became more prominent at higher energies.

48-day In^{114m}

This nuclide, along with its 72-sec. negatron-emitter daughter, was identified readily by following the decay curve through several half-lives and by confirming the radiation characteristics by absorption curves.

Cadmium Fraction: Short-lived Isotopes

At high energies at least one activity with a half-life in the range 1 to 2 hr. was detected in low yield. From the fact that 100-Mev deuterons failed to show this activity, it is deduced that the mass number is near or below the lightest stable cadmium isotope, Cd^{106}. These isotopes were not further characterized because of the low yield.

6.7-hr. Cd^{107}

Decaying by orbital electron capture, this isotope was definitely identified by separating its daughter, 40-sec. Ag^{107m}, as well as by its prominence in the decay curve taken through beryllium. The Cd^{107} was detected with difficulty by decay curves taken without absorber since it was masked by the beta-activity of the shorter- and longer-lived isotopes.

[10] E. C. Mallary and M. L. Pool, Phys. Rev. **76**, 1454 (1949).
[11] J. J. Livingood and G. T. Seaborg, Phys. Rev. **55**, 667 (1939).
[12] J. W. Mihelich and R. D. Hill, Phys. Rev. **77**, 743 (1950).
[13] E. C. Mallary and M. L. Pool, Phys. Rev. **77**, 75 (1950).

2.3-day and 42-day Isomers of Cd^{115}

The 2.3-day Cd^{115} was prominent in decay followed without absorber, but was almost undetectable in the decay curve taken through beryllium. Identification and yield determination were also aided by determining its 4.2-hr. In^{115m} daughter. Since the 42-day Cd^{115} has no prominent electromagnetic radiation, it could only be measured in the decay curve taken without absorber.

330-day Cd^{109}

This activity was apparent in the decay curve taken through beryllium soon after the 6.7-hr. Cd^{107} had disappeared. Ultimately it could be seen in the curve taken without absorber after the 42-day Cd^{115} had decayed. Identification was made certain by removal of its daughter, 40-sec. Ag^{109m}.

From the above account of the cadmium fraction it may be visualized that the decay curves taken with and without absorbers were quite different. Without absorber the short-lived activities and the Cd^{115} isomers were most prominent, while decay curves taken through beryllium showed largely the 6.7-hr. Cd^{107} and 330-day Cd^{109}.

Silver Fraction: 24-min. Ag^{106}

This positron-emitting isomer of Ag^{106} was detected with the beta-ray spectrometer as the shortest-lived positron component but it could not be analyzed satisfactorily in the decay curve followed on the Geiger counter and no yield data are presented. The 8.2-day isomer of Ag^{106} is discussed below.

70-min. Ag

This positron-emitter, probably that reported by Enns,[14] could be identified in the same manner as that described for Ag^{106}. It could not be resolved in the Geiger counter decay curve taken without absorber but was prominent in that determined through beryllium. This indicates considerable orbital electron capture branching in the decay of this isotope.

7.5-day Ag^{111} and 8.2-day Ag^{106}

It was possible to show that both of these isotopes are formed in antimony spallation and to determine the yield of each. The 7.5-day Ag^{111} is a negatron emitter with no associated gamma-rays, as a result of which it could be detected without absorber but would not be counted through a sufficient amount of beryllium. On the other hand, 8.2-day Ag^{106} decays by orbital electron capture and has gamma-rays which Feather and Dunworth[15] showed to be but slightly converted. As a result, nearly all of the 8-day activity followed without absorber was due to Ag^{111} while all of the 8-day activity followed through beryllium was due to Ag^{106}. Further proof that the two isotopes were present could be found in the ratio of the 8-day activity measured in these two ways when the projectile energy was changed.

45-day Ag^{105}

This activity could be detected only after irradiation of antimony with deuterons of 190 Mev or helium ions of 380 Mev. It was more prominent in decay curves taken through beryllium than without absorber but, even so, the resolution was difficult from 225-day Ag^{110} in the relatively short period of time the samples were followed.

225-day Ag^{110}

As mentioned above the accuracy in resolution from 45-day Ag^{105} was not as high as for most of the nuclides for which yields were calculated.

3.2-hr. Ag^{112}

This activity was observed in all irradiations of antimony with deuterons from 50 to 190 Mev. It showed up better at the lower energies because of the absence of the other short-lived isotopes of silver which only appeared at higher energies. The isotope was identified by absorption curves which showed the presence of a very hard beta-particle.

Palladium Fraction

The palladium fraction contained so many activities of similar half-life that they could not be resolved directly from decay curves. However, three activities whose half-lives lie in the range 10 to 20 hrs. have radioactive daughters which can serve as indices of the amounts of the parent nuclides present. For palladium and lower elements measurable yields were obtained only with highest energy deuterons and helium ions.

21-hr. Pd^{112}

This activity could be measured by its 3.2-hr. Ag^{112} daughter. Decrease in yield of the Ag^{112} removed from the palladium fraction at intervals defined a 21-hr. half-life and served to determine the yield of Pd^{112}.

26-min. Pd^{111}

When the palladium separation was performed sufficiently rapidly, the 26-min. negatron emitter was noted and after decay the 7.5-day Ag^{111} could be removed from the palladium fraction.

12-hr. Pd^{109}

This negatron emitter was positively identified by separation of its daughter, the 40-sec. Ag^{109m}. Its yield was determined by resolution of the decay curve taken without absorber correcting for the 21-hr. Pd^{112} present which was uniquely determined through its daughter, 3.2-hr. Ag^{112}.

[14] T. Enns, Phys. Rev. **56**, 872 (1939).
[15] N. Feather and I. V. Dunworth, Proc. Roy. Soc. **A168**, 578 (1938).

UNIVERSITY OF MICHIGAN LIBRARIES

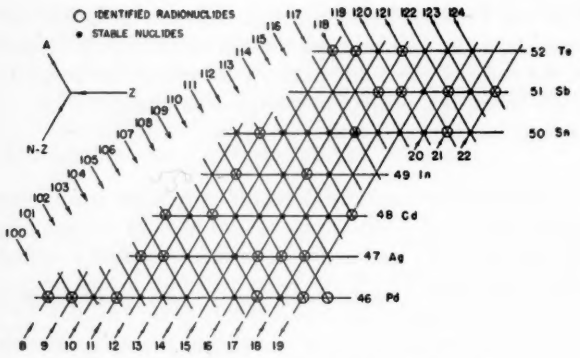

FIG. 1. Distribution of spallation products of antimony.

17-day Pd^{103}

This activity appeared as the longest-lived component of the palladium fraction and its yield was determined by measuring the x-rays.

10-hr. Pd^{101}

This isotope, which decays both by electron capture and positron-emission to its 4.3-day Rh^{101} daughter, was described in an earlier report.[5] Its yield was determined by measuring the x-rays of the Rh^{101} to which it decayed.

4.0-day Pd^{100}

Also described previously,[5] this isotope decays by orbital electron capture with the emission of gamma-rays to a 19.4-hr. daughter, Rh^{100}, which in turn decays predominantly by orbital electron capture with about 5 percent branching through positron-emission. The yield was determined best by measuring the x-rays of the Rh^{100}.

Ruthenium Fraction: 4.5-hr. Ru^{105}

This negatron emitter was the only short-lived isotope in the ruthenium fraction. The yield was checked by distilling the ruthenium from perchloric acid after decay of the Ru^{105} leaving its 36-hr. Rh^{105} daughter which could then be measured.

2.8-day Ru^{97}

This activity could be resolved out of the decay curves taken through beryllium and without absorber. It showed up well in the ruthenium distilled from the 36-hr. Rh^{105} after decay of the 4.5-hr. Ru^{105}.

42-day Ru^{103}

Detected in the decay curve taken without absorber, this isotope also appeared in the ruthenium distilled from the Rh^{105}.

1-yr. Ru^{106}

This period was found after decay of 42-day Ru^{103} and could be detected earlier through the hard beta-rays of its daughter, 30-sec. Rh^{106}. The yields determined by the two methods were in essential agreement.

Molybdenum Fraction: 67-hr. Mo^{99}

No short-lived molybdenum activities were looked for and this activity was the only one found in the molybdenum fraction. The beta-ray absorption curve was in agreement with those reported. This period was followed through about 6 half-lives following irradiation of antimony with 200-Mev deuterons.

Yttrium Fraction: 80-hr. Y^{87}

No yttrium activities of half-life less than one day were sought. Initial growth in the yttrium fraction suggested the presence of 80-hr. Y^{87} producing its daughter 2.7-hr. Sr^{87m}. This was confirmed by removal of the strontium. The decay curve of the yttrium was less than 80 hrs. which suggests that some 62-hr. Y^{90} was present but that the two yttrium activities were not resolved.

57-day Y^{91}

This period which was followed through three half-lives appeared after Y^{87} had decayed.

4. DISCUSSION OF RESULTS

In Fig. 1 is shown the distribution of identified spallation products of antimony with 190-Mev deuterons as far down as isotopes of palladium, in relation to the stable nuclides in this region. Table I gives the yields of these and other products listed in columns according to the energy and type of projectile which produced them.

In general, there is a continuous distribution of reaction products from the neighborhood of the target nuclides down to those lower by about 12 units of atomic number and 35 mass number units. For almost every element, radioactive isotopes are found on both sides of the region of beta-stability, that is, those with excess of neutrons and those that are neutron-deficient. Because of the complexity of chemical separations and the difficulty of resolving many of the radioactive mixtures, many short-lived activities which were undoubtedly present were either missed through decay or were not used in the yield calculations for lack of positive identification. As an example, there was evidence for the presence of six indium activities of a few hours half-life or less, but the yields of none could be calculated.

As pointed out in Section 1, the wide distribution of products is in keeping with the description by Serber[6] of nuclear encounters with high energy particles. According to this, if antimony is irradiated with 190-Mev deuterons, it is not to be expected that a compound nucleus will be formed in each nuclear encounter; instead, the present picture demands that all degrees of excitation up to the maximum be possible.

With respect to its reaction with a nucleus, a deuteron of 190 Mev is fairly accurately described as an independent proton and neutron each carrying approximately one-half of the kinetic energy. The principal significance of the existence of the proton and neutron as a deuteron is their spatial relation as they approach a nucleus. Another consequence of the high velocity of the neutron (or proton) is that its reaction with the struck nucleus may be described in terms of collisions with individual nucleons. This follows when the velocity of the approaching particle is greater than that of a particle within the struck nucleus, making it improbable that the kinetic energy can be distributed during the period of nucleon-nucleon interaction. For similar reasons, nuclear matter begins to be transparent at these energies, making the mean free path between collisions comparable with the nuclear dimensions.

From the above picture it is possible to visualize the multiplicity of nuclear reactions resulting from the irradiation of antimony with high energy deuterons. On one extreme a deuteron may approach a nucleus near an edge in such a way that the neutron of the deuteron, for example, penetrates and makes a single collision with a nucleon while the proton is stripped off in the process. According to Serber, the neutron would lose an *average* of about 25 Mev in the collision and, since it is near the edge of the nucleus, it would leave, carrying off most of its initial kinetic energy. The struck nucleon would, in general, give up its energy to excite the nucleus. Products from reactions of this type will be a few mass numbers lighter than the target nucleus and it is seen from Table I that representatives of this type, Sb^{119} and Sb^{120}, are formed in highest yield.

On the other extreme of energy transfer, one can visualize that both parts of the deuteron will strike the antimony nucleus near the center and in rare instances, each will undergo a sufficient number of collisions to give up its entire energy to the nucleus. This case is

TABLE I. Cross sections in millibarns for spallation products of antimony at various energies.

Nuclide		$T_{1/2}$	380-Mev alpha-particles	190-Mev deuterons*	100-Mev deuterons	75-Mev deuterons	50-Mev deuterons
52 Te	121	140 d *IT*	18	11	17	15	33
	119	4.5 d *K*	67	22	66	65	77
	118	6.0 d *K*	29	18	53	31	23
	?	2.6 hr. β^+	20	13	21	4.4	<0.07
51 Sb	124	60 d β^-	15	1.4	2.5	1.5	3.6
	122	2.8 d β^-	72	44	65	28	31
	119?	5.7 d *K*	180	110	160	40	47
	118?	3.9 hr. *K*	100	160	180	63	29
50 Sn	121	28 hr. β^-	2.2	—	0.81	0.32	0.14
	117*m*	14 d *IT*	28	17	17	5.6	2.2
	113	110 d *K*	30	17	6.2	0.7	<0.03
	108	4.5 hr. *K*	8	—	<0.01	—	—
49 In	114*m*	48 d *IT*	23	16	5.1	0.86	<0.002
	111	2.7 d *K*	160	72	0.95	<0.01	—
48 Cd	115	2.3 d β^-	0.35	0.15	0.026	0.0041	<0.0017
	115	42 d β^-	1.1	0.68	0.11	0.0088	0.0041
	109	330 d *K*	14	3.2	<0.14	—	—
	107	6.7 hr. *K*	43	5	<0.005	—	—
47 Ag	112	3.2 hr. β^-	0.57	0.28	0.038	0.0029	<0.00042
	111	7.5 d β^-	2.3	0.63	0.080	0.0035	<0.00017
	110	225 d *K*	—	4.8	0.18	—	—
	106	8.2 d *K*	3.5	11	<0.01	—	—
	105	45 d *K*	1.7	5	<0.02	—	—
46 Pd	112	21 hr. β^-	0.0043	0.0008	<0.0001		
	111	26 min. β^-	—	0.03			
	109	13 hr. β^-	0.12	0.027			
	103	17 d *K*	4.7	1.0			
	101	8 hr. β^+	1.1				
	100	4 d *K*	1.0	0.013			
44 Ru	106	1 yr. β^-		0.002			
	105	4 hr. β^-		0.008			
	103	40 d β^-		0.004			
	97	2.7 d *K*	0.32	0.01			
42 Mo	99	67 hr. β^-		0.0023			
39 Y	91	57 d β^-		0.0009			
	87	80 hr. *K*		0.0003			

* Most of the values in this column represent averages of three measurements.

TABLE II. Yields of silver isotopes from 190-Mev deuterons on antimony.

Mass	Cross section (millibarns)
Ag 112	0.28
111	0.63
110	4.8
106	11
105 (?)	1.7

identical with compound nucleus formation at lower energies in that the incident particles are captured, after which nuclear evaporation considerations explain the results. With 190-Mev deuterons it would be predicted that such collisions would cause the evaporation of 20 or more nucleons, depending upon whether they are lost as individual neutrons and protons or as more complex fragments such as alpha-particles. Representative products of such reactions are indeed found, as shown in Table I.

Formation of Antimony Isotopes

As mentioned above, the formation of the antimony isotopes measured corresponds to the transfer of comparatively small amounts of energy to the nucleus, hence the loss of only a few neutrons, or none at all, as evidenced by the formation of Sb^{124}. It is of interest to compare the yields of Sb^{122} and Sb^{124}. The latter can be formed only by the reaction: $Sb^{123}(d,p)Sb^{124}$ or its equivalent. The former, however, can be formed by two reactions: $Sb^{121}(d,p)Sb^{122}$, and $Sb^{123}(d,p2n)Sb^{122}$.

Since the yield of Sb^{124} is an order of magnitude less than that of Sb^{122}, it is apparent that Sb^{122} must be formed principally by the $(d,p2n)$ reaction. For 190-Mev deuterons, the $(d,p2n)$ reaction appears about thirty times as probable as the (d,p) reaction. This ratio appears to have decreased to about twenty for 75-Mev deuterons and ten for 50-Mev deuterons, and is in the direction which would be anticipated since the lower energy available would tend to make the (d,p) reaction more probable relative to the $(d,p2n)$ reaction.

Of further interest is the relatively large yield of Sb^{124} resulting from irradiation with 380-Mev alpha-particles as compared with that from irradiation with 190-Mev deuterons. Both can be looked upon as neutron addition reactions; however, the neutrons in the alpha-particle have a greater kinetic energy and momentum than the neutron in a deuteron. If at the instant of collision with the nucleon in the target nucleus, the momentum of the neutron is in the reverse direction from that of the center of mass, the effect will be to decrease the energy to be transferred to a nucleon struck by this neutron. In this way it is possible to capture a neutron from an alpha-particle with less energy to be radiated than if the neutron is a component of a deuteron.

TABLE III. Energy requirement for particle removal.

Particle	Binding energy	Coulomb barrier	Total necessary for expulsion
n	8	0	8
p	8	8	16
α	3	16	19

Pattern for Yields of Nuclides Formed with High Energy Particles

Reference to Table I shows that at the highest bombardment energies, yields of neutron-deficient isotopes of any product element generally are larger than yields of isotopes containing an excess of neutrons. Table II, for example, illustrates this situation for silver.

It will be seen that the yield generally increases as the mass number of the isotope decreases. The isotope Ag^{105} appears not to conform to this pattern; however, this may be due to difficulties in estimating counting efficiencies of the radiations associated with this nuclide and with resolution of the Ag^{105} from the Ag^{110}. Furthermore, the isotopic assignment of this period is still in doubt, and if its mass number is actually lower than 105, the low yield could be due to approach to the energy threshold.

The pattern illustrated above is rather general for all nuclides at these energies. Hence in Fig. 1, those nuclides lying far to the left (neutron-deficient) predominate over those lying on the right.

When the bombardment energy is decreased, it will be noticed that the yields of the neutron-deficient isotopes (except for those of Sb and Te) drop off much more rapidly than do the yields of those with neutron excess. This trend follows from energy considerations and will be discussed below.

These features of the spallation process may be explained qualitatively by considering energy requirements on the one hand and, on the other, the predilection for loss of neutrons rather than charged particles from highly excited nuclei. In discussing spallation

TABLE IV. Cross sections for isobars produced with 190-Mev deuterons.

Atomic number	Nuclide	Cross section (millibarns)
52	Te^{119}	22
51	Sb^{119}	160
47	Ag^{112}	0.28
46	Pd^{112}	0.0008
49	In^{111}	72
47	Ag^{111}	0.63
46	Pd^{111}	0.03
48	Cd^{109}	3.2
46	Pd^{109}	0.027
47	Ag^{106}	11
44	Ru^{106}	0.002
46	Pd^{103}	0.1
43	Ru^{103}	0.004

reactions with high energy particles, the inability to write a unique reaction to describe each of the products is an immediate obstacle. As an example, in the formation of Ag^{112} from the irradiation of antimony (let us say Sb^{121}) with 190-Mev deuterons, it is neither possible to define an intermediate excited nucleus nor to tell by what combination of neutron and proton evaporation Ag^{112} is reached. For purposes of discussion, let us assume that Sb^{121} itself is the primary excited nucleus, and that protons are lost as alpha-particles whenever possible. Then the Ag^{112} would arise from the loss of "$2\alpha n$" using the short-hand expression. It is seen from Table II that with 190-Mev deuterons a greater disparity between neutrons and protons is favored even though the loss of more nucleons is demanded. Thus, Ag^{106} from the loss of $2\alpha 7n$ is formed with 11 mb cross section, as compared with $Ag^{112}(2\alpha n)$ with 0.28 mb, and $Ag^{111}(2\alpha 2n)$ with 0.63 mb. From Table I it may be seen that cadmium isotopes show the same behavior.

All of these reactions require considerable nuclear excitation; in fact, 100 Mev is probably not sufficient to form Ag^{106}. From Table I it is seen that Ag^{106} and Ag^{105} are no longer measurable using 100-Mev deuterons; and although the cross sections for formation of Ag^{110}, Ag^{111}, and Ag^{112} have decreased from what they were at 190 Mev, these nuclides are now the predominant silver isotopes. Table III shows[16] roughly the energies required to expel nucleons and alpha-particles in this region. For the loss of $2\alpha 7n$ to form Ag^{106}, just about 100 Mev would be required, and it is therefore not surprising that the yield should fall off at least 1000-fold between 190 Mev and 100 Mev. On the other hand, $Ag^{110}(2\alpha 3n)$ would require 62 Mev excitation at threshold, and the yield only falls off by a factor of 25 between deuterons of 190 Mev and 100 Mev. It may further be noted that for reactions of this type, the protons are indeed most likely lost as alpha-particles since at 100-Mev excitation there is not sufficient energy to expel the protons and neutrons individually. Conceivably, in some cases less energy would be required in reaching lower atomic numbers from the target nucleus by the ejection of an even greater ratio of neutrons to protons followed by positron-emission, but in the present case Ag^{110} would be blocked by stable Cd^{110}. For that matter, Ag^{106} is shielded from positron-emission by Cd^{106} and therefore must be hit by the emission of the required amount of positive charge in the form of nucleons. In this same mass number region it may be noted that In^{114}, a completely shielded nuclide, is found in good yield.

The same pattern as that just discussed may be extended to a higher energy region. In the irradiation of antimony with 380-Mev alpha-particles, palladium isotopes could be reached in easily measurable yields; of these, the neutron-deficient isotopes Pd^{100}, Pd^{101}, and Pd^{103} were found more abundant than the heavier isotopes Pd^{109} and Pd^{112}.

[16] W. Horning, private communication.

Isobar Yields

There were a number of cases in which independent yields of isobars could be measured. Table IV summarizes the data for isobars formed with deuterons of 190 Mev.

There is, in every case except the first, a significantly larger yield of the isobar of higher atomic number. This may be taken as some measure of the ease with which a neutron is emitted from some excited nucleus in preference to the emission of charged particles.

The fact that the yield of Sb^{119} exceeds that of Te^{119} may be explained by the restrictions imposed upon the formation of the tellurium isobar. This can come about only by capture of a proton and loss of neutrons, whereas the antimony isobar may result from capture of either the proton or neutron of the projectile or neither.

Relative Yields of Isomers

There is no reason to believe that the relative amounts of two isomers produced in spallation reactions should change particularly with bombardment energy, since in all cases, after the last nucleon has left, the nucleus is left in an excited state well above the level of the highest lying isomer. Table I shows cross sections for the formation of Cd^{115} isomers using 380-Mev alpha-particles and deuterons from 190 Mev to 75 Mev. The ratio varies irregularly in this energy range and on the average, the upper state (43 day) is formed in three times the yield of the lower state.

In comparison with this ratio of Cd^{115} isomers formed in spallation, the ratios arising from slow neutron fission of uranium[17] and fission of thorium with 38-Mev alpha-particles[18] are both about 0.07. This is presumably the ratio at which these isomers arise from β^--decay of Ag^{115}, making it accordingly likely that Cd^{115} is not a primary fission product in these types of fission. On the other hand, in the fission of bismuth with 190-Mev deuterons[19] and uranium with 380-Mev alpha-particles,[20] the ratio of the upper to lower state is about 0.6, indicating that part arises from Ag^{115} decay but most as primary fission products. From slow neutron capture in cadmium, the ratio of 43-day to 2.5-day isomers was reported[21] to be approximately 0.1.

Yields of Nuclides of Low Atomic Number

The nuclide of lowest atomic weight and number which was definitely detected was $_{39}Y^{87}$. As may be inferred from the low cross section shown in Table I, the positive identification of nuclides in this region demanded extensive purification of the chemical frac-

[17] R. P. Metcalfe, reported in "Nuclei Formed in Fission," J. Am. Chem. Soc. **68**, 2411 (1946).
[18] A. S. Newton, Phys. Rev. **75**, 17 (1949).
[19] R. H. Goeckermann and I. Perlman, Phys. Rev. **76**, 628 (1949).
[20] P. R. O'Connor and G. T. Seaborg, Phys. Rev. **74**, 1189 (1948).
[21] Seren, Engelkemeir, Sturm, Friedlander, and Turkel, Phys. Rev. **71**, 409 (1947).

tions. Consequently, only isotopes with half-lives of the order of a day were detected for elements in this lower region. This region has not, therefore, been very thoroughly investigated for short-lived activities.

If such nuclides do indeed arise from the antimony rather than from some impurity, the energy threshold is very close to the deuteron energy (190 Mev) even if one assumes that the maximum number of alpha-particles are ejected. It may be that such a mechanism is not possible, and that these nuclides arise from the ejection of fragments heavier than alpha-particles perhaps approaching a reaction which might more properly be termed fission.

To shed some light on the possibility that these nuclides arise from impurities in the antimony, a spectrographic analysis was made in which no foreign lines were detected, and upper limits for the amounts of In, Cd, Pd, Rh, Ru, and Zr could be set at about 0.01 percent. Similar low limits can be set for molybdenum because of the extremely small amount of Mo^{99} found. In general, the limits of impurities are such that it is somewhat unlikely that the nuclides in question could come from this source.

ACKNOWLEDGMENTS

We wish to thank Dr. Duane Sewell and members of the 184-inch cyclotron staff for the bombardments which made this work possible.

PHYSICAL REVIEW VOLUME 78, NUMBER 5 JUNE 1, 1950

Total Cross Section of C, O, Mg, Si, and S for Fast Neutrons*

G. FREIER, M. FULK, E. E. LAMPI, AND J. H. WILLIAMS
University of Minnesota, Minneapolis, Minnesota

(Received February 20, 1950)

The total cross sections of light nuclei containing an integral number of alpha-particles was found by measuring the transmission of C, Mg, Si, S and SiO_2 samples for fast neutrons in the energy range 0.60 Mev to 1.90 Mev and in the energy range 2.5 Mev to 5.0 Mev. The cross sections have many resolved resonances, and the number of resonances per unit energy range increases rapidly with atomic number.

I. INTRODUCTION

THE experimental determinations of nuclear energy levels have as their prime objective the acquiring of sufficient information to enable one to construct detailed models of nuclei. A convenient way of finding the energy levels in a nucleus is to bombard it with neutrons of known energy and find at what energies the bombarded nucleus readily accepts the incident neutrons to form a compound nucleus in some excited energy state. If one measures the transmission of a beam of neutrons through some absorber as a function of the energy, the transmission will decrease markedly for certain incident neutron energies. The energy at which this occurs corresponds to a characteristic state of the compound nucleus, and by finding all these states one can construct an energy level diagram for the nucleus. In this experiment it was hoped that one might find some similarity in the energy levels of compound nuclei formed by bombarding light nuclei containing an integral number of alpha-particles with neutrons, and thus lend support to the hypothesis that the relatively stable alpha-particle remains an entity in the nucleus.

To make the measurements of transmission independent of the physical size and shape of the absorber, they are expressed in terms of cross section by the relation $T=e^{-nx\sigma}$ where T is the transmission, σ is the total cross section, and nx is the number of scattering centers per cm^2 presented to the incident neutron beam. Energy levels of the compound nucleus then appear as resonances in the curves for the total cross section as a function of energy. The method of measuring the total cross section as a function of energy was similar to that described previously.[1]

II. EXPERIMENTAL PROCEDURE

The $Li^7(p,n)Be^7$ reaction was used to obtain neutrons up to 1.90 Mev. Protons accelerated by the Minnesota Van de Graaff generator bombarded a thin layer of Li which had been evaporated onto a 0.010-inch thick tantalum backing. The Li target was of such thickness that incident protons of 1.88 Mev lost 30 kev energy in passing through the target. The energy of the incident protons was determined with an electrostatic analyzer, and all measured energy values are relative to 1.882 Mev, the threshold of the $Li^7(p,n)Be^7$ reaction.[2] The stability of the machine was such as to make the measured proton energy uncertain to ± 10 kev. The

* This research was done with the partial support of the ONR, Contract N5ori-147, T.O. III.

[1] Bailey, Bennett, Bergstrahl, Nuckolls, Richards, and Williams, Phys. Rev. **70**, 583 (1946); D. H. Frisch, Phys. Rev. **70**, 589 (1946); Nuckolls, Bailey, Bennett, Bergstrahl, Richards, and Williams, Phys. Rev. **70**, 805 (1946); L. W. Seagondollar and H. H. Barschall, Phys. Rev. **72**, 439 (1947).

[2] Herb, Snowden, and Sala, Phys. Rev. **75**, 246 (1949).

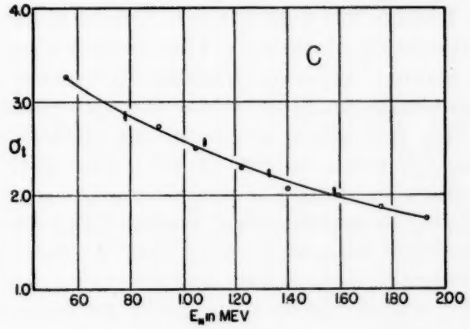

FIG. 1. Total cross section of carbon as a function of neutron energy. The product nx for the scatterer was 2.05×10^{23} atoms/cm^2.

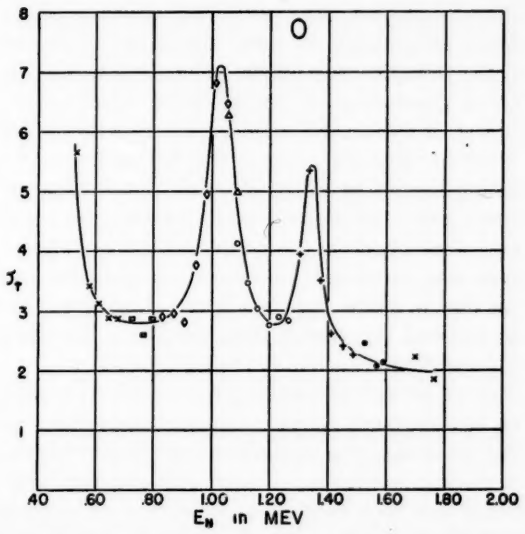

FIG. 2. Total cross section of oxygen as a function of neutron energy. The product nx for the quartz scatterer was 6.32×10^{22} atoms/cm^2.

corresponding neutron energies were then calculated for each measured proton energy.

The neutron detector was a cylindrical pulse ionization chamber 2 inches in diameter and 4 inches long filled with 2 atmospheres of argon containing 3 percent of methane. The collecting electrode was held at 135 volts, but this voltage was not critical. A thin layer of paraffin serving as a source of recoil protons covered the interior of one flat end, thus making the counter directional. The detector was placed 16 inches from the neutron source with the axis of the counter falling on the line defined by the incident proton beam. The pulses from this counter were then amplified and recorded on instruments of Los Alamos design.[3] This type of detector was energy sensitive. The smallest energy a neutron could have and still be detected was about 550 kev, and above this value the sensitivity varied approximately as the square of the neutron energy. The bias on the pulse discriminator was adjusted at each energy to keep the counting rate approximately constant, so that if a neutron entering the detector had lost energy in any scattering collision or in any other process it is quite probable that it would not have been counted.

The scatterers were disks 1.5 inches in diameter placed midway between the neutron source and detector and held in place by four strands of piano wire. The scatterers were of such thickness as to give approximately 50 percent transmission. This value of transmission was selected to give the smallest statistical error for any given number of counts while scattering into the detector from the outside edges of the scatterer was kept at a minimum. The density and thickness of each scatterer was measured and from this the number of scattering centers was calculated. The cross section of oxygen was determined by measuring the cross sec-

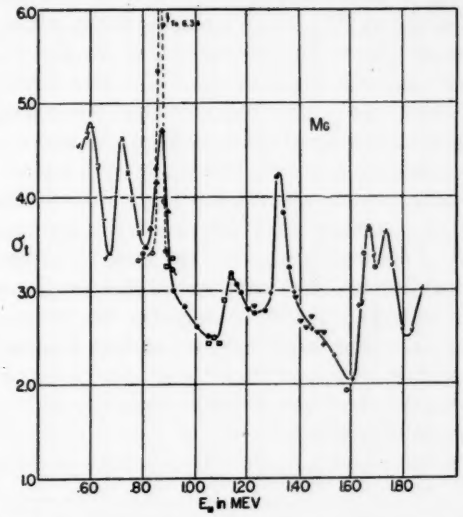

FIG. 3. Total cross section of magnesium as a function of neutron energy. The product nx for the scatterer was 2.183×10^{23} atoms/cm^2.

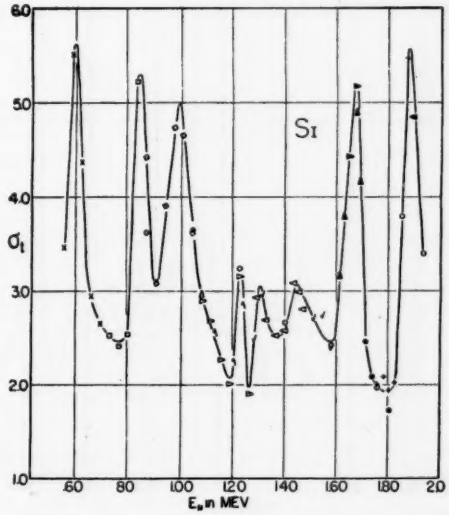

FIG. 4. Total cross section of silicon as a function of neutron energy. The product nx for the scatterer was 2.543×10^{23} atoms/cm^2.

[3] Higinbotham, Gallagher, and Sands, Rev. Sci. Inst. 18, 706 (1947).

tion of both silicon and quartz and then subtracting the scattering due to silicon from the measurements made with quartz. The scatterers were all chemically pure and contained the natural relative abundances of their isotopes.

The number of background counts was measured by replacing the scatterer with a paraffin cylinder 3 inches in diameter and 8 inches long. This paraffin cylinder was sufficiently long to reduce the intensity of the direct neutron beam between the source and detector to zero and sufficiently narrow so it would not shield any object in the room which might be scattering neutrons into the detector during a regular intensity run.

The alignment of the neutron source, scatterers, and detector was periodically checked by placing a point source of light at the position of the source and then centering the scatterer and detector in the shadow cone.

A directional BF_3 counter placed about 6 feet from the source and at approximately 90° to the incident proton beam served as a monitor. The number of counts from the pulse ionization chamber during any run was always normalized to a fixed number of counts on this monitor counter. The number of counts from the monitor counter exceeded the number from the ionization chamber by a factor of two so that this method of normalization did not greatly increase the statistical error. The runs were also monitored by measuring with a current integrator the total charge transferred to the target by the incident proton beam, but changing characteristics of the target could make this measurement less reliable than monitoring the neutron flux directly.

For measurements made with neutrons in the energy range 2.5 Mev to 5.0 Mev, the $D(d,n)He^3$ reaction was used as a source of neutrons. This required a gas target which had to be separated from the high vacuum of the Van de Graaff generator by a 0.0001-inch thick nickel foil. This foil would withstand one atmosphere of pressure. A small volume of deuterium gas 0.6-cm thick and at a pressure of one atmosphere gave a sufficient yield of neutrons when bombarded by deuterons. The energy of the neutrons was varied by changing both the incident deuteron energy and the angle at which the detector was placed with respect to the incident deuteron beam. To cover the neutron energy range, 2.5 Mev to 5.0 Mev, measurements were made at angles of 0°, 60°, and 98°.

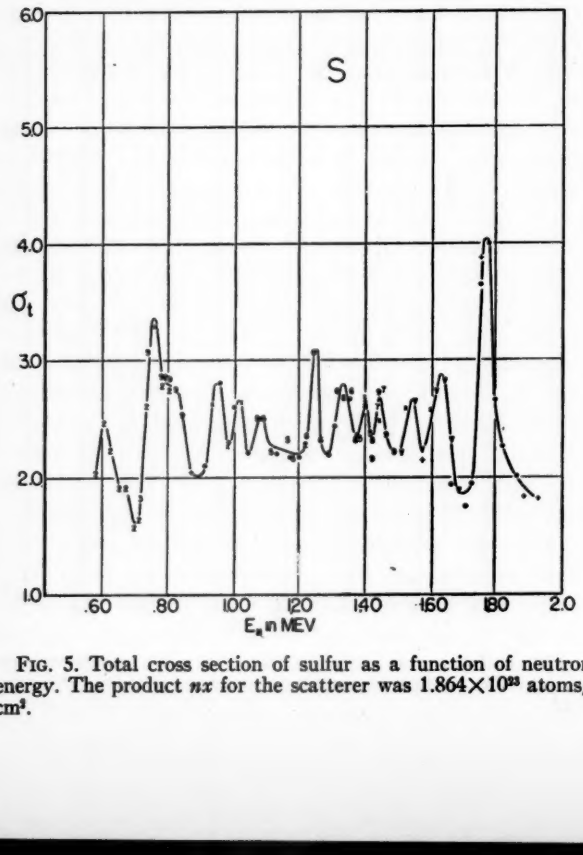

FIG. 5. Total cross section of sulfur as a function of neutron energy. The product nx for the scatterer was 1.864×10^{23} atoms/cm².

The solid angle subtended by the detector allowed a spectrum of neutrons to enter the detector, especially when the detector was placed at angles other than 0°. However, the energy at the center of the detector was very close to the mean energy of the neutrons entering the detector when the mean energy was calculated with weighting factors including the yield distribution of the neutrons from the source[4] and the effective counting area of the detector. The uncertainty of where the neutron was produced in the source, plus the energy spread due to finite angles subtended by the detector, made some of the energy determinations for the neutrons from deuterium uncertain by ±200 kev.

In order to determine the number of neutrons produced by deuterons striking any carbon nucleus in the target container, the deuterium gas in the target was replaced by hydrogen. Under these conditions the counting rate was as high as 8 percent of the regular counting rate, but if one used these counts to determine cross sections it was found that they gave approximately the same values of the cross sections as were determined by the counts when deuterium was in the gas target. It was concluded that most of this 8 percent background was from the deuterium reaction, and when hydrogen replaced the deuterium in the target, it released adsorbed deuterium from the walls of the target container. A further check on this showed that the amount of this type of background decreased with repeated flushing of the target with hydrogen gas. It was concluded that the contribution of the carbon neutrons was negligible compared to other sources of error. Furthermore, the detector (pulse ionization chamber) was energy-sensitive, and by discriminating against small pulses we could eliminate pulses from neutrons arising from the reaction of deuterons on carbon.

A background count was also taken with the paraffin cylinder as described earlier, except that the cylinder length was increased to 12 inches.

III. RESULTS

The results are shown in the following graphs. Figures 1 through 5 show the total cross sections for neutrons

[4] Blair, Freier, Lampi, Sleator, and Williams, Phys. Rev. **74**, 1599 (1948).

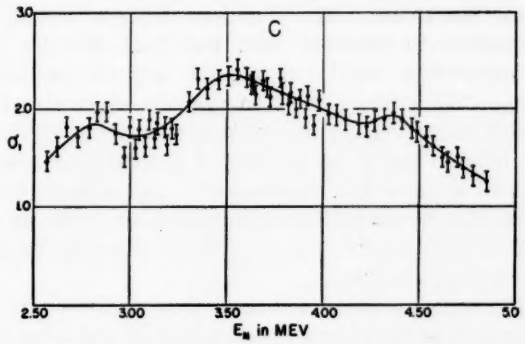

FIG. 6. Total cross section of carbon as a function of neutron energy. The product nx for the scatterer was 3.716×10^{23} atoms/cm^2.

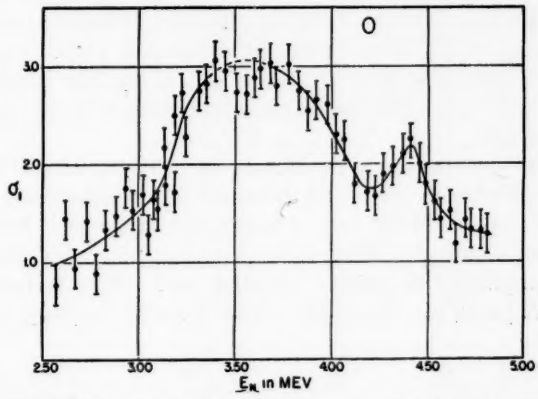

FIG. 7. Total cross section of oxygen as a function of neutron energy. The product nx for the quartz scatterer was 6.321×10^{23} atoms/cm^2.

obtained from the $Li^7(p,n)Be^7$ reaction while Figs. 6 through 8 show the total cross section for neutrons from the $D(d,n)He^3$ reaction. All cross sections are plotted as functions of incident neutron energy in the laboratory coordinate system. Sufficiently many counts were taken at each point in Figs. 1 through 5 to make the statistical error ±5 percent. The uncertainty in the energy of the incident particle is ±10 kev and the spectrum of energy due to the finite thickness of the Li target is about 30 kev wide. The different symbols for the experimentally determined points indicate measurements made on different days.

The errors in the individual points in Figs. 6 through 8 are about ±10 percent, and the spectrum of energy is about 400 kev wide. This made resolution of the resonance peaks very difficult. Figures 1 and 6 show the results for carbon. In Fig. 1 the four points with vertical bars were taken during (n,p) scattering experiments[5] when the statistical error was reduced to ±1 percent. These four points were also corrected for scattering into the detector by the outside edges of the scatterer. Since the new points fell so close to the line determined by the four more accurately determined points, no effort was made to correct the new data for scattering into the detector.

[5] Lampi, Freier, and Williams, Phys. Rev. **76**, 188 (1949).

Figures 2 and 7 show the total cross section of oxygen as a function of the incident neutron energy. The steep drop at the beginning of Fig. 2 corresponds to a resonance previously measured at Wisconsin.[6] The solid curve drawn in Fig. 7 shows only two resonances, but it is quite possible that the first broad resonance consists of two unresolved resonances as indicated by the slight dip in the experimentally determined points. The relatively narrow half-widths of all other peaks at lower energies also lead one to believe that there should be no broad resonance at this higher energy.

Figure 3 shows the total cross section of Mg as a function of incident neutron energy. The solid curve was drawn from data taken with a 30-kev Li target while the dotted curve at the third peak shows data taken with a 12-kev Li target which gave much better resolution. The measured half-width at the third peak could be accounted for by the energy spread of the neutron beam so that the true half-width is probably much smaller than that shown by these measurements.

Figures 4 and 8 show the total cross section of Si. Figure 8 shows no definite resonance structure, but the energy spread of the incident neutrons was so great that all detail of narrow resonances was probably lost and the measurements give only a mean value of the total cross section.

Figure 5 shows the total cross section of S. The density of resonance levels appears to be so great that the resonances cannot be completely resolved with a 30-kev Li target. No attempt was made to resolve these peaks further, but several of these peaks have been resolved into more resonances by the Wisconsin group.[7]

IV. DISCUSSION

Since the measurements were made, it has been observed by other workers[8–11] that there is an excited

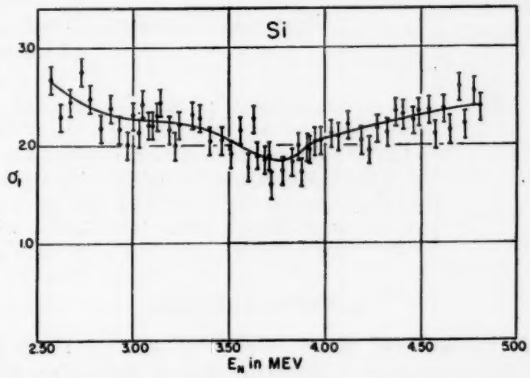

FIG. 8. Total cross section of silicon as a function of neutron energy. The product nx for the scatterer was 2.543×10^{23} atoms/cm^2.

[6] Adair, Barschall, Bockelman, and Sala, Phys. Rev. **75**, 1124 (1949).

[7] H. H. Barschall, private communication.

[8] J. C. Grosskreutz and K. B. Mather, Bull. Am. Phys. Soc. **24**, No. 7, 15 (1949).

[9] Brown, Chao, Fowler, and Lauritsen, Bull. Am. Phys. Soc. **24** No. 8, 11 (1949).

state 430 kev above the ground state in the residual Be^7 nucleus which can be excited in $Li^7(p,n)Be^7$ reaction over the energy range covered in this experiment. The measurements made at Wisconsin[11] and preliminary measurements made in this laboratory show that about 10 percent of the Be^7 nuclei are left in the excited state. This makes it possible that some of the observed resonances could be due to the slower group of neutrons producing the same resonance that had been measured previously at some lower energy with the primary group of neutrons. However, when one considers that the second group makes up 10 percent of the total number of neutrons and that the cross section at most resonance energies increases by a factor of two over the average cross section, one finds that the second group can produce a resonance in the cross section which increases by only 7 percent above the average cross-section value. All measured resonances were considerably higher than this. Measurements which included this second group of neutrons were also improbable because the detector was energy-sensitive and was biased to discriminate against the smaller pulses produced by the slower neutrons. Since the detector was completely insensitive to neutrons with less than 550 kev, the measurements could not include any of the slower group until primary neutron energies of greater than 1 Mev were used. As the neutron energy was increased the bias on the pulse selector of the detector was increased to keep the counting rate approximately constant. By discriminating against smaller pulses in this way, it is felt that no neutrons of the slower group were detected at any time.

The measurements give total cross sections only. No attempt was made to find what part of the total cross section was due to scattering and what part arose from nuclear reactions.

An analysis of this data has not yet been completed, but it appears that there is no obvious similarity in the energy levels of the different compound nuclei which are formed when light nuclei containing an integral number of alpha-particles are bombarded by fast neutrons.

This work was materially assisted by the University of Minnesota Technical Research Fund subscribed to by General Mills, Inc., Minneapolis Honeywell Regulator Company, Minneapolis Star Journal and Tribune Company, Minnesota Mining and Manufacturing Company, and Northern States Power Company.

[10] T. Lauritsen and R. G. Thomas, Bull. Am. Phys. Soc. **24**, No. 8, 11 (1949).
[11] Johnson, Laubenstein, and Richards, Phys. Rev. **77**, 413 (1950).

PHYSICAL REVIEW VOLUME 78, NUMBER 5 JUNE 1, 1950

Microwave Determination of the Structure of Borine Carbonyl and of the Nuclear Moments of the Stable Boron Isotopes

WALTER GORDY AND HAROLD RING*
Department of Physics, Duke University,† Durham, North Carolina
AND
ANTON B. BURG
Department of Chemistry, University of Southern California,‡ Los Angeles, California
(Received February 2, 1950)

From measurements on the $J=1\rightarrow2$ and the $J=2\rightarrow3$ rotational transitions of borine carbonyl its molecular structure has been determined as follows: $d_{BH}=1.194$A, $d_{BC}=1.540$A, $d_{CO}=1.131$A, and $\angle HBH=113°52'$. The moments of inertia (which assume $h=6.624_2\times10^{-27}$ erg. sec.) in g cm$^2\times10^{-40}$ are: 93.42_{66} for $B^{10}H_3C^{12}O$, 96.90_{92} for $B^{11}H_3C^{12}O$, 111.41_{13} for $B^{10}D_3C^{12}O$, and 114.35_{40} for $B^{11}D_3C^{12}O$. Nuclear quadrupole couplings determined are 3.36 ± 0.10 mc/sec. for B^{10} and 1.55 ± 0.08 mc/sec. for B^{11}. Approximate values of the nuclear quadrupole moments are 0.06×10^{-24} cm^2 for B^{10} and 0.03×10^{-24} cm^2 for B^{11}. The nuclear spin of B^{10} is determined as 3 and that of B^{11} as 3/2.

1. INTRODUCTION

IN preliminary communications[1] we have reported the experimental determination of the nuclear spins, quadrupole couplings, and approximate values for the quadrupole moments of B^{10} and B^{11}. Since our original report the spin values have been confirmed by remeasurement of the hyperfine structure with a new chemical sample of BH_3CO and by measurements on BD_3CO. Precision measurements have now been made on samples of both normal and deuterated borine carbonyl, and a complete determination of the structure of borine carbonyl has been made.

2. EXPERIMENTAL METHODS

For detecting the lines a single 1*N*26 crystal detector followed by a narrow-band, low frequency amplifier

* Frederick Gardner Cottrell Fellow. Now with the E. I. du Pont de Nemours Company, Wilmington, Delaware.
† The research at this University was supported by a grant-in-aid from the Research Corporation. It was submitted by H. Ring in partial fulfillment of the requirements for the Ph.D. degree.
‡ The work at this University was supported through a contract with the ONR.
[1] Gordy, Ring, and Burg, Phys. Rev. **74**, 1191 (1948); **75**, 1325(A) (1949).

TABLE I. Hyperfine spectrum of the $J=1\rightarrow2$ transition.

K	$F\rightarrow F'$	Frequency in mc/sec. Calculated[a]	Frequency in mc/sec. Observed	Relative intensity Calculated	Relative intensity Observed
		$B^{10}H_3C^{12}O$			
0	2→3	35,920.38	35,920.40	18	20
0	4→4	35,920.24	35,920.22	31	35
0	4→3	35,920.14		6	
0	2→2	35,919.96	35,919.95	30	25
0	4→5	35,919.64	35,919.60	100	200
0	3→4	35,919.57		51	
0	2→1	35,919.54		27	
0	3→3	35,919.47		40	
0	3→2	35,919.07	35,919.08	15	20
1	3→4	35,918.59	35,918.55	38	55
1	3→3	35,918.55		30	
1	3→2	35,918.35	35,918.29	11	25
1	4→4	35,918.26		23	
1	4→3	35,918.22		4	
1	2→3	35,918.11	—	13	—
1	4→5	35,917.96	35,917.96	75	80
1	2→2	35,917.90		23	
1	2→1	35,917.67	35,917.66	21	20
		$B^{11}H_3C^{12}O$			
0	1/2→3/2	34,629.27	34,629.27	21	40
0	5/2→5/2	34,629.23		23	
0	5/2→3/2	34,628.96	34,628.85	3	170
0	1/2→1/2	34,628.88		21	
0	3/2→5/2	34,628.85		53	
0	5/2→7/2	34,628.85		100	
0	3/2→3/2	34,628.57	34,628.58	27	30
0	3/2→1/2	34,628.18	34,628.16	4	5
1	3/2→5/2	34,627.81	34,627.81	39	35
1	3/2→3/2	34,627.68	34,627.64	20	25
1	5/2→5/2	34,627.62		17	
1	3/2→1/2	34,627.48	34,627.42	3	75
1	5/2→3/2	34,627.48		2	
1	5/2→7/2	34,627.43		75	
1	1/2→3/2	34,627.33		16	
1	1/2→1/2	34,627.13	34,627.16	16	20

TABLE I.—(*Continued*)

K	$F\rightarrow F'$	Frequency in mc/sec. Calculated[a]	Frequency in mc/sec. Observed	Relative intensity Calculated	Relative intensity Observed
		$B^{10}D_3C^{12}O$			
0	2→3	30,122.00	30,121.86	18	40
0	4→4	30,121.86		31	
0	4→3	30,121.76	30,121.56	6	25
0	2→2	30,121.58		30	
0	4→5	30,121.26	30,121.21	100	200
0	3→4	30,121.19		51	
0	2→1	30,121.16		27	
0	3→3	30,121.09		40	
1	3→4	30,120.84	30,120.86	46	60
1	3→3	30,120.80		37	
0	3→2	30,120.69	30,120.56	15	30
1	3→2	30,120.60		13	
1	4→4	30,120.51		28	
1	4→3	30,120.47		5	
1	2→3	30,120.36	—	16	—
1	4→5	30,120.21	30,120.21	92	110
1	2→2	30,120.15		28	
1	2→1	30,119.92	30,119.91	26	30
		$B^{11}D_3C^{12}O$			
0	1/2→3/2	29,346.65	29,346.65	21	40
0	5/2→5/2	29,346.61		23	
0	5/2→3/2	29,346.34	29,346.24	3	170
0	1/2→1/2	29,346.26		21	
0	3/2→5/2	29,346.23		53	
0	5/2→7/2	29,346.23		100	
0	3/2→3/2	29,345.95	29,345.93	27	30
0	3/2→1/2	29,345.56	—	4	—
1	3/2→5/2	29,345.66	29,345.68	48	40
1	3/2→3/2	29,345.53	29,345.52	24	30
1	5/2→5/2	29,345.47		21	
1	3/2→1/2	29,345.33	29,345.28	4	100
1	5/2→3/2	29,345.33		2	
1	5/2→7/2	29,345.28		92	
1	1/2→3/2	29,345.18		20	
1	1/2→1/2	29,345.00	29,345.03	20	25

[a] Calculated with $I=3$ and $3/2$, with $eQ(\partial^2V)/(\partial z^2)=3.36$ and 1.55 mc/sec. for B^{10} and B^{11}, respectively. In addition to the separation caused by quadrupole effects, the $K=1$ lines are separated from the $K=0$ lines by the centrifugal stretching term, $-4D_{J,K}$. The values used for $D_{J,K}$ are given in Table III.

was employed. Filtering[2] was used to eliminate the mode contour and effects of variations in power caused by impedance mismatch. The more sensitive modulation methods[3] could not be used on the $J=1\rightarrow2$ transition because their distortion of the lines prevented resolution of the hyperfine structure. The absorption cell, which was 60 ft. in length, was made of coin silver K-band wave guide. Raytheon millimeter wave klystrons provided the microwave power.

Measurements of the line positions were made with frequency markers produced by multiplying to the microwave region a 10-mc/sec. signal continuously monitored by station WWV. Details of the standard[4] and the monitoring method[3] are given elsewhere.

3. NUCLEAR MOMENTS

Spins

Previous to our initial report, no determination of the spins of B^{10} and B^{11} had been made, although concurrently with that report there appeared the interesting note of Goldhaber[5] in which he, independently of our work, predicted from theoretical considerations the surprising value of 3 for the spin of B^{10}. Before that time the spin of B^{10} had been generally assumed to be 1, and that of B^{11} to be 3/2. Our observation confirms the spin of 3/2 for B^{11}, but proves that the spin of B^{10} is 3, in agreement with Goldhaber's prediction.

From the point of view of simplicity of spectrum, as well as of chemical and physical behavior, borine carbonyl appeared to be the most satisfactory molecule from which to determine the spins of the boron isotopes by means of microwave spectroscopy. However, because these nuclei are small in size, a large quadrupole moment was not expected for either. And because the electron diffraction data[6] indicated a molecular structure which could be explained on the basis of tetrahedral bonds to the boron, we were not very hopeful at the outset that a resolution of the hyperfine structure

[2] W. Gordy and M. Kessler, Phys. Rev. **71**, 640 (1947).
[3] W. Gordy, Rev. Mod. Phys. **20**, 668 (1948).
[4] R. Unterberger and W. V. Smith, Rev. Sci. Inst. **19**, 580 (1948).
[5] M. Goldhaber, Phys. Rev. **74**, 1194 (1948).
[6] S. H. Bauer, J. Am. Chem. Soc. **59**, 1804 (1937).

would be possible. Fortunately, the HBH angles proved to be larger than tetrahedral and the quadrupole coupling just large enough to allow determination of the spins of both B^{10} and B^{11}. It is also fortunate that the centrifugal stretching in the BH_3CO molecule is so large that the hyperfine structure of the $K=0$ lines is completely separated from that of the $K=1$ lines. For BD_3CO this is not quite true. For this reason the spin determinations from the latter molecule are not quite as definite as those from BH_3CO, although they do provide confirming evidence. See Table I.

The transition by which we were able to establish the spins is $J=1\rightarrow2$, which for $B^{10}H_3CO$ occurs at 35919 mc/sec. The hyperfine structure of the $J=0\rightarrow1$ transition, which contains only three lines, is more widely spaced than that of the $J=1\rightarrow2$. Nevertheless, because its absorption is much weaker than that of the $J=1\rightarrow2$, we were unable to detect its lines at the extremely low pressures required for their resolution. The absorption at the $J=2\rightarrow3$ transition is of course, stronger than that at the $J=1\rightarrow2$. But in the $J=2\rightarrow3$ transition the hyperfine structure is so closely spaced that we were unable to resolve it, although we could detect a broadening of the $K=2$ and the $K=3$ lines caused by the quadrupole coupling. The sample contained B^{10} in normal concentration, about 18 percent. With our spectrometer one could obtain complete resolution of the $J=0\rightarrow1$ transition by using a sample containing a high concentration of the B^{10} isotope, also a better resolution of the $J=1\rightarrow2$ transition. Since the data obtained were considered adequate to establish the spin, we did not prepare a sample with concentrated B^{10}. By using the Stark modulation method[7] one can obtain higher sensitivity, but the consequent complication of the pattern decreases the resolution and might prevent identification of the spin. Indeed, Strandberg, Pearsall, and Weiss[8] have observed the $J=0\rightarrow1$ transition with the Stark modulation method but were unable to resolve the hyperfine structure.[9]

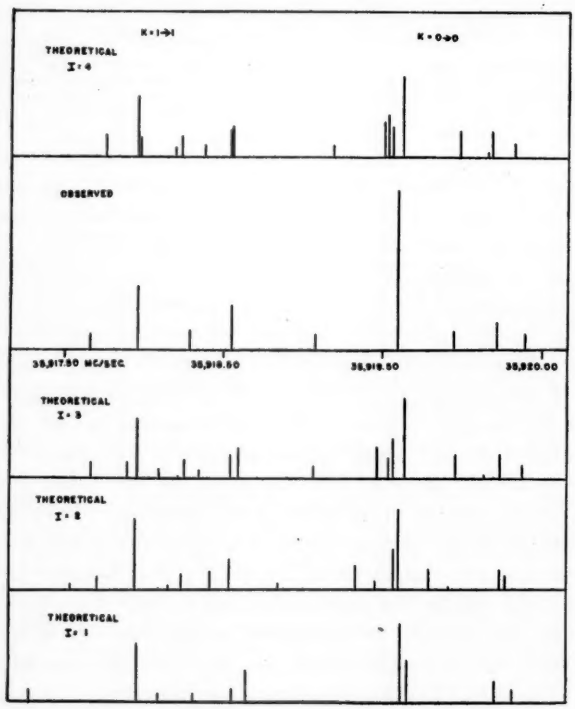

FIG. 1. Observed and calculated hyperfine structure of the $J=1\rightarrow2$ transition of $B^{10}H_3CO$.

Figure 1 shows the positions and estimated intensities of the observed lines, compared with the theoretically predicted patterns for different spin values which might be considered possible. It is apparent that the spin of 3 is the only one consistent with the observed data.[10] In Fig. 2 are shown two photographs of the C.R.O. presentation of the hyperfine structure. The measurements of the lines are more certain than the pictures indicate, since the adjustment of conditions for the over-all picture was not as favorable as was possible when adjustments were optimized for a certain portion. Also, the measurements were checked many times under different conditions of observation, and on $B^{10}D_3CO$ as well as $B^{10}H_3CO$. See Table I.

Figure 3 and Table I compare the calculated and observed hyperfine structure for the $J=1\rightarrow2$ transition of $B^{11}H_3CO$. These comparisons demonstrate that the nuclear spin of B^{11} is 3/2.

Quadrupole Moments

The nuclear quadrupole coupling $eQ(\partial^2V)/(\partial z^2)$ is calculated from the formula:

$$E_Q=eQ\frac{\partial^2V}{\partial z^2}\left(\frac{3K^2}{J(J+1)}-1\right)\times\left(\frac{\frac{3}{4}C(C+1)-I(I+1)J(J+1)}{2(2J+3)(2J-1)I(2I-1)}\right),$$

where $C=F(F+1)-I(I+1)-J(J+1)$, $F=J+I, J+I-1\cdots|J-I|$, I=spin of the interacting nucleus, and J=rotational quantum number. Table I gives the observed hyperfine structure for the $J=1\rightarrow2$ transition of $B^{10}H_3CO$, $B^{10}D_3CO$, $B^{11}H_3CO$, and $B^{11}D_3CO$ with that calculated from the above formula, using $eQ(\partial^2V)/(\partial z^2)=3.36$ mc/sec. for B^{10} and 1.55 mc/sec. for B^{11}. These we consider the most probable values for the respective couplings. They give the ratio of the quadrupole moment of B^{10} to that of B^{11} as 2.17 and show that both the moments are of the same sign.

[7] R. H. Hughes and E. B. Wilson, Phys. Rev. **71**, 562 (1947).
[8] Strandberg, Pearsall, and Weiss, J. Chem. Phys. **17**, 429 (1949).
[9] After this was written we learned by private communication that Weiss, Strandberg, Lawrance, and Loomis have now been able to check our spin assignment with the Stark modulation method.
[10] The calculated spectra for spin values of 2 and 4, which are closest to the correct value, have certain frequency ratios which differ from the corresponding observed ratios by a factor outside the range of experimental error.

To obtain the quadrupole moment Q from the measured quadrupole coupling, one must evaluate the quantity $(\partial^2V)/(\partial z^2)$, which represents the gradient along the symmetry axis of the electric field of the extra nuclear electrons. An exact calculation of this quantity is not possible for borine carbonyl, but from the molecular structure determinations given below one can obtain an approximate value. As indicated below, the structure of borine carbonyl may be considered as a resonant hybrid of structures I to V. The value of $(\partial^2V)/(\partial z^2)$ can be calculated approximately for these contributing structures. To obtain its value for the actual molecule we average the values for these structures in proportion to their estimated contributions to the ground state of the molecule.

In structures I and II, with four equivalent tetrahedral bonds to boron, the valence shell of B is symmetrically filled; and, except for second-order polarization effects, which we discuss below, $(\partial^2V)/(\partial z^2)$ would be zero. This is also true, to a first approximation, for III and IV. In the most important case, structure V, where we have essentially free BH_3 and CO, there are, from analogy with BF_3, three equivalent sp^2 bonds to boron which lie in a plane at angles of 120°. The p orbital perpendicular to this plane and along the symmetry axis of the molecule contains no electrons. Following the practice of Townes,[11] we estimate $(\partial^2V)/(\partial z^2)$ for this case from the formula,

$$(\partial^2V)/(\partial z^2)=\frac{2\epsilon\Delta\nu l(l+1)}{Z_i R\alpha^2 a_0^3(2l-1)(l+\frac{1}{2})(2l+3)},$$

used to calculate the coupling of electrons in isolated atoms.[12] It is clear that there is an equivalent deficit of one p electron along the molecular axis and hence that $(\partial^2V)/(\partial z^2)$ would be positive in sign. From the value of $\Delta\nu=15$ cm^{-1}, taken from Bacher and Goudsmit,[13] and with $Z_{\text{eff}}=3.1$, we obtain $(\partial^2V)/(\partial z^2)=1.44\times10^{15}$ e.s.u. for this case.

The contributions to $(\partial^2V)/(\partial z^2)$ by the excited electronic states can be neglected in the present approximation. Also, the effects of bond-orbital overlap are negligible. Distortion of the bond orbitals by the adjacent atoms requires consideration. In structures I and II the distortion effects would be in the same direction along each bond and would tend to cancel each other. Though the carbon is further from the boron than are the hydrogens, its greater electronegativity and its positive formal charge in II would still allow it to counterbalance approximately the effects of the hydrogens. In III and IV the distortion effects would tend to cancel each other but to a lesser extent than in I and II since the bond angles would not be exactly tetrahedral. For these structures a small negative contribution to $(\partial^2V)/(\partial z^2)$ might be expected. In structure V we neglect the effects of the CO group since here it is effectively free carbon monoxide, which is known to have a very small dipole moment (~0.1 debye). Fortunately, hydrogen and boron have almost the same electronegativities, 2.1 and 2.0, and consequently the ionic character of the BH bonds will be very small. The most apparent effects of the hydrogens would be to flatten slightly the boron atomic orbitals in the BH_3 plane and hence to increase $(\partial^2V)/(\partial z^2)$. One can estimate the order of magnitude of the hydrogen effects by a comparison with the $(\partial^2V)/(\partial z^2)$ for the hydrogen molecule, which is due almost entirely to distortion of the s orbitals. This quantity has been calculated for H_2 by Nordsieck[14] as 1.15×10^{15} e.s.u. Since the hydrogen-boron separation in BH_3 ($d_{BH}=1.194$A) is much greater than the hydrogen separation in H_2 (0.74A), the contribution of each H should be very much less than that in H_2. The effects of the hydrogens should be, however, more important than the negative contributions of III and IV, and hence one would expect the combined distortion effects to increase $(\partial^2V)/(\partial z^2)$ slightly.

For reasons given in a later section it is concluded that structure V contributes 40 to 50 percent to the ground state of the molecule. Hence we conclude that $(\partial^2V)/(\partial z^2)\approx0.7\times10^{15}$ e.s.u. for the borine carbonyl molecule. With the observed couplings this gives 0.06×10^{-24} cm^2 for B^{10} and 0.03×10^{-24} cm^2 for B^{11}. The distortion effects, which we neglect, would tend to decrease these values but not to change their sign, since their estimated total effect is to increase $(\partial^2V)/(\partial z^2)$.

Magnetic Moments

The nuclear g-factors for both B^{10} and B^{11} have been evaluated by Millman, Kusch, and Rabi[15] with the molecular beam method, and more recently by Bitter[16] using nuclear magnetic resonance. Zimmerman and Williams[17] also give a value for B^{11}/H determined by the magnetic resonance method. Using the frequency ratios given by Bitter, $B^{10}/B^{11}=0.33488$ and $B^{11}/H=0.32085$, with the spin values determined in the present work, one obtains $\mu_{B^{10}}=1.7984$ and $\mu_{B^{11}}=2.6851$ nuclear magnetons. In these calculations we neglect dimagnetic corrections and assume $\mu_H=2.7896$ nuclear magnetons (Table II).

4. MOLECULAR PROPERTIES

From the spacing of the rotational lines for the different transitions it is established that borine carbonyl has a symmetric-top structure. This was indicated by the earlier electron diffraction work of Bauer,[6] but

[11] C. H. Townes, Phys. Rev. **71**, 909 (1947); C. H. Townes and B. P. Dailey, J. Chem. Phys. **17**, 782 (1949).
[12] H. A. Bethe and R. F. Bacher, Rev. Mod. Phys. **8**, 226 (1936).
[13] R. F. Bacher and S. Goudsmit, *Atomic Energy States* (McGraw-Hill Book Company, Inc., New York, 1932).
[14] A. Nordsieck, Phys. Rev. **58**, 310 (1940).
[15] Millman, Kusch, and Rabi, Phys. Rev. **56**, 165 (1939).
[16] F. Bitter, Phys. Rev. **75**, 1326(A) (1949).
[17] J. R. Zimmerman and D. Williams, Phys. Rev. **76**, 350 (1949).

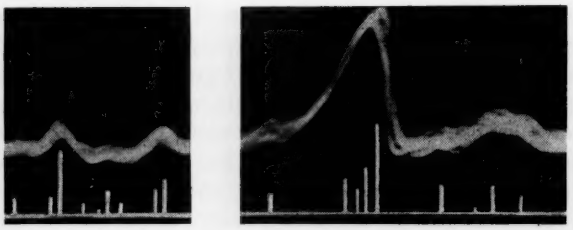

$K=1\rightarrow1$ $K=0\rightarrow0$

FIG. 2. A photograph of a cathode-ray tracing of the $J=1\rightarrow2$ transition of $B^{10}H_3CO$, with bars showing the theoretical spectrum for a nuclear spin of 3 for B^{10}.

small deviations from symmetry cannot be detected by this method.[18] Exclusive of nuclear interactions, the rotational frequencies of a symmetric-top molecule are given by the formula,[19]

$$\nu(\text{cm}^{-1})=2\text{B}(J+1)-2D_{JK}(J+1)K^2-4D_J(J+1)^3$$

where $\text{B}=h/(8\pi^2cI_\text{B})$, and $J=0, 1, 2, \cdots$. Here, I_B represents the moment of inertia about an axis perpendicular to the symmetry axis, and D_J and D_{JK} are distortion constants. Values for these constants, except for D_J, as determined from the rotational frequencies are listed in Table III. Although two rotational frequencies were measured for BH_3CO, the constant D_J is so small that its effects were less than the possible error. Its magnitude is apparently less than 10 kc/sec. The D_{JK} values found are rather large, about four

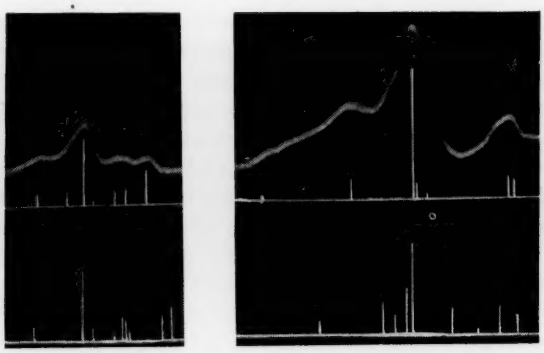

$K=1\rightarrow1$ $K=0\rightarrow0$

FIG. 3. A photograph of a cathode-ray tracing of the $J=1\rightarrow2$ transition of $B^{11}H_3CO$, with bars showing the theoretical spectrum for a nuclear spin of 3/2 (upper) and for a nuclear spin of 5/2 (lower) for B^{11}.

times those for methyl bromide and methyl iodide.[20] This indicates that the borine carbonyl bonds are much more easily distorted than are those in the methyl halides.

The internuclear distances and bond angles were calculated from the moments of inertia with the equation:

$$I_\text{B}=3M_\text{H}(x^2+(d^2_\text{BH}/2)\sin^2\alpha)+M_\text{B}(x-d_\text{BH}\cos\alpha)^2+M_\text{O}(d_\text{BC}+d_\text{CO}-x+d_\text{BH}\cos\alpha)^2+M_\text{C}(d_\text{BC}-x+d_\text{BH}\cos\alpha)^2,$$

where

$$x=\frac{M_\text{C}(d_\text{BC}+d_\text{BH}\cos\alpha)+M_\text{B}d_\text{BH}\cos\alpha+M_\text{O}(d_\text{BC}+d_\text{CO}+d_\text{BH}\cos\alpha)}{3M_\text{H}+M_\text{B}+M_\text{O}+M_\text{C}},$$

and where $\alpha=180°-\angle\text{HBC}$. This formula is readily derived from the geometry of the molecule. There are four structural parameters. Hence, the four different isotopic forms studied are just sufficient to determine the structure completely. The interatomic distances and bond lengths obtained are listed in Table IV, with those previously determined from electron diffraction. The accuracy of our values is limited by zero point energy effects. The error limits are not definitely known but are probably less than one percent.

TABLE II. Nuclear moments of boron.

Isotope	Spin I	Quadrupole coupling in BH_3CO $eQ(\partial^2V)/(\partial z^2)$	Quadrupole moment Q	Magnetic moment μ
B^{10}	3	3.36±0.10 mc/sec.	$\sim0.06\times10^{-24}$ cm²	1.7984[a]
B^{11}	3/2	1.55±0.08 mc/sec.	$\sim0.03\times10^{-24}$ cm²	2.7896[a]

[a] Given in nuclear magnetons. These values are determined from Bitter's g-values (reference 16).

[18] The symmetric top configuration is also revealed by the recent infra-red work of R. D. Cowan, J. Chem. Phys. **17**, 218 (1949).

[19] Z. I. Slawsky and D. M. Dennison, J. Chem. Phys. **7**, 509 (1939). G. Herzberg, *Infrared and Raman Spectra of Polyatomic Molecules* (D. Van Nostrand Company, Inc., New York, 1945), p. 224.

The electronic structure of borine carbonyl is rather unusual. To explain the diffraction results of Bauer,[6] Pauling[21] suggested resonance between structures I and

TABLE III. Observed rotational frequencies and molecular constants.

Molecule	ν in mc/sec.[a]		B in mc/sec.	D_{JK} in mc/sec.	I_B[b] in g cm² $\times10^{-40}$
$B^{10}H_3C^{13}O$	35,919.74±0.10	$(J=1\rightarrow2,\ K=0)$	8,979.94	0.39	93.42₆₆
	35,918.17±0.10	$(J=1\rightarrow2,\ K=1)$			
	53,879.98±0.15	$(J=2\rightarrow3,\ K=0)$			
	53,877.68±0.15	$(J=2\rightarrow3,\ K=1)$			
	53,870.70±0.15	$(J=2\rightarrow3,\ K=2)$			
$B^{11}H_3C^{13}O$	34,628.88±0.10	$(J=1\rightarrow2,\ K=0)$	8,657.22	0.36	96.90₉₂
	34,627.52±0.10	$(J=1\rightarrow2,\ K=1)$			
	51,942.84±0.15	$(J=2\rightarrow3,\ K=0)$			
	51,940.59±0.15	$(J=2\rightarrow3,\ K=1)$			
	51,934.41±0.15	$(J=2\rightarrow3,\ K=2)$			
$B^{10}D_3C^{13}O$	30,121.35±0.30	$(J=1\rightarrow2,\ K=0)$	7,530.34	0.29	111.41₁₁
	30,120.20±0.30	$(J=1\rightarrow2,\ K=1)$			
$B^{11}D_3C^{13}O$	29,346.26±0.20	$(J=1\rightarrow2,\ K=0)$	7,336.56	0.24	114.35₄₀
	29,345.33±0.20	$(J=1\rightarrow2,\ K=1)$			

[a] Frequency here represents the frequency of the rotational line corrected for nuclear quadrupole displacements.
[b] The value for Planck's constant used in calculating I_B values is $6.624_2\times10^{-27}$ erg-sec. [from R. T. Birge, Rev. Mod. Phys. **13**, 233 (1941)].

[20] Gordy, Simmons, and Smith, Phys. Rev. **74**, 243 (1948).

[21] L. Pauling, *The Nature of the Chemical Bond* (Cornell University Press, Ithaca, New York, 1939), p. 244.

TABLE IV. Molecular dimensions of borine carbonyl.

	Present value[a]	Electron diffraction value[b]
d_{BH}	1.194A	1.20A
d_{BC}	1.540A	1.57A
d_{CO}	1.131A	1.13A
∠HBH	113°52′	Tetrahedral

[a] The masses used in these calculations are: $M_H = 1.00813$, $M_{C^{12}} = 12.00386$, $M_O = 16.00000$, $M_{B^{10}} = 10.01631$, and $M_{B^{11}} = 11.01292$, all in a.m.u. [from M. S. Livingston and H. A. Bethe, Rev. Mod. Phys. 9, 373 (1937)]. The unit atomic mass used is 1.6599×10^{-24} g [from R. T. Birge, Rev. Mod. Phys. 13, 233 (1941)].
[b] From S. H. Bauer, reference 6.

II. Bauer[6] proposed, in addition, possible contributions

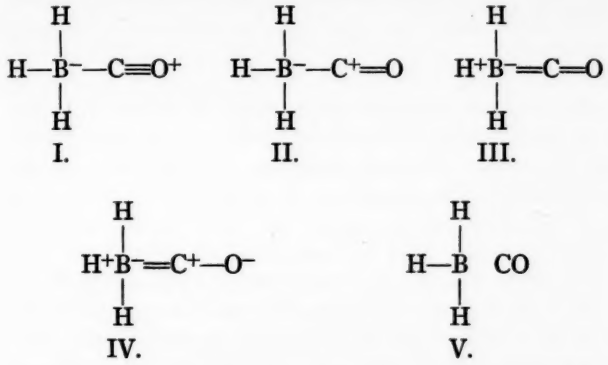

from structures III and IV. Our results indicate that structure V, which is essentially free BH_3 and CO with no formal bond between B and C, also contributes significantly to the ground state. Contributions from structure V are needed to explain the fact that ∠HBH is intermediate between the tetrahedral sp^3 type and the planar sp^2 type. If a linear variation of bond type with bond angle is assumed, structure V would contribute about 40 to 50 percent to the ground state of borine carbonyl.

The dipole moment of BH_3CO, which has been measured by Strandberg, Pearsall, and Weiss[8] as 1.795 debye, shows that I and II are not the only important contributing structures. A very large dipole moment is indicated for I or II by the product of the formal charge and the internuclear distances. These are 13 debye for I and 7.3 debye for II. The dipole moment expected for III would be about 1.4 debye in the opposite direction. Structure IV would have a still larger moment in the opposite direction from that of I and II, but from the electronegativity difference of C and O its expected contribution to the ground state would be only about 20 percent that of III. The dipole moment of structure V would be essentially that of carbon monoxide, 0.1 debye. One can account for the observed dipole moment by assuming 40 to 50 percent contribution from V, about 30 percent from I and II combined, and about 20 percent from III and IV combined.

The observed bond lengths are in agreement with the proportional contributions of I to V needed to explain the dipole moment. The BH bonds are of the length expected for normal covalent BH bonds (added radii = 1.20A). The CO length is equivalent to that in carbon monoxide (1.13A). The BC length expected for structure I is 1.66A, the added covalent radii. As pointed out by Pauling,[21] this value should be about 0.10A shorter for II because of the deficit of electrons around C. The contributions from structure V would not influence the BC length significantly because for it there are no electrons in the B orbital along BC. Contributions from structures III and IV would tend to shorten BC, since the added double-bond covalent radii is only 1.43A. However, the CO length expected for the combination of III and IV would be 1.21A (i.e., in CH_2CO and similar molecules), and for this reason large contributions from these structures would not be expected.

From consideration of bond angles, bond lengths, and dipole moments we conclude that borine carbonyl may be considered a resonant hybrid of structures I to V, with their contributions probably decreasing in the order V, II, III, I, and IV. These conclusions are in harmony with the chemical instability of the molecule and with the fact that it can be stabilized under pressure with carbon monoxide.

We wish to thank Vida Miller Gordy for assisting with the calculations and the preparation of the manuscript.

Magnetic Deflection of Cosmic-Ray Mesons Using Nuclear Plates*

IAN BARBOUR†
University of Chicago, Chicago, Illinois
(Received January 12, 1950)

An experiment has been carried out in which two nuclear plates, secured with an air gap separating their parallel emulsion surfaces in a perpendicular magnetic field, were used to obtain magnetic deflection measurements on cosmic-ray mesons near the top of the atmosphere. Details of the experimental procedure are given and sources of error are discussed. The signs of the charges of particles were determined, and confirmation obtained for the negative charge of σ-(star-producing) mesons, positive charge for π and μ (observed disintegration), while both signs were observed for ρ-mesons (stopping without visible interaction). The relative abundances of the different meson types were investigated. For particles which stopped in the emulsion, range and magnetic curvature measurements allowed mass determinations which in the most favorable case of long path length gave, for an individual meson, a probable error of 15 percent in the mass determination. The values obtained were, for π- and σ-mesons, 270 ± 20; for μ and ρ, 226 ± 15. No evidence for light or very heavy mesons has been found so far.

1. INTRODUCTION

SINCE the definite identification of the tracks of mesons in photographic emulsions,[1] much valuable information on the cosmic radiation has been obtained through the use of nuclear plates. However, most emulsion techniques such as measurement of range, grain density, scattering, etc., yield no direct evidence as to the sign of the charge of any particle, while the individual determination of the mass of a cosmic-ray particle is of relatively low precision; a magnetic deflection measurement therefore may be expected to contribute better information on the charge and mass of the particle. Since in an emulsion the scattering of any low energy meson will obscure its magnetic curvature, with any attainable field strength, curvature measurements can best be made if the particle experiences a magnetic deflection in a medium of low scattering power and low stopping power, such as an air gap between two plates. Such a method of obtaining magnetic deflection measurements on mesons was suggested by Powell and Rosenblum;[2] an investigation of the possibilities of this type of experiment and development of the necessary techniques had also been independently undertaken in this laboratory[3] and preliminary results have been published.[4]

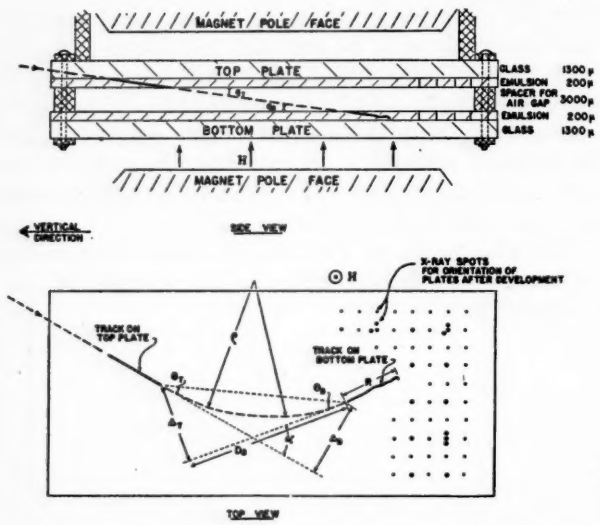

FIG. 1. Top and side view of plates as exposed in the field of the magnet. A typical meson is schematically represented, crossing the top emulsion and stopping in the bottom emulsion.

Because of the difficulty of reconstructing the orientation of the plates after development, Powell suggested[2] placing the developed emulsions in contact with each other; since this necessitated viewing the emulsion through the glass backing of standard thickness about 1 mm, the usual refracting microscope with short working distance could not be used. He therefore proposed the use of a specially constructed reflecting microscope[5] without objective lenses, having a large working distance. Prior to this time we were using emulsions on thin glass slides[3] so that an ordinary microscope could be used to view through the thin glass backing, but later the desired accuracy was achieved by the method[4] described in detail below, in which a pantograph[6] was used to map separately the events found on each plate on to large sheets of tracing paper, which were then superimposed for measuring deflection angles.

Several factors favored an experiment at stratospheric rather than mountain altitudes: (a) The frequency of events involving mesons is very considerably greater under a given quantity of matter at the top of

* Assisted by the Joint Program of the ONR and the AEC. The author is also indebted to the du Pont Company for a fellowship, and to the Research Corporation for a Cottrell Grant, during certain periods of this work.

† Now at Kalamazoo College, Kalamazoo, Michigan.

[1] Lattes, Occhialini, and Powell, Nature **160**, 453 (1947).

[2] C. Powell and S. Rosenblum, Nature **161**, 473 (1948); see also C. Franzinetti in *Cosmic Radiation* (Butterworth's, Ltd., London, 1949), p. 159. *Note added in proof.*—a more complete account has appeared after the present paper was submitted for publication: C. Franzinetti, Phil. Mag. **41**, 86 (1950).

[3] I. Barbour, Phys. Rev. **74**, 507 (1948).

[4] I. Barbour, Phys. Rev. **76**, 170 (1949); **76**, 320 (1949).

[5] C. R. Burch, Proc. Phys. Soc. London **59**, 41 (1947).

[6] I. Barbour, Rev. Sci. Inst. **20**, 530 (1949).

the atmosphere[7] and hence the number of mesons with long trajectories obtainable per plate per hour is correspondingly greater; also there is greater ease and certainty in matching the track segments due to one meson as it passes through the two emulsions, as the ratio of mesons stopping to protons stopping is very much increased under matter at balloon altitudes; (b) at mountain elevations the scattering of low energy mesons in the air of the gap between the plates is a serious problem, whereas close to the top of the atmosphere the scattering in the air of very low pressure introduces negligible errors; (c) it was desirable to investigate the presence of mesons of various masses and charges in the upper atmosphere since the creation of mesons takes place largely at the higher altitudes. Preliminary investigations with a 10-lb. magnetron magnet in a B-29 airplane showed the possibility of obtaining magnetic deflections. A larger magnet, described below, was accordingly constructed and four successful balloon flights were carried out through the cooperation of the ONR, using General Mills balloons.

2. EXPERIMENTAL PROCEDURE

Two nuclear plates were mounted as a "sandwich" in an aluminum plate-holder which held them rigidly face-to-face with a 3-mm air gap separating their parallel emulsion surfaces, as in Fig. 1. Ilford C2 plates were used throughout; on the first flight, 100-micron emulsions were employed, but in subsequent flights 200-micron emulsions were used because, as will be discussed later, better statistics could be obtained with thicker emulsions, without introducing significantly greater distortion errors. Special Ilford plates with an added quantity of plasticizer were tried on a test run, to see if this agent would increase the rigidity and thus lessen the emulsion distortion. Since there was no evidence for an appreciable effect of this sort they were not used in the magnetic deflection experiments. On the first flights, 2 in.×4 in. plates were used. For the last two flights specially manufactured 4 in.×4 in. plates were obtained so that a margin of 1 in. of emulsion surrounded the central 2 in.×2 in. emulsion area which was in the region of strong magnetic field; hence the large errors in track angles which would have been caused by emulsion distortion near the plate edges was avoided. The mounted plates, wrapped in aluminum foil, were then exposed to an x-ray beam to produce on the emulsion the grid of reference dots[2,3] by which the relative orientation of the plates could later be reconstructed, after development. For this purpose a $\frac{1}{32}$-in. Pb plate, drilled with holes 100 microns in diameter on a $\frac{1}{2}$-cm square grid (with a coded 3-hole pattern at intervals for ease in identification) was placed between the plates and a distant x-ray source. The plate-holder was then secured to the magnet for the balloon flight.

The magnet weighs 65 lb., produces a field of 13,300 gauss in an air gap $\frac{1}{4}$ in. wide, with pole pieces 2 in.×2 in. in area (25.9 cm²). The side blocks are of Alnico V; the cross-yoke and pole-pieces are of soft iron. The magnet was mounted with the gap and plates vertically downward so that there was thus a considerable quantity of iron above the plates to act as a meson generator, since at the top of the atmosphere there are few mesons of low energy found in the free air. The magnet was rigidly mounted in a Dow-metal frame which was then suspended by 16 shock-absorbing springs from a larger aluminum frame, enclosed with celluloid sheets and reflecting surfaces to provide temperature control. The equipment was flown from Camp Ripley, Minnesota, and the magnet and parachute were released in the upper atmosphere by a clock mechanism at a predetermined time. The first flight was sent to about 90,000 ft. for a trial period of 1 hour; the second was flown at this altitude for 3 hours, a third at 70,000 ft. for 6 hours, and the fourth flight for 6 hours at 90,000 ft.

A number of different development procedures were tried on 200-micron test plates, to determine the method most suitable for processing the emulsions from the deflection experiments. The "cold method," [8] in which development of the plates during the time of diffusion of the developer is inhibited by lowering the temperature, gave excellent evenness of development, but in general appeared to produce greater distortion of the emulsion than other methods, as measured by the *apparent* deflection of fast proton tracks between "sandwich" pairs of plates exposed with no magnetic field. Several variations of the "two-bath" method[9] were tried, in which developing action during diffusion in the first solution is almost absent because the alkali agent is in the second bath only. These methods produced even development and little distortion; however we were not able to prevent the appearance of a higher density of background and surface grains, which increase the difficulty in scanning the emulsions for tracks and measuring their angles of emergence from the emulsion. (The usual operation of wiping the emulsion surface to remove these surface grains would be undesirable in this experiment.) The most satisfactory method appeared to be a one-bath, one-temperature method, but with a somewhat weaker developer (D19 4:1) and lower temperature (18°C) than usually employed, so that a longer development time (around 55 minutes for 200-micron emulsions) is required; the time of diffusion is thus a smaller fraction of the total developing time, and a more even development results than in the standard method. However this procedure does produce tracks slightly denser near the surface than near the glass, and hence can not be recommended if accurate grain counts are desired *throughout* the emulsion. In this experiment, where grain counts were of secondary importance and were carried out only near the surface of the emulsion to identify the 2-track

[7] J. Lord and Marcel Schein, Phys. Rev. **75**, 1956 (1949).

[8] Dilworth, Occhialini, and Payne, Nature **162**, 102 (1948).

[9] M. Blau and C. DeFelice, Phys. Rev. **74**, 1198 (1948).

segments due to one particle passing through the two emulsions, and where freedom from emulsion distortion is of primary importance, it was found to be the most satisfactory method. Test runs were made to see if the use of a separate hardening solution between development and fixation would reduce distortion; since the improvement found was not pronounced, a standard acid fixer with hardener was used in these experiments.[9a]

3. ANALYSIS OF PLATES

After development the plates were scanned and the location of all particles stopping in the emulsion, and of heavy nuclei, stars, meson events, etc., were plotted relative to the grid of x-ray dots. This was greatly facilitated by the construction of a pantograph[6] attached to the microscope stage, by which the motion of the stage is mechanically amplified twenty times. When the scanner sees an event of interest, he has only to close a switch which activates a magnetically operated pen at the free end of the pantograph, thus recording on a large sheet of paper a plot of the position of the event. The pantograph has precision bearings, so that by using a cross-hair in the microscope eye-piece, considerable accuracy in plotting a point on the emulsion can be obtained. The azimuth direction of the emerging track, projected in the plane of the emulsion surface, is then read off with a goniometer protractor[6] on the microscope eye-piece; these angles are later reconstructed on the sheet of plotting paper. The approximate dip angle between the track and the plane of the emulsion can be determined by measuring under oil immersion the difference in depth of two track points of known horizontal separation. From these data, knowing the factor by which the emulsion shrinks on development (approximately 2.4 for these plates with 200-micron emulsions), one can calculate the approximate point at which the particle would have emerged from the opposite plate of the "sandwich" if undeflected. If in addition the range of the particle has been measured and the magnetic field strength is known, it is possible to lay off an area in which one should expect to find the matching segment of track in the second plate. The correct matching of the two track segments in the two emulsions, due to a single meson, can be ascertained from the following characteristics of the tracks:

(a) The positions and locations of the two tracks must be such that the deflection angle (θ_T in Fig. 1) between the tangent to the track as the particle leaves the top plate and the line connecting the points of leaving and entering the air gap, must equal the angle (θ_B) between the tangent to the second segment of track as it enters the opposite plate, and this same connecting line. This is, of course, a consequence of the fact that the trajectory due to the magnetic field in the gap is an arc of a circle; the two measured θ-angles should not differ by much more than twice the total probable error in each angle (see "sources of error").

(b) The dip angles between each of the two track segments and their respective emulsion surfaces should agree closely since the two emulsions had the same shrinkage factor at development. The dip angle can be determined by measuring the depth below the emulsion surface of a number of points on the track; the Leitz microscope used in these experiments has a ball-bearing fine adjustment with almost no back-lash, and depths can be determined to $\frac{1}{4}$ micron by taking several readings. For more accurate measurements of the dip angle, a tilting stage[6] has been constructed for the microscope. With an objective and eyepiece combination having slight curvature of field, the angle through which the stage must be tilted to bring the portion of the track near the surface into simultaneous focus can be accurately measured.

(c) Grain counts on portions of the two tracks near the surface should agree closely.

(d) An estimate of the multiple scattering of the particle in the emulsion is also valuable. The tracks with small dip angle which, as pointed out later, are particularly important because of the smaller percentage error in their deflection measurements, will have long path lengths in the second emulsion and hence afford a good opportunity to estimate the scattering, which is often

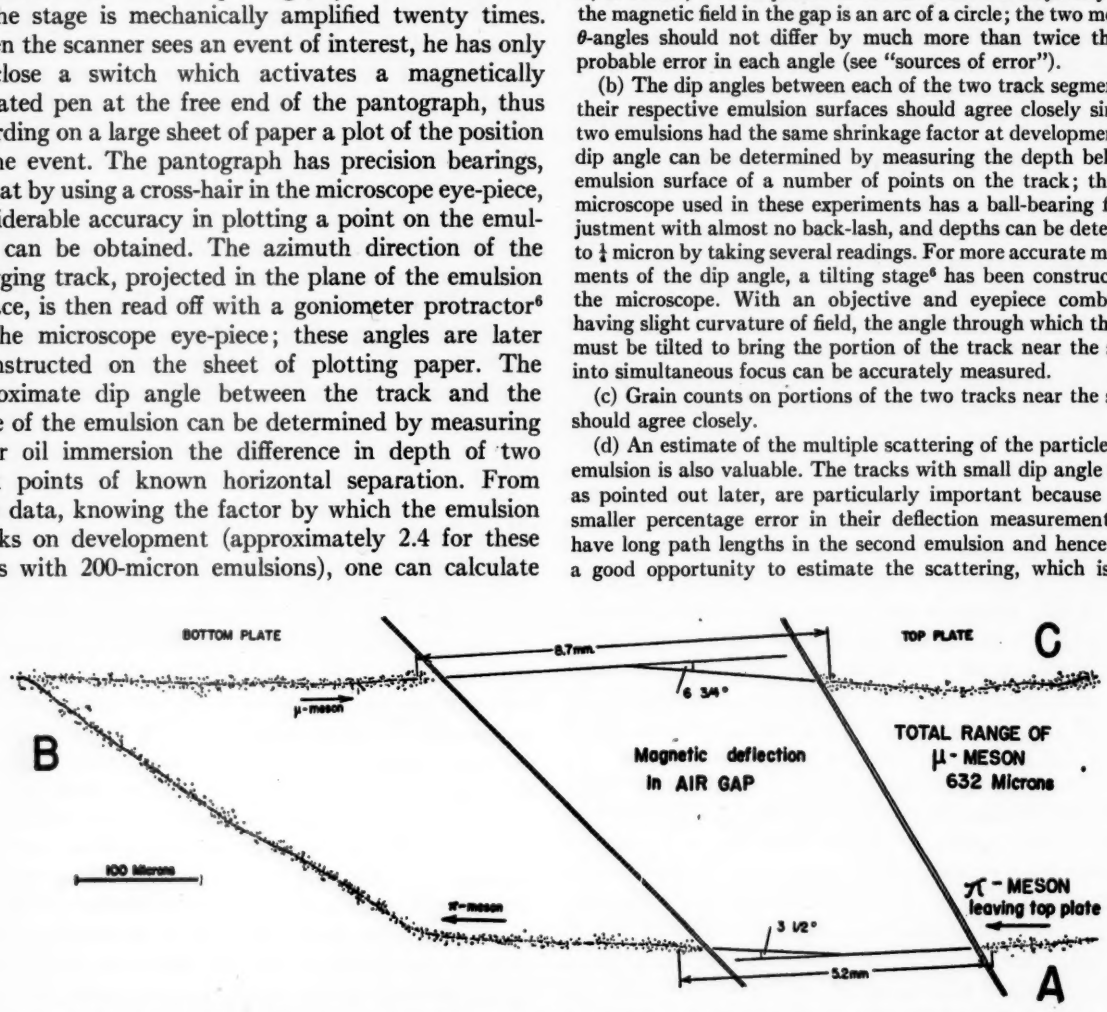

FIG. 2. Micro-projection of a $\pi-\mu$-decay occurring in 2 plates, arranged schematically to show magnetic deflection of both mesons. A π-meson traveled ~410 microns through the top emulsion to the point A and crossed the air gap, decaying in the bottom plate at B into a μ-meson which in turn re-crossed the air-gap to stop in the top emulsion at C. This case gave a mass determination of low accuracy, but was typical of cases showing the total range of a μ-meson.

[9a] It would be desirable in any extension of this type of experiment to investigate the use of a fine-grain developer with which a smaller grain size results, so that the azimuth angle at which a particle enters the emulsion could be more accurately determined from the first few grains of the track. Photo-glycine, for instance, has been recommended as giving a smaller size of grain, but in the developed emulsion the lighter tracks of low ionization appear harder to locate.

helpful in deciding which tracks passing through the emulsion might be due to mesons.

(e) The distance D_B, along the projection of one track, to the point of emergence from the opposite plate, must be consistent with the measured dip angles.

We have seldom found that there is more than *one* possible "matching" track in the second plate for which more than two or three of the characteristics above are in agreement. Matching is especially certain in the cases in which a π–μ-decay occurs in one plate and the μ-meson crosses the air-gap to stop in the second plate, for the total range in both plates of the μ-meson is known[1] to be about 600 microns. Figure 2 shows a typical case in which both mesons of a π–μ-decay traversed the air-gap and the total range of the μ-meson in both plates can be determined.

Once the tracks have been matched, the radius of magnetic curvature, ρ, in the plane of the emulsion is computed from the distance, D_B, and from measurement of the total angular change in direction, α, experienced by the particle. This angle should be equal to the sum of the angles, θ_B and θ_T, measured to the points of emergence of the tracks (see Fig. 1). However, unlike the measurements of the angle θ, the total angular deflection is not influenced by any errors in plotting positions, laying-off angles on the tracing paper, etc.; α depends only on the difference in the measured azimuth directions of the two emergent track segments. By purely geometrical considerations, one can show that $\rho=\frac{1}{2}D_B \sec\frac{1}{2}\alpha \csc\frac{1}{2}\alpha$. The exact value of the actual dip angle, q, is calculated for each case from the distance D_B and the known 3-mm separation of the plates. As shown below, the mass calculations then depend only on three quantities measured experimentally on the plates for each meson: (1) the range, R; (2) the deflection angle, α; and (3) the distance D_B; for from α and D_B one can compute ρ and q.

The calculation of the mass of the particles from these data is dependent on two assumptions: (1) that their charge is numerically equal to the electronic charge, and (2) that the energy loss is a function only of the velocity, v, as is known to be the case for ionization losses. It follows that for any particle of given mass m and range R in the non-relativistic region the relation holds: $R=mF(v)$, or $v=F'(R/m)$. Hence if H is the magnetic field strength, and v_p is the component of the velocity perpendicular to the magnetic field, we find that

$$R\cos q/H\rho=KR\cos q/mv_p=KR/mv=f(R/m), \quad (1)$$

where K is a constant. Values of the function f, were calculated and plotted using the range-energy data[10] for protons in an Ilford emulsion. Hence, using for any particle the experimentally determined values of R, ρ, q, and H, and knowing f, the unknown value of the mass m can be determined from the extreme left and right members of Eq. (1).

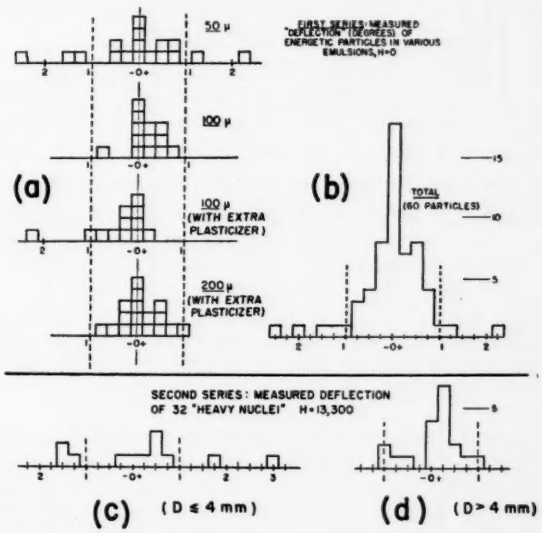
50 μ
100 μ
(a)
100 μ (WITH EXTRA PLASTICIZER)
200 μ (WITH EXTRA PLASTICIZER)
FIRST SERIES: MEASURED DEFLECTION (DEGREES) OF ENERGETIC PARTICLES IN VARIOUS EMULSIONS, H=0
(b)
TOTAL (60 PARTICLES)
SECOND SERIES: MEASURED DEFLECTION OF 32 "HEAVY NUCLEI" H=13,300
(c) (D ≤ 4 mm)
(d) (D > 4 mm)

FIG. 3. Distortion test: measured deflection angles for (a) protons in various emulsions as indicated, no field; (b) total of 60 fast particles; (c) steep tracks of heavy nuclei; and (d) heavy nuclei at glancing angles.

4. SOURCES OF ERROR

The experimental value of ρ depends on the measured total angular deflection. The following sources of error in angular measurements may be listed:

(a) *Scattering.*—The greatest source of error in measuring the azimuth direction of a particle starting or finishing its trajectory in the air gap is scattering as it enters or leaves the emulsion. In practice, the azimuth is read off, relative to a "zero" direction established from the x-ray grid, by setting the intersection of the eye-piece cross-hairs, under high magnification, on the last grain of the track as it passes into the air, and then rotating the eye-piece until the cross-hair coincides as closely as possible with the center of each grain of the adjacent track segment which usually appears "straight." Except for cases where a visible scattering occurs very near the surface, it was found that for meson tracks of the average energy encountered, the direction of emergence could best be determined from the grains of about the last 20 microns of track before emergence; if too short a segment is used the limit of resolution of the optical system and the finite size of a grain and uncertainty in the position of its "center" introduce greater uncertainty in the direction of the azimuth line, whereas if too long a segment is taken, scattering may introduce greater changes in the direction of motion of the particle. Such a length is in fair agreement with the theoretical optimum segment of track from which to measure its direction of motion at a given point, as derived by Scott.[11] For particles of lower energy and smaller residual range, shorter track segments were used. To estimate the error in azimuth due to scattering, one can start by assuming that in setting the cross-hair on, say, the last 20 microns of a track which appears "straight" over that distance, one is in reality determining on the average the direction of motion of the particle at about the mid-point of this segment; then the average error, due to scattering, in determining the actual azimuth direction of the particle at emergence will be the average angle of multiple scattering of such a particle in the last 10 microns of emulsion. Using the

[10] Lattes, Fowler, and Cuer, Proc. Phys. Soc. London **59**, 883 (1947).

[11] W. T. Scott, Phys. Rev. **76**, 214 (1949), Eq. (11b).

PLATE NO.	EMULSION THICKNESS (MICRONS)	TOTAL FLIGHT HOURS	NO. SQ. INCHES OBSERVED	CEILING ALT. (feet)	MINS. WITHIN 5000' OF CEILING	TYPE OF MESON ρ a	ρ g	π−μ a	π−μ g	σ a	σ g	EJECTED	TOTAL
1	100	8	4.5	99,000	.74	13	10	4	4	2	1	1	35
2	200	8	5	95,000	3	47	62	19	25	10	14	2	179
3	200	7	8.5	69,000	6	38	42	13	31	14	17	0	155
4	200	7	8	94,000	5	49	53	23	27	12	17	1	182
				TOTALS−		147	167	59	87	38	49	4	551
				TOTAL NO. OF MESONS OF EACH TYPE −		314		146		87		4	

FIG. 4. Number of mesons observed. Breakdown of total of 551 mesons according to plate, type of meson, etc. Mesons in columns "*a*" entered the emulsion from the air gap; those in columns "*g*" entered the emulsion from the glass backing.

results of the theory[11–13] and adapting these calculations to the C2 emulsion,[14] we can obtain for each meson the theoretical scattering angle (in the case above, for a path length of 10 microns), provided its range and an approximate value for its mass are known. For tracks of moderate range, this scattering angle, which represents an uncertainty inherent in this method, is of the order of 1 or 2 degrees.

(b) *Observational.*—There is also in practice a smaller uncertainty in reading each azimuth, depending on (1) the steepness of the track, (2) the particular pattern of the last few grains, and (3) the presence of any unusually large scattering which is directly visible in the last 20 microns, etc. An "observational" error, assigned to each measurement of the azimuth, is obtained by direct inspection of the track, and by the standard deviation or spread of 20 individual angle readings on each track (two observers each made a series of five successive readings, which were repeated with another microscope later). This source of error, while not independent of the scattering error above, is usually much smaller, and is included in the estimate of the total probable error to make allowance for the uncertainty occurring occasionally when a fairly straight track happens to have a visible sudden scatter very near the surface.

(c) *Emulsion distortion.*—During its life, development and drying, an emulsion inevitably experiences some distortion. It was found that contraction on drying causes severe distortion near the corners and lateral edges of a plate; this was the reason for obtaining plates large enough that measurements could be confined to areas of the plate at least 1 in. from the nearest plate edge. The total translatory motion of any point in the emulsion (distortion in position) does not introduce serious errors in this experiment. However, the derivative of this translation with respect to depth in the emulsion (i.e., the relative slippage of points at different depths) was found to be great enough to cause a rotary distortion in the angle of a track, particularly a steep one. In order to test the extent of this type of angle distortion, the apparent deflection was measured for a series of fast protons, passing through a sandwich in *no* magnetic field. These tests were made on several emulsions, developed in the method indicated above, as shown in Fig. 3, a. There is little variation among the emulsions of different thicknesses. At (b) the probable error of the distribution in angle is about ½°, as seen in the figure. Below, similar measurements are shown of the deflection angle of 32 heavy nuclei[15] with $H=13{,}300$ gauss. The distribution (d) refers to tracks of small or intermediate dip angles, i.e., path length D in the air-gap of at least 4 mm, which was about the minimum path length of any mesons used for deflection measurements; the distribution at (c) for very steep tracks ($D<4$) shows the greater errors in angle for steep tracks. These errors in the azimuth angles must include also any instrumental errors in the eye-piece protractor, or other parts of the microscope. These sources of error appear to be unavoidable and would represent the lowest limit (~½°) for angular errors in deflection measurements on very energetic mesons where scattering errors are small.

(d) *Scattering in air-gap.*—The scattering of particles in the air between the plates is proportional to the square root of the air pressure[12] and at these altitudes corresponding to about 1 cm Hg, turns out to be completely negligible compared to errors listed above.

In addition to errors in angle, there are four other factors which in this experiment cause smaller errors in the value of the calculated mass: (1) The *field* strength, H, was measured before and after each flight, with several different search coils calibrated with an accurate mutual inductance standard and ammeter. The field was mapped and found to be homogeneous to 2 percent to within ¼ in. of the edge of each pole-piece; and the absolute value of the field measurements are believed reliable to 2 percent. (2) The *range* of each particle in three dimensions is measured by making, for the cases of greater accuracy, a profile of depth *versus* horizontal component of path length. Since particles with reasonably long ranges were usually used, the error in range measurement produces an uncertainty in the mass value which is negligible compared with that due to the errors in measuring the deflection angle. (3) The value of the *dip angle* q in Eq. (1) is obtained from the path length D_B and the known 3-mm separation of the plates; these quantities are large enough to be measured with sufficient accuracy that the error in $\cos q$ (which is close to 1 for the tracks used) is negligible. (4) The *range-energy curve*[10] for protons, and its extrapola-

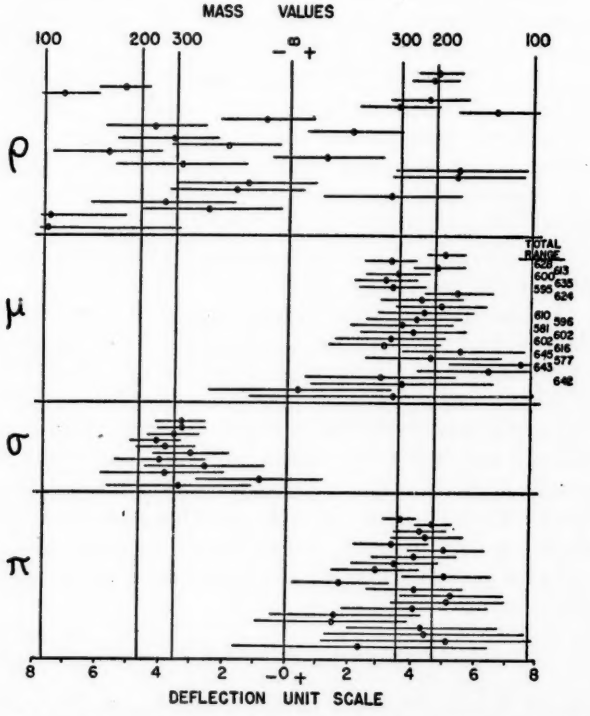

FIG. 5. Mass determinations on individual mesons, grouped vertically according to the type of meson and arranged in order of increasing precision. Values and probable errors are plotted on a deflection unit scale (see text); some corresponding mass values in units of m_e are given at the top. Positive charge is indicated if point lies to right of center-line, negative to left. For $\pi-\mu$-decays, in which the μ-meson was created in one plate and stopped in the other plate, the total range of the μ-meson is given at the extreme right of the diagram.

[12] H. Bethe, Phys. Rev. **70**, 821 (1946).
[13] E. J. Williams, Phys. Rev. **58**, 292 (1940).
[14] Goldschmidt-Clermont, King, Muirhead, and Ritson, Proc. Phys. Soc. London **61**, 183 (1948).
[15] Freier, Lofgren, Ney, Oppenheimer, Bradt, and Peters, Phys. Rev. **74**, 213 (1948).

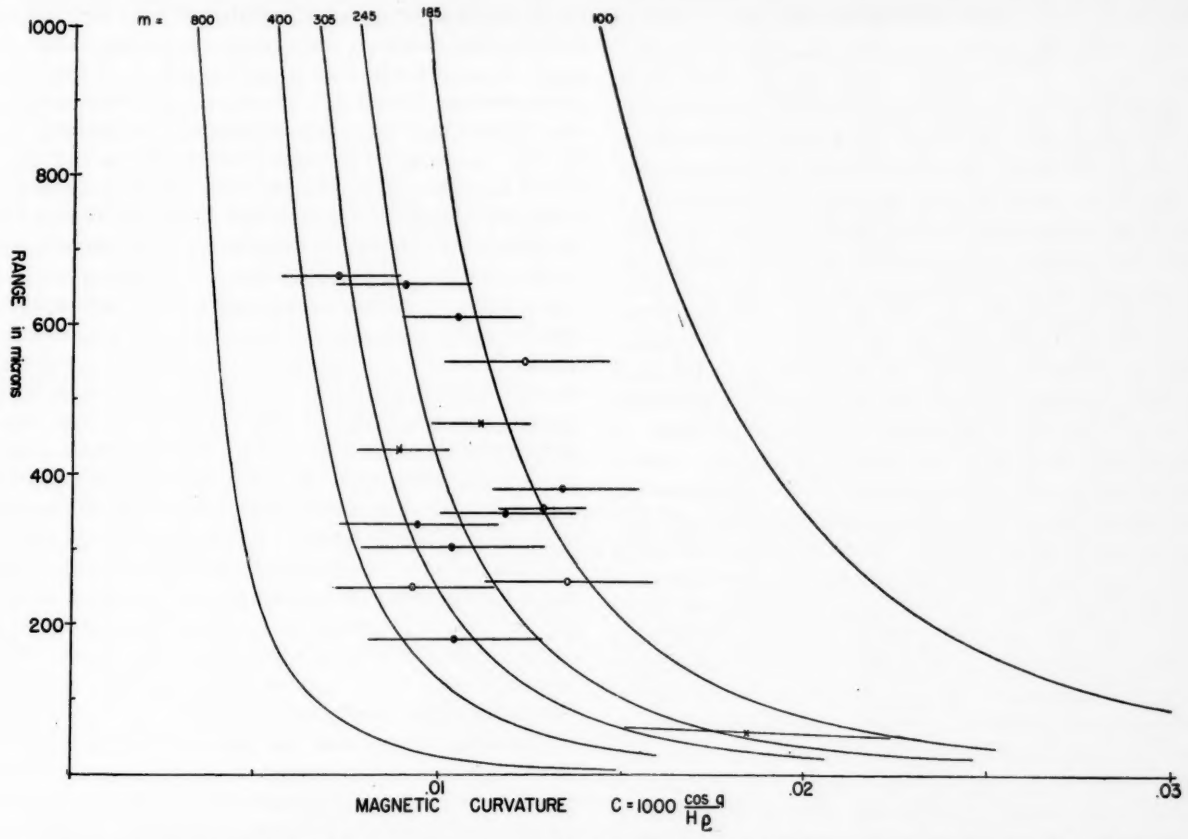

FIG. 6. Range-curvature plot. The solid curves represent the theoretical relationship between magnetic cuvature (C) and range in emulsion for a series of singly charged particles of different assumed mass values. A few experimental points and probable errors are given.

tion to higher energies, used for obtaining the function f in Eq. (1), may be assumed accurate to within a few percent.

The errors which would influence the mass determinations systematically (such as uncertainties in field or range) are in general small; the larger errors influencing the deflection angle α are Gaussian and hence tend to average out. Thus scattering errors are as likely to be positive as negative; similarly for observational errors, since the average measured angle for fast protons and heavy tracks was zero; even the occasional "mis-matching" of an unrelated track, which is possible though improbable, is as likely to occur on one side of the true corresponding track as on the other. The square of the *total* probable error in the angular deflection measurement for each meson is taken as the sum of the squares of the three sources of error in angle, *a*, *b*, and *c* above. Measurements of the apparent deflection of a few mesons in sandwiches with *no* magnetic field are consistent with this assignment of errors. (An exact experimental evaluation of angle errors in this manner would necessitate studying a very large number of such tracks, as there are these three independent sources of error in each case, and the scattering will give a Gaussian distribution of errors for each value of the range.) The plot of the final magnetic-deflection mass determinations, given in Fig. 5 below, indicates that the total probable errors have, if anything, been *over*estimated since for all types of mesons the *average* mass value for that group lies *within* the limits of probable error in the individual mass determination for considerably more than 50 percent of the cases; in fact, there are few cases in which the average value does not lie within the limits of probable error given. Of all the sources of error scattering is the most important. The average scattering angle is proportional to $1/E$, and decreases more rapidly than the curvature $(1/\rho)$ as one considers particles of greater and greater residual range; hence the percentage of error, due to scattering, in the deflection measurement is less for particles of longer range. It should also be emphasized that for a given curvature the angle of magnetic deflection is in first approximation proportional to the path length D in the air-gap. This has the important consequence that particles with small dip angle will have larger deflection angles; for such particles a given error in angle will represent a smaller percentage error in angle and hence greater accuracy in mass determination. These two factors, the range and the dip, account for the rather wide variations in the precision of individual mass determinations. A summary of all cases analyzed is given below.

5. RESULTS

Figure 4 indicates the number of events of different types found on the plates. The mesons have been grouped according to descriptive classifications,[1] where a σ is star-producing, π and μ are associated with an observed π–μ-decay, and a ρ is a particle which appears to have the scattering and density characteristic of a meson and stops with no visible interaction. For each individual stopped meson which had a trajectory in the air gap of at least 7 mm length, the mass was calculated from the observed experimental data as indicated in Eq. (1) (the plates of the 4th flight are still under analysis). The total probable error in angle, discussed in the preceding section, was then successively added to and then subtracted from the measured angle of deflection; using these two extreme angles new values of the mass were calculated which were assumed to correspond to the limits of probable error for that particular mass determination. The results are shown in Fig. 5 where, for each type of meson, the cases are arranged in order of increasing precision. In the figure there has been included a small sampling of the inaccurate cases. Since in averaging the mass determinations the values are weighted as the inverse squares of the probable errors, such cases contribute negligibly to such an average value; they are of interest because they indicate the sign of the charge (positive plotted on the right, negative on the left). The mass values have been plotted on a "deflection unit" scale in which equal increments of the deflection angle are measured by equal lengths in all parts of the scale. Since the errors in deflection angle must be Gaussian, probable errors in mass will be represented here by horizontal lines of equal length to the right and left of each point, which would not be the case on a linear mass abscissa. (The conversion from mass units to deflection units is actually made from a calculated curve relating the mass to the theoretical deflection angle measured in degrees for a particular range and dip angle which were arbitrarily chosen; hence, for mesons with other values of R and q, the reduced value expressed in these deflection units will not be equal to the actual deflection angle in *degrees*.)

The best statistical treatment of the experimental data to obtain an "average" mass value for each type of meson is performed by taking a least-squares fit in a representation where abscissa and ordinate are variables with Gaussian error distributions; in our case, this will be a range-curvature plot. Figure 6 shows such a representation of a few selected experimental points, together with a few typical theoretical range-curvature curves for a series of assumed mass values. (All the experimental points are not shown here because with four types of mesons and with different probable errors for each point this is not a convenient representation for visualizing all the data on one graph.) In contrast to cloud-chamber techniques the uncertainties in the range using photographic emulsions are very much smaller than those in the curvature, so that they can safely be neglected. This is particularly true since the constant-mass curves can be seen to have such a steep slope that a very large error in range would be required to produce an error in mass comparable to that produced by errors in curvature; the curves have a less steep slope for small values of the range, but at such low energies scattering in any case gives a larger uncertainty in the curvature. The best value of the mass of a given type of meson is then determined by the least-squares method as the parameter of that curve of constant mass which for the experimental points on the range-curvature plot minimizes the sum $\sum(V_i/\epsilon_i)^2$, where V_i is the residual and ϵ_i the probable error of the curvature of an individual meson.[16,17] Such a least-squares solution yielded for the mass of the μ-meson 229 ± 21; for π-mesons 250 ± 25; for the σ-mesons, 302 ± 39; for the ρ^+-mesons 220 ± 30, and for the ρ^--mesons 226 ± 35.

A much simpler method for obtaining the approximate value for the mass of a given type of meson is to find the arithmetic average of the individual masses as expressed on the deflection unit scale (Fig. 5), weighting them inversely as the squares of the probable errors on that scale. The validity of such an approximation can be shown to depend on the following relationship: A given experimental point (mass-value) and the limits of probable error are obtained from curvature measurements which, for any mass parameter under consideration, have a certain residual V_i and error ϵ_i in the curvature ordinate (Fig. 6). If this point is represented, not on the actual curvature ordinate, but on the arbitrary deflection unit scale, as in Fig. 5, the new residual V_i' and error ϵ_i' on this scale will, of course, not in general be the same as V_i and ϵ_i. However one finds that over a considerable range of values, $V_i/\epsilon_i \cong V_i'/\epsilon_i'$. Because of this fact that the ratio of the residuals to the errors is almost unchanged by the transformation, one can, in place of minimizing the sum, $\sum(V_i/\epsilon_i)^2$, instead minimize $\sum(V_i'/\epsilon_i')^2$, on the deflection unit scale. The calculations are greatly simplified since with only one variable the best least-squares fit is equal to the arithmetic average. Values obtained in this manner were: $\pi\sim251\pm22$; $\sigma\sim304\pm40$; $\mu\sim231\pm21$; $\rho^-\sim225\pm32$; $\rho^+\sim220\pm25$. Combining the π- and σ-values gives 270 ± 19; while the μ- and ρ-values give 228 ± 15. The approximation method is seen to agree with the least-squares method to within 1 percent.

6. DISCUSSION

From the results in Fig. 4 concerning the number of mesons of different types observed on the plates several

[16] W. E. Deming, "Least squares," Graduate School of Department of Agriculture, Washington, D. C. (1938).

[17] R. B. Brode, Phys. Rev. 75, 904 (1949). The residuals should be weighted as the inverse squares of the probable errors (ΔR and ΔC) rather than as the inverse squares of the *percent* probable errors as given. The author of the article acknowledges the mistake here (private communication).

comments can be made. The total number of mesons per hour per cc of emulsion at about 95,000 ft. found in the plates of flights 1, 2, and 4 respectively, are in good agreement. The number found on flight 3, whose ceiling was 69,000 ft., is significantly lower; comparing the rates at the two altitudes and assuming exponential absorption, a mean free path of ~ 85 g/cm^2 is indicated for the absorption of the radiation which produced these low energy mesons. It is also interesting to compare the number of mesons of different types. Thus the ratio of the total number of ρ-mesons observed to the number of π- and σ-mesons is 1.4, which is lower than the ratio reported in plates at mountain altitudes (around 4). The ratio of π- to σ-cases is 1.7. Since, if anything, one would be more likely to miss a π–μ-decay in scanning than a σ-meson, and since the identification of both types of mesons is rather certain, a positive excess is indicated for these low energy mesons, even allowing for the fact that some negative mesons may produce no visible star. It will also be noted from the figure that slightly more mesons enter the emulsion from the glass backing than from the air gap.

The mass measurements on π-, μ-, and σ-mesons are consistent with the assumption of a unique value for the mass of each type of particle; and, while the averaged value of the σ-meson mass measurements was greater than that of the π-mesons, the limits of probable error of the two groups overlap, so the data are not inconsistent with the assumption that π- and σ-mesons have the same mass of 270 ± 20 m_e, but opposite charge sign. Similarly, the μ-, ρ^+-, and ρ^--groups have mass averages which agree within the probable errors, giving for the whole group 226 ± 15. These values may be compared with the Berkeley measurements[18] on artificial mesons, where the value found for π- and σ-mesons was 285 m_e; measurements on μ^+-cases yielded 216 m_e, but no measurements on negative light mesons (ρ^-) were obtainable. From cloud-chamber measurements, which are restricted to the light μ-mesons, Retallack and Brode[19] report a value of 215 ± 4 m_e. It will be noted in Fig. 5 that in general the ρ-mesons were not as well-grouped about single values as were the other types of mesons. Since in this group were classified particles of "no visible interactions but appearance (scattering, density, etc.) characteristic of mesons," there may be included a certain percentage of heavier negative mesons captured without the emission of visible charged particles, such as have been reported from the Berkeley cyclotron experiments. There is also a slight possibility that one or two protons might have been included in this group.

Because of the fact that these experiments were carried out at very high altitudes, where one would expect mesons of all types to be produced in abundance in the 65 lb. of iron in the magnet, it is interesting to see what evidence is given in this data concerning the presence in this experiment of other types of mesons different from the usual π- and μ-types (outside of the range 200–300 m_e, like the "τ"- and "λ"-mesons reported). In the first place, the presence in an appreciable abundance of any type of meson producing nuclear disintegrations could not have escaped detection; all measured cases in which mesons produced visible stars in the emulsion had negative charges and had masses consistent with 270 m_e. Secondly, the percentage of low energy mesons present in these plates with mass less than 150 m_e must be comparatively small (<5 percent). (Very light mesons, of mass smaller than about 15 m_e, however, would have been difficult to detect in our C2 emulsions.) Thirdly, there is no evidence for the presence in appreciable abundance of *negative* mesons of greater than 400 m_e, stopping without visible interaction; such particles would be readily distinguishable from protons because of their charge sign. A *positive* heavy meson of, say, 1000 m_e would be more difficult to differentiate from a proton if it stopped without the emission of a visible particle. A series of mass determinations, carried out on a group of particles selected at random on these plates but presumed to be protons, gave values consistent with the accepted proton mass; however an extended series of measurements to obtain a more exact mass spectrum would be necessary before any definite statement could be made concerning such very heavy positive mesons.

The accuracy of these experiments was limited by the field strength and gap width of the magnet. A balloon experiment will be carried out using a stronger magnetic field and wider air-gap, which should give considerably greater accuracy to the measurements.

The author wishes to express his gratitude to Dr. Marcel Schein for his encouragement and cooperation throughout this project. Indebtedness is also acknowledged to the du Pont Company for a fellowship and to the Research Corporation for a research grant during different periods of the work. The ONR and the General Mills Company arranged for the balloon flights. W. Ferris assisted with the scanning of the emulsions and T. Kinyon, H. Martinek, and D. Orr helped with the computations.

[18] A. S. Bishop, Phys. Rev. **75**, 1468 (1949).
[19] J. G. Retallack and R. B. Brode, Phys. Rev. **75**, 1716 (1949).

Multiple Scattering in an Infinite Medium

H. W. LEWIS
Department of Physics, University of California, Berkeley, California
(Received January 24, 1950)

The integro-differential diffusion equation of the multiple scattering problem in an infinite, homogeneous, medium, is studied without the usual small-angle approximation. An expansion in spherical harmonics is carried out which is rapidly convergent in the case of large-angle scattering, whose coefficients can be exactly determined, and which leads to expressions for the various moments of the spatial and angular distributions. The latter alone has previously been obtained by Goudsmit and Saunderson, and, in the small-angle approximation, by Snyder and Scott. Our results are shown to include these.

I. INTRODUCTION

IT is the purpose of this paper to describe a direct method of obtaining exact results from the diffusion equation of the multiple scattering problem, without the usual small-angle approximation. The main limitation of the method lies in the fact that we are restricted to an infinite and uniform medium, which precludes the treatment of problems involving plates or foils, or of the reflection problem at boundaries between different media. We will take into account energy loss, simply by regarding the energy of the particle as a function of its residual range, which is permissible as long as the straggling in energy loss is small, and we do not concern ourselves with the question of the individual scattering cross section at a single atom. The former condition limits us to energies below the critical energy of shower theory in the medium in question, which is (except in the heaviest elements) the only region in which the small-angle approximation may not be adequate.

The question of the angular distribution in large-angle multiple scattering has been studied by Goudsmit and Saunderson,[1] who exploited a persistence property of the Legendre polynomials. Their method leads in the most direct way to Eq. (7) below, which we take the liberty of re-deriving, but does not seem to be easily extensible to the study of spatial distributions.

Bethe, Rose, and Smith[2] have considered the penetration of electrons through thick plates, neglecting energy loss, using the Fokker-Planck differential equation of the problem. The major disadvantage of the Fokker-Planck approximation stems from the well-known fact[3] that in the small-angle approximation it leads to a Gaussian solution, hence omits the tail of the angular distribution. Snyder and Scott[4] have recently studied the diffusion equation in its integral form, and in the small-angle approximation, and have derived exact solutions for this case, which show clearly the transition from the Gaussian-like inner region of the curve to the long single-scattering tail. We will show later that, in the small-angle case, our solution passes exactly into theirs.

II. BASIC EQUATION

If the direction of motion of the charged particle is given by the unit vector $\mathbf{v}$, the cross section for scattering, per unit solid angle, by σ, the position by $\mathbf{x}$, and the distribution function by $f(\mathbf{x}, \mathbf{v}, s)$, then the diffusion equation for the problem is

$$(\partial f/\partial s)+\mathbf{v}\cdot\nabla f = N\int[f(\mathbf{x}, \mathbf{v}', s)-f(\mathbf{x}, \mathbf{v}, s)]\sigma(|\mathbf{v}-\mathbf{v}'|)d\mathbf{v}', \quad (1)$$

where s is the arc length traversed by the particle, N the number of atoms per unit volume, and the integration is over the solid angle. We will want to solve this equation under the boundary conditions $f(\mathbf{x}, \mathbf{v}, 0) = \delta(\mathbf{x})\delta(\mathbf{v})$, corresponding to a single particle, incident at the origin, and moving in the z direction. To put the equation in a more tractable form, we expand the solution in normalized surface harmonies in $\mathbf{v}$, so that

$$f=\sum_{lm} f_{lm}(\mathbf{x}, s)Y_{lm}(\mathbf{v}) \quad (2)$$

and obtain from (1) and (2)

$$(\partial f_{lm}/\partial s)+\sum_{\lambda\mu} \nabla f_{\lambda\mu}\cdot \mathbf{Q}_{lm}{}^{\lambda\mu} = N\sum_{\lambda\mu} f_{\lambda\mu}\int\int Y_{lm}{}^*(\mathbf{v})[Y_{\lambda\mu}(\mathbf{v}')-Y_{\lambda\mu}(\mathbf{v}) \times\sigma(\mathbf{v}-\mathbf{v}')d\mathbf{v}d\mathbf{v}', \quad (3)$$

where

$$\mathbf{Q}_{lm}{}^{\lambda\mu}=\int Y_{lm}{}^*\mathbf{v}Y_{\lambda\mu}d\mathbf{v}$$

is a constant vector, which is zero if $|\lambda-l|$ or $|\mu-m|$ is greater than unity. The last integral in (3) can be carried out most easily by expanding σ in Legendre polynomials, using the addition theorem for the spherical harmonics, and finally the orthogonality and normalization. The result is

$$(\partial f_{lm}/\partial s)+\kappa_l f_{lm}=-\sum_{\lambda\mu} \nabla f_{\lambda\mu}\cdot \mathbf{Q}_{lm}{}^{\lambda\mu}, \quad (4)$$

[1] S. Goudsmit and J. L. Saunderson, Phys. Rev. **57**, 24 (1940) and **58**, 36 (1940).
[2] Bethe, Rose, and Smith, Proc. Am. Phil. Soc. **78**, 573 (1938).
[3] B. Rossi and K. Greisen, Rev. Mod. Phys. **13**, 240 (1941).
[4] H. Snyder and W. T. Scott, Phys. Rev. **76**, 220 (1949).

where

$$\kappa_l = 2\pi N \int_0^\pi \sigma(\vartheta)[1-P_l(\cos\vartheta)]\sin\vartheta d\vartheta, \quad (5)$$

and the $P_l(\cos\vartheta)$ here are the usual (unnormalized) Legendre polynomials. The Fokker-Planck approximation can be obtained by expanding the Legendre polynomial in powers of ϑ^2, and keeping only the first two terms, one of which will cancel the unity in the square bracket.

The boundary conditions to be satisfied by the f_{lm} are

$$f_{lm}(\mathbf{x}, 0) = \delta_{m0}\delta(\mathbf{x})Y_{l0}(0) = [(2l+1)/4\pi]^{\frac{1}{2}}\delta_{m0}\delta(\mathbf{x}). \quad (4')$$

III. THE ANGULAR DISTRIBUTION

To obtain the angular distribution alone, we integrate (4) over all space, thus losing the last term, and find

$$(\partial F_l/\partial s)+\kappa_l F_l = 0, \quad (6)$$

where $F_l(s) = \int f_{l0}(\mathbf{x}, s)d\mathbf{x}$. The terms with $m \neq 0$ vanish because of the cylindrical symmetry of the problem. The solution to (6) is, of course,

$$F_l(s) = [(2l+1)/4\pi]^{\frac{1}{2}} \exp\left(-\int_0^s \kappa_l ds\right),$$

which satisfies the boundary conditions, so that

$$F(\mathbf{v}, s) = \int f(\mathbf{x}, \mathbf{v}, s)d\mathbf{x}$$

$$= (1/4\pi)\sum_{l=0}^{\infty}(2l+1)P_l(\cos\vartheta)\exp\left(-\int_0^s \kappa_l ds\right), \quad (7)$$

where we have inserted the unnormalized polynomials, and regard κ_l as a function of s because of the energy dependence of the scattering cross section. This result has been obtained by Goudsmit and Saunderson[1] by a different method, and they have carried out a number of numerical examples. They have also described the approximation in which this distribution becomes Gaussian.

It is clear from (7) that the convergence of this expression depends upon the magnitudes of the expressions $\int \kappa_l ds$. These are, in turn, related to the mean scattering angles, as can be seen, for example, from the fact that

$$\langle\cos\vartheta\rangle_{Av} = \exp\left(-\int_0^s \kappa_1 ds\right),$$

or more generally,

$$\langle P_l(\cos\vartheta)\rangle_{Av} = \exp\left(-\int_0^s \kappa_l ds\right).$$

Thus, in the small-angle case, we can take

$$P_l(\cos\vartheta) \approx 1-\tfrac{1}{4}l(l+1)\vartheta^2$$

so that

$$\int \kappa_l ds \approx \tfrac{1}{4}l(l+1)\langle\vartheta^2\rangle_{Av},$$

and, in this case, convergence will set in at around $l \sim 2(\langle\vartheta^2\rangle_{Av})^{-\frac{1}{2}}$. This makes it possible (in fact mandatory) in the latter case, to replace the sum in (7) by an integral, which will turn out to be just the Snyder-Scott integral, after the appropriate transformations.

IV. EVALUATION OF THE K_l FOR A PARTICULAR CASE

If we now use the simplified potential $V = (Ze/r)e^{-r/a}$, the exponential factor schematizing the effect of screening, and calculate the scattering cross section by the Born approximation, we find, for a singly charged particle

$$\sigma(\vartheta) = \frac{Z^2e^4}{p^2v^2(1-\cos\vartheta+2\beta)^2}, \quad (8)$$

where $\beta = \hbar^2/4a^2p^2$, and p and v are the momentum and velocity, respectively, of the scattered particle. Thus

$$\kappa_l = A\int_{-1}^{1}\frac{[1-P_l(\mu)d\mu]}{(1-\mu+2\beta)^2} = A(I_l - J_l), \quad (9)$$

where $A = (2\pi NZ^2e^4)/(p^2v^2)$, and I_l and J_l are the integrals involving the two terms in the square bracket, respectively. The first is elementary and yields

$$I_l = 1/[2\beta(1+\beta)]. \quad (10)$$

The second can be simplified by inserting Rodrigues' formula for the Legendre polynomial, integrating by parts l times, and making the substitution $1-\mu = 2\lambda$. One obtains

$$J_l = \tfrac{1}{2}(l+1)\int_0^1 \frac{\lambda^l(1-\lambda)^l d\lambda}{(\lambda+\beta)^{l+2}}. \quad (11)$$

This is recognizable as a hypergeometric function,[5] and is

$$J_l = \tfrac{1}{2}\beta^{-l-2}\frac{\Gamma(l+1)\Gamma(l+2)}{\Gamma(2l+2)}F(l+1, l+2; 2l+2; -\beta^{-1}). \quad (12)$$

Since β is small, in general, it is convenient to make the hypergeometric transformation to the reciprocal argument (WW289); the formula given there does not apply when the first two parameters of the function differ by an integer, as in our case, so that it is necessary to take the given transformation and carry out a limiting process to obtain a useful result. In addition,

[5] Whittaker and Watson, *Modern Analysis* (Oxford University Press, New York, 1946), American edtion, p. 293. We will have a number of references to this book, and in the future, will simply insert them into the body of the text, as, for example (WW293), for the above.

the formula given has a number of incorrect signs, and must be modified accordingly. After the transformation one has

$$2J_l=\frac{1}{\beta}+\sum_{\nu=0}^{l-1}\frac{\beta^\nu}{\nu!(\nu+1)!}\frac{(l+\nu+1)!}{(l-\nu-1)!}[\ln\beta-\psi(\nu+1)$$
$$-\psi(\nu+2)+\psi(l-\nu)+\psi(l+\nu+2)]-M_l(\beta), \quad (13)$$

where $\psi(z)=(d/dz)\ln\Gamma(z)$ and

$$M_l(\beta)=(-)^l\sum_{\nu=l}^{\infty}\frac{(-\beta)^\nu}{\nu!}\frac{(l+\nu+1)!(\nu-l)!}{(\nu+1)!}. \quad (13')$$

Since β is small in all physical cases, M_l can be neglected, for all l. This is not true of the first sum in (13), since the coefficient of β^ν is of the order of $l^{2\nu+2}$, which may be large.

One can now use the recursion formula for the ψ-functions to write the expression in the square bracket as

$$-G_{l\nu}=-\Big[\ln(1/\beta)+\sum_1^\nu m^{-1}+\sum_1^{\nu+1}m^{-1}$$
$$-\sum_1^{l-\nu-1}m^{-1}-\sum_1^{l+\nu+1}m^{-1}\Big]. \quad (14)$$

Here it is to be understood that sums in which the upper limit is less than unity are to be omitted. Thus, from (9), (10), (13), and (14), neglecting $M_l(\beta)$ and replacing $1/(1+\beta)$ by $1-\beta$, we have

$$\kappa_l=\tfrac{1}{2}A\Big[-1+\sum_{\nu=0}^{l-1}\frac{\beta^\nu}{\nu!(\nu+1)!}\frac{(l+\nu+1)!}{(l-\nu-1)!}G_{l\nu}\Big]. \quad (15)$$

All this applies only for $l\neq 0$; for $l=0$, $\kappa_l\equiv 0$, from its definition. For moderate values of l, it is sufficient to use

$$\kappa_l\approx\tfrac{1}{2}Al(l+1)\Big[\ln\frac{1}{\beta}+1-2\sum_1^l m^{-1}\Big]. \quad (15')$$

V. TRANSITION TO SMALL ANGLES

To carry out the transition to the case in which only small-angle scattering is important, we need only notice, as mentioned in Section III, that in this case the major contributions to the sum in (7) come from large values of l. Accordingly, we replace the sum in (7) by an integral, and consider the expressions (14) and (15) in the limit of large l.

In (14) we use the fact that the sum of the partial harmonic series is given by

$$\sum_1^A m^{-1}=\ln(A+\tfrac{1}{2})+C+O(A^{-2}), \quad (16)$$

where C is Euler's constant, and is equal to 0.5772. Using this fact in the sums in (15) that involve l in the upper limit, we find

$$G_{l\nu}\approx\ln(1/l^2\beta)-2C+\sum_1^\nu m^{-1}+\sum_1^{\nu+1}m^{-1} \quad (17)$$

for $\nu\ll l$. We also replace $(l+\nu+1)!$ in (15) by $l^{\nu+1}l!$ and similarly in the denominator, which approximation is valid for $\nu^2\ll l$, obtaining

$$\kappa_l\approx\tfrac{1}{2}Al^2\sum_{\nu=0}^{\infty}[(l^2\beta)^\nu/\nu!(\nu+1)!]G_{l\nu}$$
$$\approx lA\beta^{-\frac{1}{2}}[K_1(2l\beta^{\frac{1}{2}}]+\tfrac{1}{2}l\beta^{\frac{1}{2}}], \quad (18)$$

where $K_1(z)$ is the modified Bessel function of the second kind (WW374). We must now approximate the Legendre polynomials in (7) for small angles, and then project them on a plane, in order to make our result comparable with that of Snyder and Scott. The former is achieved by

$$P_l(\cos\vartheta)\approx J_0(l\vartheta) \quad (19)$$

(WW 367) where J_0 is the Bessel function of zero order, the latter by writing $\vartheta=(\varphi^2+\chi^2)^{\frac{1}{2}}$ with φ and χ the projections of ϑ on two mutually perpendicular planes through the polar axis, and integrating with respect to χ. Thus (WW 357, 377)

$$\int_{-\infty}^{\infty}J_0[l(\varphi^2+\chi^2)^{\frac{1}{2}}]d\chi=2l^{-1}\cos l\varphi, \quad (20)$$

if we take into account the fact that

$$\int_0^\infty J_n(z)dz=1,$$

for all n. Thus, finally, the distribution in φ becomes (if we neglect energy loss),

$$F(\varphi)\approx\frac{1}{\pi}\int_0^\infty\cos l\varphi\exp(-\kappa_l s)dl \quad (21)$$

with κ_l given by (18). This is just the result given by Snyder and Scott, since our β is equal to their $\frac{1}{4}\eta_0^2$.

VI. SPATIAL DISTRIBUTIONS

A. Longitudinal Distribution

In order to find the spatial distribution of the scattered particle, we would like to solve Eq. (4) for f_{00}. However, because the differential equations for the various f_{lm} are coupled equations, this turns out to be impracticable, and one must resort to a somewhat less satisfying procedure involving the evaluation of the moments of the spatial distributions (and correlation functions with the angles). This is, in principle, completely equivalent to the evaluation of the function, though somewhat less useful. We illustrate the procedure on the longitudinal distribution.

First we integrate (4) with respect to x and y, and define

$$g_{lm}(z, s)=\int\int f_{lm}(\mathbf{x}, s)dxdy.$$

Then

$$\left(\frac{\partial}{\partial s}+\kappa_l\right)g_{lm}+\sum_{\lambda\mu}\frac{\partial g_{\lambda\mu}}{\partial z}(Q_{lm}{}^{\lambda\mu})_z=0. \tag{22}$$

The boundary conditions for the g_{lm} are

$$g_{lm}(z, 0)=[(2l+1)/4\pi]^{\frac{1}{2}}\delta_{m0}\delta(z).$$

From these, and from the fact that Q_z is zero unless $\mu=m$, we conclude that $g_{lm}=0$ for $m\neq 0$. We will simply use the notation $g_l(z, s)$ for $g_{l0}(z, s)$. Now we use the well-known expression[6] for Q_z, namely,

$$\begin{aligned}(Q_{l0}{}^{\lambda 0})_z&=\frac{l\delta_{l-1,\lambda}}{(4l^2-1)^{\frac{1}{2}}}+\frac{(l+1)\delta_{l+1,\lambda}}{[4(l+1)^2-1]^{\frac{1}{2}}}\\&=\alpha_l\delta_{l-1,\lambda}+\alpha_{l+1}\delta_{l+1,\lambda}\end{aligned} \tag{23}$$

in which we give the coefficients a name. Thus,

$$\left(\frac{\partial}{\partial s}+\kappa_l\right)g_l+\frac{\partial}{\partial z}[\alpha_l g_{l-1}+\alpha_{l+1}g_{l+1}]=0. \tag{24}$$

For $l=0$, the first term in the square brackets of course does not appear. Now define

$$H_{ln}=\int_{-\infty}^{\infty}g_l(z, s)z^n dz,$$

so that, if we multiply (24) by z^n, and integrate, one integration by parts yields

$$\left(\frac{\partial}{\partial s}+\kappa_l\right)H_{ln}-n[\alpha_l H_{l-1,n-1}+\alpha_{l+1}H_{l+1,n-1}]=0 \tag{25}$$

which is a set of differential equations for the H_{ln}, which can be solved in ascending order in n. For example, if we call

$$\exp\left(-\int_0^s\kappa_l ds\right)=k_l(s),$$

since the k_l will appear frequently,

$$H_{l0}=[(2l+1)/4\pi]^{\frac{1}{2}}k_l(s) \tag{26}$$

and

$$H_{l1}=\left(\frac{2l+1}{4\pi}\right)^{\frac{1}{2}}k_l(s)\int_0^s\frac{d\sigma}{k_l(\sigma)}[lk_{l-1}(\sigma)+(l+1)k_{l+1}(\sigma)],$$

where we have inserted the explicit values of the α_l. This process can be continued.

It follows from (26) that the mean value of z is given by $(4\pi)^{\frac{1}{2}}H_{01}$, so that, since $\kappa_0=0$, and $k_0(s)=1$,

$$\langle z\rangle_{Av}=\int_0^s k_1(\sigma)d\sigma. \tag{27}$$

[6] H. Bethe, *Handbuch der Physik* (1933), Vol. 24/1, p. 551. (*Anhang uber Kugelfunktionen.*)

We can also calculate correlation functions of z with various functions of ϑ, by considering H_{l1} for $l\neq 0$. For example,

$$\begin{aligned}\langle z\cos\vartheta\rangle_{Av}&=(4\pi/3)^{\frac{1}{2}}H_{11}(s)\\&=k_1(s)\int_0^s[1+2k_2(\sigma)][k_1(\sigma)]^{-1}d\sigma.\end{aligned} \tag{28}$$

We can also find $\langle z^2\rangle_{Av}$, for example, by calculating the H_{l2}.

In order to obtain numerical results for a particular case, one must express the various κ_l as functions of energy [according to (15) or (15′), if one wishes to use the cross section (8)], and combine these results with the range-energy curves in the medium in question, to find the $k_l(s)$, where the integral involved can be done numerically if need be. The $k_l(s)$ then appear in all the physically interesting expressions.

B. Transverse Distribution

In order to calculate the moments of the transverse distribution, we follow the same pattern as in the preceding section; namely, to integrate (4) with respect now to (say) y and z, write in the value of $(Q_{lm}{}^{\lambda\mu})_z$, then multiply by x^n, integrate, and solve the resulting differential equations for the moments. The latter turn out to be, for the x direction,

$$\begin{aligned}\left(\frac{\partial}{\partial s}+\kappa_l\right)h_{lm}{}^{(n)}(s)=\frac{n}{2}\Big\{&A_m{}^l h_{l-1,m-1}^{(n-1)}+A_{m+1}^{l+1}h_{l+1,m+1}^{(n-1)}\\&-A_{-m}{}^l h_{l-1,m+1}^{(n-1)}-A_{-m+1}^{l+1}h_{l+1,m+1}^{(n-1)}\Big\},\end{aligned} \tag{29}$$

where we have defined

$$A_m{}^l=\left[\frac{(l+m)(l+m-1)}{4l^2-1}\right]^{\frac{1}{2}}$$

and

$$h_{lm}{}^{(n)}(s)=\int_{-\infty}^{\infty}x^n f_{lm}(\mathbf{x}, s)d\mathbf{x}. \tag{30}$$

The boundary conditions are $h_{lm}{}^{(n)}(0)=0$ for $n\neq 0$, and

$$h_{lm}{}^{(0)}(s)=[(2l+1)/4\pi]^{\frac{1}{2}}\delta_{m0}k_l(s). \tag{30′}$$

These equations yield, for example $h_{lm}{}^{(1)}(s)=0$ for $m^2\neq 1$, and

$$\begin{aligned}h_{l1}{}^{(1)}=-h_{l,-1}{}^{(1)}=\frac{k_l(s)}{4}\left[\frac{l(l+1)}{\pi(2l+1)}\right]^{\frac{1}{2}}&\int_0^s\frac{d\sigma}{k_l(\sigma)}\\&\times[k_{l-1}(\sigma)-k_{l+1}(\sigma)].\end{aligned} \tag{31}$$

By going to $n=2$, one also finds, for example,

$$\langle x^2+y^2\rangle_{Av}=\frac{4}{3}\int_0^s d\sigma k_1(\sigma)\int_0^\sigma d\tau[1-k_2(\tau)]/k_1(\tau) \tag{32}$$

which can easily be shown to reduce to the correct result when the scattering is small.

Nuclear Magnetic Resonance in Weak Fields*

RICHARD M. BROWN†
Lyman Laboratory of Physics, Harvard University, Cambridge, Massachusetts
(Received February 16, 1950)

The nuclear magnetic resonance for protons in water was observed in magnetic fields of 6 and 12 gauss corresponding to Larmor frequencies of 25 and 50 kc, respectively. The line width was found to be determined by the frequency of modulation and here was approximately 3 milligausses. The ratio of magnetic fields for resonance was found to agree with the ratio of Larmor frequencies within the experimental error, estimated at 0.01 percent.

I. INTRODUCTION

THE theory of nuclear magnetic resonance in liquids[1] predicts a very narrow resonance line occurring at the Larmor frequency for the nuclear moment. While this effect has been confirmed by many investigators, no careful study has been made of the actual width of the resonance and of the linearity of the relationship between magnetic field and radiofrequency at the resonance. Since several investigators have taken advantage of the sharpness of the resonance to obtain precise ratios of nuclear g-factors,[2] an experimental check on the theory implicit in their results seemed warranted.

One of the purposes of this work was to examine the resonance in a very homogeneous field in order to verify the narrowness of the resonance line. In a second experiment the position of the resonance was observed at two different Larmor frequencies, 25 to 50 kc/sec., and the ratio of applied magnetic fields at resonance compared with the ratio of frequencies. In this way the linearity of the relationship, $\omega_0=\gamma H_0$ could be checked.

These studies were made at very weak magnetic fields of 6 and 12 gauss corresponding to Larmor frequencies for the proton of 25 and 50 kc. There are two reasons for working in this domain. First, the theory might be expected to break down in this region, for the perturbing interatomic fields which theoretically are "averaged out" by the thermal motion, are here instantaneously of the same magnitude as the applied field. One might expect, therefore, that any discrepancies between theory and experiment would be the more evident in this region. Second, greater resolution can be attained with weak fields, for the limit on resolution is ordinarily set by the absolute value of the magnetic field inhomogeneity over the sample. According to the theory, the true line width which is observable only in a completely homogeneous field, should be independent of the field strength. One must seek, therefore, to approach this ideal condition by reducing the absolute rather than the relative inhomogeneity of the field. Not only is this achieved by reducing the field, but also one is assisted by the fact that in weak fields a more easily compensated solenoid may be employed.

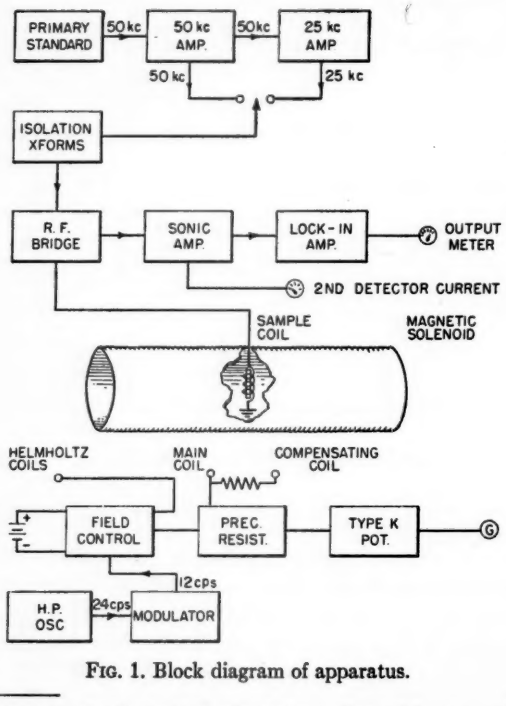

FIG. 1. Block diagram of apparatus.

II. APPARATUS

The proton resonance in one liter of distilled water at room temperature was observed using the method of Bloembergen, Purcell, and Pound.[1] A block diagram of the apparatus is shown in Fig. 1. A Wheatstone bridge arrangement was employed, one side consisting of two purely capacitive arms and the other side made of two parallel tuned resonance arms, containing the sample and the dummy coils. Analysis of the circuit shows the output of the bridge to be sensitive only to the absorption in the sample or real part of the change in impedance of the sample coil.

The sample and dummy coils consisted of approximately 500 turns of 10–32 Nylon-covered Litz wire, wound on cylindrical Bakelite forms, 4.5 in. in outside diameter and 5.62 in. in length. To achieve a high Q,

* Based on the doctoral thesis of the author while on an AEC Predoctoral Fellowship at Harvard.
† Present address: The State College of Washington, Pullman, Washington.
[1] Bloembergen, Purcell, and Pound, Phys. Rev. **73**, 679 (1948).
[2] Bitter, Alpert, Nagle, and Poss, Phys. Rev. **72**, 1271 (1947); Bloch, Graves, Packard, and Spence, Phys. Rev. **71**, 373, 551 (1947); Bloch, Levinthal, and Packard, Phys. Rev. **72**, 1125 (1947); and several others.

a three-layer bank winding was employed. The measured inductance at 50 kc per sec. was approximately 12.5 mh and the value of Q without the sample was around 280. Insertion of the sample bottle containing distilled water reduced the Q to 200.

The bridge output was amplified at the output directly by a one-stage amplifier and was further amplified and detected by a sonic amplifier designed by Noyes and Pierce.[3] This amplifier was a superheterodyne receiver, tunable from 20 kc to 70 kc with an I.F. of 175 kc. The detected audio signal resulting from the modulation was tapped directly off the grid leak in the second detector.

The final detection of the absorption signal was accomplished with a phase sensitive lock-in amplifier[4] modified to work at a modulation frequency of 12 c/sec. The signal-to-noise ratio at 50 kc was estimated from observation to be of the order of 40:1, on a voltage basis, at 25 kc it was somewhat lower, being 20:1.

A General radio primary frequency standard was used as the source of the 50-kc signal. The 25-kc signal was obtained from the 50-kc signal by dividing by two in a multivibrator circuit.

To produce a magnetic field of desired homogeneity, a single-layer solenoid 49.8 in. long and $12\frac{7}{16}$ in. in mean diameter was wound on a brass cylinder. The winding, No. 11 copper with General Electric Formex coating, was made on a threading with a pitch of ten turns in the inch. To reduce the end effect inhomogeneity, a compensating coil 16.5 in. long was wound over the central portion of the main coil. With the current in the compensating coil equal to 3.2×10^{-2} times the main current and in an opposite sense, the inhomogeneity over ±4 in. around the center of the solenoid was calculated to be 0.005 percent. Roughly 2.6 amp. were necessary to produce the 11.7 gauss field for the proton resonance at 50 kc/sec.

Modulation of the magnetic field was obtained by shunting a 0.5-ohm resistor in series with the main coil by means of a relay operated at 12 c/sec. Although square-wave modulation was thus applied to the coil, calculation showed that the attenuation of the higher harmonics in the $\frac{1}{4}$-in. thick brass cylinder was sufficient to cause the actual modulation field at the sample to be approximately sinusoidal. The modulation field was too weak for direct observation.

Since the applied magnetic fields here were only 6 and 12 gauss approximately, the earth's magnetic field of 0.5 gauss could affect the resonance position appreciably. If the solenoid axis were aligned with the earth's field, the effect of the earth's field could be eliminated by taking the mean of the applied fields at resonance obtained on reversal of the solenoid current. It was more convenient to align the solenoid axis with the horizontal component of the earth's field and to cancel the vertical component by means of Helmholtz coils.

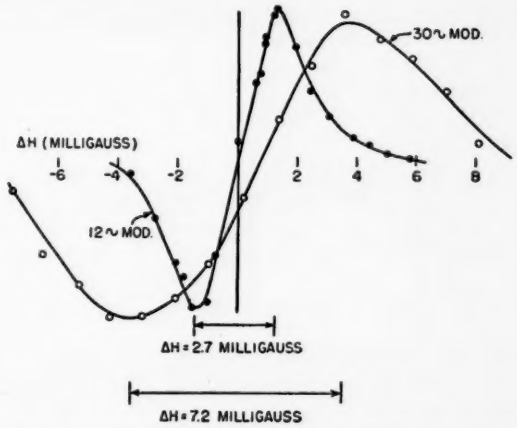

FIG. 2. Derivative of absorption curve at 50 kc for modulation frequencies of 12 and 30 c/sec.

The absence of any ferromagnetic materials permitted the measurement of magnetic fields against the solenoid currents. Accordingly, the resonances were plotted in terms of the voltages produced by the solenoid currents across two manganin resistance strips in series, each approximately 5 ft. long, mounted at the ends to brass blocks, and immersed in an oil bath to maintain uniform temperature distribution. Since two currents, whose ratio was nearly two, were to be compared, the voltage for the lesser current was measured across both resistance strips; whereas the voltage for the greater current was taken as the sum of the voltages measured across each strip. Thus all voltages were measured at the same setting of the fixed resistors in the Leeds and Northrup Type K potentiometer used.

III. EXPERIMENTAL RESULTS

A. The Nuclear Resonance in Weak Fields

The nuclear resonance absorption for protons in water was observed at frequencies of 50 and 25 kc/sec. The shape and location agreed roughly with the resonance found at higher fields. Because the magnetic field inhomogeneity was reduced to such a low value, another source of line broadening was observed, namely that due to the modulation of the magnetic field. Figure 2 shows the output of the lock-in amplifier for the proton resonance at 50 kc, plotted against the magnetic field for modulation frequencies of 12 and 30 c/sec. The curves are the derivatives of absorption curves whose half-width in gauss is approximately the ratio of the angular frequency of modulation to the gyromagnetic ratio of the proton, γ. The fact that the separation between the peaks follows the modulation frequency indicates that neither the true line width nor the inhomogeneity of the magnetic field enter into the observed width.

While modulation broadening can be explained qualitatively on the basis of the equivalence of the present type of field modulation and the use of a frequency-

[3] A. Noyes, Jr. and G. W. Pierce, J. Acous. Soc. Am. **9**, 205 (1938).
[4] R. Dicke, Rev. Sci. Inst., **17**, 268 (1946).

TABLE I. Experimental values for the ratio of magnetic fields for resonances at 50 and 25 kc/sec.

Run	H(50 kc)/H(25 kc)		
1	2.00029		
2	1.99993		
3	1.99992	Mean ratio:	2.00008±0.00020
4	2.00022	Root-mean-square deviation:	0.00023
5	2.00004		
6	2.00052		
7	1.99989		
8	1.99986		

modulated radiofrequency signal, the observed line width is one-half of that predicted. Further work on this is planned.

Despite the modulation broadening, the observed line width is still narrower by a factor of 100 than in any previous measurements. We have, therefore, obtained better confirmation of the theory of line narrowing due to thermal motion in liquids.

B. Comparison of Magnetic Fields at Resonance

The resonance was observed at frequencies of 25 and 50 kc/sec. and the ratio of the fields calculated from the currents in the solenoid. Five sets of data around resonance had to be taken for each complete measurement: two at each frequency including reversal of the solenoid current to eliminate the effects of the earth's field, and another at 50 kc to calibrate the two resistances used in obtaining the voltages.

The voltages across the precision resistances for the center of the resonance were obtained by taking the mean of the values for the derivative peaks. This was more accurate than attempting to find the point at which the derivative vanished, for the baseline was too uncertain and the slope of the curve too steep for accurate determination. These voltages were corrected for the effect of the earth's field and the ratio of voltages for the two Larmor frequencies taken. This ratio represented the ratio of magnetic fields at resonance. No correction is necessary for the diamagnetic effect of the electrons around the nucleus,[5] since this effect appears as a factor on both fields which cancels on taking the ratio. Table I shows the results for all the runs in which sufficient data for all calculations was taken.

IV. ERRORS

If the temperature of the solenoid should change during a set of runs the ratio of currents would not be a measure of the ratio of fields, because of the change in solenoid dimensions. The temperature of the solenoid was recorded during the runs and found to vary less than 1.5°C. The error here should be less than three parts in 10^5.

The temperature of the oil bath for the manganin resistances never varied more than 0.7°C, so that the error introduced in voltage measurements could not be greater than one part in 10^5. Extensive measurements were made on thermoelectric voltages and at no time did they exceed one microvolt out of the 0.13 volt measured.

Since all voltages were measured at the same setting of the fixed resistors in the Type K potentiometer, and since the ratio of voltages was taken, the only appreciable error in the voltage measurements arose from non-uniformity of the slide wire. Leeds and Northrup quote a maximum variation in uniformity of the slide wire of 0.2 percent from turn to turn so that here, where the slide wire of 11 turns was one-fourteenth of the total resistance, the error introduced was less than 1.3 parts in 10^5.

The points read from the plots of the resonance curves were estimated to have an error of two parts in 10^5. The errors arose from the roughness of the curve and were presumed to be statistical in nature.

The error in the frequencies used was negligible for the 25-kc signal was locked as a submultiple of the 50-kc signal, which was stable to better than one part in a million.

With these possible errors in mind, the limits of error on the measurement of the ratio of magnetic fields at resonance were set at ± 1 part in 10^4. From Table I it is seen that within these limits the value for the ratio of fields is the same as the ratio of frequencies; i.e., 2:1.

One concludes, therefore, that the resonance magnetic field is indeed a linear function of the frequency even at these weak field strengths, where the theory of the resonance might be expected to break down. There is no evidence of second-order effects which might cause a departure from the resonance condition. This result provides strong support for the assumptions upon which measurements of nuclear g-factors by nuclear absorption and induction methods have been based.

This work was supported by a Frederick Gardner Cottrell Special Grant-in-Aid from the Research Corporation. The author is indebted to Professor E. M. Purcell for the original suggestion of the problem and for invaluable advice during the research.

[5] Kusch, Millman, and Rabi, Phys. Rev. **55**, 1176 (1938).

Symmetrical Tripartition of U^{235} by Thermal Neutrons

LOUIS ROSEN AND ALVIN M. HUDSON*
Los Alamos Scientific Laboratory,† Los Alamos, New Mexico
(Received February 23, 1950)

Making use of an ionization chamber divided into three sections and triple coincidence circuit in conjunction with either a gated ten-channel amplitude discriminator or a double coincidence circuit, it has been found possible to determine the frequency of symmetrical triple fissions in U^{235} relative to the frequency of binary fissions. The results of the experiment are that triple fissions occur to the extent of 6.7 ± 3.0 per 10^6 binary fissions in the case where the fragments come off with comparable masses.

1. INTRODUCTION

THE process of binary fission, namely, the splitting of a heavy nucleus into two lighter nuclei, is now well established. In the case of uranium, for example, the maximum energy liberated is in the neighborhood of 200 Mev, approximately 160 Mev of which is evidenced as kinetic energy of the fission fragments with the remainder going into internal excitation of the fission fragments and kinetic energy of the neutrons emitted during fission. The possibility of fission into three charged particles has been predicted from theoretical considerations based on the liquid-drop model of fission.[1–3] In fact, from a calculation of mass differences one might expect a maximum energy liberation in triple fission of 10–20 Mev greater than that for binary fission.

Evidence for triple fission into two heavy particles and one light particle was first published in the literature by San-Tsiang, Zah-Wei, Chastel, and Vigneron.[4–6] The first discovery of this mode of fission was, however, made by Alvarez during the war. Detailed studies of these light particles using coincidence counting methods were conducted by Farwell, Segrè, and Wiegand[7] who determined the frequency with which long-range charged particles come off during the fission process and also established that these were, for the most part, alpha-particles. Prior to the publication of the work of Farwell, Segrè, and Wiegand, a detailed investigation of the particles emitted during fission was independently carried out by Green and Livesey[8,9] using photographic plate techniques. They concluded that in approximately one percent of fission events a light nucleus of specific ionization similar to that of the alpha-particle is emitted. They also concluded that the average mass number of these light particles is very nearly 4 and that approximately one-fourth of them have a range exceeding that of the fission fragments. These results are in fair agreement with the results of Farwell, Segrè, and Wiegand. Other investigators[10–15] using either coincidence counting or photographic plate techniques verified at least the broader aspects of these conclusions, although Marshall,[15] on the basis of a study of 18,500 fission tracks, takes issue with Green and Livesey[9] on the existence of short-range alpha-particles. She concludes that practically all of the short-range particles are protons or heavier atoms from the photographic emulsion scattered by the fission fragments.

The present paper is concerned with the frequency of tripartition of U^{235} nuclei under thermal neutron bombardment, where the definition of tripartition is here limited to the division of a compound U^{236} nucleus into three fragments of approximately equal masses. This is not to be confused with the emission of low mass particles discussed above. San-Tsiang, Zah-Wei, Chastel, and Vigneron[16] have published a photomicrograph of one case of ternary fission into three heavy fragments. However, no mention is made of the frequency of such events, although the frequency for quadripartition of U^{235} nuclei was given as 0.0003 ± 0.0002 the frequency of bipartition.[17–20] Green and Livesey[5] also attempted, again using photographic plates, to find triple tracks which could be ascribed definitely to ternary fission into three heavy fragments. No such track was found in an examination of 5,000 fission events. These authors point out the difficulty of positively distinguishing

* Now at Stanford University, Stanford, California.
† This document is based on work performed at Los Alamos Scientific Laboratory of the University of California under AEC Contract W-7405-Eng-36.
[1] N. Bohr and J. A. Wheeler, Phys. Rev. **56**, 426 (1939).
[2] R. D. Present and J. K. Knipp, Phys. Rev. **57**, 751, 1188 (1940).
[3] R. D. Present, Phys. Rev. **59**, 466 (1941).
[4] San-Tsiang, Chastel, Zah-Wei, and Vigneron, Comptes Rendus **223**, 986 (1946).
[5] San-Tsiang, Zah-Wei, Chastel, and Vigneron, Comptes Rendus **224**, 272 (1947).
[6] San-Tsiang, Zah-Wei, Chastel, and Vigneron, Phys. Rev. **71**, 382 (1947).
[7] Farwell, Segrè, and Wiegand, Phys. Rev. **71**, 327 (1947). Their preliminary classified report was dated May 18, 1944.
[8] L. L. Green and D. L. Livesey, Nature **159**, 332 (1947).
[9] L. L, Green and D. L. Livesey, Phil. Trans. **A241**, 323 (1948).
[10] P. Demers, Phys. Rev. **70**, 974 (1946).
[11] Cassels, Dainty, Feather, and Green, Proc. Roy. Soc. **A191**, 428 (1947).
[12] Wallan, Moak, and Sawyer, Phys. Rev. **72**, 447 (1947).
[13] K. W. Allen and J. T. Dewan, Phys. Rev. **75**, 337 (1949).
[14] J. T. Dewan and K. W. Allen, Phys. Rev. **76**, 181 (1949).
[15] L. Marshall, Phys. Rev. **75**, 1339 (1949).
[16] San-Tsiang, Zah-Wei, Chastel, and Vigneron, Nature **159**, 773 (1947).
[17] Zah-Wei, San-Tsiang, Vigneron, and Chastel, Comptes Rendus **223**, 1119 (1946).
[18] San-Tsiang, Zah-Wei, Chastel, and Vigneron, Phys. Rev. **71**, 382 (1947).
[19] San-Tsiang, Zah-Wei, Chastel, and Vigneron, J. de phys. et rad. **8**, 165 (1947) and **8**, 200 (1947).
[20] Tsien San-Tsiang, J. de phys. et rad. **9**, 6 (1948).

between a triple track due to a triple fission event and a triple track due to a binary fission event plus a heavy recoil originating in the emulsion at approximately the point of fission.

2. EXPERIMENTAL METHOD

Since tripartition into heavy fragments was known to occur extremely rarely, if indeed it occurred at all, it was clear that in order to make a determination of the frequency of these events by observing two, or even all three, of the fragments in coincidence, it would be necessary to eliminate most of the accidental coincidences produced by two binary fissions occurring within the resolving time of the coincidence equipment.[21]

A triple ionization chamber, connected to three linear amplifiers and counting circuits, was used as the detector. In conjunction with this was used either a gated ten-channel pulse amplitude discriminator or a double coincidence circuit. Since most of the results were obtained with the arrangement using the double coincidence circuit, the experiment will be discussed in terms of this arrangement, a brief discussion being appended to indicate how the ten-channel pulse amplitude discriminator was utilized instead of the double coincidence circuit during the preliminary phases of this investigation.

A plan view of the triple ionization chamber is shown in Fig. 1. It is composed of three sections, designated as Chamber I, Chamber II, and Chamber III. Pure U^{235}

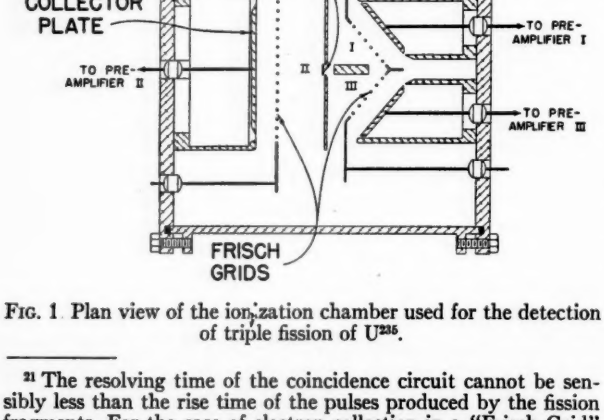

FIG. 1. Plan view of the ionization chamber used for the detection of triple fission of U^{235}.

[21] The resolving time of the coincidence circuit cannot be sensibly less than the rise time of the pulses produced by the fission fragments. For the case of electron collection in a "Frisch Grid" ionization chamber in which the fission particles are completely stopped prior to reaching the grid (a prerequisite if the pulse heights are to be proportional to the energy of the particles) this rise time is of the order of one microsecond, and with such a resolving time accidental coincidences, if not somehow eliminated, would effectively limit the sensitivity of detection of triple fission events to approximately 1 in 50,000 binary fissions. This estimate is based on an experimental running time of approximately two weeks using optimum counting rates.

was coated uniformly[22] to an average thickness of 0.003 mg per cm^2 on 0.1 mg per cm^2 Al, which was glued to the high voltage electrode of the chamber over a $\frac{3}{8}$-in. wide slot along a diameter. This electrode was common to all three sections of the chamber. Figure 2 shows a block diagram of the electronic equipment utilized.

On filling the chamber with a mixture of argon plus two percent CO_2 and exposing the chamber to a source of thermal neutrons, fission pulses were obtained from all three sections. Each of the three discriminators in the triple coincidence circuit was so adjusted that its channel would respond to a pulse size, from the appropriate section of the chamber, corresponding to a heavy fission particle of initial energy approximately 40 Mev or higher for the case of Chambers I and III, and 48 Mev or higher for the case of Chamber II. The U^{235} was so placed that whenever a binary fission occurred such that one fragment entered either Chamber I or Chamber III, the mate to that fragment, if it was not unduly scattered, was obliged to enter Chamber II. Chamber II is seen to be a standard-type Frisch-Grid counter from which a pulse, under proper conditions, would be proportional to the ionization produced in the chamber and hence to the energy lost by the fission fragment responsible for the ionization.

The triple coincidence circuit registered events occurring simultaneously in each chamber if, of course, sufficient energy was liberated by particles in each of the chambers within the resolving time of the coincidence circuit. Under the conditions of our experiment, a triple coincidence could mean one of three things: (1) A compound U^{236} nucleus actually underwent fission into three comparable masses; (2) Two binary fissions occurred within the resolution time of the triple coincidence circuit; (3) immediately after occurrence of a binary fission, one of the fragments collided with either a U^{235}, aluminum, or argon nucleus in such a manner that the three particles each entered a separate chamber with sufficient energy to activate the coincidence channel with sufficient energy to activate the coincidence channel associated with that chamber. It is shown in Appendix I that the third mechanism could not effect our results. By far the overwhelming majority of the observed triple coincidences resulted by the second mechanism, namely, two binary fissions occurring within the resolving time of the triple coincidence circuit. In order to eliminate most of these, utilization was made of the fact that, under ideal conditions, the sum of the energies of two fission fragments is almost always greater than 100 Mev, which is the average energy of the high energy group of fission particles.

In order to take advantage of the fact that, in almost all cases, the sum of the energies of any two fragments is greater than the energy of any one fragment which

[22] The U^{235} coating was made by Robert Potter using the "Zapon Technique" in which the uranium as UNO_3 is dissolved in a solution of alcohol and Zapon and this solution is then painted on the aluminum foil.

would result from tripartition into three heavy fragments, the output from the triple coincidence circuit, in addition to going to a scaling circuit, was also fed into one channel of a double coincidence circuit, the discriminator for that channel being set so that the channel was activated by the output pulse from the triple coincidence circuit.[23] Into the second channel of the double coincidence circuit were fed the amplified pulses from Chamber II, the discriminator for this channel being set at such a bias that the channel would only be activated when it received a pulse corresponding to at least the minimum energy (under idealized conditions) liberated by the sum of the energies of two of the fragments from two binary fissions, this being also approximately equal to the maximum energy which one might expect from one fragment resulting from a tripartition into comparable masses. Under the above conditions more than 85 percent of the triple coincidences which resulted from two binary fissions occurring within the resolving time of the triple coincidence circuit were accompanied by a double coincidence. Every triple coincidence not so accompanied represented either, (a) an actual tripartition of a uranium nucleus into three heavy fragments,[24] or (b) two binary fissions occurring within the resolution of the triple coincidence circuit under one of the following conditions: (1) The sum of the fragment energies in Chamber II was less than 100 Mev. (2) One of the fragments which was destined to enter Chamber II was scattered by the Al or U^{235} through such an angle as to make this impossible. (3) One of the binary fissions occurred in Chamber I or III as a result of contamination. It is seen that the triple coincidence counting rate due to factor (b) will vary as the product of the counting rates of Chambers I and III, whereas the triple coincidence counting rate due to factor (a) will be a linear function of only one of those counting rates. The number of triple coincidences due to actual tripartitions could therefore, in principle at least, be separated from the number of triple coincidences due to two binary fissions which gave rise to either conditions (1), (2), or (3) by the well-known technique of plotting the number of triple coincidences per count in Chamber I, for example, as a function of counting rate in Chamber III (see Appendix II).

In order to be certain that the double coincidence circuit received from Chamber II a pulse corresponding to the full sum of any two fragments whose individual mates respectively entered Chambers I and III within the resolving time of the triple coincidence circuit, the clipping time of Amplifier II was made two microseconds, while Amplifiers I and III each had one-microsecond clippers, and the resolving time of the double coincidence circuit was made 2.2 microseconds. The electron collection-time for each of the chambers was approximately 0.8 microsecond. In order that the mate of every fragment which entered Chambers I or III would be certain, if it did not scatter excessively, to enter Chamber II, the active material was masked on the double-chamber side by a disk containing a slot one-half inch shorter and only half as wide as the slot in the plate to which was glued the uranium foil. (This masking plate is not shown in Fig. 1.)

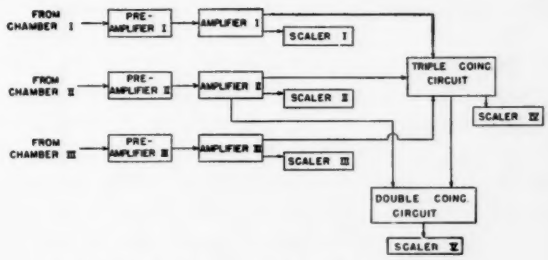

FIG. 2. Block diagram of the electronic equipment.

On the basis of scattering considerations, and in the interests of obtaining reasonable pulse height distributions in Chambers I and III, it was deemed desirable to mount the U^{235} foil with the aluminum side facing Chamber II. As a result the pulse height distribution curve for Chamber II was distorted. Furthermore, in order to obtain reasonably meaningful pulse height distributions from Chambers I and III, it was found necessary to decrease the pressure in the chamber to such an extent that not all of the fission fragments in Chamber II were now stopped prior to reaching the grid. This, of course, also had an adverse effect on the pulse height distribution curve from this chamber. Figure 3 shows the pulse height distribution due to fission fragments as observed in Chamber II under the actual conditions of the experiment. Figure 4 shows the pulse height distribution as obtained from Chambers I or III. The triple coincidence circuit discriminators for Channels I and III were set so that these channels responded to all pulses from Chambers I and III with energy corresponding to an initial particle energy of greater than 40 Mev as determined from the pulse height distributions from the two chambers and the known average energies of the two groups of particles emitted in binary fission (see Fig. 4). The triple coincidence circuit discriminator for Channel II was set so that this channel responded to all pulses from Chamber II with energy corresponding to a fission fragment energy greater than 48 Mev.

In order to separate accurately triple coincidences due to actual tripartitions from so-called accidental triple

[23] During the preliminary experiments a gated ten-channel pulse amplitude discriminator was used instead of the double coincidence circuit. Under these conditions the gate was supplied by the output of the triple coincidence circuit and into the amplitude analyzer were fed all the amplified pulses from Chamber II. In this way we obtained the pulse height distribution of the pulses from Chamber II for the pulses occurring simultaneously with triple coincidences. It was then a simple matter to identify most of the triple coincidences which occurred as a result of two binary fissions.

[24] An alpha-particle, no matter what its kinetic energy, could only liberate a maximum of four Mev in any of the chambers. This follows from stopping power and specific ionization considerations.

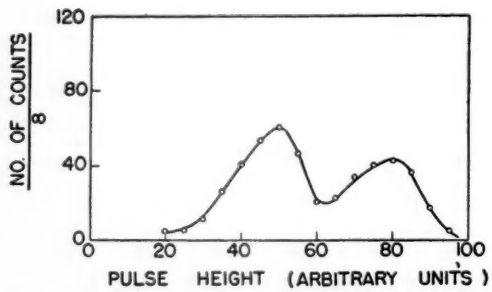

FIG. 3. Pulse height distribution of fission fragments in Chamber II.

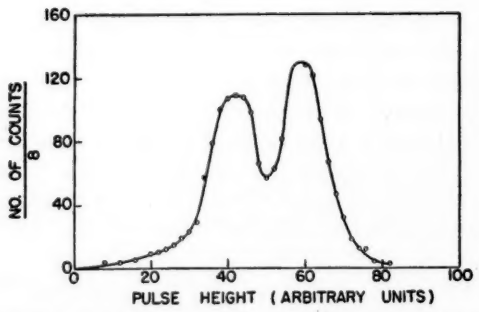

FIG. 4. Pulse height distribution of fission fragments in Chamber I or Chamber III. Identical curves were obtained for these two chambers within the statistical error of the experiment.

coincidences, runs were taken at different counting rates, the thermal column of the Los Alamos slow neutron reactor being used as the neutron source.[25] The power level of the reactor was kept constant to ±0.1 percent during each run. The use of the thermal column and pure U^{235} insured that any effect observed would be due to thermal neutron fission of U^{235}. Appendix II shows the method used to isolate the frequency of "real" triple coincidences from "accidental" triple coincidences.

The procedure used for collecting data was to make a run at a given counting rate for such a time as to obtain approximately 10^6 counts in Chambers I and III. The number of fission fragment pulses in each of the three chambers, the number of triple coincidences and the number of double coincidences were all recorded. Also recorded was the precise duration of the run and, as an additional check, the power level of the reactor. After completing a run, the reactor was turned off and, without moving the chamber, a calibration was made by determining the counting rate of the alpha-particles from the U^{235} foil for given settings of amplifier gains and discriminators. This not only checked the preamplifiers, main amplifiers and counters, but also served as a check on the discriminator and scaling circuits. If the observed counting rate for each chamber did not vary at these conditions, we proceeded to take another run with the reactor operating at a different power level. The fission counting rate from Chambers I and III was varied from 100–350 counts per second. Not less than three runs were taken at each counting rate. The discriminator settings at the inputs to the triple and double coincidence circuits were checked regularly by feeding a pulse from a precision pulser through each channel (from preamplifier to coincidence stage). The pulse size necessary to activate the coincidence stage of any given channel never varied by more than two percent from the predetermined pulse size for a given discriminator setting when the amplifiers were operating properly. As a check on both coincidence circuits and the experimental set-up in general, the discriminator on the double coincidence circuit into which were fed the pulses from Chamber II was periodically adjusted to accept all pulses corresponding to a fission fragment energy of greater than 40 Mev. Under these conditions, virtually every triple coincidence count should be accompanied by a double coincidence count and this was indeed the case when all circuits were operating properly.

3. INSTRUMENTATION DETAILS

The triple ionization chamber was made of dural and all parts were thoroughly decontaminated in nitric acid before assembly. The Frisch Grids, which shielded the collecting electrodes from the positive ions and thus made possible high speed electron collection in such a way that the pulse heights were approximately proportional to the ionization produced in the chamber were made of No. 36 parallel copper wires spaced 0.75 mm apart. The high voltage electrode on which was mounted the fissionable material was kept at minus 2200 volts by a well-filtered r-f type power supply. Additional Π-filter networks were utilized at the input to each chamber. The screens were kept at a constant minus 1000 volts by a second well-filtered r-f power supply. This made the field between screen and collecting electrodes slightly higher than the field outside the screen. However, this was desirable in order to insure that the screen should capture a minimum number of electrons. Without the uranium foil in the chamber, no triple coincidences were observed during an exposure to an integrated thermal neutron flux from the reactor of intensity sufficient to produce 200 triple coincidences at a counting rate from Chamber II of 200 counts per second under normal operating conditions with the active material in the chamber. The chamber was filled with argon plus two percent of CO_2 to a pressure of 50 cm Hg. This was not quite sufficient to stop the highest energy fragments if they traveled in a straight line from fission material to grid. However, as was pointed out above, this was necessary in order to obtain reasonable pulse height distributions from Chambers I and III. The dural plate between Chambers I and III was inserted for the purpose of preventing these two chambers from sharing the ionization produced by any one fission fragment. This plate was at the same poten-

[25] In the preliminary work when the ten-channel discriminator was used instead of the double coincidence circuit, the Los Alamos cyclotron was utilized as the neutron source.

TABLE I. Combined results of the runs taken at different counting rates. C_3=counting rate of Chamber III. C_t=triple coincidence counting rate minus double coincidence counting rate. C_1=counting rate of Chamber I. E=efficiency of chamber for recording a symmetrical tripartition.

C_3 Counts/sec.	C_t/C_1E	Probable error
94.3	3.4×10^{-5}	$\pm0.5\times10^{-5}$
108.0	4.3	0.4
123.8	4.8	0.5
133.0	5.4	1.0
198.6	6.9	0.5
259.2	9.5	0.4
347.3	11.8	0.6

tial as the high voltage electrode. The saturation voltage for each chamber was established by determining the position of the energy peaks of the fission fragment energy spectrum as a function of plate voltage, the grid being maintained at a constant fraction of the plate voltage. It was found that making the plate voltage more negative than minus 1800 volts shifted the positions of the peaks very little. Also, for grid voltages between minus 800 and minus 1300 volts the positions of the peaks showed little change. The chamber pulses were amplified by "Model 100" [26] preamplifiers and main amplifiers. These amplifiers were stabilized by inverse feedback and had a rise time of 0.5 microsecond. By using a shorted delay-line clipping unit, the inverse reflection of the incoming pulse was superimposed upon itself after two microseconds for Amplifier II and after one microsecond for Amplifiers I and III. The amplifiers were shown to be linear to ±1 percent over the amplification interval utilized. The combined amplified noise level due to alpha-particles in the chambers, gamma-rays, amplifier noises, etc., was less than one-fourth of the minimum pulses which could pass the discriminators.

The coincidence circuits, which were designed and built by the Los Alamos electronics group, contained in each channel a blocking oscillator circuit which could produce a square pulse of fixed duration. These pulses were then applied to a coincidence stage. Five Higginbothom-type scalars were used as shown in Fig. 2 to count triple coincidences, double coincidences, and fission pulses from each of the three counters. Double coincidences were counted by a scale-of-eight incorporated into the double coincidence circuit. The triple coincidences were counted by a scale of 32 while the fission pulses were counted by a scale of 128. The triple coincidence circuit had an effective resolving time of approximately 1.0 microsecond. The double coincidence circuit had a resolution of 2.2 microseconds as stated earlier.

4. RESULTS AND DISCUSSION

Table I gives the results of all the runs taken under the conditions previously outlined. These results comprise three complete sets of runs, over a wide range of counting rates.

Figure 5 gives a plot of $C_t/(C_1E)$ as a function of C_3 (see Eq. (8)). From the Y-intercept of the straight line obtained by a least-squares fit and a consideration of the statistical accuracy of each point for which the data are plotted, one arrives at a frequency of ternary fission of 6.7 ± 3.0 per 10^6 binary fissions, assuming that all such fissions occurred symmetrically. (This is the case for which E is calculated; E would be smaller for an asymmetrical division.) Every point in Fig. 5 represents the weighted average of all the data taken at that counting rate for the bias setting prevailing during all the counting rates represented on the curve.

In order to evaluate the validity of the above results it is necessary first to determine to what extent triple coincidences which were due neither to ternary fission events nor to accidental coincidences produced by two or more binary fission events, could occur. In view of the tests carried out on the counters and electronic equipment, the only conceivable cause for such triple coincidence counts is in nuclear collision between fission fragments and U, Al, or A recoils, and this has already been shown to be highly improbable (Appendix I). The second question to be answered is whether or not triple fissions into heavy fragments could have occurred without having been detected with the efficiency which the chamber geometry would permit. Since close attention was paid to the coincidence resolving time, rise times of the pulses produced by the fission fragments, as well as frequency response and time delays in the detector circuits, this possibility must also be ruled out. It must be understood, however, that the frequency of tripartition may be considerably higher than we have given it, if this mode of fission occurs asymmetrically, since our calculation of E is based on a symmetrical division of the U^{236} nucleus, and the efficiency of the chamber for detecting triple fission events diminishes with increasing asymmetry of the disintegration. It is very difficult, however, to imagine any systematic error which would have led us to a lower value for the frequency of tripar-

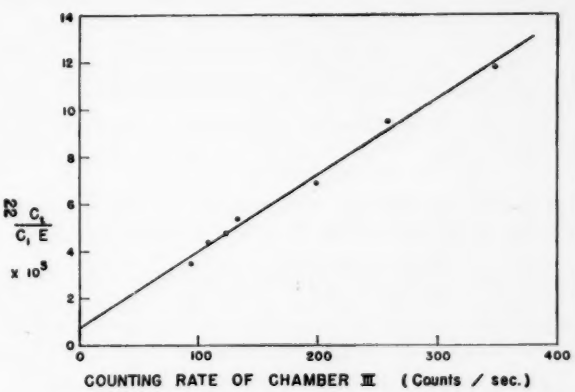

FIG. 5. Plot of $C_t/(C_1E)$ as a function of C_3. The intercept on the vertical axis gives the number of symmetrical triple fissions per binary fission.

[26] Los Alamos designation.

tition into heavy fragments than the value given by our data. Nevertheless, it is quite obvious that tripartition of uranium does not occur with sufficient frequency to be of practical importance.

APPENDIX I

Let us consider the collision of a fission fragment with another nucleus. Let M=mass of fission fragment, m=mass of recoil nucleus, θ=angle between recoil nucleus and original direction of fission fragment, E=energy of fission fragment before collision, E_1=energy of recoil nucleus, E_2=energy of fission fragment after collision, Z=charge of fission fragment, Z'=charge of recoil nucleus, e=electron charge, ϕ=angle through which M is scattered in C.M. system. Then from the law of conservation of momentum and the relationship between energy and momentum we have

$$M(E-E_1)=ME+mE_1-2(mMEE_1)^{\frac{1}{2}}\cos\theta,$$

and

$$E_1=4MmE\cos^2\theta/(M+m)^2. \tag{1}$$

We have seen that the discriminators for Channels I and III are set such that they will pass pulses corresponding to fission fragment energies of greater than 40 Mev, while the discriminator for Channel II is set such that it will pass pulses corresponding to fission fragment energies of greater than 48 Mev. It is apparent, therefore, that if a fission fragment is to project a U, Al, or A nucleus into Chamber II, for example, while it is itself scattered into Chamber I or III, and if the pulse produced by each particle is to be large enough to pass its discriminator, the original fission fragment must have an energy of at least 88 Mev. Now, the maximum energy of a fragment is 105 Mev. Since 40 Mev must go to Chamber I or III, this means that the nucleus entering Chamber II can have any energy from 65 to 48 Mev. It is then calculated from Eq. (1) that the scattering angle θ can have, as a rough approximation, any angle from 25° 16′ to 39° 0′ if uranium is the scattered nucleus and from 24° 47′ to 38° 43′ if aluminum is the scattered nucleus. In obtaining the above values a mass number of 81 and an atomic number of 40 were used to correspond to a fission fragment energy of 105 Mev. We will now calculate the cross section for scattering through these angles for U and Al nuclei.

The cross section for coulomb scattering of M into the ϕ-interval (ϕ_1, ϕ_2) is given by the well-known equation

$$2\pi\int_{\phi_1}^{\phi_2} I(\phi)\sin\phi d\phi, \tag{2}$$

where

$$I(\phi)=\left(\frac{ZZ'e^2}{2E}\right)^2\left(\frac{M+m}{m}\right)^2\frac{1}{4\sin^4(\phi/2)}. \tag{3}$$

The cross section for projecting m into the laboratory angular interval (θ_1, θ_2) is also given by

$$2\pi\int_{\theta_1}^{\theta_2} I(\theta)\sin\theta d\theta, \tag{4}$$

where $I(\theta)$ must be related to $I(\phi)$ by the following:

$$I(\theta)\sin\theta d\theta=I(\phi)\sin\phi d\phi,$$

and

$$\phi=180°-2\theta.$$

After making the indicated transformation the cross section for scattering m into the interval (θ_1, θ_2) is determined to be

$$\pi\left[\left(\frac{M+m}{m}\right)\frac{ZZ'e^2}{2E}\right]^2(\tan^2\theta_2-\tan^2\theta_1). \tag{5}$$

With each value of E is associated an interval (θ_1, θ_2) and hence a cross section for scattering into that interval. We then find that the number of fission fragments scattered in such a manner that the recoil fission fragment has an energy greater than 40 Mev and the knock-on nucleus has an energy greater than 48 Mev is given by

$$\sum_{E=88}^{105}\sigma(E)\cdot\Delta N(E)\cdot\frac{t}{A}\cdot 6.023\times10^{-23}, \tag{6}$$

where $\sigma(E)$=average cross section for scattering in the interval (θ_1, θ_2) corresponding to an average fission fragment energy E, $\Delta N(E)$=fraction of fission fragments in the energy interval E for which the scattering cross section is $\sigma(E)$, t=thickness in g/cm² of scattering material, and A=atomic weight of scattering material.

It can be shown that for our geometry we would observe in Chambers I or III less than one scattering from U^{235} per 2×10^6 fissions recorded by those counters, while in the case of Al there would occur less than one such scattering per 10^8 fissions recorded by Chambers I and III. Similar considerations show the possibility of accidental triple coincidences originating from the collision of fission fragments with argon nuclei to be completely negligible. All the approximations made in the above calculations were on the side of making the effect calculated as bad as possible. No account, for example, was taken of the energy lost by both fission fragment and scattered nucleus in the aluminum foil which one or the other must traverse. Also, no account was taken of the screening of the nuclear charge by the electronic field in the calculation of coulomb scattering cross section.

APPENDIX II

Let C_t=triple coincidence counting rate minus double coincidence counting rate, C_1=counting rate of Chamber I, C_3=counting rate of Chamber III, τ=resolving time of triple coincidence circuit when it is used as a double coincidence circuit between Channels I and III (Channel II always receives a pulse whenever Channel I or Channel III receives a pulse), N=average number of triple fissions per binary fission, and E=probability, that if a triple fission occurs and one of the fragments enters Chamber I, Chambers II and III will each receive one of the remaining fragments.[27] Then we have the following relation

$$C_t=2C_1C_3\tau+ENC_1, \tag{7}$$

from which

$$C_t/C_1E=(2C_3\tau/E)+N. \tag{8}$$

If one then plots $C_t/(C_1E)$ as a function of C_3, he obtains a straight line for which the Y-intercept will immediately yield the number of ternary fissions per binary fission. It is to be noticed that the standard counting error for each point on the curve is $\pm C_t^{\frac{1}{2}}$. This value is not determined solely by either the triple coincidence counting rate or the double coincidence counting rate. The two counting rates are not independent since every double coincidence must, *a priori*, have been accompanied by a triple coincidence. Therefore, the counting error depends only on the difference of these counting rates.

ACKNOWLEDGMENT

The authors take pleasure in thanking Dr. L. D. P. King for making the Los Alamos slow neutron reactor available for the above experiment and for numerous helpful suggestions during the course of the experiment.

[27] E was calculated by the Theoretical Division computing group under the supervision of B. Carlson. This calculation was based on the solid angle subtended by the various chambers at the uranium film for the case of symmetrical tripartition.

The Fine Structure of Singly Ionized Helium*†

WILLIS E. LAMB, JR. AND MIRIAM SKINNER‡
Columbia Radiation Laboratory, Columbia University, New York, New York
(Received January 26, 1950)

The displacement $2^2S_{\frac{1}{2}}-2^2P_{\frac{1}{2}}$ in singly ionized helium has been determined to be 14,020±100 mc/sec. The method is analogous to that employed for hydrogen by Lamb and Retherford, except that no beam of metastable ions is formed. Instead, helium atoms are bombarded by electrons of a few hundred volts energy. In about one percent of the ionizing collisions, the remaining atomic electron is excited to the metastable $2^2S_{\frac{1}{2}}$ state of the ion. When the bombardment region is illuminated with microwave radiation of the proper frequency, transitions to the $2^2P_{\frac{1}{2}}$ state are induced, and the ultraviolet photons emitted in the subsequent decay to the ground state $1^2S_{\frac{1}{2}}$ are detected by a suitable photoelectric detector. Background effects due to metastable atoms and radiation from HeI are reduced by the use of a collodion film filter. Our experimental value for the $2^2S_{\frac{1}{2}}-2^2P_{\frac{1}{2}}$ level shift is about 1.4 percent higher than the present theoretical value.

1. INTRODUCTION

IN their experiment on the fine structure of hydrogen, Lamb and Retherford[1] showed that contrary to the predictions of the Dirac theory, states with the same principal quantum number, n, and the same total angular momentum quantum number, j, were not degenerate. In particular, they measured the energy difference between the $2^2S_{\frac{1}{2}}$ and the $2^2P_{\frac{1}{2}}$ states, using microwave techniques. In their first paper they reported a value of about 1000 mc/sec. for the frequency corresponding to this energy difference. After refining the measurement considerably, they obtained a value[2] of 1062±5 mc/sec.

Shortly after the deviation from the Dirac theory had been established, Bethe[3] presented an explanation based on the interaction of the atomic electron with the radiation field. Using non-relativistic quantum electrodynamics, he showed that such an interaction would result in an upward shift of the energies of the $^2S_{\frac{1}{2}}$ states in a hydrogen-like atom, and a much smaller downward shift of the $^2P_{\frac{1}{2}}$ states, thus removing the degeneracy predicted by the Dirac theory. The numerical value obtained for this level shift was in qualitative agreement with the measured $2^2S_{\frac{1}{2}}-2^2P_{\frac{1}{2}}$ energy difference.

Kroll and Lamb,[4] and French and Weisskopf[5] applied relativistic quantum mechanics to the calculation of the electromagnetic shift, and derived the following expression for the energy difference between the $n^2S_{\frac{1}{2}}$ and $n^2P_{\frac{1}{2}}$ levels of a hydrogen-like atom:

$$\Delta W_n=\frac{8\alpha^3}{3\pi}\frac{Z^4}{n^3}Ry\left[\log\frac{1}{\bar{\epsilon}}-\log 2+\frac{23}{24}-\frac{1}{5}\right], \qquad (1)$$

where α is the fine structure constant, Ry is the ionization energy of hydrogen, Z is the nuclear charge, n is the principal quantum number, and $\bar{\epsilon}$ is proportional to an average excitation energy of the atom. For hydrogen, using the latest[6] values of 135.549 mc/sec. for $\alpha^3Ry/3\pi$ and 7.6915 for $\log 1/\bar{\epsilon}$, this theory gives 1051 mc/sec. for the level shift of the $2^2S_{\frac{1}{2}}$ state above the $2^2P_{\frac{1}{2}}$ state. There is therefore, to date, an 11 mc/sec. discrepancy between the theoretical and experimental values.

In order to subject the theory to further tests, it becomes of interest to examine the fine structure of singly ionized helium, a hydrogen-like atom of nuclear charge 2. In the experiment described below, microwave techniques were used to measure the energy difference between the $2^2S_{\frac{1}{2}}$ and $2^2P_{\frac{1}{2}}$ levels of singly ionized helium.

The theoretical value for the shift in He^+ can be found immediately from Eq. (1), noting that $Z=2$, and that $\bar{\epsilon}(He^+)=4\bar{\epsilon}(H)$. The predicted level shift of the $2^2S_{\frac{1}{2}}$ state above the $2^2P_{\frac{1}{2}}$ state is then 13,820 mc/sec.

Several groups of spectroscopists have worked in the visible and ultraviolet regions on the fine structure of He^+. Paschen,[7] in 1916, investigated the fine structure of the λ4686 line. His results constituted strong evidence

TABLE I. Measured fine structure in the He^+ spectrum.

	ΔW_n (in cm^{-1})	ΔW_2 (in 10^3 mc/sec.)
Mack and Austern[a]	0.113±0.014($n=3$)	11.4±1.4
Kopfermann and Paul[b]	0.137±0.015($n=3$)	13.9±1.5
Fowles[c]	0.445±0.050($n=2$)	13.3±1.5
Kopfermann[d]	0.119±0.003($n=3$)	12.0±0.3
Hirschberg and Mack[e]	$0.125<\Delta W_3<0.134$($n=3$)	$12.6<\Delta W_2<13.6$

[a] J. E. Mack and N. Austern, Phys. Rev. **72**, 972 (1947).
[b] H. Kopfermann and W. Paul, Nature **162**, 33 (1948).
[c] G. R. Fowles, Phys. Rev. **74**, 219 (1948).
[d] Kopfermann, Krüger, and Ohlmann, Zeits. f. Physik **126**, 760 (1949).
[e] J. G. Hirschberg, Jr. and J. E. Mack, Phys. Rev. **77**, 745 (1950). We are indebted to Professor Mack for sending us these data.

* Work supported jointly by the Signal Corps and the ONR under Signal Corps Contract W 36-039 sc-32003.
† Submitted by Miriam Skinner in partial fulfillment of the requirements for the degree of Doctor of Philosophy in the Faculty of Pure Science, Columbia University.
‡ Present address: Radiation Laboratory, University of California, Berkeley, California.
[1] W. E. Lamb, Jr. and R. C. Retherford, Phys. Rev. **72**, 241 (1947).
[2] R. C. Retherford and W. E. Lamb, Jr., Phys. Rev. **75**, 1325 (1949).
[3] H. A. Bethe, Phys. Rev. **72**, 339 (1947).
[4] N. M. Kroll and W. E. Lamb, Jr., Phys. Rev. **75**, 388 (1949).
[5] J. B. French and V. F. Weisskopf, Phys. Rev. **75**, 1240 (1949).
[6] Bethe, Brown, and Stehn, Phys. Rev. **77**, 370 (1950). We are indebted to the authors for an opportunity to see their paper prior to publication. These authors conclude that $\bar{\epsilon}$ should not depend appreciably on the principal quantum number n. Unpublished calculations by B. S. Gourary confirm this expectation for $n=2$ and $n=3$, although the value for $n=1$ is somewhat different.
[7] F. Paschen, Ann. d. Physik **50**, 901 (1916).

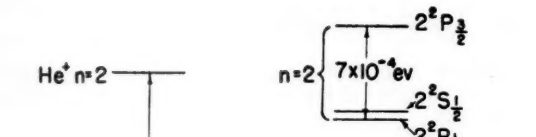

FIG. 1. Energy levels of He and He^+.

of the essential correctness of the theoretical fine structure splitting of the energy levels of hydrogen-like atoms as developed by Sommerfeld, and later by Dirac. The results of the more recent work, pursued in the attempt to establish the anomalous fine structure of He^+, are given in Table I. Fowles measured ΔW_2 by analysis of the ultraviolet $\lambda 1640$ line ($n=3\rightarrow n=2$). The others measured ΔW_3 by analysis of the visible $\lambda 4686$ line ($n=4\rightarrow n=3$). To facilitate comparison with the theoretical electromagnetic shift (and later with our result) the value in the last column represents in each case the corresponding shift of the $n=2$ level. This is obtained by assuming[6] a negligible change in $\tilde{\epsilon}$ when n changes from 2 to 3, in which case, according to Eq. (1), $\Delta W_3/\Delta W_2$ is just 8/27. It is to be noted that the last two, more accurate, measurements are then low compared to the theoretical value of 13,820 mc/sec.

The experiment to be described below is capable of greater precision than those just mentioned for two reasons: the Doppler effect becomes negligible, and there is no complex of components to be analyzed.

2. METHOD

The possibility of applying microwave techniques to the measurement of the fine structure of He^+ is suggested by the theoretical value of 13,820 mc/sec. for the shift of the $2^2S_{\frac{1}{2}}$ state above the $2^2P_{\frac{1}{2}}$ state. This corresponds to a wave-length of 2.2 cm, which is in an accessible range for microwave oscillators.

As in the case of hydrogen, the experimental method for ionized helium is based on the metastability of the $2^2S_{\frac{1}{2}}$ state. The energy levels of interest are shown in Fig. 1. An energy of 24.6 ev is required to remove one electron from the atom, and an additional 40.8 ev is required to excite the remaining electron to the group of states with $n=2$. The lifetime of the 2^2P states is

$$\tau=1/A=10^{-10}\text{ sec.},\qquad(2)$$

where A is the decay rate. (This is 16 times smaller than the lifetime of these states in hydrogen.) The $2^2S_{\frac{1}{2}}$ state, however, is metastable, the transition to the $1^2S_{\frac{1}{2}}$ ground state of the ion being forbidden by the selection rule $\Delta L=\pm 1$. The most probable decay method is double quantum emission, as shown for H by

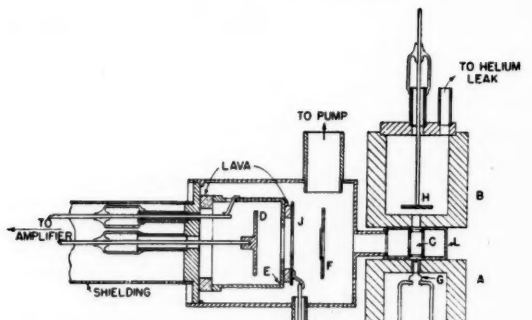

FIG. 2. Cross-sectional diagram of the apparatus. The data reported here were taken with r-f radiation of about 1.6-cm wavelength, transmitted through the K-band guide C. This guide could be slipped out of the apparatus, however, and longer wave-lengths transmitted through the X-band guide L. J, a disk with a circular hole, defined the solid angle subtended by the detector plate at the excitation region. J was maintained at a positive potential with respect to D and E so that electrons ejected from J would not reach D.

Breit and Teller.[8] Making the appropriate changes in frequencies and matrix elements so as to use their calculations for He^+, one finds that the expected lifetime of the $2^2S_{\frac{1}{2}}$ state is 2.2×10^{-3} sec., smaller by a factor of 64 than the lifetime of the metastable state of H.

The energy difference between the $2^2S_{\frac{1}{2}}$ and the $2^2P_{\frac{1}{2}}$ states can be measured in principle by obtaining a sufficient number of helium ions in the metastable $2^2S_{\frac{1}{2}}$ state (by electron bombardment of normal helium atoms), irradiating these with microwave radiation of the correct frequency in order to induce the transition to the $2^2P_{\frac{1}{2}}$ state and then, in some manner, detecting the decrease in the population of the $2^2S_{\frac{1}{2}}$ state.

The main difference between the work on hydrogen and that on singly ionized helium lies in the method of detection. In the hydrogen experiment, a beam of metastable atoms falls on a metal target and ejects electrons. The decrease in the population of the $2^2S_{\frac{1}{2}}$ state is inferred from the reduction in the electron current. Unfortunately, this detection method is not suitable in the case of He^+. Although it is known that ions can eject electrons from metals, the relative ejection efficiencies of metastable and non-metastable ions are not known. Since, as we shall see below (Appendix II, Eq. (32)), the number of metastable ions produced by electron bombardment of normal helium atoms is about 1 percent of the number of non-metastable ions formed, large background currents would be unavoidable using this method of detection.

Because of this difficulty a photoelectric method of detection was adopted for the work with ionized

[8] G. Breit and E. Teller, Astrophys. J. 91, 215 (1940).

helium. If a transition is induced from the $2^2S_{\frac{1}{2}}$ state to the $2^2P_{\frac{1}{2}}$ state, the ion then decays in 10^{-10} sec. to the ion ground state with the emission of a 41-ev photon. The photoelectric current produced by these photons striking a metal plate was used as a measure of the number of induced transitions. We shall refer to such induced transitions as r-f "quenching" of the metastable ions.

A cross-sectional diagram of the apparatus is shown in Fig. 2. A and B are pole pieces of a magnet. C is a wave guide. G is a hot filament maintained at a negative potential, so that electrons of a few hundred volts energy stream across the wave guide into the opposite pole piece and are collected on a metal plate at H. In contrast to the work with hydrogen, no attempt is made to form a beam of atoms in the $2^2S_{\frac{1}{2}}$ state. Instead, helium atoms circulate freely through the apparatus with thermal velocities. Some of the atoms in the bombardment region are excited or ionized, and a very small fraction of them are left in the $2^2S_{\frac{1}{2}}$ and 2^2P states of the ion. Those ions in the 2^2P states decay immediately to the $1^2S_{\frac{1}{2}}$ state with the emission of 41-ev photons. Those in the $2^2S_{\frac{1}{2}}$ state remain there until they diffuse out of the region and strike a wall or come into the presence of some other perturbing field which will cause them to decay. If, however, r-f of the proper frequency is introduced into the wave guide, the transition from the $2^2S_{\frac{1}{2}}$ state to the $2^2P_{\frac{1}{2}}$ state is induced, and the resultant $2^2P_{\frac{1}{2}}$ state decays to the ground state with the emission of an additional 41-ev photon. The photons are detected with a photoelectric detector which consists simply of a copper plate D and an electron collector E. The current from D to E is measured with an electrometer tube and a sensitive galvanometer.

The experiment is carried out in the presence of a magnetic field. One advantage derived from this is that charged particles cannot reach the detector. The main reason for the use of the magnetic field, however, arises from the difficulty of taking data by the direct method of varying the oscillator frequency. The $2^2P_{\frac{1}{2}}$ state has a natural width $A/2\pi=1600$ mc/sec. Thus, in order to obtain a resonance curve by varying the frequency, one would require either a single oscillator tunable over a range of about 3000 mc/sec., centered at a frequency in the vicinity of 14,000 mc/sec. or a set of ten or twelve fixed frequency oscillators covering this range. In either case the practical difficulties are very great, owing to the wide range of frequencies involved, and to the requirement that the power be the same for all the measurements. In the presence of a magnetic field, it is possible to work at a fixed oscillator frequency and vary the field strength to obtain a resonance for one of the Zeeman component transitions, from which one can then easily obtain the zero magnetic field energy shift. In this case one has considerable latitude in the choice of the fixed oscillator frequency (limited only by the maximum magnetic field available and by the desirability of working in a region isolated from neighboring Zeeman transitions), and the variation of the magnetic field over a wide range involves no problems comparable to those which one would encounter in varying the frequency.

3. ZEEMAN EFFECT

In the presence of a magnetic field, the $2^2S_{\frac{1}{2}}$ state and the $2^2P_{\frac{1}{2}}$ state are each split into two components (see Fig. 3). Transitions are possible between each of the components of the S state and each of the components of the P state. The transition frequencies as a function of the magnetic field are shown in Fig. 4. The significant data of this experiment were obtained by working with the upper (ad) transition,

$$2^2S_{\frac{1}{2}}(m=+\tfrac{1}{2})\rightarrow 2^2P_{\frac{1}{2}}(m=-\tfrac{1}{2}).$$

If the magnetic field is sufficiently weak, the energy of a given state is a linear function of the field strength, given by the expression

$$E=E_0+mg\mu_0H, \tag{3}$$

where μ_0 is the Bohr magneton, m is the magnetic quantum number, and g is the Landé g-factor. For small magnetic fields, the resonance energy for the (ad) transition is also a linear function of H, given in frequency units by

$$\nu_r=\nu_0+(4/3)\mu_0H/h=\nu_0+aH, \tag{4}$$

where

$$a=1.866 \text{ mc/sec. per gauss.} \tag{5}$$

In strong magnetic fields, the spin and orbital angular momentum vectors are decoupled, and Eqs. (3) and (4) no longer hold. For the magnetic fields used in this experiment (up to 4000 gauss) there is sufficient decoupling to require only a small correction to Eq. (4),

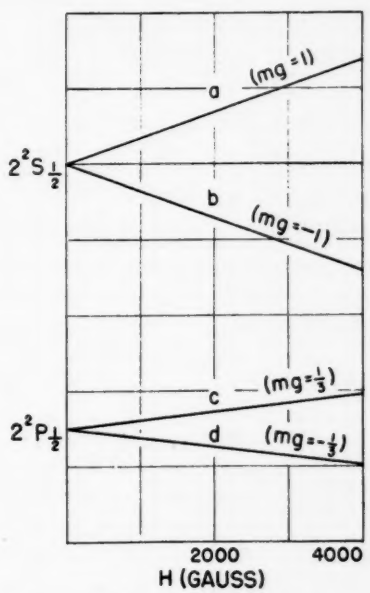

FIG. 3. Zeeman effect for the $2^2S_{\frac{1}{2}}$ and $2^2P_{\frac{1}{2}}$ states.

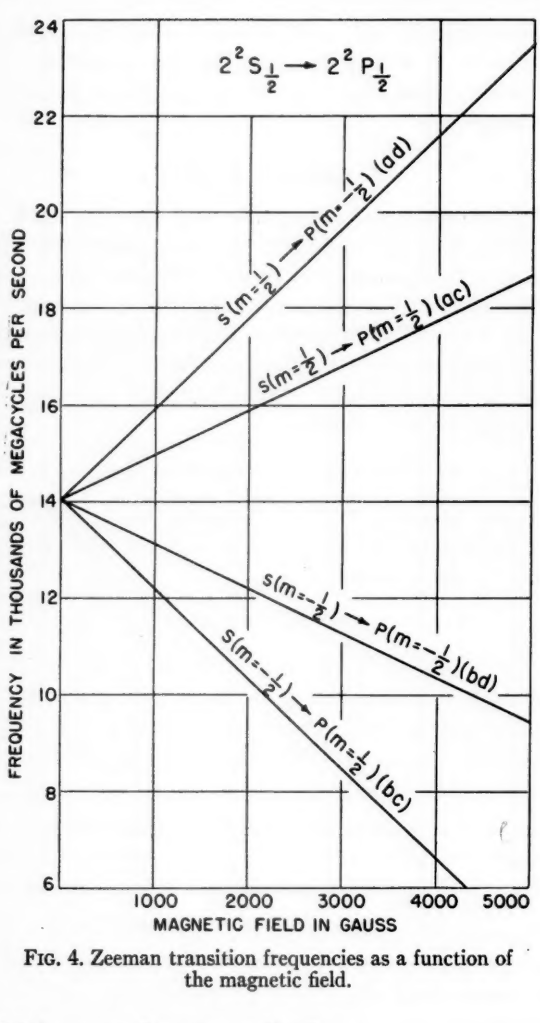

FIG. 4. Zeeman transition frequencies as a function of the magnetic field.

which becomes (see Appendix I)

$$\nu_r = \nu_0 + aH + bH^2, \tag{6}$$

where $b = 2.5\times10^{-6}$ mc/sec./gauss^2.

If the probability per second of an induced transition from $2^2S_{\frac{1}{2}}(m=+\frac{1}{2})$ to $2^2P_{\frac{1}{2}}(m=-\frac{1}{2})$ is μ, then[9]

$$\mu \propto 1/[(\nu-\nu_r)^2+(A/4\pi)^2], \tag{7}$$

where ν is the frequency of the incident radiation, ν_r is the resonant frequency, and $A=10^{10}$ sec.$^{-1}$ is the radiative half-width of the $2^2P_{\frac{1}{2}}$ state. Substituting Eq. (6) for ν_r, and H_0 for $(\nu-\nu_0)/a$, this becomes

$$\mu \propto 1/[(\nu-\nu_0-aH-bH^2)^2+(A/4\pi)^2] \tag{8}$$

or

$$\mu \propto 1/[(H_0-H-bH^2/a)^2+(\Gamma/2)^2], \tag{9}$$

where $\Gamma = A/2\pi a = 855$ gauss.

There are some possible corrections to (9) which must be considered. Use of the Bohr magneton in Eqs. (3) and (4) neglects effects due to the motion of the nucleus. The error introduced in Eq. (5) by using μ_0 is completely negligible, however, being less than 0.01 percent. Secondly, recent experimental results and theoretical considerations show that the gyromagnetic ratio of the electron spin is not 2, which was used to find Eq. (5), but $2+\alpha/\pi$. Neglect of the term α/π introduces about 0.06 percent error in Eq. (5), which is again negligible.

For low r-f power, Eq. (9) gives the shape of the resonance obtained by varying H. The peak of the curve is at $H=H_1$, where $H_1+bH_1^2/a=H_0$. The term bH^2/a is considerably smaller than H; at 4000 gauss, bH^2/a is about 20 gauss. Since this is the case, it can be shown that, for low r-f power, the half-width of the resonance is very nearly $\Gamma=855$ gauss.

From the definition of H_0, we see that the zero magnetic field resonant frequency is

$$\nu_0 = \nu - aH_1 - bH_1^2, \tag{10}$$

where ν is the oscillator frequency and H_1 is the magnetic field at the resonance peak. This is the expression that was used to determine the shift of the $2^2S_{\frac{1}{2}}$ state above the $2^2P_{\frac{1}{2}}$ state, from the experimental curves.

TABLE II. Cross sections for excitation and ionization in helium.

Atomic cross sections[a] (in units of πa_0^2)	Ionic cross sections (in units of πa_0^2)
$\sigma(2^1S)=0.49\times10^{-2}$	$\sigma^+(2^2S)=0.37\times10^{-2}$
$\sigma(2^1P)=6.9\times10^{-2}$	$\sum_{n=2}^{\infty}\sigma^+(n^2P)=2.8\times10^{-2}$
$\sigma(3^1P)=2.1\times10^{-2}$	
$\sigma(4^1P)=0.86\times10^{-2}$	
$\sigma(5^1P)=0.46\times10^{-2}$	

[a] H. S. W. Massey and C. B. O. Mohr, Proc. Roy. Soc. **140A**, 613 (1933).

[9] See article by G. Wentzel in *Handbuch der Physik* (1933), second edition, 24/1, p. 757.

4. DETECTION

The metastable ions are formed by the collisions of electrons with normal helium atoms. An electron energy greater than 65 ev is required, and electron energies of 150 or 200 ev were used. As mentioned before, we look for an increase in 41-ev photons when the metastable ions are quenched by the r-f induced transition to the $2^2P_{\frac{1}{2}}$ state. Unfortunately, the signal to background ratio is not very large. (The signal is that part of the detector current affected by the r-f. The background is the detector current when there is no r-f quenching.) This is a necessary result of the fact that the metastable state of the ion is just one of many states excited by collisions between electrons and helium atoms.

A. Theoretical Signal

The maximum signal, obtained when the r-f power is high enough to quench all the metastable ions formed, is directly proportional to the cross section for excitation of the metastable state of the ion in a collision between a normal helium atom and a 200-ev electron, and is given by

$$\begin{aligned} i_0 &= NIl(\omega/4\pi)\eta_{41}\sigma^+(2^2S) \\ &= K\eta_{41}\sigma^+(2^2S). \end{aligned} \tag{11}$$

In this expression N is the density of helium atoms, I is the bombarding electron current, l is the length of the electron beam from every point of which an unobstructed path can be drawn to the detector, ω is the solid angle subtended by the detector at the excitation region, η_{41} is the photoelectric efficiency of 41-ev photons, and $\sigma^+(2^2S)$ is the cross section for excitation to the metastable state of the ion.

In Appendix II, the value of $\sigma^+(2^2S)$ is estimated to be

$$\sigma^+(2^2S)=0.37\times10^{-2}\pi a_0^2. \tag{12}$$

In order to obtain a quantitative estimate of i_0 we assume that η_{41} is of the order of 0.1. (See Section 4-C.) The values of l and $\omega/4\pi$ for the apparatus used are respectively 0.38 cm and 1.4×10^{-3}. Then, for an electron bombarding current of 0.2 ma and a pressure of 5×10^{-3} mm Hg, the expected value of i_0 is 6×10^{-14} ampere. If the background current were small, such a signal could be easily measured.

B. Sources of Background Current

There are three sources of background current to the detector: (a) Most of those atoms excited to the n^2P states of the ion decay to the ion ground state. The decay photons of energy 41 ev or greater produce photoelectric current at the detector. (b) Those atoms excited to the atomic metastable 2^1S_0 state cause background current by ejecting electrons from the detector plate.[10] (c) Most of the atoms excited to singlet n^1P_1 states of the atom decay to the ground state of the atom with the emission of photons of about 20-ev energy. Effects arising from the excitation of the atoms to the triplet states or to states with $L>1$ are negligible since, at the electron energies used, such excitations are very much less probable than excitation to the singlet states with L equal to zero or one.

In order to estimate the relative contributions from these three processes, we need to know the cross sections for the n^2P states of the ion and for the 2^1S_0 metastable state and the n^1P_1 states of the atom. From Appendix II, where the cross sections in question are discussed, we have the results given in Table II, where a plus sign indicates that the cross section is for excitation to a state of the ion.

Since $\sigma(2^1P)$ is the largest cross section, it might be expected that most of the background current would be caused by the 20-ev radiation from the $2^1P_1\rightarrow1^1S_0$ transition. This is resonance radiation, however, and is highly absorbed in the gas between the excitation region and the detector. In Appendix III we compute the fraction, T_n, of photons arising from the transition $n^1P_1\rightarrow1^1S_0$ which reach the detector without being absorbed at least once in the gas at a pressure of 5×10^{-3} mm. For instance, only 0.08 percent of the photons from the $2^1P_1\rightarrow1^1S_0$ transition which are emitted in the direction of the detector reach it without being absorbed. The absorption and re-emission of a photon does not necessarily mean that it is lost to the detector. An exact analysis of the situation is difficult, since one cannot define a mean free path for resonance radiation. It is likely, however, that a photon that strikes the walls of the apparatus is lost. This indicates that most of the photons reaching the detector do so without absorptions. We therefore define an effective cross section for excitation to the n^1P_1 states given by

$$\sigma^*(^1P)=\sum_{n=2}^{\infty}T_n\sigma(n^1P). \tag{13}$$

We shall assume, then, that the photoelectric current from $n^1P_1\rightarrow1^1S_0$ photons is $K\eta_{20}\sigma^*(^1P)$, where K is the proportionality factor given in Eq. (11) and η_{20} is the photoelectric efficiency of 20-ev photons. In Appendix III it is shown that $\sigma^*(^1P)=0.95\times10^{-2}\pi a_0^2$.

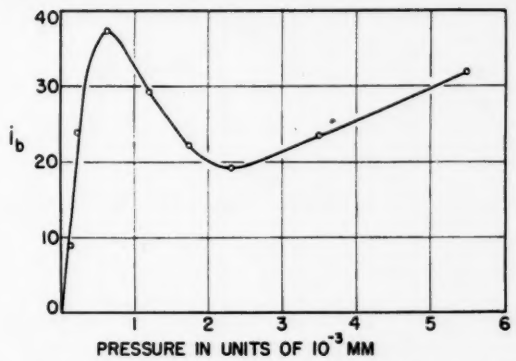

FIG. 5. Background current as a function of the pressure.

The effect of the absorption of resonance radiation on the background current is shown in Fig. 5, where the experimental detector current is plotted as a function of the pressure. Assuming, as we have, that the current is due to (a) photo-electrons from photons of energy 41 ev or greater arising from the transitions $n^2P\rightarrow1^2S_{\frac{1}{2}}$ of the ion, (b) electrons ejected by metastable atoms, and (c) photo-electrons from the 20-ev photons emitted in the transitions $n^1P_1\rightarrow1^1S_0$ of the atom, this curve is easily interpreted. At low pressures the detector current increases linearly with the pressure. In the vicinity of 4×10^{-4} mm there commences to be a significant amount of absorption of 20-ev photons. Since the cross sections for the lower n^1P_1 atomic levels are much larger than either

$$\sum_{n=2}^{\infty}\sigma^+(n^2P)$$

or $\sigma(2^1S)$, the signal actually decreases as the pressure is increased from 5×10^{-4} mm to 2.5×10^{-3} mm. At sufficiently high pressures, when the contributions from (a) and (b) become significant, the current increases again with pressure. (One would not expect any considerable absorption of 41 ev photons by either ions or atoms; the ion population is low, and the atomic ab-

[10] R. Dorrestein, Physica **9**, 433 and 447 (1942).

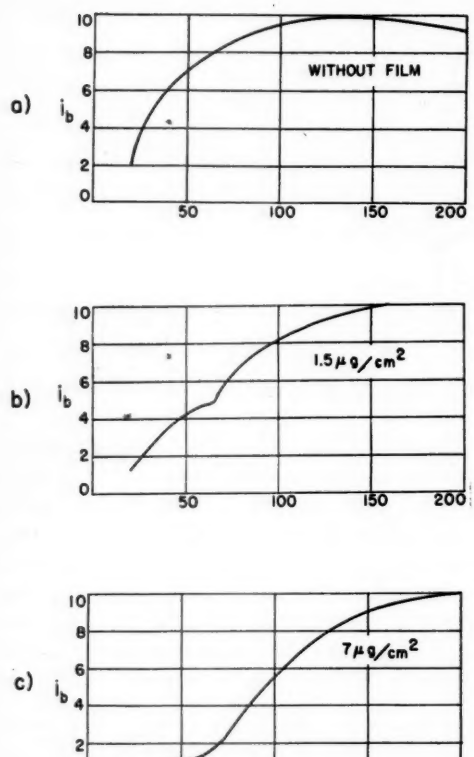

FIG. 6. Excitation curves showing the effect of the collodion film. The electron bombarding current for (a) was 3 μa, for (b) 100 μa, and for (c) 350 μa.

sorption cross section[11] is only about 3×10^{-18} cm^2. It is possible that deflecting collisions between the excitation region and the detector reduce the contribution from the metastable atoms.[10] We shall assume in what follows, however, that this is not important.)

For the background current we can now write

$$i_b=K\left[\eta_{41}\sum_{n=2}^{\infty}\sigma^+(n^2P)+\eta_{20}\sigma^*(^1P)+\eta_m\sigma(2\,^1S)\right], \quad (14)$$

where K is the proportionality factor given in Eq. (11), η_{41} and η_{20} are the photoelectric efficiencies of 41-ev and 20-ev photons, and η_m is the electron ejection efficiency of metastable atoms.

C. Theoretical Signal to Background Ratio

The maximum signal to background ratio is given by

$$r=i_0/i_b$$
$$=\eta_{41}\sigma^+(2^2S)\Big/\left[\eta_{41}\sum_{n=2}^{\infty}\sigma^+(n^2P)+\eta_{20}\sigma^*(^1P)+\eta_m\sigma(2^1S)\right]. \quad (15)$$

We now need the relative values of η_{41}, η_{20}, and η_m. The detector plate was made of copper and was not outgassed. Dorrestein[10] found an efficiency of 0.4 for metastable helium atoms and a photoelectric efficiency of 0.08 for 20-ev photons on outgassed platinum. For the purposes of our rough estimate, we assume that Dorrestein's value of 5 for η_m/η_{20} holds in our case also. The only information available on the photoelectric efficiency of 41-ev photons is that of Kenty[12] who found that the photoelectric efficiencies of several metals were rising sharply with photon energy in the vicinity of 584A (20 ev). Since, however, one can draw no definite conclusions from this about the behavior of 41-ev photons, we shall assume that $\eta_{41}=\eta_{20}$. Thus

$$r=\sigma^+(2^2S)\Big/\left[\sum_{n=2}^{\infty}\sigma^+(n^2P)+\sigma^*(^1P)+5\sigma(2^1S)\right]. \quad (16)$$

Substituting our values for the cross sections we find that $r=6\times10^{-2}$. It should have been possible, thus, to obtain a 6 percent increase in the detector current when the r-f power was turned on.

D. Experimental Signal to Background Ratio

With the apparatus as described in Section 2, a signal was obtained which was in good agreement with the estimated theoretical value. The maximum signal to background ratio observed, however, was 1.5 percent. The theoretical estimate made in the last section was apparently optimistic by a factor of 4, which is not surprising considering the assumptions that had to be made in deriving the various cross sections and efficiencies.

If the maximum signal to background ratio is 1.5 percent, less than half of this can be used in taking data for resonance curves. Only half of the metastable ions have magnetic quantum number $m=+\frac{1}{2}$, and only these are quenched in the transition between the Zeeman components $2^2S_{\frac{1}{2}}(m=+\frac{1}{2})$ and $2^2P_{\frac{1}{2}}(m=-\frac{1}{2})$. In order to obtain sharp resonances, well-isolated from

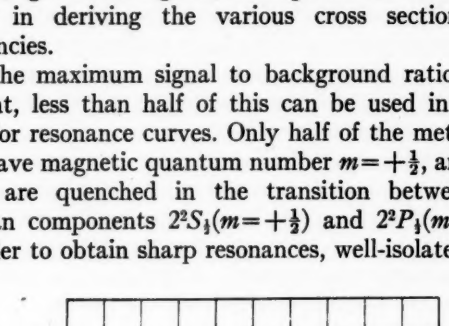

FIG. 7. R-f quenching as a function of the bombarding electron energy. The ordinate is the percent increase in the detector current when the r-f power was turned on. This curve was taken with a thick collodion film in the apparatus, and with a large amount of r-f power.

[11] S. Huang, Astrophys. J. 108, 354 (1948). We are indebted to Dr. Huang for informing us of his results prior to the publication of his paper.

[12] C. Kenty, Phys. Rev. 44, 891 (1933).

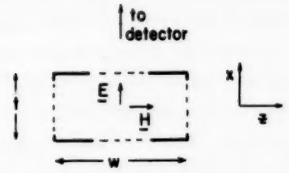

FIG. 8. Cross section of the wave guide in the excitation region.

neighboring resonances, the r-f power is made lower than that required to quench all of the $2^2S_{\frac{1}{2}}(m=+\frac{1}{2})$ ions at the peak of the resonance.

Some very rough resonances were obtained, with peak quenching of about 0.3 percent. The data obtained were quite unsatisfactory, however. With a peak quenching of only 0.3 percent, one must hope to obtain good data on the wings of the resonance with less than 0.1 percent quenching. This means that variations in the background current must be held down to less than 0.05 percent, and this is difficult to accomplish.

E. Improvement of Signal to Background Ratio with Collodion Film

In order to improve this unfavorable signal to background ratio, a thin collodion film was placed in the apparatus at F (Fig. 2), between the excitation region and the detector. This would eliminate any contribution to the detector current from metastable atoms. In addition, the work by O'Bryan[13] on thin celluloid films indicated that collodion, similar in composition to celluloid, should have a higher absorption coefficient for 20-ev photons than for 41-ev photons.

The actual behavior of the collodion in eliminating contributions to the background current from metastable atoms and 20-ev photons is shown in Fig. 6. A rough excitation curve is shown in (a), giving the current as a function of the energy of the exciting electrons, with no collodion film in the apparatus. The current starts at 20 ev with the production of excited atomic levels. There is no observable contribution from the excitation of the ionic levels at 65 ev. A similar excitation curve with a thin collodion film, 1.5 μg/cm^2 (about 100A), in the apparatus is given in (b). Here for the first time effects due to the excitation of the ionic levels are observable. Presumably, in this case the current is due only to 20- and 41-ev photons, the film having cut out the metastable atoms. Finally, in (c), we see that with a thicker film, 7 μg/cm^2, the background current from sources other than excited states of the ion has been reduced to about ten percent.

With a sufficiently thick film in the apparatus, the background current should be almost entirely due to 41-ev photons arising from the $n^2P\rightarrow 1^2S_{\frac{1}{2}}$ transitions of the ion. Under these conditions, the signal to background ratio is

$$r'=\sigma^+(2^2S)\Big/\sum_{n=2}^{\infty}\sigma^+(n^2P). \tag{17}$$

[13] H. M. O'Bryan, J. Opt. Soc. Am. **22**, 739 (1932).

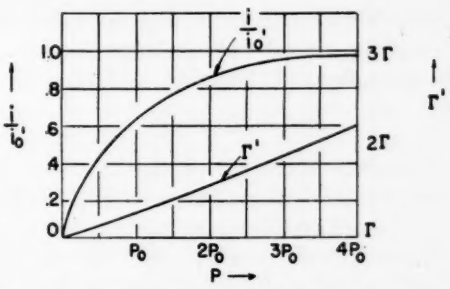

FIG. 9. Peak signal and resonance half-width as a function of the r-f power.

According to our estimates of these cross sections, the maximum signal to background ratio should be 13 percent. The experimental signal to background ratio was 12 percent, in good agreement with this theoretical estimate. (The signal to background ratio is increased slightly by working at lower pressures, which indicates that some of the metastable ions are lost by collisions at high pressures. We did not investigate this behavior very thoroughly. At pressures of 5×10^{-3} mm, however, less than half the metastable ions were lost. The reason for working at high pressures was simply to obtain a large enough signal to make random fluctuations in the galvanometer current insignificant. In Appendix IV, there is a discussion of the possibility of losing metastable ions due to Stark effect quenching. It is shown that, under the conditions of this experiment, this effect is negligible.)

Figure 7 shows the percentage increase in detector current with r-f quenching as a function of the energy of the bombarding electrons, when the r-f power is high and when there is a thick collodion film in the apparatus. For electron energies above 100 ev there is a 12 percent quenching signal. There is no indication of any quenching below 65 ev, the threshold for the production of metastable ions.

The resonance curves for the $2^2S_{\frac{1}{2}}(m=+\frac{1}{2})\rightarrow 2^2P_{\frac{1}{2}}(m=-\frac{1}{2})$ transitions were obtained with a peak r-f quenching of 4 or 5 percent.

5. RADIOFREQUENCY POWER REQUIRED

The probability per second of the induced transition $2^2S_{\frac{1}{2}}(m=+\frac{1}{2})\rightarrow 2^2P_{\frac{1}{2}}(m=-\frac{1}{2})$ is[9]

$$\mu=\frac{2\pi S_0}{\hbar\omega}\frac{e^2}{\hbar c}\frac{A\omega}{(\omega-\omega_0)^2+(A/2)^2}|\mathbf{r}_{ad}\cdot\mathbf{E}|^2, \tag{18}$$

where A is the width of the P state, ω_0 the resonant frequency and ω the frequency of the r-f, all in radians per second, S_0 is the incident power in ergs/cm^2 per second, $\mathbf{r}_{ad}$ is the vector whose components are the matrix elements for the transition, and $\mathbf{E}$ is a unit vector along the direction of polarization. In this case, with the wave guide transmitting radiation in the TE_{01} mode, $|\mathbf{r}_{ad}\cdot\mathbf{E}|=|x_{ad}|$ (see Fig. 8). At resonance we have

$$\mu=(8\pi e^2/\hbar^2c)S_0|x_{ad}|^2A^{-1}. \tag{19}$$

Now $x_{ad}=(\sqrt{3}/2)a_0$. Using this and the values $A=10^{10}$ sec.$^{-1}$ and P (in watts)$=\frac{1}{2}S_0w\times t\times 10^{-7}$, where w and t are the dimensions of the guide, we obtain

$$\mu=17\times 10^6 P \text{ sec.}^{-1}. \tag{20}$$

The photoelectric current produced at the detector when there is sufficient r-f power to quench all of the $2^2S_{\frac{1}{2}}(m=+\frac{1}{2})$ metastable ions that are formed in the wave guide is $i_0/2=i_0'$ (see Eq. (11)). The photoelectric current for any value of the r-f power is then

$$i=i_0'(1-e^{-\mu\tau_d}), \tag{21}$$

where τ_d is the time spent by a metastable ion in a region in the wave guide from which there is an unobstructed path to the detector. There is a circular opening in the wave guide whose diameter is 0.38 cm, facing the detector, and τ_d will be equal roughly to this length divided by v, the velocity with which the ions diffuse out of the region.

There are two velocities which must be considered before calculating τ_d. The first of these is the thermal velocity of the ions. In a magnetic field, the ions will spiral about the flux lines. Thus, only the z-component of the velocity has to be considered. The average speed in the z-direction at 300°K is given by

$$\langle v_z^2\rangle_{Av}^{\frac{1}{2}}=(kT/M)^{\frac{1}{2}}=8\times 10^4 \text{ cm/sec.} \tag{22}$$

The average recoil velocity of the ions due to the electron collisions is harder to evaluate. The maximum recoil velocity occurs, however, when the incident electron is scattered through 180° and when the momentum of the electron knocked out of the atom is equal in direction and magnitude to that of the scattered electron. In this case

$$v=(m/M)[v_0+(2v_0^2-4Q/M)^{\frac{1}{2}}], \tag{23}$$

where m and v_0 are the mass and initial velocity of the bombarding electron, M is the mass of the atom (or ion), and Q is the transition energy from the ground state of the atom to the excited state of the ion. In this case $Q(65 \text{ ev})=1.05\times 10^{-10}$ erg and for a 200-ev incident electron $v_0=8.4\times 10^8$ cm/sec. Substituting these values in Eq. (23), we find that the maximum recoil velocity is 2.5×10^5 cm/sec.

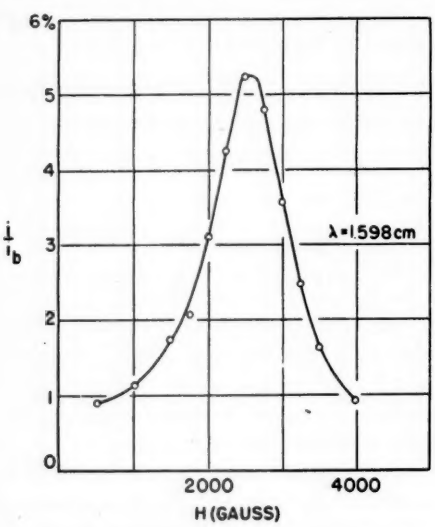

FIG. 10. Experimental resonance curve.

Since the recoil velocity distribution is not known, we do not know how to combine the recoil and thermal velocities to obtain an average value for the resultant. Instead, since the maximum recoil velocity is larger than the average thermal velocity, we shall use it to calculate τ_d. The average recoil velocity is probably much smaller than 2.5×10^5 cm/sec. Therefore, we should in this way find a value for the order of magnitude of the power required to obtain a given photoelectric current which is higher than the actual power requirement.

Using $v=2.5\times 10^5$ cm/sec., we find that $\tau_d=1.5\times 10^{-6}$ sec. The condition for $i=0.63i_0'$ is that $\mu\tau_d$ be equal to unity. Thus, in order to quench 63 percent of the $(m=+\frac{1}{2})$ metastable ions, we need about 40 milliwatts of r-f power.

For $\mu\tau_d\ll 1$, we have $i=i_0'\mu\tau_d$. In this case the shape of a resonance obtained by varying the magnetic field is given by Eq. (9). With low r-f power, the half-width of the resonance should thus be about 855 gauss. For higher r-f power, the resonance is broadened. In Fig. 9 the resonance value of i/i_0' and the half-width, Γ', as determined by Eqs. (20), (21), and (9), are plotted as a function of the power. The power is in units of P_0, the power required to quench 63 percent of the metastable $2^2S_{\frac{1}{2}}(m=+\frac{1}{2})$ ions, and the half-widths are given in units of Γ, where $\Gamma=855$ gauss.

6. DETAILED DESCRIPTION OF THE APPARATUS

With the pole piece arrangement used, the electromagnet gave fields up to 4000 gauss. The magnet current, which at 4000 gauss was 1.5 amperes, was supplied by a rectifying unit consisting of a voltage doubling transformer, a selenium rectifier and two filter sections. The 115-volt a.c. input to the rectifier was stabilized with a Sola transformer. The field was calibrated by means of a rotating flip coil which had been previously calibrated in a standard field. An upper limit on the error in the magnetic field calibration is 0.5 percent. The uniformity of the field was investigated by means of a flip coil and a General Electric flux meter. In the wave guide region the field was uniform to better than 0.5 percent.

The source of radiofrequency power was a continuous wave magnetron. The meaningful results of the experiment were obtained using cw magnetrons in the 1.6-cm wave-length range. These tubes[14] were made for the experiment in the Columbia Radiation Laboratory under the direction of M. J. Bernstein, to whom we are indebted for keeping us supplied.

A wave guide was used to transmit the r-f radiation

[14] Columbia Radiation Laboratory Report (September 30, 1948), p. 8.

from the magnetron to the excitation region. In the excitation region, the guide dimensions were 0.180 in. by 0.360 in. Circular holes 0.150 in. in diameter were cut in the walls of the guide to allow the electron beam to pass through the guide and to allow the photons passage to the detector. At $\lambda=1.60$ cm, the guide wave-length is 1.31 in., which is long compared to the diameter of the holes, so the holes should not disturb the transmission of the r-f power in the TE_{01} mode to any considerable extent. Connections were made from the vacuum regions of the guide to the non-vacuum regions through mica windows. The r-f power was monitored by the crystal current from a standing wave machine which was situated between the magnetron and the excitation region. Beyond the excitation region the r-f fed into a TE_{01n} two centimeter cylindrical wave meter,[15] by means of which the wave-length could be determined to about 0.1 percent. On the other side of the wave meter the r-f fed into a matched load.

The current heating the filament of the electron gun was supplied by storage batteries, which were charged continuously through a selenium rectifier. The electrical connections in the filament circuit were made with great care, since the detector current was extremely sensitive to variations in this filament current, being directly proportional to the filament emission. The current to the filament was varied by means of an Ohmite resistor in an oil bath.

Two grades of helium were used, the welding grade, 99.95 percent pure, and the XX grade, 99.99 percent pure, obtained from the Ohio Chemical and Manufacturing Company.

Aside from the mica windows in the wave guide, all vacuum seals were either soldered or brazed, if permanent, or waxed with Apiezon W, if temporary. The apparatus was pumped continuously, with a forepump and a three-stage oil diffusion pump, and could be pumped down to a pressure of 2×10^{-6} mm in 3 or 4 hours. Helium was admitted to the apparatus directly from the tank through a leak which was made by inserting a short length of 0.010-in. tungsten wire in a Pyrex capillary tube of about 0.030-in. bore and making a leaky glass-to-metal seal. The helium pressure in the apparatus was read by means of an ionization gauge, using the calibration data supplied by Distillation Products, Inc. for the VG-1A gauge, and correcting for the distance from the ionization gauge to the excitation region.

For the measurement of the detector current, a Victoreen VX 41 electrometer tube was used in a Penick[16] d.c. amplifier circuit. The Penick circuit is designed to operate in a balanced condition such that the galvanometer current is independent of small fluctuations in the tube filament current. Although for most of the work in this experiment the circuit was not so balanced, the amplifier gave entirely satisfactory results. All electrode voltages were supplied by two 6-volt "A" batteries. The leads to the electrometer tube were shielded electrically, and the tube itself was shielded magnetically by being placed in a cylinder of soft iron. The lead from the apparatus to the control grid of the tube was at all points insulated from other metal parts by at least a quarter of an inch of air. No attempt was made to mount the tube in vacuum, or to use drying agents in its vicinity. In spite of this, the galvanometer current was very steady. There was no noticeable change in the sensitivity of the whole detection system in a period of more than a year. The response of the amplifier was linear up to a control grid voltage of about 0.1 volt. Above this voltage, the slope of the response curve increased with control grid voltage.

The galvanometer used was a Leeds and Northrup Type R. The sensitivity of amplifier and galvanometer was 1.2×10^{-5} volt/mm. A grid resistor of 10^{11} ohms was used, giving a current sensitivity of 1.2×10^{-16} ampere/mm. With no signal coming to the detector, galvanometer and amplifier unsteadiness amounted to random ffuctuations of about 1 mm, with occasional 2- or 3-mm fluctuations.

The collodion for the thin films was diluted to the required strength with amyl acetate. With an eye-dropper, a drop was placed on the surface of clean distilled water. When the interference fringes disappeared from the film that formed on the water, it was picked up on a copper frame which had been suspended under the water surface. This was done in such a way that a double film covered the frame. After a short drying time, the frame was placed in the apparatus. The process of making the films was quite simple, except in the case of very thin films which displayed many fine cracks if they were allowed to harden too much on the water before being raised on the frame. The thickness of the films was determined only very roughly by weighing several drops of the diluted collodion on an analytical balance and dividing the weight per drop by the area over which the drop spread. We are very much indebted to Dr. C. S. Wu for information about mounting collodion films.

7. DISCUSSION OF THE DATA

In obtaining resonances, several fixed r-f frequencies were used, resulting in quite widely differing peak mag-

TABLE III. Level shift of $2^2S_{\frac{1}{2}}-2^2P_{\frac{1}{2}}$ in He^+.

ΔW_2 (in mc/sec.)	
14,070	14,050
14,010	14,050
14,010	14,040
14,030	14,030
13,980	14,050
13,970	13,980
Average = 14,020	
(Statistical error = ±10)	

[15] Columbia Radiation Laboratory Report (September 30, 1948), p. 11.

[16] D. B. Penick, Rev. Sci. Inst. 6, 115 (1935).

netic fields. The slope of the line obtained by plotting the frequency as a function of the peak magnetic field was equal to 1.87 mc/sec. per gauss (see Eq. (5)), showing that the resonances did indeed belong to the (ad) $2^2S_{\frac{1}{2}}(m=+\frac{1}{2})\rightarrow 2^2P_{\frac{1}{2}}(m=-\frac{1}{2})$ transition.

The most accurate data were taken with r-f wavelengths between 1.52 cm and 1.61 cm, corresponding to peak magnetic fields between 3050 gauss and 2450 gauss. Figure 10 shows a typical resonance curve.

Before applying Eq. (10) to the resonance curves, in order to obtain the zero magnetic field level shift, the influence of two neighboring Zeeman transitions must be considered. First, there is the (ac) $2^2S_{\frac{1}{2}}(m=+\frac{1}{2})\rightarrow 2^2P_{\frac{1}{2}}(m=+\frac{1}{2})$ transition, also originating in the $m=+\frac{1}{2}$ component of the $2^2S_{\frac{1}{2}}$ state (see Fig. 4). The only matrix element of the vector $\mathbf{r}$ which does not vanish for the (ac) transition is z_{ac} where z is in the direction of the magnetic field. Since the electric field is along x (see Fig. 8 and Eq. (18)), this transition is not induced by the r-f. Secondly, there is the (bc) $2^2S_{\frac{1}{2}}(m=-\frac{1}{2})\rightarrow 2^2P_{\frac{1}{2}}(m=+\frac{1}{2})$ transition, originating in the $m=-\frac{1}{2}$ component of the $2^2S_{\frac{1}{2}}$ state. For r-f frequencies above 14,000 mc/sec., the peak of this transition occurs at "negative" magnetic fields. Since $x_{bc}=x_{ad}$, this transition can be induced if there is enough r-f power to compensate for the large off-resonance term which appears in the denominator of Eq. (18). It was in this way that we were able to quench all of the metastable ions with high r-f power and see a 12 percent signal to background ratio instead of the 6 percent maximum which would have been observed if only those metastable ions with $m=+\frac{1}{2}$ had been quenched. The (bc) transition spoils the symmetry of the (ad) resonance in the wings by raising the low magnetic field wing above the high magnetic field wing (see Fig. 10). It can be shown, however, that with sufficient power to obtain about 5 percent quenching for the (ad) transition, or a signal due to quenching five-sixths of the $m=+\frac{1}{2}$ metastable ions, the shift in the (ad) resonance peak magnetic field due to the influence of the (bc) transition amounts to only about 2 gauss, if the peak is in the vicinity of 2500 gauss. This corresponds to about 4 mc/sec., which can be neglected for this experiment. Therefore, no corrections for neighboring transitions are necessary before applying Eq. (10).

The value of the peak magnetic field, H_1, to be used in Eq. (10) was found graphically for each resonance.

The narrowest resonance curve that we observed had a half-width of about 1150 gauss. This was with a peak quenching of 2.8 percent. Consulting Fig. 9, it is seen that for $i/i_0'=2.8/6=0.47$, the width should be 1.2Γ, or about 1020 gauss. We did not investigate the widths for very low r-f powers since, with the collodion film in the apparatus, a higher detector sensitivity would have been required to do so.

8. RESULTS

Applying Eq. (10) to twelve resonances, the values shown in Table III were obtained for the $2^2S_{\frac{1}{2}}-2^2P_{\frac{1}{2}}$ level shift.

There are three possible sources of error: (a) Accidental errors, made in locating the resonance peak magnetic field, which are evidenced by the fluctuations in the values in Table III, (b) error in the calibration of the wave meter used to measure the r-f wave-length, and (c) error in the calibration of the magnetic field. We take ± 100 mc/sec. for the maximum total error introduced by the above.

Our experimental value for the $2^2S_{\frac{1}{2}}-2^2P_{\frac{1}{2}}$ level shift in ionized helium is thus

$$\Delta W_2=14{,}020\pm 100 \text{ mc/sec.} \tag{24}$$

The average value is about 1.4 percent higher than the present theoretical value of 13,820 mc/sec. In addition, both the theoretical result and our experimental value are larger than the last two values in Table I.

It should be possible to obtain a more precise value for the level shift for ionized helium than for hydrogen, since, in the former case, the complicating factor of hyperfine structure is missing. The work reported here is of an exploratory nature. A new apparatus is being built in this laboratory for a more accurate measurement of the level shift in ionized helium.

APPENDIX I. CORRECTION TO EQ. (4) FOR PASCHEN—BACK EFFECT

The two components of the $2^2S_{\frac{1}{2}}$ state experience only a linear Zeeman effect. Therefore we need only the correction to Eq. (3) for the $m=-\frac{1}{2}$ component of the $2^2P_{\frac{1}{2}}$ state.

Let E_+ and E_- be the energies of the $2^2P_{3/2}$ and $2^2P_{\frac{1}{2}}$ states in the absence of a magnetic field. Then it can be shown[17] that the energy of the $2^2P_{\frac{1}{2}}(m=-\frac{1}{2})$ state for a magnetic field H is

$$E=\tfrac{1}{2}(E_++E_-)+\mu_0Hm-\tfrac{1}{2}[(E_+-E_-)^2 +(4/3)\mu_0Hm(E_+-E_-)+(\mu_0H)^2]^{\frac{1}{2}}. \tag{25}$$

For ionized helium, the zero-field energy difference between the $2^2P_{3/2}$ and $2^2P_{\frac{1}{2}}$ states is, in frequency units,

$$(E_+-E_-)/h=175\times 10^3 \text{ mc/sec.} \tag{26}$$

At 4000 gauss, the highest magnetic field used, the magnetic energy, also in frequency units, is $\mu_0H/h=5.6\times 10^3$ mc/sec.

Since $(E_+-E_-)\gg\mu_0H$ for all magnetic fields used, we may expand the square root in Eq. (25), keeping only linear and quadratic terms in H:

$$E=E_-+\tfrac{2}{3}\mu_0Hm-2\mu_0^2H^2/9(E_+-E_-). \tag{27}$$

Thus, the correction to Eq. (3) for the $2^2P_{\frac{1}{2}}(m=-\frac{1}{2})$ state is $-bH^2$, where $b=2\mu_0^2/9h(E_+-E_-)=2.5\times 10^{-6}$ mc/sec./gauss^2.

Equation (4) then becomes Eq. (6) of the text

$$\nu_r=\nu_0+aH+bH^2.$$

For $H=2500$ gauss, $bH^2=16$ mc/sec.

APPENDIX II. EXCITATION CROSS SECTIONS

We are interested in the cross sections for the production of certain excited levels of helium by collisions between 200-ev

[17] See article by H. A. Bethe in *Handbuch der Physik* (1933), 24/1, second edition, p. 397.

electrons and normal helium atoms. The cross sections in question are those for the $2^2S_{\frac{1}{2}}$ (metastable) and n^2P states of the ion and for the 2^1S_0 (metastable) and n^1P_1 states of the atom.

Considering the atomic levels first, cross sections for the 2^1S_0 metastable state and for the first four n^1P_1 states ($n=2$ to $n=5$) were calculated by Massey and Mohr. Their results are given in Table II. Massey and Mohr's values for the $\sigma(n^1P)$ are very nearly equal to k/n^3 where $k=0.57\pi a_0^2$. When we have occasion to consider cross sections for excitation to the n^1P_1 states with $n>5$, we shall therefore use

$$\sigma(n^1P)=0.57\pi a_0^2/n^3 \quad (n>5). \tag{28}$$

As far as we know, there is no work reported in the literature on excitation cross sections for the ionic levels. It is possible, however, to obtain rough estimates for these cross sections quite easily.

Consider first $\sigma^+(2^2S)$, the cross section for excitation to the metastable $2^2S_{\frac{1}{2}}$ state of the ion. Originally the helium atom is in a state which can be approximated by the product of two hydrogen ground state wave functions with nuclear charge 1.69:

$$\psi_0=\psi_{10}(1.69, \mathbf{r}_1)\psi_{10}(1.69, \mathbf{r}_2), \tag{29}$$

where $\psi_{nl}(Z, \mathbf{r})$ is a hydrogen wave function for an electron whose position vector is $\mathbf{r}$, in the field of a nucleus with charge Z. If, in a collision with an electron, the primary process is the excitation of electron 1 into the continuum, the second electron suddenly finds itself bound to a nucleus of charge 2, instead of effective charge 1.69, and is therefore no longer in a definite quantum state. To find the probability that the electron is left in the $2^2S_{\frac{1}{2}}$ state we use the "sudden" approximation,[18] in which the initial wave function of the second electron is expanded in terms of the eigenfunctions of the second electron in the new force field:

$$\psi_{10}(1.69, \mathbf{r}_2)=\Sigma a_{nl}\psi_{nl}(2, \mathbf{r}_2). \tag{30}$$

Then,

$$\sigma^+(2^2S)=\sigma^+|a_{20}|^2=\sigma^+\left|\int\psi_{20}^*(2, \mathbf{r}_2)\psi_{10}(1.69, \mathbf{r}_2)d\tau_2\right|^2, \tag{31}$$

where σ^+ is the cross section for ionization. This yields

$$\sigma^+(2^2S)=0.01\sigma^+. \tag{32}$$

Using Massey and Mohr's value of $0.37\pi a_0^2$ for σ^+, we find the result of Eq. (12) of the text.

The validity of the use of the sudden approximation is open to some question, since it assumes that the initial process that changes the Hamiltonian of the second electron, namely the excitation of the first electron to a state in the continuum, happens in a "short" time. We can show, however, that the use of the sudden approximation does yield predictions for two other similar double excitation processes which agree within a factor of two with results obtained by different methods.

Consider first the double ionization of the helium atom. Bleakney and Smith[19] found by mass spectrographic measurements that 0.5 percent of the ions formed at 200-ev bombarding electron energy were doubly charged. The sudden approximation treatment of this problem yields

$$\sigma^{++}=\sigma^+\sum_{\text{continuum}}\left|\int\psi_c^*(2, \mathbf{r}_2)\psi_{10}(1.69, \mathbf{r}_2)d\tau_2\right|^2. \tag{33}$$

Since the $\psi(2, \mathbf{r}_2)$ form a complete set, this becomes

$$\sigma^{++}=\sigma^+\left[1-\Sigma_n\left|\int\psi_{n0}^*(2, \mathbf{r}_2)\psi_{10}(1.69, \mathbf{r}_2)d\tau_2\right|^2\right]$$

$$=\sigma^+[1-\Sigma_n|b_n|^2]. \tag{34}$$

Only the first few terms of the sum are significant. It can be shown that $b_1=0.989$, $b_2=-0.104$, and $b_3=-0.038$. Thus

$$1-\Sigma_n|b_n|^2=1-0.978-0.011=0.011. \tag{35}$$

The sudden approximation yields the result that 1.1 percent of the ions should be doubly ionized, which agrees well with Bleakney and Smith's value of 0.5 percent.

Next consider the double excitation of the helium atom to the state $(2s4p)^1P$. The cross section for this process was calculated by Massey and Mohr[20] using the Born approximation. The sudden approximation treatment assumes a primary excitation of one electron to a $4p$ state, the cross section for this process being very nearly $\sigma(4^1P)$. In the final state, the s-electron will see a charge on the nucleus which is close to 2. Using the sudden approximation, we therefore obtain

$$\sigma(2s4p)=\sigma(4^1P)\left|\int\psi_{20}^*(2, \mathbf{r}_2)\psi_{10}(1.69, \mathbf{r}_2)d\tau_2\right|^2$$

$$=0.01\sigma(4^1P). \tag{36}$$

Massey and Mohr's values for $\sigma(2s4p)$ and $\sigma(4^1P)$ are $0.45\times10^{-4}\pi a_0^2$ and $0.86\times10^{-2}\pi a_0^2$. The ratio of these two cross sections 0.52×10^{-2} is in sufficiently good agreement with the above value of 0.01.

Although the sudden approximation is apparently applicable to the calculation of such cross sections as $\sigma^+(2^2S)$, σ^{++}, and $\sigma(2s4p)$, it is not clearly applicable to the calculation of the excitation cross sections for the low n^2P states of the ion. Consider, for example, $\sigma^+(2^2P)$. To calculate this by the sudden approximation, we would take as the primary process the excitation of one electron to a $2p$-state. As compared with the above cases for which the primary excitation is to a continuum or high principal quantum number p-state, one would now expect more interaction between the two atomic electrons during the excitation process, and therefore less validity for the sudden approximation procedure. In addition there is the practical objection that the presence of the first electron in the $2p$-state makes it difficult to find good approximations to the eigenfunctions of the second electron in the new potential field.

Since a treatment of the problem by more exact methods than the sudden approximation becomes very involved, we find a rough estimate of $\sigma^+(2^2P)$ in the following way. Massey and Mohr[20] calculated the double excitation cross sections $\sigma(2s3p)$ and $\sigma(3s2p)$ for helium, and found that

$$\frac{\sigma(2s3p)}{\sigma(3s2p)}=\frac{0.68\times10^{-4}\pi a_0^2}{5.3\times10^{-4}\pi a_0^2}=0.13. \tag{37}$$

Our rough estimate is obtained by assuming that

$$\frac{\sigma^+(2^2S)}{\sigma^+(2^2P)}=\frac{\sum_{\text{continuum}}\sigma(2s\infty p)}{\sum_{\text{continuum}}\sigma(\infty s2p)}\lessapprox\frac{\sigma(2s3p)}{\sigma(3s2p)}\lessapprox0.13. \tag{38}$$

With Eq. (12) this yields

$$\sigma^+(2^2P)=2.8\times10^{-2}\pi a_0^2. \tag{39}$$

We assume that the total cross section for excitation to the n^2P states of the ion with $n>2$ is much less than $\sigma^+(2^2P)$, and therefore write

$$\sum_{n=2}^{\infty}\sigma^+(n^2P)=2.8\times10^{-2}\pi a_0^2. \tag{40}$$

(One cannot, by a similar argument, neglect the excitation of the atomic n^1P_1 states with $n>2$. It is shown in Appendix III that the absorption of the resonance radiation from the $n^1P_1\rightarrow1^1S_0$ transitions increases the relative importance of excitation to states with high n.)

[18] F. Bloch, Phys. Rev. **48**, 187 (1935) used the sudden approximation to treat an analogous problem in the theory of x-ray satellites.

[19] W. Bleakney, Phys. Rev. **43**, 378 (1933). W. Bleakney and L. G. Smith, Phys. Rev. **49**, 402 (1936).

[20] H. S. W. Massey and C. B. O. Mohr, Proc. Camb. Phil. Soc. **31**, 604 (1935).

TABLE IV. Probability (T_n) that photons reach the detector.

Transition	k_0	T_n
$2^1P_1 \rightarrow 1^1S_0$	50 cm^{-1}	0.08×10^{-2}
$3^1P_1 \rightarrow 1^1S_0$	12 cm^{-1}	0.38×10^{-2}
$4^1P_1 \rightarrow 1^1S_0$	4.5 cm^{-1}	1.2×10^{-2}
$5^1P_1 \rightarrow 1^1S_0$	2.3 cm^{-1}	2.5×10^{-2}

APPENDIX III. ABSORPTION OF THE RESONANCE RADIATION ARISING FROM THE $n^1P_1-1^1S_0$ TRANSITIONS IN HELIUM

In a paper on the imprisonment of resonance radiation, Holstein[21] derived the following expression for the probability that a photon emitted in a transition from an excited state of principal quantum number n to the ground state of the atom traverse a distance ρ without being absorbed

$$T_n(\rho) = (k_0\rho)^{-1}(\pi \log k_0\rho)^{-\frac{1}{2}}. \tag{41}$$

In this expression k_0 is determined by

$$k_0 = \lambda_n^3 N g_n / 8\pi^{\frac{3}{2}} g_1 v_0 \tau_n, \tag{42}$$

where λ_n is the resonance wave-length of the radiation, N is the number of absorbing atoms per cm^3, g_n and g_1 are the statistical weights of the two states, $v_0 = (2kT/M)^{\frac{1}{2}}$, and τ_n is the lifetime of the excited state.

Equation (41) was developed on the basis of a Doppler spectral distribution, and holds only for values of $k_0\rho$ large compared to unity. Before using Eq. (41) for photons from the $n^1P_1 \rightarrow 1^1S_0$ transitions of helium, we must first show that the spectral distribution of each of the lines arising from these transitions is essentially a Doppler distribution.

We shall first consider the line $2^1P_1 \rightarrow 1^1S_0$. The natural width of this line is $A_2/2\pi$, where

$$A_2 = (64\pi^4 e^2 \nu_2^3/3hc^3)(|x|^2 + |y|^2 + |z|^2). \tag{43}$$

In this expression, x is given by

$$x = \int \psi_1^*(\mathbf{r}_1, \mathbf{r}_2)(x_1 + x_2)\psi_2(\mathbf{r}_1, \mathbf{r}_2) d\tau_1 d\tau_2. \tag{44}$$

Vinti[22] has calculated these matrix elements for the first few excited singlet P states. For the $2^1P_1 \rightarrow 1^1S_0$ transition, he obtained

$$|x|^2 + |y|^2 + |z|^2 = 0.224\pi a_0^2. \tag{45}$$

Substituting this, and the value $\nu_2 = 5.14 \times 10^{15}$ sec.$^{-1}$ (corresponding to a wave-length of 584A), we have

$$A_2 = 0.23 \times 10^{10} \text{ sec.}^{-1}. \tag{46}$$

Thus, the natural half-width of the resonance line is

$$\Delta\nu_N = A_2/2\pi = 0.36 \times 10^3 \text{ mc/sec.} \tag{47}$$

For a thermal velocity distribution of the normal and excited atoms, the Doppler width is given by

$$\Delta\nu_D = 2(2 \ln 2)^{\frac{1}{2}}(kT/M)^{\frac{1}{2}}\nu_2/c. \tag{48}$$

One might expect that the excited atoms would not have a thermal velocity distribution because of the recoil velocity given them in the excitation collision with an electron. The great majority of the excited atoms, however, result from collisions in which the electron is scattered through less than 20 degrees (see Table II). For these collisions, the recoil energy of the atom is less than 0.003 ev, which is well below thermal energies. We shall, therefore, assume a thermal velocity distribution corresponding to a temperature of 300°K. We then find

$$\Delta\nu_D = 3.1 \times 10^4 \text{ mc/sec.} \tag{49}$$

Since the Doppler width is much larger than the natural width, the spectral distribution can be taken as a Doppler distribution, and if $k_0\rho$ is large, Eq. (41) can be applied. For the $n^1P_1 \rightarrow 1^1S_0$ lines, the ratio of $\Delta\nu_D$ to $\Delta\nu_N$ increases with n, so that the above statement holds for all n.

Using $g_n = 3$, $g_1 = 1$, $N = 1.8 \times 10^{14}$ corresponding to a pressure of 5×10^{-3} mm, and Vinti's values for the lifetimes of the excited states $\tau_n = 1/A_n$, we find the values given in Table IV for the probability T_n that photons from the $n^1P_1 \rightarrow 1^1S_0$ transition emitted in the direction of the detector will reach it without being absorbed. Since the detector plate is 6 cm from the excitation region, we have taken $T_n = T_n(6)$.

We define the total effective cross section for excitation to any of the n^1P_1 states by Eq. (13) of the text. The first four terms of this sum are known. Since T_n is 0.025 for $n = 5$, and is rapidly increasing, we approximate the contribution from terms with $n > 5$ by setting T_n equal to unity. We can then use Eq. (28) to evaluate

$$\sum_{n=2}^{\infty} \sigma(n^1P).$$

In this way, we find that

$$\sigma^*(^1P) = 0.95 \times 10^{-2} \pi a_0^2. \tag{50}$$

APPENDIX IV. STARK EFFECT QUENCHING OF METASTABLE IONS

Bethe[23] has developed the theory of the Stark effect mixing of the metastable $2^2S_{\frac{1}{2}}$ and the $2^2P_{\frac{1}{2}}$ states of a hydrogen-like atom for the case that these states are degenerate. In the non-degenerate case, let $h\nu_r$ be the energy difference between the two states. Then it can be shown[24] that the lifetime of the metastable state, as shortened by the Stark effect mixing, is given by

$$\tau_{2s} = \tau[\nu_r^2 + (A/4\pi)^2]/|V/h|^2, \tag{51}$$

where V is the matrix element of the perturbation energy, $H' = +e\mathbf{E}\cdot\mathbf{r}$, and $\tau = 1/A$ is the lifetime of the $2^2P_{\frac{1}{2}}$ state.

We shall consider the lifetime of the $2^2S_{\frac{1}{2}}(m = +\frac{1}{2})$ state of the ion for zero magnetic field. This will give a minimum lifetime since a magnetic field increases ν_r. Assuming that $\mathbf{E}$ is in the x direction (see Fig. 8), $V = +eEx = \sqrt{3}/2eEa_0$. For E in volts/cm,

$$|V/h| = 1.1 \text{ mc/sec.} \tag{52}$$

For ionized helium, $A = 10^4$ mc/sec., and in the absence of a magnetic field $\nu_r = 1.4 \times 10^4$ mc/sec. Equation (51) now yields

$$\begin{aligned} \tau_{2s} &= (1.6 \times 10^8/E^2)\tau \\ &= 1.6 \times 10^{-2} E^{-2} \text{ sec.} \end{aligned} \tag{53}$$

There will be no appreciable loss of metastable ions by Stark effect quenching if the $2^2S_{\frac{1}{2}}$ lifetime is long compared to the ion diffusion time τ_d. Therefore, the condition which must be satisfied is

$$\tau_d/\tau_{2s} \ll 1. \tag{54}$$

If for τ_d we use the value 1.5×10^{-6} sec. given in Section V, the requirement for small Stark quenching is found to be

$$E \ll 100 \text{ volt/cm.} \tag{55}$$

Since the stray electric fields in the apparatus due to space charge or other sources were considerably less than 100 volt/cm, the Stark effect quenching was negligible.

It is interesting to note that according to Eq. (51) the Stark effect lifetime of the He^+ metastable state is 42 times as large as that of hydrogen in the same perturbing electric field.

[21] T. Holstein, Phys. Rev. 72, 1212 (1947).
[22] J. P. Vinti, Phys. Rev. 42, 632 (1932).
[23] H. A. Bethe, reference 17, p. 454.
[24] W. E. Lamb, Jr. and R. C. Retherford (to be published).

A Study of the Polarization-Direction Correlation of Successive Gamma-Ray Quanta*

FRANZ METZGER AND MARTIN DEUTSCH
Department of Physics and the Laboratory for Nuclear Science and Engineering, Massachusetts Institute of Technology, Cambridge, Massachusetts

(Received February 6, 1950)

A gamma-ray polarimeter utilizing Compton scattering as the analyzing process is described. Measurements of the polarization-direction correlations of the gamma-rays emitted in the disintegration of Sc^{46}, Co^{60}, Rh^{106}, and Cs^{134} are reported.

1. INTRODUCTION

THE angular correlation of two gamma-rays, successively emitted by a nucleus, is intimately connected with the multipolarity of the two transitions and with the total angular momenta of the nuclear levels involved,[1,2] but does not depend on the parity changes occurring. Information concerning the electric or magnetic nature of the radiating multipoles may be obtained, as was shown by Falkoff[3] and Hamilton,[4] through an investigation of the polarization properties of the emitted radiation. Such a study, involving the simultaneous measurement of several gamma-rays, became possible through the development of the scintillation counters. These detectors with their high efficiency for gamma-rays and excellent properties regarding high speed counting are especially suited for coincidence measurements with gamma-rays. Their use increases the coincidence rates by several orders of magnitude as compared with Geiger-Müller counters in a similar arrangement.

As any process analyzing the polarization of gamma-rays is apt to reduce the intensity by a large factor, the simultaneous measurement of the polarization of both quanta[3] is most unfavorable in view of the small counting rates expected even if one uses the scintillation counters available today.

We therefore restricted ourselves to a combination of a polarization-insensitive detector, used to define the direction of one of the quanta, with a polarization-sensitive device for the analysis of the polarization of the other quantum. This combination had been suggested by Hamilton,[4] who gave the explicit form of the correlations expected in this case for dipole and quadrupole radiation.

As a polarization-sensitive process we chose the Compton scattering of the gamma-rays, a method that had previously proven adequate in the investigation of the polarization of the annihilation radiation.[5]

The arrangement used is shown schematically in Fig. 1. A, B, and C are the crystals of three scintillation counters. A is the polarization-insensitive detector, B and C together form the polarization-sensitive detector, which we shall call the analyzer. S is the source which is surrounded by enough material to stop all beta-rays. Crustal C is heavily shielded against direct radiation from the source and scattered radiation from A; therefore it detects preferentially the radiation scattered from B. However, as the counting rate in C due to direct radiation is still large (see Table I), it is necessary to use a counter B instead of a simple scatterer, selecting in this way the significant events. For a polarized beam of gamma-rays coming from B, the coincidence counting rate BC depends, as we shall discuss later, on the angle ϕ, the amount of asymmetry being directly related to the degree of polarization.

All the information about the polarization of the quantum going to B (the other quantum going to A) can be expressed in terms of the intensities $J_{\parallel}$ and $J_{\perp}$ of the linear polarizations parallel and perpendicular to the plane defined by the two gamma-rays.[3] The direction of polarization is identified with the direction of the electric vector; $J_{\parallel}$ corresponds to J_{θ}, $J_{\perp}$ to J_{ϕ} in the notation of Hamilton.[4] For a given degree of polarization we expect the largest ratio of coincidence rates (triple coincidences ABC) between the two positions $\phi=0$ and $\phi=\pi/2$, ϕ being the angle between the planes BSA and BSC (Fig. 1).

The intensities $J_{\parallel}$ and $J_{\perp}$ in general depend on the coefficients $a_2, a_4 \cdots$ of the angular correlation which are

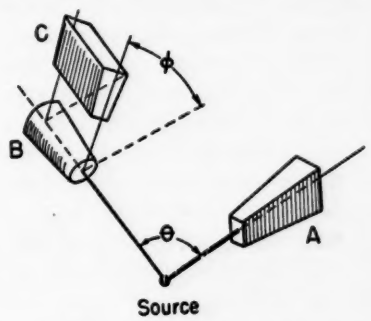

FIG. 1. Schematic diagram of experimental arrangement of polarimeter.

* This work was supported in part by the joint program of the ONR and the AEC and by grants to one of us (F.M.) from the Swiss "Arbeitsgemeinschaft für Stipendien der Physik und Mathematik." Preliminary results were reported in Phys. Rev. 74, 1542 (1948) and Phys. Rev. 76, 187 (1949).

[1] D. R. Hamilton, Phys. Rev. 58, 122 (1940).
[2] E. L. Brady and M. Deutsch, Phys. Rev. 74, 1541 (1948).
[3] D. L. Falkoff, Phys. Rev. 73, 518 (1948).
[4] D. R. Hamilton, Phys. Rev. 74, 782 (1948).
[5] Snyder, Pasternack, and Hornbostel, Phys. Rev. 73, 440 (1948), E. Bleuler and H. L. Bradt, Phys. Rev. 73, 1398 (1948) and R. C. Hanna, Nature 162, 332 (1948).

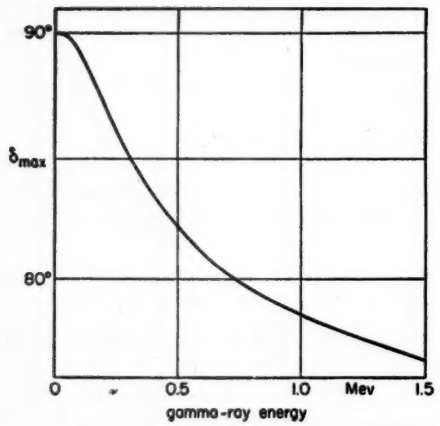

FIG. 2. Angle of maximum asymmetry, δ_{max}, for ideal geometry, as a function of the gamma-ray energy of the primary photons.

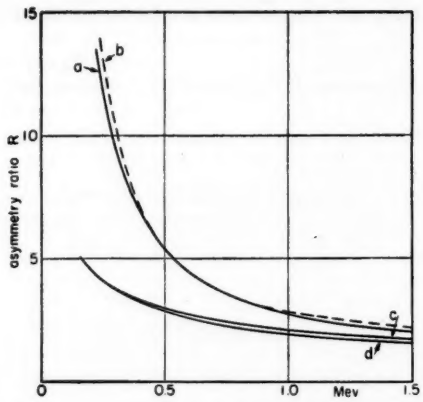

FIG. 3. Compton scattering of polarized gamma-rays. Asymmetry ratio R as a function of gamma-energy for different geometries: (a) $\delta=80°$, ideal geometry; (b) $\delta=\delta_{max}$, ideal geometry; (c) $\delta=80°$, $\Delta\delta=55°$, $\Delta\phi=60°$; (d) like (c) but corrected for scattering from C to B.

defined by the equation

$$W(\theta)=1+a_2\cos^2\theta+a_4\cos^4\theta\cdots,$$

where $W(\theta)$ is the relative probability of the second quantum being emitted at an angle θ with respect to the first one.

If both detectors (A, $B+C$) have the same dependence of gamma-ray efficiency on energy, then in exactly half of the 16 possible combinations of dipole and quadrupole transitions $J_{\parallel}$ is equal to $J_{\perp}$, independently of a_2 and a_4, i.e., there exists no polarization correlation. In the other half, $J_{\parallel}/J_{\perp}$ has the form

$$J_{\parallel}/J_{\perp}=[1+a_2+a_4-\tfrac{1}{2}a_4\sin^2 2\theta]/[1+(a_2+a_4)\cos 2\theta], \quad (1)$$

or its reciprocal, depending on the type of the two transitions.

A closer inspection shows that for all the cascades for which $J_{\parallel}$ is equal to $J_{\perp}$ an over-all parity change is brought about by the two transitions, while the cascades with $J_{\parallel}\neq J_{\perp}$ are characterized by no over-all change in parity. The mere statement of the existence or non-existence of a polarization correlation therefore unambiguously describes the cascade with respect to the over-all parity change provided that not all the coefficients a_n of the angular correlation vanish.

As soon as the existence of a polarization correlation is established for a given cascade, the sign of the difference $J_{\parallel}-J_{\perp}$ is also determined. If we then know the multipole order from the coefficients of the angular correlation, the sign of $J_{\parallel}-J_{\perp}$ enables us to characterize the two transitions in more detail. In the case of two quadrupole transitions, for instance, the sign of $J_{\parallel}-J_{\perp}$ tells us whether the two transitions are both magnetic or both electric quadrupoles.

The sign of $J_{\parallel}-J_{\perp}$ and the coefficients a_2, $a_4\cdots$ of the angular correlation rigorously determine the detailed shape of the polarization correlation. A careful investigation of the angular dependence of the polarization and the absolute value of $J_{\parallel}/J_{\perp}$ may therefore be used to confirm the results of the angular correlation experiments, but does not yield any information which could not be derived from the sign of $J_{\parallel}-J_{\perp}$, if a_2, a_4 are precisely known.

2. THE POLARIMETER

A. Compton Scattering as Analyzing Process

The differential cross section $d\sigma$ for the scattering of a photon of energy k_0 through an angle δ is given by the Klein-Nishina formula[6] which, averaged over all polarizations of the scattered quantum, can be expressed as

$$d\sigma=\frac{r_0^2}{2}d\Omega\frac{k^2}{k_0}\left[\frac{k}{k_0}+\frac{k_0}{k}-2\sin^2\delta\cos^2\phi\right],$$

where $k=k_0[1+k_0/mc^2(1-\cos\delta)]$ is the energy of the photon after scattering. ϕ is the angle between the direction of polarization of the incident photon and the plane of scattering, $r_0=e^2/mc^2$ is the classical radius of the electron and $d\Omega$ the element of solid angle.

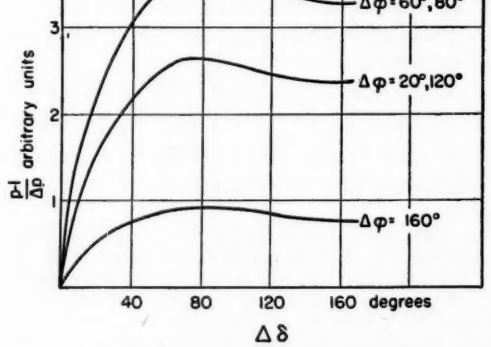

FIG. 4. Figure of merit of the polarimeter, for finite geometry, as a function of the spread in the angle δ for various spreads of ϕ.

[6] O. Klein and Y. Nishina, Zeits. f. Physik 52, 853 (1929).

For a fixed value of δ the differential cross section assumes its extreme values for $\phi=0$ and $\phi=90°$. The ratio of the counting rates which we obtain in the two extreme angular positions for a linearly polarized gamma-ray beam is a measure of the sensitivity of the analyzer. This ratio we shall call asymmetry ratio R and define it such that it is always larger than unity. For the ideal geometry dealt with in this section, R is simply the ratio of two differential cross sections, i.e., $R=(d\sigma)_{\phi=\pi/2}/(d\sigma)_{\phi=0}$.

Owing to the δ-dependence of k, the asymmetry ratio R, which is unity for $\delta=0$ and $\delta=\pi$, reaches its maximum value at an angle δ somewhat smaller than $\pi/2$. In Fig. 2 the dependence of this angle δ_{max} for maximum asymmetry is given as a function of the energy of the primary photons.

For our analyzer we chose a mean angle δ of 80°. The energy dependence of the asymmetry ratio R for this angle is illustrated in Fig. 3. In this figure the dotted line, which almost coincides with the curve for $\delta=80°$, represents the upper limit for the sensitivity of any analyzer which uses Compton scattering as the analyzing process; it was calculated taking for each energy the corresponding value of δ_{max} (Fig. 2).

In the actual design of an analyzer one has to allow rather large spreads of both δ and ϕ in order to obtain practical counting rates. If p denotes the ratio $J_{\parallel}/J_{\perp}$ of the components polarized perpendicular to each other and Δp the standard deviation of p, then $p-1/\Delta p$ may be used as a criterion for the usefulness of a polarization sensitive arrangement.

Using the Klein-Nishina formula we calculated the value of this ratio $p-1/\Delta p$ for a point scatterer and a variety of values $\Delta\delta$ and $\Delta\phi$. The results of these calculations are represented in Figs. 4 and 5. The characteristic quantity $(p-1)/\Delta p$ is plotted as a function of the spreads of δ and ϕ. Both figures refer to a gamma-ray energy of 1 Mev and a value $p=1.2$. Within the energy range which is of main interest in the present study (0.3–1.5 Mev), the shapes of the curves do not change appreciably. The optimum spreads in both δ and ϕ lie between 50 and 80°.

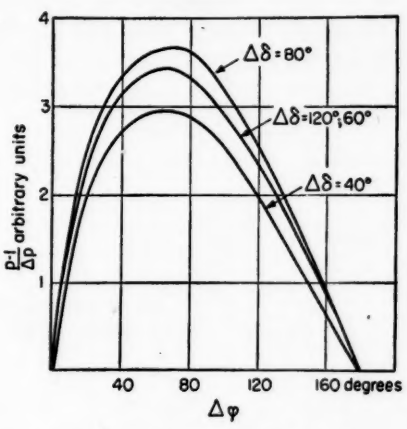

FIG. 5. Figure of merit of the polarimeter, for finite geometry, as a function of the spread in the angle ϕ for various spreads in δ.

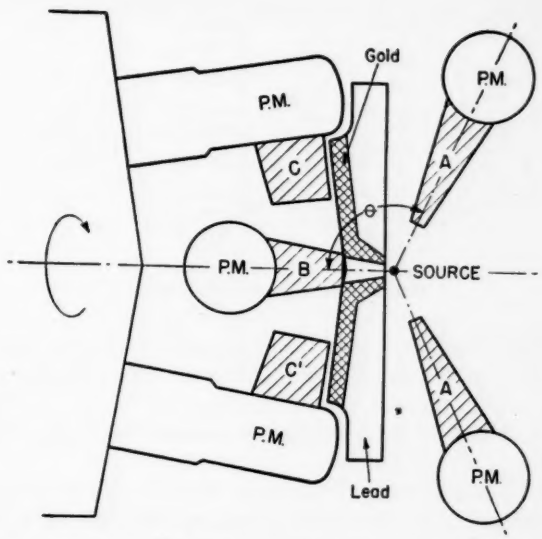

FIG. 6. Cross section through the polarimeter in the position $\phi=0$. P.M.: Photo-multiplier tube 931-A.

The spans of δ and ϕ realized in the actual analyzer are $\Delta\delta=55°$ and $\Delta\phi=60°$. Experimental evidence for these values will be presented later. The asymmetry ratio R for this finite geometry may be compared in Fig. 3 with the ratio for the ideal arrangement.

The ratio $N_{\parallel}/N_{\perp}$ of the triple coincidence rates in the two extreme positions ($\phi=0$, $\phi=\pi/2$) of the analyzer, the asymmetry ratio R, and the ratio of the polarization intensities $p=J_{\parallel}/J_{\perp}$ are connected through the relation

$$N_{\parallel}/N_{\perp}=(p+R)/(pR+1). \qquad (2)$$

For $p=0$ and $p=\infty$, i.e., for linearly polarized gamma-rays, $N_{\parallel}/N_{\perp}$ takes on the values R and $1/R$ as is to be expected from the definitions of p and R. We might point out that owing to the preference of scattering at right angles with respect to the plane of polarization the ratio $N_{\parallel}/N_{\perp}$ is smaller than unity when $p=J_{\parallel}/J_{\perp}$ is larger than unity, and vice versa.

B. Design of the Polarimeter

The arrangement of the counters and shields in our polarimeter is illustrated in Fig. 6, which represents a cross section through the polarimeter, the plane of the two gamma-rays coinciding with the plane of the paper. The rotating element (with counters C and C') is shown in the position corresponding to $\phi=0$ (see Fig. 1).

TABLE I. Data on scandium[46] taken at $\theta=120°$; numbers represent counts per second. Total number of counts: 10^6 in each single channel, 2.10^4 in each double coincidence channel.

Pos.	n_A	n_B	n_C	n_{AB}	n_{AC}	n_{BC}	$n_{ABC}\cdot10^2$ Total	Chance	True
∥	6420	3552	735	13.4	4.08	19.0	8.95±0.11	2.79	6.16±0.11
⊥	6490	3550	732	13.3	4.05	19.2	9.39±0.11	2.82	2.82±0.11

This measurement: $(N_{\parallel}/N_{\perp})_{120}=0.938\pm0.024$
Final value: $(N_{\parallel}/N_{\perp})_{120}=0.934\pm0.014$

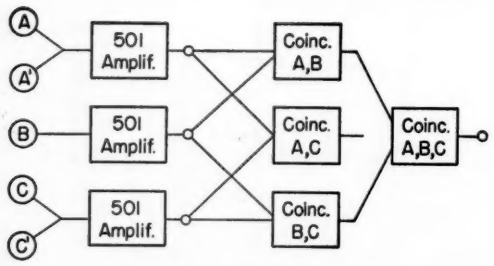

FIG. 7. Schematic circuit diagram.

The counters A' and C', displaced with respect to A and C by 180° in azimuth, add to the original polarimeter ABC the equivalent combinations ABC', $A'BC$, and $A'BC'$, thus increasing the coincidence counting rates by a factor of four.

The addition of C' not only increases the counting rate, but at the same time improves the symmetry of the apparatus, since any small asymmetry due to misalignment of the axis of the rotating part is canceled to a first approximation.

Naphthalene was used as fluorescent substance for all five gamma-ray detectors. At the time of the construction of the polarimeter this substance had the advantages of being readily available and of having good mechanical properties. Today it might be preferable to replace naphthalene by anthracene or one of the other substances which in the meantime have been found to have good counting properties. Most of the inorganic phosphors, however, are excluded in view of their rather long "decay-times."

The photo-multiplier tubes are selected 931-A, 1P21, and 1P28 RCA tubes. The whole polarimeter is cooled to dry ice temperature. Owing to the fact that the quanta scattered into C and C' have rather low energies, the improvement obtained by the cooling is quite remarkable, especially with naphthalene as the counter substance.

The shield is rotationally symmetrical with respect to the main axis of the apparatus, which coincides with the axis of the conical crystal B. The shield mainly serves the following two purposes: (a) It attenuates the direct radiation which would go to the counters C and C', and (b) it prevents scattering from A to C.

Poor shielding of the counters C and C' against the direct radiation from the source would give rise to a large number of triple coincidences due to quanta scattered from C to B through almost 180°. As scattering of polarized photons through zero or 180° shows no azimuthal asymmetry, the additional coincidences would reduce the sensitivity of the analyzer appreciably. Moreover, due to the angular correlation of the gamma-rays, the number of these undesirable coincidences would depend on the position ($\phi=0$, $\phi=\pi/2$) of the counters C, C' and would therefore change the ratio $N_{\parallel}/N_{\perp}$ and consequently suggest a different polarization correlation.

A similar falsification of the data arises from insufficient shielding of C against the radiation scattered from A. The consequences of this effect can be much more detrimental than those of the effect mentioned. In this case, not only the solid angle subtended by C at A changes, when C goes from $\phi=0$ to $\phi=\pi/2$, but also the energy of the radiation and the amount of absorber change radically. One expects in this case more additional coincidences in the position $\phi=0$ than in the position $\phi=\pi/2$; i.e., a trend of $N_{\parallel}/N_{\perp}$ toward larger values than those corresponding to the polarization correlation of the substance being investigated. The effect is largest for $\theta=90°$, in which case A is nearest to C and the energy of the quanta scattered into C is highest. The rises at $\theta=\pi/2$ in the measured correlations of Sc^{46} and Co^{60} (Figs. 9 and 10) are probably due to residual effects of the two types just described.

The existence of strong asymmetries due to these effects made it necessary to replace part of the lead in the shield by gold. (See Fig. 6.) The reduction in sensitivity (i.e. in R) due to the additional coincidences C, B is still about 12 percent for the hardest gamma-rays (Co^{60}), the asymmetry in the triple coincidences is of the order of one percent.

C. Counting Devices

A schematic diagram of the arrangement of the circuits is shown in Fig. 7. The tubes of A and A' and of C and C' are connected in parallel; their pulses are fed into Los Almos Model 501 amplifiers (0.1-μsec. rise time). The outputs of these amplifiers are taken by pairs into separate coincidence circuits. The pulses of two of these coincidence channels are then mixed again in a fourth coincidence arrangement. In this way one is able to count all the double coincidences separately, a possibility which is essential for monitoring the performance of the polarimeter. The difference in the number of double coincidences A, C for the two positions $\phi=0$ and $\phi=90°$ gives, for instance, information concerning the amount of undesired scattering from A to C.

The resolving time of the final coincidence channel is not important as the question of the existence or nonexistence of a triple coincidence is decided in the previous coincidence stages. One can therefore use rather broad and large output pulses of the three double coincidence channels, a fact that contributes to the reliability of the whole device.

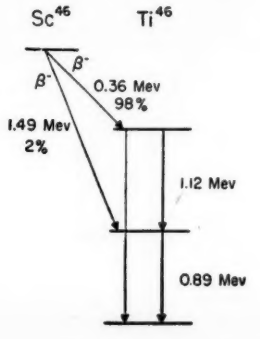

FIG. 8. Disintegration scheme of Sc^{46}.

All the double coincidence channels have the same resolving time of 0.1 μsec. as well as can be measured. Denoting this common resolving time by τ, the triple coincidence chance rate for a simple cascade is given by

$$n_{ABC}^{\text{chance}}=2\tau(n_{AB}n_C+n_{AC}n_B+n_{BC}n_A-4\tau n_An_Bn_C),$$

where n_{AB}, n_{AC}, n_{BC} are the numbers of double coincidences between the corresponding counters and where n_A, n_B, n_C are the single counting rates.

In the case of positron emitters the existence of two annihilation quanta per cascade adds five possible combinations of two gamma-rays to the pair representing the cascade. Consequently the cascade gamma-rays will contribute only a small fraction of the total coincidence rate and any asymmetry in this contribution will be very hard to detect. As the shielding of counter C is not perfect we might expect true triple coincidences not due to scattering in B which cause an additional reduction of the actual sensitivity. With the present apparatus we therefore can hope to detect a polarization correlation in a positron emitter only if this correlation is very large.

Table I contains typical counting rates and demonstrates the degree of symmetry obtained as well as the large contribution of the direct radiation to the counting rate in C.

In order to obtain a sufficient number of coincidences, the apparatus was arranged to take the data automatically, the position of the analyzer changing every half hour. Sources giving about 8.10^5 disintegrations per second were used.

3. THE SENSITIVITY OF THE ANALYZER

Owing to the rather complicated geometry of the polarimeter it is difficult to make a reliable estimate of the effective spreads $\Delta\delta$ and $\Delta\phi$, which determine the sensitivity of the analyzer. The values $\Delta\delta=55°$ and $\Delta\phi=60°$, on which we based our calibration, were derived from the following experiment.

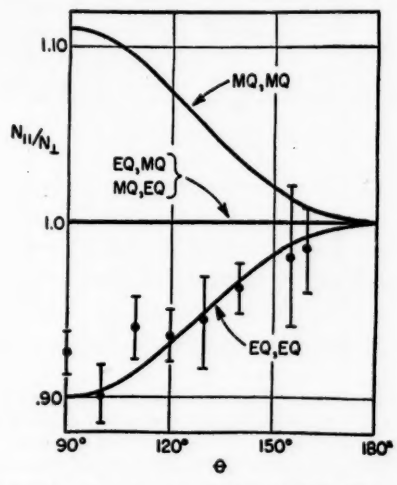

FIG. 9. Polarization-direction correlation for Sc^{46}. The three curves correspond to the different parity assignments.

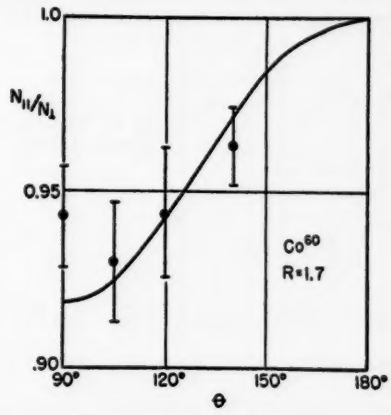

FIG. 10. Polarization-direction correlation of Co^{60}.

A collimated beam of gamma-rays from a strong ($\frac{3}{4}$ curie) Co^{60} source is scattered through an angle of 90°, becoming partially polarized in a manner predictable from the Klein-Nishina formula. For this beam of known polarization the ratio $N_{II}/N_\perp$ is measured in our analyzer. In this way the asymmetry ratio R is determined for the energy of the scattered quanta (360 kev for Co^{60}).

If the two gamma-rays of Co^{60} (1.117 and 1.332 Mev)[7] are detected with equal over-all efficiency, the average polarization $p=J_{II}/J_\perp$ is 2.2 for scattering through 90°. The measured ratio $N_\perp/N_{II}=1.61\pm0.06$ of the counting rates in the two extreme positions then leads to an asymmetry ratio R_{exp} of 4.3 ± 0.7 for a gamma-ray energy of 360 kev. The spreads in δ and ϕ for our apparatus are approximately equal and their value R_{exp} is compatible with $\Delta\delta=\Delta\phi=45\pm15°$.

When the analyzer is used in the polarimeter, the finite size of crystal A increases the spreads of both δ and ϕ, the change in δ being 10°, with the one in ϕ being 15°. Thus we arrive at effective spreads $\Delta\delta=55\pm15$ and $\Delta\phi=60\pm15°$. The asymmetry ratio $R(60/55)$ for these spreads is plotted in Fig. 3 as a function of the gamma-ray energy. This asymmetry ratio is, however, still not the actual one. In order to arrive at the true value of the asymmetry ratio for our polarimeter, we have to correct $R(60/55)$ for the reduction in sensitivity due to the scattering from C to B which we mentioned earlier in connection with the shielding problem.

For the "regular" scattering from B to C the asymmetry ratio R_{BC} is equal to $R(60/55)$. For the undesirable scattering from C to B, however, R_{CB} is practically unity. The actual value of R is then the weighted average of these two asymmetry ratios R_{BC} and R_{CB}. The geometry of the analyzer suggests as appropriate weights the single counting rates n_B and n_C in the counters B and C. The actual asymmetry ratio is therefore given by

$$R_{\text{actual}}=(n_B\cdot R_{BC}+n_C\cdot R_{CB})/(n_B+n_C)$$

[7] Lind, Brown, and DuMond, Phys. Rev. **76**, 591 (1949).

FIG. 11. Disintegration scheme of Rh^{106}.

or, if we use the values 1 and $R(60/55)$ for R_{CB} and R_{BC}

$$R_{\text{actual}}=[n_B\cdot R(60/55)+n_C]/(n_B+n_C).$$

This actual asymmetry ratio is also plotted in Fig. 3; it was used for the calculation of the expected polarization correlations in all the cases presented in this paper.

4. RESULTS

A. Scandium 46

The disintegration scheme of Sc^{46} is shown in Fig. 8. The angular correlation of the two gamma-rays has been studied by Brady and Deutsch.[2] Their data are consistent with the correlation function

$$W(\theta)=1+(1/8)\cos^2\theta+(1/24)\cos^4\theta,$$

which is expected[1] for two quadrupole transitions between states with spins 4, 2, and 0.

The knowledge of the coefficients $a_2=1/8$ and $a_4=1/24$ enables us to predict the polarization direction correlation for each of the four different types of quadrupole cascades:

$$EQ, EQ \quad p=J_{\parallel}/J_{\perp}=(1.17-0.02\sin^2 2\theta)/(1+0.17\cos 2\theta),$$

$$EQ, MQ \quad p=J_{\parallel}/J_{\perp}=1,$$
$$MQ, EQ$$

$$MQ, MQ \quad p=J_{\parallel}/J_{\perp}=(1+0.17\cos 2\theta)/(1.17-0.02\sin^2 2\theta).$$

The ratios $N_{\parallel}/N_{\perp}$ expected for these four cases are plotted against the angle θ in Fig. 9. An asymmetry ratio $R=1.9$ (see Fig. 3) was used for the conversion of the ratios $J_{\parallel}/J_{\perp}$ into coincidence counting ratios. The experimental points with their standard deviations are indicated on the same graph. The agreement with the correlation expected for two electric quadrupole transitions is as good as can be expected for this kind of experiment. If one does not consider multipoles of orders higher than quadrupole, the assignment 4, 2, 0; *EQ, EQ* is the only one consistent with the correlation experiments.

The lack of calculations for higher multipoles and the possibility of interference for mixed radiation[8] cause ambiguities in the interpretation of the correlation experiments for all the substances studied. As magnetic octupole transitions and electric or magnetic radiation of higher multipole order are extremely improbable from lifetime considerations, the most important transitions of higher multipolarity which have to be considered are electric octupoles.

Many of the cascades involving electric octupoles can be excluded: The existence of a polarization-direction correlation rules out[8a] the combinations with an over-all parity change; i.e., *EO, EQ*; *EQ, EO*; *EO, MD*; *MD, EO*; the sign of the polarization is inconsistent with the sequence *EO, EO*.

The conversion coefficients reported by Peacock and Wilkinson[9] would call for higher multipole orders, in disagreement with the fact that coincidences are observed with resolving times as small as 10^{-7} sec. In view of the difficulty of the measurement of very small conversion coefficients it seems advisable to repeat these experiments.

There is good reason to believe that calculations for the combinations with octupoles will soon be available and that the assignment of spins and parities will then be unambiguous.

Fluharty and Deutsch[10] have searched for the 2.01-Mev cross-over transition in Sc^{46}. They were able to establish the existence of gamma-rays with energies larger than 1.63 Mev and smaller than 2.2 Mev in 1.2×10^{-5} percent of the disintegrations. This abundance is of the order of magnitude which one expects, based on the approximate formulas for the transition probabilities, for the (4, 2, 0; *EQ, EQ*) assignment.

B. Cobalt 60

Both Co^{60} and Sc^{46} disintegrate to even-even nuclei by the emission of a soft beta-ray spectrum followed by

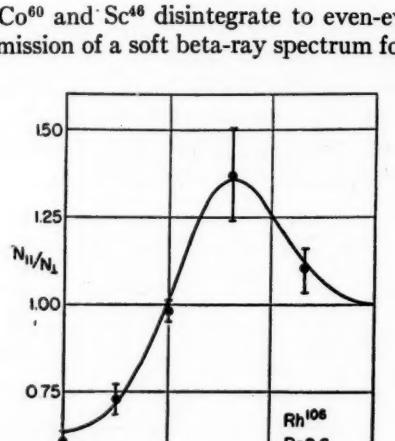

FIG. 12. Polarization-direction correlation of Rh^{106}.

[8] D. S. Ling and D. L. Falkoff, Phys. Rev. **74**, 1224 (1948).

[8a] We assume here, that the general relations between the character of the transitions and the polarization-direction correlation (existence, sign), which are correct for dipole and quadrupole radiation, are also valid for combinations with higher multipoles.

[9] C. L. Peacock and R. G. Wilkinson, Phys. Rev. **74**, 297 (1948).

[10] R. G. Fluharty and M. Deutsch, Phys. Rev. **76**, 182 (1949).

a cascade of two gamma-rays with energies of about 1 Mev.

Within the experimental uncertainty the angular correlations[2] of the gamma-rays from Sc^{46} and Co^{60} are identical. The same is true for the polarization-direction correlations of these two substances (Figs. 9 and 10). It is therefore very likely that the levels of Ni^{60}, involved in the disintegration of Co^{60}, have the same properties as those of Ti^{46} connected with the decay of Sc^{46}, i.e., that the three levels have the same parity and spins 4, 2, and 0.

The discussion of the cascades including electric octupoles follows the one of Sc^{46}. Deutsch and Siegbahn[11] measured the coefficients of internal conversion. Their results indicate that there is no over-all change in parity in the cascade and that both gamma-rays are probably quadrupoles.

Fluharty and Deutsch[10] limited the intensity of the cross-over gamma-ray of 2.45 Mev, if present, to less than 2.5×10^{-5} percent of the Co^{60} disintegrations. The cross-over transition in Sc^{46}, though present, has an abundance smaller than the limit of detection quoted for Co^{60}. It is still possible, therefore, that the two cross-over transitions have about the same abundance as one would expect from the similarity of the disintegration schemes.

C. Rhodium 106

The disintegration scheme[12] of the 30-sec. daughter of Ru^{106} (Fig. 11) has not been definitely established, the identification of the 1.25-Mev gamma-ray as the cross-over transition being justified only by an agreement of energy values which might be fortuitous.

Due to the low abundance of the 1.25-Mev gamma-ray the main contribution to both angular and polarization-direction correlation has to be attributed to the two gamma-rays of 0.51 and 0.73 Mev even if the decay scheme should be modified with respect to the high energy gamma-ray.

Rh^{106} exhibits a very strong angular correlation[2] which can be represented quite well by a probability function of the form

$$W(\theta)=1-1.5\cos^2\theta+2.0\cos^4\theta.$$

The occurrence of a $\cos^4\theta$ term excludes dipole transitions. None of the correlations expected for two quadrupole transitions fits the experimental distribution. The theoretical coefficients for a spin assignment $0-2-0$ are just twice as large as the experimental ones. As long as we have no explanation[12a] for this fact we may as well assume that the inclusion of higher multipoles will provide a solution.

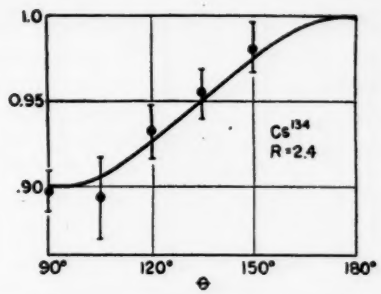

FIG. 13. Polarization-direction correlation of Cs^{134}.

Having found large coefficients $a_2=-1.5$ and $a_4=2$ for the angular correlation, one expects either a very large polarization for Rh^{106} or none. The experimental results as illustrated in Fig. 12 reveal a large polarization with an angular dependence which is represented quite well by

$$p=J_{\parallel}/J_{\perp}=(1.5-\sin^2 2\theta)/(1+0.5\cos 2\theta),$$

i.e., the distribution obtained from the general relation (1) using the experimentally determined angular correlation coefficients.

D. Cesium 134

As the disintegration scheme[13] of Cs^{134} comprises several gamma-rays coinciding with each other, one cannot hope to arrive at a clear decision concerning the properties of the nuclear levels from correlation experiments alone. However, any future analysis must be able to account for the experimentally established correlations and it is for this reason that we present our data on Cs^{134} in Fig. 13. The asymmetry ratio R for the average gamma-ray energy of Cs^{134} is 2.4. The experimental value of $N_{\parallel}/N_{\perp}$ at $\theta=90°$ therefore corresponds to a polarization $p=1.3$, which in turn leads to[14] a ratio $W(\pi)/W(\pi/2)=1.13$ for the angular correlation. This value is in good agreement with that measured by Brady and Deutsch.[2] The solid line in Fig. 13 was calculated under the somewhat arbitrary assumption of a distribution of the form $1+0.13\cos^2\theta$ for the angular correlation. More precise measurements of the angular correlation are needed for this isotope. A decision concerning the position of the cross-over transition would reduce considerably the number of possible interpretations.

5. CONCLUSIONS

In combination with reliable measurements of the angular correlation of successive gamma-rays, the investigation of the polarization-direction correlation

[11] M. Deutsch and K. Siegbahn, Phys. Rev. **77**, 680 (1950).
[12] W. C. Peacock, Phys. Rev. **72**, 1049 (1947).
[12a] If one of the transitions proceeds with a mixture of different radiations, the correlations may be changed radically as was shown by D. S. Ling and D. L. Falkoff (reference 8). Still another change in the correlation coefficients might be caused by atomic-nuclear interactions. See G. Goertzel, Phys. Rev. **70**, 897 (1946).
[13] K. Siegbahn and M. Deutsch, Phys. Rev. **71**, 483 (1947); **73**, 410 (1948). L. G. Elliott and R. E. Bell, Phys. Rev. **72**, 979 (1947).
[14] At $\theta=90°$, $p=(1+\Sigma a_i)/(1-\Sigma a_i)$ or its reciprocal, and $W(\pi)/W(\pi/2)=1+\Sigma a_i$.

yields very definite information concerning the parities of the nuclear levels involved. The ambiguities left in the examples discussed in this paper arise from a paucity of theoretical predictions for higher multipole transitions, to the possibility of interference for mixed radiation, and to the preliminary character of the angular correlation data. If these obstacles are eliminated the experiments with the polarimeter have only to decide the existence or non-existence of a polarization in the position (θ) at which we expect the largest effect.[15] For this purpose the polarimeter described in this paper has sufficient sensitivity. For gamma-ray energies above a few hundred kev the correlation method compares favorably with other methods which lead to the assignment of spins to nuclear levels and of parity changes to the transitions between these levels.

[15] p is largest at $\theta=90°$ in most of the cases, but not in all of them.

PHYSICAL REVIEW VOLUME 78, NUMBER 5 JUNE 1, 1950

Angular Correlation of Successive Gamma-Rays*

E. L. BRADY† AND M. DEUTSCH
Laboratory for Nuclear Science and Engineering, Department of Physics and Chemistry Department, Massachusetts Institute of Technology, Cambridge, Massachusetts

(Received February 6, 1950)

The angular correlation of successive gamma-rays emitted by six even-even nuclei has been investigated and found to be anisotropic in every case, and of the magnitude expected theoretically. Effects of external magnetic fields and of chemical binding on the correlations are found to be smaller than the experimental uncertainty for some exploratory experiments. Interpretation of the results in terms of the nuclear states involved is in general possible by use of additional evidence such as relative transition probabilities.

1. INTRODUCTION

CONSIDERABLE progress has been made during the last few years in studies of nuclear radiation spectra from radioactive processes. The experiments have mainly yielded results concerning the energies of excited states. Only little unambiguous systematic evidence on the spins of these states has appeared. Coefficients of internal conversion have revealed the multipole character of nuclear gamma-rays in some cases. Although this method is in principle universally applicable, limitations on the precision of both theoretical and experimental results have so far restricted it to the more favorable cases. No values of nuclear angular momenta are obtained directly by this method, but probable values can frequently be assigned from the multipole orders.

If the life time of a gamma-ray transition is long enough to be measured a probable multipole order can be obtained. This is usually done by means of Bethe's life-time formulas as modified by Segrè. With a few notable exceptions only transitions of rather low energy or high multipole order have been studied so far by this method because of the difficulty in measuring extremely short life-times. There is considerable uncertainty about the exact validity of the life-time formula because it neglects necessarily all details of the nuclear configuration.

It would be most desirable to have a method of the general validity and applicability available to atomic spectroscopy in the Zeeman effect. Unfortunately, it seems at present entirely unfeasible to separate the nuclear magnetic substates by application of external fields sufficiently to observe the transitions between the individual m-values separately. It has been proposed to change the relative populations of the several magnetic substates of an excited state by applying a magnetic field at very low temperatures where the magnetic energy μH is comparable to the thermal agitation energy kT.[1] Information about the multipole nature of the radiation and about the angular momenta of the initial and final states could then be obtained from the space distribution and the polarization of the emitted radiation. This method has not yet been tried. It presents formidable experimental difficulties and is probably limited to long-lived excited states.

Although it is difficult to change the relative populations of the several substates it is frequently possible to make measurements on a sample of nuclei for which these relative populations are different from their equilibrium values. This is in general the case when two successive rays are emitted by one nucleus. If we observe the first ray to be emitted in the z-direction the probability of the intermediate state being in any one of the possible m_z states is no longer the same as in the absence of this information. Thus, by observing the space distribution and polarization of those gamma-rays which

* Supported in part by the joint program of the ONR and the AEC.

† Present address: E. L. Brady, Research Laboratory, General Electric Company, Schenectady, New York.

[1] J. A. Spiers, Nature **161**, 807 (1948).

coincide with the emission of another gamma-ray in the z-direction the results are similar to those obtained if the populations of the states had been changed by an external field. In fact, if nuclear spectroscopy had to deal practically only with dipole radiation as does optical spectroscopy, unique spin assignments could be made in virtually every case from the angular correlation of successive gamma-rays. Because of the occurrence of higher multipoles the situation is somewhat more complicated. Hamilton[2] and Goertzel[3] have calculated explicitly the angular correlation of successive gamma-rays for all possible combinations of pure dipole and quadrupole radiations. A general discussion of the correlations of successive radiations has been given by Yang.[4]

The probability, per unit solid angle, that two successive gamma-rays are emitted at an angle θ is proportional to

$$W(\theta)=1+\sum_{1}^{l} a_i \cos^{2i}\theta$$

where $2l$ is the order of the lowest multipole in the cascade. Thus, if both gamma-rays are quadrupoles $W(\theta)=1+a_1\cos^2\theta+a_2\cos^4\theta$. If one is a dipole $W(\theta)=1+a_1\cos^2\theta$, etc. A further restriction on the number of terms in $W(\theta)$ is $a_i=0$ for $i>J_2$. J_2 is the spin of the intermediate state in the cascade. Thus if J_2 is zero or $\frac{1}{2}$, the angular correlation will always be isotropic; if J_2 is 1 or $\frac{3}{2}$, the correlation will at most contain terms in $\cos^2\theta$. The coefficients a_1 and a_2 have been given by Hamilton[2] for all possible combinations of angular momenta. In Table I we have listed the values of these coefficients from Hamilton's paper for the values of J which are of interest in connection with our experiments. Coefficients for octupole radiation should be very useful, but have not yet been published. If the transition involves mixed multipoles, e.g., electric quadrupole and magnetic dipole components, the situation becomes very complicated and the coefficients depend not only on the relative intensities of the two components but also on their relative phases.[5]

Following the original suggestion of Dunworth[6] that an angular correlation between gamma-rays might exist a number of experiments were performed to find the effect.[7-9] In all cases but one it was reported that any anisotropy in the correlation, if it existed, was smaller than the estimated experimental uncertainty. This was true for Na^{24}, Br^{82}, Y^{88} and Co^{60}. In one case, Cl^{38}, Kikuchi *et al.*[7] reported a smaller probability for emission at 180° than at 90°. They gave the result

$$(W(\pi)-W(\pi/2))/W(\pi/2)=\sum a_i=-0.15\pm0.06.$$

TABLE I. Coefficients for the angular correlation with the spin of the ground state $J_1=0$.

J_2	J_3	Multipoles	a_1	a_2
1	0	Dipole–Dipole	1	0
1	1	Dipole–Dipole	−1/3	0
1	2	Dipole–Dipole	−1/3	0
1	1	Quadrupole–Dipole	−1/3	0
1	2	Quadrupole–Dipole	3/7	0
1	3	Quadrupole–Dipole	−3/29	0
2	3	Dipole–Quadrupole	−3/29	0
2	2	Dipole–Quadrupole	3/7	0
2	1	Dipole–Quadrupole	−1/3	0
2	0	Quadrupole–Quadrupole	−3	4
2	1	Quadrupole–Quadrupole	5	−16/3
2	2	Quadrupole–Quadrupole	−15/13	16/13
2	3	Quadrupole–Quadrupole	0	−1/3
2	4	Quadrupole–Quadrupole	1/8	1/24

However, Beringer[8] reported isotropic correlation for this case, claiming slightly greater precision.

It seemed extremely difficult to reconcile these results with the theoretical predictions. In all cases studied the ground state of the nucleus in question has almost certainly zero spin, containing even numbers of neutrons and protons so that the intermediate state must have at least $J=1$. Except in the case of Br^{82} the gamma-rays are all emitted in simple two-quantum cascades. Theory would predict isotropic correlation in such cases only for accidental combinations of multipoles. The entire theory is, of course, based on the assumption that the orientation of the nucleus is not appreciably disturbed during the lifetime of the intermediate state. In a free atom a disturbance which may interfere with the correlation is provided by the magnetic field of the orbital electrons which has random direction with respect to the chosen axis of quantization. The rate at which this field will cause transitions between the nuclear m states is of the order of the frequency of the Larmor precession which is known from the observed hyperfine structure splittings to be at most about 10^9 sec.$^{-1}$. According to present views the life times of the nuclear states should in general be of the order of 10^{-12} sec. so that this disturbance should be negligible. Furthermore it is well known that in nonparamagnetic solids the atomic moments are largely quenched so that the rate of transition should be of the order of the reciprocal relaxation times observed in nuclear resonance experiments, i.e., 10^{-5} sec. or even much longer. One must, of course, consider the fact that the atom in question may be in an excited state due to recoil and the recent change in atomic number but it is still hard to visualize a process which will reduce the relaxation time much below the precession time in a free atom. If we had to accept the above negative results of search for an angular correlation we should be forced to assume either that the gamma-ray widths are much smaller than is generally assumed or that some unknown mechanism creates extremely strong magnetic fields or electric field gradients at the recoiling nuclei or, even less probable, that some

[2] D. R. Hamilton, Phys. Rev. **58**, 122 (1940).
[3] G. Goertzel, Phys. Rev. **70**, 897 (1946).
[4] C. N. Yang, Phys. Rev. **74**, 764 (1948).
[5] D. S. Ling and D. L. Falkoff, Phys. Rev. **74**, 1224 (1948).
[6] J. V. Dunworth, Rev. Sci. Inst. **11**, 167 (1940).
[7] Kikuchi, Watase, and Itoh, Zeits. f. Physik **119**, 185 (1942).
[8] R. Beringer, Phys. Rev. **63**, 23 (1943).
[9] W. M. Good, Phys. Rev. **70**, 978 (1948).

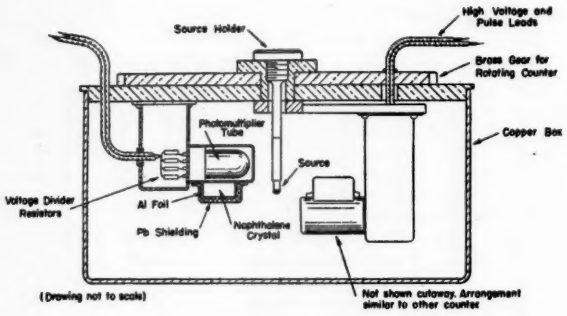

FIG. 1. Apparatus for observing angular correlations.

unknown circumstance favors particular nuclear configurations which will give rise to isotropic emission.

In view of this conclusion it seemed desirable to reexamine the problem with improved experimental techniques. Our results, confirming the basic predictions of the theory have already been briefly reported.[10,11]

2. EXPERIMENTAL PROCEDURE

The principal limitation in previous attempts to observe angular correlation between successive gamma-rays arose from the low intrinsic efficiency of the Geiger-Müller counters used. This efficiency for gamma-rays is about one percent. The experiment consists in observing the coincidence rate between two counters when the angle θ between the lines joining the counters with the source is varied. In order to maintain a useful angular resolution the solid angle subtended by each counter must be limited to about 0.25 steradian. The net efficiency of each counter, including solid angle is therefore about 2×10^{-4}. Since the shortest useful resolving time of a coincidence circuit used with Geiger counters is about 3×10^{-7} sec., the source strength must be kept to about 10^6 disintegrations per second in order to keep the accidental coincidence rate manageable.[6] Thus the genuine coincidence rate was only about 0.1 count per second. While we were able to prove the existence of a correlation of the expected order of magnitude in preliminary experiments[10] further, improved measurements were all made with the use of scintillation counters. Such counters, in the arrangement used by us have an intrinsic efficiency five to ten times as great as does a Geiger counter. Furthermore, they permit the use of shorter coincidence resolving times, 1×10^{-7} sec. in our arrangement. Thus true coincidence rates of the order of 5 counts per second are obtained while keeping the accidental rate substantially smaller than the true rate. In the experiments reported here pure naphthalene blocks and selected 931A photomultipliers were used. It is expected that the recent great strides in scintillation counter techniques will permit further refinement of the experiments. The multipliers were operated at a total voltage of about 600 volts. Los Alamos model 501 amplifiers and preamplifiers were used with a total gain of about 3×10^4. The coincidence circuit consisted of blocking oscillator pulse shapers and a 6AS6 mixer tube. The experimental arrangement is shown in Fig. 1. The dimensions of the naphthalene blocks were approximately $1\times1\times2$ cm. One counter is mounted in a fixed position on the brass cover while the other counter is mounted on a heavy brass gear which can be rotated from the outside. The angular position is read on a revolution counter. The entire assembly was placed in a thermally insulated box filled with dry ice to reduce the dark current of the multiplier tubes.

The angular resolution of the arrangement was determined by observing the coincidence rate due to annihilation quanta from a Na^{22} source as a function of angle. Since these quanta are known to be practically exactly collinear[12,13] the curve shown in Fig. 2 represents directly the angular resolution of the apparatus. The small residual coincidence rate at large angles is due to the nuclear gamma-ray accompanying the decay of Na^{22}. Correction for the finite angular resolution was made in all cases but only in one case did the correction exceed the experimental uncertainty of the data. In this one case (Rh^{106}) the validity of the correction was verified by repeating the experiment with better angular resolution. Sources were mounted in small cups of brass, aluminum or plastic, covered with wax and inserted in the source holder shown in Fig. 1. It is important that the size and self-absorption of the source be very small. Otherwise the counts recorded by the two counters will, on the average, come from different parts of the source when the counters are 180° apart, but from the same part of the source when the counters are close together. Thus the coincidence rate at large angles would appear smaller than at small angles, even though the individual counting rates would be unaffected.

The other main danger of systematic error arises from the possibility that a single primary quantum may

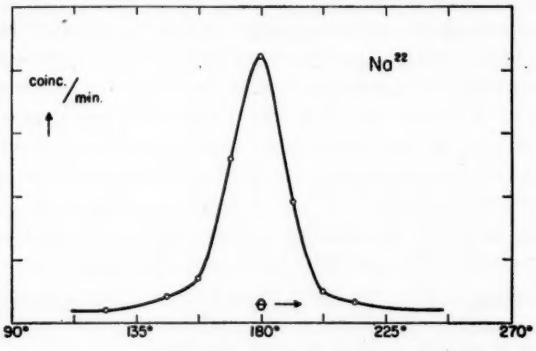

FIG. 2. Angular correlation of coincidences due to annihilation quanta from Na^{22}.

[10] E. L. Brady and M. Deutsch, Phys. Rev. **72**, 870 (1947).
[11] E. L. Brady and M. Deutsch, Phys. Rev. **74**, 1541 (1948).
[12] R. Beringer and C. G. Montgomery, Phys. Rev. **61**, 222 (1942).
[13] deBenedetti, Cowan, and Konneker, Phys. Rev. **76**, 440 (1949).

cause a coincidence by Compton scattering from one counter to the other. This effect will generally be greatest when the two counters are close together. It was minimized by covering the sides of the naphthalene blocks with tapered lead shields about $\frac{1}{8}$ in. to $\frac{1}{4}$ in. thick. In angular positions near 180° the backscattered quanta can enter through the front opening of this lead shield. The energy of the scattered quanta at this angle will always be less than 0.25 Mev and definite improvement was obtained by covering the front of the crystals with $\frac{1}{32}$ in. to $\frac{1}{16}$ in. lead foil. The primary radiation is not appreciably attenuated by this but the soft scattered quanta which have to traverse *both* shields are greatly reduced. The small residual effect of scattering of primary photons, remaining after these precautions, can be determined and corrected for by observing the coincidence rate due to a source emitting only single gamma-rays. Fe^{59} and Mn^{54} were used for this purpose and the very small correction found was applied to all data. This correction should be practically exact for gamma-rays near 1 Mev, i.e., for Co^{60} and Sc^{46} but may be slightly in error for some of the other substances. This error is almost certainly less than the indicated experimental uncertainty due to other causes. It should be emphasized that unless proper precautions are taken scattering effects may completely mask the true angular correlation. The magnitude of the effect depends on the energy of the primary radiation and the type of detector used.

A slight asymmetry in the source position will affect the observed correlation. However, the effect on the coincidence rate will, in first order, be the same as on the individual counting rates. The observed number of coincidences was therefore always divided by the product of the individual counts. This procedure also corrects in first order for changes in counter efficiency and effects of scattering by the apparatus and surrounding material. The latter phenomenon may reduce the effective angular resolution at small angles compared with that shown in Fig. 2. It is very unlikely that the disturbance due to this can be comparable to our estimated experimental uncertainty.

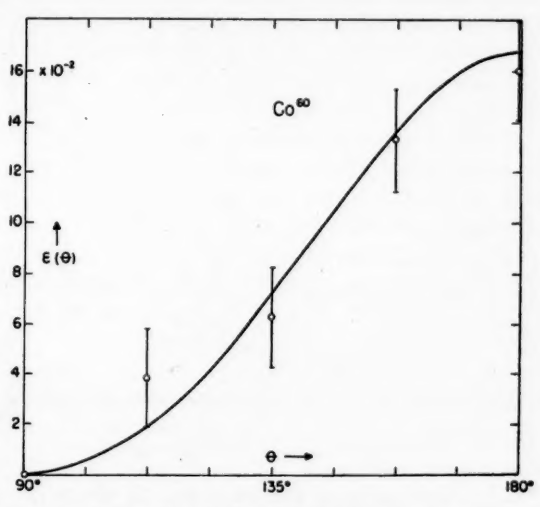

FIG. 3. Correlation of Co^{60} gamma-rays.

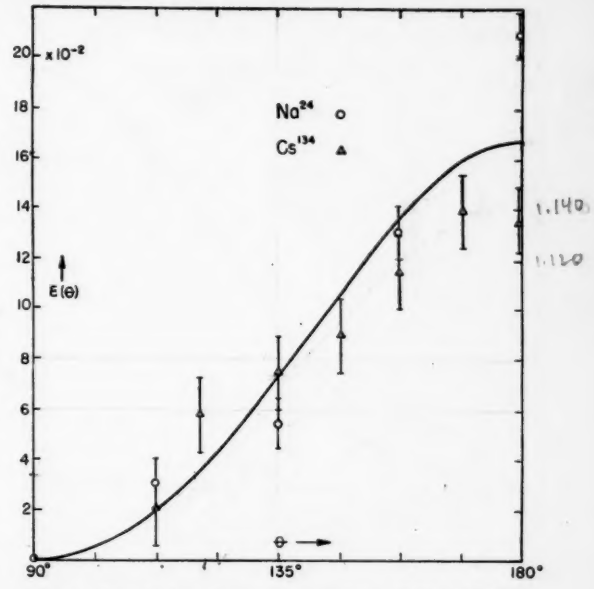

FIG. 4. Correlation of gamma-rays from Cs^{134} and Na^{24}.

3. RESULTS

Figures 3 to 6 show the results obtained with a number of substances. The ordinate represents

$$\epsilon(\theta)=[n(\theta)-n(\tfrac{1}{2}\pi)]/n(\tfrac{1}{2}\pi)=W(\theta)-1.$$

The solid lines in Fig. 3 and 4, and the upper line in Fig. 5 represent the equation

$$\epsilon(\theta)=0.125\cos^2\theta+0.042\cos^4\theta$$

characteristic of two successive quadrupole transitions with angular momenta $J_1=0$, $J_2=2$, $J_3=4$ for the three states in order of increasing excitation energy. The line in Fig. 6 has the equation $\epsilon(\theta)=-1.5\cos^2\theta+2\cos^4\theta$. Its significance and that of the lines in Fig. 4 will be discussed below.

Co^{60}

The decay of this nuclide was shown by Deutsch, Elliott, and Roberts[14] to lead to an excited state of Ni^{60} which decays by the successive emission of two quanta whose energies have been measured by Lind, Brown, and duMond[15] to be 1.172±0.001 Mev and 1.332±0.001 Mev, respectively. Ni^{60} being an even-even nucleus its ground state probably has spin zero.

Deutsch *et al.*[14] showed that the beta-decay of the 10.7′ isomer of Co^{60} probably leads to the intermediate excited state of Ni^{60} and W. C. Peacock (private communication) confirmed this, showing that the energy of

[14] Deutsch, Elliott, and Roberts, Phys. Rev. **68**, 193 (1945).
[15] Lind, Brown, and duMond, Phys. Rev. **76**, 591 (1949).

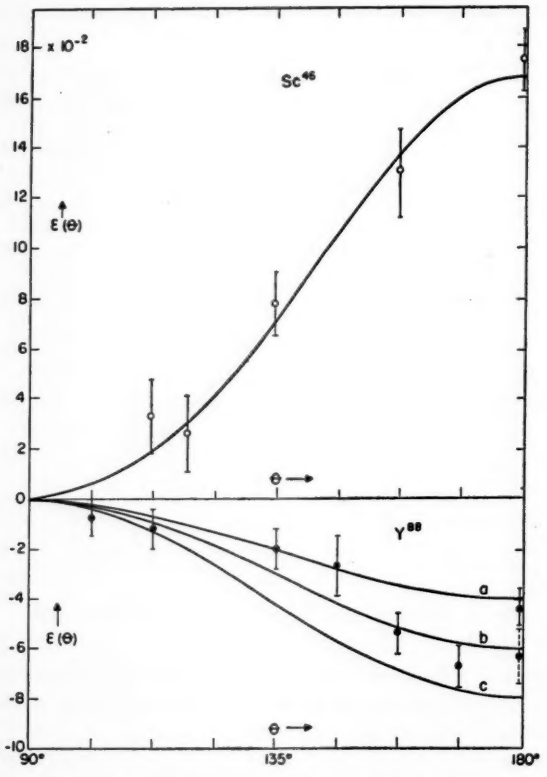

FIG. 5. Correlation of gamma-rays from Sc^{46} and Y^{88}. The point marked by the broken line has been corrected for an estimated effect of positrons.

this level corresponds to the 1.332-Mev gamma-ray. The electromagnetic transition from the 10.7′ state to the 5 yr. state of Co^{60} probably involves no parity change and an angular momentum change of 3 or 4. Our experimental points in Fig. 3 follow the solid line within the experimental error and it appears very probable that the angular momenta of the excited states are 2 and 4, respectively. Metzger and Deutsch[16] have observed a polarization-direction correlation for Co^{60} which indicates that if the above spin assignment is correct the parities of all three states of Ni^{60} are the same, i.e., both transitions electric quadrupole. Siegbahn and Deutsch[17] have measured the internal conversion of the two gamma-rays and their results also indicate that the multipole nature of the two transitions is the same. The observations of Fluharty[18] indicating that the direct transition from the 2.5-Mev level to the ground state of Ni^{60} occurs in less than 2.5×10^{-7} of the disintegrations favor the assignment of different parities to the 2.5-Mev state and the ground state. However, this conclusion is based on the very rough lifetime formula of Bethe and Segrè. The matrix element for the "cross-over" transition may easily be a hundred times smaller than calculated from this formula. A spin and parity assignment consistent with all our present information is shown in Fig. 7.

[16] F. Metzger and M. Deutsch, Phys. Rev. **78**, 551 (1950).
[17] M. Deutsch and K. Siegbahn, Phys. Rev. **77**, 680 (1950).
[18] R. G. Fluharty and M. Deutsch, Phys. Rev. **76**, 182 (1949).

Cs^{134}

A sample of this nuclide was obtained from the Isotopes Division. Its decay scheme is somewhat more complex[19] than those of the other activities reported here but the main mode of decay is very similar to that of Co^{60}, the energies of the two gamma-rays being 0.79 Mev and 0.60 Mev, respectively. The results shown in Fig. 6 are not too dissimilar to those for Co^{60} and Sc^{46}. Because of the complexity of the decay scheme it is difficult to draw definite conclusions. One might assume that the main cascade involves the same spins as in the case of Co^{60}. In this case the polarization measurements of Metzger[16] indicate that the parities are also the same. Such a spin and parity assignment would imply that the 1.35 Mev gamma-ray reported by Siegbahn and Deutsch[20] should accompany only the 0.09-Mev beta-ray spectrum reported by Elliott and Bell.[19] This is consistent with the fact that Fluharty[18] found indication of a transition from the 1.96 Mev level directly to the ground state with an abundance just under one per million disintegrations. While these interpretations are still somewhat speculative, it can be stated with certainty that the main gamma-ray cascade cannot involve spins giving rise to very great anisotropy, e.g., 0, 2, 0. Our failure to observe the correlation in the preliminary experiments with Geiger counters[10] is inexplicable.

Na^{24}

The decay of this nuclide is well known to involve the successive emission of two gamma-rays of 1.38 Mev and 2.76 Mev. It was prepared in the cyclotron by deuteron bombardment of sodium. As seen in Fig. 4 the angular correlation is again rather similar to that obtained with Co^{60} and Sc^{46}, indicating that the spins of the states involved may also be 0, 2, 4. No indirect support for this assignment is available, though, as in

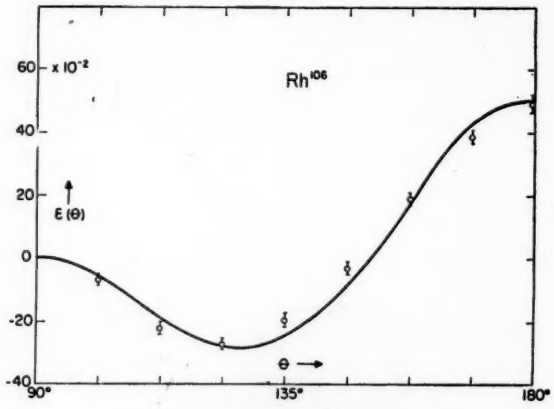

FIG. 6. Correlation of Rh^{106} gamma-rays.

[19] L. G. Elliott and R. G. Bell, Phys. Rev. **72**, 979 (1947).
[20] K. Siegbahn and M. Deutsch, Phys. Rev. **71**, 483 (1947).

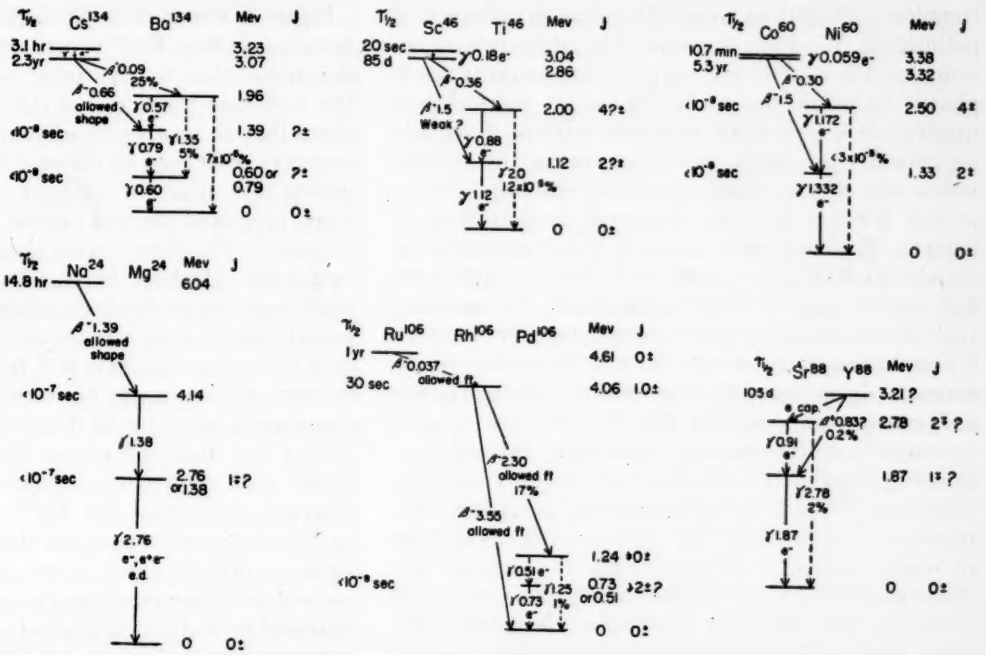

FIG. 7. Summary of information concerning the decay schemes discussed. States of opposite parity are indicated by ± and ∓, respectively.

the case of Co^{60} and Sc^{46}. The point at 180° in Fig. 4 is definitely higher than would be expected from this assignment. This may be caused by internal pair conversion of the 2.76-Mev gamma-ray. The annihilation radiation due to the resulting positrons may cause the observed effect. By changing the thickness and material of the source cup it was shown that the increased counting rate at 180° was not due to pairs created by the gamma-rays in the cup. This point should be investigated further since this type of measurement may be used as a sensitive determination of internal pair creation.

Sc^{46}

This nuclide was obtained from the Isotopes Division of the Atomic Energy Commission. Its decay scheme has been shown[21–23] to be very similar to that of Co^{60}, the gamma-ray energies being 1.2 Mev and 0.88 Mev. The results, shown in Fig. 5 are again consistent with spin assignments 0, 2, 4 to the three states of Ti^{46}. Metzger[16] demonstrated from the polarization correlation that the parities of all three states must be the same as in the case of Co^{60}. Fluharty[18] found evidence of a "cross-over" gamma-ray, corresponding to a direct transition from the 2.0 Mev level to the ground state in about 1.2×10^{-7} of the transitions. This is consistent with the proposed spin and parity assignments. Figure 7 summarizes our present knowledge of this nuclide.

Y^{88}

This nuclide was obtained by deuteron bombardment of strontium metaborate in the M.I.T. cyclotron. The target was allowed to cool for three weeks. After removing strontium by precipitation in conc. HNO_3 and copper by precipitation with H_2S, yttrium was precipitated with HF, dissolved in $HClO_4$ and finally reprecipitated with NH_4OH.

The orbital electron capture decay of Y^{88} has been shown[24] to lead to the successive emission of two gamma-rays of 0.91 Mev and 1.86 Mev energy.[25] Gamertsfelder[26] has also shown that in about 2 percent of the disintegrations a single "cross-over" gamma-ray of 2.8 Mev is emitted instead of the two quantum cascade. This relatively high abundance of the "cross-over" transition makes it obvious that the spins must be different from those in Co^{60} and Sc^{46}, where there is only very little direct one-quantum de-excitation. Indeed the points shown in Fig. 5 indicate a very different angular correlation. They cannot be fitted by any of the curves calculated by Hamilton for pure dipoles and quadrupoles (see Table I). It is, of course, possible that higher multipoles for which calculations are not available, are involved in Y^{88} or that the ground state of Sr^{88} does not have $J=0$. But the results can also be fitted by assuming that the first gamma-ray of the cascade is a mixture of electric quadrupole and magnetic dipole radiation. If the ground state has spin zero, the second gamma-ray must, of course be a pure multipole and agreement is obtained by assuming it to be a dipole. The angular momenta involved must then be 0, 1, 2. Ling and Falkoff[5] have calculated the coefficients of the correlation to be expected in such a case. We are indebted to them for having made their more

[21] I. Feister and L. F. Curtiss, J. Research Nat. Bur. Stand. **38**, 411 (1947).
[22] A. E. Miller and M. Deutsch, Phys. Rev. **72**, 527 (1947).
[23] C. Peacock and R. G. Wilkinson, Phys. Rev. **72**, 251 (1947).
[24] Downing, Deutsch, and Roberts, Phys. Rev. **60**, 470 (1947).
[25] W. C. Peacock and J. W. Jones CNL-14 (1948), also declassified manuscript.
[26] G. R. Gamertsfelder, Phys. Rev. **66**, 288 (1944).

complete calculations available to us in advance of publication. We made the somewhat arbitrary assumption that the electric and magnetic components are in phase. Although the coefficient a_1 for pure electric quadrupole or pure dipole radiation with the above spin assignments is positive, it is negative for the mixture unless the relative intensity of the quadrupole component is either less than 2 percent or more than 85 percent. The lower solid curves in Fig. 5 represent the correlation $W(\theta)=1-a\cos^2\theta$, with $a=0.04$, 0.06, 0.08. Our results may be fitted satisfactorily by assuming that the relative quadrupole intensity is either between 1 and 2 percent or between 80 and 85 percent of the magnetic dipole intensity. The resulting spin and parity assignments are shown in Fig. 7. They are in good agreement with the observed "cross-over" intensity and in fair agreement with the observed internal conversion coefficients.[25] The latter agreement had previously been reported to be excellent but the improved calculations of Rose, Goertzel *et al.* have made it somewhat less disintegrations a single "cross-over" gamma-ray of 2.8 favorable. The observed conversion coefficients definitely indicate that no multipoles higher than quadrupole are involved. The possibility that the positron spectrum observed by Peacock and Jones[25] may really be at least partly due to internal pair conversion cannot be entirely ruled out.

Rh^{106}

Rh^{106} is the 30″ daughter of the 1 yr. Ru^{106} fission product. It was used in equilibrium with its parent which emits only very soft beta-radiation and no gamma-rays.[27] The ruthenium was received from Oak Ridge in a solution containing long lived Tc, Ru, Rh, and Te, all carrier free. Ruthenium was separated from the mixture by distillation of ruthenium tetroxide from perchloric acid solution, and subsequent reduction with ethyl alcohol. The sample was old enough for the 42 day Ru^{103} to be negligible. Rh^{106} has been reported by Peacock[28] to decay to the ground state of Pd^{106} with the emission of a 3.55-Mev beta-ray in 82 percent of the disintegrations. Eighteen percent of the beta-decays lead to a state of Pd^{106} with 1.25 Mev excitation. This state decays mostly with the emission of two successive gamma-rays of 0.73 Mev and 0.52 Mev. Peacock presents evidence for a 1.25 Mev "cross-over" gamma-ray appearing in about 1 to 2 percent of the total number of disintegrations. Both beta-transitions appear to be allowed and the existence of this gamma-ray is a strong argument for Gamow-Teller selection rules since it indicates that the 1.25-Mev state cannot have $J=0$ if the ground state of even-even Pd^{106} is assumed to have zero spin. Unfortunately the abundance of the hard gamma-ray is so low that it is difficult to be certain of its assignment in the decay scheme.

Figure 6 shows that the angular correlation of the gamma-rays from Rh^{106} is very different and much more anisotropic than for any other substance investigated. The fact that the curve of $\epsilon(\theta)$ *vs.* θ crosses the axis shows that at least two coefficients in the expansion in powers of $\cos^2\theta$ must be different from zero so that both gamma-rays must be at least quadrupole radiation. Thus the spin of the first excited state of Pd^{106} must be at least 2. The data cannot be fitted with any of the coefficients calculated by Hamilton (see Table I). This would seem to establish definitely that the spin of the second excited state cannot be zero since the correlations for the assignments 0, 1, 0 and 0, 2, 0 are unique because no cross terms between electric and magnetic components can occur in these cases.

Ling and Falkoff[29] report that no combination of dipole and quadrupole radiations can explain the observed correlation for Rh^{106} even if one includes interference terms. One must then conclude that either higher multipoles occur in the decay of Rh^{106} or that our results do not represent the true correlation but are distorted by instrumental effects or by disturbing fields at the nucleus. Indeed the solid line in Fig. 6 represents the correlation expected for spins 0, 2, 0 but with the *coefficients reduced to half* of their calculated values. The rather good agreement with the experimental points is probably fortuitous but sufficiently suggestive to have caused us to investigate carefully the possibility of instrumental effects. The observed correlation could have been reduced by scattering of the gamma-rays in the source cup which has to be fairly heavy to stop all of the energetic beta-rays from the source. However, no measurable change occurred when the necessary absorber was placed at the counters instead of the source. Another possibility is the presence in the decay of some undiscovered gamma-ray cascade with nearly isotropic correlation, superimposed on the main process. However the observed correlation was not measurably affected when the amplifier gain was changed to favor higher energy gamma-rays. This indicates that the disturbing gamma-rays must have very nearly the same energy as those giving rise to the correlation, an unlikely coincidence which we may disregard. The possibility of internal magnetic fields disturbing the nucleus during the life time of the intermediate state was investigated by the method discussed in the next section. The result was negative. The solution of the riddle of Rh^{106} will probably be provided by measurements of internal conversion coefficients. If octupole radiation is indeed involved it must be the second gamma-ray and the spin of the first excited state must be 3, provided the ground state has spin 0, since the fact that both beta-transitions are allowed fixes the spin of the second excited state as 0, 1 or 2. Higher multipoles are definitely ruled out by life-time considerations.

[27] L. E. Glendenin, NNES-PPR Vol. 9B (1946).
[28] W. C. Peacock, Phys. Rev. 72, 1049 (1947).
[29] D. S. Ling and D. L. Falkoff, Phys. Rev. 76, 431 (1949).

4. EFFECT OF A MAGNETIC FIELD

It was pointed out in the introduction that the theory of angular correlation as used here can be expected to hold only if there is no appreciable reorientation of the nuclear moment during the lifetime of the intermediate state. In particular such reorientation might occur unless the width of the intermediate state is considerably greater than the hyperfine structure splitting of the state involved. While reasons were adduced in Section 1 which make it very unlikely that the known fields existing in solids could destroy the correlation in most cases, it does not follow necessarily that the observed correlation represents the one which would be obtained with an entirely undisturbed nucleus. Particularly with quadrupole and higher multipole radiation of relatively low energy, as in Rh^{106} and possibly Cs^{134}, the lifetime of the intermediate state may accidentally be long enough for a residual hyperfine structure splitting of 0.01 cm^{-1} to cause an appreciable distortion of the correlation. Deutsch and Stevenson[30] have recently demonstrated an abnormally long lifetime for a transition whose internal conversion[31] shows it to be almost certainly magnetic dipole or electric quadrupole radiation. Goertzel[3] has calculated the effect of a disturbing field on the coefficients of the angular correlation and has also pointed out that an external magnetic field of the order of 10^4 gauss may in many cases be sufficient to remove the perturbation to a considerable extent provided one of the gamma-rays is observed in the direction of the field. Since it is only necessary to make the coupling between the electronic shell and the external field stronger than the hyperfine structure coupling to make the direction of the average magnetic field at the nucleus coincide with that of the applied field, such moderate fields suffice to fix a "good" axis of quantization. Furthermore it is evident that one need in general only observe the coincidence rate for one position of the counters with and without the magnetic field to establish the effect of the field on the angular correlation since the total intensity of radiation must remain unchanged and for every increase in one position there must be a corresponding decrease in another.

Since it did not seem practicable to provide simultaneously cooling and adequate magnetic shielding for the multiplier tubes while maintaining a favorable geometry, Geiger counters were used in these experiments. The experimental arrangement is shown in Fig. 8. The counter tubes were placed inside the hollow pole pieces of the magnet, at opposite sides of the source and the coincidence rate was measured with and without a magnetic field of about 12,000 gauss. The results are summarized in Table II. The statistical accuracy of the results is not as good as might be desired since only Geiger counters were used. It seems probable, though, that there is no drastic change in the angular correlation due to reorientation of the intermediate state. Recent progress in scintillation counter technique should make it possible to investigate the effect further.

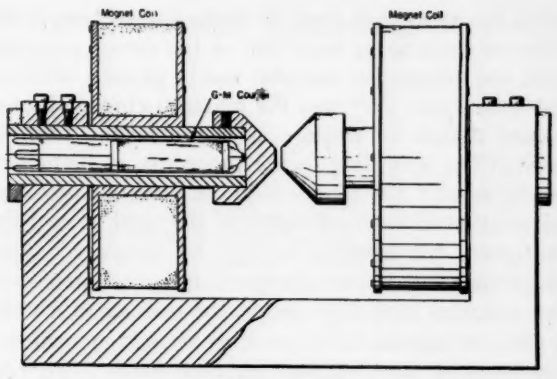

FIG. 8. Apparatus for studying the effect of a magnetic field on the coincidence rate.

TABLE II. Effect of magnetic field on coincidence rate at 180°.

Sample	Conc. per minute Magnet off	Magnet on	Percent difference
Co^{60} (solution)	5.4±0.13	5.2±0.2	−4±4
Co^{60} (gas)	8.9±0.2	8.6±0.3	−3±5
Y^{88} (solid)	13.6±0.2	14.1±0.3	4±3
Cs^{134} (solid)	5.2±0.2	5.2±0.2	0±6
Cs^{134} (solution)	5.2±0.2	5.2±0.3	0±6
Sc^{46} (solid)	8.4±0.2	8.3±0.2	−1±3
Rh^{106} (solid)	10.0±0.4	9.6±0.4	4±6

It should be noted that while a relatively weak external field will remove the distortion of the angular correlation by perturbing atomic fields, a field of this magnitude will not affect an undistorted correlation unless the life-time of the intermediate state is at least of the order of 10^{-8} sec. Indeed, if it should be found that the magnetic fields in solids or solutions are sufficiently weak even at the position of a recoiling nucleus to permit observation of the angular correlation when the lifetime of the intermediate state exceeds this time, then it should become possible to measure the magnetic moment of the nucleus in the intermediate state by a careful observation of the effect of an external field. The experiment would essentially compare the Larmor precession period of the nucleus with the lifetime of the state. If delayed coincidences are observed it will be found that the effect of the field is greatest on the correlation of coincidences with the longest delay. Experiments of this type are in preparation in this laboratory.

5. EFFECT OF CHEMICAL BINDING

If the angular correlation is greatly disturbed by some unsuspected mechanism involving collisions of the recoiling nucleus one might expect that the observed correlation would depend strongly on the medium in

[30] M. Deutsch and D. T. Stevenson, Phys. Rev. **76**, 184 (1949).
[31] Boehm, Huber, Marmier, Preiswerk, and Steffen, Helv. Phys. Acta **22**, 69 (1949).

which the atom finds itself. It seemed, therefore, worth while to examine at least one of the decay processes when the radioactive material was in gaseous, solution and solid form. Co^{60} was the material chosen since it seemed easiest to prepare as a gas in the form of $CoNO(CO)_3$ according to the procedure of Blanchard and Gilmont.[32] The solid was in the form of Co_2O_3 and the solution of $CoCl_2$. Because of the need to cool the multipliers the samples had to be compared using Geiger counters. In order to speed the collection of data four counters were arranged in the manner of a cross around the source. All six possible twofold coincidence combinations were counted simultaneously, two corresponding to $\theta=\pi$ and four to $\theta=\pi/2$. The samples were changed repeatedly to average possible drift in the apparatus and were chosen to give very nearly the same counting rates to avoid effects due to possible differences in recovery time of the several counters. Within the accuracy of the experiment, about 2 percent, no differences among the samples were found. As in the case of the effect of magnetic fields such experiments should be carried out in cases where the intermediate state has a measurable lifetime.

6. CONCLUSIONS

In these experiments we have investigated gamma-ray cascades in even-even nuclei only. If the ground states of all of these have zero angular momentum an anisotropic correlation should be observed in every case except for accidental cancellation of terms by interference. Such a correlation was observed in all cases, proving the applicability of the theory to experiments of this type in contradiction to previous results by other observers. The choice of even-even nuclei also reduces the number of possible combinations of spins which must be considered. Table I lists the coefficients for all the possible combinations up to quadrupole transitions. It appears from the table that for example, the Co^{60}, Sc^{46}, Cs^{134}, Na^{24} correlations can only be fitted by the 0, 2, 4 spin sequence. All other combinations differ at least by a factor two from the data. This result alone does not establish the spins because only the simplest combinations are considered in Table I. On the other hand Y^{88} and Rh^{106} *must* involve either octupole radiations or interference terms. It should be noted that for zero spin ground states the second of the two gamma-rays must always be a pure multipole. This again reduces the number of possibilities that need be considered. Despite this simplification, unique spin assignments cannot be made from the angular correlation alone, but certain conclusions can be drawn. For example, the first-excited state of Pd^{106} must have a spin of at least 2. The second-excited state of Ni^{60}, Ti^{46}, and Mg^{24} cannot possibly have spin zero, etc. It is also interesting that at least half, and probably all but one, of the gamma-rays involved are quadrupole or higher multipole transitions. The evidence very strongly supports the view that the spins of the odd-odd nuclei Co^{60}, Sc^{46}, and Na^{24} are high. The spin of Rh^{106} must, of course be 0 or 1 because of the allowed beta-transition from the ground state of Ru^{106} and to the ground state of Pd^{106}. The most urgently needed data are precise measurements of the internal conversion coefficients. It seems certain that the combination of such data with the angular correlation and polarization experiments will make all spin and parity assignments unique.

It is a pleasure to acknowledge the help of Professor J. W. Irvine with the chemical phases of this work. All of the theoretical physicists quoted have contributed further through private discussions.

Note added in proof.—Since this paper was written a number of related results and suggestions have been published: Waggoner, Moon, and Roberts (Bull. Am. Phys. Soc. **25**, No. 3, 45 (1950)) measured the internal conversion coefficients for Co^{60} and find both gamma-rays to be electric quadrupole radiations. Rae (Phil. Mag. **40**, 1155 (1949)) measured the internal pair conversion of the 2.76-Mev gamma-ray of Na^{24} and showed it to be an electric dipole transition. Calculations of Spiers (Phys. Rev. **78**, 75 (1950)) indicate that our results for Rh^{106} could not be explained by octupole terms.

[32] A. A. Blanchard and P. Gilmont, J. Am. Chem. Soc. **62**, 1192 (1940).

On the Interpretation of Conduction and Thermionic Emission of (Ba—Sr)O Cathodes

F. K. du Pré, R. A. Hutner, and E. S. Rittner
Philips Laboratories, Inc., Irvington on Hudson, New York

(Received February 3, 1950)

A new semiconductor model for (Ba-Sr)O cathodes is proposed comprising a conduction band, donor levels, acceptor levels, and a full band. The combination of this model with the Vink-Loosjes concept of conduction by an electron gas in the pores of the oxide coating appears to explain in a natural way many of the existing experimental facts pertaining to the conductivity and thermionic emission of these cathodes. Also some predictions which follow from this picture are indicated.

1. INTRODUCTION

THE usual semiconductor model[1] for (Ba-Sr)O cathodes consists of a donor level widely separated from the conduction band ($\Delta\epsilon\sim 1.4$ ev). Although this model appears to describe a number of the experimental facts successfully, it fails to explain others, notably the change in Richardson work function,[2] ϕ_{Rich}, and in conductivity slope with activation,[1] and also the temperature dependence of $\phi_{c.p.d.}$, the work function determined from contact *p.d.* data.[3] Furthermore, as it is completely at variance with the recent results of Vink[4] and of Wright,[5] this model must certainly be revised. Such a revised model will be proposed in this paper, but first the pertinent results of Vink and of Wright will be stated briefly.

Vink has extensively investigated the resistivity, R, of (Ba-Sr)O cathodes over a wider temperature range than that employed previously, and has found that a log$R$ *vs.* $1/T$ plot consists of three regions: a straight line part of low slope, Region I (observed between 600° and about 800°K); a straight line part of steeper slope, Region II (observed between about 800° and 1000°K); and a third part of gradually diminishing slope, Region III (observed above about 1000°K). Regions I and II are clearly visible in Fig. 1. The values of the slope in Region I decrease with activation and can be as low as 0.1 ev. Vink and Loosjes present the view supported by experiments and calculations, that the conduction in Region I occurs almost completely through the grains, whereas in Regions II and III the conduction through the electron gas in the pores is the determining mechanism.[6]

Wright has obtained evidence from Hall effect data for p-type conductivity below 850°K, at which temperature a $p-n$ transition was found, with n-type conductivity at higher temperatures.

The low slopes in Vink's Region I for well-activated cathodes have already led us[7] to suggest the presence of a donor level close to the conduction band. Here we have retained this idea and have added other features to form an improved semiconductor model, which when combined with the Vink-Loosjes concept, permits an

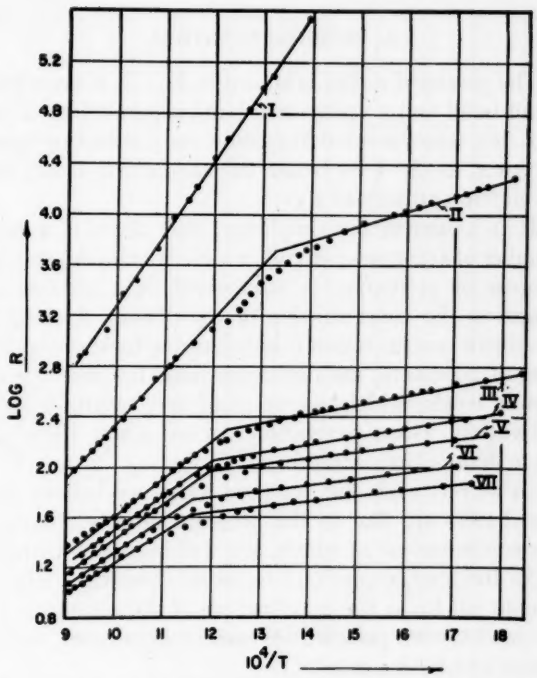

FIG. 1. Experimental values of the logarithm of the resistance *vs.* inverse absolute temperature for different stages of activation. (After Vink, reference 4.)

	Slope Region I	Slope Region II	Corrected slope Region II	Experimental work function
II	0.22	0.84	0.98	1.07
III	0.14	0.60	1.14	—
IV	0.12	0.54	1.24	1.10
V	0.11	0.56	0.96	0.90
VI	0.10	0.54	0.96	1.02
VII	0.09	0.48	0.94	0.87

[1] A. S. Eisenstein, *Advances in Electronics. I. Oxide Coated Cathodes* (Academic Press, Inc., New York, 1948.)
[2] J. P. Blewett, J. App. Phys. **10**, 831 (1939).
[3] H. Huber, Thesis, Berlin (1941). H. Huber and S. Wagener, Zeits. Techn. Physik **23**, 1 (1942). W. Heinze and S. Wagener, Zeits. f. Physik **110**, 164 (1938).
[4] H. J. Vink, Thesis, Leiden (1948). See also R. Loosjes and H. J. Vink, J. App. Phys. **20**, 884 (1949), and Philips Research Reports **4**, 449 (1949).
[5] D. A. Wright, Nature **164**, 714 (1949).
[6] Hannay, MacNair and White (reference 15) have criticized this view based on their experimental work. We do not believe their criticism to be valid for the reasons which have been outlined by Loosjes and Vink in Philips Research Reports (reference 4).
[7] Rittner, du Pré, and Hutner, Phys. Rev. **76**, 996 (1949).

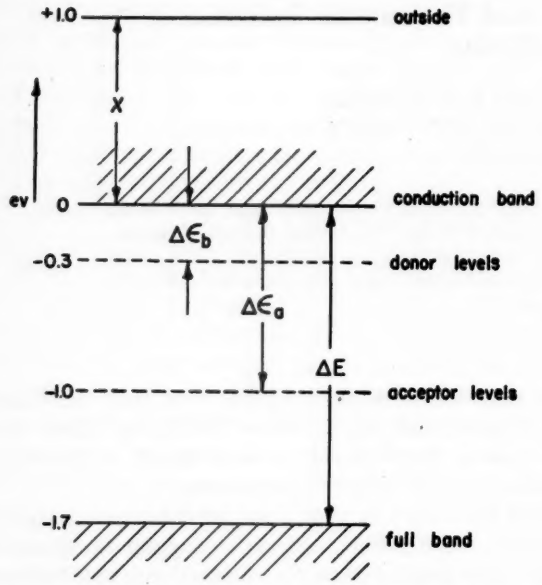

FIG. 2. Proposed semiconductor model for (Ba-Sr)O cathodes.

explanation of Wright's results and removes the above-mentioned and other difficulties.

2. PROPOSED MODEL

The proposed model is shown in Fig. 2. It comprises a full band and a conduction band separated by a gap of 1.7 ev, donor levels 0.3 ev below the conduction band, acceptor levels[8] 1 ev below the conduction band, and an electron affinity of 1 ev.

It is assumed, for simplicity, that there is a fixed number of acceptors per cm³ in a given cathode, and the process of activation is interpreted as a gradual increase in the concentration of the donors. As long as the donor concentration is less than the fixed concentration of acceptors, the donor electrons fall into the acceptor levels, which, as we shall see, results in poor activation. Good activation occurs when there are more donors than acceptors.

In accord with the accepted view, we believe that the donors are due to the presence of excess barium, the concentration of which, in a well-activated cathode, is 3×10^{17}/cm³, according to a recent chemical analysis.[9] We do not know the exact nature of the acceptors, but the well-known possibilities include impurities, surface states and lattice defects.[10]

The choice of the energy values shown in Fig. 2 was based on the following considerations. The work function is known to vary with activation roughly between 2 and 1 ev. The lower value was taken[7] as the electron affinity, χ, and the higher one as the energy difference between the acceptor level and a point just outside the cathode. The position of the donor level was chosen[7] so as to give the required low slopes of Region I. The full band was assumed to be 0.7 ev below the acceptor level in order to obtain the maximum slope observed by Vink in Region I, for poorly activated cathodes; this is also in accord with the p-type conductivity observed by Wright. The thermal separation between the full and conduction bands is accordingly 1.7 ev, which is considerably smaller than the generally supposed optical gap, but which is not in disagreement with the Franck-Condon principle.

The choice of the donor and acceptor concentrations was determined as follows: the maximum value of the donor concentration, n_b, was taken to be 3×10^{17}/cm³, based on chemical evidence,[9] whereas the minimum value, 10^{17}/cm³, and the acceptor concentration, n_a, of 1.5×10^{17}/cm³ were chosen by trial to give the best fit of the data. It is likely that the above parameters could be varied somewhat without impairing materially the agreement with the experimental facts.

3. FORMULAS

The general formula for the conductivity arising from both electrons (concentration n_e, mobility b_e) and holes (concentration n_h, mobility b_h) is

$$\sigma=n_e e b_e+n_h e b_h. \tag{1}$$

In the absence of data concerning the mobilities, we have taken

$$b_e=b_h$$

and have neglected the temperature dependence of these quantities, which probably is slight compared to that of n_e and n_h. Thus

$$\sigma\propto(n_e+n_h), \tag{2}$$

and the specific resistivity, ρ, is correspondingly,

$$\rho\propto 1/(n_e+n_h). \tag{3}$$

The expressions for n_e and n_h are (see Fowler[11])

$$n_e=2[2\pi m_e kT/h^2]^{\frac{3}{2}}e^{\zeta/kT}, \tag{4}$$

$$n_h=2[2\pi m_h kT/h^2]^{\frac{3}{2}}e^{\zeta/kT}, \tag{5}$$

where ζ is the position of the Fermi level with respect to the bottom of the conduction band. (In the actual calculation we have taken $m_e=m_h=m$.)

In addition, the general formula for the saturated thermionic emission current density[11] has the form,

$$i=AT^2e^{-(\chi-\zeta)/kT} \tag{6}$$

where, neglecting the reflection coefficient, $A=120$

[8] We have just learned that J. A. Burton has already proposed, in a private communication to Eisenstein (reference 1), that the presence of a few electron traps would give a qualitative explanation of the change in conductivity slope with increasing impurity concentration.

[9] R. O. Jenkins and R. H. S. Newton, Nature **163**, 572 (1048).

[10] As was pointed out by Dr. J. W. Mitchell (Bristol) in a private discussion with one of us, a semiconductor model containing donors and acceptors simultaneously is not always chemically stable. If either or both impurity centers are sufficiently mobile, they may destroy each other by recombination.

[11] R. H. Fowler, *Statistical Mechanics* (Cambridge University Press, London, 1936) pp. 399–401.

amp./cm². (Note that with the zero of energy at the bottom of the conduction band, ζ is usually negative.)

Thus the quantities n_e, n_h and i may be calculated from a knowledge of the position of the Fermi level, ζ, as a function of the temperature. The Fermi level positions were determined from the expression[11]

$$2[2\pi mkT/h^2]^{\frac{3}{2}}e^{\zeta/kT}=[n_b/(1+e^{(\zeta+\Delta\epsilon_b)/kT})]-[n_a/(1+e^{-(\zeta+\Delta\epsilon_a)/kT})]+2[2\pi mkT/h^2]^{\frac{3}{2}}e^{-(\zeta+\Delta E)/kT}, \quad (7)$$

where the symbols $\Delta\epsilon_b$, $\Delta\epsilon_a$, and ΔE are defined in Fig. 2.

Equations (4), (5), and (7) are based on classical statistics which proved to be always applicable in the present problem.

4. CONDUCTIVITY[12]

Figure 3 shows calculated values of $\log[10^{17}/(n_e+n_h)]$ plotted as a function of $10^4/T$ for different donor concentrations, and hence for different stages of activation. The graph indicates that the model presented here predicts decreasing slopes in Region I with increasing activation, in agreement with Vink's experimental results. (See also Table I.) In fact, low slopes occur for most stages of activation except the very poor ones, which is also in accord with Vink's data. (In concordance with the Vink-Loosjes concept that the conductivity above about 800°K is primarily determined by conduction through the electron gas in the pores, the curves of Fig. 3 have not been extended above 800°K.)

Furthermore, the type of conductivity in Region I can be either n- or p-type, as is indicated in Fig. 3 and in Table I; it is evident that the model predicts p-type conductivity for the more poorly activated cathodes.[13] For these cathodes, however, the conductivity at higher temperatures may become n-type since in Region II the effective cross section for the electron current increases enormously and in addition the mean mobility of the electrons becomes much greater than that of the holes. Thus these cathodes may show a $p-n$ transition at about the same temperature where the transition from Region I to Region II occurs. On the other hand, well-activated cathodes should always show n-type conductivity.

5. THERMIONIC EMISSION

The thermionic emission current was calculated, in the temperature range from 800° to 1100°K, from Eq. (6) using the values of $\zeta(T)$ determined from Eq. (7). These calculated currents were then used to make Richardson plots ($\log i/T^2$ *vs.* $1/T$), and straight lines were obtained. Thus the calculated values of the current can also be represented by

$$i=A_{Rich}T^2\exp(-\phi_{Rich}/kT). \quad (8)$$

The quantities, A_{Rich}, ϕ_{Rich}, and $i_{1000°K}$, as determined from these calculations for different stages of activation, i.e., for different values of n_b, are shown in Table I. The magnitude of ϕ_{Rich} varies from 2.1 to 0.93 ev with increasing activation, in good agreement with experiment. Similarly, the corresponding values of A_{Rich} check reasonably well with observations, as may be seen from the calculated values of i at 1000°K. Moreover, a semilogarithmic plot of A_{Rich} *vs.* ϕ_{Rich} for different stages of activation is essentially a straight line (see Fig. 4) and in good agreement with Veenemans' data.[14]

We wish to emphasize that since A_{Rich} and ϕ_{Rich} are constants independent of temperature,

$$\phi_{Rich}\neq\chi-\zeta(T), \text{ and therefore } A_{Rich}\neq A, \quad (9)$$

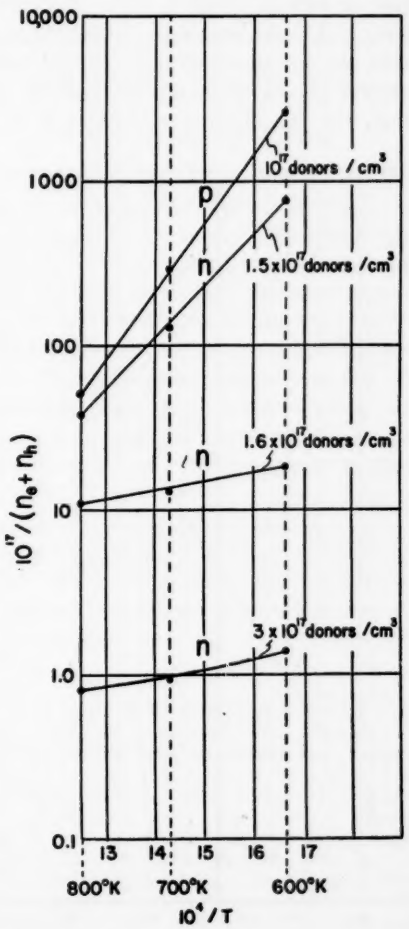

FIG. 3. Calculated values of the logarithm of the "resistance" *vs.* inverse absolute temperature for different donor concentrations. Electron and hole mobilities taken equal and constant.

[12] In addition to the points mentioned in this section Vink (reference 4) has already explained many of the experimental facts. His picture accounts for a corrected slope in Region II equal to the Richardson work function for all stages of activation; it yields a reasonable value of the calculated conductivity in Region II; it explains the occurrence of linear I–V plots in Region I, non-linear ones in Region II, and linear ones again in Region III; finally, it accounts for the gradually diminishing slope in Region III.

[13] Although Wright reports p-type conductivity in cathodes with work functions from 1 to 1.2 ev, which would normally be considered well activated, the possibility exists that the portion of the cathode actually used for the Hall effect measurements, which had to be on an insulating base, was not as well activated as the over-all work function would imply.

[14] C. F. Veenemans, Ned. Tijdschr. Natuurk. **10**, 1 (1943).

TABLE I. Calculated thermionic emission and "conductivity" for different stages of activation. The direction of increasing conductivity is that of increasing n_b.

n_b	T	$\zeta(T)$	$\phi_{c.p.d.}=(\chi-\zeta)$	ϕ_{Rich}	A_{Rich}	$i_{1000°K}$	Slope in Reg. I	Type of conduction
$1\times10/^{17}$cm^3	600°K	−0.97 ev	1.97 ev	ev	amp./cm^2	amp./cm^2	0.76 ev	p
	700	−0.96	1.96					
	800	−0.95	1.95					
	900	−0.93	1.93	2.10	1,105.	0.0288		
	1100	−0.88	1.88					
1.5×10^{17}	600	−0.67	1.67				0.58	n
	700	−0.70	1.70					
	800	−0.73	1.73					
	900	−0.76	1.76	1.50	4.18	0.115		
	1100	−0.81	1.81					
1.6×10^{17}	600	−0.49	1.49				0.11	n
	700	−0.56	1.56					
	800	−0.64	1.64					
	900	−0.71	1.71	1.21	0.211	0.17		
	1100	−0.80	1.80					
3×10^{17}	600	−0.36	1.36				0.12	n
	700	−0.41	1.41					
	800	−0.47	1.47					
	900	−0.53	1.53	0.93	0.049	1.01		
	1100	−0.67	1.67					

as may also be seen in Table I. Thus the temperature independent work functions, ϕ_{Rich}, obtained from Richardson plots do not measure directly the energy difference between the Fermi level and a point just outside the cathode. On the other hand, there is a different technique for determining work functions, namely by contact $p.d.$ measurements.[3] The $\phi_{c.p.d.}$'s so determined are temperature dependent and actually measure the position of the Fermi level, for, according to theory,

$$\phi_{c.p.d.}=\chi-\zeta(T); \tag{10}$$

and therefore

$$\phi_{c.p.d.}\neq\phi_{Rich}.$$

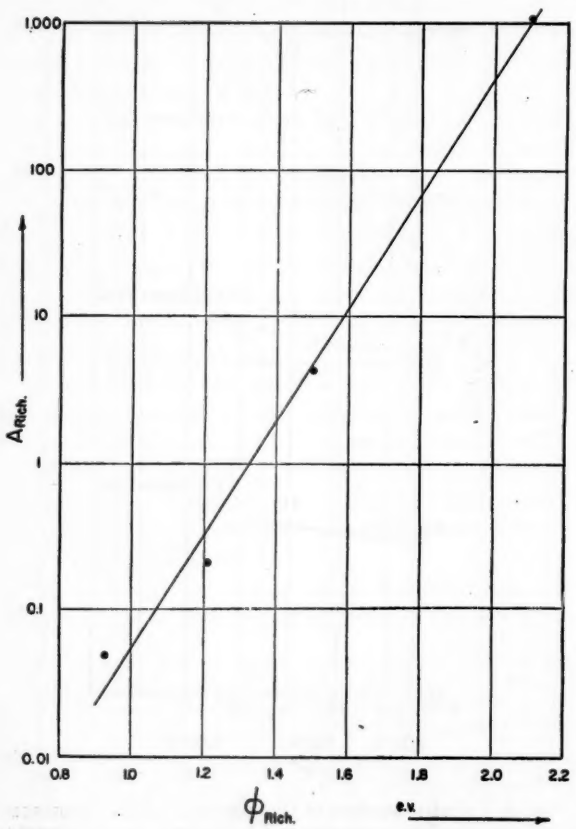

FIG. 4. Semilogarithmic plot of the calculated values of A_{Rich} vs. ϕ_{Rich} for different stages of activation.

A plot of the variation of the Fermi level with temperature is presented in Fig. 5. A comparison of the values of $\phi_{c.p.d.}$ as read from this figure for $n_b=3\times10^{17}$/cm^3 with the two values of $\phi_{c.p.d.}$ measured by Huber[3] is shown in Table II. The absolute magnitude of the calculated $\phi_{c.p.d.}$ and its temperature variation agree remarkably well with Huber's values, although the excellence of the agreement is, no doubt, fortuitous.

In Fig. 5, note that in the temperature range from 800°K to 1100°K, $\zeta(T)$ is closely approximated by a straight line, and can be represented by the formula

$$\zeta=\zeta_0-\alpha kT. \tag{11}$$

Inserting this in Eq. (6), we have

$$i=AT^2\exp(-(\chi-\zeta_0+\alpha kT)/kT)$$
$$=Ae^{-\alpha}T^2\exp(-(\chi-\zeta_0)/kT). \tag{12}$$

Thus

$$A_{Rich}=Ae^{-\alpha} \quad \text{and} \quad \phi_{Rich}=\chi-\zeta_0. \tag{13}$$

This last equation clearly shows that ϕ_{Rich} may also be obtained by extrapolating linearly to 0°K the high temperature part of each ζ curve. Numerical confirmation of this statement is shown by a comparison of the extrapolated ϕ_{Rich} values in Fig. 5 with the results in column 5 of Table I. It may also be seen from Fig. 5 that whereas in a well-activated cathode $\phi_{c.p.d.}>\phi_{Rich}$, the model predicts for a cathode, so poorly activated as to be p-type in Region I, that $\phi_{c.p.d.}<\phi_{Rich}$.

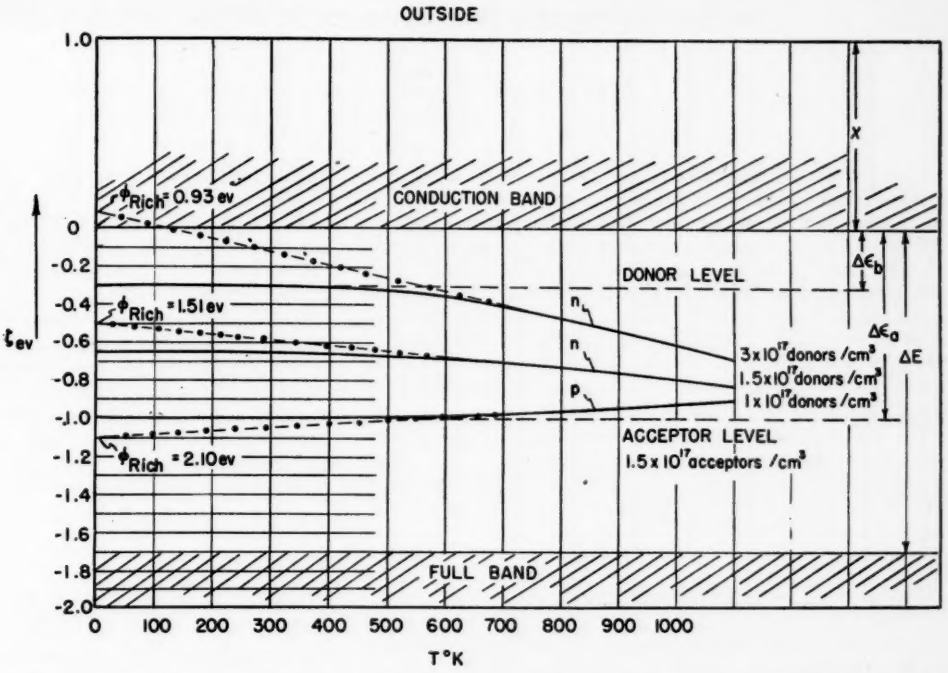

FIG. 5. Variation of Fermi level, ζ, with temperature for three donor concentrations.

The relationship between $\phi_{c.p.d.}$ and ϕ_{Rich} is obtained by substituting Eq. (11) in Eq. (10). Thus we obtain

$$\phi_{c.p.d.}=\chi-\zeta_0+\alpha kT, \tag{14}$$

and using Eq. (13)

$$\phi_{c.p.d.}=\phi_{Rich}+\alpha kT. \tag{15}$$

It should be pointed out that Huber[3] has already made a clear distinction between $\phi_{c.p.d.}$ and ϕ_{Rich} and has correlated the two by means of an equation similar to Eq. (15).

The relation between log$i$ and logσ at a given temperature for different stages of activation has been investigated,[1,15] and found to be linear with a slope of 45°. This has been explained on the basis of the semiconductor formulas for σ and i, in each of which the Fermi energy, ζ, appears only in the factor $e^{\zeta/kT}$, see Eqs. (1), (4), (5), and (6). Since ζ is assumed to be the only quantity that varies on activation, at a given temperature the conductivity, σ, varies in direct proportion to the thermionic emission, i. We believe that this explanation applies only at the temperatures of Region I. Since for temperatures in Region II, Vink's calculations show that the conductivity through the electron gas in the pores is also proportional to the thermionic emission, i, we still expect the above linear relation at these temperatures, although the underlying physical picture is different. As Hannay, MacNair, and White[15] carried out their experiments at 1000°K, we believe the latter explanation to apply in their case.

TABLE II. Comparison of values of $\phi_{c.p.d.}$.

T°K	$\phi_{c.p.d.}$ (Huber)	$\phi_{c.p.d.}$ (Fig. 5)
770°	1.46 ev	1.45 ev
640°	1.38	1.38

[15] Hannay, MacNair, and White, J. App. Phys. **20**, 669 (1949).

6. CONCLUDING REMARKS

The combination of the proposed semiconductor model, Fig. 2, with the Vink-Loosjes concept of the conduction by an electron gas in the pores appears to explain in a natural way many of the existing experimental facts pertaining to the conductivity and thermionic emission of (Ba-Sr)O cathodes.

In addition the picture leads to a number of predictions which can be experimentally tested. Thus, for a well-activated cathode, the conductivity should be n-type for all temperatures. Furthermore, for a cathode activated so poorly as to be p-type in Region I, the temperature coefficient of $\phi_{c.p.d.}$ should be negative and $\phi_{c.p.d.}<\phi_{Rich}$. Finally, if an inert gas is introduced at sufficiently high pressure, the pore conduction should be impeded thus causing both the break in the conductivity curve and the $p-n$ transition to occur at higher temperatures, if at all. An experiment of this type has been started in this laboratory.

Note added in proof.—This paper was presented at the Symposium on Thermionics sponsored by the Division of Electron Physics of the American Physical Society held January 31 and February 1, 1950 in New York City, at which time experimental results were announced by L. Apker showing that the optical and thermal gaps in BaO are about equal. Also, C. Herring stated that this result is in accord with theoretical expectations. Our choice of 1.7 ev for the thermal gap was based entirely on an attempt to incorporate Wright's Hall data into a consistent picture. In view of the greater difficulty involved in obtaining reliable Hall data compared to that encountered in the other experiments in question, there may be reason at the present time for preferring a thermal gap about equal to the optical gap (*ca.* 3.8 ev). We wish to point out that even if the model is so modified, all of the numerical results of this article, save those dealing with the p-type conduction, remain substantially unaltered due to the minuteness of the full band contributions in all n-type cases.

On the Ferromagnetic Resonance in Nickel and Supermalloy*

N. BLOEMBERGEN†
Cruft Laboratory, Harvard University, Cambridge, Massachusetts
(Received February 14, 1950)

Both the real and imaginary part of the high frequency permeability of flat specimens of nickel and supermalloy have been investigated at 9030 mc/sec. and 24400 mc/sec., with a constant field H_0 parallel to the plane of the specimen. For the higher frequency, experiments were extended beyond the Curie point (358°C for nickel and about 400°C for supermalloy). The decrease in saturation magnetization causes the maximum and the minimum of ferromagnetic absorption to shift toward higher field strengths. The g factor is independent of temperature within the limit of error (2 percent); $g=2.12$ for supermalloy and $g=2.20$ for nickel.

The line width in nickel increases first slowly, but above 200°C more rapidly from 250 gauss at room temperature to 700 gauss at the Curie point, the width being defined as half the width between the points where the imaginary part of the susceptibility has dropped to half its maximum value. In supermalloy the width is 110 gauss between 20°C and 300°C and then rises sharply to 350 gauss at 420°C. There is no discontinuity at the Curie point, but the intensity of the absorption drops very rapidly beyond that temperature. At the lower frequency the width is reduced by approximately a factor 1.6.

The observed data are compared with existing theories. Only interactions of the ferromagnetic spins with the lattice vibrations or the conduction electrons could probably account for the observed order of magnitude of the width. It is not clear, however, how the width could be independent over a large temperature interval, if these interactions were the only broadening agent. A pseudo-dipolar interaction, introduced by Van Vleck, might give an explanation for the line width at lower temperatures.

I. INTRODUCTION

As early as 1935, Landau and Lifshitz[1] wrote a fundamental paper on ferromagnetic permeabilities and predicted the existence of resonance effects. The first experimental observation was made by Griffiths[2] in 1946. Kittel[3] extended Landau's theory and showed how the ratio of the frequency and the magnetic field at which resonance occurs depends critically on the demagnetizing factors, and therefore on the geometry of the sample. The classical equation of motion for the magnetic moment of a ferromagnetic body expresses the balance between the exerted torque and the rate of change of angular momentum

$$(dM_{x,y}/dt)=\gamma[\mathbf{M}\times\mathbf{H}_{eff}]_{x,y}-M_{x,y}/T_2, \quad (1a)$$

$$(dM_z/dt)=\gamma[\mathbf{M}\times\mathbf{H}_{eff}]_z-(M_z-M_0)/T_1 \quad (1b)$$

with

$$\gamma=ge/2mc, \quad (1c)$$

where g is the Landé factor and M_0 is the static saturation magnetization. These equations have the same form as those describing the nuclear magnetic resonance and the notation is the same as in Bloch's paper.[4] In the nuclear case H_{eff} can usually be put equal to the externally applied magnetic field H^{ext}, consisting of a constant field H_0 and a radiofrequency component which are mutually perpendicular,

$$H_x^{ext}=H_1e^{i\omega t}, \quad H_y^{ext}=0, \quad H_z^{ext}=H_0. \quad (2)$$

In the ferromagnetic case we have to add three terms to the external field in order to get the effective field:

$$\mathbf{H}_{eff}=\mathbf{H}^{ext}-N_{x,y,z}\mathbf{M}+\mathbf{H}^{anis}+\alpha\nabla^2\mathbf{M}. \quad (3)$$

The terms $-N_xM_x$, $-N_yM_y$, $-N_zM_z$, where N is the demagnetizing factor, represent the internal field produced by the magnetization of the sample. In the ferromagnetic case these terms have the same order of magnitude as the applied field.

The anisotropy energy of a ferromagnetic sample adds the torque $\partial f/\partial\vartheta_{x,y,z}$ to the equations of motion, where $\partial\vartheta_{x,y,z}$ denotes a rotation around the x, y or z axis, respectively. Kittel[3] showed that this torque can in many cases be written as $\mathbf{M}\times\mathbf{H}^{anis}$. Finally an inhomogeneous distribution in the magnetization gives rise to an increase in the exchange energy of the spin system, the effect of which may be described[1] by a contribution $\alpha\nabla^2\mathbf{M}$ to the effective field with

$$\alpha=4JS^2/aM_0^2, \quad (4)$$

where J is the exchange energy and a the distance between two neighboring spins.

The damping terms in Eqs. (1) have a simpler form than the corresponding expression (21) in Landau's paper.[1] It should be pointed out that T_1 and T_2 may be arbitrary functions, usually depending on the frequency of the applied field and on the temperature, and that in general T_1 and T_2 are not equal, but that

$$1/T_2=1/(2T_1)+1/T_2^*. \quad (5)$$

Interactions between the spin system and the lattice vibrations determine the quantity T_1 and magnetic and exchange interactions within the system of spins determine T_2^*. A discussion of these interactions will be postponed to Section IV. Presently we shall consider T_1 and T_2 only from the phenomenological point of view.

We shall now omit the last two terms in Eq. (3). The

* This research was supported jointly by the Navy Department (ONR), the Signal Corps (U. S. Army), and the U. S. Air Force, under ONR Contract N5-ori-76, T. O. 1.
† Society of Fellows.
[1] L. Landau and E. Lifshitz, Physik. Zeits. Sowjetunion 8, 153 (1935).
[2] J. H. E. Griffiths, Nature 158, 670 (1946).
[3] C. Kittel, Phys. Rev. 73, 155 (1948).
[4] F. Bloch, Phys. Rev. 70, 460 (1946).

influence of these terms will be discussed in Section IV and will be shown to be small. A stationary solution of Eqs. (1) can then be obtained by putting $M_{x,y}=M_{x,y}e^{i\omega t}$. Combining (1), (2), and (3) we get the solution

$$M_x=\frac{\gamma^2M_z\{H_0+(N_y-N_z)M_z\}}{[i\omega+(1/T_2)]^2+\gamma^2\{H_0+(N_x-N_z)M_z\}\{H_0+(N_y-N_z)M_z\}}H_1, \tag{6}$$

$$M_y=\frac{\gamma M_z(i\omega+1/T_2)}{(i\omega+1/T_2)^2+\gamma^2\{H_0+(N_x-N_z)M_z\}\{H_0+(N_y-N_z)M_z\}}H_1, \tag{7}$$

while M_z can be obtained by substituting these expressions into

$$(M_z-M_0)/T_1=-\gamma\langle H_1M_y\rangle_{Av}+\gamma(N_x-N_y)\langle M_xM_y\rangle_{Av}. \tag{8}$$

The average is taken over the time, and we neglect small periodic variations in M_z. For small values of the radiofrequency field H_1, when

$$\gamma^2H_1^2T_1T_2\ll 1,$$

the right-hand side of Eq. (8) may be put equal to zero and we have $M_z=M_0$, which is valid for all experiments described in the present paper. At a very high power level saturation phenomena will occur which play such an important role in nuclear resonance. It may be pointed out that experiments at high power levels, as have been carried out by Slichter[5] in paramagnetic salts, would give information on T_1 in ferromagnetic materials. Using Eq. (6) with $M_z=M_0$ and the well-known relation for the susceptibility

$$\mu-1=\mu_1-1-i\mu_2=4\pi\chi=4\pi M_x/H_1, \tag{9}$$

we obtain the following expressions for the real and imaginary parts of the ferromagnetic high frequency permeability,

$$\mu_1=\frac{4\pi\gamma^2M_0\{H_0+(N_y-N_z)M_0\}(\omega_0^2-\omega^2)}{(-\omega^2+\omega_0^2)^2+4\omega^2/T_2^2}+1, \tag{10}$$

$$\mu_2=\frac{4\pi\gamma^2M_0\{H_0+(N_y-N_z)M_0\}2\omega/T_2}{(-\omega^2+\omega_0^2)^2+4\omega^2/T_2^2} \tag{11}$$

with a resonant frequency ω_0 given by

$$\omega_0^2=\gamma^2\{H_0+(N_x-N_z)M_0\}\times\{H_0+(N_y-N_z)M_0\}+1/T_2^2. \tag{12}$$

We shall now discuss how these permeabilities are obtained from experiment. This research was originally undertaken to get an understanding of the quantity T_2 in ferromagnetic materials. Experiments around the Curie temperature seemed therefore advisable, since the causes which determine T_2 are best understood for paramagnetic substances.

II. EXPERIMENTAL METHOD

A standard method of determining the high frequency magnetic susceptibility of an insulator is to fill part of the space—preferably where the electric field is zero—inside a resonance circuit with the material to be investigated.[6] The real part of the susceptibility is then determined by the shift in resonant frequency and the imaginary part by the change in the Q of the resonant circuit.

In the case of a ferromagnetic metal the important electric losses, caused by the finite resistance of the material, cannot be separated physically from the magnetic losses. The sample is now conveniently made one of the walls of the resonant circuit. If we extend a well-known formula for the effect of the finite skin depth on the losses and the resonant frequency of a cavity[7] to the case where the permeability of the wall is different from unity, we find in an approximation to the first order in $1/Q$

$$1/Q_{fer}=\mu_R^{\frac{1}{2}}/Q_0, \tag{13}$$

$$-2\Delta\omega/\omega_0=\pm\mu_L^{\frac{1}{2}}/Q_0, \tag{14}$$

with

$$\mu_R=(\mu_1^2+\mu_2^2)^{\frac{1}{2}}+\mu_2, \tag{15}$$

$$\mu_L=(\mu_1^2+\mu_2^2)^{\frac{1}{2}}-\mu_2, \tag{16}$$

and

$$Q_0=(2/\delta_0)\int\int H^2dS\Big/\int\int\int H^2dV. \tag{17}$$

The surface integral extends over the ferromagnetic surface, δ_0 is the skin depth and Q_0 the quality factor of the wall, if its permeability were unity. The + sign in Eq. (14) holds if μ_1, as given by Eq. (10), is positive, the − sign, if μ_1 is negative. In this latter case of *anomalous dispersion* the skin depth losses are accompanied by a decrease of the effective length of the cavity

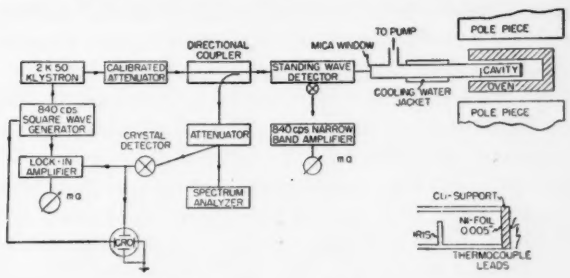

FIG. 1. Block diagram of the apparatus.

[5] C. P. Slichter, thesis, Harvard University (1949).

[6] H. G. Beljers, Physica 14, 629 (1949).

[7] See, e.g., J. C. Slater, Rev. Mod. Phys. 18, 441 (1946), especially the derivation of formula (III-59); also J. Bernier, *Onde Electrique* 26, 305 (1946).

and an increase of its resonant frequency. The quantities on the left-hand side of Eqs. (13) and (14) can be measured experimentally by any of the usual methods.[8] Our particular experimental arrangement is shown in the block diagram of Fig. 1. It is essentially the same as one used by Yager.[9] Also the technique of evaluation of the data is at many points the same as indicated in his papers.

A 2K50 klystron generates power at about 24,400 mc/sec. All voltages for the klystron, including the heater voltage, are derived from an electronically regulated power supply. A square wave of 840 c.p.s. is applied to the repeller, which provides an off-on modulation. The microwave power which can be varied by a calibrated attenuator is partly reflected by the cavity system which terminates the end of the wave guide. The reflected power is fed into a crystal detector by means of a directional coupler and the rectified signal passes through an 840 c.p.s. narrow band amplifier and lock-in detector. The standing wave pattern set up by the reflections from the cavity can be measured by a standing wave detector also followed by an 840 c.p.s. amplifier. The over-all response of the crystal-amplifier combinations was determined with the calibrated attenuator, and deviated slightly from a square law. The microwave power could alternatively be fed into a spectrum analyzer which had a calibrated wave meter for frequency measurements.

The rectangular cavity consists of a section of guide, one guide wave-length long, shorted at one end by a slab of ferromagnetic material. On the other side it is coupled by an asymmetrical window through which it is excited in the E_{102} mode. The size of the diaphragm is so chosen that the cavity is undercoupled to such an extent that the reflected power in zero external field is between 10 and 20 percent of the incident power. The cavity is placed between the pole pieces of an electromagnet. If we call the plane of the ferromagnetic wall the xz plane, then the microwave field at the wall is in the x direction and the constant field in the z direction. The pole pieces were 7 inches in diameter and 2 inches apart. A current of 10 amp. at 200 volts through the excitation coils provided a field of about 10,000 gauss. This current could be maintained for several minutes without a special cooling arrangement for the coils. Since the ferromagnetic resonance curves are wide, there are no special requirements on the homogeneity or regulation of the field. The field strength was measured with less than 0.5 percent error with a flip coil and fluxmeter combination, which was calibrated at one point with a proton magnetic resonance. The width of the gap is ample so that a small oven can be put around the cavity. The oven consists of 50 turns of non-magnetic wire (total resistance 20Ω), sandwiched between two asbestos cylinders, $1\frac{3}{4}$ inches outside diameter and 6 inches long. A current of 4 amp. was sufficient to heat the cavity to 450°C. The temperature was measured with a platinum-platinum-rhodium thermocouple. One of the joints was clamped against the end wall of the cavity. To prevent oxidation of the end wall and copper side walls of the cavity, the pressure in it was kept below 0.01 mm Hg with a small roughing pump. Microscopic examination of the inside walls showed no trace of oxidation after completion of the runs. The choke flange with sealed mica window (0.0015-inch thick) was 15 inches away from the cavity. In between, a cooling jacket was soldered around the guide through which a convection current of water was circulated. A dummy mica window was placed a quarter wave-length away from the one which kept the pressure to minimize microwave reflections.

Great care should be taken in the preparation of the samples. They should be kept free from strains and surface contaminations, since the microwaves penetrate only 10^{-4} to 10^{-5} cm. The surface should also be as smooth as possible. Electrolytic nickel foil** (0.005-inch thick) was used, spectroscopically analyzed to be 99.8 percent pure, the main contaminant being 0.17 percent of cobalt. Supermalloy (0.004-inch thick) was generously put at our disposal by Dr. Bozorth of the Bell Telephone Laboratories. The samples were cut to size between two brass disks, carefully avoiding shearing forces. They were soldered with gold to a copper disk which served as support and annealed for one hour at 850°C, then slowly cooled to room temperature. They were electropolished in a bath of 90 percent phosphoric and 10 percent chromic acid, kept at 90°C. The current of 5 amp./cm^2 was maintained for 20 sec. Finally, they were silver-soldered to the end of the wave-guide where care was taken that the solder would not flow over the inside wall. The soldering operations were all carried out in an atmosphere of purified hydrogen. To check whether they had any spurious effect on the ferromagnetic resonance, data were also taken at room temperature with a cavity which could not be evacuated and where the sample foil was pressed tightly against a narrow edge of the guide wall. The contact resistance did not appreciably lower the value of Q. No change in the resonance curve was observed for nickel. The value of $\mu_R{}^{\max}$ for supermalloy was 25 percent lower for the soldered cavity, probably due to a slight strain in the material. Data reproduced well after each run at higher temperature.

The demagnetizing factors would be $N_x=0$, $N_y=4\pi$, $N_z=0$, if the foils were infinitely thin. This assumption is valid for the x and y direction, since the foil is only one skin-depth thick for the microwave components. The z component requires a small correction:[10] $N_z=-\pi^2(d/a)\sim 0.08$, where a and d are the axes of an

[8] G. C. Montgomery, *Technique of Microwave Measurements* (McGraw-Hill Book Company, Inc., 1947).
[9] W. A. Yager, Phys. Rev. 75, 316 (1949).

** The nickel was made available by the courtesy of the Superior Tube Company.
[10] J. C. Maxwell, *Electricity and Magnetism* (Clarendon Press, Oxford, 1881), Volume 2, p. 69.

oblate spheroid, d corresponding to the thickness of the sample, and a to its diameter. Most conveniently this correction amounting to about 50 gauss is directly applied to the value of the external field H_0.

The experiments at X band were carried out only at room temperature with a similar arrangement of the electric circuits. The power at 9030 mc/sec. was generated by a 2K25 klystron.

The procedure is now to vary the frequency of the klystron slowly by changing the repeller voltage, or the thermal tuning grid voltage in the case of the 2K50, until minimum reflection into the directional coupler indicates resonance in the cavity. The voltage standing-wave ratio at resonance, β, is equal to the ratio of the unloaded Q of the cavity, Q_u, and the external or radiation Q_e,

$$\beta=Q_e/Q_u=Q_e/Q_c+Q_e/Q_{\text{fer}}, \tag{18}$$

where $1/Q_c$ and $1/Q_{\text{fer}}$ represent the losses in the copper and ferromagnetic walls, respectively. A correction has been made for the attenuation in the guide between the detector and the cavity. The value of β is measured as a function of the constant magnetic field H_0 at various temperatures. Actually in each run β was measured with the standing wave detector only for one or two values of H_0. In other points the reflected power P_r was measured with the directional coupler output and β was determined from the formula

$$\frac{P_r}{P_i}=\frac{(1-\beta)^2}{(1+\beta)^2}.$$

This procedure was not only much faster, but also gave more accurate results near maximum absorption, where the VSWR becomes very high and P_r/P_i may be as large as 0.6. In addition we determine the total Q by varying the frequency through the resonance of the cavity and measuring the VSWR as a function of frequency. From Eq. (18) and the relation

$$1/Q=1/Q_u+1/Q_e,$$

Q_e and Q_u are known. Q_c could be calculated from the geometry of the cavity and the conductivity of copper. Then Q_{fer} would be known from Eq. (18) and μ_R from (13). The y component of the magnetization does not contribute to Q_{fer}, since the cavity is only excited in a mode with a vanishing y component of the magnetic field at the sample. In practice this procedure does not work very well and gives erroneous values for μ_R. It is a common phenomenon that the theoretical values for Q are usually 10 to 30 percent higher than the experimental values. Causes for this discrepancy are scratches and roughness of the surface[11] and perhaps also spurious losses in soldered or clamped joints. An error of 30 percent in Q_c would cause an error of a factor 3 or more in μ_R. The following procedure would therefore be preferable. Let μ_R and $'\mu_R$ be two values of the permeability, belonging to two values of the magnetic field H_0 and $'H_0$, with measured SWR β and $'\beta$. From Eqs. (13) and (18) we then obtain an expression from which Q_c is eliminated,

$$\mu_R=\{'\mu_R^{\frac{1}{2}}+(\beta-\beta')(Q_0/Q_e)\}^2. \tag{19}$$

The quantity Q_0 has still to be computed from Eq. (17). Values for the d.c. conductivity, which enter into δ_0, have been taken from the *Physikalisch Chemische Tabellen* in the case of nickel. For supermalloy[12] only the value at room temperature is known $1/\sigma=65\times10^{-6}$ Ω/cm^{-1}. The assumption, verified in similar alloys, that the resistance is equal to that of nickel at the same temperature plus a temperature independent part, makes it possible to calculate δ_0 for supermalloy at higher temperatures. It is true that the calculated value of Q_0 may again be somewhat too high. But now we have only one wall with a well-polished, well-defined surface, so that the systematic error in μ_R is probably less than 10 percent too high. Typical Q values at K band are $Q_u=2440$, $Q_e=6730$, $Q_0=25{,}000$ for nickel at 24°C and $Q_u=1750$, $Q_e=6650$, $Q_0=12{,}000$ for nickel at 350°C.

As the reference value $'\mu_R$ in Eq. (19) the limiting value of the permeability for very high fields H_0 may be used. From (10), (11) and (15) we see that $'\mu_R$ then approaches unity. At 9100 mc/sec. this procedure has been used. But at 24,000 mc/sec. the available field strength was unfortunately not sufficiently larger than

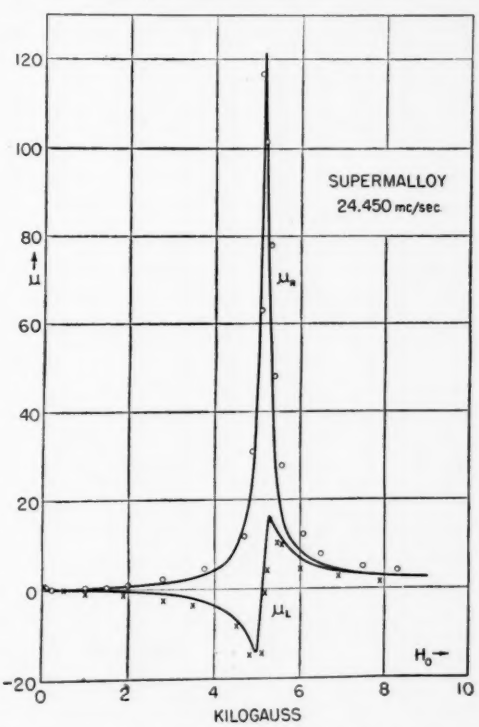

FIG. 2. The real and imaginary parts of the effective permeability in supermalloy at 24400 mc/sec.

[11] S. P. Morgan, J. App. Phys. **20**, 352 (1949).

[12] O. L. Boothby and R. M. Bozorth, J. App. Phys. **18**, 173 (1947).

the resonance field to warrant an extrapolation of β' to its value for infinitely high fields. Here we assumed $'\mu_R$ to be near unity in zero external field. It should be kept in mind that for very low values of H_0 the domains will not be aligned and the magnetization M_0 will tend to a very small value. Inspection of (10), (11), and (15) shows that μ_R will be close to unity in that case. Actually, better agreement between theory and experiment is obtained when $'\mu_R$ is taken to be slightly smaller, between 0.8 and 0.9. The value is adjusted for a good fit at the minimum of the curves (Figs. 3 and 5) which will be discussed in the next section. The maximum value of the absorption near resonance is very insensitive to small variations in $'\mu_R$. Nevertheless, the error in the absolute value of μ_R is rather high and could be as large as 25 percent. It is subject to systematic errors, one of which, the determination of Q_0, has already been mentioned. Another error arises from spurious reflections from choke flanges, pumping slot, and mica window. The SWR from these causes was measured to be less than 1.05, by putting a tapered load in the guide. The directivity of the coupler was better than 30 db. The phases

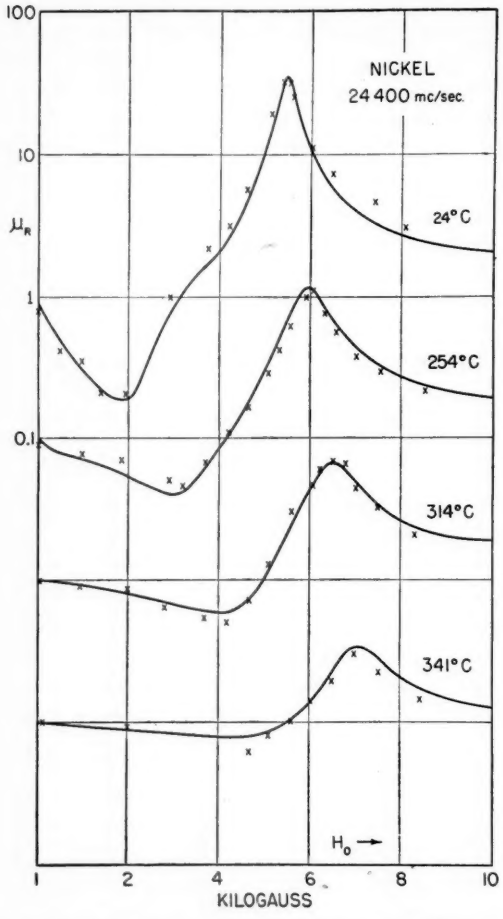

FIG. 3. The effective permeability of nickel at 24400 mc/sec. for various temperatures. Each curve is lowered by one decade with respect to the one above it. The numbers along the ordinate axis apply to the top curve. The drawn lines have been calculated theoretically.

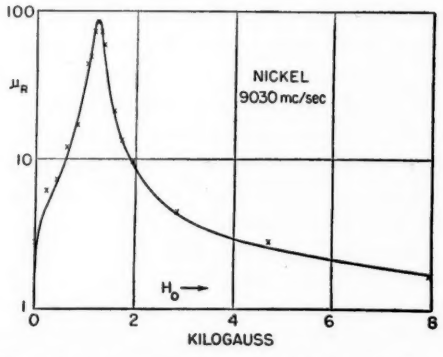

FIG. 4. The effective permeability of nickel at 9030 mc/sec. at room temperature.

with which these spurious reflections add to the signal reflected from the cavity vary largely, as the effective length of the guide is enlarged by heating. If the cavity were well matched, intolerable errors would result in the measured reflected power. Therefore the coupling was chosen such that the reflected power was always more than 10 percent of the incident power. The error is smaller near the maximum, where the reflection is larger, and cancels to a considerable extent when the difference $\beta-'\beta$ is taken in Eq. (19) for the variation in μ_R. But the error in μ_R is twice as large as that in the power measurement because the square must be taken on the right side of (19). Adding an uncertainty of about 5 percent in the calibration of the attenuator and 5 percent in the measurement of Q_e, one obtains a rather large possible error in μ_R of 30 percent in extreme cases. More precise measurements should be carried out with a transmission type of cavity and different couplings should be used in the range of low and very high values of μ_R.

III. EXPERIMENTAL RESULTS

In Fig. 2 the real and imaginary parts of the *effective* permeability are plotted, calculated from Eqs. (10), (11), (15), and (16), together with some experimental points for supermalloy at 24,400 mc/sec. It is seen that the theory is generally confirmed. The ratio $|\mu_R/\mu_L|$ is much larger than the more familiar quantity $|\mu_2/\mu_1|$. The detuning of the cavity was 8 mc/sec. from the maximum to the minimum in μ_L and the anomalous dispersion is demonstrated quantitatively by this ex-

TABLE I. Nickel.

Temp.	Frequency mc/sec.	H_0^{max} gauss	$4\pi M_s$ gauss	g	μ_R^{max}	$1/T_2$
24°C	24410	5400	6000	2.24	34	$5.0^5\times10^9$ sec.$^{-1}$
114	24380	5550	5700	2.20	32	5.0^5
190	24350	5800	5100	2.19	21	6.4^5
254	24330	5950	4500	2.20	12	9.7
314	24320	6600	3300	2.16	7	11.0
341	24310	7000	2200	2.18	3.5	13.8
358	24280	7200	1000	2.26	1.5	14.5
24	9050	1160	6000	2.23	85	3.3^5

TABLE II. Supermalloy.

Temp. °C	Freq. mc/sec.	H_0^{max} gauss	H_0^{min} gauss	$4\pi M_s$ gauss	g	μ_R^{max}	$1/T_2$ sec.$^{-1}$
28	24310	5150	300	7900	2.13	110	2.1×10^9
126	24290	5400	1000	7250	2.11	79	2.6
179	24280	5550	1350	7000	2.10	71	2.7
246	24250	5700	2000	6250	2.11	71	2.4
311	24230	6150	3000	5450	2.07	46	3.0
355	24210	6300	3600	4680	2.10	38	3.0
407	24200	7100	5300	3280	2.06	8.7	8.1
				(2500)	(2.11)		(6.2)
420	24190	7400	6100	2250	2.05	4.5	10.5
				(1500)	(2.15)		(7.0)
440	24180	8200	?	——		2.0	
24	9050	1040	——	7800	2.10	300	1.3

periment. We shall now proceed with a more systematic discussion and plot μ_R on a logarithmic scale to bring out more detail in the wings of the absorption curve.

(a) Nickel

The experimental values for μ_R at 24,400 mc/sec. together with the theoretical curves, are shown in Fig. 3 for various temperatures. The three parameters, γ, T_2, and M_0, occurring in (10) and (11) have to be determined. Note that ω is a constant and ω_0 is a variable, changing with H_0 in our experiment. The values for M_0 have been taken from the static magnetization experiments of Weiss and Forster.[13] At low temperatures the magnetization is practically constant but drops off rapidly in very small fields. For temperatures close to the Curie temperature, M_0 increases continually with increasing H_0. Then γ and T_2 are determined from the position and the value of the maximum absorption according to the relations

$$\omega=\gamma\{H_0^{max}(H_0^{max}+4\pi M_0)\}^{\frac{1}{2}} \tag{20}$$

and

$$(1/T_2)=4\pi\gamma^2 M_0(H_0^{max}+4\pi M_0)/\omega\mu_R{}^{max}. \tag{21}$$

The main uncertainty in g, which is proportional to γ according to Eq. (1c), comes from inaccurate knowledge of M_0; H_0^{max} was measured with an error of 0.5 percent, except at the highest temperatures, where the line becomes broad and the intensity small. The error in g is probably between 1 and 2 percent. The values of g are listed in Table I; $g=2.20$ remains constant over the whole temperature range, within the limits of error. The uncertainty in T_2 is much larger, the same as in μ_R, as discussed in the preceding section. Nevertheless, it can be established beyond doubt from the listed values that the half-width between the points where μ_2 has dropped to half its maximum value increases from 250 gauss at room temperature, first slowly and then above 200°C more rapidly, to about 750 gauss at 358°C. At the Curie point no discontinuity occurs in the absorption curve, but at higher temperatures the signal soon becomes unobservably small because of the rapid decrease in magnetization M_0. It is furthermore seen that the shape of the absorption curve is also well represented by the theoretical formulas (10) and (11). The minimum is brought out clearly and shifts more rapidly than the maximum toward higher field strengths as the temperature is increased and the magnetization decreased.

The results for room temperature at 9030 mc/sec. are shown in Fig. 4, and are also included in the table. The g factor is the same, but the line width $\Delta\omega$ calculated from the maximum is decreased by a factor 1.5.

(b) Supermalloy

Unfortunately no values for the saturation magnetization have been published, except at room temperature.[12] In order to determine M_0 we use in addition to Eq. (20) the relation

$$\omega=\gamma(H_0^{min}+4\pi M_0), \tag{22}$$

where H_0^{min} is the field at the minimum in the absorption curve. Then γ and M_0 are solved from (20) and

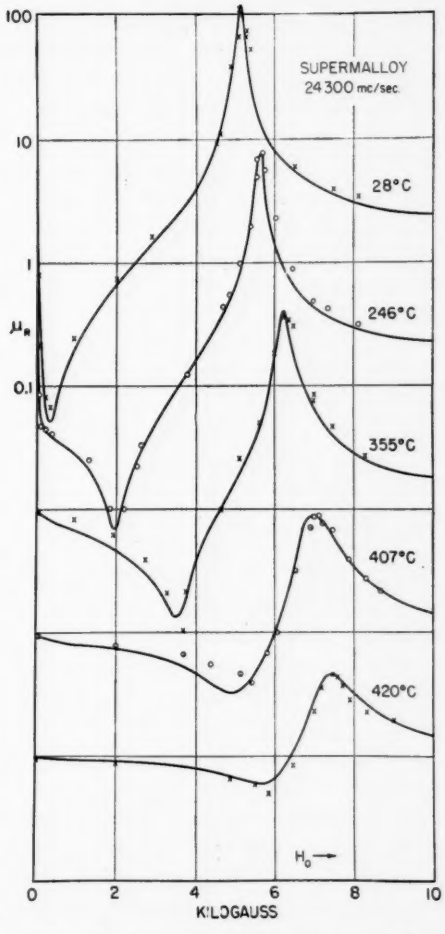

FIG. 5. The effective permeability of supermalloy at 24300 mc/sec. for various temperatures. Each curve is lowered by one decade with respect to the one above it. The numbers along the ordinate axis apply to the top curve. The drawn lines have been calculated theoretically.

[13] See, e.g., R. Becker and W. Döring, *Ferromagnetismus*, (Julius Springer, Berlin, 1939), p. 25.

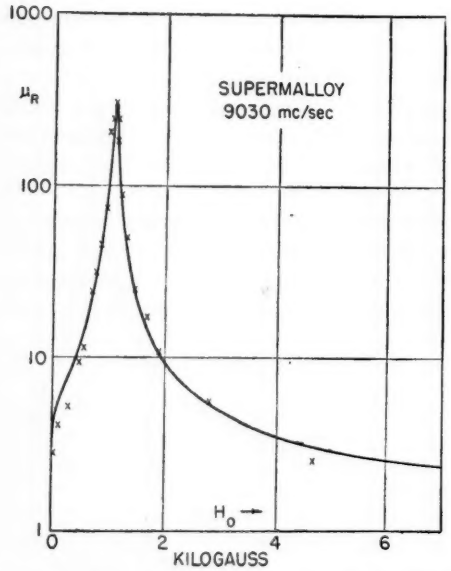

FIG. 6. The effective permeability of supermalloy at 9030 mc/sec. at room temperature.

(22). Equation (22) was first derived by Kittel,[3] and is based on the assumptions that the line-width is small and that the variation in μ_2 may be neglected at the position of the minimum, and also that M_0 is independent of H_0. This procedure can therefore not be applied at higher temperatures where the line gets broader, the maximum and minimum are close together and M_0 is not constant. In general the calculated values for M_0 listed in Table II will be too high. At room temperature there is good agreement, but comparison with preliminary unpublished data from the Bell Telephone Laboratories shows that our values between 200°C and 400°C are a few hundred oersteds too high. Much larger deviations must be expected near 400°C. To show the influence on g and T_2 of lower values of M_0, more probable values of M_0 have tentatively been added to the table between brackets for the highest temperatures. Within this uncertainty in M_0 the value of $g=2.12$ is constant over the whole temperature range. Yager reported earlier $g=2.17$, but informed the author that this value is not final. Experimental points and theoretical curves for μ_R in supermalloy have been plotted in Fig. 5. There is fair agreement even far out in the wings of the curve. The half-width at room temperature is 105 gauss, 2.5 times smaller than for nickel. It remains practically constant up to 300°C, then rises rather abruptly by a factor of 3 near the Curie point, which is at about 400°C. Again no discontinuities occur at this point, but the intensity decreases rapidly proportional to the magnetization. In Fig. 7 the line-widths in supermalloy and nickel are plotted as functions of temperature.

The values of μ_R at 9050 mc/sec. are shown in Fig. 6. The g-factor is independent of the frequency, but the width $\Delta\omega$ is decreased by a factor 1.6. The minimum does not appear, since even in zero field the condition (22) cannot be satisfied at this frequency.

IV. COMPARISON WITH THEORY

The anomalous g values have been discussed by Kittel.[14] New and more precise measurements seem to converge to the lower end of the range of experimental values quoted in Kittel's paper. So do ours, but the experimental g values are still too high to fit the relation $g-2=2-g'$, where the magneto-mechanical ratio $g'=1.92$ for nickel. A quantum mechanical derivation of this relation has been given recently by Van Vleck.[15] No reason can be given for the discrepancy. The effect of the finite skin depth[16]—the term with $\nabla^2\mathbf{M}$ in Eq. (3)—would lower g by only 0.1 percent. The term with the anisotropy energy will change g, depending on the orientation of the crystalline sample with respect to the magnetic field. Since we work with a polycrystalline material, this effect will tend to broaden the line, but the center position will remain unaffected. A unidirectional stress on the sample, however, might produce a shift of the whole line. This effect did not occur, as

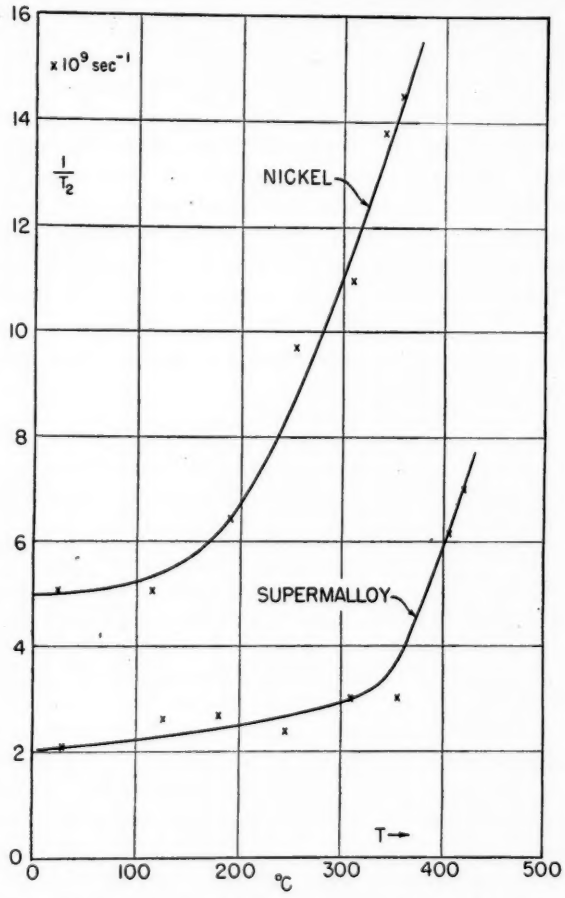

FIG. 7. Line-widths in nickel and supermalloy as functions of temperature at 24400 mc/sec.

[14] C. Kittel, Phys. Rev. **76**, 743 (1949).
[15] J. H. Van Vleck, Phys. Rev. **78**, 266 (1950).
[16] C. Herring and C. Kittel, Phys. Rev. **77**, 725 (1950).

could be demonstrated by rotating the whole sample; no shift of the resonance line occurred. It seems reasonable that the g value does not change with temperature, because the very small variation in lattice configuration by heating is not expected to alter the contribution of the orbital motion to the g value.

Various causes which contribute to the line width can be listed in the following way:

(a) The dipolar interaction between the spins has been discussed by Van Vleck.[15] At the absolute zero the contribution to the second moment from the magnetic interaction between neighboring spins vanishes. This may be understood directly from the physical fact that all spins are perfectly aligned and so the enrivonment of every spin is exactly the same. As the temperature is increased more and more spins turn antiparallel, causing a decrease in M_s and contributing to a dispersion of the local field values for the different spins. Finally, above the Curie temperature about as many spins are parallel as antiparallel and the second moment is then given by Van Vleck's formula for paramagnetic salts.[17] There should then be a continuous increase of the second moment from zero to the paramagnetic value, which is of the order of 2000 gauss. But the exchange forces, which enhance the fourth moment,[17] will narrow the line by a large factor, approximately given by $h\Delta\omega/J=10^4$, where J is the exchange energy and $\Delta\omega$ is the observed width. Therefore, the contribution to the effective width from the dipolar interaction should be less than 1 gauss even above the Curie temperature. No rigorous calculation of the fourth moment is available and the estimate is admittedly very rough. But in some organic paramagnetic salts, where the exchange integral is a hundred times smaller, line widths of only a few gauss have been reported.[18] Since, moreover, the temperature dependence of the dipolar broadening should be different, we can be certain that the observed widths must be explained in a different way. Akhieser[19] calculated the interaction within the spin system by considering collisions between spin waves. He gives a value of $T_2{}^*=10^{-7}$ sec. at 10°K. If we use his formula for the temperature dependence, we find $T_2=10^{-9}$ sec. at room temperature, corresponding roughly to 10 gauss. This is much too small, in agreement with our previous remark and Akhieser's observation that the spin-lattice interactions play a more important role at 300°K.

(b) Van Vleck introduced anisotropic quasi-dipolar interactions to explain the magnetic anisotropy in a cubic crystal like nickel. It has already been pointed out that the anisotropy energy will have an influence on the resonance condition. The shift in the resonance field is of the order of $2K_1/M_s$, where K_1 is the anisotropy constant decreasing rapidly with increasing temperature for nickel. In a polycrystalline sample of nickel we would expect the line to be broadened by about 40 gauss at 20°C and much less at higher temperatures. But apparently this effect is very much smaller than the observed widths in nickel. In supermalloy the anisotropy constant is still much smaller than in nickel.

Van Vleck points out, however, that the anisotropic spin interactions, in the presence of impurities, may give a broadening of the line. This contribution, dependent on the density of crystalline imperfections, would not vanish at the absolute zero.

(c) The effect of the finite skin depth on the line width can be estimated in different ways. Using the picture of Bloch waves, the microwave field will create a spin wave near the surface. The time it takes for the excited wave to travel one interatomic distance a is h/J, and to diffuse outside the skin depth $T_2{}^*\sim\delta^2h/Ja^2$. When we take $J/h=10^{13}$, $\delta=2\times10^{-5}$ cm, $a=4\times10^{-8}$ cm, this corresponds to a width of 0.1 gauss. The same order of magnitude is obtained if we put $c\nabla^2M=4\pi i\mu\omega M$ in Eq. (3) and go through the steps of the derivation of (10) with this term included. A term $\delta(y)\partial M/\partial y$ should be added to account for the discontinuity in $\partial M/\partial y$ at the boundary.

All causes discussed so far determined $T_2{}^*$. We shall now turn to the interaction of the spin system with the outside world, which determines T_1.

(d) The interaction of the spin waves with the lattice vibrations has been treated by Akhieser. He obtains $T_1=10^{-6}$ sec. at 10°K. Unfortunately his formula is not valid at higher temperatures and does not include the case in which an external constant field H_0 is present. We should have $T_1=1.5\times10^{-10}$ sec. at 300°K in order to explain the observed width in nickel. This does not seem unreasonable. But Polder[20] claims that Akhieser's theory yields too small relaxation times, because only spin waves with long wave-lengths should be taken into account for ferromagnetic resonance. The width in nickel changes approximately proportionally to the square of the absolute temperature at 300°K and more nearly directly proportionally to T at room temperature. But in supermalloy there seems to be a large temperature range with little variation in the width, which would be hard to explain with spin-lattice interaction.

(e) Finally, another mechanism of relaxation is suggested: the interaction of the ferromagnetic spins with the conduction electrons. No theory is available for the collision process of the spin waves with the conduction electrons. However, if we describe the process as one in which the magnetic quantum number m of the ferromagnetic spin system changes by unity and the corresponding magnetic energy quantum $h\nu_0$ is taken up by the conduction electron, we can obtain an estimate of the probability by using the formula which Heitler and Teller derived in their theory of nuclear magnetic

[17] J. H. Van Vleck, Phys. Rev. **74**, 1168 (1948).
[18] Holden, Kittel, Merritt, and Yager, Phys. Rev. **77**, 147 (1950).
[19] A. Akhieser, J. Phys. U.S.S.R. **10**, 217 (1946).
[20] D. Polder, Phil. Mag. **40**, 99 (1949).

relaxation in metals, and which has been verified experimentally.[21] One finds

$$1/2T_1=\frac{|V_{ij}|^2}{E_0^2}\frac{kT}{h}, \tag{23}$$

where E_0 is the Fermi energy and V_{ij} is the matrix element of interaction between a ferromagnetic and conduction electron, connecting states with $\Delta m=\pm 1$. This interaction consists of a magnetic dipolar term of the order of $\beta^2 a^{-3}\sim 1$ cm^{-1}, where β is the Bohr magneton and a the atomic radius, and an exchange interaction. Only if we take for the latter a large value so that $V_{ij}\approx 100$ cm^{-1}, would we find the right order of magnitude $T_1\sim 5\times 10^{-10}$ sec. to explain the observed width, which should vary proportionally to the absolute temperature.

V. CONCLUSION

The discussion of the preceding section may be summarized in the following conclusions. The increase in width, approximately as T^2, for temperatures higher than 300°C can be understood as a decrease in spin-lattice relaxation time. The absence of a discontinuity at the Curie point is in agreement with this explanation. Above that point, where the substance is paramagnetic, the causes of line broadening are well known and spin-lattice interactions alone can account for the observed width. Collisions with lattice phonons seem to be a more likely cause than collisions with conduction electrons, although a theoretical treatment for the latter process is wanting.

The very slight, if any, variation of the width in supermalloy below 350°C remains unexplained. The dipolar interaction and the finite skin depth exchange effect do not give the right order of magnitude. Only Van Vleck's suggestion of a combination of anisotropic forces and imperfections of the lattice remains a possibility. However, the variation of T_2 with frequency, approximately as $\omega^{-\frac{1}{2}}$ at room temperature, is not to be expected from any of the causes (a), (b), or (c), but could be reconciled with a spin-lattice mechanism.

There is no reason to expect perfect agreement of the *shape* of the experimental curve with theory. The shape given in Eqs. (10) and (11) is merely a consequence of the phenomenological introduction of damping terms in Eq. (1). The broadening by dipolar interaction alone would, for example, produce a Gaussian-like distribution, but the exchange interaction would make the intensity in the wings larger and produce more resemblance with the resonance curve of a damped harmonic oscillator. This curve one should expect for the spin-lattice relaxation mechanism and it is therefore gratifying that the experimental data fit this type of curve rather well. It is not warranted to assume the damping term $1/T_2$ to be proportional to H_0, if one uses the Bloch equation; $1/T_2$ is a function of the frequency and temperature only.

More experimental data are needed, first of all measurements on the width at low temperatures. A single crystal of nickel should be used to avoid dispersion of the resonance frequencies by increasing anisotropy. In the second place, experiments on insulators like the ferrites at low temperatures would be useful. The effect of the conduction electrons is then eliminated. Finally, saturation experiments at a high level of the microwave power will give definite information about T_1 separately, so that the spin-lattice theories may be tested directly.

The author is greatly indebted to Professor Van Vleck and Dr. Kittel for illuminating discussions on the theoretical aspects, to Mr. Yager for discussion and communication of his experimental results before publication, and to Mr. Cooke and the staff of the Electronics Research Laboratory for advice and aid in microwave techniques.

[21] N. Bloembergen, Physica **15**, 588 (1949).

Magnetic Resonance Absorption in Nitric Oxide

ROBERT BERINGER AND J. G. CASTLE, JR.*
Sloane Physics Laboratory, Yale University,† New Haven, Connecticut
(Received January 24, 1950)

The nine-line magnetic resonance spectrum of $N^{14}O^{16}$ is observed at fields in the range of 8600 oersted at a frequency of 9360 megacycle/sec. The spectrum arises from magnetic-dipole transitions between Zeeman levels in the $J=\frac{3}{2}$ state of the $^2\Pi_{3/2}$ spin component. The line positions allow a determination of the magnetic IJ coupling constant, which is 29.8 ± 0.3 megacycle/sec., and the nuclear electric quadrupole coupling, which is -1.7 ± 0.5 megacycle/sec. The line position and triplet spacings, which arise from molecular perturbations, are in good agreement with the theory of Margenau and Henry. The absolute intensity of the three stronger lines is measured to be $\chi''=1.2\times10^{-10}$ which also agrees with theory.

1. INTRODUCTION

THIS paper describes an investigation[1] of the magnetic levels of one of the rotational states of the paramagnetic gas NO. The experiments employ the principle of magnetic resonance and have much in common with other recent applications of this principle.[2] They fall into the general class which is termed magnetic resonance absorption experiments.

When a gas composed of molecules possessing permanent magnetic moments is placed in a magnetic field, the degeneracies associated with the magnetic quantum numbers are removed and the energy levels are split into a number of Zeeman components. Transitions between pairs of these component levels are generally permitted for magnetic-dipole radiation. Since the permanent magnetic moments are of the order of Bohr magnetons, the frequencies of these transitions lie in the microwave region for field strengths of a few thousand oersteds. For such frequencies the Einstein coefficient of spontaneous emission is negligibly small as compared with the equal coefficients of induced emission and of absorption, so that the transition probabilities for absorption and emission are essentially equal. However, molecular collisions bring the gas to an equilibrium state in which there is a preferential population of the less energetic states. Thus there are more absorption than emission transitions, which produces a net absorption of an electromagnetic wave which satisfies the polarization rules and the Bohr frequency condition for the two levels involved. There is also an anomolous dispersion[3] but this is not exploited in the present experiments.

The paramagnetic molecule NO follows Hund's coupling case (a) to a fair approximation.[4] The electronic orbital motion and spin are strongly coupled to the internuclear axis and weakly coupled to the nuclear rotation. In the ground electronic state $\Lambda=1$ and $\Sigma=\frac{1}{2}$. The resulting doublet has a large ($\sim$120 cm^{-1}) separation. The upper or $^2\Pi_{3/2}$ doublet component possesses an electronic magnetic moment and is responsible for the paramagnetism of the gas. At room temperatures ($kT\sim200$ cm^{-1}) a number of rotational

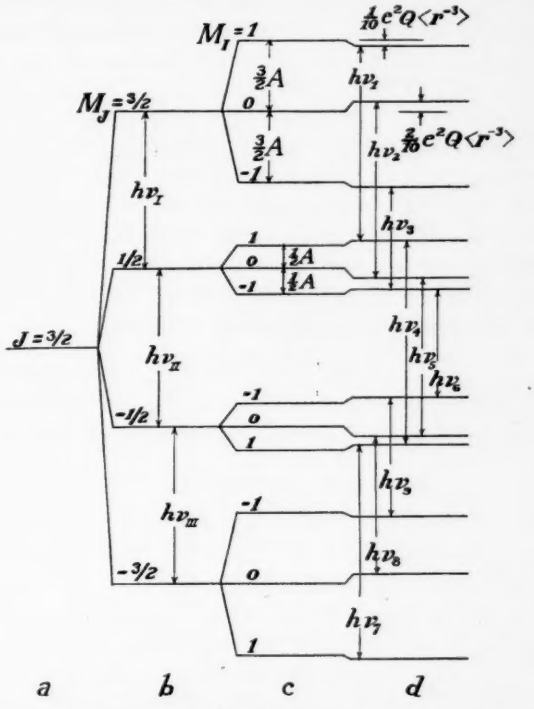

FIG. 1. Energy level diagram of the $J=\frac{3}{2}$ level of the $^2\Pi_{3/2}$ state of $N^{14}O^{16}$. Stage (a) is in the absence of magnetic field. Stage (b) shows the magnetic levels considering only molecular effects. Stage (c) includes the nuclear electric quadrupole IJ coupling. The nine transitions $\Delta M_J=\pm1$, $\Delta M_I=0$ are shown in stage (d). Arabic indices on the transitions correspond to the labeling of the observed absorption lines.

Note: The quadrupole energies labeled $1/10e^2Q\langle r^{-3}\rangle$ and $2/10e^2Q\langle r^{-3}\rangle$ should be written $1/20eQq$ and $2/20eQq$ respectively in accord with Eq. (14) of reference 4a.

* Dupont Company Fellow in Physics (1949–1950).

† Assisted by the ONR.

[1] A preliminary report is given by R. Beringer and J. G. Castle, Jr., Phys. Rev. **76**, 868 (1949).

[2] These include the experiments of Purcell, Torrey, and Pound, Phys. Rev. **69**, 37 (1946) on nuclear magnetic resonance absorption; those of Bloch, Hansen, and Packard, Phys. Rev. **69**, 127 (1946) on nuclear induction; those of E. Zavoisky, J. Phys. U.S.S.R. **9**, 211, 245 (1945) on magnetic resonance by paramagnetic ions; and those of J. H. E. Griffiths, Nature **158**, 670 (1946) on ferromagnetic resonance.

[3] The general Kramers-Kronig relation, H. A. Kramers, Atti Congr. Fis., Como (1927) 545 connects the absorption and dispersion.

[4] G. Herzberg, *Molecular Spectra and Molecular Structure* (Prentice-Hall, Inc., New York, 1939), pp. 241, 242, 326, 502.

states of this upper component are appreciably populated; of these, the lowest ($J=\frac{3}{2}$) is of concern here.

Vector model considerations[4] give a system of four magnetic levels, $M_J=\frac{3}{2}, \frac{1}{2}, -\frac{1}{2}, -\frac{3}{2}$, spaced by $(\frac{4}{5})H\mu_0$ erg for the $J=\frac{3}{2}$ rotational level of the $^2\Pi_{3/2}$ state; μ_0 is the Bohr magneton $eh/2mc$ and H the applied field in oersted. This level system is shown in stage (b) of Fig. 1. Such a level system would give rise to three coincident transitions of frequency ($4H\mu_0/5h$) cycle/sec. for magnetic-dipole radiation ($\Delta M_J=\pm 1$). As might be expected, however, this coincidence is removed by field-uncoupling in the molecule and the perturbations of nearby states. Thus ν_I, ν_{II}, and ν_{III} of Fig. 1 differ from each other and from $4H\mu_0/5h$. The accompanying paper by Margenau and Henry[4a] sets forth an exact theory of the magnetic energy states in NO.

In addition to these molecular distortions, hyperfine structure is to be expected, since the nucleus N^{14} possesses a spin ($I=1$), a magnetic moment, and an electric quadrupole moment. In distinction to the usual case of molecules in $^1\Sigma$ states the magnetic IJ coupling will be large in this molecule because of the electronic magnetic moment. The nuclear electric quadrupole coupling will add to this. The result of these two interactions is to split each M_J state into three M_I components. A twelve-level pattern results and transitions $\Delta M_J=\pm 1$, $\Delta M_I=0$ give rise to a nine-line absorption spectrum (see stages (c) and (d) of Fig. 1). For pure magnetic IJ coupling and strong magnetic fields the M_I components would be symmetrical around the M_J levels, and the nine-line spectrum would be composed of triplets of constant spacing. Electric quadrupole coupling removes this constant spacing. It should be noted that the spectrum $\Delta M_I=\pm 1$; $\Delta M_J=0$ lies in the radiofrequency range and is not observed here.

2. APPARATUS

The experiment consists in noting the absorption which results from transitions brought about by a microwave magnetic field in a gas-filled resonant cavity when a transverse d.c. magnetic field is adjusted for resonance with one of the transitions.

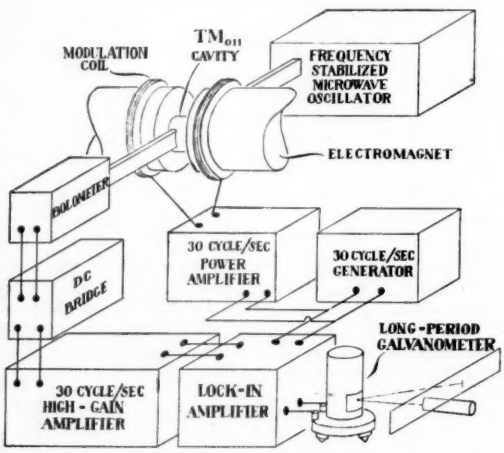

FIG. 2. Schematic diagram of the microwave magnetic resonance absorption apparatus.

The main components of the apparatus are shown in Fig. 2. The oscillator, a 723A/B klystron, is stabilized by a microwave discriminator and d.c. amplifier following the method of Pound.[5] A brass wave guide leads from the oscillator to the circular-cylinder cavity which is resonant at 9360 mc/sec. in the TM_{011} mode. The cavity is machined from commercial copper and is isolated by vacuum-tight mica windows. It is coupled to the incident and emergent wave guides by circular irises of 0.250 inch diameter. The measured loaded and unloaded Q-values at room temperature are 3500 and 8400 respectively. The cavity is placed between the poles of a Weiss design (Société Genevoise) electromagnet with plane parallel pole faces of 5.7 inches diameter spaced by 1.8 inches. The microwave H field in the cavity lies entirely in planes normal to the H field of the magnet.

The wave guide emergent from the cavity goes to a matched bolometer[6] mounted in a tuneable wave guide circuit. This bolometer forms one arm of a high impedance d.c. bridge which is in balance for a bolometer resistance of 200 ohms. In place of the usual balance meter there is connected a high gain (voltage gain of 2.2×10^6) audio amplifier of 2 cycle/sec. noise-band width[7] centered at 30 cycle/sec. The output from this amplifier is impressed on a balanced lock-in[8] mixer which receives its local-oscillator voltage from a small 30 cycle/sec. a.c. generator driven by a synchronous motor. The d.c. output from the lock-in mixer deflects a critically damped galvanometer of 0.04 cycle/sec. band width. A conventional audio power amplifier takes a 30 cycle/sec. signal from the same generator and energizes a pair of modulation coils wound on the magnet poles. These produce a 30 cycle/sec. sinsudoidal modulation of the d.c. magnetic field, uniform in space and variable from 1 to 200 oersted, peak-to-peak.

The main coils of the magnet are energized by a compound-wound d.c. generator which receives its excitation from a conventional degenerative voltage stabilizer using the terminal voltage of the magnet coils as a control voltage. A voltage derived from dry batteries is balanced against the magnet voltage and is used to set the magnet current. The short-term stability of the magnetic field is about one part in ten thousand. The magnet current is monitored with a L and N type-K potentiometer connected across a resistor in series with the magnet coils. Recently we have used an improved current stabilizer of the type described by Lawson and Tyler[9] as modified by Wadey.

In operation the microwave oscillator is tuned to the

[4a] H. Margenau and A. Henry, Phys. Rev. **78**, 587 (1950).

[5] R. V. Pound, Rev. Sci. Inst. **17**, 490 (1946).

[6] Similar to the Sperry No. 921 barretter.

[7] J. M. Sturtevant, Rev. Sci. Inst. **18**, 124 (1947).

[8] Similar to that of R. H. Dicke, Rev. Sci. Inst. **17**, 268 (1946).

[9] J. L. Lawson and A. W. Tyler, Rev. Sci. Inst. **10**, 304 (1939); W. G. Wadey, Thesis, University of Michigan (1948).

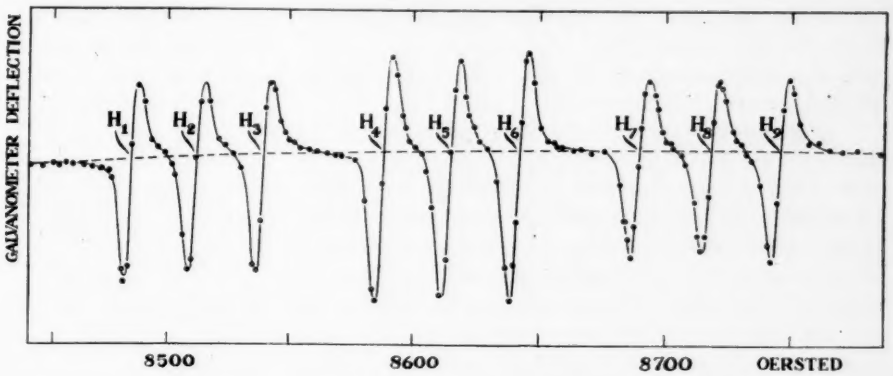

FIG. 3. Observed spectrum of $N^{14}O^{16}$ at a pressure of 1.0 mm Hg. The modulation amplitude is 3.2 oersted peak-to-peak.

cavity resonance where some four milliwatts of microwave power is transmitted to the bolometer. The d.c. magnetic field is then raised to the region of a magnetic absorption line. Modulation of the d.c. magnetic field produces amplitude modulation of the microwave power which modulates the bolometer resistance; hence a 30 cycle/sec. signal appears at the input of the amplifier. As the d.c. magnetic field is increased the galvanometer deflection traces essentially the derivative of the absorption line; phase is preserved by the lock-in mixer.

3. SENSITIVITY

The apparatus described has a high signal-to-noise ratio resulting from the mode of operation of the bolometer and the narrow noise-band width of the amplifying system. Because of the relatively high values of the signal power, it does not suffer from the usual low sensitivity of single-detection receivers.[10] For most microwave spectra these high power levels would not be permissible because of energy saturation of the absorption, and a bolometer system would be quite insensitive. However, the weak magnetic absorption lines require large energy densities for saturation. In contrast to crystal detectors, bolometers do not produce low frequency noise in great excess of thermal noise. In the present system flicker noise in the amplifier is the principal noise contribution.

The resistance-power law for bolometers is given by[11]

$$R-R_0=K(P+i^2R)^n$$

where R is the operating resistance, R_0 the cold resistance, K a constant, P the microwave power, i the bolometer current, and n a constant (<1) describing the deviations from square-law response. A simple analysis shows that for a fixed total power, the sensitivity (idR/dP) of a bolometer in a constant-current circuit is a maximum for equal d.c. and microwave power. For the bolometer used this optimum sensitivity is 46 volt/watt at the bolometer terminals for a total power of 9 milliwatts.

The microwave power absorbed by the bolometer can be written as

$$P+P2(Q_L/Q_A)S\cos\omega_m t$$

where Q_L is the loaded Q of the cavity, Q_A the Q of the absorption line, $\omega_m/2\pi$ the modulation frequency and S a constant depending on the field configuration in the cavity and the value of the magnetic field modulation. In the present case S attains a maximum value of 0.5. Q_A may also be expressed as

$$Q_A=1/(4\pi\chi'')$$

where χ'' is the imaginary part of the magnetic susceptibility describing the absorption. The r.m.s. signal voltage at the bolometer terminals is

$$\epsilon_s=9.0\times10^3\chi''=720/Q_A \text{ volts.}$$

for the present system. The observed r.m.s. noise voltage at the same terminals is 2×10^{-8} volt. Thus for a signal-to-noise ratio of unity χ'' is 3×10^{-12} and Q_A is 3×10^{10}.

4. EXPERIMENTAL RESULTS

The nitric oxide was produced by the slow reaction of metallic copper with dilute nitric acid. The reaction was carried out at 0°C. The gaseous products were purified of nitrogen and the other oxides of nitrogen by fractional distillation at liquid nitrogen temperatures. The resulting NO is believed to be quite pure.

Several runs at different values of NO pressure and modulation amplitude were taken. All showed the characteristic nine-line spectrum shown in Fig. 3.

TABLE I. Values of resonance field in oersted for the nine absorption lines in NO. Observing frequency is 9360 megacycle/sec. The absolute errors in the field values may be as much as 1 oersted.

$H_1=8481.5$	$H_5=8614.2$
$H_2=8508.2$	$H_6=8641.2$
$H_3=8536.8$	$H_7=8689.4$
$H_4=8586.8$	$H_8=8717.5$
	$H_9=8744.4$

[10] The well-known superiority of a superhetrodyne receiver over a single-detection receiver for small signal detection is not carried over to the detection of small modulations of a large signal, since in the latter case the square-law response of the single-detection receiver is no longer operative. The modulation sidebands beat with the strong signal carrier giving a first-order demodulation signal.

[11] Radiation Laboratory Series (McGraw-Hill Book Company, Inc., New York, 1947), Vol. 11, p. 161.

The line locations are described by the numbers giving the field at the center of each line. Table I collects the average values of these data. The arabic indices correspond to those of Figs. 1 and 3.

The magnetic field intensity was measured at the position of the cavity in terms of the magnetic-resonance field of the proton moment. A regenerative detector, whose grid coil contained distilled water, and an audio amplifier were used to display the proton resonance on an oscilloscope.[12] A U. S. Signal Corps BC221 frequency meter was coupled loosely to the regenerative detector and the regeneration frequency located by zero-beat on the oscilloscope. The frequency meter was in turn calibrated against the standard frequency broadcasts of WWV. The conversion formula[13] $H=2.3487\times10^{-4}f$ served to convert the frequency values to field intensities. The principal error in the magnetic field values arises from geometrical uncertainties. The random errors are less than this and result from current fluctuations in the magnet which set a limit of perhaps 0.2 oersted.

The microwave frequency was monitored with a M.I.T. Radiation Laboratory TSX-4SE spectrum analyzer and measured with a TFX-19GA cavity wave meter. The absolute value of the microwave frequency is subject to an unknown calibration uncertainty but is believed to be accurate to 2 megacycle/sec. The cavity was calibrated against a standing wave machine to a precision of 6 megacycle/sec. Unfortunately no crystal-controlled microwave frequency standard was available at the time of the experiments.

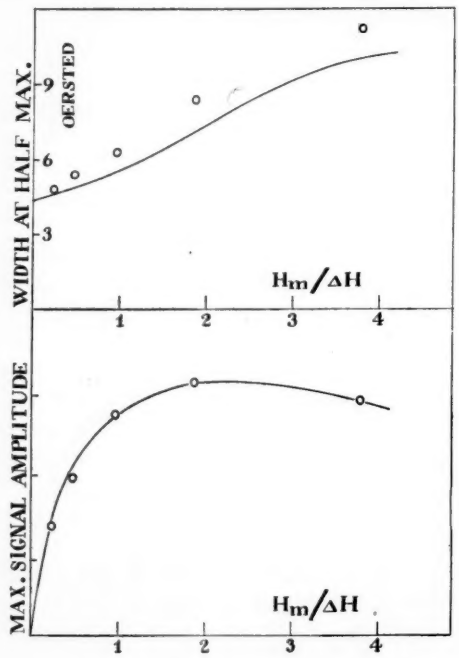

FIG. 4. Variation of line width and amplitude of magnetic resonance lines of NO with modulation amplitude. The pressure is 0.85 mm Hg and the temperature 298°K. $2H_m$ is the peak-to-peak modulation amplitude and ΔH the Van Vleck line half-width. Solid lines are drawn for pure pressure broadening with $\Delta H=3.5$ oersted. The deviations in the upper curve arise from broadening due to magnetic field inhomogeneity.

[12] Similar to that of N. J. Hopkins, Rev. Sci. Inst. **20**, 401 (1949).
[13] Thomas, Driscoll, and Hipple, Phys. Rev. **75**, 902 (1949).

5. LINE WIDTHS

Because of distortions introduced by the large magnetic field modulation, which is required for optimum sensitivity, the output galvanometer deflections do not trace the derivative curve of an absorption line. Actually, one observes the fundamental-frequency Fourier amplitude of the modulated absorption-function of the line.

If one assumes that pressure broadening is the only source of line broadening, then at the low pressures used the Lorentz or Van Vleck-Weisskopf line shape[14] should be correct, and one can write the imaginary part of the magnetic susceptibility (normalized to unity and expressed in terms of field strengths rather than frequencies) as

$$\frac{\Delta H}{(H-H_0)^2+\Delta H^2},$$

where H is the applied d.c. and modulation field and H_0 its value at resonance. Thus

$$H=H_0+H_1-H_m\cos\omega t,$$

where $2H_m$ is the peak-to-peak modulation amplitude and $\omega/2\pi$ the modulation frequency. The coefficient of the signal voltage at the modulation frequency is proportional to

$$\frac{1}{\pi}\int_{-\pi}^{\pi}\frac{\cos\omega t\,d(\omega t)}{[H_1/\Delta H+H_m/\Delta H-H_m/\Delta H(1+\cos\omega t)]^2+1}.$$

This integral is evaluated[15] for various values of $H_1/\Delta H$ and $H_m/\Delta H$. It is found that the maximum value of the signal voltage occurs for $H_m=2\Delta H$. For higher modulation amplitudes the signal amplitude decreases slowly and the lines are broadened. For smaller modulations the signal amplitude decreases rapidly and assumes the shape of the derivative curve.

The line half-width ΔH may be obtained by plotting certain parameters of the theoretical signal amplitude curves *vs.* the modulation amplitude. Figure 4 shows two such curves drawn for $\Delta H=3.5$ oersted at the pressure 0.85 mm Hg and temperature 298°K. From various line contour measurements it appears that the line shapes cannot be fitted in exact detail by the above procedure. Some other source of broadening is present, probably arising from magnetic field inhomogeneities. This might reduce ΔH by as much as 1.0 oersted. The line width appears to be proportional to pressure in the

[14] J. H. Van Vleck and V. F. Weisskopf, Rev. Mod. Phys. **17**, 227 (1945).
[15] Similar integrals appear in a paper by W. D. Hershberger, J. App. Phys. **19**, 411 (1948).

TABLE II. Formulas for the resonance field values for the nine absorption lines.

$M_J \to M_J-1$	M_I	Resonance field
$\frac{3}{2}\to\frac{1}{2}$	1	$H_1 = H_I - H_D + (2/10)H_Q$
	0	$H_2 = H_I - (4/10)H_Q$
	−1	$H_3 = H_I + H_D + (2/10)H_Q$
$\frac{1}{2}\to-\frac{1}{2}$	1	$H_4 = H_{II} - H_D$
	0	$H_5 = H_{II}$
	−1	$H_6 = H_{II} + H_D$
$-\frac{1}{2}\to-\frac{3}{2}$	1	$H_7 = H_{III} - H_D - (2/10)H_Q$
	0	$H_8 = H_{III} + (4/10)H_Q$
	−1	$H_9 = H_{III} + H_D - (2/10)H_Q$

range around 1 mm Hg. This proportionality has not been checked at higher pressures because of overlapping of the lines. Assuming that the line width is proportional to pressure it becomes 0.11 cm^{-1} at 76 cm Hg and 25°C.

6. LINE INTENSITIES

The intensities of the transitions, $\Delta M_J = \pm 1$, observed can be calculated from radiation theory using the matrix elements derived in the accompanying paper of Margenau and Henry. We will follow a scheme similar to that used by Bloembergen, Purcell, and Pound[16] in their calculation of the intensity in nuclear magnetic-resonance absorption.

Consider a system of N nitric-oxide molecules per cm^3 characterized by quantum numbers M_J; the hyperfine splitting will be neglected at this stage of the calculation. The molecules are in a d.c. and modulation field along z represented by H and a microwave field of frequency $\omega/2\pi$ given by

$$H_x = 2H_1 \cos\omega t,$$

which, near resonance, can be replaced[17] by a rotating field

$$H_x = H_1 \cos\omega t \quad H_y = H_1 \sin\omega t.$$

The probability per sec. of a transition $M_J \to M_J - 1$ for a single molecule is given by radiation theory as

$$W_{M_J \to M_J-1} = (8\pi^3/3h^2)\,|(M_J|\mathfrak{M}|M_J-1)|^2 \rho_\nu$$

where $\rho_\nu d\nu$ is the isotropic energy density and $\mathfrak{M}$ the magnetic moment operator producing the transition.

In this case the local energy density is replaced by

$$\rho_\nu = (3H_1^2/4\pi)g(\nu),$$

where $g(\nu)$ is a shape factor of the line normalized so that

$$\int_0^\infty g(\nu)d\nu = 1.$$

In contrast to optical absorption, the observing frequency is sharp and the dispersion in final states arises from the breadth of the line.

In the Margenau and Henry paper the square of the matrix elements for the transition is shown to be (see Eq. (15) of that paper).

$$0.386(\tfrac{3}{2}+M_J)(\tfrac{5}{2}-M_J)\mu_0^2$$

for the $J=\frac{3}{2}$ states.

For a Lorentz line shape

$$g(\nu) = \frac{1}{\pi}\frac{\Delta\nu}{(\nu_0-\nu)^2+\Delta\nu^2}$$

so that, at resonance

$$W_{M_J \to M_J-1} = 0.772\pi \frac{H_1^2\mu_0^2}{\Delta\nu h^2}(\tfrac{3}{2}+M_J)(\tfrac{5}{2}-M_J).$$

This probability, when multiplied by $h\nu$ and by the excess of upward over downward transitions per sec., gives the absorbed power per cm^3.

The population in the $J=\frac{3}{2}$ level of the $^2\Pi_{3/2}$ state is computed using the case (a) energy function[4]

$$B[J(J+1)-\Omega^2] \pm A\Lambda\Sigma.$$

We define f to be the fractional number of molecules in the J level of the $^2\Pi_{3/2}$ state. At room temperatures

$$f \cong \frac{(2J+1)\exp\{-BJ(J+1)hc/kT\} \times \exp\{-(A+2B)hc/kT\}}{(kT/hcB)[1+\exp\{-(A+2B)hc/kT\}]}.$$

With $J=\frac{3}{2}$, $T=293°K$, $B=1.70$ cm^{-1}, $A=120$ cm^{-1} we find that $f=0.011$.

In the $J=\frac{3}{2}$ state there are four M_J levels. The difference in population of two adjacent M_J levels is

$$fNh\nu/4kT$$

and the energy absorbed per cm^3 per sec. in the gas is

$$\frac{fN(h\nu)^2}{4kT} W_{M_J \to M_J-1}$$

for one M_J transition.

The absorption Q of the transition is defined by

$$Q_A = 2\pi\nu \frac{\text{energy stored per cm}^3}{\text{energy absorbed per cm}^3 \text{ per sec.}}.$$

TABLE III. Comparison of theoretical and experimental resonance field values in the absence of hyperfine splitting.

	H_{II}	$H_{II}-H_I$	$H_{III}-H_{II}$
Theory	8619.5	105.5	103.1
Meas.	8614.1	105.3	103.0

[16] Bloembergen, Purcell, and Pound, Phys. Rev. **73**, 679 (1948).
[17] F. Bloch and A. Siegert, Phys. Rev. **57**, 522 (1940).

Evidently the energy stored per cm³ is

$$(1/8\pi)(2H_1)^2.$$

Thus at resonance for a M_J transition

$$\frac{1}{Q_A}=\frac{0.606fN\mu_0^2\nu}{kT\Delta\nu}(\tfrac{3}{2}+M_J)(\tfrac{5}{2}-M_J).$$

Because of the hyperfine structure an individual absorption line has a Q three times as large as this.

For a pressure of 0.85 mm Hg and a temperature 298°K, $\nu/\Delta\nu=8620/3.5$, $N=0.30\times10^{17}$, and $f=0.011$. For one of the individual lines of the central triplet ($M_J=\frac{1}{2}\rightarrow M_J=-\frac{1}{2}$) the calculated absorption Q is

$$Q_A=7.0\times10^8.$$

The observed r.m.s. signal referred to the bolometer for one of these lines at optimum modulation is 1.1×10^{-6} volt. This corresponds to a measured Q_A of 6.5×10^8 which agrees with the calculated value to much less than the experimental uncertainty.

The relative intensities are observed as dictated by the term $(\frac{3}{2}+M_J)(\frac{5}{2}-M_J)$ which predicts relative intensities of 3:4:3 for the M_J transitions $\frac{3}{2}\rightarrow\frac{1}{2}$, $\frac{1}{2}\rightarrow-\frac{1}{2}$, $-\frac{1}{2}\rightarrow-\frac{3}{2}$, respectively. The observed intensity ratios are 1.33 ± 0.02.

7. ANALYSIS

The line positions are determined by three splitting energies: (a) the molecular energies neglecting nuclear spin (stage *b* of Fig. 1), (b) the magnetic IJ coupling (stage *c* of Fig. 1), (c) the nuclear electric quadrupole IJ coupling (stage *d* of Fig. 1). Expressions for the molecular energies are given in the paper of Margenau and Henry and are not repeated here. The magnetic IJ energy can be written as

$$AM_IM_J.$$

The electric quadrupole energy[18] for $J=\frac{3}{2}$, $I=1$ is

$$\tfrac{1}{60}eQq[15/4-3M_J^2][2-3M_I^2]$$

Taking account of the three energies, the resonance fields for the nine lines are as given in Table II. H_I, H_{II}, and H_{III} are given by the molecular energies in the absence of nuclear spin and

$$H_Q=-\tfrac{1}{2}eQq(H_{II}/h\nu_0)$$
$$H_D=A(H_{II}/h\nu_0),$$

where ν_0 is the frequency of observation.

The average values of H_D and H_Q are obtained by taking differences of the nine equations. The results are

$$H_Q=0.78\pm0.2 \text{ oersted}$$
$$H_D=27.4\pm0.3 \text{ oersted}.$$

Converting these numbers to "coupling constants" expressed in megacycle/sec., as is the usual practice, the magnetic IJ coupling constant A is 1.98×10^{-19} erg or 29.8 ± 0.3 megacycle/sec. and the nuclear electric "quadrupole coupling" is -1.7 ± 0.5 megacycle/sec. The assignment of a negative quadrupole coupling[19] is unambiguous from the experiment.

The average values of H_{II}, $H_{II}-H_I$, and $H_{III}-H_{II}$ are given in Table III and compared with the theory of Margenau and Henry.

The agreement between the theoretical field values of Margenau and Henry and the experiments is quite good. The general features of the interpretation are supported by this agreement and also by the relative intensities of the nine absorption lines. Recently we have observed the corresponding spectrum $N^{15}O$, which further verifies the interpretation. A six-line spectrum is observed with pairs of lines centered at field values slightly lower than H_I, H_{II} and H_{III}; the pairs arising from magnetic IJ coupling with the N^{15} nucleus ($I=\frac{1}{2}$). The details of this spectrum will be published elsewhere.

[18] See Eq. (14) of reference 4a.
[19] The notation is that of B. T. Feld, Phys. Rev. **72**, 1116 (1947).

Theory of Magnetic Resonance in Nitric Oxide*

HENRY MARGENAU AND ALLAN HENRY
Sloane Physics Laboratory, Yale University, New Haven Connecticut
(Received January 24, 1950)

The paper presents a theoretical study of the effect of a magnetic field on the lowest of the $^2\Pi_{3/2}$ levels of $N^{14}O^{16}$. The molecular Zeeman effect is calculated in detail and found to yield good agreement with experiment. Consideration is given to the energy of interaction, (a), of the spin of the N^{14} nucleus with the total electronic angular momentum in the external field, and (b) of the quadrupole moment of N^{14} with the electric field at the N^{14} nucleus. The last section contains an evaluation of the matrix elements needed in the computation of absolute intensities for the transitions within the $^2\Pi_{3/2}$ level.

1. SURVEY

THE splitting of the term $^2\Pi_{3/2}$ in the NO molecule, observed by Beringer and Castle,[1] has its origin in the level system schematically represented in Fig. 1 of reference 1. In a magnetic field, the energy of a state with given J takes on as many values as there are magnetic sub-levels characterized by M_J, four in the present instance. This splitting is shown in stage *b* of the figure; it would describe the situation fully if there were no nuclear spin with its associated magnetic moment and no nuclear quadrupole moment.

Before considering the nuclear effects we focus attention once more on stage *b*. The diagram represents a condition commonly known as the weak field case, a condition in which the coupling between the various angular momenta is not disturbed by the external magnetic field. The fields used in the experiments under discussion, having magnitudes below 10,000 oersted, are indeed weak with respect to the internal molecular couplings in the ordinary sense of the word. The scheme of Fig. 1b of reference 1 is therefore adequate.

However, another question concerns the equality of the frequency differences, ν_I, ν_{II}, and ν_{III}. Only for *very* weak fields are they equal. We shall show that under the circumstances of Beringer and Castle's experiments the external field did alter the internal molecular couplings to an extent reflected in an inequality of ν_I, ν_{II} and ν_{III}, though not sufficiently to cause a Paschen-Back effect.

The hyperfine structure of our level with the exclusion of quadrupole effects is shown in stage *c* of Fig. 1 in reference 1. Here the field is strong enough to uncouple **I** and **J** completely, so that M_I and M_J are both good quantum numbers resulting quite accurately in the scheme of levels drawn. Their spacing is the familiar one, but it will be explained in detail in Section 4. We shall demonstrate also, notwithstanding the fact that we are dealing with magnetic dipole transitions, the validity of the usual selection rule, $\Delta M_I=0$. Thus one is led to expect the nine transitions marked in stage *d* of the figure.

These would be of three different frequencies: $\nu+A/h$, ν, and $\nu-A/h$ if the equality $\nu_I=\nu_{II}=\nu_{III}\equiv\nu$ were true. The appearance of nine lines is therefore at once an indication of the distortion of the molecular Zeeman levels, of the inequality of the ν's. Observation shows three similar groups of lines which exhibit two different intervals, one interval of about 27 and one of approximately 100 oersted. One of these must clearly correspond to the difference between successive ν_i, the other to the value of the (hyperfine-structure) constant A. The observed line pattern is indifferent to the assignment of intervals; hence other considerations are necessary to settle this assignment.

We shall see later that the intensities of the lines are given by the formula

$$\text{Int}\,(M_J\rightarrow M_J-1)\approx(J+M_J)(J-M_J+1). \quad (1)$$

Accordingly, the lines associated with ν_{II} should be stronger by a factor 4/3 than those associated with ν_I and ν_{III}. Hence the frequencies $\nu_{II}+A/h$, ν_{II} and $\nu_{II}-A/h$ should be equally strong and slightly more intense than the others. If A were the large interval, we should expect the middle line of each triplet to be of greater intensity; otherwise the middle group of three should contain all the lines of greater intensity. The latter is the alternative present in the measurements. We must conclude, therefore, that the hyperfine-structure constant corresponds to 27 oersted, the separation of about 100 oersted being assignable to molecular distortion. Our detailed calculations, too, will bear this out.

2. THE HAMILTONIAN

The NO molecule presents an instance of Hund's case *a*. Nevertheless it is simpler for the purposes of calculation to employ zero-order state functions corresponding to case *b*, and to treat the interaction which distinguishes the two cases as one of the perturbations. In the initial representation, therefore, the molecular quantum numbers[2] J, K, S, and Λ and M_J are sharp; as the calculation proceeds, states corresponding to different values of some of these constants are combined in variational fashion.

The perturbing Hamiltonian has the form:

$$\mathcal{H}'=\mathcal{H}_m+\mathcal{H}_n$$
$$\mathcal{H}_m=D\mathbf{\Lambda}\cdot\mathbf{S}+\boldsymbol{\mu}_J\cdot\mathbf{H} \quad (2)$$

* Supported by the ONR.
[1] R. Beringer and J. G. Castle, Jr., Phys. Rev. **78**, 581 (1950).

[2] The notation follows G. Herzberg, *Molecular Spectra and Molecular Structure* I (Prentice-Hall, Inc., New York, 1939).

$$\mathcal{H}_n = A\mathbf{J}\cdot\mathbf{I} + \boldsymbol{\mu}_I\cdot\mathbf{H} + q'. \tag{3}$$

$\mathcal{H}_m$ is the molecular, $\mathcal{H}_n$ the nuclear part of the perturbation. The two differ greatly in magnitude, the contribution of $\mathcal{H}_m$ to the energy differences sought being several hundred times that of $\mathcal{H}_n$. Of the two terms comprising $\mathcal{H}_m$, the first accounts for the rotational distortion of the molecule and carries the molecule from case *b* toward case *a*. The term $\boldsymbol{\mu}_J\cdot\mathbf{H}$ represents the energy of the electronic magnetic moments $\boldsymbol{\mu}_J$ in a magnetic field $\mathbf{H}$. Customarily it is written in the form

$$g_J\mu_0\mathbf{J}\cdot\mathbf{H}, \tag{4}$$

and if one consults books on band spectra[3] one will find for g_J the formula

$$g_J = \frac{(\Lambda+\Sigma)(\Lambda+2\Sigma)}{J(J+1)} \tag{4a}$$

as valid for Hund's case *a*. The level studied by Beringer and Castle is of type $^2\Pi_{3/2}$, hence $\Lambda=1$, $\Sigma=\frac{1}{2}$; $J=\frac{3}{2}$, and g_J should be 4/5. Our work will show that the effective value of g_J will depart appreciably, though not widely, from this ideal value.

We note here that the form (4) is not a suitable one for use on the present occasion because the intermingling of states occurring in the perturbation calculus will cause g_J to be a function of the magnetic quantum number M_J, an incident which deprives this quantity of its usual significance. We must therefore turn to a more detailed analysis of the operator $\boldsymbol{\mu}_J\cdot\mathbf{H}$.

When $\mathbf{H}$ is taken along the Z axis, this operator may be expanded to read

$$\boldsymbol{\mu}_J\cdot\mathbf{H} = [\mu_0(\Lambda_z+2S_z)+\mu_n(K_z-\Lambda_z)]H_z.$$

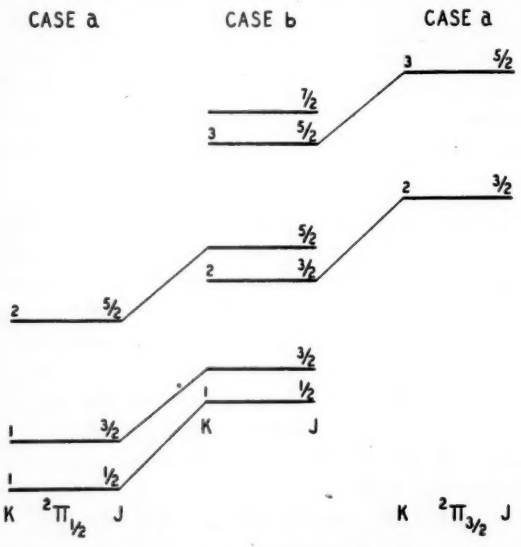

FIG. 1. Relation between level arrangements in case *a* and case *b* [see R. S. Mullikan, Rev. Mod. Phys. **2**, 113 (1930)].

[3] E.g., W. Jevons, *Band Spectra of Diatomic Molecules* (Cambridge University Press, London, 1932), p. 252.

The quantity $\mathbf{K}-\boldsymbol{\Lambda}$ is the angular momentum (sometimes called $\mathbf{N}$) resulting from the slow rotation of the entire molecule, and μ_n is the magnetic moment produced by it. This quantity consists of two parts, $\mu_n'+\mu_n''$, which arise separately from the rotation of the nuclei and of the electrons. A simple consideration shows that μ_n' is a nuclear magneton, multiplied by $N_p/(N_p+N_n)$, the ratio of the number of revolving protons to that of nucleons. On the other hand, μ_n'' is very difficult to calculate, but is known[4] to cancel part of μ_n'. It is clear, therefore, that the term $\mu_n(K_z-\Lambda_z)H_z$ is quite small in comparison with the remainder of $\boldsymbol{\mu}_J\cdot\mathbf{H}$. It will later be seen to be small also relative to the important part of $\mathcal{H}_n$ and will now be ignored. Hence we take

$$\mathcal{H}_m = D\boldsymbol{\Lambda}\cdot\mathbf{S}+\mu_0(\Lambda_z+2S_z). \tag{5}$$

The matrix elements for this operator have been evaluated by Hill and by Van Vleck.[5]

The three terms composing $\mathcal{H}_n$ (Eq. 3) represent (a) the interaction between the magnetic moment of the N^{14} nucleus ($\mu=0.403$ nuclear magnetons; I, the nuclear spin quantum number, $=1$) and the magnetic field produced by the electrons; (b) the energy of alignment of the nuclear magnet in the external field $\mathbf{H}$; (c) the operator q' which represents the interaction between the nuclear quadrupole moment of N and the electronic field. This last effect is very small but, it turns out, just measurable. Nothing is known about the numerical value of the constant A for NO, but we recall from elementary theory its significance:

$$A \approx -\mu_I H_0/IJ. \tag{6}$$

Here H_0 is the field produced by all electrons in the molecule at the place of the N-nucleus. The experimental data lead to $A=1.98\times10^{-19}$ erg and $H_0\cong150{,}000$ oersteds.

The procedure followed in this paper is to combine "case *a* functions" for the NO molecules so as to diagonalize $\mathcal{H}_0$ (the unperturbed Hamiltonian)$+\mathcal{H}_m$, this being the large part of the energy. Then we compute the diagonal energy components corresponding to $\mathcal{H}_n$ in the usual way. The first of these two tasks is performed in Section 3.

Throughout this calculation we have neglected the energy difference resulting from Λ-type doubling. This corresponds to inclusion in $\mathcal{H}_m$ of an operator proportional to $\mathbf{L}\cdot\mathbf{N}$ and requires consideration of electronic states other than the one involved in the lines here studied. The fact that this doubling would not appear in our approximation is of course no guarantee of its

[4] See G. C. Wick, Zeits. f. Physik **85**, 25 (1933).

[5] E. L. Hill and J. H. Van Vleck, Phys. Rev. **32**, 250 (1928); E. L. Hill, Phys. Rev. **34**, 1507 (1929).

Equation (3), which is customary and upon which the present treatment will be based, is only approximately true. It will be shown in a later paper that the term $\mathbf{J}\cdot\mathbf{I}$ requires a slight correction which further improves the agreement of our results with experiment.

smallness. Mulliken and Christie,[6] however, have published parameters from which its size can be computed roughly. The actual splitting should be of the order of 10^{-4} cm^{-1} for the $^2\Pi_{3/2}$ term of NO, and this corresponds to about 2 oersted in the experiments of Beringer and Castle. It would thus be on the verge of being measurable if the difference communicated itself somehow *in toto* to the various Zeeman levels. We have not investigated this point in detail.

3. MOLECULAR ZEEMAN EFFECT

In this, the main part of the calculation, we deal with the Hamiltonian $\mathcal{H}_T+\mathcal{H}_m$, which we abbreviate in the present section as $\mathcal{H}$. Here $\mathcal{H}_T$ is the energy operator for the symmetric top, whose eigenvalues are given by $B[K(K+1)-\Lambda^2]=E_T$. As usual, $B=\hbar/4\pi cI$ and is measured in cm^{-1}. The eigenfunctions of $\mathcal{H}_T$ are characterized by the values of K (and other parameters, to be sure); but since in our case the electron spin $S=\frac{1}{2}$, two values of $\mathbf{J}=\mathbf{K}+\mathbf{S}$ are assignable to every K, namely $K\pm\frac{1}{2}$. This is the degeneracy peculiar to the use of case *b* eigenfunctions, a degeneracy which is removed by the interaction between $\mathbf{K}$ and $\mathbf{S}$. The eigenfunctions will be written in the form $\psi(K, J)$.

To locate the energies associated with the various quantum numbers we have drawn in Fig. 1 the anatomy of the terms of the NO molecule (without external field) in the neighborhood of the one here selected for study. The central system, labeled case *b*, is the arrangement reflected by our functions $\psi(K, J)$, except that these functions do not take account of the J-splitting indicated in the diagram. As this splitting becomes important (case *a*) the central arrangement transforms itself into the $^2\Pi_{\frac{1}{2}}$ and the $^2\Pi_{3/2}$ systems as shown in the figure. Our interest is in the lowest level on the right. Its ancestor of the case *b* generation has quantum numbers $K=2$, $J=\frac{3}{2}$, and is degenerate with the level $(2, \frac{5}{2})$. Its closest neighbors are the states $(1, \frac{3}{2})$ and $(3, \frac{5}{2})$; these are important in our variational calculation despite the fact that, in the case *a* scale, one of these states, $(1, \frac{3}{2})$ moves out of the neighborhood of the state in question.

The procedure to be described is suggested by a comparison of the sizes of the various matrix elements $(K, J|\mathcal{H}_m|K', J')$ and by the magnitude of the differences $E_T(K, J)-E_T(K', J')$. Hill[7] has calculated all matrix elements needed for the present purposes and extensive use is made of his results.

The work proceeds in three steps toward the final approximation.

Step 1.—A linear combination is formed from the functions $\psi(1, \frac{3}{2})$ and $\psi(2, \frac{3}{2})$. Of the two roots of the secular determinant, $|\mathcal{H}_{ij}-E|$ which we will call E_a and E_a', we select the one which originates at $E_T(2, \frac{3}{2})$ in the absence of the perturbation $\mathcal{H}_m$, and we call this root E_a. The corresponding linear combination shall be ψ_a. Clearly, E_a is a better approximation to the energy we are seeking than is $(2, \frac{3}{2}|\mathcal{H}|2, \frac{3}{2})$, but it is far from adequate for our purposes.

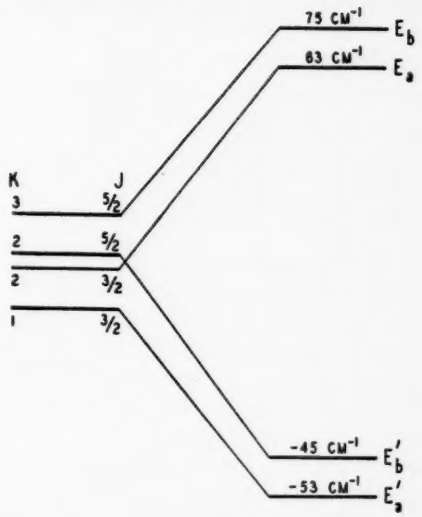

FIG. 2. Behavior of energy levels under perturbation (first stage).

Step 2.—To improve the accuracy, we first combine the functions $\psi(2, \frac{5}{2})$ and $\psi(3, \frac{5}{2})$ in the same manner in which step 1 combined $\psi(1, \frac{3}{2})$ and $\psi(2, \frac{3}{2})$ to yield ψ_a. In this way, then, two energies, E_b and E_b', are obtained, and the root selected, E_b, shall be the one closest to E_a. The corresponding linear combination is ψ_b. In completion of step 2, ψ_a is combined with ψ_b, and the combination which reduces to $E_T(2, \frac{3}{2})$ is called ψ, or "the grand ψ." The corresponding energy is E_{ab}. This E_{ab} is a much better approximation than E_a, but it is not quite good enough. In the absence of an external field, states *a* and *b* do not combine; the improvement just noted has relevance only for the Zeeman effect.

Step 3.—Upon the grand ψ one may impose a perturbation in the manner of the Rayleigh-Schrödinger scheme. In terms of the variational procedure thus far employed this scheme is equivalent to a neglect of all non-diagonal elements in the secular determinant except those in the first row and the first column, ψ being the first state. There is then added to E_{ab} the perturbation

$$\Delta E=\sum_\lambda \frac{|\int \psi^*\mathcal{H}_m\psi_\lambda d\tau|^2}{E_{ab}-E_\lambda} \tag{7}$$

and

$$E=E_{ab}+\Delta E.$$

By ψ_λ is meant any function $\psi(K, J)$ which combines with ψ but is not already included in ψ.

The first two steps are illustrated in Fig. 2, intended to show schematically what happens to the various levels under the influence of $\mathcal{H}_m$. To arrive at the grand ψ, the two states corresponding to the two highest levels, E_a and E_b, were selected because of their prox-

[6] R. S. Mulliken and A. Christie, Phys. Rev. **38**, 87 (1931).
[7] E. L. Hill, Phys. Rev. **34**, 1507 (1929).

TABLE I. Calculated magnetic fields (oersteds) and comparison with experimental values.

	H_{II}	$H_{II}-H_I$	$H_{III}-H_{II}$
Step 1	8612.3	17.1	17.5
Step 2	8618.9	127.1	128.6
Step 3	8619.5	105.5	103.1
Experiment	8614.1	105.3	103.0

imity. In his successful work on the Zeeman effect in doublet states, Hill has used what amounts to the procedure here employed up to step 2, although this may not be at once apparent from his language and indeed his formulas. But there is one difference. He combined the states corresponding to E_a and E_b' to obtain the equivalent of the grand ψ. This produces indeed the better approximation for molecules near case b, for then the energies E_a and E_b' fall closer together than they do in NO; in fact the difference E_a-E_b' can be much smaller than E_b-E_a. In our case, however, E_a-E_b' is of the order 100 cm^{-1} while E_b-E_a is less than 10 cm^{-1}. As a consequence, Hill's formula produces in the present instance an approximation inferior to E_{ab}; it is but little better than E_a alone.

The analytic details of the work need only be summarized, for they are routine matters and involve well-known methods. As to notation, the functions will be labeled

$$\psi(1,\tfrac{3}{2})=\psi_1;\quad \psi(2,\tfrac{3}{2})=\psi_2;\quad \psi(2,\tfrac{5}{2})=\psi_3;\quad \psi(3,\tfrac{5}{2})=\psi_4.$$

We recall: $\mathcal{H}=\mathcal{H}_T+\mathcal{H}_m$ and $\mathcal{H}_{ij}=\int\psi_i^*\mathcal{H}\psi_j d\tau$, as usual. One then finds

$$E_a=\tfrac{1}{2}(\mathcal{H}_{11}+\mathcal{H}_{22})+(\rho_{12}^2+1)^{\frac{1}{2}}\mathcal{H}_{12} \tag{8}$$

with the abbreviation:

$$\rho_{12}\equiv(\mathcal{H}_{22}-\mathcal{H}_{11})/2\mathcal{H}_{12}. \tag{8a}$$

The corresponding function is

$$\psi_a=(1+S_{12}^2)^{-\frac{1}{2}}[\psi_1+S_{12}\psi_2] \tag{9}$$

with

$$S_{12}\equiv\rho_{12}+(\rho_{12}^2+1)^{\frac{1}{2}}. \tag{9a}$$

In a similar manner ψ_b is formed from the functions ψ_3 and ψ_4; hence ψ_b and E_b are also given by formulas (8) and (9) provided the subscripts 1, 2 are changed to 3, 4 respectively.

Finally,

$$E_{ab}=(\mathcal{H}_{aa}+\mathcal{H}_{bb})-(\rho_{ab}^2+1)^{\frac{1}{2}}\mathcal{H}_{ab}$$
$$\psi=(1+S_{ab}^2)^{-\frac{1}{2}}[-S_{ab}\psi_a+\psi_b]$$

the quantities appearing here being again given by Eqs. (8a) and (9a) with the indicated changes in subscripts. Explicity,

$$\mathcal{H}_{ab}=(1+S_{12}^2)^{-\frac{1}{2}}(1+S_{34}^2)^{-\frac{1}{2}}\times(\mathcal{H}_{13}+S_{34}\mathcal{H}_{14}+S_{12}\mathcal{H}_{23}+S_{12}S_{34}\mathcal{H}_{24}).$$

Only three functions, $\psi(1,\frac{1}{2})$, $\psi(3,\frac{7}{2})$, and $\psi(4,\frac{7}{2})$ form non-vanishing matrix elements with ψ. The summation in formula (7) has therefore only three terms.

In carrying out the numerical calculations the following values of the constants were adopted: $B_{\frac{1}{2}}=1.6696$ cm^{-1}, $B_{3/2}=1.7200$ cm^{-1}, $D=123.8$ cm^{-1}, and $\mu_0/hc=4.66846\times10^{-5}$ (cm oersted)$^{-1}$. The two values of B refer to the $\Pi_{\frac{1}{2}}$ and $\Pi_{3/2}$ states and are taken from Gillette and Eyster.[8] Our choice of different B's in the diagonal matrix elements represents a minor refinement which proved to have only a slight effect on the final answer. The constant D is not identical with the doublet splitting of 120.5 cm^{-1}, which is directly measured in the band spectrum. It may be calculated from Hill's formula or, as was done here, from the difference E_a-E_a', this being the doublet splitting. If x is written for $H\mu_0/hc$, all expressions for the energies are of the form

$$\text{constant}+f_1(x)+f_2(M_J,x),$$

the constant being independent of M_J and x, and f_1 independent of M_J. To obtain the energy differences between magnetic states the constant and f_1 are not needed and will not be listed here. The results are given below (M_J is now replaced by M).

Step 1, leading to E_a:

$$f_2=0.776495Mx+0.001963M^2x^2-0.0000124M^3x^3+\cdots$$

Step 2, leading to E_{ab}:

$$f_2=0.776495Mx+0.014508M^2x^2-(0.003859M+0.000184M^2-0.000605M^3-0.000021M^4)x^3+\cdots$$

Step 3, leading to $E_{ab}+\Delta E$.

Here ΔE was computed separately for different values of M, since expansion in the form of a power series is not feasible:

$$\Delta E(M=\pm\tfrac{3}{2})=0.000024x^2+0.0000020Mx^3+\cdots$$
$$\Delta E(M=\pm\tfrac{1}{2})=0.005371x^2-0.0000284Mx^3+\cdots$$

(Dots indicate omission of terms in higher powers of x.)

Beringer and Castle measure the fields necessary to make the energy differences between magnetic levels equal to the frequency of observation, $\nu_0=0.3122$ cm^{-1}. Hence, to compare the theoretical results with experiment, the differences of our energies (E_a, E_{ab}, and E in the various stages of calculation) for successive M's must be equated to ν_0, and each equation must be solved for H. This process leads to the three values H_I, H_{II} and H_{III} tabulated in the first three rows of Table I. Since there is some interest in the manner of convergence of our calculation we have stated the results computed at every stop.

The use of formula (4a) leads to $H_2=8359.3$ oersted, with zero values for the difference.

[8] R. H. Gillette and E. H. Eyster, Phys. Rev. **56**, 1113 (1939).

4. HYPERFINE STRUCTURE

The operator $\mathfrak{IC}_n$ contributes the hyperfine structure of the molecular term. In a field of several thousand oersteds **I** and **J** are completely uncoupled. The nuclear situation corresponds to that of a total Paschen-Back effect, and the correct representation of the state is that in which J, I, M_J and M_I are sharp. The term $\mathfrak{y}_I \cdot \mathbf{H}$ may be written as $(g_I/1840)\mu_0 I_Z H$. Since

$$(M_J M_I|\mathbf{J}\cdot\mathbf{I}|M_J M_I)=M_J M_I$$

and

$$(M_I|I_Z|M_I)=M_I$$

we find

$$E_n=AM_JM_I+(g_I/1840)\mu_0 M_I H \tag{10}$$

to be the energy of the hyperfine levels for the case under consideration, exclusive of the effect of q' in Eq. (3). When account is taken of E_n, we arrive at stage *c* of Fig. 1 in the preceding paper.

Since the N^{14} nucleus has an electric quadrupole moment, a hyperfine structure resulting from its interaction with the electronic field is to be expected in addition to what we have just calculated.

Employing the customary notation, we have[9]

$$\left.\begin{aligned} q'&=-\frac{eQ\langle\Sigma_k e_k(3\cos^2\theta_k-1)r_k^{-3}\rangle_{\text{molecule}}}{2J(2J-1)I(2I-1)}U \\ \text{where}\quad U&=3(\mathbf{I}\cdot\mathbf{J})^2+\tfrac{3}{2}\mathbf{I}\cdot\mathbf{J}-I(I+1)J(J+1)\end{aligned}\right\}. \tag{11}$$

Now

$$\langle 3\cos^2\theta-1\rangle_{\text{molecule}}=\frac{2J}{2J+3}\left[\frac{3(\Lambda+\Sigma)^2}{J(J+1)}-1\right] \tag{12}$$

for a molecule typefying Hund's case *a*, and

$$(M_JM_I|U|M_JM_I)=\tfrac{1}{2}[J(J+1)-3M_J^2][I(I+1)-3M_I^2]. \tag{13}$$

Hence the quadrupole energy in the J, I, M_J, M_I representation is given by

$$-\frac{eQq}{4(2J-1)I(2I-1)(2J+3)}[J(J+1)-3M_J^2]\times[I(I+1)-3M_I^2]\left[\frac{3(\Lambda+\Sigma)^2}{J(J+1)}-1\right]. \tag{14}$$

Here

$$q=\sum_k l_k\frac{3\cos^2\theta_k'-1}{r_k^3}.$$

When this effect is added onto the levels in stage *c* of Fig. 1 of reference 1, stage *d* results. As is well known, the quadrupole effect causes a departure from the interval rule as illustrated.

5. INTENSITIES

The lines observed by Beringer and Castle arise from transitions in which the magnetic dipole moment changes, the electric moment remaining unaltered. Their intensities are therefore given by the squares of the matrix elements of

$$-\frac{e}{2mc}\mathfrak{M}=-\frac{e}{2mc}(\mathbf{\Lambda}+2\mathbf{S})-\frac{e}{2Mc}g_I\mathbf{I}.$$

Here M is the mass of a nucleon, while m is the mass of an electron. The last term is therefore negligible.

The operotor $\mathbf{\Lambda}+2\mathbf{S}$, like the electric dipole moment, forms a vector of type **T** in the terminology of Condon and Shortley.[10] The matrix elements are therefore the same, except for constants, as those for the electric moment vector.

In particular,

$$\Delta M_I=0$$

for all allowed transitions because $\mathfrak{M}$ commutes with **I** when the last term of the former operator is neglected. The intensities become

$$\text{Int}\,(M_J\to M_J-1)=\text{const.}\,(J+M_J)(J-M_J+1).$$

This justifies our use of Eq. (1).

An accurate calculation is required for the purpose of comparing the absolute intensities of the measured lines with theory. This involves the computation of the proper matrix elements of $\mathfrak{M}_x$ and $\mathfrak{M}_y$ for the actual molecular states under consideration. We must find

$$(\gamma M|\mathfrak{M}_x|\gamma M\pm1)=\mp i(\gamma M|\mathfrak{M}_y|\gamma M\pm1),$$

and take γ to represent the state given by the grand ψ

$$\psi=\psi_\gamma=\sum_{i=1}^{4}a_i\psi_i$$

the ψ_i being defined just prior to Eq. (8). It is understood, of course, that the ψ_i are now written in their explicit dependence on the magnetic quantum number M. As to the coefficients a_i, which were used in Section 4 (but not displayed), their values are

$$a_1=0.853,\quad a_2=0.521,\quad a_3=a_4=0$$

to an approximation sufficiently good for present

[9] Equation (11) comes from H. B. G. Casimir, *On the Interaction between Atomic Nuclei and Electrons* (Haarlem, DeErven F. Bohn N.V. 1936). Equation (12) is obtained by a calculation similar to that of J. M. Jauch, Phys. Rev. **72**, 716 (1947) and Eq. (13) can be checked by employing matrix elements given in Condon and Shortley. The relationship between θ_k in Eq. (11) and θ in Eq. (12) is given by A. Nordsieck, Phys. Rev. **58**, 310 (1940) as $\sum_k e_k(3\cos^2\theta_k-1)r_k^{-3}=(3\cos^2\theta-1)\sum_k e_k\frac{3\cos^2\theta_k'-1}{2r_k^3}$. See this paper for details and notation.

[10] E. U. Condon and G. H. Shortley, *Theory of Atomic Spectra* (Cambridge University Press, London, 1935), p. 59 ff.

purposes. We also need the formulas[11]

$$(J, K, M|\mathfrak{M}_x|J, K, M\pm1)$$

$$=\frac{1}{2}\left\{\frac{\Lambda^2}{K(K+1)}\,\frac{J(J+1)-S(S+1)+K(K+1)}{2J(J+1)}+\frac{S(S+1)-K(K+1)+J(J+1)}{J(J+1)}\right\}(J\pm M+1)^{\frac{1}{2}}(J\mp M)^{\frac{1}{2}}$$

$$(J, K, M|\mathfrak{M}_x|J, K+1, M\pm1)$$

$$=\frac{\Lambda}{4J(J+1)(K+1)}\left\{\frac{[(K+1)^2-\Lambda^2](J-S+K+1)(J+S+K+2)(K+S-J+1)(J+S-K)}{(2K+1)(2K+3)}\right\}(J\pm M+1)^{\frac{1}{2}}(J\mp M)^{\frac{1}{2}}.$$

When numbers are inserted we obtain for the quantity we are seeking

$$2|(\gamma M|\mathfrak{M}_x|\gamma M\pm1)|^2=0.386(J\pm M+1)(J\mp M). \quad (15)$$

It is interesting to observe that the state ψ_2 contributes far less to the intensity than does ψ_1, as is very evident when the matrix elements are evaluated. An explanation of this apparent anomaly is provided by the vector model which shows state ψ_1 to suffer a large change in magnetic moment on change of M because of the relative orientation of the vectors which constitute M, in contradistinction to the situation in ψ_2.

[11] These were here derived with the use of the matrix elements given by Reiche and Rademacher, Zeits. f. Physik **41**, 453 (1927) and the quantum addition rules for angular momenta.

PHYSICAL REVIEW VOLUME 78, NUMBER 5 JUNE 1, 1950

The Quantum Mechanics of Localizable Dynamical Systems

T. S. CHANG
Peking University, Peking, China
(Received November 25, 1949)

Expressions for the operators in Dirac's general theory of quantum mechanics of localizable dynamical systems are explicitly constructed and their commutation laws directly worked out (§2). Conditions for the expectation values of dynamical variables or their densities to be independent of the parametrization of the surface are given and it is shown that of the two conjugate field variables in Weiss' theory, one is a parametrization-independent variable and the other is a parametrization-independent density (§3).

Finally it is shown that P^n in Dirac's theory does not have any simple expression other than that given in Weiss' theory. This, together with the results described in the above paragraph, shows that for all practical purposes the two theories are equivalent (§5).

1. INTRODUCTION

IN the quantum mechanical theory of localizable dynamical systems, a wave function is introduced on each space-like surface in the four-dimensional space, and equations are set up for its change as the surface changes. Such a general theory was first given by Dirac,[1] who introduced the deformation operators Π^r, Π^n to describe the changes of the surface and the operators P^r, P^n giving the corresponding changes of the wave function. Conditions which these operators must satisfy were given, and if we call the equation giving the change of the wave function on a surface as the surface changes the wave equation, these conditions are precisely the conditions of integrability of the wave equation.[2]

For fields whose field equations are derived from the variation of a Lagrangian, wave equations of the above nature were effectively given by Weiss.[3] The exact form of the wave equation and a proof of its integrability were given in two papers by the author.[4,5] It is easy to construct P^r and P^n from this wave equation and to verify that the conditions for them are satisfied.

In this theory, as well as in Dirac's paper, parametrization of the surface is introduced and the wave function changes as the "parametrized" surface changes. It is thus important to ask whether the expectation values of different dynamical variables at a point P inside a surface S are independent of the parametrization of the surface S. Conditions for such independence of dynamical variables (and their densities) are worked out (§3) and it is found that in Weiss' theory one of the

[1] P. A. M. Dirac, Phys. Rev. **73**, 1092 (1948).
[2] The relativity requirements on the wave equation were overlooked by Dirac and will be supplied here.
[3] P. Weiss, Proc. Roy. Soc. **A156**, 192 (1936).
[4] T. S. Chang, Phys. Rev. **75**, 967 (1949).
[5] T. S. Chang, Chinese J. Phys. **7**, 265 (1949). This paper contains an extension of Weiss's theory to fields, the Lagrangian of which contains various derivatives of the field quantities.

two conjugate field quantities satisfies the conditions for a density. This feature is not too satisfactory and and one would like to know if it is possible to develop Dirac's general theory without this feature.

In §4 we introduce conjugate variables into Dirac's theory. We determine P^r and the dependence of the conjugate variables on the metric so that their commutation law is satisfied and their expectation values as well as the expectation values of the energy and momentum densities are all independent of the parametrization of the surface. It is revealed that a simple change of variable carries P^r and the conjugate variables determined in such a theory into corresponding quantities in Weiss' theory.

This settles incidentally the important question whether Dirac's theory is actually more general than Weiss' theory. Any difference between the Weiss theory and Dirac's theory as developed in §4 lies in the determination of P^n. It will be shown that there does not exist any simple expression for P^n beside that of Weiss' theory. Thus for all practical purposes, we may consider the two theories as equivalent.

2. COMMUTATION LAWS BETWEEN Π^r, Π^n

To clarify Dirac's paper as well as to provide for the subsequent sections, we shall construct explicit expressions for the operators Π^r, Π^n and develop their commutation laws.

Let x^μ be (x, y, z, ct), and $g_{00}=-g_{11}=-g_{22}=-g_{33}=1$ as usual, and let surfaces be represented by

$$x^\mu \doteq x^\mu(u). \quad u=(u_1, u_2, u_3). \tag{1}$$

Let us write the wave functional Ψ as $<m(u), x^\mu(u)|>$, where $m(u)$ is the label for the different coordinates of the wave functional. Consider a surface S given by $x^\mu=b^\mu(u)$ deformed to a surface S' given by $x^\mu=b^\mu(u)+\Delta x^\mu(u)$. Writing Δx^μ as

$$\epsilon\{a_r(\partial x^\mu/\partial u_r)+a_n n^\mu\}, \quad (r, s, \cdots=1, 2, 3), \tag{2}$$

where $n^\mu(u)$ is the unit normal to the surface at the point u, $(n_\mu n^\mu=1,\ n^0>0)$ and defining $\Delta\Psi$ as $<m(u), b^\mu+\Delta x^\mu|>-<m(u), b^\mu|>$ we have

$$\Delta\Psi=\int \Delta x^\mu(u)\frac{\delta\Psi}{\delta x^\mu(u)}du$$

$$=\int \epsilon\left\{a_r\frac{\partial x^\mu}{\partial u_r}+a_n n^\mu\right\}\frac{\delta\Psi}{\delta x^\mu(u)}du,$$

$$(du=du_1du_2du_3) \tag{3}$$

where $\delta\Psi/\delta x^\mu(u)$ is the usual functional derivative of Ψ with respect to $x^\mu(u)$ at the point u. Defining Π^r, Π^n according to Dirac by

$$\Delta\Psi=-\epsilon i\int(a_r\Pi^r+a_n\Pi^n)\Psi du, \tag{4}$$

we get

$$\Pi^r(u)=i(\partial x^\mu/\partial u_r)(\delta/\delta x^\mu(u)),\ \Pi^n(u)=in^\mu(\delta/\delta x^\mu(u)). \tag{5}$$

It is possible to calculate the commutation relations between the Π's from (5). For example, defining $[A, B]\equiv -i(AB-BA)$ and noting that

$$(\delta/\delta x^\mu(u))(\delta/\delta x^\nu(u'))=(\delta/\delta x^\nu(u'))(\delta/\delta x^\mu(u)),$$

we have

$$[\Pi^r(u), \Pi^s(u')]=i\left\{\frac{\partial x^\mu(u)}{\partial u_r}\left[\frac{\delta}{\delta x^\mu(u)}\frac{\partial x^\nu(u')}{\partial u_s'}\right]\frac{\delta}{\delta x^\nu(u')}\right.$$

$$\left.-\frac{\partial x^\nu(u')}{\partial u_s'}\left[\frac{\delta}{\delta x^\nu(u')}\frac{\partial x^\mu(u)}{\partial u_r}\right]\frac{\delta}{\delta x^\mu(u)}\right\}$$

$$=-i\delta_s(u-u')x_r{}^\nu(\delta/\delta x^\nu(u'))$$

$$+i\delta_r(u'-u)x_s{}^\nu(u')(\delta/\delta x^\nu(u)), \tag{6}$$

where $x_s{}^\mu$ stands for $\partial x^\mu/\partial u_s$, $\delta(u-u')$ for $\delta(u_1-u_1')$, $\delta(u_2-u_2')$, $\delta(u_3-u_3')$, and $\delta_s(u)$ for $\partial\delta(u)/\partial u_s$. The right-hand side of (6) added to

$$\delta_s(u-u')\Pi^r(u')+\delta_r(u-u')\Pi^s(u) \tag{7}$$

can be proved to be zero by showing that the sum vanishes after performing the integration with respect to either u or u'.[6] Thus

$$H^{rs}(uu')\equiv[\Pi^r(u), \Pi^s(u')]+\delta_s(u-u')\Pi^r(u')$$
$$+\delta_r(u-u')\Pi^s(u)=0. \tag{8}$$

We can find the other Poisson brackets in a similar way. For simplicity, let us write x', $\Pi^{r\prime}$, $\cdots$ in place of $x(u')$, $\Pi^r(u')$, $\cdots$ and let x, Π^r, $\cdots$ denote $x(u)$, $\Pi^r(u)$, $\cdots$. Let us introduce the symbols $\partial x_\mu/\partial w$, u_μ, $\partial u_r/\partial x_\mu$, $\partial w/\partial x_\mu$ by

$$\partial x_\mu/\partial w=n_\mu, \quad u^\mu=u_\mu=(w, u_1, u_2, u_3), \tag{9}$$

$$(\partial u_\rho/\partial x_\mu)(\partial x_\nu/\partial u_\rho)=\delta_\nu{}^\mu,$$
$$(\partial x_\rho/\partial u_\mu)(\partial u_\nu/\partial x_\rho)=\delta_\nu{}^\mu.$$
$$(\mu, \nu, \rho=1, 2, 3, 0) \tag{10}$$

Then

$$n^\mu=\partial w/\partial x_\mu=\partial x^\mu/\partial w, \quad n_\mu=\partial w/\partial x^\mu=\partial x_\mu/\partial w. \tag{11}$$

With this notation we get

$$\delta n^\mu(u)/\delta x_\nu(u')=\delta_s(u'-u)n^\nu(u)(\partial u_s/\partial x_\mu),$$

$$H^{rn}(uu')\equiv[\Pi^r(u), \Pi^n(u')]+\delta_r(u-u')\Pi^n(u)=0, \tag{12}$$

[6] A more standard proof is to cast the sum into

$$\gamma(u)\delta(u-u')+\gamma^{(r)}(u)\delta_r(u-u')+\gamma^{(rs)}(u)\delta_{rs}(u-u')+\cdots$$
$$(\delta_{rs}(u-u')=\partial^2\delta(u-u')/\partial u_r\partial u_s, \cdots)$$

and to show that all the coefficients are zero. The casting is performed by expanding all functions except $\delta(u-u')$ and its derivatives into a power series of (u_r-u_r') with coefficients as functions of u and removing these powers by using relations of the type

$$(u_r-u_r')\delta(u-u')=0,$$
$$(u_r-u_r')\delta_s(u-u')=-\delta_{rs}\delta(u-u'), \text{ etc.}$$

$$H^{nn}(uu')\equiv[\Pi^n(u),\Pi^n(u')]$$
$$-\delta_s(u-u')\left\{\frac{\partial u_r}{\partial x_\mu}\frac{\partial u_s}{\partial x^\mu}\Pi^r+\frac{\partial u_r'}{\partial x_\mu'}\frac{\partial u_s'}{\partial x^{\mu'}}\Pi^{r'}\right\}=0. \quad (13)$$

If ξ is any quantity and $\Pi^{r'}\xi$, $\Pi^{n'}\xi$ are given, it is obvious that ξ may exist as a functional of $x^\mu(u)$ if and only if $H^{rs}(u'u'')$, $H^{rn}(u',u'')$, $H^{nn}(u',u'')$ operating on $\xi(u)$ yield zero. Hence the vanishing of the brackets of $H^{rs}(u'u''),\cdots$ with $\xi(u)$ supplies the integrability condition.

If, following Dirac, we write the wave equation as

$$\int(a_r\Pi^r+a_n\Pi^n)\Psi du=\int(a_rP^r+a_nP^n)\Psi du, \quad (14)$$

the condition of integrability for the wave equation is

$$G^{rs}(uu')\equiv[P^r,P^{s'}]-[\Pi^r,P^{s'}]+[\Pi^{s'},P^r]$$
$$-\delta_s(u-u')P^{r'}-\delta_r(u-u')P^s=0, \quad (15)$$

$$G^{rn}(uu')\equiv[P^r,P^{n'}]-[\Pi^r,P^{n'}]$$
$$+[\Pi^{n'},P^r]-\delta_r(u-u')P^n=0, \quad (16)$$

$$G^{nn}(uu')\equiv[P^n,P^{n'}]-[\Pi^n,P^{n'}]+[\Pi^{n'},P^n]$$
$$+\delta_s(u-u')\left\{\frac{\partial u_s}{\partial x_\mu}\frac{\partial u_r}{\partial x^\mu}P^r+\frac{\partial u_s'}{\partial x_\mu'}\frac{\partial u_r'}{\partial x^{\mu'}}P^{r'}\right\}=0. \quad (17)$$

Obviously, we must assume P^r, P^n as functionals of u and $x^\mu(u)$, hence their brackets with $H^{rs}(u',u''),\cdots$ are zero. These relations and (15)–(17) are the conditions for P^r, P^n.

For completeness, we mention the relativity requirements. Consider two surfaces S and S^* with S^* obtained from S by a translation of a rotation about a certain point. The relativity principle requires that with suitably chosen representations of the wave functions on S and S^*, i.e., with a suitably chosen label $m(u)$ in $<m(u),x^\mu(u)|>$ the operators P^n, P^r on S and the corresponding operators P^{n*}, P^{r*} on S^* take the same form. Let S^* be obtained from S by the infinitesimal transformation

$$x_\mu{}^*=x_\mu+\epsilon_{\mu\nu}x^\nu+\eta_\mu. \quad (18)$$

We expect the existence of an operator O acting on $m(u)$ and depending on $\epsilon_{\mu\nu}$, η_μ so that we have

$$\left[P^r(u),O+\int du'(\epsilon_{\mu\nu}x^{\nu'}+\eta_\mu)\right.$$
$$\left.\times\{(\partial u_r'/\partial x_\mu')\Pi^{r'}+n^{\mu'}\Pi^{n'}\}\right]=0 \quad (19)$$

and a similar equation for P^n.

THE INDEPENDENCE OF EXPECTATION VALUES OF DYNAMICAL VARIABLES OF THE PARAMETRIZATION OF SURFACES

In general, the dynamical variables are functions of u as well as functionals of $x^\mu(u)$. To emphasize the dependence on the metric $x^\mu(u)$ we write a variable ξ as $\xi(u,M)$, with M denoting the metric $x^\mu(u)$. The operators Π operate on ξ through M, while there may be operators operating on ξ through u. Thus if a function $\xi(u,M)$ is known to satisfy the relation

$$\Pi^{r'}\xi(u,M)=K^{r'}\xi(u,M), \quad (20)$$

where K operates on ξ through u, the condition of integrability

$$[H^{rs}(u'u''),\xi(u,M)]=0 \quad (21)$$

becomes, because of the relation

$$\Pi^{r'}\Pi^{s''}\xi=\Pi^{r'}K^{s''}\xi=K^{s''}\Pi^{r'}\xi=K^{s''}K^{r'}\xi,$$

the relation

$$[-[K^{r'},K^{s''}]+\delta_s(u'-u'')K^{r''}$$
$$+\delta_r(u'-u'')K^{s'},\xi]=0. \quad (22)$$

Let us work out the condition that the expectation value of a dynamical variable B at a point P inside a surface S be independent of the parametrization of the surface. Let the parameters u_r be changed to

$$u_r{}^*=u_r-a_r(u)\epsilon. \quad (23)$$

Since

$$x_\mu{}^*(u^*)=x_\mu(u),$$

we have

$$\Delta x_\mu=x_\mu{}^*(u)-x_\mu(u)=(\partial x_\mu/\partial u_r)a_r\epsilon.$$

The change of the wave function is thus

$$-\epsilon i\int a_rP^r du\Psi.$$

If the expectation value of B at a point P inside a surface is unchanged, we have

$$\left(1+\epsilon i\int a_r'P^{r'}du\right)B(u^*,M^*)$$
$$\times\left(1-\epsilon i\int a_r''P^{r''}du''\right)=B(u,M), \quad (24)$$

M^* denoting the new metric. Thus

$$[P^{r'}-\Pi^{r'},B(u,M)]=-(\partial B/\partial u_r)\delta(u-u'). \quad (25)$$

Similarly, suppose that the expectation value of $A(u,M)du$ is some physical quantity independent of the parametrization. (For brevity, we call such $A(u)$ a parametrization-independent density.) We have

$$\left(1+\epsilon i\int a_r'P^{r'}du'\right)A(u^*,M^*)du^*$$
$$\times\left(1-\epsilon i\int a_r''P^{r''}du''\right)=A(u,M)du, \quad (26)$$

where

$$du^*=\frac{D(u_1{}^*,u_2{}^*,u_3{}^*)}{D(u_1,u_2,u_3)}du=(1-\epsilon(\partial a_r/\partial u_r))du. \quad (27)$$

From (26) and (27) we get

$$[P^{r'}-\Pi^{r'}, A(u, M)]=A(u', M)\delta_r(u'-u). \quad (28)$$

This can be written as

$$[P^{r'}-\Pi^{r'}, Adu]=-(\partial(Adu)/\partial u_r)\delta(u-u'),$$

with $\partial du/\partial u_r$ understood as zero and

$$[\Pi^{r'}, du]=du\delta_r(u'-u).$$

The last relation can be obtained by comparing (27) and

$$du^*-du=\epsilon\int a_r'du'[\Pi^{r'}, du].$$

In the usual quantum mechanics, the energy and momentum operators are defined by the coefficients of Δx_μ in the expressions

$$i\int\Delta x_\mu\frac{\delta\Psi}{\delta x_\mu}du=\int\Delta x_\mu\left(\frac{\partial u_r}{\partial x_\mu}\Pi^r+n^\mu\Pi^n\right)\Psi du$$

$$=\int\Delta x_\mu\left(\frac{\partial u_r}{\partial x_\mu}P^r+n^\mu P^n\right)\Psi du. \quad (29)$$

Thus (28) should hold for $A=\Delta x_\mu\{(\partial u_r/\partial x_\mu)P^r+n^\mu P^n\}$. By using Eqs. (15) to (17) and (25), with B replaced by Δx_μ, a straightforward calculation from (28) for this A leads to the condition

$$-\Delta x_\mu\{(\partial u_s/\partial x_\mu)[\Pi^s, P^{r'}]+n^\mu[\Pi^n, P^{r'}]\}=0,$$

or

$$[\Pi^s, P^{r'}]=0, \quad (30.1)$$

$$[\Pi^n, P^{r'}]=0. \quad (30.2)$$

From (29), the energy and the momentum along the direction $\partial x^\mu/\partial u_1$ inside an area du are given by

$$P^n du \quad \text{and} \quad -P^l\left(-\frac{\partial x^\mu}{\partial u_1}\frac{\partial x_\mu}{\partial u_1}\right)^{-\frac{1}{2}}du \quad (31)$$

respectively. It may be noted that (30.1), (30.2) are consistent, since they enable the brackets between $H^{rs}(u', u'')$, $\cdots$ and $P^l(u)$ to vanish simultaneously. (The suffix l is here of the same nature as r, s, $\cdots$.)

In the formulation of the wave equation in Weiss' theory as given in reference 2, we have

$$\left.\begin{aligned}p(u)q(u')-q(u')p(u)&=\hbar\delta(u-u'),\\ P^r&=-(i/\hbar)(\partial q/\partial u_r)p,\end{aligned}\right\} \quad (32)$$

$$[\Pi^{r'}, p]=[\Pi^{n'}, p]=0, \quad [\Pi^{r'}, q]=[\Pi^{n'}, q]=0 \quad (33)$$

for a Bose field, with similar relations for a Fermi field. From (32), (33), it is found that q satisfies (25) for B and p (28) for A. From this, p cannot have significance as a dynamical variable at a point, but rather as a density. This feature of the Weiss theory is certainly not too satisfactory. It may be noticed that Eqs. (30) are satisfied, and thus (31) may be interpreted as the energy and the momentum inside as area du.

4. CONJUGATE VARIABLES IN DIRAC'S THEORY

To push Dirac's theory further, let us ask if there can exist dynamical variables ξ, $\bar\xi$ satisfying the condition

$$\left.\begin{aligned}\xi(u, M)\bar\xi(u', M)+\bar\xi(u', M)\xi(u, M)&\\ =f(u, M)\delta(u-u'),&\\ \xi\xi'+\xi'\xi=\bar\xi\bar\xi'+\bar\xi'\bar\xi=0,&\end{aligned}\right\} \quad (34)$$

where both ξ and $\bar\xi$ are dynamical variables having expectation values independent of parametrizations and f is a c-number. Here we confine ourselves to Fermi-Dirac fields where ξ, $\bar\xi$ play symmetrical roles, the extension to Bose field being obvious.

Let us leave aside P^n and Π^n for the moment. The equations to be considered are (15), (34), (21) and a similar one for $\bar\xi$, and (25) for ξ or $\bar\xi$, and if we want parametrization-independent energy and momentum densities we include further (30.1). So far it is not at all obvious that the above equations are consistent and can yield an expression for P^r, $[\Pi^{r'}, \xi]$, etc.

Condition (25) for ξ or $\bar\xi$ are

$$[P^{r'}-\Pi^{r'}, \xi(u)]+(\partial\xi/\partial u_r)\delta(u-u')=0, \quad (35.1)$$

$$[P^{r'}-\Pi^{r'}, \bar\xi(u'')]+(\partial\bar\xi''/\partial u_r'')\delta(u''-u')=0. \quad (35.2)$$

We now define the positive Poisson bracket (p.P.B.) $[A, B]_+\equiv-i(AB+BA)$, take the p.P.B. of the left side of (35.1) with $\bar\xi(u'')$, that of left side of (35.2) with $\xi(u)$ and add. We get, on using (34),

$$[\Pi^{r'}, f(u, M)]=(\partial f/\partial u_r)\delta(u-u')-f\delta_r(u-u'). \quad (36)$$

$f(u)$ thus satisfies an equation of the type (20) with $[K^{r'}, f]$ given by the right side of (36). From this it is easily verified that (22) is satisfied for f, and since $[\Pi^{r'}, f]$ is yet entirely arbitrary, (36) may have a solution f.

From (36) and (28), we find that $f^{-1}du$ has a significance independent of parametrization. The surface element is certainly independent of parametrization, and thus we expect that one solution for f is

$$f=(N_\mu N^\mu)^{-\frac{1}{2}},$$
$$N_\mu=\epsilon_{\mu\nu\rho\theta}(\partial x^\nu/\partial u_1)(\partial x^\rho/\partial u_2)(\partial x^\theta/\partial u_3), \quad (37)$$

where $\epsilon_{\mu\nu\rho\theta}$ is the antisymmetrical tensor. In fact, it may be directly verified that (37) gives a solution of (36). For this solution, $\Pi^{n'}f$ is a function of u times $\delta(u-u')$.

Among the equations to be considered, (21) and a similar one for $\bar\xi$ are redundant; i.e., they are consequences of (15), (34) and (35). To show this, denote the left side of (35.1) by $H^r(u', u)$, and we then have

$$\begin{aligned}0=&[G^{rs}(uu'), \xi(u'')]-[P^r(u), H^s(u'u'')]\\ &+[P^s(u'), H^r(uu'')]=-\delta_s(u-u')[P^{r'}, \xi'']\\ &-\delta_r(u-u')[P^s, \xi'']-\delta(u'-u'')[P^r, \xi_s'']\\ &+\delta(u-u'')[P^{s'}, \xi_r'']+[\Pi^{s'}, [P^r, \xi'']]\\ &-[\Pi^r, [P^{s'}, \xi'']],\end{aligned} \quad (38)$$

where ξ_s stands for $\partial\xi/\partial u_s$ etc. Eliminating $[P^r, \xi'']$,

$[P^r, \xi_s'']$ etc. by (35.1) we reduce the right side of (38) to terms of the type $[\Pi, \xi]$, $[\Pi, [\Pi, \xi]]$, ξ. The vanishing of this right side yields exactly Eq. (21).

The remaining equations are (15), (34), (35), (30.1). From (15), (30.1) we get

$$[P^r, P^{s'}]-\delta_s(u-u')P^{r'}-\delta_r(u-u')P^s=0. \quad (39)$$

From (34), (39) we get a solution[7]

$$P^r=-if^{-1}\xi_r\bar{\xi}. \quad (40)$$

From this and (35), we get

$$[\Pi^{r'}, \xi]=0, \quad (41.1)$$

$$[\Pi^{r'}, \bar{\xi}]=\bar{\xi}[\Pi^{r'}, \log f]. \quad (41.2)$$

From these, one verifies that (30.1) is satisfied, and thus (40), (41) give us a correct solution. Obviously $-if^{-1}\bar{\xi}_r\xi$ is another solution for P^r, owing to the symmetry between ξ and $\bar{\xi}$.

To search for the general solution, write P^r as a series in ξ, ξ_s, $\xi_{sl}(\equiv\partial^2\xi/\partial u_s\partial u_l)$, $\cdots$, $\bar{\xi}$, $\bar{\xi}_r$, $\cdots$. Substitution into (39) gives us relations among the coefficients, which we call a_s'. Substitution into (30.1) and making use of (35) give us an equation containing ξ, ξ_s, $\cdots$, $\bar{\xi}$, $\bar{\xi}_s$, $\cdots$, a_s' and $\Pi a_s'$, and thus give us relations between a_s' and $\Pi a_s'$. If all these relations for a_s' and $\Pi a_s'$ have a common solution, the series gives us a solution for P^r. In this way, we find that P^r have only the two above solutions.

For $[\Pi^{n'}, \xi]$, etc. we are forced to assume

$$[\Pi^{n'}, \xi]=0, \quad (42.1)$$

$$[\Pi^{n'}, \bar{\xi}]=\bar{\xi}[\Pi^{n'}, \log f], \quad (42.2)$$

so that (41) and (42) are integrable and (30.2) is satisfied. (41.2), (42.2) show that $\bar{\xi}/f$ is independent of the metric. If we let $\hbar\bar{\xi}/f=\xi^*$, ξ^* satisfies

$$\xi\xi^{*\prime}+\xi^{*\prime}\xi=\hbar\delta(u-u')$$

and (28), behaving exactly as the conjugate variable to $q=\xi$ in the Weiss theory. After this transformation, P^r takes the form $-(i/\hbar)\xi_r\xi^*$ in Weiss' theory. Thus so far as P^r, $\Pi^{r'}\xi$, $\Pi^{n'}\xi$, $\Pi^{r'}\bar{\xi}$, $\cdots$ are concerned, a simple transformation of the variables carries the Dirac theory into the Weiss theory.

[7] If we had required P^r, P^n to be parametrization-independent densities, we could have done so. From (15) and (28) with A replaced by P^s, we get

$$[\Pi^s, P^{r'}]=P^r\delta_s(u'-u),$$

which is the counterpart of (30.1). (39) is replaced by

$$[P^{r'}, P^s]=0$$

and (40) by

$$P^s=f^{-1}b_\nu{}^s(\partial u_l/\partial x_\nu)(\xi_l\bar{\xi}+\xi\bar{\xi}_l),$$

where $b_\nu{}^s$ are arbitrary quantities.

5. THE DETERMINATION OF P^n

For definiteness, let us restrict ourselves to Fermi-Dirac fields. A simple choice of P^n is

$$P^n=(\hbar/f)(c^0\xi\bar{\xi}+c^s\xi_s\bar{\xi}). \quad (43)$$

We have such a form for P^n in Weiss' theory, and since the wave equation in such a theory is integrable, this form of P^n satisfies together with (34), (40), (41), (42) the Eqs. (15) to (17) with suitably choosen c's. On substituting (43) into (15)–(17) and making use of (34), (40), (41), (42), we find

$$[\Pi^{r'}, c^0]=(\partial c^0/\partial u_r)\delta(u-u'), \quad (44.1)$$

$$[\Pi^{n'}, c^0]=b\delta(u-u')+ic^0c^s\delta_s(u'-u), \quad (44.2)$$

$$[\Pi^{r'}, c^s]=(\partial c^s/\partial u_r)\delta(u-u')-\delta_{rs}c^l\delta_l(u-u'), \quad (44.3)$$

$$[\Pi^{n'}, c^s]=b^s\delta(u-u')+\left\{-i\frac{\partial u_s}{\partial x_\mu}\frac{\partial u_l}{\partial x^\mu}+ic^lc^s\right\}\delta_l(u-u'), \quad (44.4)$$

b and b^s being arbitrary. The solutions of (44) are far from unique; thus a solution for the c^s from (44.3) is $\alpha_\nu(\partial u^s/\partial x_\nu)$, with the α_ν as arbitrary constants. The vanishing of the brackets $H^{rs}(u', u'')\cdots$ with the c's give us conditions of Πb, Πb^s, etc. The simultaneous solution for b and c from such conditions together with (44) will not be pursued here.

To get wave equations essentially different from those in Weiss' theory, let us introduce terms $h^s\xi\bar{\xi}_s$ and $h^{sl}\xi_s\bar{\xi}_l$ into P^n. Equation (16) is satisfied if

$$[\Pi^r, h^{s'}]=(\partial h^s/\partial u_r)\delta(u-u')-h'^s\delta_r(u-u')+\delta_{rs}h'^l\delta_l(u-u'),$$

$$[\Pi^r, h^{sl'}]=(\partial h^{sl}/\partial u_r)\delta(u-u')-h'^{sl}\delta_r(u-u')+(h'^{ml}\delta_{rs}+h'^{sm}\delta_{rl})\delta_m(u-u'),$$

both of which are integrable. However (17) is not easily satisfied. To satisfy (17), a simple addition of a term $h^s\xi\bar{\xi}_s$ compels us to introduce simultaneously terms like $\xi\bar{\xi}_{rs}$, $\xi_{rs}\bar{\xi}$, and these, in turn, compel us to introduce terms like $\xi\bar{\xi}_{rsln}$, $\xi_{rslm}\bar{\xi}$, etc. Thus, there are no simple expressions for P^n except (43). If P^n is given by (43), the theory resembles closely that of Weiss. In particular, the expectation value of ξ at a point P inside a surface S constructed from the wave function on S is independent of S so long as S passes through P and satisfies a Lagrangian principle.

Effects of Initial Energies on Mass Spectra*

CLIFFORD E. BERRY
Consolidated Engineering Corporation, Pasadena, California
(Received January 16, 1950)

The slit system of a conventional mass spectrometer discriminates against ions having initial kinetic energies. Relations between the amount of the discrimination and the geometry of the system are developed and confirmed experimentally for ions having only thermal energy. Curves showing the discrimination against high energy fragments from a number of simple molecules are given. These curves show that measured relative abundances depend strongly on the geometry of the system and on the accelerating voltage.

In theory, the initial velocity distribution can be obtained from discrimination data. This method is shown to be impractical, and a better method is described, which involves electrostatic deflection of the ion beam in a direction parallel to the magnetic field. Curves of ion intensity *vs.* deflecting potential give directly the shape of the distribution for one component of initial velocity. Distribution curves are given for the same ions for which discrimination curves were obtained.

1. INTRODUCTION

CONVENTIONAL mass spectrometers exhibit a phenomenon called *discrimination*, in which ions having initial energies may fail to pass through the slit system of the ion source and analyzer tube because of the effects of the components of velocity normal to the principal motion through the system. It is found in general that ions having no initial kinetic energy except that due to thermal motions are discriminated against, even at accelerating voltages of several thousands of volts. In addition it is well known[1] that many molecules, when fragmented by electron impact, produce ions having as much as several volts excess kinetic energy. Such ions may be discriminated against to such an extent that very few are observed reaching the collector.

In the practical design and operation of mass spectrometers it is of interest to know what discrimination effects may take place, and to know their relation to the geometry of the system. This is particularly true of instruments used for isotope ratio measurements or for gas analysis. In addition, there is the possibility of utilizing the discrimination effect to determine average values of initial kinetic energies, and possibly to determine energy distributions, from which information regarding the potential energy curve for certain states of the molecule may be deduced.

The literature on the subject of discrimination itself is somewhat limited. Hagstrum and Tate,[2] in studying ionization processes, discussed qualitatively the discrimination against high energy ions at the first slit of a mass spectrometer. Coggeshall[3] was the first to show that even thermal velocities are great enough to cause measurable discrimination at the second slit of a conventional mass spectrometer, and that appreciable errors in isotope ratio measurement might result. Washburn and Berry[4] pointed out that discrimination at the collector slit could be of the same order of magnitude as the discrimination at the second slit. They showed a set of discrimination curves for a number of ions from *n*-butane and attempted to estimate the initial energies of the various ions.

In work on molecular structure there have been numerous studies of the ionization process by electron impact, and while much of this work has been concerned with appearance potential measurements, some attention has been given to kinetic energy measurements, both in the mass spectrometer and in the retarding field apparatus of Lozier.[5,6] However, since Lozier's method cannot distinguish between ions of different mass-to-charge ratio, its use is somewhat limited.

Hagstrum and Tate[2] were able to make some deductions concerning the shape and position of the upper potential energy curves for a number of diatomic molecules by studying the peak shapes of the high energy ions in a mass spectrometer. Newhall[7] used the retarding

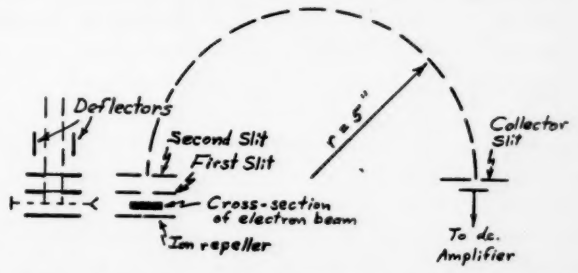

FIG. 1. Arrangement of slits in the mass spectrometer used in the experiments. For most of the discrimination experiments the dimensions were as follows: First slit, 0.008×0.250 in.; second slit, 0.008×0.250 in.; collector slit, 0.030×0.250 in. The separation of the first and second slits was 0.250-in. For the deflection experiments, the lengths of the second slit and collector slit were changed from 0.250 to 0.040 in.

* An abridgement of a thesis submitted to the Graduate Faculty of Iowa State College in partial fulfilment of the requirements for the degree of Doctor of Philosophy.

[1] E. E. Hanson, Phys. Rev. **51**, 86 (1937).
[2] H. D. Hagstrum and J. T. Tate, Phys. Rev. **59**, 354 (1941).
[3] N. D. Coggeshall, J. Chem. Phys. **12**, 19 (1944).
[4] H. W. Washburn and C. E. Berry, Phys. Rev. **70**, 559 (1946).
[5] W. W. Lozier, Phys. Rev. **36**, 1285 (1930).
[6] W. W. Lozier, Phys. Rev. **46**, 268 (1934).
[7] H. F. Newhall, Phys. Rev. **62**, 11 (1942).

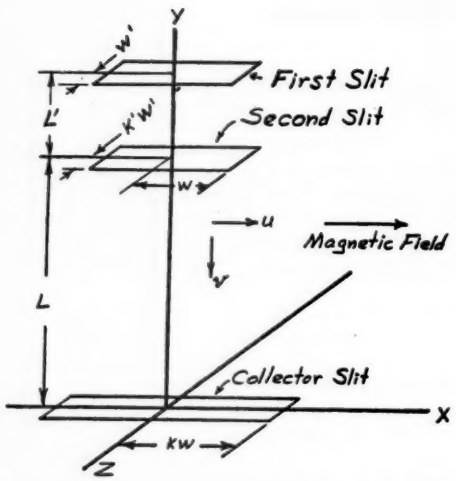

FIG. 2. Coordinate system used in deriving the discrimination equations for the collector slit and the second slit. The y axis has been shown straight for convenience; actually it is an arc of a circle.

potential produced by the space charge of the electron beam in a special mass spectrometer to study high energy protons. Hipple *et al.*[8] described the use of a retarding field near the collector in a mass spectrometer. Although their purpose was to suppress metastable ions, they demonstrated that the CH_3^+ ion in *n*-butane may result from two processes, one giving ions of low initial energy and the other ions of high initial energy.

The problem which was undertaken in the present work was twofold: (a) To investigate theoretically and experimentally the effects of discrimination by the slits of a mass spectrometer, and (b) to explore methods of determining the distribution of initial velocities, in the hope of extending the usefulness of the mass spectrometer in the study of molecular structure.

2. THEORETICAL TREATMENT

A. Derivation of Discrimination Equations

(a) *Discrimination at the Collector Slit*

Figure 1 shows the slit system of the mass spectrometer used in this study. The ions formed in the electron beam are forced through the first slit by a weak electric field, and are then accelerated in the region between the first and second slits by a voltage V. Between the second slit and the collector slit the ions travel at constant speed, but are caused to move in a circular path by the uniform magnetic field in which the entire apparatus is immersed. This is a conventional 180° mass spectrometer; the treatment that follows, however, applies to any mass spectrometer of the sector type, since the only geometrical factors concerned in the discrimination effect are the relative slit dimensions and spacings.

An approximate derivation of the discrimination at the collector slit will be given first. Figure 2 shows the coordinate system and defines the pertinent quantities. It is assumed that ions pass through the second slit with a velocity v derived from the accelerating voltage, and in addition possess a small component of velocity $\bar{u}$ at right angles to v in the direction of the plane of the slits.[9] We may consider $\bar{u}$ to be the average molecular velocity corresponding to the temperature of the gas in the ionization region.

If we define collection efficiency N as the ratio of the number of ions of given mass passing through the collector slit in unit time to the number passing through the second slit, we can write from simple geometrical reasoning that

$$N=\left\{\begin{matrix}1\\k\end{matrix}\right\} \text{ for } L\bar{u}/v<|k-1|w, \tag{1}$$

$$N=\tfrac{1}{2}(1+k-L\bar{u}/v) \text{ for } |k-1|w<L\bar{u}/v<(k+1)w, \tag{2}$$

$$N=0 \text{ for } L\bar{u}/v>(1+k)w, \tag{3}$$

where the upper term in the bracket in Eq. (1) corresponds to $k>1$ and the lower to $k<1$, and where k is the ratio of the length of the collector slit to the length of the second slit. Thus for either case, the collection efficiency is constant out to a critical value of $L\bar{u}/v$ then, regarded as a function of $L\bar{u}/v$, decreases linearly to zero. If $k=1$, the initial flat portion of the curve disappears.

The relations just derived are applicable only when the spread in thermal velocities is small compared with v, so that the average value, $\bar{u}$, is representative. For

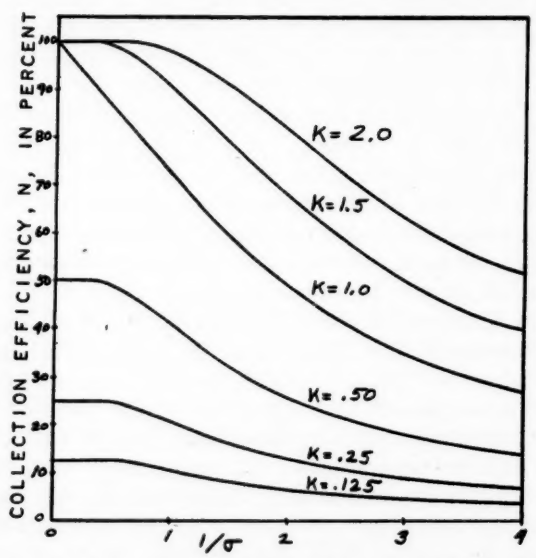

FIG. 3. Collection efficiency calculated from Eq. (4) in terms of the dimensionless parameter σ.

[8] Hipple, Fox, and Condon, Phys. Rev. **69**, 347 (1946).

[9] Initial components in the y and z directions merely broaden the beam at the focal point, but since the beam is normally somewhat narrower than the collector slit, these components cause no loss of ions at the collector except at very low accelerating voltages.

small values of v, the actual distribution of initial velocities must be considered. In the Appendix, the problem is solved for the general case of an arbitrary initial velocity distribution and also for a Maxwellian distribution. For the latter case, the result is found to be

$$N=\tfrac{1}{2}(k+1)\ erf[(k+1)\sigma]-\tfrac{1}{2}|k-1|\ erf[(k-1)\sigma] +(1/2\pi^{\frac{1}{2}}\sigma)[\exp[-(k+1)^2\sigma^2] -\exp[-(k-1)^2\sigma^2]], \quad (4)$$

in which σ is a dimensionless parameter defined as $(108w/L)(V/T)^{\frac{1}{2}}$, V is the accelerating potential in volts, and T is the absolute temperature of the gas in degrees Kelvin. A plot of Eq. (4) for several values of the parameter, k, is shown in Fig. 3.

(b) *Discrimination at the Second Slit*

The discrimination effect at the second slit can be derived in a similar manner. Here the initial velocity component of interest is that at right angles to the plane of the slits. (Since the spacing of the first and second slits is normally nearly the same as the length of the slits, a velocity component parallel to the plane of the slits has relatively small effect.) The principal difference between this case and the previous one is that here the ions, instead of traversing the region with constant forward velocity, travel under constant acceleration. Thus the effects of initial velocity components are relatively twice as great. Equation (4) applies provided that σ is defined as $(54w'/L')(V/T)^{\frac{1}{2}}$ and k' is substituted for k.

Coggeshall[3] derived an approximate expression for the discrimination effect at the second slit for the case $k=1$. If Eq. (4) is expanded in powers of σ, the first-order term is identical with Coggeshall's Eq. (16) when proper interpretation of symbols is made. Furthermore, the first-order approximation to Eq. (4) is identical with Eq. (2), the approximation derived previously.

Discrimination at the first slit can be treated in the same manner as that at the second slit if the thickness of the electron beam is assumed to be negligible. In the mass spectrometer used in the experimental work to be described, no discrimination at the first slit was observed because of the relatively great width of the electron beam as compared with the width of the first slit.

B. Determination of Initial Energy Distributions

(a) *Method Based on Discrimination Effect*

Since the efficiency of collection, N, depends on the initial velocity distribution function $\rho(u)$, it should be possible, in theory at least, to find the distribution function from an experimental curve of N *vs.* V. If it is assumed that discrimination occurs only at the collector slit and that the value of the parameter k is unity, the problem is readily solved. The general expression for the collection efficiency (Eq. (9) in the Appendix) in effect can be turned inside out to give an explicit expression for the initial *speed* distribution, $F(s)$, with the result

$$F(s)=-s^2\frac{d^3N(s)}{ds^3}-3s\frac{d^2N(s)}{ds^2}, \quad (5)$$

in which $N(s)$ is the collection efficiency function.

For determining $F(s)$ from an experimental curve for N, the use of Eq. (5) appears to be impracticable, since extremely smooth data would be required in order for the second and third differences to have meaning. Also,

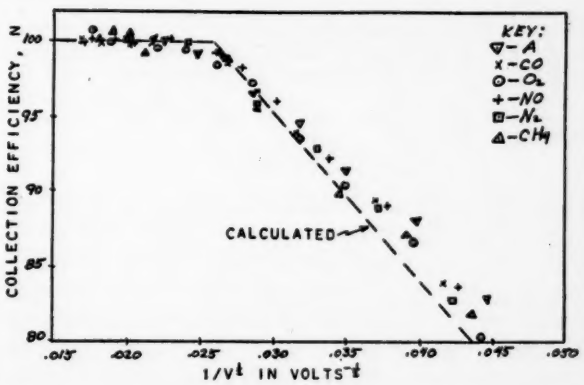

FIG. 4. Comparison of discrimination curves for a number of ions having only thermal energy. The calculated curve is based on the approximate treatment of Eqs. (1)–(3).

the problem would become much more complicated if k were different from unity or if discrimination at more than one slit occurred.

(b) *Method Based on Deflection of Beam in Analyzing Region*

A more promising method of determining initial velocity distributions is based on the use of a pair of small deflecting electrodes as shown in Fig. 1, placed immediately behind the entrance slit to the analyzing region so as to deflect the ion beam in the x direction. Such electrodes are used in some mass spectrometers in order to center the ion beam on the exit slit by compensating for mechanical misalignment.

As discussed earlier, the x component of initial velocity causes the beam to fan out in the x direction in the analyzing region. By making w/L sufficiently small, and thus the collection efficiency, N, likewise small, the collector slit in effect takes a small sample of the original beam, the sample consisting of those ions entering the analyzer with very small x components of velocity. By means of the deflecting electrodes, the fanned-out beam can be moved past the collector in the x direction, allowing each part of the original beam to be sampled.

It is easily shown that the curve of ion current *vs.* deflecting voltage gives directly the shape of the initial velocity curve for one component. The relation between the velocity scale and other pertinent factors is found

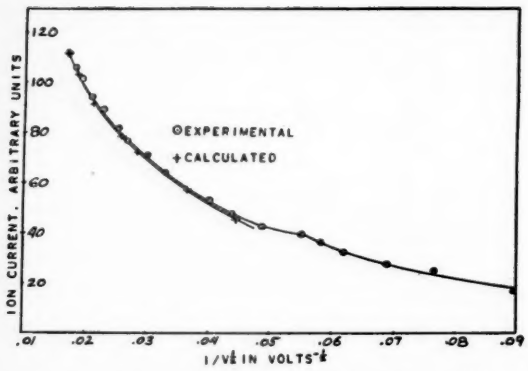

FIG. 5. Discrimination curve for CO^+, using 0.040-in. long second slit and collector slit. The calculated curve was obtained from Eq. (4).

to be

$$u = AP(e/mV)^{\frac{1}{2}}, \tag{6}$$

where A is a constant of the instrument, P the deflecting potential in volts, e the charge on the particle in e.s.u., m the mass of the particle in grams, and V the accelerating potential in volts. In general the accurate calculation of the constant A is difficult. However, by calibrating the instrument with an ion of known velocity distribution and known energy, e.g., an ion with thermal energy, A can be determined empirically.

It is important to note in Eq. (6) that for an ion of given initial energy distribution, the experimental curve should be an invariant function of $P/V^{\frac{1}{2}}$, regardless of the constant value of V used. This is an excellent criterion for judging whether an instrument is measuring the true initial velocity distribution. If the collection efficiency is too high so that too broad a section of the distribution curve is sampled, then the distribution will appear different for different values of V, since the collection efficiency varies with V. Likewise, if end effects occur at the slits, the apparent distribution may be affected by the value of V, since some ions may receive x components of velocity from the accelerating field.

3. EXPERIMENTAL APPARATUS

The mass spectrometer used for the experimental work has been described in other publications.[10–12] The principal information needed in connection with the present work is that given in Fig. 1, which shows the slit dimensions and radius of curvature. The temperature of the ion source was 534°K, as determined by a thermocouple. It had been determined previously that the gas entering the ionizing region was in thermal equilibrium with the walls of the ion source.

The energy of the ionizing electrons was 100 volts for all experiments. The gas samples were approximately 99 percent or better in purity.

[10] C. E. Berry, Electronic Industries **3**, 94 (June, 1944).
[11] Washburn, Wiley, Rock, and Berry, Ind. Eng. Chem., Anal. Ed. **17**, 74 (1945).
[12] Washburn, Wiley, and Rock, Ind. Eng. Chem. Anal. Ed. **15**, 541 (1943).

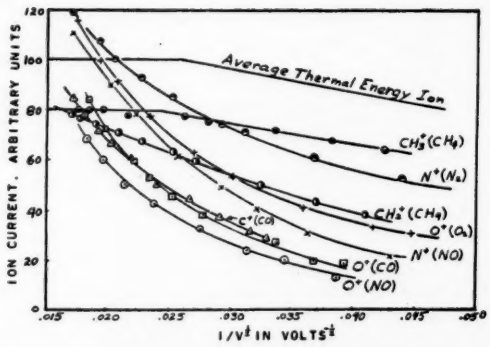

FIG. 6. Discrimination curves for the high energy fragments produced from a number of molecules. The discrimination curve for an average molecular ion is given for comparison. The scales are in arbitrary units, but the actual ratio of the current for a given fragment to the current for its parent molecule can be obtained by multiplying the scale for the fragment by the appropriate factor given: C^+ from CO −0.059; O^+ from CO −0.030; O^+ from O_2 −0.12; N^+ from N_2 −0.15; O^+ from NO −0.047; N^+ from NO −0.14; CH_2^+ from CH_4 −0.11; CH_3^{2+} from CH_4 −1.1.

4. EXPERIMENTAL RESULTS

A. Discrimination Experiments

(a) *Ions with Thermal Energy*

Equation (4), giving the collection efficiency for an ion with a Maxwellian distribution of initial velocities, reveals that the mass of the ion does not enter into the relation between collection efficiency and accelerating voltage. Thus, if no other effect than that postulated takes place, the curves of collection efficiency *vs.* accelerating voltage should be the same for all ions receiving no energy from dissociation processes.

Figure 4 compares the results of runs on the molecular ions formed in CO, A, O_2, N_2, NO, and CH_4 which have only thermal energy. The points are seen to cluster very closely in a band two to three percent wide, thus confirming that primarily the discrimination effect, with only small extraneous effects, was taking place.

The abrupt change of slope observed in Fig. 4 was unexpected, inasmuch as previous work had shown no discrimination caused by the second ion slit. Furthermore, the nominal value of k for the collector slit was unity. However, the curves obtained are just what would be obtained from Eqs. (1) and (2) for $k \neq 1$. Since previous studies of deposits in the ion source had indicated that the ion beam was not perfectly collimated, the most reasonable explanation of the sharp break in the curves is that the beam of ions was either slightly diverging or slightly converging in the x direction (Fig. 2), so that effectively k differed from unity. A simple calculation shows that a half-angle of convergence in the x direction of 0.25° would give the calculated curve shown in Fig. 4 and would correspond to an effective value of 1.56 for k.

The discrimination curve for the molecular ion $n\text{-}C_4H_{10}^+$ was found to contain a break, but the left-hand portion of the curve was not horizontal. Such an

effect could be caused by metastable ions, which are known to be formed in this molecule. Using Hipple's value[13] for the half life of the metastable $n-C_4H_{10}^+$ ions, the experimental curve was corrected to give a curve closely matching those of Fig. 4. However, it was necessary to assume that 29 percent of the $n-C_4H_{10}^+$ ions were originally in a metastable state, rather than 9 percent as Hipple estimated.

(*b*) *Discrimination at the Second Slit*

The results of all runs thus far described were completely explained by assuming that only the collector slit was active in discriminating against ions with thermal energy. This was considered reasonable in view of previous observations of deposits on the second slit. These observations indicated that because of lens action at the first slit, the beam striking the plane of the second slit was considerably wider than the slit itself. In this case there should be an effective value for k' somewhat less than unity.

In order to test this hypothesis, several runs were made, using the CO^+ ion at much lower accelerating voltages (down to 60 volts) than were used previously. A second sharp break in the curve appeared at an accelerating voltage of about 340 volts, which is somewhat below the values commonly used in the normal operation of the mass spectrometer. From the position of this break, an effective value of 0.46 for k' was computed, which checks fairly well with measurements of deposits in the ion source.

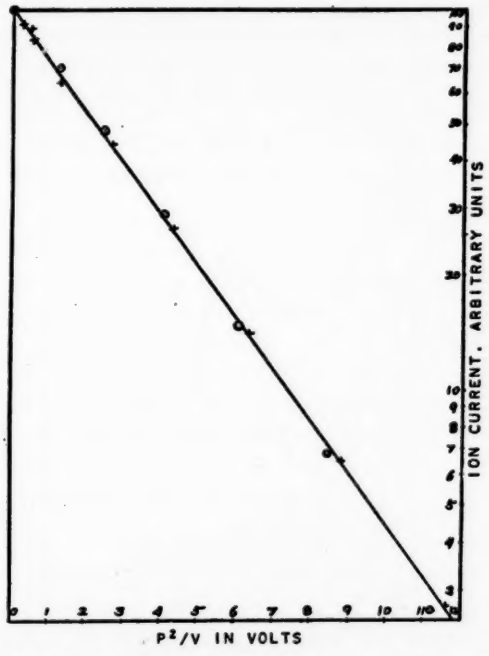

FIG. 7. Deflection experiment for CO^+ ion. By plotting the log of the intensity *vs.* the square of the deflecting voltage, the curve should be linear if the distribution is Maxwellian.

[13] J. A. Hipple, Scientific Paper #1264, Westinghouse Research Laboratories, East Pittsburgh, Pa. (1946).

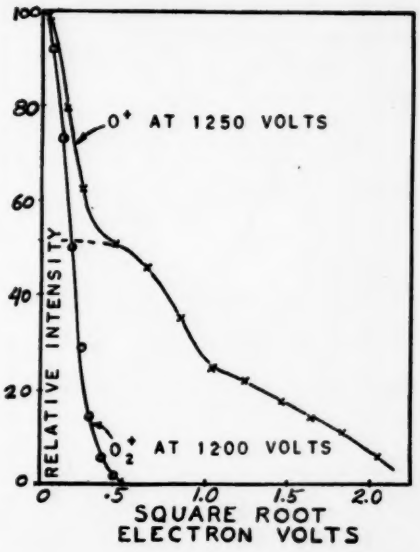

FIG. 8. Velocity distribution curves for O^+ and O_2^+ from O_2. The dotted line is an estimated distribution assuming the central hump to be O^{++} ions with thermal energy.

A further check on the discrimination effect for thermal energy ions was obtained by running CO^+ with the entrance slit and collector slits cut down in length from 0.250 to 0.040 in. by means of apertured disks placed in the analyzer. The results of this run are shown in Fig. 5. The lower break, attributed to the second slit, did not change in position, but the upper one completely disappeared.

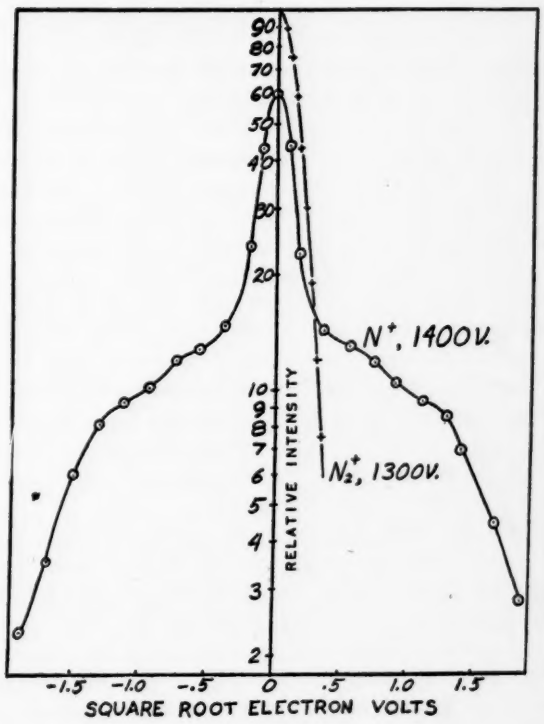

FIG. 9. Velocity distribution curves for N^+ and N_2^+ from N_2.

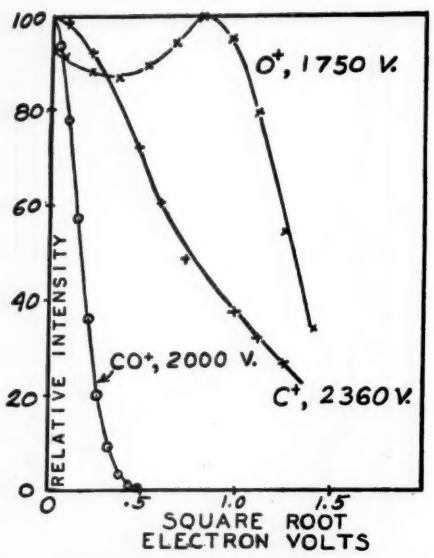

FIG. 10. Velocity distribution curves for C^+, O^+, and CO^+ from CO.

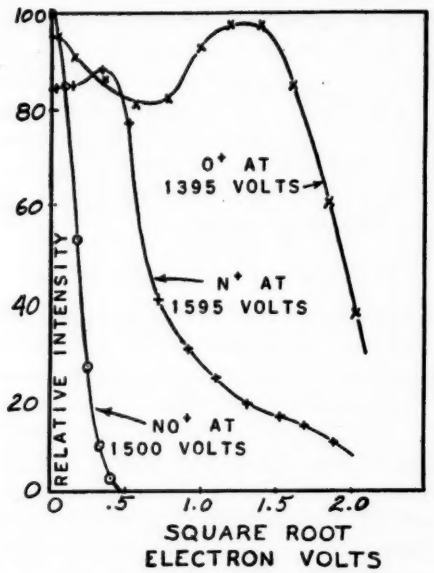

FIG. 11. Velocity distribution curves for N^+, O^+, and NO^+ from NO.

That portion of the curve to the left of the break, for which only the collector slit was responsible, afforded an excellent check on Eq. (4). The effective value of k was assumed to be unity, since only ions near the axis of the tube were collected. With this assumption, Eq. (4) for the collection efficiency was computed for the values of w, L, and T used in the experiment. The theoretical points are shown as crosses in Fig. 5. The vertical scale factor was adjusted to fit at an arbitrarily chosen point; the agreement is seen to be good.

(c) *Discrimination Against High Energy Ions*

Figure 6 shows the result of discrimination runs on the high energy fragments resulting from ionization of CO, O_2, N_2, NO, and CH_4. Plotted on the same sheet is the average curve for the thermal energy molecular ions. The scale factor for the molecular ions has been normalized, whereas the scale factors for the high energy ions are in arbitrary units. However, in each case a conversion factor is given by which the actual ion currents of the low and high energy ions can be related.

In general, the curves for the high energy ions are seen to be extremely steep when compared with that for thermal energy ions. It is probable that for the high energy ions shown, except the CH_3^+ ion from methane, each curve is in the region below the second break; that is, in the region where both the collector slit and the second slit are discriminating.

The CH_3^+ ion from methane appears to have but little excess energy, since the first break has moved only to a slightly higher voltage. Because of the scatter of points the position of the break for the CH_3^+ curve is not definite. However, by comparing the slope of this curve with that of the CH_4^+ curve, the average energy of the CH_3^+ was found to be approximately 46 percent higher than thermal energy. This gives a value of 0.032 ev for the average excess kinetic energy of the CH_3^+ ions.

It may be concluded that, insofar as the discrimination effect is concerned, the simple theory presented here adequately describes the effect. It is plain from a study of the curves given that the observed spectrum of a given substance will depend strongly on the geometry of the instrument used to obtain that spectrum.

The use of discrimination curves to estimate average initial energy appears to be valid for low energy ions. For high initial energies the method proposed becomes

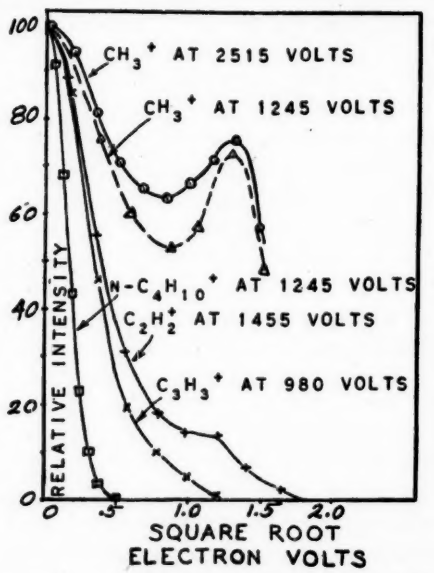

FIG. 12. Velocity distribution curves for various ions from $n-C_4H_{10}$. The dotted curve shows the effect of changing the accelerating voltage on the anomalous distribution for the CH_3^+ ion.

too indirect to be of any use. In this connection it should be pointed out that the data presented by Washburn and Berry,[4] on the average initial energies of some ions from *n*-butane, were based on imperfect knowledge of the effects of discrimination and the influence of the energy distributions on the slopes of the curves, and the figures given can only be rough approximations.

B. Deflection Experiments

(*a*) *Test of the Method*

The principal test of the deflection method was to see whether the measured distribution curve for an ion having a Maxwellian distribution gave the correct curve experimentally. Figure 7 shows a typical result on an ion with thermal energy, the CO^+ ion. For a Maxwellian distribution, plotting the log of the intensity against the velocity squared should give a straight line. The curve shown was drawn through the experimental points with a straightedge by estimating the best average position. The good linearity over a range of intensity of nearly 40 to 1 shows a close agreement with Maxwell's distribution law and gives confidence in the method.

Further tests, using ions of different masses, and the same ion at different accelerating voltages, gave reasonably consistent results. Runs of this sort were used to establish the energy scales for the distribution curves of the high energy ions.

(*b*) *Distributions for High Energy Ions*

Figures 8 through 12 show the results of runs on the high energy ions observed in O_2, N_2, CO, NO, and $n-C_4H_{10}$, respectively. Plotted on each sheet are also the distributions for the respective molecular ions. Each curve gives the shape of the distribution for one component of velocity, plotted in square root electron volts so that energy distributions can be calculated readily.

O^+ from O_2

The distribution curve of Fig. 8 shows the probable presence of three groups of ions, one having essentially thermal energy (probably O_2^{++} ions) one having a minimum energy of about 0.17 ev, and one having a minimum energy of about 1.1 ev. These latter groups correspond to transitions giving rise to the "Type II" peak shapes of Hagstrum and Tate.[2]

N^+ from N_2

The curve of Fig. 9 is similar to the curve for O^+ from O_2, showing again three distinct groups of ions, one having essentially thermal energy, one having a minimum energy at about 0.5 ev, and the third having a minimum energy of about 1.9 ev.

C^+ and O^+ from CO

The C^+ ion shows a smooth curve (Fig. 10) rising to a maximum at zero with no abrupt changes in slope,

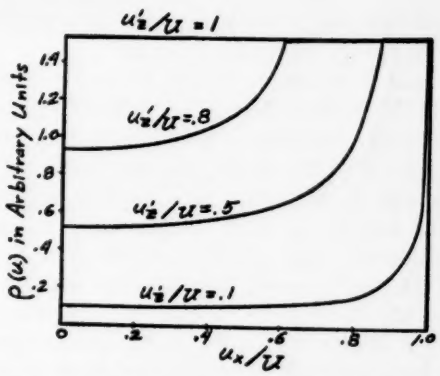

FIG. 13. Theoretical distribution functions, showing the distortion produced by discrimination.

indicating that many ions are formed with energies near zero. This is in general agreement with the results of Hagstrum and Tate for this particular ion.

The result for the O^+ ion from CO is anomalous in that a minimum occurs at zero velocity. In any physical situation where spherical symmetry obtains, the distribution of one component of velocity cannot have a positive slope at any point, as this implies a negative value for a portion of the speed distribution function. Neglecting this for the moment, it is apparent that very few, if any ions of less than about 0.65 ev are formed, and that appreciable numbers are formed with more than 2.5 ev. This also is in general agreement with the result of Hagstrum and Tate on CO.

N^+ and O^+ from NO

Both curves of Fig. 11 for NO show the same anomaly as observed with the O^+ ion from CO. As the ion currents for the O^+ and N^+ peaks were rather weak, the scatter of points is somewhat worse than for some of the other gases. However, there is a definite dip in each distribution. In the case of the N^+ ion, there appear to be no ions formed with less than 0.1 ev, while for the O^+ ion, all appear to have at least 2 ev. This result for O^+ disagrees with that of Hagstrum and Tate, since they suggest that appreciable numbers of O^+ ions are formed with zero energy. They give no result for the N^+ ion.

CH_3^+, $C_2H_2^+$, $C_3H_3^+$ from $n-C_4H_{10}$

The curves of Fig. 12 for the $C_2H_2^+$ ion and the $C_3H_3^+$ ion show that ions of several volts energy are produced, but that many low energy ions are also produced. Since it is probable that many different types of processes can give rise to these ions, the curves are undoubtedly the superposition of several different distributions.

The distribution curve for the CH_3^+ ion is more interesting. Here again the same anomaly is observed as with some of the previous ions. However, there is a rise in the center, suggesting the presence of a group of CH_3^+ ions with low, perhaps only thermal, energies. This is in agreement with the results of Hipple,[8] who

found evidence for the existence of a high energy group and a low energy group for this ion.

The most likely reason for the anomalous curves obtained for N^+ and O^+ from NO, O^+ from CO, and CH_3^+ from $n-C_4H_{10}$ becomes apparent when the effects of discrimination at the second slit are considered. It has been tacitly assumed thus far that the ions emerging from the second slit have a spherically symmetrical distribution of initial velocities. However, if any component is discriminated against the distribution of every other component is changed. In the present instance it is known that the second slit discriminated against ions with high initial velocities in the z direction. Thus it should be expected that the x component of velocity, which is the component affected by the deflecting potential, would suffer a distortion of its distribution function.

The effect, on the x velocity distribution, of losing all ions with z components of velocity above a certain amount is readily calculated. Figure 13 summarizes the results. It is assumed that all ions have initially the same velocity U, uniformly distributed in direction, and that those ions with z components of velocity greater than u_z' are lost. The curves show the distribution in x components of velocity for $u_z'/U=0.1$, 0.5, 0.8, and 1.0. It is seen that the distributions have minima at zero velocity and reach a maximum at a point dependent upon u_z'/U. Beyond this point the distribution is uniform out to $u_x/U=1$.

In any actual case, the distribution of initial velocities would have a spread of values, so that a superposition of distributions such as those shown in Fig. 13 would occur. However, if there were a minimum value of the initial speeds the superposition would then result in a velocity distribution curve with a minimum at zero velocity, such as that found for O^+ from CO, for example. On the other hand, of large numbers of ions with both low and high velocities were formed the over-all distribution of one component of velocity, while distorted by the discrimination effect, still would not necessarily show a dip in the center.

The effect just mentioned should become greater the lower the accelerating voltage. This is borne out by the dotted curve of Fig. 12, which shows the distribution for the CH_3^+ ion from $n-C_4H_{10}$ at 1245 volts. The solid curve, taken at 2515 volts, shows the same general shape but has a less pronounced dip.

It is clear that precise use of the deflection method in the present apparatus is limited to those ions with such low energies that discrimination at the second slit does not occur. Consideration of the discrimination curves for the second slit indicates that, at an accelerating voltage of about 2000 volts, negligible second slit discrimination would occur against those ions which had their principal energies below about six times thermal energy. In order to obtain accurate distribution curves for higher energy ions a modification of the ion source would have to be made to reduce the second slit discrimination.

The direction in which to proceed to reduce the second slit discrimination is indicated by Eq. (1). By increasing the width of the first slit, and making k' smaller (assuming it to be less than unity originally), the maximum value of the initial velocity that will be free of discrimination can be increased. For example, increasing the first slit width by a factor of three and decreasing the second slit width by a factor of two should result in an increase of a factor of 5.5 in the maximum initial velocity that would be discrimination free. This corresponds to a 30-fold increase in the initial energy. Reference to the velocity distribution curves shown in Figs. 8–12 shows that such a modification should allow much more accurate distribution curves to be obtained.

Despite the fact that the velocity distributions shown are distorted from the true distributions, they are of interest in indicating the magnitudes of the initial dissociation energies of the molecules studied. Furthermore, the sharp breaks occurring in some of the curves undoubtedly indicate the presence of certain transitions taking place within the molecules.

The writer wishes to express his gratitude to Dr. H. W. Washburn for many suggestions during the course of the work, to Dr. Sam Legvold for his encouragement and suggestions regarding the manuscript, and to Consolidated Engineering Corporation for the use of the mass spectrometer and for permission to publish this work.

APPENDIX

Derivation of the discrimination equation for an arbitrary initial velocity distribution and for a Maxwellian distribution.

For an arbitrary distribution of velocities, $\rho(u)$, Eqs. (1) and (2) can be rewritten as

$$dN_u=\begin{Bmatrix}1\\k\end{Bmatrix}\rho(u)du \quad \text{for} \quad Lu/v<|k-1|w, \tag{7}$$

$$dN_u=\tfrac{1}{2}(1+k-Lu/vw)\rho(u)du \quad \text{for} \quad |k-1|w<(Lu/v)<(k+1)w. \tag{8}$$

Integrating (7) and (8) between the limits indicated, and adding, there results for the over-all collection efficiency

$$N=2\begin{Bmatrix}1\\k\end{Bmatrix}\int_0^{|k-1|\omega v/L}\rho(u)du + 2\int_{|k-1|\omega v/L}^{(k+1)\omega v/L}\tfrac{1}{2}(1+k-Lu/wv)\rho(u)du, \tag{9}$$

where the factor 2 appears because only positive velocities are considered in the limits.

Now if the distribution of velocities is Maxwellian the indicated integrations can be carried out. The distribution of one component of velocity is given by

$$\rho(u)=(hm/\pi)^{\frac{1}{2}}\exp(-hmu^2), \tag{10}$$

where m is the mass of the particle in grams, and $h=1/2RT$, in which R is Boltzmann's constant in ergs/deg. C/molecule, and T is degrees Kelvin. Making this substitution, and setting

$\sigma=(w\nu/L)(hm)^{\frac{1}{2}}$, the final expression for N becomes

$$N=\tfrac{1}{2}(k+1)\,erf[(k+1)\sigma]-\tfrac{1}{2}|k-1|\,erf[(k-1)\sigma]+(1/2\pi^{\frac{1}{2}}\sigma)[\exp[-(k-1)^2\sigma^2]-\exp[-(k-1)^2\sigma^2]]. \quad (11)$$

This is a simple result, since all possible conditions are encompassed by the two dimensionless parameters k and σ. The parameter k is simply the ratio of the collector slit length to the entrance slit length; σ can be expressed in other terms, by substituting for h its equivalent expression given above, and for v in terms of the mass and charge of the particle and the accelerating voltage. When this is done, we obtain

$$\sigma=(w/L)(eV/300RT)^{\frac{1}{2}}. \quad (12)$$

Substitution of numerical factors for e and R gives

$$\sigma=108w/L(V/T)^{\frac{1}{2}}.$$

The general discrimination equation, Eq. (9), for the special case of $k=1$, can be inverted to give an explicit expression for the initial speed distribution $F(s)$ in terms of the collection efficiency function $N(s)$. Though tedious, the process simply involves repeated differentiation of the integrals of Eq. (9), and suitable rearrangement. The final result is

$$F(s)=-s^3\frac{d^3N(s)}{ds^3}-3s\frac{d^2N(s)}{ds^2}. \quad (13)$$

PHYSICAL REVIEW VOLUME 78, NUMBER 5 JUNE 1, 1950

On the Statistics of Luminescent Counter Systems*

FREDERICK SEITZ
University of Illinois, Urbana, Illinois
AND
D. W. MUELLER
Los Alamos Scientific Laboratory, University of California, Los Alamos, New Mexico

(Received February 10, 1950)

The method of generating functions is employed to analyze the composite statistical variations which arise in a counting system that consists of a source, a luminescent crystal, and a photo-multiplier tube. The methods are applied to several photo-type assemblies and indicate that the techniques can be used to treat any problem of this type in a simple way. It is found that once the crystal has accepted energy, the effectiveness of the assembly is measured by the number of photo-electrons ejected from the photo-cathode of the multiplier. This quantity, which depends upon the luminescent efficiency of the crystal, the geometry of the crystal-multiplier arrangement and the efficiency of the photo-cathode, should be at least 5 for faithful counting of particles absorbed in the crystal. The number of photoelectrons must be much larger than 5 for good statistics if the current from the multiplier is measured. The results of Schiff and Evans for the statistical variations in the voltage of a condensor which is charged with the pulses from the multiplier are generalized to cover the case in which the size of pulses varies.

1. INTRODUCTION

THE type of crystal counter which depends upon the combination of luminescent crystals and a photo-multiplier tube shows promise of being of great service in the detection of radiations both because of its high sensitivity and its speed of registry and recovery. This device has been developed by a large number of individuals, almost too numerous to mention; however, the origin of the system appears to rest with Coltman and Marshall,[1] who employed powdered luminescent materials of the type used in previous commercial luminescent systems, and with Broser and Kallmann,[2] who first appreciated the advantages of employing large transparent luminescent crystals and introduced organic materials.

The purpose of the present paper is to analyze some of the factors which influence the statistical behavior of luminescent counter systems in order to evaluate the limits within which a counter may be used in making a particular type of measurement. The problems of interest range over a wide spectrum of possibilities. However, the problem on which we shall focus attention for immediate purposes in order to provide a practical objective is the following: A crystal counter system is employed to count the gamma-rays emitted from a source in time T. If N gamma-rays are emitted, what is the most probable number that will be counted and what is the range of variation to be expected? We shall attempt to examine this problem in a sufficiently general way that the results will have value for a much broader group of problems.

It is interesting to consider the component parts of this problem in order to be able to examine the sources of statistical variations. The components are as follows.

(A) The source, even if constant in the sense that it remains unchanged during the time T will contribute to the statistical variation since the gamma-rays are usually emitted at random. For simplicity, we shall assume that the time T is sufficiently short that varia-

* This document is based on work performed at Los Alamos Scientific Laboratory of the University of California under U. S. Government contract W-7405-Eng-36.

[1] J. W. Coltman and F. Marshall, Phys. Rev. **72**, 528 (1947); F. Marshall, J. App. Phys. **18**, 512 (1947).

[2] I. Broser and H. Kallmann, Zeits. f. Naturforschung **2a**, 439 (1937); 642 (1947); Broser, Herforth, Kallmann, and Martius, Zeits. f. Naturforschung **3a**, 6 (1948).

tions in the source strength can be neglected and that the statistical variations in emission of gamma-rays can be treated on the basis of a Poisson distribution.

(B) Unless the source is completely surrounded by the luminescent material, some of the gamma-rays will not pass through this material and hence will certainly fail to be registered. We shall designate the average fraction which passed through the material by f, so that the average number of gamma-rays which pass through the detecting system, if N are emitted from the source, is

$$\nu = fN. \tag{1}$$

If the source is isotropic, f will be determined simply by the solid angle subtended by the crystal system; otherwise a somewhat more involved calculation is needed to determine f.

(C) A given gamma-ray may or may not produce an ionizing pulse within the luminescent crystal. The possible mechanisms for producing such a pulse are the photoelectric effect, the Compton effect and pair production. In the first and third cases the gamma-ray transmits all of its energy to the crystal, provided the energetic electrons produced by the gamma-ray do not escape from the crystal. A greater statistical variation is possible when the range of gamma-ray energy and atomic number is such that the Compton effect predominates. This would be the case for example if the luminescent material were one of the organic types such as naphthalene or anthracene and if the gamma-rays had an energy in the neighborhood of 2 Mev.

The probability of a Compton encounter may be described in terms of the mean free path λ for the process namely

$$\lambda = 1/n_e\sigma_c, \tag{2}$$

where n_e is the density of electrons in the luminescent material and σ_c is the Compton cross section per electron. If d is the thickness of the luminescent material in the direction in which the incident gamma-rays are traveling, the probability that a given gamma-ray will pass through the system without producing a Compton electron is $e^{-\alpha}$ where

$$\alpha = d/\lambda. \tag{3}$$

The initial energy k_0 of the gamma-ray and the energy k after the collision are related by the equation[3]

$$\frac{k}{k_0} = \frac{1}{1+\gamma(1-\cos\theta)}, \tag{4}$$

where θ is the angle between the incident and scattered quantum and γ is the energy of the incident gamma-ray expressed in units of the rest mass of the electron (507 kev). The energy gained by the electron is $\epsilon = k_0 - k$. From (4) we readily derive the relation

$$d(\cos\theta) = (k_0/\gamma k^2)dk. \tag{5}$$

[3] The notation employed here is that of W. Heitler, *The Quantum Theory of Radiation* (Oxford University Press, New York, 1936).

The differential cross section $d\varphi$ for scattering into solid angle $d\Omega$ is

$$d\varphi = \frac{r_0^2 d\Omega}{2}\frac{k^2}{k_0^2}\left(\frac{k_0}{k}+\frac{k}{k_0}-\sin^2\theta\right)$$

in which r_0 is the classical electron radius e^2/mc^2. If we use the relation $d\Omega = 2\pi\sin\theta d\theta$ and replace $d\theta$ by dk with the use of (5), we obtain

$$d\varphi = \pi r_0^2\frac{1}{k_0\gamma}\left(\frac{k_0}{k}+\frac{k}{k_0}-\sin^2\theta\right)dk. \tag{7}$$

This is to be employed in the range of k from k_0 to $k_0/(1+2\gamma)$, corresponding to the range of θ from 0 to π. When θ takes the values 0, $\pi/2$ and π the quantity in parentheses in Eq. (7) takes the values

$$2(\theta=0);\quad \frac{1+\gamma+\gamma^2}{1+\gamma}(\theta=\pi/2);\quad 2\frac{1+2\gamma+2\gamma^2}{1+2\gamma}(\theta=\pi). \tag{8}$$

For values of γ not larger than about 4, this variation is sufficiently small that it is reasonably satisfactory to assume that k has equal probability of falling in any part of the allowed range, or that the knocked-on electron has equal probabilities of receiving any energy in the range from zero to $2\gamma/(1+2\gamma)$, in units of k_0. For very large values of γ the $\sin^2\theta$-term in parenthesis in (7) may be neglected for the most interesting collisions. It is then clear from the remaining terms in parenthesis that collisions in which k is small compared with k_0 are preferred over those in which k is near k_0.

The degree of preference is not exceedingly great for values of γ in the normal radioactive range and we shall assume that the probability per unit energy range is constant within the allowed limits. This gives the maximum statistical variation to be expected in a given Compton process.

The gamma-ray may conceivably make a number of Compton encounters in passing through the crystal. There are two interesting extreme cases to consider which we shall refer to as the "thin" and "thick" approximations. In the thin case, which corresponds to values of α appreciably less than unity the gamma-ray has much smaller probability of making two collisions than one collision. We shall treat this case by assuming that α may be chosen to be a constant for each successive collision as if its energy were not greatly affected by successive Compton encounters. In this event the probability that the gamma-ray will make n encounters can be described by the distribution function

$$P_n = (\alpha^n e^{-\alpha})/n! \tag{9}$$

for the range of values of n of practical interest.

In the thick approximation the gamma-ray transfers all of its energy to the luminescent material in a succession of encounters once it has made the first encounter. Thus this case is equivalent to that in which

the gamma-ray transfers its energy by means of the photoelectric effect or pair production, provided the electrons produced do not escape. These last two cases differ from the thick approximation only with respect to the geometrical distribution of points within the crystal at which the electrons are released—a difference which we shall not consider here.

The thin approximation is best achieved by employing a very thin crystal so that α is small compared with unity and also employing soft gamma-rays, for which γ is unity or less, which lose relatively little energy in a Compton encounter. It is probably not a case which would be met in practice, but is interesting as one statistical extreme. It should be remarked that this limit cannot be achieved by going to very soft radiation for such radiation is scattered almost isotropically. The distance which the scattered photon must traverse is usually different from that which the original photon would have had to travel to pass through the crystal because it is traveling in a different direction. Thus α is not a constant in this limit even though the energy of the photon is not greatly altered by a Compton collision. The thick case can evidently be achieved by using a thick crystal and is the one that will be met more commonly in practice.

(**D**) The number of luminescent quanta which the crystal emits can vary even when the energy transmitted to the crystal is fixed because of statistical fluctuations in the manner in which the exciting radiation is distributed among the different excited states of the medium. This type of statistical fluctuation is partly responsible for the straggling in range of heavy ionizing particles as they pass through matter. In order of magnitude the fractional variation in the number of light quanta is $1/\eta^{\frac{1}{2}}$, where η is the average number. Since we shall be interested in cases in which η is 1000 or larger, corresponding to Compton encounters in which the knocked-on electron gains several hundred kev of energy, this source of statistical variation will be neglected for the present. It could be significant in cases in which the particle being detected produces very few light quanta, as for very soft beta-rays or x-rays.

(**E**) Only a fraction of the light quanta produced in the luminescent crystal will reach the photoelectric surface. The fraction Ω which do is determined primarily by geometrical factors involving the angular distribution of emitted light and the angle subtended by the photosurface relative to the luminescent material. The value of Ω will be in the neighborhood of 0.5 for a relatively thin layer of luminescent material which is immediately adjacent to the photo-surface, but may be considerably smaller if the luminescent crystal is somewhat farther away. It may be enhanced by placing a reflecting backing on the luminescent material or by employing other devices which cause the light to be "funneled" toward the photo-cathode.

(**F**) Only a fraction p of the photons striking the photo-surface will eject electrons from it. This parameter appears[4] to be about 0.03 for the type of photo-surface in which the photons penetrate the photo-surface and electrons are ejected from the back side, and about 0.05 for the type of photo-surface for which electrons are ejected from the front surface.

(**G**) The electrons ejected from the photo-cathode will give rise to pulses of various size, depending upon the accidents which befall the primary photo-electron and the secondaries which it emits from the multiplying surfaces. Actually there are two problems associated with an analysis of the pulse distribution: first, that of determining the probability that the photo-electron will actually create a measurable pulse, and second, that of determining distribution of pulse sizes when pulses are generated. If the secondary emission ratio is s, the probability that the photo-electron will not eject a secondary from the first stage of the multiplier is e^{-s}, provided we assume the emission of secondaries to be random. This probability is of the order of a few percent for normal values of s (between 3 and 5), and is essentially equal to the probability that the primary electron will not generate a pulse. Since the percentage uncertainty in p is at least as large as this, we may combine this factor with p in the following discussion and assume that a measurable pulse is produced whenever an electron is ejected. The distribution of pulse sizes has been measured by Engstrom[4] using a light source. Presently we shall approximate his results with an appropriate mathematical function. Evidently the pulse distribution is not important if the luminescent counter is employed simply as a counter of events and if a pulse of arbitrary size can be employed as the signal for a significant count. Knowledge of the distribution becomes important, however, if a pulse discriminator is employed so that only pulses larger than a certain size are counted (as when a noise background is eliminated) or if the integrated current of the photo-multiplier is recorded. The first of these cases can be treated by redefining the parameter p as the probability that an observable pulse is measured when a photon strikes the cathode and introducing measured values of this quantity. The second case will be discussed in detail.

2. THE GENERATING FUNCTION AND ITS APPLICATIONS TO THE PRESENT PROBLEM[5]

The aggregate contribution of the various unit parts of the photo-multiplier system to the statistical varia-

[4] P. W. Engstrom, J. Opt. Soc. Am. 37, 420 (1947). G. A. Morton and J. A. Mitchell, RCA Review 9, 632 (1948) have shown that the pulse-height distribution is broader than that expected on the basis of a Poisson distribution of electrons at each stage.

[5] The generating function was introduced into probability theory very early in its development and some of its properties are described in textbooks (see for example, J. V. Uspensky, *Introduction to Mathematical Probability* (McGraw-Hill Book Company, Inc., New York, 1937)). The writers have benefited by reading a mimeographed survey of the subject by O. R. Frisch. An account of some of the relations employed here is given by

tion of the system can be determined most simply with the use of generating functions appropriate to each stage. If p_n is the probability that a given observation shall yield n events; for example, that the source shall emit n gamma-rays in time T, the generating function $G(\epsilon)$ for the process of observation is defined by the series

$$G(\epsilon)=p_0\epsilon^0+p_1\epsilon^1+p_2\epsilon^2+\cdots+p_n\epsilon^n+\cdots. \quad (10)$$

The generating function is readily found to possess the following properties

$$G(0)=p_0; \quad G(1)=1. \quad (11)$$

The mean value m of a series of observations, namely,

$$m=\sum_n np_n \quad (12)$$

is readily seen to satisfy the relation

$$m=(dG/d\epsilon)_{\epsilon=1}. \quad (13)$$

Similarly the variance of a sequence of observations, defined by the relation

$$v=\sum_n(n-m)^2p_n=\sum_n n^2p_n-m^2 \quad (14)$$

is readily found to be related to the generating function by the equation

$$v=\left[\frac{d^2G}{d\epsilon^2}+\frac{dG}{d\epsilon}-\left(\frac{dG}{d\epsilon}\right)^2\right]_{\epsilon=1}=\left(\frac{d^2G}{d\epsilon^2}\right)_{\epsilon=1}+m-m^2. \quad (15)$$

In the case of the Poisson distribution

$$p_n=(\alpha^n e^{-\alpha})/n! \quad (16)$$

$G(\epsilon)$ is readily found to be

$$G(\epsilon)=e^{\alpha(\epsilon-1)}, \quad (17)$$

whence

$$m=\alpha, \quad v=\alpha. \quad (18)$$

In the following we shall employ the ratio $v^{\frac{1}{2}}/m$ to provide a measure of the fractional deviation from the mean or the *fractional deviation*. In the case of the Poisson distribution this quantity is the familiar ratio $1/\alpha^{\frac{1}{2}}$. Although the generating function is interesting and useful because of the properties outlined above, its real service appears when the following two additional properties are considered.

(I). Suppose that instead of making one observation of the number of events of interest (such as the number of gamma-rays emitted from the source in time T) we make two observations (e.g., for two time intervals T) and ask for the probability that n events are observed *in toto*. The probability for this is the sum

$$p_np_0+p_{n-1}p_1+p_{n-2}p_2+\cdots+p_0p_n,$$

which is the coefficient of ϵ^n in the expansion of $G^2(\epsilon)$. This is a special case of the more general theorem: The generating function governing the probability distribution of the *sum* of r identical observations is $G^r(\epsilon)$ if $G(\epsilon)$ is the generating function for a single observation.

(II). Suppose next that we are dealing with a situation in which each member of a set of initial events which are statistically distributed (such as gamma-rays from a source) can give rise to a series of events of possibly different type (for example, the production of Compton electrons), and ask for the statistical distribution of the second type of event. Let $G_1(\epsilon)$ be the generating function for the first type of event (e.g., the number of gamma-rays emitted by the source in a given time for the example under consideration) and $G_2(\epsilon)$ be the generating function for the number of events of the second type associated with one primary event (e.g., the number of Compton recoils produced by a single gamma-ray). It is readily shown that the generating function $G_{II}(\epsilon)$ for the number of events of the second type when the statistical variation of the number of events of the first type is taken into account is given by

$$G_{II}(\epsilon)=G_1[G_2(\epsilon)]. \quad (19)$$

The validity of this theorem can be demonstrated readily by writing G_{II} in the form

$$G_{II}(\epsilon)=p_0G_2^0(\epsilon)+p_1G_2^1(\epsilon)+p_2G_2^2(\epsilon)+p_3G_2^3(\epsilon)+\cdots+p_nG_2^n(\epsilon)+\cdots, \quad (20)$$

in which p_n is the probability of n events of the first type, so that

$$G_1(\epsilon)=p_0\epsilon^0+p_1\epsilon^1+p_2\epsilon^2+\cdots+p_n\epsilon^n+\cdots.$$

The coefficient of p_n in (20) is the generating function for the total number of events of the second type when it is known that n events of the first type have occurred, in accordance with theorem I. This coefficient appears suitably weighted with the probability that n primary events shall occur.

We may readily find, using Eqs. (13) and (14), the mean and variance associated with the generating functions

$$G_I(\epsilon)=G^r(\epsilon) \quad \text{and} \quad G_{II}(\epsilon)=G_1[G_2(\epsilon)], \quad (21)$$

which occur in the cases I and II described above. The results are respectively

$$m_I=rm \quad v_I=rv \quad (22)$$

in which m and v are the mean and variance associated with a single observation in case I, and

$$m_{II}=m_1m_2, \quad v_{II}=v_1m_2^2+v_2m_1. \quad (23)$$

It is clear that if case II were extended to that in which the second type of event can give rise to a third type (e.g., if a Compton electron can give rise to ion pairs or to luminescent quanta) which is statistically distributed in accordance with a generating function

T. Jorgenson, Am. J. Phys. 16, 285 (1948). We are indebted to Dr. S. Ulam for pointing out the value of the generating function to us.

$G_3(\epsilon)$ the complete generating function which takes account of the statistical variation in events of the three types is

$$G_{III}=G_1(G_2[G_3(\epsilon)]), \tag{24}$$

for which the mean and variance are, by analogy with (23)

$$m_{III}=m_{II}m_3, \quad v_{III}=v_{II}m_3^2+v_3m_{II}. \tag{25}$$

We shall now examine the appropriate form of generating function to be employed in each of the constituent processes described in Section 1.

(1) *Emission from source.* Since the gamma-rays are emitted at random, the appropriate generating function is of the Poisson type (17), namely

$$G_1(\epsilon)=e^{N(\epsilon-1)}, \tag{26}$$

in which N is the average number of gamma-rays emitted in the time T.

(2) *Passage of gamma-rays into system.* A given gamma-ray either does or does not enter the crystal. If the probability that it does is f, the generating function for this event is simply

$$G_2(\epsilon)=(1-f)+f\epsilon. \tag{27}$$

Using (19) we readily find that the generating function $G_2'(\epsilon)$ giving the distribution of probabilities that the gamma-rays emitted at random by the source enter the crystal is

$$G_2'(\epsilon)=G_1[G_2(\epsilon)]=\exp[Nf(\epsilon-1)]=\exp[\nu(\epsilon-1)], \tag{28}$$

where $\nu=fN$.

(3) *Generation of photons.* As stated in Section 1, we shall assume that a fixed fraction of the energy which the gamma-photon gives up to the crystal is transformed into light quanta. If this energy is E, the number of light quanta produced is then

$$\eta=\beta E, \tag{29}$$

where β is a factor measuring the efficiency with which the luminescent crystal converts the excitation energy it receives into light quanta. If $h\nu$ is the average energy of the luminescent quanta emitted, $\beta h\nu$ is the fraction of the energy of excitation which appears in the form of luminescent radiation. This may be as large as 0.20 for some of the most efficient materials, but can easily be much smaller. According to Broser, Kallmann, and Martius,[6] the efficiencies of energy conversion in zinc sulfide activated with silver and in the organic materials naphthalene, diphenyl, and phenanthrene are shown in Table I. The investigators find somewhat different efficiencies for beta-ray excitation. Similarly, Coltman, Ebbighausen, and Altar[7] have found the energy conversion in calcium tungstate to be 5.0 percent for x-rays. We shall be concerned with detailed values of the efficiency in Section 3.

TABLE I. Efficiency of energy conversion in luminescent materials under gamma-ray excitation. (After Broser, Kallmann and Martius. Values in fractions.)

Material	$\beta h\nu$
ZnS:Ag	0.135
naphthalene	0.05
diphenyl	0.075
phenanthrene	0.11

As mentioned in Section 1, there are two extreme approximations that are of interest, namely those designated as "thin" and "thick." In the second case, all of the energy of the gamma-ray is transmitted to the crystal once a first collision has occurred. The number of quanta emitted is then equal to η_0, the value of η when k_0 is the energy of the gamma-ray. If c is the probability that such a collision occurs, the generating function for the number of quanta is evidently

$$S_3(\epsilon)=(1-c)+c\epsilon^{\eta_0}. \tag{30}$$

If this is combined with (28) the complete generating function for the production of luminescent quanta in the thick case is

$$S_3'=\exp[\nu c(\epsilon^{\eta_0}-1)]. \tag{31}$$

In the thin case there are two sources of statistical variation, for both the number of Compton encounters and the energy transferred to the counter per collision may vary. The first of these quantities is distributed in accordance with the Poisson law (17) in the ideal thin case, for which the generating function is

$$H_3=e^{\alpha(\epsilon-1)},$$

where α is the ratio (3). The energy which the Compton electron receives is randomly distributed between zero and the maximum value $2k_0\gamma/(1+2\gamma)$ in the approximation described in paragraph 3 of the introduction. This means that the number of quanta generated will vary between zero and a maximum η_m, where

$$\eta_m=\beta\frac{2k_0\gamma}{1+2\gamma} \tag{32}$$

in which β is the efficiency factor appearing in Eq. (29). A generating function for this random distribution is readily constructed by treating η as a continuous variable and is

$$K_3(\epsilon)=\frac{1}{\eta_m}\int_0^{\eta_m}\epsilon^\eta d\eta=\frac{\exp(\eta_m\log\epsilon)-1}{\eta_m\log\epsilon}, \tag{33}$$

for which the mean and variance are $\eta_m/2$ and $\eta_m^2/12$, respectively. The complete generating function for the number of quanta associated with a single gamma-ray is $H_3(K_3(\epsilon))$.

(4) *Emission of photo-electrons.* A given light quantum

[6] See the paper by L. Herforth and H. Kallmann, Ann. d. Physik 4, 231 (1949).

[7] Coltman, Ebbighausen, and Altar, J. App. Phys. 18, 530 (1947).

either does or does not emit a photo-electron from the photo-surface of the multiplier. The probability that it does is Ωp, so that the generating function for this process is

$$G_4(\epsilon)=((1-\Omega p)+\Omega p\epsilon). \tag{34}$$

As stated in sub-section (G) of Section 1, we shall assume that a measurable pulse is associated with each photo-electron ejected from the cathode of the multiplier.

(5) *Generating function for pulse distribution.* Engstrom[4] has measured the pulse-height distribution of a typical multiplier tube. We shall represent his empirical distribution by the analytical function

$$f(h)=Ah^2\exp(-h/\rho), \tag{35}$$

in which h is the pulse height on an arbitrary scale, ρ is a constant measuring the width of the distribution and A is a normalization factor $\frac{1}{2}\rho^3$. A generating function

$$G_5(\epsilon)=1/(1-\rho\log\epsilon)^3, \tag{36}$$

can readily be constructed for this distribution. The mean and variance are

$$m_5=3\rho \quad \text{and} \quad v=3\rho^2. \tag{37}$$

We shall see later that it is not necessary to know ρ in order to determine the fractional deviation which is of interest to us.

3. CORRELATION BETWEEN GAMMA-RAYS FROM SOURCE AND PULSES IN MULTIPLIERS

Let us now ask for the probability that a gamma-ray from the source will produce a pulse in the multiplier. We shall treat separately the thick and thin cases.

(A). *Thick Case.* In the thick case, a gamma-ray passing through the crystal has probability c of making an encounter in which case it generates η_0 photons. The distribution of such encounters is random, being governed by the Poisson distribution. The average number is $Nfc=\nu c$ and the variance is νc. Thus as far as luminescent pulses are concerned the effective strength of the source is νc.

The probability that n of the η_0 light quanta will eject photo-electrons from the multiplier is given by the generating function

$$[G_4(\epsilon)]^{\eta_0}=[(1-\Omega p)+\Omega p\epsilon]^{\eta_0}. \tag{38}$$

The probability that none will eject electrons is $(1-\Omega p)^{\eta_0}$, so that the probability of observing a pulse, if one electron is sufficient to produce an observable pulse, is

$$P=1-(1-\Omega p)^{\eta_0}. \tag{39}$$

Since η_0 is usually large compared with unity, this may be approximated by

$$P=1-\exp(-\eta_0\Omega p), \tag{40}$$

in which the quantity

$$\eta_0\Omega p, \tag{41}$$

is the average number of photo-electrons emitted from the cathode.

With the use of the rule (25) for determining the mean and variance of a chain of events, we find that the mean number of counts is

$$M=Nfc(1-\exp(-\eta_0\Omega p))=NfcP, \tag{42}$$

whereas the variance is

$$V=NfcP. \tag{43}$$

The fractional variance is

$$V^{\frac{1}{2}}/M=[1/(NfcP)]^{\frac{1}{2}} \tag{44}$$

(B). *Thin Case.* There are four statistical processes in the chain extending from the passage of gamma-rays into the crystal to the ejection of electrons from the photo-cathode; namely, those described by the generating functions G_2', H_3, K_3 and G_4 of the preceding section. The number of electrons ejected from the cathode when a single gamma-ray passes through the crystal is governed by the generating function

$$E(\epsilon)=H_3[K_3(G_4(\epsilon))]. \tag{45}$$

The probability that no electron will be ejected, and hence that no pulse will be recorded, is $E(0)$, so that the probability of a pulse is $[1-E(0)]$ and the generating function for pulses is

$$[E(0)+(1-E(0))\epsilon]. \tag{46}$$

Hence the mean and variance in the number of pulses are given by

$$M=V=Nf(1-E(0)). \tag{47}$$

Since Ωp is of the order of three percent even when Ω is unity, we readily find that $K_3(G_4(0))$ can be approximated by the expression

$$K_3(G_4(0))=\frac{[1-\exp(-\eta_m\Omega p)]}{\eta_m\Omega p}. \tag{48}$$

A simple examination of $E(0)$ shows that it approaches $e^{-\alpha}$ when $\eta_m\Omega p$ is large compared with unity and approaches $\exp(-\alpha\eta_m\Omega p/2)$ when $\eta_m\Omega p$ is small.

We conclude that in both the thick and thin cases the counts are governed by a Poisson distribution and that it is desirable to have the quantities c and $(1-e^{-\alpha})$ as near unity as possible; the quantities $\eta_0\Omega p$ and $\eta_m\Omega p$ should be somewhat larger than unity, although there probably is little advantage to having them as large as 10.

As a concrete example, suppose one is dealing with gamma-rays in the vicinity of 1.5 Mev. In this case the mean free path for the Compton effect in a material such as naphthalene is of the order of 15 cm. Hence if the crystal is a cube 5 cm on an edge, the factor $e^{-\alpha}$

is 0.72. The Compton electron will have an average energy of the order of 0.7 Mev so that the average number of luminescent quanta produced is 10,000 if the energy efficiency is taken to be 0.05. Choosing p to be 0.03, we find that $\frac{1}{2}\eta_m\Omega p$ is 300Ω. Hence Ω should be at least 10^{-2} if we expect each Compton electron to register with reasonable faithfulness. If we assume that the photo-surface of the multiplier has an active area of about 15 cm², and that this surface is 5 cm from the center of the crystal, the factor Ω should be as large as 0.05 even if the photons are isotropically distributed, which would guarantee faithful counting of Compton encounters. The same photo-surface would be more nearly borderline if the crystal were chosen to be a 10-cm cube and the surface were placed 10 cm from its center, for then Ω would be about 0.01, which is very close to the limit set above. In fact, those Compton encounters which take place at points within the crystal that are most distant from the surface may fail to register if the photon distribution is isotropic. In this event it may prove profitable to employ a method of light funneling; for example, by covering all surfaces of the crystal except that opposite the multiplier with a reflecting metallic covering.

4. PHOTO-MULTIPLIER CURRENT

Consider next the current in the photo-multiplier, or rather, the charge which arrives at the anode end when N gamma-rays are emitted from the source. We shall treat the "thick" and "thin" cases separately once again.

(A). *Thick Case.* In this case the distribution of charge in the photo-multiplier may be regarded as though it were compounded of the three statistical processes which are described by the generating functions S_3', G_4 and G_5 of Section 2. The first of these gives the distribution of photons in the crystal associated with the N gamma-rays, the second gives the distribution of the photo-electrons from the cathode of the multiplier, and the third gives the distribution of pulses in the multiplier. The means and variances of these distributions are shown in Table II. The quantity $(\Omega p)^2$ can be neglected in comparison with Ωp since the latter is at most a few percent.

By compounding these statistical quantities in accordance with the rule (25) we readily obtain the following values of the mean and variance for the charge in the multiplier

$$\begin{aligned} M&=3\rho\nu c\eta_0\Omega p,\\ V&=3\rho^2\nu c\eta_0\Omega p(4+3\eta_0\Omega p). \end{aligned} \tag{49}$$

TABLE II. Means and variances for the thick case.

	Mean	Variance
S_3'	$\nu c\eta_0$	$\nu c\eta_0^2$
G_4	Ωp	$\Omega p-(\Omega p)^2\cong\Omega p$
G_5	3ρ	$3\rho^2$

The fractional variance is

$$\frac{V^{\frac{1}{2}}}{M}=\left[\frac{4+3\eta_0\Omega p}{3\nu c\eta_0\Omega p}\right]^{\frac{1}{2}}. \tag{50}$$

This quantity is independent of ρ, as pointed out previously. Moreover, it becomes independent of the quantity $x=\eta_0\Omega p$ when this quantity is large compared with unity. The condition placed upon x for this limit to be valid is somewhat more stringent than the condition that is required for faithful counting of luminescent pulses. That is x must be larger than 5 for this approximation to be precise.

(B). *Thin Case.* In this approximation the distribution of pulses is governed by a generating function that is compounded of the generating functions G_2', H_3, K_3, G_4 and G_5. These correspond respectively to the distribution of gamma-rays in the crystal, the distribution of Compton encounters, the distribution of luminescent quanta produced in the crystal, the distribution of photo-electrons from the cathode, and the distribution of pulses in the multiplier. The corresponding means and variances are shown in Table III.

The mean and variance for the distribution of pulses are found to be

$$\begin{aligned} M&=\tfrac{3}{2}\rho\nu\alpha\eta_m\Omega p,\\ V&=\tfrac{3}{2}\rho^2\nu\alpha\eta_m\Omega p(4+\tfrac{1}{2}\eta_m\Omega p(4+3\alpha)). \end{aligned} \tag{51}$$

One again we note that ρ drops out of the fractional variance. Whenever the quantity $y=\eta_m\Omega p$ is very small compared with unity the fractional variance may be approximated by the expression

$$\frac{V^{\frac{1}{2}}}{M}=\left(\frac{8/3}{\nu\alpha\eta_m\Omega p}\right)^{\frac{1}{2}}. \tag{52}$$

In the opposite extreme, in which y is very large compared with unity, the fractional variance is

$$\frac{V^{\frac{1}{2}}}{M}=\left(\frac{4+3\alpha}{3\nu\alpha}\right)^{\frac{1}{2}}, \tag{53}$$

which approaches $2/(3\alpha\nu)^{\frac{1}{2}}$ if α is small compared with unity, and approaches $1/\nu^{\frac{1}{2}}$ if α is very large. The latter case, in which α is large, is in contradiction with the assumptions of the thin approximation; however, it is of mathematical interest.

TABLE III. Means and variances for the thin case.

	Mean	Variance
G_2'	ν	ν
H_3	α	α
K_3	$\eta_m/2$	$\eta_m^2/12$
G_4	Ωp	Ωp
G_5	3ρ	$3\rho^2$

5. FLUCTUATIONS IN CHARGE ON CONDENSER

When dealing with a high intensity source, it is frequently convenient to feed the current pulses from the photo-multiplier into a condenser which is shunted with a high resistance, and then measure the voltage across the condenser in order to provide a measure of the average current which arrives at the condenser. This voltage exhibits fluctuations because the pulses are distributed statistically both in magnitude and in time. The influence of the distribution-in-time has been investigated by Schiff and Evans[8] for the case in which the pulses are equal in magnitude. We are interested in the generalization of their results when the pulses vary in size.

If the capacity of the condenser is C and the shunting resistance is R, the decay time for the shunted capacity is $\tau=RC$. A charge which is fed into the condenser at time t' will have decayed by a factor $\exp[-(t-t')/\tau]$ by the later time t.

We shall assume that the charge associated with each pulse of the multiplier arrives in a time that is short compared with the decay time of the condenser. We shall also assume that the pulses are distributed in time in accordance with the distribution law governing the frequency with which gamma-rays enter the luminescent crystal; that is, in accordance with the generating function $G_2'(\epsilon)$ of Section 2 (see Eq. (28)). Since we shall be interested in specific intervals of time t, we shall replace ν in Eq. (28) by nt, where n is the average number of gamma-rays entering the crystal per unit time. Those gamma-rays which do not excite the crystal will give rise to pulses of zero size. For the purposes of this section, we shall designate the generating function for the pulse in the photo-multiplier associated with the passage of a single gamma-ray into the crystal by $G(\epsilon)$. The pulse size will be assumed to be expressed in units of charge. $G(\epsilon)$ will differ in the soft and hard approximations, but may be left arbitrary for the moment.

Consider the gamma-rays which arrive in the time interval dt' between t' and $t'+dt'$. The generating function associated with the current they contribute to the condenser at the time t' is

$$1+ndt'[G(\epsilon)-1], \tag{54}$$

which is the expansion of $G_2'(G(\epsilon))$ in terms of dt' when ν is replaced by ndt'. The mean value of the charge associated with this generating function is

$$ndt'G'(1). \tag{55}$$

This mean contribution will have decayed by a factor $\exp((t'-t)/\tau)$ by the time t. Thus the mean charge at time t resulting from the accumulation for all previous times is

$$nG'(1)\int_{-\infty}^{0}\exp((t'-t)/\tau)dt'=n\tau G'(1). \tag{56}$$

[8] L. I. Schiff and R. D. Evans, Rev. Sci. Inst. **7**, 456 (1937); L. I. Schiff, Phys. Rev. **50**, 88 (1936).

$G'(1)$ evidently is the mean charge pulse $\bar{Q}$ in the photo-multiplier associated with the entrance of a single gamma-ray.

Similarly, the variance in the charge on the condenser at time t is the integral of the variance of (54) from $t'=-\infty$ to $t'=t$, with a weighting coefficient $\exp[2(t'-t)/\tau]$, since the decay constant for the square of the charge is twice as large as that for the charge. The result is

$$\tfrac{1}{2}\tau n[G''(1)+G'(1)]. \tag{57}$$

The quantity $[G''(1)+G'(1)]$ is the mean of the square of the charge pulse associated with a single gamma-ray, which we shall designate as $\langle\bar{Q}^2\rangle_{Av}$. This is also equal to the variance of the charge pulse associated with a single gamma-ray plus $(\bar{Q})^2$.

We find, then, that the fractional variance of the charge on the condenser is

$$V^{\frac{1}{2}}/M=[\langle Q^2\rangle_{Av}/2\tau n\bar{Q}^2]^{\frac{1}{2}}. \tag{58}$$

The coefficient $(\frac{1}{2}\tau n)^{\frac{1}{2}}$ represents the result obtained by Schiff and Evans for pulses of constant amplitude. We may now investigate the coefficient $\langle Q^2\rangle_{Av}/(\bar{Q})^2$ for the thick and thin case.

(A). *Thick Case.* In this case the generating function $G(\epsilon)$ is $S_3[G_4(G_5(\epsilon))]$. The means and variances of G_4 and G_5 were tabulated in the previous section. The corresponding quantities for G_3 are $\eta_0 c$ and $\eta_0^2 c(1-c)$. By combining the means and variances, we obtain

$$M=\bar{Q}=3\rho\eta_0 c\Omega p,\quad V=3\rho^2\eta_0 c\Omega p(4+3\eta_0\Omega p(1-c)). \tag{59}$$

Moreover

$$\langle Q^2\rangle_{Av}=V+M^2=3\rho^2\eta_0 c\Omega p(4+3\eta_0\Omega p), \tag{60}$$

so that

$$\left(\frac{\langle Q^2\rangle}{\bar{Q}^2}\right)^{\frac{1}{2}}=\left(\frac{4+3\eta_0\Omega p}{3\eta_0 c\Omega p}\right)^{\frac{1}{2}}. \tag{61}$$

As should be expected, this approaches $1/c^{\frac{1}{2}}$ when $\eta_0\Omega p$ becomes sufficiently large, for the pulses then approach the constant size and the only source of statistical variation is, in the random production of luminescent bursts.

(B). *Thin Case.* In this case $G(\epsilon)$ is $H_3[K_3(G_4(G_5(\epsilon)))]$ whose averages were tabulated in the previous section. We obtain

$$\begin{gathered}M=\bar{Q}=\tfrac{3}{2}\rho\alpha\eta_m\Omega p,\quad V=3\rho^2\alpha\eta_m\Omega p(2+\eta_m\Omega p),\\ Q^2=3\rho^2\alpha\eta_m\Omega p[2+\eta_m\Omega p(1+\tfrac{3}{4}\alpha)],\\ \left(\frac{Q^2}{\bar{Q}^2}\right)^{\frac{1}{2}}=\left[\frac{4}{3}\,\frac{2+\eta_m\Omega p(1+\frac{3}{4}\alpha)}{\alpha\eta_m\Omega p}\right]^{\frac{1}{2}}.\end{gathered} \tag{62}$$

Here $Q^2/\bar{Q}^2$ approaches $[(4+3\alpha)/3\alpha]$ when $\eta_m\Omega p$ becomes sufficiently large.

A Note on Commutators in Quantized Field Theories

S. SCHWEBER
Princeton University, Princeton, New Jersey
(Received February 14, 1950)

It is shown that the commutators of quantized field theories are not uniquely determined by the specification of the Hamiltonian and the field equations and the requirement of Lorentz invariance. However, this lack of uniqueness cannot be used to obtain a high frequency cut-off as in the non-relativistic case.

1. INTRODUCTION

IT has been pointed out recently[1] that the specification of the Hamiltonian and the equation of motion of a classical non-relativistic system does not uniquely determine the commutators of the canonical variables in the quantum theory. Indeed, it is possible to make use of this lack of uniqueness in the commutators to change the values of the matrix elements of certain operators. For example, in the case of the harmonic oscillator with

$$H=\tfrac{1}{2}(p^2+\omega^2q^2) \tag{1}$$

the most general commutator of p and q, such that Heisenberg equations of motion

$$(i/\hbar)[H,q]=\dot{q};\quad (i/\hbar)[H,p]=\dot{p} \tag{2}$$

shall yield the correct equations of motion

$$\dot{q}=p;\quad \dot{p}=-\omega^2q \tag{3}$$

can be written in the form

$$[p,q]=-i\hbar(1+W). \tag{4}$$

Here W is a matrix which anti-commutes with p and q. As W commutes with H the two can be simultaneously diagonalized. It is easily found that in the energy representation with

$$E_n=n\hbar\omega+E_0, \tag{5}$$

$$W_n=[(2E_0/\hbar\omega)-1](-1)^n. \tag{6}$$

As we are free to choose E_0, the zero-point energy, as we please as long as it is greater than zero and less than or equal to $\frac{1}{2}\hbar\omega$, we may for example put

$$E_0=\tfrac{1}{2}\hbar\omega_0\exp(-\omega^2/\omega_0^2),$$

where ω_0 is a constant with the dimensions of angular frequency. In this particular case we then have for the matrix element of q between the states $n=0$ and $n=1$

$$q_{10}=q_{01}=(E_0/\omega^2)^{\frac{1}{2}}=(\hbar\omega_0/2\omega^2)^{\frac{1}{2}}\exp(-\omega^2/2\omega_0^2).$$

It is thus seen that when this procedure is applied to an infinite set of harmonic oscillators without regard to relativistic invariance, a cut-off at high frequencies for some processes will occur and thus might eliminate some of the divergences in present field theories. It is the purpose of this note to point out that relativistic invariance prevents such a cut-off in quantized field theories, though once again the commutators are not uniquely determined by the Hamiltonian and the equations of motion of the fields.

[1] E. P. Wigner, Phys. Rev. 77, 711 (1950).

2. SCALAR FIELDS

For the sake of simplicity we consider the case of a real scalar field. The Hamiltonian is then

$$H=\int d\mathbf{r}\tfrac{1}{2}\{\pi^2+|\nabla\psi|^2+\kappa^2\psi\};\quad (c=\hbar=1), \tag{7}$$

where $\pi\equiv\partial\psi/\partial t\equiv\psi_t$. The most general canonical commutator bracket of $\pi(\mathbf{r})$ and $\psi(\mathbf{r})$ such that the correct equations of motion of the field

$$\pi_t(\mathbf{r})=(\nabla^2-\kappa^2)\psi(\mathbf{r}),\quad \text{with}\quad \pi_t\equiv\partial\pi/\partial t, \tag{8}$$

are obtained from the Heisenberg equations of motion:

$$\begin{aligned} i[H,\psi(\mathbf{r})]&=\psi_t(\mathbf{r}),\\ i[H,\pi(\mathbf{r})]&=\pi_t(\mathbf{r}) \end{aligned} \tag{9}$$

is

$$i[\pi(\mathbf{r}),\psi(\mathbf{r}')]=\delta(\mathbf{r}-\mathbf{r}')+W(\mathbf{r}-\mathbf{r}'). \tag{10}$$

Here the matrix function $W(\mathbf{r}-\mathbf{r}')$ satisfies the following equations

$$\int\{\pi(\mathbf{r}')W(\mathbf{r}-\mathbf{r}')+W(\mathbf{r}-\mathbf{r}')\pi(\mathbf{r}')\}d\mathbf{r}=0,$$

$$\int\{\pi_t(\mathbf{r}')W(\mathbf{r}-\mathbf{r}')+W(\mathbf{r}-\mathbf{r}')\pi_t(\mathbf{r}')\}d\mathbf{r}=0. \tag{11}$$

In order to analyze the Lorentz invariance of these commutator relations, it will be easier to work with the commutator of the field variables at two different points in space time. Calling

$$[\psi(x_\mu'),\psi(x_\mu'')]=iF(x_\mu',x_\mu''),$$

where $(x_\mu)=(t,x,y,z)=(x_0,x_1,x_2,x_3)$, the functional dependence of F on x_μ', x_μ'' can be obtained as follows:

(a) From the requirement that the commutator must be invariant under a translation $\bar{x}_\mu=x_\mu+\epsilon_\mu$ (ϵ_μ = constant 4-vector) it follows that $F(x_\mu',x_\mu'')=F(x_\mu'-x_\mu'')=F(x_\mu)$, where $x_\mu=x_\mu'-x_\mu''$,

(b) From the requirement that the commutator must be invariant under a Lorentz transformation

$\bar{x}_\mu = l_\mu{}^\nu x_\nu$ it follows that $F(x_\mu' - x_\mu'') = F(x_\mu x^\mu)$ and that F is an invariant scalar function,

(c) From the fact that $\psi(x_\mu)$ satisfies the equation $(\Box - \kappa^2)\psi(x_\mu) = 0$ it follows that $F(x_\mu)$ likewise satisfies $(\Box - \kappa^2)F(x_\mu) = 0$,

(d) From the property of a commutator that $[\psi(x_\mu'), \psi(x_\mu'')] = -[\psi(x_\mu''), \psi(x_\mu')]$ it therefore follows that F is an odd function namely $F(x_\mu' - x_\mu'') = -F(x_\mu'' - x_\mu')$,

(e) In order that we shall obtain the correct field equation from the Heisenberg equations of motion, it follows from Eq. (10) that

$$\left\{\frac{\partial}{\partial t'}[\psi(\mathbf{r}', t'), \psi(\mathbf{r}'', t'')]\right\}_{t'=t''=0}$$

$$= i\left\{\frac{\partial F(x_\mu' - x_\mu'')}{\partial x_0'}\right\}_{x_0=0} = -i\delta(\mathbf{r}' - \mathbf{r}'') - iW(\mathbf{r}' - \mathbf{r}'').$$

To satisfy these conditions, we shall write

$$F(x_\mu x^\mu) = (1/2\pi)^3\left\{\int F_+(\mathbf{k})\exp[i(\mathbf{k}\cdot\mathbf{x} - k_0 x_0)]d\mathbf{k}/k_0 + \int F_-(\mathbf{k})\exp[i(\mathbf{k}\cdot\mathbf{x} + k_0 x_0)](d\mathbf{k}/k_0)\right\},$$

where $k_0 = (k^2 + \kappa^2)^{\frac{1}{2}}$. We note that condition (c) is satisfied immediately in this Fourier representation of $F(x_\mu x^\mu)$. Consider now the first integral, which is independent of the second, on the right-hand side of this last equation. Upon performing a Lorentz transformation

$$\bar{x}_\mu = l_\mu{}^\nu x_\nu \quad \text{(or symbolically } \bar{x} = lx\text{)}$$

the requirement that the integral be Lorentz invariant (condition b) is that

$$F_+(\mathbf{k}) = F_+(l\mathbf{k}),$$

from which it follows that $F_+(\mathbf{k})$ is a matrix independent of $\mathbf{k}$: $F_+(\mathbf{k}) = F_+$. Similarly, we must have $F_-(\mathbf{k}) = F_-$ a matrix independent of $\mathbf{k}$. The condition (d) that $F(x_\mu x^\mu)$ be an odd function now requires that

$$F_- + F_+ = 0,$$

and thus

$$F(x_\mu x^\mu) = -\frac{F}{(2\pi)^3}\int_{-\infty}^{+\infty} e^{i\mathbf{k}\cdot\mathbf{x}}\frac{\sin[x_0(k^2+\kappa^2)^{\frac{1}{2}}]}{(k^2+\kappa^2)^{\frac{1}{2}}}d\mathbf{k},$$

where F is a matrix independent of k. It should be noted that in our case (that of a real field) the commutability of two observables separated by a space-like distance, which follows from the vanishing of the above integral for $x_\mu x^\mu$ space-like, is the result of our requirements (a), (b), (c) and is not a separate assumption. Finally, from the requirement (e) it follows that

$$(F/(2\pi)^3)\int e^{i\mathbf{k}\cdot\mathbf{x}}d\mathbf{k} = \delta(x) + W(x),$$

and therefore that W is a matrix independent of k, namely $W(x) = W\delta(x)$ and

$$F = 1 + W.$$

Thus the most general canonical commutator bracket satisfying all our previous requirement is

$$i[\pi(\mathbf{r}), \psi(\mathbf{r}')] = (1+W)\delta(\mathbf{r} - \mathbf{r}').$$

If we now Fourier analyze our field, with

$$\psi(\mathbf{r}) = (1/V^{\frac{1}{2}})\sum_k q_k e^{i\mathbf{k}\cdot\mathbf{r}}; \quad q_{-k} = q_k^*$$

$$\pi(\mathbf{r}) = (1/V^{\frac{1}{2}})\sum_k p_k e^{-i\mathbf{k}\cdot\mathbf{r}}; \quad p_{-k} = p_k^*$$

it follows from the above that

$$H = \frac{1}{2}\sum(p_k^* p_k + \omega_k^2 q_k^* q_k); \quad \omega_k = k_0 = (k^2+\kappa^2)^{\frac{1}{2}}$$

$$i[p_k, q_{k'}] = F\delta_{kk'} = (1+W)\delta_{kk'}$$

and that

$$[W, q_k]_+ = [W, p_k]_+ = 0$$
$$= [W^2, p_k] = [W^2, q_k] = [W, H] = 0.$$

By a suitable contact transformation this last Hamiltonian can be brought to the form

$$H = \frac{1}{2}\sum_k(\bar{p}_k^2 + \omega_k^2\bar{q}_k^2).$$

Since W is independent of k, it follows from (6) that $E_k{}^0$, the zero point energy of the state k, must be of the form

$$E_k{}^0 = \text{constant} \times \omega_k,$$

where the value of the constant must be greater than zero. However, this is of no consequence. We, therefore, conclude that the present field commutators, though not completely unique, cannot be changed so as to introduce a high frequency cut-off.

The author wishes to express his appreciation to Professor Wigner, who suggested this problem, for the many valuable suggestions he has made during this investigation.

Letters to the Editor

PUBLICATION of brief reports of important discoveries in physics may be secured by addressing them to this department. The closing date for this department is five weeks prior to the date of issue. No proof will be sent to the authors. The Board of Editors does not hold itself responsible for the opinions expressed by the correspondents. Communications should not exceed 600 words in length.

A Suggestion Regarding the Spectral Density of Flicker Noise

F. K. DU PRÉ
Philips Laboratories, Inc., Irvington on Hudson, New York
April 17, 1950

AN explanation of the flicker noise in oxide cathodes was first given by Schottky.[1] He assumed that the work function is influenced by the presence on the outer surface of impurity atoms, the density of which was subject to fluctuation because of diffusion effects. The expression for the mean square noise current per unit frequency interval based on this assumption is

$$\langle i^2\rangle_{Av}\sim\tau I^2/(1+\tau^2\omega^2), \tag{1}$$

where I is the average current and τ is the average time spent by an atom on the surface. Assuming $\tau\omega\gg 1$ we find

$$\langle i^2\rangle_{Av}\sim I^2/\tau\omega^2. \tag{2}$$

The experimental results, however, follow more closely the law $\langle i^2\rangle_{Av}\sim I^2/\omega^{1.25}$. Similar discrepancies[2] are found in other cases where the same assumptions might be used to explain a fluctuating barrier height e.g., metal semiconductor rectifiers, lead sulfide cells and carbon microphones. The frequency dependence may be close to ω^{-1}. Also the dependence on the current may differ somewhat from the square law, but this may be due to slight deformations caused by changing the applied electric field, as was suggested by Christensen and Pearson.[3]

Recently, MacFarlane[4] has extended and modified Schottky's theory in order to obtain the correct frequency dependence. His result is

$$\langle i^2\rangle_{Av}\sim I^{2m+2}/\omega^{2m+1}, \quad \text{with} \quad 0<m<\tfrac{1}{2}. \tag{3}$$

Although this improves the agreement with experiment considerably, neither theory explains the relative insensitivity of the flicker noise to the temperature. This is so because in Schottky's expression (2) the relaxation time for the diffusion will depend on the temperature according to

$$\tau=\tau_0\exp(Q/kT),$$

and because in (3) the proportionality factor depends strongly on T.

More recently Richardson[5] has obtained a $1/\omega$ dependence without a strong temperature influence by considering the contact between two rough surfaces and making rather special assumptions about the statistical properties of the surface irregularities.

It is our aim to show that a slight modification of Schottky's theory will describe both the frequency and the temperature dependence correctly. Our fundamental hypothesis is that there will be a certain spread in the values of the diffusion activation energy, Q, at different points of the barrier surface. More precisely we suppose that the fraction of the barrier surface having a value of Q between Q and $Q+dQ$ is given by $f(Q)dQ$. This leads immediately instead of (1) to

$$\langle i^2\rangle_{Av}\sim\int_0^\infty dQ f(Q)\tau I^2/(1+\tau^2\omega^2)=(I^2/\omega)\int_0^\infty dQ f(Q)\tau\omega/(1+\tau^2\omega^2).$$

The expression $\tau\omega/(1+\tau^2\omega^2)$ as a function of Q, will show a sharp maximum at $Q_m=-kT\ln(\tau_0\omega)$, corresponding to the value τ_m of τ determined by $\tau_m\omega=1$. Assuming that $f(Q)$ varies relatively little in a range of the order of kT, we can also write

$$\langle i^2\rangle_{Av}\sim(I^2/\omega)f(Q_m)\int_0^\infty dQ\tau\omega/(1+\tau^2\omega^2).$$

The integral can be evaluated by taking as a new variable $z=\tau/\tau_m$ and using $\tau_m\omega=1$. This leads to

$$\int_0^\infty dQ\tau\omega/(1+\tau^2\omega^2)=kT\int_\delta^\infty dz/(1+z^2), \quad \text{where} \quad \delta=\exp(-Q_m/kT).$$

As we must expect that $Q_m\gg kT$ we can integrate from zero to infinity and obtain $kT\pi/2$. Therefore

$$\langle i^2\rangle_{Av}\sim(I^2/\omega)Tf[-kT\ln(\tau_0\omega)]. \tag{4}$$

We will obtain the often observed proportionality with ω^{-1} when $f(Q)$ in a certain range does not depend on Q. We wish to emphasize that in order to have the ω^{-1} law from $\omega=10^7$ to $\omega=1$ sec.$^{-1}$ we only need a "homogeneous" spread in Q of about 0.25 ev. For according to (4) the extreme values of Q that we have to consider are $-kT\ln(10^7\tau_0)$ and $-kT\ln(\tau_0)$. Their difference is $kT\ln(10^7)=0.25$ ev. It is known that such a variation in Q may occur under the influence of inhomogeneous strains.

Using results reported by Miller,[6] we find it possible to describe the noise spectrum of a silicon rectifier at room temperature and at liquid air temperature, in the range $\omega=10^6$ to $\omega=10^2$ sec.$^{-1}$, by having $f(Q)$ vary gradually in a range of Q values about equal to the one mentioned.

The author is indebted to Professor G. E. Uhlenbeck for his advice.

[1] W. Schottky, Phys. Rev. **28**, 74 (1926).
[2] D. K. C. MacDonald, Report on Progress in Physics **XII**, 56 (1949).
[3] D. J. Christensen and G. L. Pearson, Bell Sys. Tech. J. **15**, 197 (1936).
[4] G. G. MacFarlane, Proc. Phys. Soc. **59**, 366 (1947).
[5] J. M. Richardson, Bell Sys. Tech. J. **29**, 117 (1950).
[6] S. J. Angello, Elec. Eng. **68**, 865 (1949).

Nuclear Magnetic Moments of the Gallium Isotopes

P. KUSCH
Columbia University, New York, New York
April 17, 1950

IN a recent letter with the above title, Béné, Denis, and Extermann[1] discuss an interpretation of the observed discrepancy between the moments of the isotopes of gallium as determined from magnetic resonance experiments and from observations on the Zeeman effect of the hyperfine structure of gallium in the $^2P_{\frac{1}{2}}$ state. The latter of these observations yields both the h.f.s. splitting at zero field ($\Delta\nu$) and the ratio of the nuclear g_I to the electronic g_J. Béné *et al.* apply corrections arising from the finite nuclear size to the value of the magnetic moment as calculated from $\Delta\nu$. Unfortunately, the calculation of a magnetic moment from $\Delta\nu$ is subject to rather considerable uncertainties and a discrepancy of 0.65 percent between the directly measured moment and the calculated one cannot be considered as evidence of the existence of an effect arising from finite nuclear size. However, the g values, obtained from h.f.s. measurements, given by Becker and Kusch[2] are obtained directly from the observed ratio g_I/g_J, and the correction given by Béné *et al.* is entirely meaningless when applied to these experimental quantities.

The nuclear resonance experiments and the h.f.s. experiments determine, in each case, the quantity $g_I\mu_0H'/h$ where H' is the external applied magnetic field, H_0, modified by diamagnetic, or possibly paramagnetic, effects of the electron configuration. A different g_I can be obtained in the two methods, only if H'/H_0 is different in the molecule studied in the nuclear resonance experiments ($GaCl_3$) and in the atoms used in h.f.s measurements. In the nuclear resonance method, large shifts have been observed[3] in the resonance frequency of a nucleus in a metal and in a salt. These effects have been discussed[4] in terms of a paramagnetic field at the nucleus due to conduction electrons in a metal.

It may be worth while to indicate the present status of the measurements of the moments of the gallium isotopes. From the results of Pound[5] and of Bitter[6]

$$\mu(\mathrm{Ga}^{71})/\mu(H^1)=0.9148\pm0.0004$$

and

$$\mu(\mathrm{Ga}^{69})/\mu(H^1)=0.7203\pm0.0006,$$

where the moments are uncorrected for diamagnetic effects.

Becker and Kusch have calculated the moments of the gallium isotopes on the basis of the assumption that $g_J(^2P_{\frac{1}{2}})=\frac{2}{3}$. Since this assumption is subject to correction because of the anomalous spin moment of the electron, and since an arithmetical error exists in the previously published values, the data have been recalculated. With the help of the known auxiliary ratios $g_J(^2P_{\frac{1}{2}}, \mathrm{Ga})/g_J(^2S_{\frac{1}{2}}, \mathrm{Na})$ and $g_I(H^1)/g_J(^2S_{\frac{1}{2}}, \mathrm{Na})$:

$$\mu(\mathrm{Ga}^{71})/\mu(H^1)=0.9078\pm0.0015$$

and

$$\mu(\mathrm{Ga}^{69})/\mu(H^1)=0.7146\pm0.0015.$$

In each case the discrepancy between the nuclear resonance values and the h.f.s. values is about three times the sum of the stated uncertainties. The discrepancy appears to be real, especially in view of the excellent agreement between the ratio of the moments of the two isotopes of gallium.

In the experiments on the determination of the magnetic moment of the electron,[7] a large volume of data on the frequencies of lines in the h.f.s. spectrum of Ga was obtained. Nine sets of data exist from which it is possible to determine the ratio g_I/g_J for Ga^{69}. It is then found that $\mu(\mathrm{Ga}^{69})/\mu(H^1)=0.7143\pm0.0015$. The agreement with the ratio previously obtained from h.f.s. data is excellent and points to the reality of the discrepancy of about 0.7 percent between the ratio obtained from the nuclear resonance method and h.f.s.

[1] Béné, Denis, and Extermann, Phys. Rev. **78**, 66 (1950).
[2] G. Becker and P. Kusch, Phys. Rev. **73**, 584 (1948).
[3] W. D. Knight, Phys. Rev. **76**, 1259 (1949).
[4] Townes, Herring, and Knight, Phys. Rev. **77**, 852 (1950).
[5] R. V. Pound, Phys. Rev. **73**, 1112 (1948).
[6] F. Bilter, Phys. Rev. **75**, 1326 (1949).
[7] P. Kusch and H. M. Foley, Phys. Rev. **74**, 250 (1948).

Cosmic Radiation and Radio Stars

H. Alfvén and N. Herlofson
Royal Institute of Technology, Stockholm, Sweden
April 17, 1950

THE normal radio wave emission from the sun amounts to 10^{-17} of the heat radiation, and increases during bursts[1] to as much as 10^{-13}. If a radio star, e.g., the source in Cygnus, is situated at a distance of 100 light years, its radio emission is of the order of 10^{-4} of the heat radiation of our sun. It is very unlikely that the atmosphere of any star could be so different from the sun's atmosphere as to allow a radio emission which is 10^9 to 10^{13} times greater, and it seems therefore to be excluded that the source could be as small as a star. The recent discovery[2] that the intensity variations of radio stars is a "twinkling" makes it possible to assume larger dimensions.

Ryle has suggested that there should be a connection between radio stars and cosmic radiation.[3]

According to a recent development of Teller and Richtmyer's theory of cosmic radiation, the sun should be surrounded by a "trapping field" of the order 10^{-6} to 10^{-5} gauss, which confines the cosmic rays to a region with dimensions of about 10^{17} cm (0.1 light year).[4] It is likely that almost every star has a cosmic radiation of its own, trapped in a region of similar size. We suggest that the radio star emission is produced by cosmic-ray electrons in the trapping field of a star.

Electrons with an energy $W\gg m_0c^2$ moving in a magnetic field H radiate at a rate

$$-dW/dt=(2e^2/3c)\omega_0^2\alpha^2, \qquad (1)$$

where[5] $\omega_0=eH/m_0c$ is the gyro-frequency corresponding to the rest mass m_0, and $\alpha=W/m_0c^2$. Most of the energy is emitted with a frequency of the order

$$\nu=\omega_0\alpha^2/2\pi=2.8\times10^6H\alpha^2 \text{ sec.}^{-1}. \qquad (2)$$

As soon as the energy is much higher than the rest energy the emitted frequency becomes much higher than the gyro-frequency, a phenomenon which is observed in large synchrotrons, where the electron beam emits visual light.[6]

According to (2) an emission of radio waves of 100 Mc/sec. requires

$$H\alpha^2=36 \text{ gauss}. \qquad (3)$$

The acceleration process of cosmic radiation should accelerate electrons as well as positive particles. In the solar environment the electron component is eliminated by Compton collisions with solar light quanta as discussed by Feenberg and Primakoff.[7] In the neighborhood of a star which does not emit much light, the electrons would be accelerated until their energy is so high that they radiate. The wave-length falls in the meter band if, for example, $\alpha=300$ ($W=1.5\times10^8$ ev) and $H=3\times10^{-4}$ gauss. This field is about 100 times the estimated strength of the sun's trapping field. As the strength is determined by the "interstellar wind," a radio star should be situated in an interstellar cloud moving rather rapidly relative to the star.

In order to account for the total energy emitted by a radio star we must suppose either that the radio emission is a transitory phenomenon, lasting a time which is short compared to the lifetime of cosmic rays in the trapping field (10^8 years), or that the cosmic-ray acceleration close to the star is supplemented by a Fermi process[8] further out in the trapping field.

According to the views presented here, a radio star must not emit very much light, and should be situated in an interstellar cloud. This would explain why it is so difficult to find astronomical objects associable with the radio stars.

[1] T. S. Hey, M. N. R. A. S. **109**, 179 (1949).
[2] Smith, Little, and Lovell, Nature **165**, 424 (1950).
[3] M. Ryle, Proc. Phys. Soc. London **A62**, 491 (1949).
[4] Alfvén, Richtmyer, and Teller, Phys. Rev. **75**, 892 (1949); R. D. Richtmyer and E. Teller, Phys. Rev. **75**, 1729 (1949); H. Alfvén, Phys. Rev. **75**, 1732 (1949) and **77**, 375 (1950).
[5] D. Iwanenko and I. Pomeranchuk, Phys. Rev. **65**, 343 (1944); J. Schwinger, Phys. Rev. **75**, 1912 (1949).
[6] Elder, Langmuir, and Pollock, Phys. Rev. **74**, 52 (1948).
[7] E. Feenberg and H. Primakoff, Phys. Rev. **73**, 449 (1948).
[8] E. Fermi, Phys. Rev. **75**, 1169 (1949).

The Doublets of N^{15} and O^{16}

D. R. Inglis
Argonne National Laboratory, Chicago, Illinois
April 18, 1950

THE nuclear energy-level spectra[1,2] of N^{15} and O^{16} are each characterized by two or more doublets having splittings of 30 to 200 kev and separated by about 1 Mev or more, in the region of excitation 5 to 8 Mev. The lack of structure[1] in the ground state of N^{15} and the importance of spin-orbit coupling in the heavier nuclei[3] suggest that the spin-orbit coupling energy is probably too large for these to be spin-orbit doublets. It is noteworthy that these nuclei at the end of the p-shell in the usual shell model[4] have a much wider gap from the ground level to the first known excited state than have other light nuclei, and the first excitation energy, 5 or 6 Mev, seems to be the energy required to excite a nucleon from the p-shell to the next shell. The nuclear spin and magnetic moment of F^{19}, being similar to a proton's, indicate that the next nucleon state is an s-state. In O^{16}, such an excited s-nucleon, if loosely coupled to the remaining $^2P_{\frac{1}{2}}$ hole of the p-shell (similar to N^{15} or O^{15}) would give rise to adjacent states having $I=0$ and 1, a sort of doublet which might be called an "intershell j-j coupling doublet" or simply a "j-j doublet." Calculations neglecting tensor forces show that for most types of central attractive forces between nucleons the

$I=0$ state lies below that for $I=1$, thus providing the 0−0 transition necessary to explain the well-known pair emission of the lowest excited state in O^{16}, and that the order of magnitude of the splitting is compatible with reasonable assumptions about the interactions. In N^{15} one may have an excited s-nucleon coupled to a p-shell resembling C^{14} or N^{14} having $J=0$ or 1 (or more) and giving rise to single levels and doublets.

Such an interpretation has a simplicity appropriate to the simple doublet pattern observed and to other indications of nuclear shell structure, but in detailed consideration of the lower doublet of O^{16} it unfortunately encounters obstacles which, unless otherwise overcome, make it desirable to seek instead a mechanism capable of pairing states of quite different angular momentum, since the doublets seem too numerous to be fortuitous. Wayne Arnold has recently observed[5] a pronounced alpha-gamma-angular correlation in $F^{19}(p,\alpha)O^{16}$ which seems to indicate $I=3$ rather than $I=1$ for the 6.1_4 Mev state of O^{16}, in striking contrast to $I=0$ for the 6.0_6 Mev state. Furthermore, the odd parity of the configuration p^5s, while consistent[6] with the existence of the three known pair resonances, requires that the two known pair-plus-long-range-alpha-resonances be chance superpositions of states of different parity-angular-momentum in the rather crowded spectrum of Ne^{20}.

[1] R. Malm and W. W. Buechner, Phys. Rev. **78**, 337 (1950) as reported at New York (2.71 Mev is C^{13} contamination), and personal communication through the kindness of D. M. Van Patter, who has also observed a doublet in B^{11}, perhaps significantly at 6.8 Mev; Kinsey, Bartholomew, and Walker, Phys. Rev. **77**, 723 (1950); Guggenheimer, Heitler, and Powell, Proc. Roy. Soc. **190**, 196 (1947); L. D. Wyly, Phys. Rev. **76**, 316 (1949).
[2] Chao, Tollestrup, Fowler and Lauritsen, Phys. Rev. **78**, 88 (1950); Streib, Fowler, and Lauritsen, Phys. Rev. **59**, 253 (1941); Becker, Fowler, and Lauritsen, Phys. Rev. **62**, 186 (1942); R. Walker and B. McDaniel, Phys. Rev. **74**, 617 (1948); Freeman and Baxter, Nature **162**, 696 (1948).
[3] M. G. Mayer, Phys. Rev. **78**, 16 (1950); Haxel, Jensen, and Suess, Naturwiss. **36**, 155 (1949).
[4] W. M. Elsasser, J. de phys. et rad. **4**, 549 (1934); W. Heisenberg, Zeits. f. Physik **96**, 473 (1935); E. Feenberg and E. Wigner, Phys. Rev. **51**, 95 (1937).
[5] Private communication at the suggestion of Arthur Roberts.
[6] J. R. Oppenheimer and J. S. Schwinger, Phys. Rev. **56**, 1066 (1939); D. M. Dennison, Phys. Rev. **57**, 454 (1940).

The Half-Life of Cm^{242}

G. C. Hanna, B. G. Harvey, and N. Moss
Atomic Energy Project, National Research Council of Canada, Chalk River, Ontario, Canada
April 10, 1950

DURING recent work on the neutron irradiation of americium it was noticed that the Cm^{242} produced decayed at a rate significantly different from that expected from the published half-life of 150 days.[1] Accordingly an attempt was made to measure this half-life with reasonable precision.

Three sources were available whose disintegration rates were known with adequate accuracy at a sufficiently early date to give a good value for the half-life. These were all unseparated sources containing the whole of the parent americium. This is not a serious drawback as the curium α-rays are more energetic and were well resolved from the α-rays from any isotope of americium present. A small correction has to be made, however, for the growth of Cm^{242} from the long-lived ground state of Am^{242} which is present.[2]

The activity of the sources was measured in a low geometry proportional counter using a 30 channel pulse analyzer. The counter, designed in this laboratory by Mr. A. G. Ward several years ago, can be trusted to maintain a constant geometry over an indefinite period of time. It consists essentially of a vertical cylinder with a removable base on which is placed the source to be counted. The lower half of the cylinder contains a collimator defining the geometry. The space above the collimator hole contains a proportional counter. The whole is filled with methane at a suitable pressure. The pulse size is a measure of how far an α-particle has penetrated the counting volume and consequently the several disintegration rates of the components of a mixed source can be measured simultaneously.

Table I. Disintegration data on Am^{241} and Cm^{242}.

Source	Date	Days	Am^{241} disin./min.	Cm^{242} disin./min.	Ratio Cm/Am	Half-life calculated from time zero
			($\times10^{-5}$)	($\times10^{-5}$)		
	16:2:49	0	1.492±0.017	2.550±0.021	1.709±0.022	—
A	1:11:49	257	1.465±0.014	0.832±0.008	0.568±0.008	161.8±2.7
	16:2:50	365	1.481±0.014	0.537±0.005	0.362±0.005	163.1±2.2
			($\times10^{-5}$)	($\times10^{-7}$)		
B	18:7:49	0	5.5±0.2	6.522±0.020	—	—
	25:11:49	130.2	not measured	3.747±0.010	—	162.9±1.5
			($\times10^{-5}$)	($\times10^{-6}$)		
	3:6:49	0	1.5±0.1	21.58±0.14	—	—
C	20:11:49	180	1.6±0.1	9.987±0.020	—	162.0±1.5
	14:2:50	256	1.6±0.1	7.254±0.020	—	162.7±1.0
	16:3:50	286	not measured	6.364±0.015	—	162.3±0.9

The three sources were all prepared by evaporation from solution on mirror-finish platinum disks and ignited to red-heat. *Source A*, produced by a very short irradiation, gave comparable Am^{241} and Cm^{242} disintegration rates. *Sources B and C* were aliquots of much more heavily irradiated sample of americium.

Source A was rather small, requiring very long counting times for good statistical accuracy, but the americium and curium counting rates could be measured with comparable precision. With sources B and C the very intense curium activity was accompanied by a finite low energy tail which precluded a very accurate estimation of the americium. The total activity of these two sources was measured and the result corrected for the presence of americium and the growth of Pu^{238}. The uncertainty in these corrections was not large enough to produce a significant error. The geometry of the counter was checked by counting a standard Pu^{239} source on each occasion. The results are given in Table I.

We are somewhat apprehensive that the sources would be weakened by aggregate recoil and give a spuriously short half-life. The constancy of the americium counting rate of source A suggests that this effect is small since it is likely that americium would accompany any curium removed in this way. However, a more satisfactory check that this effect was not significant was obtained by monitoring the inside of the containers in which the sources had been kept: no activity was detected with an instrument sensitive to a few hundred α-disintegrations per minute.

It is possible that sources B and C contain some Cm^{243} formed by a second neutron capture during irradiation. However, the α-activity from this isotope is not expected to exceed a few tenths of one percent of the Cm^{242} activity. The agreement between the half-lives from B and C and the lightly irradiated source A suggest an upper limit of about $\frac{1}{2}$ percent.

Seaborg, James, and Morgan[2] have shown that in neutron irradiated americium there occurs about one β-disintegration of the long-lived ground state of Am^{242} for every 1000 α-disintegrations of Cm^{242} in a fresh unseparated sample. In our measurements the correction for this growth of curium amounts to −0.2 day in the half-life.

Our "best value" is 162.7−0.2 days=162.5 days. The limits of error are probably ±2 days.

[1] G. T. Seaborg and I. Perlman, Rev. Mod. Phys. **20**, 639 (1948).
[2] Seaborg, James, and Morgan, "The new element Americium," AECD 2185.

Measurement of Gamma-Ray Energies with One Crystal*

John A. McIntyre and Robert Hofstadter
Palmer Physical Laboratory, Princeton University, Princeton, New Jersey
April 13, 1950

THE use of scintillations in a single crystal to measure gamma-ray energies[1] may have important applications in nuclear physics because of the possibility of examining sources of very weak radioactivity. In view of this attractive possibility we have studied the pulse-height distributions in clear NaI(Tl)

crystals of various sizes and with various degrees of collimation of the gamma-rays investigated. The crystal pulses were analyzed by a single-channel discriminator.[2] The photo-multiplier employed has been the *EMI* 5032. The crystals were freshly cleaved from Harshaw supplied material, coated with a thin layer of Nujol and kept in a dry atmosphere. The quality of the surfaces has been of great importance in obtaining the following results.

Figure 1 shows the results observed with a 1° collimated beam of Co^{60} (1.17, 1.33 Mev) gamma-rays in a ½-in. crystal cube of NaI(Tl). Figure 2 shows the results obtained with an 8-microcurie point source of Co^{60} in an uncollimated arrangement with the source 3 cm from the crystal. The two peaks near 60.5 and 68.5 volts in each figure correspond to the full energy of the gamma-rays from Co^{60}, while the third larger peak, near 49 volts, is the maximum of the Compton recoil electron distribution. The reproducible asymmetry lying near 54.0 volts in Fig. 1 is believed to be due to the peak of the Compton recoil electron distribution associated with the higher energy gamma-ray component (1.33 Mev). These assignments, consistent among themselves, are also consistent with the established positions of the Compton recoil lines in Fig. 3 of the accompanying paper.[1]

The peaks at 60.5 and 68.5 volts are interpreted as partially due to the photoelectric effect in the iodine constituent of NaI. Merged with these peaks are some pulses caused by Compton forward recoil electrons and their associated ~200-kev back-scattered gamma-rays, the latter of which are also captured by the crystal. The sum of the electron and photon pulses is again the whole energy of the gamma-ray.

The reproduction in Fig. 2 of the important features of Fig. 1 shows that gamma-energies in extremely weak sources may indeed be studied without the losses involved in collimation. There is however an attendant loss in resolution of detail. Nevertheless, it is easy to miss detection of the detailed structure present by using imperfect crystals and by unfortunate choice of crystal size.[3] This is exemplified by Fig. 3 which shows how the spectrum of Fig. 1 is distorted by employment of a larger crystal ($1\times1\times\frac{11}{16}$ in.). In this case multiply-scattered Compton gamma-rays are partially captured in the crystal, broadening and smearing out

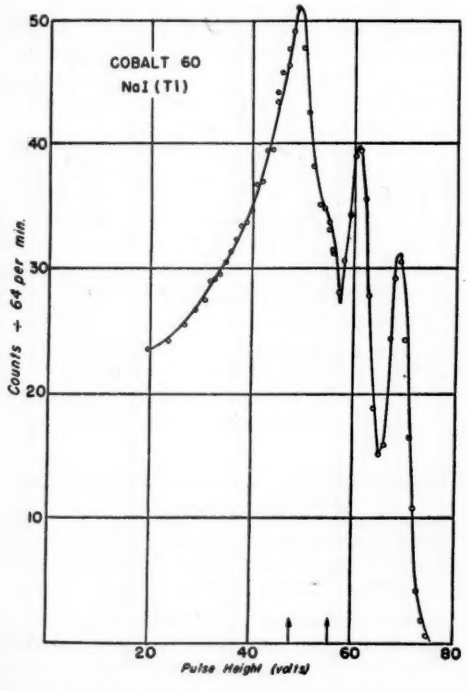

FIG. 1. Pulse-height distribution due to 1° collimated Co^{60} gamma-ray beam in 0.5-in. crystal cube of NaI(Tl).

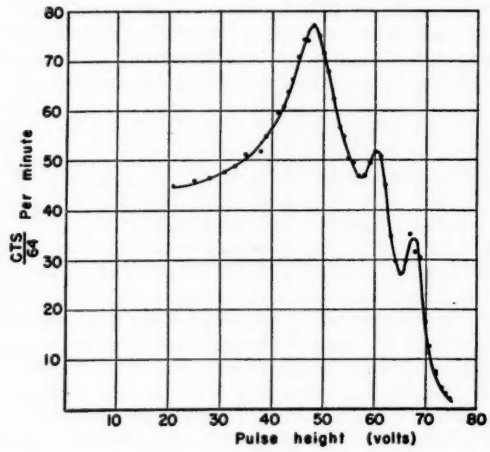

FIG. 2. Pulse-height distribution of uncollimated Co^{60} gamma-rays in NaI(Tl) using 8-microcurie source. Crystal used is identical with the crystal of Fig. 1.

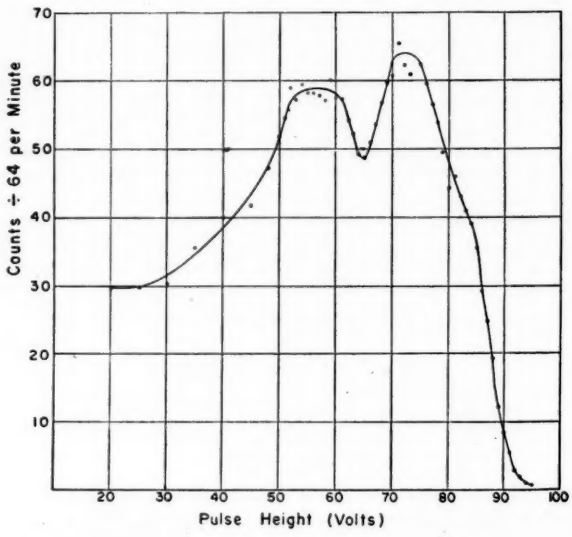

FIG. 3. Pulse-height distribution due to 1° collimated Co^{60} gamma-ray beam in $1\times1\times\frac{11}{16}$ in. crystal of NaI(Tl). Abscissa scale not the same as those in Figs. 1 and 2.

the structure presented by the smaller crystal. Energy measurements would have dubious value if carried out with such large crystals, particularly when the source itself has a complex spectrum. Previously reported Co^{60} curves[4] do not show the structure given in Fig. 1; the lack of collimation, thick diffuse source, and perhaps poor crystal are probably reasons for the differences. On the other hand, a very large crystal (perhaps a 2- or 3-in. cube) might give essentially a line for a single gamma-ray since all the scattered products would be absorbed within the crystal. In organic scintillators this possibility is rather remote because of their small densities. The published curves of Bell and Cassidy[5] on K^{40} and Zn^{65} also show no structure.

Of incidental interest is the fact that the narrow width of the lines in Fig. 1 indicates that approximately 480 photo-electrons per Mev are produced at the photo-cathode of the multiplier tube, if the entire width is assigned to statistical effects. Allowing a five percent photo-efficiency and 50 percent light collection, the resulting luminous efficiency of NaI(Tl) on an energy basis is about six percent.

After this work had been completed it was found that Johann-

son[6] had also observed "photo-electron lines" using NaI(Tl). His results show considerably less detail than those presented here.

* This work received partial support from a U. S. Army Signal Corps Contract and from the joint program of the ONR and AEC.
[1] See also the accompanying paper by R. Hofstadter and J. A. McIntyre, Phys. Rev. **78**, 619 (1950).
[2] Design to be reported by L. W. Hamner.
[3] The double-crystal arrangement of the accompanying paper gives a unique spectrum of gamma-ray lines and avoids the difficulties described in connection with the single crystal.
[4] Pringle, Standil, and Roulston, Phys. Rev. **77**, 841 (1950).
[5] P. R. Bell and J. M. Cassidy, Phys. Rev. **77**, 409 (1950).
[6] S. A. E. Johannson, Nature **165**, 396 (1950).

Measurement of Gamma-Ray Energies with Two Crystals in Coincidence*

ROBERT HOFSTADTER AND JOHN A. MCINTYRE
Palmer Physical Laboratory, Princeton University, Princeton, New Jersey
April 13, 1950

THE known properties of the Compton effect may be used in connection with scintillation counters to measure accurately and without confusion the energies of gamma-rays. A method by which this may be accomplished is shown in Fig. 1.

The line, labeled $h\nu$ in Fig. 1, represents a collimated beam of incident gamma-rays whose energy it is desired to measure. In a

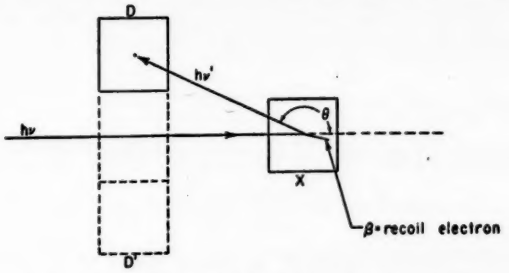

FIG. 1. Schematic of coincidence method for determining gamma-ray energies.

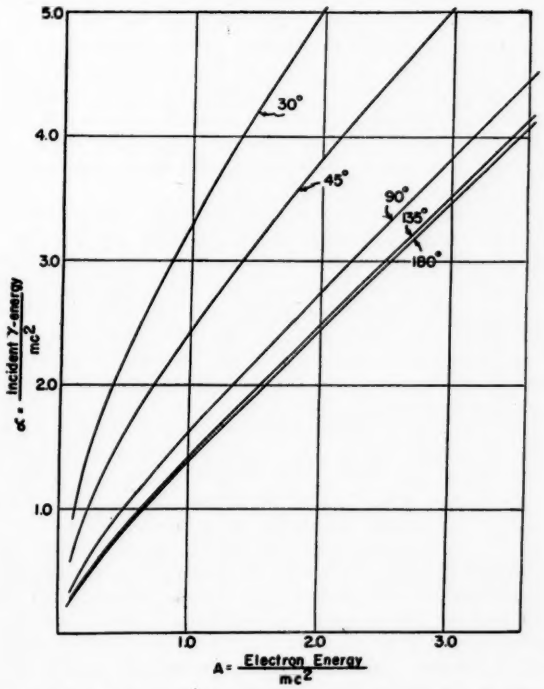

FIG. 2. Energy of incident gamma-ray plotted against electron recoil energy with angle θ as parameter. Energies are expressed in mc^2 units.

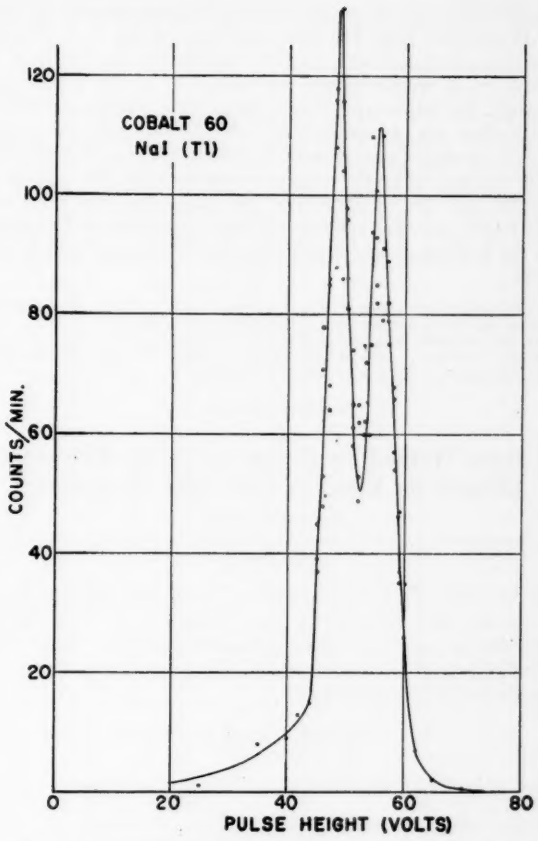

FIG. 3. The spectrum of Co^{60} obtained with the coincidence method.

Compton encounter involving $h\nu$ and crystal X, the scattered gamma-ray $h\nu'$ and recoil electron β appear simultaneously. A fraction of the total number of $h\nu'$ gamma-rays engage in further Compton encounters in "detector" crystal D, or in photoelectric encounters in this crystal. In either case crystal D produces a light flash due to $h\nu'$ while crystal X produces a simultaneous light flash due to β. These coincident light flashes are the ones selected for study. If the pulse in D is used as a gate to trigger a single-channel (or multi-channel) discriminator, the resulting pulse size distribution in X (β-pulses) provides the energy of the incident gamma-ray beam. This follows from the fact that pulse height is proportional to the energy of the recoil electron. If more than one energy is present in the incident beam, each energy provides in X a unique pulse distribution appropriate to this energy.

Using the energy-momentum equations of the Compton effect the energy of the original gamma-ray beam can be calculated from the energy of the recoil electron. Let $h\nu=\alpha(mc^2)$ and β-energy $=A(mc^2)$. Then

$$\alpha=\tfrac{1}{2}A\{1+[1+2/(Ah\alpha v\theta)]^{\frac{1}{2}}\}. \quad (1)$$

Figure 2 shows a set of curves of α *versus* A obtained from Eq. (1) for various values of θ. It may be observed that between 135° and 180° the dependence on θ is extremely small. This corresponds to the well-known fact that a quantum of approximate energy $\frac{1}{2}mc^2$ is scattered in the back hemisphere for a large range of values of $h\nu \geq mc^2$. Hence a large solid angle for detector D may be employed without sacrificing much energy resolution. To gain still higher efficiencies of detection the ring counter DD' may be used. We are now using the single block D shown in Fig. 1 at an approximate angle of 150° at a center-to-center distance of crystals of 1.5 in.

With this arrangement, a single-channel discriminator, and

clear NaI(Tl) crystals, we have studied the gamma-rays of Co^{60} at 1.17 and 1.33 Mev. The results are given in Fig. 3. A 15-millicurie source was used with about 1° collimation. The choice of 1° collimation is accidental and we believe 5° or 10° collimation sufficient. The latter type of collimation and a ring counter (DD′) should allow use of considerably less than one-millicurie source strength to obtain similar results. A multi-channel discriminator should further reduce the required source strength. The radium C spectrum and Sb^{124} gamma-spectrum have also been examined with results agreeing closely with those obtained by Latyshev[1] and the Indiana group.[2] Further details will be published in due course.

* This work received partial support from a U. S. Army Signal Corps Contract and the joint program of the ONR and AEC.
[1] G. D. Latyshev, Rev. Mod. Phys. 19, 132 (1947).
[2] Kern, Zaffarano, and Mitchell, Phys. Rev. 73, 1142 (1949). C. S. Cook and L. M. Langer, Phys. Rev. 73, 1149 (1949).

A Short Method for Evaluation of the Townsend Integral for Electron Avalanche Formation*

EDWARD E. DODD
Department of Physics, University of California, Berkeley, California
April 6, 1950

IT was observed by C. G. Miller[1] of this laboratory that the starting potentials of the burst pulse corona with coaxial cylindrical geometry in certain gases decreased more slowly than inversely proportional to pressure. Since Loeb[2] has given the relation for this threshold as

$$\beta f \exp\left(\int_a^r \alpha dx\right)=1,$$

it was of importance to show that if the dominant term,

$$\exp\left(\int_a^r \alpha dx\right),$$

was to remain constant in setting the threshold, the potential was required to decrease more slowly than the pressure decreased. The establishment of this conclusion on the basis of functional reasoning led to a much simplified procedure for calculating the integral for coaxial cylindrical geometry and one which will be applicable to other geometries. The integral

$$\int_a^r \alpha dx \tag{1}$$

is called the Townsend integral for avalanche formation, with dx a line element in the gap, α the first Townsend coefficient, $a=x$ at the high field electrode, and $r=x$ at a point where α, in virtue of lowered field intensity, becomes negligible.

Knowing the field along the line of integration, $E=\Delta V g(x)$, where ΔV is the gap potential, the variable of integration can be changed to the quotient $(E/\Delta V)$ by the transformation $dx=h(E/\Delta V)d(E/\Delta V)$. Then if the electrode system used is such that the function $h(E/\Delta V)$ is homogeneous, $h(Kt)=K^n h(t)$, the ΔV can be transferred outside the integral and the integrand further transformed to a function of the quotient of the field divided by the gas pressure, p,

$$\int_a^r \alpha dx=(p/\Delta V)^{n+1}\int_{g(a)\Delta V/p}^{E(r)/p} \alpha h(E/p)d(E/p).$$

But the relationship between α, p, and E has the form

$$\alpha/p=f(E/p), \tag{2}$$

so that

$$\int_a^r \alpha dx=-p(p/\Delta V)^{n+1}\int_{E(r)/p}^{g(a)\Delta V/p} f(E/p)h(E/p)d(E/p). \tag{3}$$

In Eq. (3) the integrand is independent of both the gas pressure and the gap potential and, therefore, can be set up for a particular gap directly from the general relation (2) for the gas used. The variables p and ΔV appear only in the external factor and in the upper limit of integration (at the high field electrode), the lower limit being zero or some preassigned constant. Thus, the dependence of the value of the Townsend integral on p and ΔV can be more easily observed from Eq. (3) than from the expression (1) alone. Conversely, if the variation of the value of the Townsend integral with, say, gas pressure is known for a particular discharge phenomenon, the dependence of the gap potential producing this phenomenon on pressure can be determined.

For example, consider a coaxial circular cylindrical electrode system having inner and outer radii a and b, respectively. At a distance x from the axis,

$$E=\Delta V/[x\ln(b/a)],$$

and

$$dx=\{-1/[(E/\Delta V)^2\ln(b/a)]\}d(E/\Delta V).$$

Hence $n=-2$ and we have the result

$$\int_a^r \alpha dx=[\Delta V/\ln(b/a)] \times\int_0^{(\Delta V/p)/a\ln(b/a)} (E/p)^{-2}f(E/p)d(E/p). \tag{4}$$

(In this case the integrand is also independent of the electrode dimensions.) It can be seen from Eq. (4) that for a phenomenon such as burst pulse onset, where the Townsend integral has essentially a constant value, the gap potential must decrease as the gas pressure decreases, but $\Delta V/p$ must increase.

* This work was done under ONR contract.
[1] C. G. Miller, doctoral dissertation, University of California at Berkeley (September, 1949).
[2] L. B. Loeb, Phys. Rev. 73, 798 (1948).

Nuclear Magnetic Moments and Shell Structure

ROALD K. WANGSNESS
University of Maryland, College Park, Maryland
April 6, 1950

THE magnetic moments of certain nuclei of intermediate mass, $34<A<132$, provide further evidence for the existence of proton shells at values of $Z=20$ and 50.[1] Table I gives the values of the magnetic moments and spins of pairs of isotopes which differ by two neutrons.[2] It will be seen that for $Z<20$ and $Z>50$, the addition of two neutrons decreases the value of $|\mu|$, while for $20<Z\leqslant 50$, $|\mu|$ is increased instead; this is particularly noticeable at $Z=50$. This general behavior is found regardless of whether the magnetic moment is to be ascribed to an odd proton or to an odd neutron. For all these nuclei for which $Z\leqslant 50$, with the exception of $_{37}Rb^{87}$ (for which $N=50$), the spin is unaffected by the addition of the two neutrons.

By comparison of the actual moments with those predicted by the one-body model for the two limiting cases in which the odd particle's spin is parallel or antiparallel to the orbital angular momentum, i.e., $l=I\mp\frac{1}{2}$, it has been found that the actual state function for the odd particle is generally a mixture of these two possibilities.[1] The addition of the two neutrons will, in general, change the proportions of the mixture and shift the actual magnetic moment toward one or the other of the limits. If we now examine the moments in Table I with this in mind, we find for $20<Z\leqslant 50$ (with the exception of Ag) the proportion of the state with lower orbital angular momentum is increased so that parallel orientation of spin and orbital angular momentum is favored. For $Z<20$ and >50, the opposite is true, the states with larger l and hence antiparallel orientation being favored instead.

As Nordheim points out, the nuclear electric charge will be distributed throughout the volume of the nucleus and will produce a quasi-elastic repulsive force on the odd proton which would tend to favor higher angular momentum orbits. Since this repulsive force is proportional to the mean charge density, the addition of two neutrons, by increasing the nuclear volume without changing the charge, will decrease this force and thereby favor the states with lower angular momentum as is observed for $20<Z\leqslant 50$. This would be the case for a proton inside the nucleus;

TABLE I. Spins and magnetic moments of nuclei differing by two neutrons.

Nucleus	I	μ	Nucleus	I	μ
$_{17}Cl^{35}$	3/2	0.82103	$_{47}Ag^{107}$	1/2	−0.084
$_{17}Cl^{37}$	3/2	0.681	$_{47}Ag^{109}$	1/2	−0.159
$_{19}K^{39}$	3/2	0.391	$_{48}Cd^{111}$	1/2	−0.595
$_{19}K^{41}$	3/2	0.215	$_{48}Cd^{113}$	1/2	−0.623
$_{29}Cu^{63}$	3/2	2.2233	$_{49}In^{113}$	9/2	5.02
$_{29}Cu^{65}$	3/2	2.3817	$_{49}In^{115}$	9/2	5.52
$_{31}Ga^{69}$	3/2	2.016	$_{50}Sn^{115}$	1/2	−0.89
$_{31}Ga^{71}$	3/2	2.561	$_{50}Sn^{117}$	1/2	−1.000
$_{35}Br^{79}$	3/2	2.108	$_{50}Sn^{119}$	1/2	−1.0465
$_{35}Br^{81}$	3/2	2.2668	$_{51}Sb^{121}$	5/2	3.7
$_{37}Rb^{85}$	5/2	1.3515	$_{51}Sb^{123}$	7/2	2.8
$_{37}Rb^{87}$	3/2	2.7471	$_{54}Xe^{129}$	1/2	−0.9
			$_{54}Xe^{131}$	3/2	−0.8

if, however, the odd particle were required to remain on the edge or the outside of the main body of the nucleus, the increase in nuclear radius resulting from the addition of the two neutrons would then favor orbits with higher angular momentum, as is observed for $Z<20$ and >50. These qualitative requirements on the orbits seem to be somewhat more in accord with the shell scheme of Nordheim than with those of either Feenberg and Hammack or of Mayer.[3]

Although their low natural abundances would probably make their measurement difficult, it would be desirable to know the magnetic moments of the two pairs $_{22}Ti^{47,49}$ and $_{52}Te^{123,125}$ because of their proximity to the proton shells in question.

I wish to thank Dr. J. S. Smart for several interesting discussions.

[1] M. G. Mayer, Phys. Rev. **74**, 235 (1948); **75**, 1969 (1949); E. Feenberg and K. C. Hammack, Phys. Rev. **75**, 1877 (1949); L. W. Nordheim, Phys. Rev. **75**, 1894 (1949).
[2] Data taken from a compilation by W. G. Proctor.
[3] Feenberg, Hammack, and Nordheim, Phys. Rev. **75**, 1968 (1949).

Pair Production in the Field of the Electron by X-Rays from a 100-Mev Betatron*

E. R. GAERTTNER AND M. L. YEATER
Research Laboratory, General Electric Company, Schenectady, New York
March 13, 1950

A STUDY has been made of positron-electron pair production in the field of the electron, in air, by x-rays from a 100-Mev betatron. The x-rays are passed through a 2-mil aluminum window into a cloud chamber[1] filled with air and saturated water and alcohol vapor at one atmosphere pressure. The beam is limited to a cross section of $\frac{1}{8}\times\frac{3}{4}$ in. and cleared of secondary electrons by a system of lead shields and permanent magnets. A pulsed magnetic field of 1700 gauss is provided for the cloud chamber. The energy of the pairs and the faster triplet[2] recoils is determined by magnetic deflection, and the energy of the slower recoils is measured by their range, down to about 10 kev (2 mm).[3]

The data have been divided into two groups according to the energy of the pairs. These groups contain, respectively, those pairs and triplets for which the primary x-ray energy lies in the range 5 to 20 Mev, and those for the range 20 to 100 Mev. For each range we have counted the number of triplets and the corresponding number of pairs. The triplet to pair ratios so obtained are averages over the continuous x-ray spectrum of the betatron.

The number of events counted as pairs is 315 between 5 and 20 Mev; the number between 20 and 100 Mev is 788. The corresponding number of observed triplets is 27 between 5 and 20 Mev, and 63 between 20 and 100 Mev. There appears to be a preponderance of recoils with momentum in the neighborhood of mc or less. A few have larger momenta, extending to about 6 mc.

The ratio of the average pair to triplet cross sections can be computed from our data for each of these energy intervals if the number of undetected triplets can be evaluated. Some recoil electrons are unobserved because their range is short, and others are lost because their orientation in space is such that the projection of the track in the horizontal plane is too short for detection. If the projected length of the recoil is less than 1 mm, we expect it to be unnoticed. If the space length of a recoil is less than 2 mm, corresponding to an energy of 10 kev, the identification of the event as a triplet is not positive and it is counted as a pair. The ratio of the observed number to the total number of triplets is by definition our detection efficiency. This can be written as $\eta=\eta_1\eta_2$, where η_1 is the geometrical efficiency and η_2 is the fraction of the triplets for which the recoil energy is equal to or greater than 10 kev. The calculated average value of η_1 is 85 percent. The efficiency η_2 has been calculated by numerical integration of Bethe's equations[4] for an unscreened nucleus of unit charge. For our detection limit, η_2 varies from 98 percent at 20 Mev to 75 percent at 100 Mev, with an average of 87 percent in the range 20 to 100 Mev and nearly 100 percent for the range 5 to 20 Mev.

From our data and these efficiencies we have calculated ratios of the average triplet to pair cross sections for our air-vapor mixture (effective atomic number $Z=7.32$). Multiplying these ratios by Z, we obtain average values for the quantity A in the expression for the dependence on Z of the total pair plus triplet cross section, $\sigma_p\propto Z(Z+A)$. We find $A=0.75$ for the energy range 5 to 20 Mev, and $A=0.8$ for the range 20 to 100 Mev. The estimated errors are ±25 and ±20 percent, respectively, based on the number of events counted, the uncertainty in the identification of a few of the triplets, and the uncertainty in our calculation of the efficiencies.

Our result for the energy range 5 to 20 Mev (mean energy 11 Mev) may be compared with the theoretical results of Borsellino.[5] From his data we derive an average value of $A=0.61$ for this interval. For x-ray energies in the range 20 to 100 Mev, our value of A may be compared with the theoretical results of Borsellino and Wheeler and Lamb.[6] Up to an energy of 50 Mev, Wheeler and Lamb's data yield $A=1$, since screening can be neglected in this case; at 100 Mev their value is only slightly greater than 1. Borsellino has shown, however, that the cross section for pair production in the field of the electron is less than in the field of the proton.[7] The difference is 15 percent at 50 Mev and increases with decreasing quantum energy. Although we do not have the corresponding data for the interval 50 to 100 Mev, it appears that the theoretical A lies between 0.85 and 1.05 in this region. With this assumption we have calculated limiting theoretical values for A, averaged over the continuous x-ray spectrum from 20 to 100 Mev. The result is $0.80<A_{\text{theor}}<0.86$.

We wish to thank Dr. E. E. Charlton and the betatron group for their cooperation. We are grateful to Professor H. A. Bethe and Dr. H. Hurwitz for discussions of the theoretical aspects of the problem.

* This work was supported in part by Contract N7 ONR 332 with the ONR.
[1] This cloud chamber is described by the authors in Rev. Sci. Inst. **20**, 588 (1949).
[2] "Triplet" is defined as a pair with a visible electron recoil which indicates the pair to have been formed in the field of the recoiling electron. The calculated probability of a spurious triplet, resulting from a coincidence between a pair and a stray electron, is one in 7500 pairs.
[3] N. N. Das Gupta and S. K. Ghosh, Rev. Mod. Phys. **18**, 280 (1946).
[4] H. Bethe, Proc. Camb. Phil. Soc. **30**, 524 (1934). In the neighborhood of 50 Mev Bethe's equations for the unscreened nucleus of unit charge give a result identical with that of Wheeler and Lamb for the electronic case. See J. Wheeler and W. Lamb, Phys. Rev. **55**, 858 (1939).
[5] A. Borsellino, Helv. Phys. Acta **20**, 136 (1947).
[6] J. Wheeler and W. Lamb, Phys. Rev. **55**, 858 (1939).
[7] Professor H. A. Bethe has pointed out to us that the values of A derived from Wheeler and Lamb should be reduced in accordance with the results of Borsellino.

Scintillation Counting with Solutions*

HARTMUT KALLMANN
Department of Physics, New York University, New York, New York
April 12, 1950

IT is a drawback of scintillation counting with crystals that large-sized crystals are found not to be very transparent. They exhibit a considerable light scattering which gives rise to

additional absorption. This drawback could be overcome if instead of crystals one were able to use liquids, which can be applied in large thicknesses without considerable absorption. In the course of the investigation of the fluorescent efficiency of liquid solutions when excited by gamma-radiation and by neutrons, special solutions were used which exhibited a fluorescent efficiency high enough to make them applicable for counting work.

Circuit.—The experimental arrangement used consisted of a multiplier tube of Type 5819. On its light-sensitive top surface a glass or porcelain tube of almost equal diameter was cemented. The glass tube was supplied with a reflecting layer (white paint or metal surface), or it can even be used with transparent walls. The liquid filled this tube and thus contacted the top surface of the multiplier directly. The upper surface of the liquid was covered with a reflecting layer. With the best solutions the following results were obtained.

Gamma-radiation.—With gamma-radiation from a radium source maximum scintillation peaks were obtained which were about five times larger than the maximum noise peaks. This means that these light flashes of maximum intensity released about 30 to 40 primary electrons from the photo-cathode. Also with softer x-ray sources the peaks could easily be detected without using a coincidence arrangement.

Neutron radiation.—With a polonium and beryllium neutron source larger peaks were obtained. The maximum size was about 15 to 20 times larger than the largest noise pulse, corresponding to a primary emission of 100 to 150 electrons per light flash. In the case of neutrons, as well as in that of gamma-radiation, the number of peaks were considerably larger than that obtained with normally available organic crystals.

Alpha-radiation.—Alpha-particles from a polonium source bombarded the surface of a solution of about 1-cm thickness. This means that the alpha-particles hit the surface of the liquid about 1 cm away from the photo-sensitive layer. In this case the alpha-particles gave rise to peaks about five times the size of the maximum noise peaks. Since the alpha-particles have an energy of about five million electron volts their efficiency in producing light emission is about three times smaller than that of gamma-radiation (gamma-radiation of about two million volts gives the same peak height). When the thickness of the solution was increased to about 6 cm the alpha-peak intensity decreased to approximately three times the size of the maximum noise peaks. Since in this case the light flashes are only produced at the upper surface, the solid angle subtended by the light at the photo-cathode is much smaller. A considerable part of the light only hits the photo-cathode after one or even several reflections at the side walls and it is quite probable that a part of the loss in intensity with increasing thickness of solution may be due to losses connected with the reflection at the walls. It may be that in large thicknesses of more than 10 cm a certain amount of absorption in the solution is already taking place.

General considerations.—Similar experiments in glass tubes without a reflecting layer at the walls gave intensities about 25 percent less than those with reflecting walls. This indicates that the walls of the tube partly operate as reflector by total reflection.

When all radiation sources are removed, a certain number of very large peaks were observed which sometimes were larger than 50 times the maximum noise pulse peaks, which means the emission of several hundreds primary electrons from the photo-cathode. These pulses were characteristic of the solution and disappeared when the solution was removed. It is supposed that these large peaks originated in cosmic-ray particles crossing the solution. Their frequency amounted to three peaks per minute which, with a solution of 50-mm thickness, would be a reasonable number of peaks to be induced by cosmic radiation.

Time constants of the solutions.—Very preliminary and rough checks of the time constants of these solutions were made. The electric circuit contained a resistor of 50,000 and in some cases of 10,000 ohms. In these cases the decay time of the observed pulses were those caused by the time constant of the electric circuit. The rise times of the peaks were practically that of the operating amplifier. This means that a very considerable part of the light emission of these solutions takes place within a period of time smaller than 10^{-7} sec.

The solutions.—A variety of solutions were found applicable for counting work. Solutions of toluene and xylene with fluorene, carbazole, phenanthrene, and anthracene prove to be nearly equally successful. Also mixtures of these solutions could be used advantageously. All solutions exhibited a maximum concentration for light efficiency, which in the case of carbazole was as low as 0.2 gram per liter. With phenanthrene the maximum concentration came out to be 8 gram per liter. The light efficiency was also increased when paraffin oil was added to the solution. Another type of equally good fluorescent solution was paraffin oil with dissolved xylene and with the addition of small amounts of anthracene, fluorene, phenanthrene, and carbazole. It is most essential for those experiments to work with pure substances, since very small amounts of contamination give rise to quenching effects. Thus, most of the substances used exhibited their maximum light efficiency only after being purified in our laboratory.

I was greatly assisted in these experiments by Mr. Milton Furst and Miss Miriam Sidran.

* This work was sponsored by the Signal Corps Engineering Laboratory, Fort Monmouth, New Jersey. Contract No. DA 36-039 sc-35.

Nuclear Coupling and Shell Model

GIULIO RACAH
The Hebrew University, Jerusalem, Israel
April 14, 1950

IN a recent paper[1] Feenberg examined some general aspects of nuclear structure from the point of view of strong spin-orbit coupling, and we wish to add some remarks to his considerations.

Feenberg considered as a "reasonable supposition" that the statistical weight of the singlet component for states in the antisymmetric j^2 function space attains a maximum at $I=0$. With the aid of Dirac's vector model it is very easy to prove this supposition and also to extend the calculation to the antisymmetrical j^n function space; i.e., to n-like particles in equivalent orbits.

The statistical weight of the singlet component in the coupling of two particles is given by the expectation value of

$$S_{12}=\tfrac{1}{4}-(\mathbf{s}_1\cdot\mathbf{s}_2), \tag{1}$$

and in extreme jj coupling this expectation value is

$$\begin{aligned}\langle S_{12}\rangle_{Av}&=\tfrac{1}{4}-(\mathbf{s}_1\cdot\mathbf{j}_1)(\mathbf{s}_2\cdot\mathbf{j}_2)(\mathbf{j}_1\cdot\mathbf{j}_2)/[j(j+1)]^2\\&=\tfrac{1}{4}-(\mathbf{j}_1\cdot\mathbf{j}_2)/(2l+1)^2\\&=\tfrac{1}{4}+[2j(j+1)-I(I+1)]/2(2l+1)^2,\end{aligned} \tag{2}$$

and attains therefore a maximum for $I=0$, in agreement with Feenberg's supposition.

For n-like particles in equivalent orbits the weight of the singlet couplings is

$$\langle\Sigma S_{ik}\rangle_{Av}=\tfrac{1}{8}n(n-1)+[nj(j+1)-I(I+1)]/2(2l+1)^2 \tag{3}$$

and attains a maximum for the minimal I allowed by the exclusion principle.

If now strong Majorana forces coexist with strong spin-orbit forces, the spin I of the ground state of an odd nucleus should equal the j of the uncoupled particle only in the trivial cases of one particle in an empty shell or one hole in a filled shell, and should be $\frac{3}{2}$ in the cases of three particles in an empty shell or three holes in a filled shell, and $\frac{1}{2}$ in any other case.

The situation is different in the space orbital approximation. In this case the weight of the singlet couplings,

$$\Sigma S_{ik}=\tfrac{1}{8}n(n+2)-\tfrac{1}{2}S(S+1), \tag{4}$$

is not a sufficient criterion for determining the lowest state, as it has the same value for all terms with the same S, and the sta-

tistical weight of the ^1S couplings should be considered. This weight is proportional to the eigen value of

$$Q=\Sigma q_{ik}, \tag{5}$$

where q_{ik} is defined as an operator which has the eigenvalue $2l+1$ when the two equivalent particles i and k are coupled in a ^1S state, and the eigenvalue 0 in any other case.

It has been shown elsewhere[2] that for a given configuration the eigenvalues of Q depend only on the "seniority number," v, of the term; i.e., on the number of particles of the configuration l^v in which the term appeared for the first time. As

$$Q=\tfrac{1}{4}(n-v)(4l+4-n-v), \tag{6}$$

the terms with maximal statistical weight of ^1S couplings are those with minimal v; i.e., a ^1S ($v=0$) for n even, and a ^2l ($v=1$) for n odd.

The experimental fact that the L of an odd nucleus seems to equal the l of the uncoupled particle is therefore an argument in favor of the LS coupling against the jj coupling model.

Owing to the fact that the minimal value of v is zero for n even, and unity for n odd, Eq. (6) gives also a quantitative expression for the odd-even structure of the energy surface.

It may also be pointed out that the fact that $Q(n, v)$ reaches its maximal value exactly for $n=2l+2$ may perhaps give the possibility of explaining the magic numbers also without assuming strong jj coupling.

[1] E. Feenberg, Phys. Rev. **76**, 1275 (1949).
[2] G. Racah, Phys. Rev. **63**, 367 (1943), Eq. (50).

On the Detection of γ-Ray Polarization by Pair Production

T. H. Berlin and L. Madansky
The Johns Hopkins University, Baltimore, Maryland
April 13, 1950

THE measurement of the polarization of γ-radiation can be important in that it would allow a determination of the change in parity between states involved in a radiative transition.[1] Although Compton scattering is a means of detecting a preferred orientation of polarization, it begins to fail at high energies because the polarization correlation of the scattered photon decreases with increasing energy, and the cross section itself decreases. For the high energy range, we believe that pair production may provide a useful technique. This conclusion has also been reached by Yang, who recently discussed the possibility of determining whether the neutral meson is scalar or psuedoscalar.[3]

The differential cross section for pair production is, in Heitler's[4] notation,

$$d\sigma=\frac{Z^2}{137}\frac{e^4}{4\pi^2}\frac{p_+p_-dE_+d\Omega_+d\Omega_-}{k^3q^4}\left\{\frac{(\boldsymbol{\varepsilon}\cdot\mathbf{p}_+)^2(q^2-4E_-^2)}{(E_+-p_+\cos\theta_+)^2}\right.$$
$$+\frac{(\boldsymbol{\varepsilon}\cdot\mathbf{p}_-)^2(q^2-4E_+^2)}{(E_--p_-\cos\theta_-)^2}-\frac{2(\boldsymbol{\varepsilon}\cdot\mathbf{p}_+)(\boldsymbol{\varepsilon}\cdot\mathbf{p}_-)(q^2+4E_+E_-)}{(E_+-p_+\cos\theta_+)(E_--p_-\cos\theta_-)}$$
$$\left.+\frac{k^2[p_+^2\sin^2\theta_++p_-^2\sin^2\theta_-+2p_+p_-\sin\theta_+\sin\theta_-\cos(\varphi_+-\varphi_-)]}{(E_+-p_+\cos\theta_+)(E_--p_-\cos\theta_-)}\right\}.$$

$\boldsymbol{\varepsilon}$ is a unit vector in the direction of polarization of the incident photon.

We suppose that the normal to the plane of the pair is perpendicular to $\mathbf{k}$, and we consider only pairs such that $\varphi_-=\varphi$, $\varphi_+=\varphi+\pi$ with φ measured from $\boldsymbol{\varepsilon}$. A cross section determined for a particular experimental arrangement can be written as

$$\Sigma=A+B\cos2\varphi,$$

where φ is the angle between the plane of polarization and the plane of the pair. The ratio, R, of the cross section for the pair to appear in a plane perpendicular to the plane of polarization ($\varphi=\pi/2$) to the cross section for the plane of the pair parallel to the plane of polarization ($\varphi=0$) is

$$R=\Sigma_\perp/\Sigma_{\parallel}=(A-B)/(A+B).$$

The cross sections for the experimental arrangements to be described are obtained from the differential cross section by appropriate integrations. We make use of the relativistic and small angle approximations in performing the integrations.

We consider several different cases.

Case I.—The photon is plane polarized. The plane of the pair is determined by a coincidence of two counters placed symmetrically with respect to the axis determined by the incident photon such that $\theta_+=\theta_-=\theta$. It is assumed that the counters will accept all values of the electron or positron energy and that the angle subtended by the counters is small compared with the range of angles in which an appreciable number of pairs are emitted ($\theta\sim m/k$). The coincidence count is a measure of the number of pairs emitted in a particular plane (φ). With these assumptions, one finds that R ranges from 1.13 for $\theta=1.4(m/k)$, to 6.73 for $\theta=0.4(m/k)$. Outside of this range for θ the cross section falls rapidly. One finds more pairs in the plane perpendicular to the plane of polarization.

Case II.—We consider again a completely polarized photon. The experiment is arranged so that *all* pairs lying in a particular plane (φ) are counted. This can be done by magnetic separation where counters can be arranged to pick up almost all energies of the positron or electron independently of the angle of emission; that is, one can use the properties of semicircular focusing that occur for high energy pairs. The plane of the pair is again determined by coincidence of the electron-positron counters. By rotating the magnet about the symmetry axis, one can determine the counting rate for a given plane. In this case, the expected $R=1.23$.

Case III.—The incident photon is assumed to be plane polarized. We suppose that of all pairs lying in a particular plane (φ) only those pairs are counted for which the electron and positron have equal energy. This can be achieved by magnetic separation of the pair. For this arrangement $R=1.30$.

Case IV.—Assuming the incident photon to be plane polarized, we shall also assume that only those pairs in a particular plane (φ) are counted for which the electron and positron have equal energies and make equal angles θ with $\mathbf{k}$. The cross section for this situation is simply proportional to $\cos^2\varphi$, so that, contrary to the previous cases, more pairs are found in the plane of polarization. Although this case is theoretically the most favorable ($R=0$), it is of little practical importance because, in order to achieve this result, it is necessary that $|p_+-p_-|<m(m/k)$ and that $|\theta_+-\theta_-|/\theta<(m/k)^2$, where $\theta\sim m/k$.

Table I.

Percent polarization	100	90	80	70
R	1.23	1.18	1.13	1.08

For a fixed energy of the incident photon, most of the pairs will be emitted in a narrow cone whose angular spread is approximately m/k. The solid angle which the pair-producing target subtends at the source of the photons must be smaller than this angle, and may introduce difficulties because of intensity considerations. Hence, from an experimental point of view, *Case II* is the most useful since there is no restriction of energy or angle for the electron and positron.[5] The sensitivity of the method outlined in *Case II* is exhibited in Table I where R is given for various states of polarization of the incident photon.

[1] See, for example, D. Hamilton, Phys. Rev. **74**, 782 (1948); D. L. Falkoff, Phys. Rev. **73**, 518 (1948).
[2] Private communication.
[3] C. N. Yang, Phys. Rev. **77**, 722 (1950).
[4] W. Heitler, *The Quantum Theory of Radiation* (Oxford University Press, London, 1936), p. 196.
[5] For the experiment described by Yang (reference 3), *Case II* yields $\beta^2=1/94$.

Specific Activity of Potassium

WILLIAM R. FAUST
Nucleonics Division, Naval Research Laboratory, Washington, D. C.
April 12, 1950

ABSOLUTE beta- and gamma-ray disintegration rates of potassium have been measured by immersing suitable counters in a large tank of water (53 in. deep and 48 in. diameter) containing 4.55 kg of KCl in solution. Geometrical conditions of the experiment were such that the source could be considered as homogeneously distributed in an infinite medium. By utilizing previous results,[1] on multiple Compton scattering under such conditions, the absolute disintegration rate of the 1.50-Mev gamma-ray was deduced. The specific beta-ray activity was found from the observed beta-ray counting rate by a calculation involving the counter geometry, and the mean range of the beta-rays in water. The results of Alburger[2] were used to compute the mean beta-ray range. A calculated correction of about 15 percent was also made for the Compton electrons. It is estimated that the error in these determinations is less than 10 percent.

The method has been tested[3] by determining specific beta- and gamma-ray disintegration rates of Na^{24} under the same conditions. A Na^{24} source (Na_2CO_3) was calibrated by three methods (coincidence counting, comparison with a known source in an ionization chamber and by means of a calibrated gamma-ray counter) which gave results differing by less than three percent from each other. After dissolving this source in a known volume of water, the specific activity determined by the methods described above differed from that calculated from the measured source strength and amount of solute by less than five percent for both beta- and gamma-rays.

Results obtained for the specific disintegration rate of potassium are: 31.2±3.0 beta-rays/sec.-g K, and 3.6±0.4 gamma-rays/sec.-g K. The beta-ray activity is in agreement with results of Stout,[4] Spiers,[5] and Ahrens and Evans.[6] The gamma-ray activity reported here is in agreement with recent observations[6-8], but is considerably higher than the results of Spiers. The mean gamma-ray activity of all recent measurements is 3.4±0.2 gamma-rays/sec.-g K, while the specific beta-ray activity is 31.8±1.0. These averages include the estimates of Ahrens and Evans.

The author is indebted to Drs. M. H. Johnson and F. N. D. Kurie for many helpful suggestions and to G. E. Halloway and C. C. Porter for aid in performing the experimental work.

[1] W. R. Faust and M. H. Johnson, Phys. Rev. **75**, 467 (1949).
[2] D. E. Alburger, Phys. Rev. **75**, 1442 (1949).
[3] To be published elsewhere.
[4] R. W. Stout, Phys. Rev. **75**, 1107 (1949).
[5] F. W. Spiers, Nature **165**, 356 (1950).
[6] L. H. Ahrens and R. D. Evans, Phys. Rev. **74**, 279 (1948).
[7] E. Gleditsch and T. Graf, Phys. Rev. **72**, 641 (1947).
[8] G. A. Sawyer and M. L. Wiedenbeck, Phys. Rev. **76**, 1535 (1949).

A Long-Lived Zirconium Activity in Fission

E. P. STEINBERG AND L. E. GLENDENIN
Argonne National Laboratory, Chicago, Illinois
April 10, 1950

ALTHOUGH much information has been obtained regarding the fission products,[1] the decay characteristics of those of very short or very long half-lives have not yet been fully investigated. Several of these "missing" activities (Se^{79}, Zr^{93}, Pd^{107}, I^{129}, Cs^{135}) have been predicted for some time to have low decay energies and probably very long half-lives. Recently Sugarman[2] has isolated Cs^{135} from uranium fission and established its half-life and beta-energy as 2.1×10^6 yr. and 0.21 Mev, respectively. In the present investigation, we have isolated from uranium fission a zirconium activity of $\sim5\times10^6$-yr. half-life, emitting beta-rays of 60±5 kev maximum energy, which is probably Zr^{93}.

The zirconium activity was isolated by a carrier-free method from uranium which had been irradiated for 10 months in a pile. The separation was carried out four years after the end of the irradiation, at which time the activity of 65-day Zr^{95} had decayed to a sufficiently low intensity that the observation of a very long-lived isotope was possible. The chemical procedure involved the carrying of zirconium on MnO_2 precipitated from a 1*N* HNO_3 solution of a fission product concentrate of the irradiated uranium. Niobium activity was removed by carrying on MnO_2 precipitated from 10*N* HNO_3, and final purification of the zirconium was achieved by repeated extractions of the cupferron complex into $CHCl_3$. These operations permit the isolation of zirconium activity in high radiochemical purity without the presence of an isotopic carrier.[3]

Observations of the radiations of the zirconium activity were made with a thin (0.85 mg/cm²) end-window proportional counter and an internal Geiger counter ("*Q*-gas counter"[4]). Figure 1 shows a comparison of the zirconium activity isolated in these experiments with that of pure 65-day Zr^{95} tracer using the proportional counter. Points not shown in Fig. 1 indicated that the two absorption curves were identical over the region of heavier absorbers. A soft component is seen in the fission zirconium curve, but not in the pure Zr^{95} curve. In successive separations of zirconium, the abundance of the soft component was found to increase over a period of two months relative to that of the Zr^{95} by an amount consistent with the 65-day half-life of Zr^{95}. This observation is evidence that the soft activity is due to a zirconium isotope, since the two activities were not fractionated by the chemical operations. Examination in a methane-flow alpha-proportional counter eliminated alpha-contamination as a possible source of the soft activity.

Figure 2 shows the absorption curves of the fission Zr and Zr^{95} tracer obtained with a *Q*-gas counter. The curves have been normalized so that the Zr^{95} curve can be subtracted from the observed data to give the absorption curve of the soft beta-radiation from the long-lived isotope. A half-thickness in aluminum of 0.35 mg/cm² is observed. In order to establish the maximum energy of the beta-radiation from its observed half-thickness, a curve of half-thickness *vs.* energy is desirable. Two points on such a curve were established using Ru^{106} and Sm^{151}. The half-thicknesses of the beta-radiations from these nuclides were determined to be 0.20 and 0.50 mg/cm², respectively; maximum energies of 40.1 and 76.6 kev, respectively, were available from beta-ray spectrometer measurements.[5] Linear interpolation gives a value of 60±5 kev for the maximum beta-energy of the long-lived zirconium.

Previous attempts to find any zirconium activity assignable to mass 93, both from neutron irradiation of zirconium[6] and from uranium fission in the half-life range from 3 min. to 100 yr.,[7] have been unsuccessful. Also, a very low decay energy is predicted for Zr^{93} from the mass formula of Bohr and Wheeler.[8] From these considerations it is probable that the new long-lived zirconium fission product is Zr^{93}. It is planned to make a positive mass assignment by examination in the mass spectrometer.

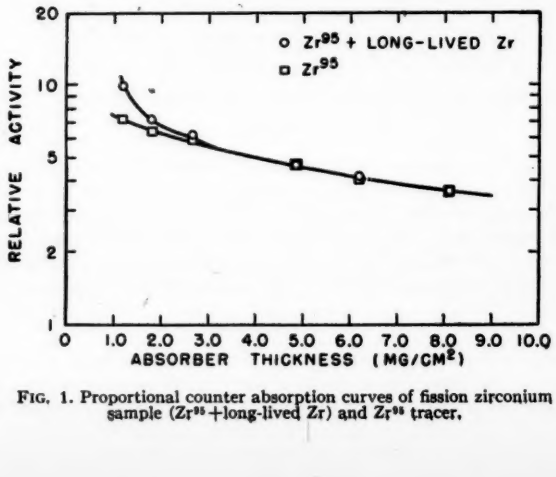

FIG. 1. Proportional counter absorption curves of fission zirconium sample (Zr^{95}+long-lived Zr) and Zr^{95} tracer.

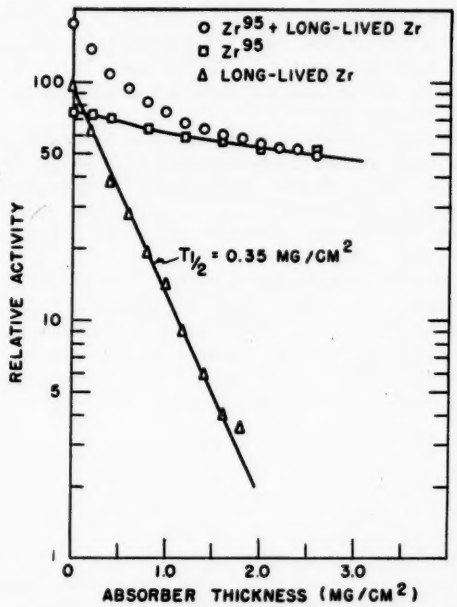

FIG. 2. Absorption curve of long-lived Zr as determined in an internal Geiger counter ("Q-gas counter").

Assuming this long-lived fission product is Zr^{93}, whose fission yield in uranium may be obtained from the smooth yield-mass curve,[1] the ratio of its activity to that of Zr^{95} at a given time after a known period of irradiation permits an estimation of its half-life. The ratio of activities observed at 4.2 yr. after an irradiation of 0.83 yr. was 1.4. This value gives a half-life for Zr^{93} of 5.2×10^6 yr. A possible error in the value of the half-life of the order of a factor of two is estimated from the uncertainty in the half-life of Zr^{95} (65±2 days). Another possible source of error lies in self-absorption by the source, which consisted of ~10 μg of solid material deposited over a small area. This effect should lower the calculated half-life by no more than a factor of two. Thus, the true half-life of Zr^{93} should lie in the range 1.5 to 8.5×10^6 yr. Further work is in progress to eliminate these sources of possible error and to establish the half-life with greater accuracy.

[1] The Plutonium Project, J. Am. Chem. Soc. **68**, 2411 (1946).
[2] N. Sugarman, Phys. Rev. **75**, 1473 (1949).
[3] *Radiochemistry: The Fission Products*, Part VI (McGraw-Hill Book Company, Inc., New York, in press), National Nuclear Energy Series, Division IV, Vol. 9.
[4] Available from Nuclear Instrument and Chemical Corporation, Chicago, Illinois.
[5] Freedman, Wagner, Steinberg, and Glendenin (unpublished work).
[6] W. H. Sullivan, *Trilinear Chart of Nuclear Species* (John Wiley and Sons, Inc., New York, 1949); G. T. Seaborg and I. Perlman, Rev. Mod. Phys. **20**, 585 (1948).
[7] Coryell, Sakakura, and Ross, Phys. Rev. **77**, 755 (1950).
[8] N. Bohr and J. A. Wheeler, Phys. Rev. **56**, 426 (1939).

Optical Absorption Edge for BaO as Determined by the Method of Ives and Briggs

E. A. TAFT AND J. E. DICKEY
General Electric Research Laboratory, Schenectady, New York
April 20, 1950

TYLER[1] has located the optical absorption edge of evaporated films of BaO at $h\nu\cong3.8$ ev. We have confirmed his result by measuring the photoelectric emission from very thin metallic films deposited on the surface of BaO layers. This method, originated by Ives and Briggs[2] in their investigation of Na films on Ag, has not been applied in the case of ionic substrates. (It is interesting to note that the narrow transmission band of Ag has almost the same location as the absorption edge of BaO.) Figure 1

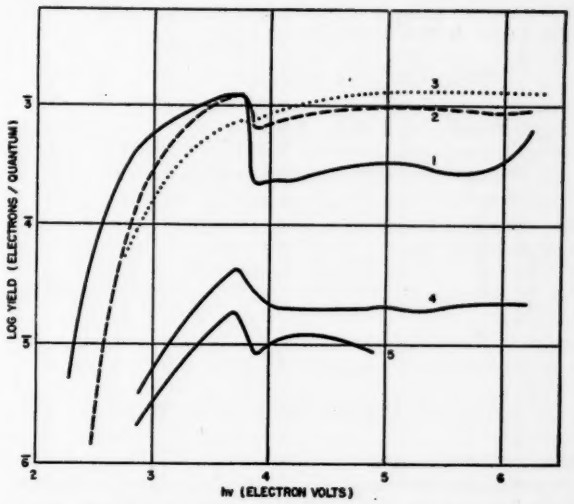

FIG. 1. Photoelectric yield of Ba films on BaO layer; curves 1, 2, and 3 are in order of increasing thickness of Ba. Curves 4 and 5 are results for Na on Ag taken in this laboratory and by Ives and Briggs respectively—the absolute magnitude of the yields being displaced arbitrarily. Note that the characteristics of the logarithms are negative.

shows the spectral distribution of the photoelectric yield from thin films of Ba metal deposited on BaO layers formed by thermal decomposition of $BaCO_3$. The thinnest Ba films were invisible. They had only a small effect on the incident ultraviolet radiation. However, they suppressed almost entirely the photoelectric emission from the BaO itself. Thus, loosely speaking, one may say that they behaved like metallic photo-emitters with the optical constants of the layer of ionic crystals. The photoelectric yield drops by several-fold between 3.7 and 3.9 ev, in good agreement with the absorption edge found by Tyler. As the films become thicker, the effect becomes less pronounced and finally disappears. The surface then has the properties of bulk Ba metal. We have obtained analogous results with films of Mg on BaO, and with Ag and Pb on KI.

[1] W. W. Tyler, Phys. Rev. **76**, 1886 (1949).
[2] H. E. Ives and H. B. Briggs, Phys. Rev. **38**, 1477 (1931).

X-Ray Determination of Hg Arc Temperature

C. KENTY AND W. J. KARASH
General Electric Company, Lamp Development Laboratory, Nela Park, Cleveland, Ohio
April 17, 1950

THE absorption of a beam of x-rays passing along the axis of a carbon arc in air was used by von Engel and Steenbeck[1] to determine the gas density and thence the arc temperature. The method has been applied to the Hg arc by the writers,[2] by Fischer[3] at about the same time, and more recently by Koch.[4] This letter outlines the writers' work as extended in early 1942 and terminated by the war.

The apparatus is shown in Fig. 1. Here an x-ray beam from a 30-kv Mo anode tube passes through a ZrO_2 filter, to render it more monochromatic, through a defining diaphragm, thence along the axis of the arc, entering and leaving the quartz tube through thin inblown windows and passing through hollow electrodes, and finally into an argon-filled ionization chamber where its strength is measured by a string electrometer. Because of the mounting of the x-ray tube, the arc is run horizontally. A special magnet confines the arc well in the axial position except near the cathode, where ordinarily the arc bows upward more strongly. This is corrected by using three cathodes operating in parallel with separate ballasts. The Hg pressure is controlled by the temperature of the furnace F_1, and measured to ~0.3 percent

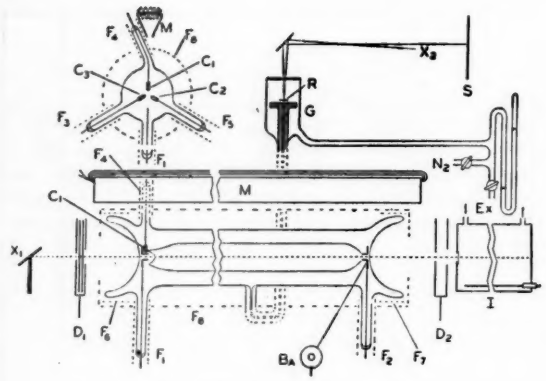

FIG. 1. Schematic diagram of the apparatus.

by a membrane manometer.[5] Furnaces F_2–F_7 prevent Hg from condensing in remote areas. The "cathode" and anode "buttons" of Mo have ~3 mm holes and clear the windows by ~1 mm.

The arc current is ~5 amp. d.c. and the Hg pressure ~1 atmos. (no rare gas). The x-ray tube current is ~28 ma, and the primary voltage 80. The former is held to about 0.3 percent and the latter to about 0.1 percent. The length L of the tube between windows is ~27 cm and the inside diameter 2.0 cm.

The method is to operate the arc at a pressure p_1, measuring the strength of the emergent x-rays, then to shut off the arc and adjust the Hg pressure downward to a pressure p_2, such that the x-ray reading is the same as before. Meanwhile heat is applied by the removable furnace, F_8, to keep the tube at a temperature T_2 well above the Hg condensation point. Then since the x-ray beam traverses the same number of Hg atoms in both cases, it follows that

$$p_1\left[\int\frac{dl}{T}+\frac{L_1}{T_1}\right]=\frac{p_2L}{T_2}, \tag{1}$$

where L_1 is the length of the uniform section of the arc (~25.5 cm) and T_1 its axial temperature. The integral is taken graphically over the end sections, with the help of fine thermocouple measurements of window temperatures and pyrometer measurements of "button" temperatures, extrapolating the temperature curves so found smoothly to T_1. A value of T_1 is thus found by trial which will satisfy (1).

The mean of four series of runs occupying about 10 hours each gave for T_1 the value 6600±200°K. This appears to be at least 800° higher than would be predicted for this arc either from the work of Koch[4] or from the latest work of Elenbaas.[6]

A fuller account will be published elsewhere. We are indebted to Professor C. Nusbaum and the Case Institute of Technology Physics Department for the use of their x-ray facilities, and to Mr. P. D. Cargill for assistance in making the later measurements.

[1] A. von Engel and M. Steenbeck, Siemens-Veröff **10**, 155 (1931).
[2] C. Kenty and W. J. Karash, Phys. Rev. **60**, 66 (1941). Through an error in the calculations, the temperature was quoted about 600° too low.
[3] H. Fischer (unpublished).
[4] O. Koch, Zeits. f. Physik **126**, 507 (1949).
[5] C. Kenty, Rev. Sci. Inst. **11**, 377 (1940).
[6] W. Elenbaas, Philips Research Reports **2**, 20 (1947).

The Temperature of the Mercury Arc

CARL KENTY
General Electric Company, Lamp Development Laboratory, Nela Park, Cleveland, Ohio
April 17, 1950

USING a quartz Hg lamp as its own gas thermometer,[1] the average temperature of the vapor is calculated from the volume of the bulb, the observed pressure, and the weight of Hg. Pressures are measured to 0.3 percent with a quartz membrane manometer.[2] Corrections are calculated for the relatively cold vapor in the end sections, with the aid of fine thermocouple measurements made all over the lamp. The lamps were 2.0 cm i.d., approximately 25 cm long, and contained about 3 mg Hg per cm of length. (No rare gas.)

The average temperature of the vapor in the uniform section, based on three different lamps operating horizontally with magnetic control on d.c. at 40 w/cm (~5 amp.) is 2850±50°K. This is 12 percent higher than the value obtained by Elenbaas[1] for a similar arc. The difference is ascribed to differences in the method of making end corrections.

With an axial temperature of 6600°K determined by x-rays (see preceding letter), and a wall temperature of 845°K, taken from the thermocouple measurements, a $T(r)$ curve is now found by trial, using graphical integration, which will give an average temperature of 2850°K and satisfy a $T^{9/8}$ power law[3] of heat conductivity from the edge of the arc core (at $r\cong0.5$ cm) to the wall.

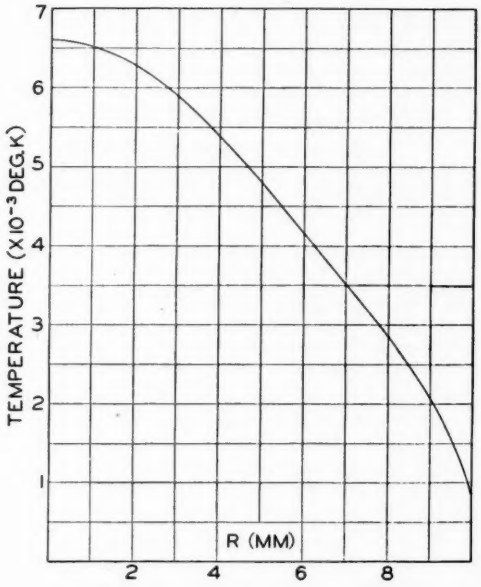

FIG. 1. Temperature distribution in the Hg arc.

This temperature curve (Fig. 1) and the measured gradient (7.94 v/cm) and current (5.07 amp.), together with the Saha and Langevin equations, are used to calculate the cross section σ for elastic collisions of electrons with Hg atoms. The result is 12×10^{-15} cm² (420 cm²/cm³) in quite good agreement with the results of Brode,[4] but threefold larger than the value found by Elenbaas in studying a dissimilar arc.[3]

With the above value of σ, Cravath's formula predicts the observed elastic heat loss[5] of ~10 w/cm if the electron temperature exceeds the gas temperature by ~40°K.

The output of the yellow lines as measured for a dissimilar arc by Elenbaas[3] can be accounted for on the basis of Boltzmann populations for the $6^3P_{2,1,0}$ states and cross sections for two-stage excitation of 6^3D which are tenfold greater[6] than for single-stage excitation, provided a temperature is used which is 450°K higher than that used by Elenbaas, whose calculations failed to account for the excitation by a factor of 100.

With this same temperature increase, σ as calculated from Elenbaas' experiments agrees with the value found here.

The present results indicate that the A values for the yellow lines, found by Schouten and Smit[7] and used by Elenbaas in calculating Hg arc temperatures are several-fold too high. This appears possible from calculations which indicate that there was self-absorption of the 2537A line in Schouten and Smit's experiments and that there were far too few electronic collisions to give

Boltzmann populations for the 6^3D states of Hg, as assumed by these authors for their Hg doped carbon arc.

Details will be published elsewhere.

[1] W. Elenbaas, Physica **1**, 211 (1934).
[2] C. Kenty, Rev. Sci. Inst. **11**, 377 (1940).
[3] W. Elenbaas, Philips Research Reports **2**, 20 (1947).
[4] R. B. Brode, Rev. Mod. Phys. **5**, 243 (1933).
[5] W. Elenbaas, Physica **2**, 757 (1935).
[6] B. Yavorsky, Comptes Rendus U.S.S.R. **48**, 175 (1945).
[7] W. Schouten and J. A. Smit, Physica **10**, 661 (1943).

The Gamma-Rays from $Be^9(\alpha, n)$

R. W. Pringle, K. I. Roulston, and S. Standil
Physics Department, University of Manitoba, Winnipeg, Canada
April 17, 1950

We have recently applied a scintillation gamma-ray spectrometer[1] to the study of high energy gamma-rays which give rise to electron pairs in the scintillation element of NaI (Tl), as a result of their interaction with the I atoms in the crystal lattice. The total kinetic energy of the pairs ($E_\gamma - 1.02$ Mev) appears as the energy of pair production lines when the differential pulse-height distribution of the crystal scintillations is examined in an arrangement similar to the one which we have been using in the lower energy region.[1] Used in this manner the device might be termed a scintillation pair spectrometer.

A satisfactory resolution has been achieved as a direct consequence of the high energies involved and of certain improvements to the original equipment, and we wish to report some interesting results which have been obtained with the very weak gamma-rays produced in the bombardment of beryllium with polonium alpha-particles. These gamma-rays are attributed to the de-excitation of the excited levels of the residual C^{12} nucleus which is formed in the reaction. Previous measurements of these gamma-ray energies[2] have yielded somewhat confusing results, but much work has been done on the level scheme involved by a study of the neutron groups which are produced.[3] It was therefore thought to be of interest to investigate the gamma-rays with the scintillation pair spectrometer, which is ideally suited to a study of very weak sources.

The ThC″ gamma-ray of 2.62 Mev was used for the purpose of calibration (Fig. 1), and a small pair production peak, *A*, due to this gamma-ray can be identified at 1.60 Mev on the pulse-height scale. This is superimposed on a well-defined Compton distribution, *B*. As the pair production cross section is relatively low for this gamma-ray energy, an accurately known gamma-ray of somewhat higher energy, if available, would be better suited for calibration purposes. The source used was about 10 grams of thorium nitrate, which illustrates the extreme sensitivity of the device. The Po-Be source strength was not known accurately but was believed to give approximately 5×10^3 neutrons/sec. The direct effect of these neutrons on the crystal was shown to be small and the pulse-height distribution curve obtained with this source is substantially due to gamma-rays alone. The predominant feature of the C^{12} curve is the pair production peak, *C*, corresponding to a gamma-ray energy of 4.40 ± 0.05 Mev superimposed on a sharp Compton distribution, *D*. The resolution of this line, defined in terms of its full width at half-height, appears to be about eight percent. This sharply resolved peak gives us confidence that the linear relation[1] between pulse height and energy extends to this region, as otherwise a broad distribution would be obtained as a result of the nature of the pair production process. No significant gamma-ray of energy in the range 2 to 4 Mev is found. However, there is evidence for the existence of a very weak gamma-ray at approximately 7.2 Mev. A detailed study of this region was difficult because of the weakness of the available source, and the low relative intensity of the gamma-ray which has been estimated as about one percent of the lower energy component.

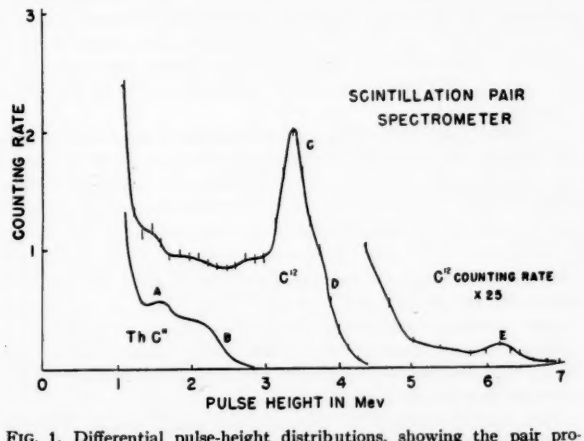

FIG. 1. Differential pulse-height distributions, showing the pair production peaks obtained with high energy gamma-rays. The ThC″ 2.62-Mev gamma-ray has been used to calibrate the pulse-height scale. A. Pair production due to ThC″ 2.62-Mev gamma-ray. B. Compton edge due to ThC″ 2.62-Mev gamma-ray. C. Pair production due to C^{12} gamma-ray (4.40 Mev). D. Compton edge due to C^{12} gamma-ray (4.40 Mev). E. Pair production due to weak C^{12} gamma-ray (7.2 Mev).

The existence of an excited level of C^{12} at 4.40 ± 0.05 Mev and the absence of other levels except the weak high energy 7.2-Mev level is in complete agreement with results which have been obtained recently by Bradford and Bennett[3] from a study of the neutron groups involved.

A considerable amount of work has been done on the study of the photo-electron lines produced by low energy gamma-rays in the scintillation spectrometer and a report of this work will be published shortly. The National Research Council of Canada has given us support in this project.

[1] Pringle, Roulston, and Taylor, Rev. Sci. Inst. **21**, 216 (1950). Pringle, Standil, and Roulston, Phys. Rev. **77**, 841 (1950); **78**, 303 (1950). R. W. Pringle, *Physics in Canada* (1950). P. R. Bell and J. M. Cassidy, Phys. Rev. **77**, 409 (1950).
[2] See W. F. Hornyak and T. L. Lauritsen, Rev. Mod. Phys. **20**, 191 (1948). T. L. Lauritsen, Nuclear Science Series, No. 5.
[3] C. E. Bradford and W. E. Bennett, Phys. Rev. **77**, 753 (1950).

Can the Rectifier Become a Thermodynamical Demon?

L. Brillouin
International Business Machines Corporation, New York and Poughkeepsie, New York
April 17, 1950

A resistor *R*, maintained at the absolute temperature *T*, is a source of random electromotive forces e_ν

$$\langle e_\nu^2\rangle_{Av} = 4RkT\,d\nu \tag{1}$$

for a small frequency interval $d\nu$. This is the well-known Nyquist formula. Let us connect the resistor in series with a rectifier. It seems as if the rectifier should rectify these random oscillations and produce a direct voltage. With a large number of such circuits in series one might obtain a voltage high enough to charge a battery. This means a possibility of doing work with just one source of heat at one temperature, in obvious contradiction with the second principle of thermodynamics.

Let us investigate how this problem can be solved. We consider the circuit of Fig. 1 with an impedance, at frequency ν,

$$Z = R + jX \tag{2}$$

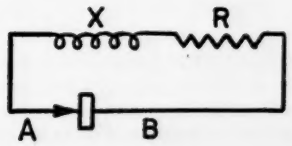

FIG. 1. Circuit with rectifier.

in series with a rectifier, for which we assume a relation

$$V_A - V_B = f = ri + bi^2 \tag{3}$$

between the difference of potential f and the current i.

At a temperature T, electromotive forces φ will be generated in the circuit, for the frequency band $d\nu$, and may contribute to the d.c. electromotive force. We assume

$$\varphi = \varphi_0 + \varphi_\nu$$
$$\langle\varphi\rangle_{Av} = \varphi_0 \quad \langle\varphi_\nu\rangle_{Av} = 0 \quad \langle\varphi_\nu^2\rangle_{Av} = 0, \tag{4}$$

thus splitting the d.c. component of φ_0 from the oscillating term φ_ν.

These electromotive forces produce a current i with a d.c. component i_0 and an oscillating component i_ν

$$\varphi_\nu = (R + r + jX) i_\nu \tag{5}$$

and

$$\langle\varphi\rangle_{Av} = \varphi_0 = (R + r) i_0 + b\langle i_\nu^2\rangle_{Av} \tag{6}$$

assuming $X = 0$ for direct currents.

The second principle of thermodynamics requires that i_0 be zero on the average, in order to give no average potential difference, $V_A - V_B$, so that

$$\langle i_0\rangle_{Av} = 0$$

and Eq. (5) yields, after averaging,

$$\langle\varphi\rangle_{Av} = \varphi_0 = b\langle i^2\rangle_{Av}. \tag{7}$$

This means that the d.c. component of the fluctuation exactly cancels the rectified voltage due to the thermal oscillating current. Furthermore, the Nyquist formula (1) must apply to the r term of the rectifier [Eq. (3)] as well as to the resistor R. Suppose for a moment that the thermal noise in the rectifier is stronger than in a resistance of similar r-value. This would mean that the noise from the rectifier should heat up the resistor R and produce, after a while, a difference in temperature between rectifier and resistor; this would again be a contradiction of the second principle. This proves that

$$\langle\varphi_\nu^2\rangle_{Av} = 4(R + r) kT d\nu, \tag{8}$$

a formula similar to (1), applied to the whole circuit. Hence

$$\langle i_\nu^2\rangle_{Av} = \frac{\langle\varphi_\nu^2\rangle_{Av}}{(R+r)^2 + X^2} = 4\frac{R+r}{(R+r)^2 + X^2} kT d\nu \tag{9}$$

and finally with the help of Eqs. (7) and (9)

$$\varphi_0 = b\langle i_\nu^2\rangle_{Av} = 4b\frac{R+r}{(R+r)^2 + X^2} kT d\nu. \tag{10}$$

The direct component of the noise, corresponding to the frequency band $d\nu$, depends on the properties R, X of the whole circuit. There is no rectified current in the circuit, and no direct voltage across the rectifier. For an actual electric circuit, X depends on ν, and an integration performed on Eq. (10), from $\nu = 0$ to $\nu = \infty$ yields the total direct φ_0-term. Application of the formula to special examples always shows a complete compensation of direct average voltage.

The whole procedure is an example of the general method of detailed balancing discussed by Bridgman.[1]

[1] P. W. Bridgman, Phys. Rev. 31, 101 (1928).

Nuclear Recoil Momentum in Pair Production

B. ROSENBAUM
Department of Physics, University of Illinois, Urbana, Illinois
April 17, 1950

RECENTLY[1] Modesitt and Koch investigated the production of electron pairs by γ-ray quanta in an air filled cloud chamber. They made measurements of the momentum transferred to nuclei in the creation of pairs by quanta of energies ranging from 1.02 to 19.5 Mev. The momentum imparted to the nucleus is related to the distance from the nucleus at which the electron pairs are formed. The data on recoil momenta of nuclei then constitute a test of a feature of the theory of pair production.

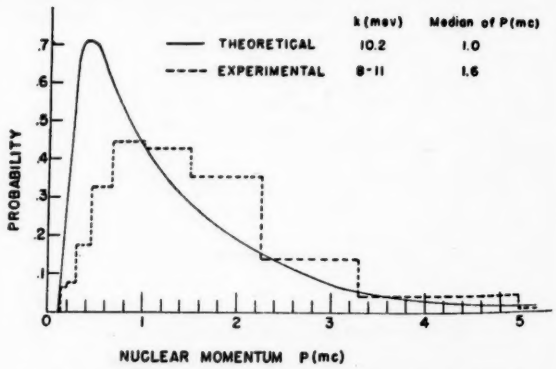

FIG. 1. The theoretical and experimental probability distribution curve of nuclear recoil momentum for pair production in air.

Bethe and Heitler[2] have given the theory of pair production by a γ-ray quantum in the Coulomb field of a nucleus. For large enough quantum energy the theory predicts a simple probability distribution for the nuclear recoil momentum[3]

$$\phi(p)dp = \text{const.}\, dp/p,$$

provided

$$1 \gg p/mc \gg \delta/mc = mc^2 k/2E_+E_-.$$

Here δ is the minimum possible momentum transfer. However, the quantum energies used in the experiments[1] are too small to justify comparison with the simple formula above, since the minimum value of δ/mc (at say $k = 20\ mc^2$) is 0.1, which hardly allows p to satisfy the conditions.

In order to obtain a formula which can justly be compared with experiment an exact numerical calculation of $\phi(p)$ was made for a quantum energy typical for the experiments, $k = 20$ cm^2. Bethe[3] has given, by simple alterations of his Eq. (32), a form of the differential cross section for pair production which is convenient for integration. Part of the necessary integrations in calculating $\phi(p)$ were performed analytically by Bethe. Further work then consisted essentially of numerical integration.

The theoretical probability curve at $k = 10.2$ Mev and the experimental results for the range 8 to 11 Mev are shown in Fig. 1. The calculated median momentum 1.0 mc and the experimental 1.6 mc are in disagreement. The validity of the Born approximation is hardly in doubt since the pair production took place in air; furthermore, screening is negligible in the range of recoil momenta involved. It is clear from the figure that the simple dp/p law at this energy is a poor approximation to the actual theoretical curve.

At higher quantum energies the theoretical distribution function approaches the simple asymptotic formula given by Bethe. The concentration of momentum transfers in the neighborhood of the minimum momentum increases with increasing quantum energy and the median, consequently, decreases. In the data of Modesitt and Koch there is no such variation of the median momentum with quantum energy. The form of their histograms is essentially the same from 3 to 19.5 Mev. Their set of observed median momenta are larger than predicted by the theory, the difference being greatest for highest energy range, 17.0 to 19.5 Mev. This disagreement between theoretical predictions and experiment has not been explained.

The author wishes to express his gratitude to Professor A. Nordsieck for suggesting this problem and for his interesting and helpful discussions.

[1] G. E. Modesitt and H. W. Koch, Phys. Rev. 77, 175 (1950).
[2] H. Bethe and W. Heitler, Proc. Roy. Soc. 146A, 83 (1934).
[3] H. Bethe, Proc. Camb. Phil. Soc. 30, 524 (1934).

Beta-Ray Spectrum of K^{40}

DAVID E. ALBURGER
Brookhaven National Laboratory, Upton, Long Island, New York*
April 10, 1950

IN a previous communication[1] the results of a spectrometer measurement on K^{40} beta-rays were presented. The source was KCl, 18.5 mg/cm² in thickness, enriched to 1.2 percent K^{40}, giving a maximum yield less than background. The end point occurred at 1.40±0.03 Mev and the apparent shape was that of an allowed type spectrum above 500 kev. Such a shape is in contradiction to the theory of forbidden beta-decay and the predictions of Marshak[2] for K^{40}. Since the known spin change is 4, Marshak showed that with parity change the transition should be third-forbidden and, for either the axial vector or tensor interactions permitted in this case, the factor $c=q^6+7q^4p^2+7q^2p^4+p^6$ [where $q=W_0-W$, $p=(W^2-1)^{\frac{1}{2}}$, W is the energy in units of mc^2, and W_0 is the end-point energy] multiplies the usual Fermi function. The actual spectrum should therefore be distinctly different from the allowed form.

During publication of this earlier result on K^{40} the first of the newly discovered series of first-forbidden type beta-ray emitters, namely Y^{91}, was reported by Langer and Price.[3] Making use of Y^{91} mixed in various amounts of KCl, Feldman and Wu[4] showed that thicknesses of 20 mg/cm² distorted the Y^{91} spectrum into the allowed shape in the upper two-thirds range of energies. They concluded from this that the K^{40} beta-ray spectrum probably did not have the allowed shape. The first clear evidence was given recently by Bell, Weaver, and Cassidy.[5] Using a scintillation spectrometer and 2.5-mg/cm² thick sources of KCl enriched to 1.3 percent K^{40}, they found a forbidden type spectrum agreeing with the factor, c, from 700 kev to the end point at 1.36±0.05 Mev.

Improved techniques of electromagnetic separation have recently enabled C. P. Keim and co-workers at Oak Ridge to increase substantially the K^{40} enrichment factor. The result is that a small quantity of potassium (in KCl) containing 7.13 percent K^{40} has become available.[6] This has made possible conventional spectrometer measurements without excessive distortion due to source thickness. In the present work a source 4 cm² in area was deposited on 0.5-mg/cm² Nylon by precipitating a saturated drop of KCl solution with acetone and rapidly evaporating the remaining liquid by hot air. Examination showed that small crystals were formed although a certain amount of clustering of crystals could not be prevented resulting in noticeable nonuniformities. The average thickness was 2.4 mg/cm².

To study the effects of this type and thickness of deposit, comparison runs were made on P^{32} which is known to have the allowed shape.[7] In the lower curve of Fig. 1 is shown the Kurie plot for a thin source (~0.3 mg/cm² deposited on 0.5-mg/cm² Nylon)

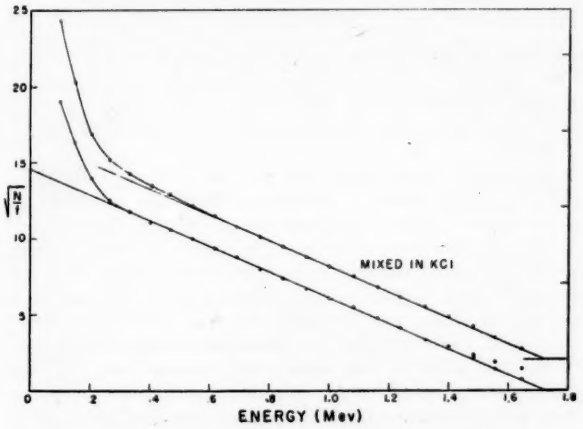

FIG. 1. Kurie plots of P^{32} beta-ray spectrum showing effects of 17 percent resolution and 2.5-mg/cm² source thickness.

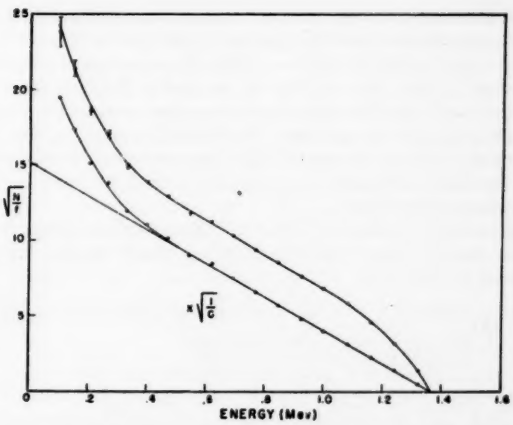

FIG. 2. Kurie plot of K^{40} beta-ray spectrum with and without the theoretical correction factor.

obtained using 17 percent resolution and the same geometry as for K^{40}. Points were corrected for resolution by a graphical integration method similar to previous work[8] on Be^{10}. Only the highest four points are appreciably affected and it is seen that with the corrections included the plot is linear down to about 300 kev. P^{32} was then mixed in ordinary KCl and a 2.5-mg/cm² deposit made by the same procedure used on K^{40}. Deviations are larger and occur up to about 550 kev, as shown in the upper curve of Fig. 1, but the remainder of the curve is linear to the end point. Counter window corrections at low energies have been made in both cases.

The K^{40} source gave at the maximum a yield of 15.8 counts per minute above a background of 18.2 per minute, requiring a total of approximately 170 hours of counting to obtain suitable statistics. The ordinary Kurie plot, including resolution and 2.8-mg/cm² counter window corrections, is shown in the upper curve of Fig. 2. The lower curve includes the correction factor, c, and is linear from about 500 kev to the end point at 1.36±0.03 Mev. Calibration was taken from the P^{32} Kurie plot using an end point of 1.715 Mev, representing the mean of values given by Siegbahn[7] and Agnew.[9] Comparison of this data with the P^{32} thick source result indicates probable agreement of the K^{40} spectrum with the factor, c, to energies well below 500 kev.

To test the uniqueness of the K^{40} spectrum shape the correction factors $\alpha=q^2+p^2$ and $D_2=q^4+10/3q^2p^2+p^4$, generally associated with first- and second-forbidden beta-ray spectra, respectively, were applied to the data. The α-curve shown in Fig. 3 is non-linear, but the D_2 corrected curve appears to be linear above 500 kev

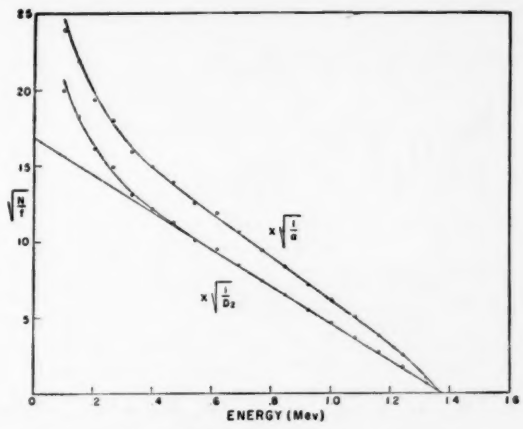

FIG. 3. K^{40} Kurie plot corrected by first-forbidden (α) and second-forbidden (D_2) correction factors.

within the statistical errors. Due to the close similarity of the second- and third-forbidden correction functions it will be difficult to reject the former in the case of K^{40}. The two fourth-forbidden correction factors (spin change 4, no parity change) given by Marshak need not be considered since they are readily distinguished from the second- and third-forbidden factors. For the present the beta-ray spectrum of K^{40} may be regarded as agreeing with the theory although unique proof of this is not possible with the data presented here.

The author is indebted to Dr. C. P. Keim of Oak Ridge for his special efforts in furnishing the enriched source making this experiment possible.

* Work performed at Brookhaven National Laboratory under the auspices of the AEC.

[1] D. E. Alburger, Phys. Rev. **75**, 1442 (1949).
[2] R. E. Marshak, Phys. Rev. **70**, 980 (1946).
[3] L. M. Langer and H. C. Price, Phys. Rev. **75**, 1109 (1949).
[4] L. Feldman and C. S. Wu, Phys. Rev. **76**, 697 (1949).
[5] Bell, Weaver, and Cassidy, Phys. Rev. **77**, 399 (1950).
[6] Carbide and Carbon Chemicals Corporation, Oak Ridge, Tennessee.
[7] K. Siegbahn, Phys. Rev. **70**, 127 (1946).
[8] Hughes, Eggler, and Alburger, Phys. Rev. **77**, 726 (1950).
[9] H. M. Agnew, Phys. Rev. **77**, 655 (1950).

Evidence from Cosmic-Ray Bursts for a Nuclear Cascade Process*

G. N. Whyte
Palmer Physical Laboratory, Princeton University, Princeton, New Jersey
April 10, 1950

THERE exists considerable indirect evidence for a substantial multiplication of the star-producing component of the cosmic radiation by a nuclear cascade process. For example, Hazen[1] has reported that more than half of the stars observed in a cloud chamber at 10,000 ft. are producted by neutrons; since most, if not all, of such neutrons are believed to *originate* in stars, this observation implies a nuclear cascade. Bernardini *et al.*[2] conclude from photographic plate data on stars that "each primary proton gives rise on the average to more than 10 secondary nucleons having energies of the order of magnitude of some hundreds of Mev." A number of cloud-chamber pictures[3,4] have actually shown an ionizing particle from one star giving rise to another star. The experiments described below provide a somewhat more direct measure of the build-up of the star-producing component in the atmosphere.

A number of thin-walled, spherical ionization chambers have been flown to altitudes exceeding 90,000 ft. at geomagnetic latitudes 0°, 29° and 35°N, extending the work done by Coor[5] at 52°. Each chamber was 30 cm in diameter and was filled with pure argon at 1.4 atmospheres. Electron collection was used. Burst sizes were measured in terms of standard pulses due to polonium alpha-particles, with which the chambers were calibrated periodically. Bursts ranging in size from 0.7 to 20 Po alpha were recorded.

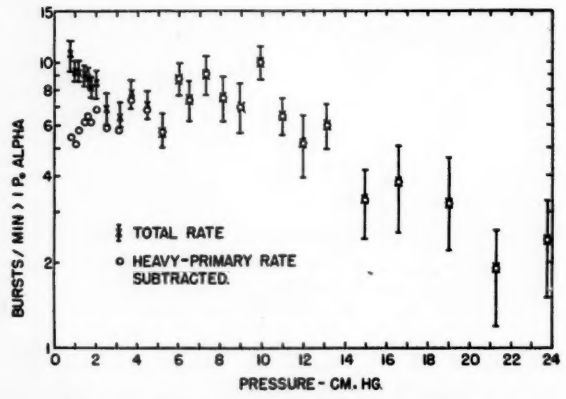

FIG. 1. Variation of burst rate with atmospheric depth.

The flights were sent up by balloon from the U. S. S. Norton Sound in the Pacific during July and August of 1949.

The crosses in Fig. 1 show the variation of the burst rate at 0° as a function of atmospheric depth for bursts greater than 1 Po alpha. The points have been obtained by averaging the results of 3 flights. The initial rapid fall-off in the rate with increasing depth is believed to be due to heavy primary nuclei of $Z \geq 12$, which can cause bursts by ionization in passing through the chamber and which are quickly absorbed by collisions with air nuclei. Bradt and Peters[6] have measured the primary fluxes and mean free paths for collision of such particles at 30° and 51°. From the approximate energy spectrum deduced from these measurements by Vallarta[7] and the geomagnetic cut-off energies at 30° and 0°, one can estimate the flux at 0°. Using this flux and the appropriate mean free paths, one can calculate the burst rate to be expected from heavy primaries as a function of atmospheric depth.

The circles in Fig. 1 have been obtained by subtracting the heavy primary rate from the total rate. Coor has estimated the burst rate due to electron showers at these altitudes to be quite negligible, so that the corrected rate is believed to be due predominantly to nuclear disintegrations and furnishes a measure of the flux of star-producing particles. It will be observed that this flux increases with increasing depth to a maximum around 7 cm Hg before falling off in the usual fashion. Such behavior is consistent with a nuclear cascade picture, according to which each primary particle produces a star, some of the secondaries from which are in turn able to produce stars, the process continuing to the stage where the secondaries have insufficient energies to cause further disintegrations.

A more complete and quantitative report on this work is in preparation.

Sincere thanks are due Dr. G. T. Reynolds for his interest and advice, Mr. Robert Price for his assistance with the flights, and the personnel of the U. S. S. Norton Sound for their unfailing cooperation.

* Assisted by the joint program of the AEC and the ONR.
[1] W. E. Hazen, Phys. Rev. **65**, 67 (1944).
[2] Bernardini, Cortini, and Manfredini, Phys. Rev. **76**, 1792 (1949).
[3] W. B. Fretter and W. E. Hazen, Phys. Rev. **70**, 230 (1946).
[4] C. Y. Chao, Phys. Rev. **74**, 492 (1948).
[5] T. Coor, Princeton University thesis (1948).
[6] H. L. Bradt and B. Peters, Phys. Rev. **77**, 54 (1950).
[7] M. S. Vallarta, Phys. Rev. **77**, 419 (1950).

Optical Absorption in Strontium Oxide Films

Robert L. Sproull
Department of Physics, Cornell University, Ithaca, New York
April 13, 1950

MEASUREMENTS of the optical absorption of strontium oxide were undertaken as part of a study of the properties of the alkaline earth oxides. The technique and apparatus used were identical with those used by Tyler[1] in his study of barium oxide films.

A platinum-rhodium (Baker No. 750 alloy) filament, 0.005 in. $\times$0.092 in., was outgassed in vacuum at 1600°C for two hours. It was then coated to a depth of about 20 mg/cm^2 with Mallinckrodt "ultra-pure" strontium oxide in a minimum of nitrocellulose, amyl acetate binder (tested for the absence of barium). The filament was heated slowly in the vacuum system, the carbonate converted to oxide, and outgassed for four hours at 1350°C. During this period, any barium oxide should evaporate preferentially. This selective evaporation has recently been analyzed by Moore and Allison,[2] whose work indicates that the concentration of barium oxide in a BaO-SrO mixture should be considerably reduced by this procedure. Fused quartz plates were coated by evaporation from the strontium oxide source thus prepared.

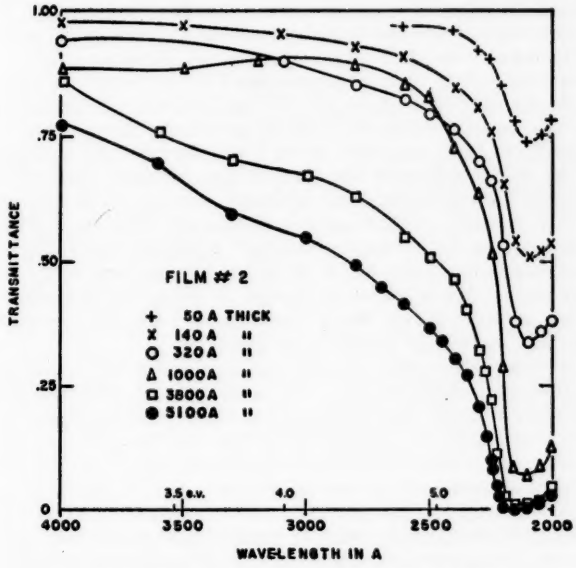

FIG. 1. Optical transmittance *vs.* wave-length for different thicknesses of a SrO film.

The observed transmittance as a function of wave-length for one film is given in Fig. 1, for six different film thicknesses. All but the thickest films show no absorption at wave-lengths longer than 2500A, indicating that barium oxide contamination is small. The crossing of the lines from the 1000A and 320A thick films is almost certainly an interference effect. The effect of scattered light has been minimized by the use of a magnesium oxide crystal[3] filter which passes $\lambda > \sim 2500$A but cuts off shorter wave-lengths. Transmittance readings were taken with the MgO filter in the optical path and without it; the *difference* in these readings gave the effect of light in the absorption band of MgO. Even with this technique scattered light was still serious with the thickest films in the wave-length range 2100 to 2000A, but caused very little error with films <1000A thick.

Measurements of the transmittance near $\lambda = 2200$A were made at room temperature and at liquid air temperature. No shift in the transmittance spectrum was observed; a shift of 7A could have been detected. The magnitude of A was also unchanged.

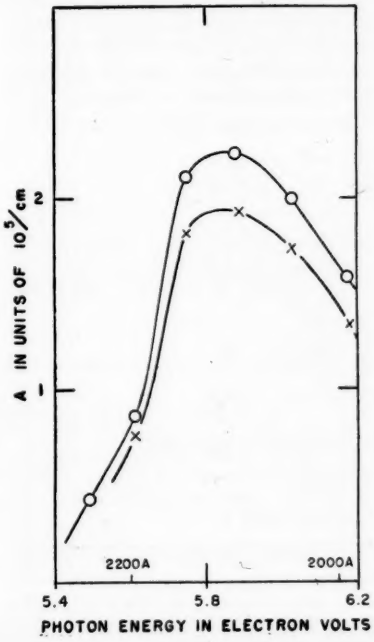

FIG. 2. Absorption constant *vs.* photon energy for two different films of SrO. X—Film No. 1. Thickness 30 to 1800A. O—Film No. 2. Thickness 50 to 5100A.

Figure 2 shows the absorption constant A (as defined by the equation $T = \exp(-Ax)$, where T is the transmittance and x is the film thickness) for two different films. The shapes of the two curves are the same, and the magnitudes of A agree within the experimental error of measuring the thickness of the films (by weighing as $Sr(OH)_2$). Data at wave-lengths longer than 2250A have not been included in Fig. 2. The existence of true absorption at longer wave-lengths is questionable; there may be a "tail" of absorption of the order of 10^4/cm, but it seems more likely that the transmittance curves for the thickest films indicate only the presence of impurities (such as barium oxide or platinum),[2] or light scattering in the films. The abrupt rise at about 5.5 ev, the absorption peak at about 5.9 ev, and the magnitude of the absorption constant near the peak are thought to be the principal conclusions from this work. The peak absorption constant is so large that the absorption cannot be caused by impurities.

The author wishes to express his appreciation for the assistance of Dr. W. W. Tyler and Mr. S. S. Stevens, and for the support by ONR and the Research Corporation.

[1] W. W. Tyler, Phys. Rev. **76**, 1887 (1949).
[2] G. E. Moore and H. W. Allison, Phys. Rev. **77**, 246 (1950).
[3] Supplied by the Norton Company, Niagara Falls, Canada.

An Unusual Effect in the Creep of Zinc Single Crystals

L. SLIFKIN AND W. KAUZMANN
Frick Chemical Laboratory, Princeton University, Princeton, New Jersey
March 27, 1950

IN an investigation of the creep of zinc single crystals, a curious "rest-hardening" effect has been found. A constant tensional load, chosen to give rates of elongation of the order of 10^{-5}/min. during the first few minutes, was applied to a single crystal rod of 99.999 percent zinc,[1] which had been annealed in nitrogen for 3 hr. at 210°C. After letting the crystal creep for 150 min. the load was removed and the crystal allowed to rest for various times, from 1 min. to 70 hr., whereupon the load was re-applied and the crystal permitted to creep again for several hours. The crystal was then annealed in nitrogen for 3 hr. at 210°C and the experiment was repeated with a different rest time. All creep experiments were conducted at 35°C.

If the logarithm of the creep rate before the rest period is plotted against the logarithm of the time after application of the load, a straight line of slope about $-\frac{2}{3}$ is obtained (Fig. 1).[2] This leads to Andrade's law for transient (or "β") creep.[3,4] Cottrell and Aytekin[5] found a similar behavior at much higher rates of elongation. We have observed, however, that at high creep rates the transient creep gradually gives way to a constant ("quasi-viscous") rate of flow. The discrepancy may lie in the fact that they used monocrystalline wires whereas our crystals were $\frac{1}{4}$ in. in diameter.

It was found that the annealing treatment after each run usually returned the crystal to the same state, in that very satisfactory reproducibility was obtained in the creep rates during the first 150 min. The total elongations produced were so small that there were no appreciable changes of crystallographic orientation or cross-sectional area, with constant load thus implying constant shear stress.

Now, zinc exhibits recovery at room temperature and one therefore expects the creep rate to be larger after resting than just before, falling eventually to the extrapolation of the original straight line. This behavior was found for rest periods of from 1 to 500 min. (curves 1 and 2 in Fig. 1). Longer rest periods thus give greater recovery, as measured by the increased creep rate

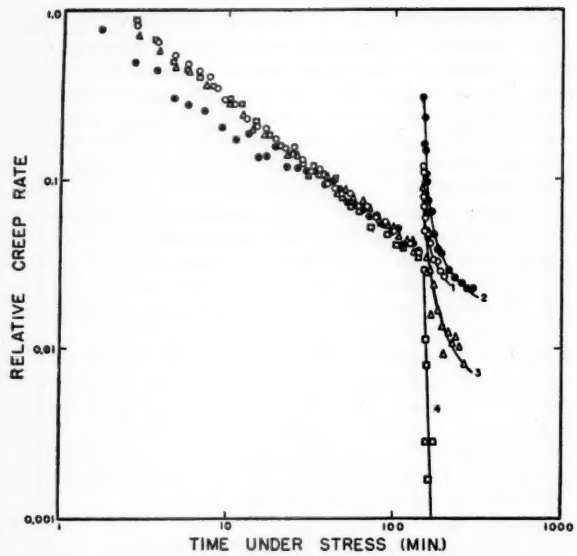

FIG. 1. Creep rate of zinc crystal with rests of various durations interposed after 150 min. of creep. The points denoted by ○, ⊕, △, and □ represent runs in which the rest periods were 1 min., 100 min., 25 hr., and 70 hr., respectively. The curves were displaced vertically to make them coincide at 150 min. The actual creep rates (in units of 10^{-5}/min.) are given by these relative rates multiplied by 1.0, 2.0, 0.89, and 0.88, respectively.

and longer time required for the rate to fall to the linear extrapolation.

If the crystals were allowed to rest for a very long time at 35°C, complete recovery would presumably take place; therefore, the effects of still longer rest periods (up to 70 hr.) were studied. A totally unexpected result was obtained. With rests of about 24 hr., the rate immediately after re-application of stress was approximately the same as, or somewhat larger than, that before resting, but it soon fell below the extrapolation of the original log rate-log time curve (curve 3 in Fig. 1). With rests of about 43 and 70 hr., even the initial rate after resting was below the value just before removing the load, and it continued to decrease sharply with time (curve 4 in Fig. 1). It thus appears that the crystal, after softening somewhat upon resting, hardens again upon further resting. This behavior was observed eight times with all of the three crystals tested. It shows some similarity to Orowan's thermal hardening effect[6,7] found in investigating stress-strain curves of zinc and cadmium. There are, however, important differences such as the absence here of softening upon further deformation.

Further investigations of this effect are in progress.

[1] This zinc was a gift from the New Jersey Zinc Company.
[2] Other crystals gave slopes even more nearly equal to $-\frac{1}{3}$ than the data in Fig. 1 indicate.
[3] E. N. da C. Andrade, Proc. Roy. Soc. **A84**, 1 (1910).
[4] E. Orowan, J. West Scot. Iron Steel Inst., 45 (1947).
[5] A. H. Cottrell and V. Aytekin, Nature **160**, 328 (1947).
[6] E. Orowan, Proc. Phys. Soc. London **52**, 8 (1940).
[7] A. H. Cottrell and D. F. Gibbons, Nature **162**, 488 (1948).

Fast Neutron Cross Sections and Nuclear Shells

D. J. HUGHES* AND D. SHERMAN†
Argonne National Laboratory, Chicago, Illinois
April 10, 1950

IN a previous paper[1] a method for measuring fast neutron activation cross sections was described. The neutron source is a plate of uranium enriched in U^{235} which, when placed in a beam of thermal neutrons from the pile, emits fission neutrons of effective energy 1 Mev for the radiative capture process. The flux of unmoderated fission neutrons is calibrated in terms of the known thermal flux and is high enough so that activation cross sections as low as 10^{-4} barn can be measured. The isotopic activation cross sections reported in reference 1 showed a rapid increase with atomic weight up to 100 and approximate constancy for heavier nuclei, with several striking exceptions. The exceptions were Ba^{138}, Pb^{208}, and Bi^{209}, all of which showed cross sections about a 100-fold lower than neighboring isotopes. The unexpectedly low results were soon explained[2] however, by the nuclear shell hypothesis, as Ba^{138} contains 82 neutrons, and Pb and Bi, 126 neutrons, both "magic numbers." A nucleus containing a complete shell of neutrons (20, 50, 82, or 126 neutrons) would be expected to show a low binding energy for an additional neutron, a low excitation energy after neutron capture, a small level density, and hence a low capture cross section.

In order to investigate further the relationship between cross sections and shell structure, additional isotopes with neutron numbers in the 50 and 82 regions have been measured. Most of the elements which were activated were used in solid form in exactly the same manner as was previously described[1] and no additional details are necessary. However, several noble gases were measured and the activation and counting of these proved somewhat difficult, especially Xe with its inconvenient 3.5 min. period. The gases were irradiated in a flat glass cylinder, cadmium covered for fast neutrons and bare for thermals (see reference 1), which was filled to two atmospheres pressure. The cylinder was carried from the pile after irradiation to a system where the gas could be transferred rapidly to a space around a thin-walled G-m tube by freezing and evaporation.

The recent cross-section measurements are listed in Table I and are plotted against neutron number in Fig. 1 along with the results of reference 1. Most of the fast cross sections were measured relative to the known thermal values listed by Way and Haines.[3] For a few cases, such as the Ce isotopes, for which no recent results were available, thermal cross sections were measured also by irradiating and counting thin foils on a calibrated end window G-M tube. It is clear from Fig. 1 that the nuclei with 50 and 82 neutrons have extremely small cross sections, in agreement with the early results for Ba, Pb, and Bi, and in support of the idea that the level density is unusually low in the compound nuclei formed by neutron capture in these isotopes. It follows that the neutron binding energy in these cases must be lower than that of neighboring nuclei by enough to cause a discontinuity in level density by a factor of 50 to 100. If the concept of neutron shells is taken literally, it would be expected that a nucleus with 84 neutrons (two more than a closed shell) would have a cross section lower than normal, but one of 80 neutrons would have a high cross section. The few nuclei of this type measured so far do not seem to fit this simple picture because, while Ce with 84 neutrons has a very small cross section, Rb and

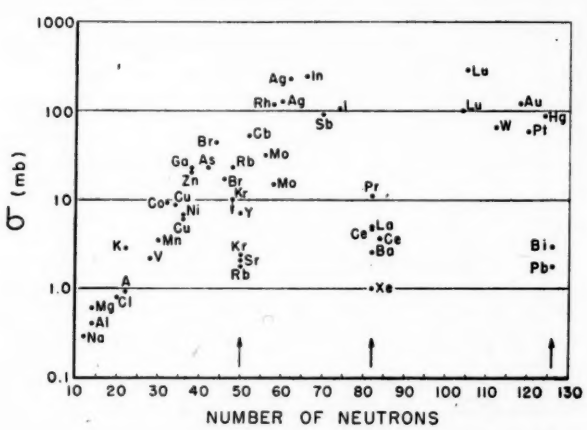

FIG. 1. Neutron cross sections *vs.* number of neutrons.

TABLE I. Isotopic activation cross sections at 1 Mev.

Isotope	No. of neutrons	Activity	Cross sections	Remarks
A^{40}	22	110 min.	0.93 mb	
Kr^{84}	48	(4.5 hr.)	1.9	
		(9.4 yr.)	<8	Activity not detected in thermal or fast irradiation; upper limit estimated from fast flux and counter geometry.
Rb^{85}	48	19.5 day	23.1	
Kr^{86}	50	74 min.	2.4	
Rb^{87}	50	17.5 min.	1.8	
Y^{89}	50	62 hr.	7.0	
Sr^{88}	50	53 day	2.1	
Xe^{136}	82	3.8 min.	1.0	
La^{139}	82	40.4 hr.	5.0	
Ce^{140}	82	28 day	4.8	Thermal $\sigma=0.24$ b measured also
Pr^{141}	82	19.3 hr.	11.0	
Ce^{142}	84	33 hr.	3.6	Thermal $\sigma=0.72$ b measured also
Lu^{175}	104	(3.7 hr.)	101	This value (101 mb) plotted on Fig. 1 for Lu^{175} is a lower limit because the fraction of neutron captures forming the 10^{10} yr. activity is unknown.
		(10^{10} yr.)	—	
Lu^{176}	105	6.8 day	296	

Kr, with 48 neutrons, instead of being higher than normal, are actually somewhat lower.

All of the nuclei discussed so far have an even number of neutrons, measurement of capture cross sections of odd neutron number nuclei being difficult because stable nuclei are formed. The neutron binding energy for an odd neutron nucleus would be about 1 to 2 Mev (twice δ_A of Bohr and Wheeler[4]) higher than for an even neutron number, and the cross section would be correspondingly higher. The change in level density corresponding to this difference in excitation energy was investigated with Lu^{175} (104 neutrons, stable) and Lu^{176} (105 neutrons, radioactive). Table I shows that the cross section of Lu^{175} is normal and that of Lu^{176} larger by a factor of at most 3. Thus a change of 1.2 Mev ($2\delta_A$ for $A=175$) in excitation energy produces a change in level density small compared to that produced at the completion of a shell, indicating that the latter discontinuity must be of the order of several Mev. In fact, the usual statistical nuclear model,[5,6] gives a level density variation with excitation energy which would require a 4-Mev change in binding energy to produce a factor of 50 in level density at $A=140$, and 3 Mev at $A=200$. From Way's[7] analysis of the binding energies in the lead region, however, it is seen that the binding of the 127th neutron in Pb and Bi is only about 2 Mev lower than the average for other odd neutrons in the same region. Thus, the change in level density at the shells, as shown by the fast neutron capture cross sections, is quite marked, and in fact larger than would be expected from other evidence based on binding energy and the statistical model.

* Now at Brookhaven National Laboratory, Upton, Long Island, New York.
† Now at Radiation Laboratory, Berkeley, California.
[1] Hughes, Spatz, and Goldstein, Phys. Rev. **75**, 1781 (1949).
[2] K. Way (private communication).
[3] K. Way and G. Haines, AECD 2138 (February, 1948) Oak Ridge, Tennessee.
[4] N. Bohr and J. A. Wheeler, Phys. Rev. **56**, 426 (1939).
[5] H. A. Bethe, Rev. Mod. Phys. **9**, 69, 86–90 (1937).
[6] D. ter Haar, Phys. Rev. **76**, 1525 (1949).
[7] K. Way, Phys. Rev. **75**, 1448 (1949).

Binding Energy of the Triton

TSI-MING HU* AND KUNG-NGOU HSU
Mathematics Department, University College, London, England
December 5, 1949

CALCULATIONS have been carried out to investigate the sensitivity of the binding energy of the triton to assumptions about the shape and range of the nucleonic interaction, assuming tensor forces. Assuming a tensor interaction the ground state of the triton will be a mixture of eight angular and spin functions, *viz.*,† $^2S'$, $^2\bar{S}$, $^2P'$, ^4P, $^4D(r_{12})$, $^4D(r_{31})+{}^4D(r_{23})$, $^4D(r_{31})-{}^4D(r_{23})$, where

$$^4D(r_{12})=[3(\sigma_1\cdot r_{12})(\sigma_3\cdot r_{12})-r_{12}^2(\sigma_1\cdot\sigma_3)]\chi$$

and

$$\chi=2^{-\frac{1}{2}}(\alpha_1\beta_2-\alpha_2\beta_1)\alpha_3.$$

Previous investigations[1,2] have considered only the contribution from the $^2S'$ and $^4D(r_{31})-{}^4D(r_{23})$ components. However, if the problem is regarded in an iteration scheme both $^4D(r_{31})+{}^4D(r_{23})$ and $^4D(r_{31})-{}^4D(r_{23})$ appear as first-order terms, considering the $^2S'$ wave as primary.[3] In the present work a combination of all the components was taken as trial function.

The effect of range of interaction on triton binding energy has been investigated for a Yukawa interaction with interaction constants adjusted to give correctly the binding energy and quadrupole moment of the deuteron, and the incoherent low energy $n-p$ scattering cross section. Calculations have also been carried out for a Yukawa interaction which gives the correct deuteron binding energy, but assumes central forces only. This is equivalent to making the ratio of the ranges r_N/r_C of the tensor force to the central force infinite. Any other value for this ratio intermediate between 1 and ∞ should lie between the two curves giving triton binding energy as a function of r_C for these two extreme cases. This is in fact found for calculations made using $r_N/r_C=2$ and $r_C=0.80\times10^{-13}$ cm.

The results are summarized in Table I.

TABLE I. Binding energy of the triron.[a]

Well shape	r_C in 10^{-13} cm	r_N/r_C	Exchange nature	$E(H^3)$ in Mev	$E(He^3)$ in Mev	Terms included in trial wave function
Y	1.36[b]	1	Ex.	7.0	—	Including first-order terms for $^2P'$, $^2\bar{P}$, ^4P and second-order terms for $^2S'$, $^2\bar{S}$, $^4D(r_{12})$, $^4D(r_{31})\pm{}^4D(r_{23})$.
Y	1.36	1	Ord.	6.7	—	
Y	1.36	1	Ex.	5.28	4.26	Including first-order terms for all eight spin and angular functions.
Y	1.36	1	Ord.	4.52	3.50	
Y	1.74[c]	1	Ord.	6.5	—	
Y	2.18[c]	1	Ord.	6.4	—	
Y	3.05[c]	1	Ord.	5.4	—	
Y	1.36	∞	Ord.	12.16	—	Including first-order terms for ^2S waves.
Y	1.74	∞	Ord.	9.00	—	
Y	2.18	∞	Ord.	7.43	—	
Y	3.05	∞	Ord.	5.44	—	
Y	0.80[d]	2	Ord.	10.2	—	Including zero-order terms in $^2S'$ and first-order terms in $^4D(r_{31})\pm{}^2D(r_{23})$.
S.W.	2.80[e]	1	Ord.	4.0	—	Including zero-order terms in $^2S'$ and $^4D(r_{31})-{}^4D(r_{23})$ and first-order terms in $^4D(r_{31})+{}^4D(r_{23})$

[a] Y = Yukawa; S.W. = spherical well; Ex. = exchange; Ord. = ordinary.
[b] K. N. Hsu (unpublished).
[c] T. M. Hu and H. S. W. Massey, Proc. Roy. Soc. **A196**, 135 (1949).
[d] H. N. Yadav (in press).
[e] W. Rarita and J. Schwinger, Phys. Rev. **59**, 436 (1941).

It is seen from the table that the difference produced by assuming different exchange properties is comparatively small, so that most of the calculations were carried out assuming ordinary forces.

It is also clear that the convergence is much better for the long range than for the short range cases. This is a characteristic feature of the variation method. For the case $r_C=r_N=1.36\times10^{-13}$ cm the convergence limit cannot be precisely extrapolated. It may attain a value as high as 8 Mev, but the possibility of determining the range from the triton problem is made difficult by the poor convergence at short ranges. For the long range case $r_C=r_N=3.05\times10^{-13}$ cm the convergence is at least as good as for the pure central force.

The binding energy of He^3 has also been calculated assuming exchange forces and Yukawa interaction of range $r_C=r_N=1.36\times10^{-13}$ cm. In this case the ground state is a mixture of charge doublet and charge quartet, but the effect of the latter is very small and the binding energy obtained was the same as that

calculated from H^3 using a perturbation method to take account of the Coulomb interaction.

We would like to thank Professor H. S. W. Massey for his interest in the work and Dr. H. N. Yadav for providing us with his interaction constants in advance of publication.

* Now at Chekiang University, China.
† The notation should be clear by reference to Gerjuoy and Schwinger, reference 1. (Owing to typographical difficulties the symbols S and P with superposed tildas have been replaced by S' and P'—Ed.)
[1] E. Gerjuoy and J. Schwinger, Phys. Rev. **61**, 138 (1942).
[2] H. Feshbach and W. Rarita, Phys. Rev. **75**, 1384 (1949).
[3] R. E. Clapp, Phys. Rev. **76**, 873 (1949).

Equivalence of Protons and Neutrons in Nuclei*

WILLIAM D. HARKINS
University of Chicago, Chicago, Illinois
April 3, 1950

IN 1917 it was found[1] that in the meteorites and on earth the elements of even atomic (proton) number are very much more abundant than those of odd number. This became known as Harkins' rule. In 1922 it was found that this rule applies as well to neutrons as to protons. In general, elements of even number P_e are, in the universe, very much more abundant than those of adjacent odd number $P_e \pm 1$, and those of even number N_e of neutrons are very much more abundant than those of odd number $N_e \pm 1$. If on one chart the abundance A is plotted against the proton number and on another against the neutron number, the two charts have an almost identical appearance to a casual observer. The even-odd relation is the same on both, and the general regions of high and low abundance are similar; e.g., high at 8 to 18 and very low at 21 for either N or P. In this sense protons and neutrons may be said to be equivalent.

These relations are made much more prominent by use of the recent data of Harrison Brown.

A remarkable relation is exhibited by the most recent data, which indicate that in the universe 99 percent of all complex nuclei exhibit equality of the numbers of protons and neutrons ($N=P$). Only in about one percent is N greater than P.

In only one relatively abundant element, iron, is N not equal to P.

If helium, the most abundant species in which $N=P$, is omitted, even then 95 percent of the other species exhibit equality of N and P.

In nearly all complex nuclei both the number of protons (P) and of neutrons (N) is even (Class I $E_p \cdot E_n$). From $P=8$ to 29, or for 22 elements (oxygen to cobalt) consider 22 million nuclei, an average of one million per element of the $E \cdot E$ class (Fig. 1).

Relative Number of Nuclei per Element

Elements 8 to 29			
$E \cdot E$	$E \cdot O$	$O \cdot E$	$O \cdot O$
1,000,000	6800	6400	0
Elements 30 to 92			
28	2.8	1.3	0

FIG. 1. If helium ($P=2$) is included, the even-even ($E \cdot E$) class rises to 70 million, owing to the great abundance of this element in the universe.

The number of Class II $E_p O_n$ species becomes 6800 and of Class III $O_p E_n$, 6400. These two numbers are equal within the limits of accuracy of the data. Thus in the production of these nuclei in the universe it has been a matter of indifference as to whether the protons or the neutrons are even.

Between these limits of $P=8$ to 20, the number of stable nuclei of Class IV, $O_p \cdot O_n$ is zero. No nuclei are stable if the number of protons and of neutrons is odd and larger than 7.

Thus 7 is a special number, which as an odd number exhibits a relation similar to the "magic" number 20, since 7 is the highest odd number for which stability is exhibited with $N_p=N_n$ and 20 is the highest even number for which this is true.

The newer data exhibit very plainly the relatively great rarity of elements 30 to 92 since for Class I, $E \cdot E$, 1,000,000 is reduced to 28, for Class II, $E \cdot O$, 6800 is reduced to 2.8 and for Class III 6400 to 1.3. When the relatively low accuracy for heavier nuclei is considered, 1.3 is not essentially different from 2.8.

Nuclear Shells. The numbers which according to Feenberg, Maria Mayer, and Nordheim represent the closing of nuclear shells (2, 8, (10), 20, (28), 50, and 82) are the same for neutrons and protons, and thus represent entire equivalence between the two types of particles. The only exception is 126 for neutrons, which, due to their charge, is too high for protons.

Departures from equivalence, as is well known, are due largely to the charge on the proton.

* From a paper on special numbers, presented as an introduction to the symposium on nuclear shells, New York Meeting of the American Physical Society (February 4, 1950).
[1] W. D. Harkins, J. Am. Chem. Soc. **39**, 856 (1917).

Pressure behind a Shock Wave Diffracted through a Small Angle*

C. H. FLETCHER, D. K. WEIMER, AND W. BLEAKNEY
Palmer Physical Laboratory, Princeton University, Princeton, New Jersey
March 10, 1950

THE problem of the reflection of a shock wave on a rigid wall has been reviewed by Bleakney and Taub,[1] and brief mention was made by them of the theory of Bargmann[2] for nearly glancing incidence together with some experimental verification of this phenomenon. Recently Lighthill[3] has reported on a method for calculating the pressures on a wall when a shock wave travels along the wall and passes by a convex corner. Both of these treatments require that the deflection at the corner be small, and both should apply to either positive or negative angles.

As an extension of the work reported by the present authors,[4] an experimental test has been performed to compare with these theoretical treatments. The shock wave was produced in the shock tube described by Bleakney, Weimer, and Fletcher[5] and the densities in the diffracted flow were measured interferometrically. The shock waves used were of strength $p_2/p_1=2$, corresponding to Fig. 2 of Lighthill's paper. The shock waves were diffracted at a convex angle of 0.1 radian ($\epsilon=+0.1$) or were reflected at a concave angle of the same magnitude ($\epsilon=-0.1$).

In the case of the concave angle, the density of the gas along the wall was measured on an interferogram with parallel fringes as described in reference 5. In the case of the convex angle, the measurements were made along the wave normal through the corner. This was done to avoid the boundary effects along the wall and should introduce a negligible error. Pressures were obtained from the densities by assuming the behavior of the gas behind the original shock to be isentropic. The results are pre-

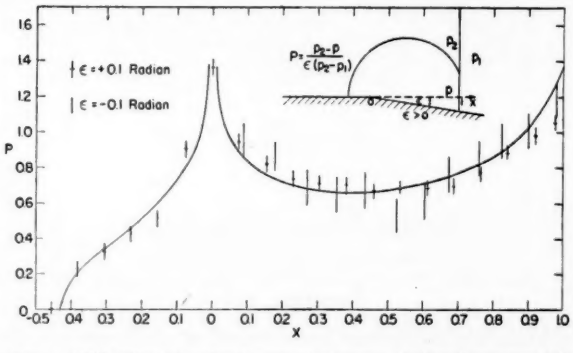

FIG. 1. Diffraction of a shock wave at a corner. Reduced pressure defect along the wall as a function of position along the wall. $p_2/p_1=2$, $\epsilon=\pm 0.1$ radian. The vertical length of the experimental points indicates approximately the reliability of the measurements.

sented in Fig. 1. The abscissa represents distance along the normal to the original shock with the origin at the corner, the scale being so arranged that the original shock has advanced a unit distance. The ordinate is the reduced pressure defect as determined by Lighthill, $P=(p_2-p)/\epsilon(p_2-p_1)$, where p is the pressure along the wall, p_1 and p_2 are respectively the pressures ahead of and behind the original shock and ϵ is the angle of the bend in the wall. The sign of the quantity P is observed to be positive for both concave and convex corners. The theoretical treatment shows a logarithmic infinity in the pressure at the corner. This, of course, would not be obtained experimentally, but a relative maximum in the pressure does exist there.

* This research was supported by the ONR of the Navy Department.
[1] W. Bleakney and A. H. Taub, Rev. Mod. Phys. **21**, 584 (1949).
[2] V. Bargmann, "On nearly glancing reflection of shocks," AMP report 108.2 R National Defense Research Committee (March, 1945).
[3] M. J. Lighthill, Proc. Roy. Soc. **A198**, 454 (1949).
[4] Bleakney, Fletcher, and Weimer, Phys. Rev. **76**, 323 (1949).
[5] Bleakney, Weimer, and Fletcher, Rev. Sci. Inst. **20**, 807 (1949).

Superconductivity of Lead

H. A. Boorse, D. B. Cook, and M. W. Zemansky
Columbia University, New York, New York*
April 11, 1950

NUMEROUS determinations of the zero-field transition temperature of lead have been made. A summary of these is given in Table I. All of these observations, except that of Daunt, were made by the direct measurement of electrical resistance. Daunt's method involved the shielding effect of persistent currents in a hollow cylinder.

In our work on columbium to be described in a forthcoming paper, an a.c. induction method[1] was used for the measurement of superconducting transitions. The superconductor was mounted as a cylindrical core of a coil which functioned as the secondary of a mutual inductance. The primary coil was actuated by an oscillator which provided a maximum a.c. field within the secondary of 1.5 oersteds at a frequency of 1000 cycles per second. The secondary e.m.f. which was dependent for its magnitude on the permeability of the core, was amplified, rectified, and observed on a recording potentiometer. During the application of this method to the study of columbium it appeared that a further check on the zero-field transition temperature of lead would be worth while, especially if agreement between results for very pure samples could be obtained using this method. Such a result would help in establishing the lead transition temperature as a reasonably reproducible reference point in the region between 4° and 10°K.

The lead used in the present investigation was made available to us through the courtesy of Dr. C. H. Hack and Mr. E. J. Dunn, Jr., of the National Lead Company. It had been analyzed as follows (No. A-586A):

Ag 0.00065%	Zn 0.0001%	As, Cd, Co, Ni, Sn: no perceptible amounts.
Cu 0.00022%	Bi 0.0002%	
Fe 0.00018%	Mn 0.00005%	

The samples were in the form of cylinders 1.5 mm in diameter and 5 cm long, attached by a copper rod to the desorption cryostat described in the forthcoming report on the superconductivity of columbium. Temperatures were determined to the nearest 0.01°K with the aid of a helium gas thermometer which was filled to 1 atmos. at 20.4°K. Corrections were applied for gas imperfection, room temperature volume, and temperature gradients in the capillary. The hydrogen triple point was checked within 0.02°K.

The collected results of the transition temperatures observed in the present experiments are given in Table II. The observations were made on two samples in a series of experiments in which the gas thermometer was refilled at the beginning of each run, usually to 1 atmos. but in one case to ½ atmos. to check the consistency of the thermometer corrections. A typical transition is shown in Fig. 1. Neither specimen showed hysteresis, but since thermometer response was more immediate on warming cycles, the data shown were taken on transitions proceeding from the superconducting to the normal state. Changes of oscillator frequency from 500 to 2000 cycles/sec. and of amplitude over the full range available did not affect the transitions.

As a further check on the magnetic purity of the material, observations were made of the $H-T$ curve in the vicinity of the zero-field transition temperature both in transverse and in longi-

TABLE I. Transition temperature of lead.

Investigators	Year	Source, purity	Temperature °K
Onnes, Tuyn[a]	1922	Kahlbaum: 99.99%	7.22; 7.26
de Haas, de Boer, van den Berg[b]	1934	Kahlbaum: 99.99%	7.19₈; 7.20₆
Daunt[c]	1937	Hilger: 99.999%	7.22
Bruksch, Ziegler[d]	1942	(evaporated films)	7.23 ±0.03
Bruksch, Ziegler, Hickman[e]	1942	Baker (thin wires)	7.20 ±0.01
van Itterbeck, de Greve, Lambeir, Celis[f]	1949	(sputtered films)	7.20
		Average:	7.216°

[a] K. Onnes and W. Tuyn, Leiden Comm. No. 160b (1922).
[b] de Haas, de Boer, and van den Berg, Leiden Comm. No. 233b.
[c] J. G. Daunt, Phil. Mag. **28**, 24 (1939).
[d] W. F. Bruksch, Jr., and W. T. Ziegler, Phys. Rev. **62**, 348 (1942).
[e] Bruksch, Ziegler, and Hickman, Phys. Rev. **62**, 354 (1942).
[f] van Itterbeck, de Greve, Lambeir, and Celis, Physica **15**, 962 (1949).

TABLE II. Zero-field transition temperatures of lead by a.c. induction method.

Transition temperature, °K	No. of separate observations
7.26	1
7.25	1
7.24	5
7.22	5
7.21	1
7.20	2
7.17	1
Average: 7.224°K	
Mean deviation: 0.02°K	

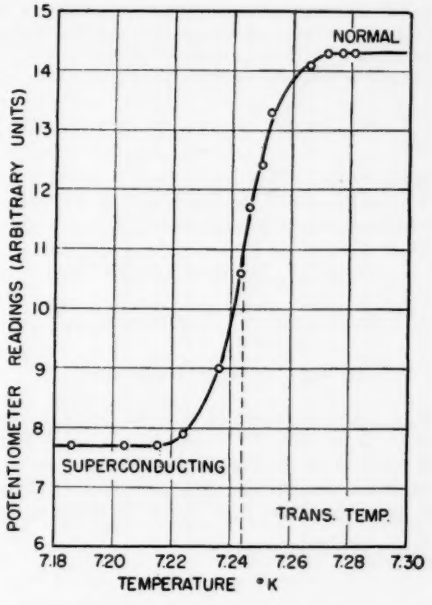

FIG. 1. Typical zero-field transition curve for Pb.

tudinal fields. The two types of transitions agreed with published values, the longitudinal field transitions showing the shape reported by Shoenberg.[2]

* Assisted by the ONR.
[1] Webber, Reynolds, and McGuire, Phys. Rev. **76**, 293 (1949).
[2] D. Shoenberg, Proc. Camb. Phil. Soc. **33**, 577 (1937).

A Lower Bound on the Range of the Triplet Neutron-Proton Interaction*

LESLIE L. FOLDY
Case Institute of Technology, Cleveland, Ohio
April 20, 1950

IT has been pointed out by Schwinger[1] that the existence of a quadrupole electric moment for the deuteron requires that the triplet neutron-proton interaction be of finite range. On the basis of approximate expressions for the quadrupole moment and the percentage of D-state in the deuteron, Schwinger was able to derive an approximate relationship between the range and these two quantities and so make an estimate of a lower bound for the range assuming the experimental value for the quadrupole moment and that the percentage of D-state was less than 5 percent. Recently, Broyles and Kivel[2] have obtained a *rigorous* lower bound for the triplet range from the experimental quadrupole moment by a very simple argument. However, the value obtained, 1.1×10^{-13} cm, is very much lower than that estimated by Schwinger who found for the lower bound 2.5×10^{-13} cm. A large part of this difference can well be attributed to the rather severe, but justifiable, restriction placed by Schwinger on the percentage of D-state, which was not imposed in the calculation of Broyles and Kivel.

Since the experimentally determined magnetic moment of the deuteron makes it unlikely[3] that the percentage of D-state in the deuteron much exceeds about 5 percent, it is of interest to determine what influence this restriction has on the rigorous calculation of Broyles and Kivel. The procedure, following Broyles and Kivel, consists in maximizing the expression for the quadrupole moment with respect to the S- and D-wave functions, assuming that these have their asymptotic form outside of the interaction range, but now with the restriction that the percentage of D-state has a fixed value. Using Lagrange's method of undetermined multipliers, the procedure is essentially identical with that of Broyles and Kivel. The optimum choice of functions is again found to be S- and D-functions which vanish inside the interaction range, as is to be expected. The maximum value of the quadrupole moment is found to be given by the equation

$$Q_{\max}=\frac{1}{80\alpha^2}\{\beta'(2\alpha r_0)[\delta(1-\delta)/\gamma(2\alpha r_0)]^{\frac{1}{2}}-\delta\gamma'(2\alpha r_0)/\gamma(2\alpha r_0)\},$$

where r_0 is the range of the interaction, $\alpha=[ME_B/\hbar^2]^{\frac{1}{2}}$ where E_B is the binding energy of the deuteron, δ is the fraction of D-state, and the functions $\gamma(x)$, $\beta'(x)$, and $\gamma'(x)$ are defined by

$$\gamma(x)=e^x\int_x^\infty[1+6/x+12/x^2]^2e^{-x}dx$$

$$\beta'(x)=8^{\frac{1}{2}}e^x\int_x^\infty[x^3+6x+12]e^{-x}dx$$

$$\gamma'(x)=e^x\int_x^\infty[x+6+12/x]^2e^{-x}dx.$$

Equating $Q_{\max}$ to the experimental value for the deuteron quadrupole moment,[4] $Q_{\exp}=2.77\times10^{-27}$ cm^2, yields a lower limit to the range of interaction, r_0. In Fig. 1, the full curve shows the dependence of this lower limit on the percentage of D-state. The dotted line gives the lower limit found by Broyles and Kivel

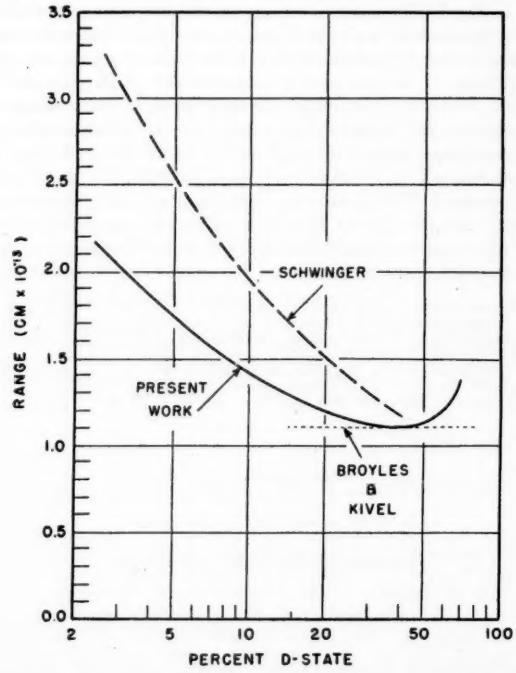

FIG. 1. Relations between range of triplet neutron-proton interaction and percentage of D-state in deuteron. *Full curve:* lower limit on range from present work; *dotted curve:* lower limit on range obtained by Broyles and Kivel; *dashed curve:* approximate relation between range and percentage of D-state obtained by Schwinger.

which is seen to correspond to about 35 percent D-state. The dashed curve represents the approximate relation between range and D-state percentage found by Schwinger. (The fact that this curve falls below our rigorous lower limit for more than 50 percent D-state shows that Schwinger's approximations break down for a high D-state percentage.) If the percentage of D-state in the deuteron is less than 5 percent, we may conclude that the triplet range is certainly greater than 1.75×10^{-13} cm. This is still considerably below Schwinger's approximate value.

We may also note that our curve becomes asymptotic to a vertical line at $\delta=8/9$ (89 percent D-state). For higher D-state percentage, the quadrupole moment is necessarily negative.

For a potential which cuts off sharply at a given range (such as a square well), the range for which the lower bound is obtained above is well defined. For a well with a "tail" (such as the Yukawa or exponential wells) the range referred to above is that at which the S- and D-functions take their asymptotic forms. This requires that the potential at the above range must be small in absolute value compared with the absolute value of the deuteron binding energy. It should be noted that it is not assumed that the central and tensor interactions have the same range; the range referred to is simply that of the longest range potential.

* This work has been supported by the AEC and by a Grant-in-Aid from the Research Society of America of the Society of the Sigma Xi.
[1] J. Schwinger, Phys. Rev. **60**, 164A (1941).
[2] A. A. Broyles and B. Kivel, Phys. Rev. **77**, 839 (1950).
[3] The uncertainty as to the additivity of proton and neutron moments in the deuteron and relativistic corrections to the deuteron moment do not at present allow one to fix definitely the D-state percentage from the deuteron magnetic moment. These corrections would not however be likely to lead to a value much greater than 5 percent. See, H. Margenau, Phys. Rev. **57**, 383 (1940); P. Caldirola, Phys. Rev. **69**, 608 (1946); G. Breit, Phys. Rev. **71**, 400 (1947); R. G. Sachs, Phys. Rev. **72**, 91 (1947); H. Primakoff, Phys. Rev. **72**, 118 (1947); F. Villars, Helv. Phys. Acta **20**, 476 (1947).
[4] A. Nordsieck, Phys. Rev. **58**, 310 (1940); Kellog, Rabi, Ramsey, and Zacharias, Phys. Rev. **57**, 677 (1940); E. Ishiguro, J. Phys. Soc. Japan **3**, 133 (1948); G. F. Newell, Phys. Rev. **77**, 141 (1950).

Proceedings of the American Physical Society

MINUTES OF THE MEETING AT OAK RIDGE, MARCH 16–18, 1950

THE 298th meeting of the American Physical Society was held at Oak Ridge, Tennessee, on Thursday, Friday, and the morning of Saturday, March 16, 17, and 18, 1950. This, the first meeting which we have held at Oak Ridge and one of the few which have so far occurred in the Southeast, was one of the pleasantest and most congenial of recent years: it exhibited in fullest measure the advantages of the meetings of bygone days, with a moderate number of sessions (few simultaneous with others) and ample time and opportunity for conversation interspersed among them. Unique features of the meeting included sessions in a movie theater (and very comfortable it was!); a smoker held on Thursday evening at the expense of Carbide Chemical Divisions (it proved an admirable scheme for bringing our members together in a state of relaxation); and the opening and staffing of a residence hall for the sole purpose of serving our members. We must praise the Local Committee particularly for this last achievement, and in general for the competence and kindness with which they served the Society in all the usual ways and in others which are not usual—for instance, in arranging for our members to be conveyed from and to railway stations and airports. The Chairman of this Committee was E. J. Murphy; its other members, Joe Bair, L. E. Burkhart, Dixon Callihan, Rex Fluharty, W. M. Good, Hugh Henry, J. R. McNally, and John Roberson. A cocktail party and banquet were held on Friday evening, affording our members the opportunity of hearing scientific achievements of the Oak Ridge community expounded by A. M. Weinberg under the title "Physics in Current Atomic-Energy Development at Oak Ridge." The attendance at this meeting was about three hundred.

Our Division of Solid-State Physics figured largely in the programme, this meeting comprising its own 1950 Annual Meeting. It arranged a Symposium extending over three half-days; the names of the speakers and the titles of their speeches are reprinted hereinafter, except for one paper of which the author was prevented by illness from coming. The balance was partially redressed by a Symposium on diverse aspects of beta-emission, particularly stressing nuclear disintegrations of extremely short and extremely long half-lives; A. M. Weinberg and M. Goldhaber contributed to the design of this Symposium. There were fifty-six ten-minute papers, about two-thirds of which were in the field of solid-state physics.

The Council met on Saturday and elected to Membership ninety-seven candidates and to Fellowship three; their names are appended.

The Society has lost through death A. J. Dempster, thirty-first President of the American Physical Society, and A. M. Nicolson.

Elected to Fellowship: R. M. Bowie, B. T. Feld, and L. C. Yuan.

Elected to Membership: Bernard M. Abraham, Leonilda Altman, Richard L. Arnowitt, Joseph Felix Aschner, Peter L. Auer, Joseph P. Baker, Georges J. Bene, George B. Benedek, Ami Emanuel Berkowitz, William M. Deuesch, Dale S. Bowman, Rafael H. Brand, Alexander Bratenahl, Allen V. Buskirk, Tsu-shen Chang, *Niels Gunnar Christensen, Joseph F. Clayton, William W. Clendenin, David Cohen, Francis T. Cole, Albert John Coleman, James G. Cottingham, James H. Crawford, Jr., E. K. Darby, Donald Holm Davis, James A. DeJuren, Paul S. Delaup, Pierre M. Denis, Arthur James Dyer, August A. Ebel, Jerome Eisenbach, William W. Ennis, Richard C. Exterman, Chang-Yun Fan, Milton D. Fisher, Melvin D. Fleisher, Stephen H. Forbes, Martyn H. Foss, Naz Frazzini, Robert W. Fritts, Morton Fuchs, John D. Gabbe, Elaine Gilinson, Frank W. Glaser, Robert C. Good, Jr., Lawrence Gould, Walter Grattidge, Paul Gray, M. R. Gustavson, William P. Heising, Joseph Mallam Hendrie, George W. Hewitt, John W. Hicks, Jr., Thomas E. Hicks, Leon Hillman, Louis V. Holroyd, Alfred Holzer, John W. Horton, Henry Palmer Hotz, Bruce T. Hulse, Edwin L. Iloff, Edward T. Jablonski, Francis J. Jankowski, Glenn H. Jenks, Frank F. Johnson, Richard T. Jones, George Kachickas, Henry Kahn, John V. Kane, David G. Karraker, Otto J. Karst, Jr., Gerald Katz, John Katzman, John W. Keller, Jr., B. H. Ketelle, Seishi Kikuchi, William C. Knopf, Jr., James H. Kraakevik, William E. Kreger, Edward Kuhn, Robert S. Landauer, Jr., Edward A. Lewis, Frank J. Lynch, John W. MacArthur, Jr., Philip A. Macklin, John R. Madigan, Charles A. McClure, James E. McKeown, Gershon Meckler, A. Hamid Medjid, Dickerson P. Miles, Maurice M. Miller, Anthony J. Mony, Robert H. Nelson, Leland K. Neher, Marcel Neve de Mevergnies, Raymond H. Opperman, James D. O'Reilly, Edward Ornstein, William Pavluk, John R. Penning, Jr., Cornelius J. Pickrell, George F. Pieper, Jr., Paul H. Pitkanen, Fred T. Porter, John O. Rasmussen, Jr., George W. Rathjens, Jr., Paul L. Roggenkamp, Arthur Z. Rosen, Bernard Rosenbaum, Adolph H. Rosenthal, Leonard Rudlin, Paul N. Russell, Marvin Schnee, Wendell B. Sell, James M. Sharp, Yoshio Shimamoto, William O. Solano, Richard S. Stone, Harry Suhl, Robert J. Taylor, Walter E. Thirring, Thomas L. Thourson, George L. Trigg, Robert Davison Turner, Arthur Uhlir, Jr., Jean Vignal, Margaret Ann Waggoner, Harold E. Way, Bernard Weinstock, H. Robert Westerman, George W. Wheeler, Robert Neal Whitehurst, Frank C. Whitmore, G. W. Williams, Ernst H. Winkler, Eva M. Winkler, Louis Witten, Artemus W. Wren, Jr., William R. Wright, James R. Young, *Herman C. Zentz, Jr., James P. Zietlow, and James E. Zimmerman.

KARL K. DARROW, *Secretary*
American Physical Society
Columbia University
New York 27, New York

* One sponsor only.

Invited Papers of the Division of Solid-State Physics

Theory of antiferromagnetism. P. W. ANDERSON, *Bell Telephone Laboratories.*

Nuclear relaxation in solids. N. BLOEMBERGEN, *Harvard University.*

Research on ferroelectricity. A. VON HIPPEL, *M.I.T.*

Nucleon bombardment of semiconductors. K. LARK-HOROVITZ, *Purdue University.*

Statistics of luminescent crystal counters. F. SEITZ, *University of Illinois.*

Neutron diffraction studies of ferromagnetic and antiferromagnetic substances. C. G. SHULL, *Oak Ridge National Laboratory.*

Theory of ferroelectricity. J. C. SLATER, *M.I.T.*

Recent work on diffusion. R. SMOLUCHOWSKI, *Carnegie Institute of Technology.*

Order and disorder in alloys. B. E. WARREN, *M.I.T.*

Recent experiments on ferromagnetic domains and domain walls. H. J. WILLIAMS, *Bell Telephone Laboratories.*

Ring diffusion in metals. C. ZENER, *University of Chicago.*

Symposium on Diverse Aspects of Beta-Emission

Isomeric transitions in nuclei. P. AXEL, *University of Illinois.*

Measurement of forbidden beta-spectra with the scintillation spectrometer. P. R. BELL, *Oak Ridge National Laboratory.*

Double beta-decay. E. L. FIREMAN, *Princeton University.*

Theory of forbidden beta-ray transitions. E. J. KONOPINSKI, *Indiana University.*

Measurement of short-lived isomeric states. F. K. MCGOWAN, *Oak Ridge National Laboratory*, AND S. DE BENEDETTI, *Carnegie Institute of Technology.*

Solid-State Physics, Largely Metallurgical

A1. Low Temperature Oxidation of Copper. T. N. RHODIN, JR., *University of Chicago* (*Introduced by A. W. Lawson*).—The formation of thin stable oxide films on small single crystal plates of copper has been studied in the temperature range 78°K to 300°K. The surface areas were determined from micro-adsorption isotherms of nitrogen and argon at 78.1°K and 89.2°K. The rate isotherms were followed with a quartz vacuum microbalance. Oxidation was extremely rapid at first but after a few minutes dropped to negligible values, a stable film being formed with a limiting thickness from 5A to 50A with an error of 3 percent. An explanation of this behavior was first given by N. F. Mott (1947) and depends on the hypothesis that a strong field is set up in the oxide film which enables the metal ions to move through it without much help from temperature. A modified oxidation rate expression based on that hypothesis was found to be valid in this case: $dx/dt = A \exp(-W/kT) \exp(V/xT)$, where x = film thickness, t = time, V = contact potential, T = temperature, W = activation energy, A = proportionality constant. The energy of activation for oxidation (1.1 ev) and the contact potential (0.8 v) between copper and cuprous oxide were calculated from the experimentally determined oxidation rates and the values of the effective limiting oxide thickness. (Army Air Force Contract.)

A2. Growth of Alkali Halides onto Single Crystal Substrates. L. G. SCHULZ, *University of Chicago.*—During a study of the mechanism of crystal growth from the vapor state eight different alkali halides were deposited by evaporation in a vacuum onto cleavage surfaces of single crystal substrates of LiF, NaCl, KCl, and KBr. Using electron diffraction it was found that for all combinations of substances examined the crystals in a deposit below 100A in thickness were oriented with their axes parallel to those of the substrate. This was true even for substances having widely different lattice constants, a_0. For example, KBr (a_0 equal to 6.58A) was found to orient on LiF (a_0 equal to 4.02A). With the technique employed it was possible to examine deposits ranging in average thickness from a few angstroms up to several thousand angstroms. When the atomic mismatch at the interface exceeded about 20 percent the following sequence of orientations was observed: below a thickness of 100A, complete orientation; in the range 100A to 300A, [100] fiber structure; and above 300A, a continuous change toward random orientation with increased thickness. When the mismatch was less than 20 percent there was complete orientation below about 200A; above that thickness there was a gradual change to random structure.

A3. Magnetostriction of Permanent Magnet Alloys. E. A. NESBITT, *Bell Telephone Laboratories.*—In order to obtain a better understanding of the mechanism of coercive force in modern permanent magnets, magnetostriction measurements have been made on various alloys having coercive forces from 50 to 600 oersteds. The results can be summarized by discussing two types of alloys. First are the older carbon-hardening permanent magnets and for these alloys high coercive force and high magnetostriction occur together. Second are the newer carbon-free permanent magnets, and for these alloys high coercive force does not occur with high magnetostriction. In fact for the Mishima alloys having compositions near 29 percent nickel, 12.5 percent aluminum and 58.5 percent iron and cooled at the rate of 3°C per second (coercive force, 400 oersteds) the magnetostriction actually passes through zero. This is contrary to the classical strain theory of coercive force which states that the latter is proportional to the product of the magnetostriction and internal stress. To explain the mechanism of coercive force for these alloys it is necessary to resort to more recent theories.

A4. Statistical Theory of Magnetic Saturation in Alloys. R. SMOLUCHOWSKI, *Carnegie Institute of Technology.*—It has been previously shown* that various magnetic properties in a binary alloy depend upon the state of order. The theory indicates that the local electron concentration rather than the average electron concentration plays the main role. This paper is concerned with the statistical interpretation of the experimental saturation magnetization in several alloys. The theory is based on the calculation of the probability of various fluctuations of the electron density by taking into account the nearest and the second nearest neighbors in a body-centered lattice. These probabilities together with the band theory interpretation of the saturation moments allow to deduce the relation between local electronic density and the saturation moments. The agreement with experiment is satisfactory.

* J. E. Goldman and R. Smoluchowski, Phys. Rev. **75**, 140, 310 (1949).

A5. A Pulse-Annealing Method for the Study of Changes in Physical Properties Resulting from Heat Treatment.* N. S. RASOR AND W. E. PARKINS, *North American Aviation, Inc.*—An apparatus has been designed for the precise measurement of thermal conductivity, electrical resistivity, and thermoelectric power of small specimens near room temperature and in a vacuum. These specimens are then heated in place for short periods to specified temperatures. After cooling, the changes in these physical properties resulting from the annealing pulse are determined. The apparatus and method are useful in the comparison of changes in physical properties which occur simultaneously during a particular heat treatment. Rates of recrystallization, phase change, or chemical reaction occurring within the specimen can be determined. Measurements are made on a specimen volume of 0.008 cc. The present method is limited to materials which can be heated directly by

an electric current. It has been found informative to determine the property changes resulting from single pulses to successively higher temperatures. Measurements have been made utilizing one minute pulses and 25°C temperature increments to as high as 2000°C. Special features of the design reduce heat losses sufficiently to permit measurement of very small thermal conductivities.

* Research carried out under contract with the AEC.

A6. The Crystallographic Mechanism of the Martensite Transformation in Iron-Carbon Alloys. J. S. BOWLES, *University of Chicago.*—Determination of the crystallographic mechanism of the martensite transformation in iron-carbon alloys involves the determination of: (1) the total atomic displacements; (2) the paths taken by the atoms during these displacements. Further confirmation of Jaswon and Wheeler's[1] minimum displacements hypothesis is given by demonstrating that these displacements produce the lattice-plane transformations determined by Greninger and Troiano.[2] These displacements cannot occur as a simple homogeneous distortion since this would not be consistent with the observed relief effects produced by the transformation. Geometrical consistency can be achieved by ascribing paths to the atoms during these displacements. Certain assumptions are made which permit these paths to be determined from a stereographic analysis of the Kurdjumow-Sachs orientation relationship, and the conclusion is reached that each atom moves first in the austenite twinning direction and then in the martensite twinning direction. The proposed mechanism is consistent with all the geometrical features of the transformation; good agreement is found between the predicted and observed angles through which polished surfaces are tilted by the production of martensite plates.

[1] M. A. Jaswon and J. H. Wheeler, Acta Cryst. 1, 216 (1948).
[2] A. B. Greninger and A. R. Troiano, Trans. A.I.M.E. 185, 590 (1949).

A7. Transformation Characteristics of a Lithium-Magnesium Alloy. C. S. BARRETT AND D. F. CLIFTON, *University of Chicago.*—Further investigation by x-ray spectrometry has disclosed new details of the diffusionless transformation in Li-Mg alloys.[1] Studies in an alloy containing 12.4 atom percent magnesium have shown that the temperature at which the transformation from cubic to hexagonal starts on cooling (Ms) is independent of cooling rate between about 1° and 30° per min. However, Ms is altered by annealing at different temperatures prior to cooling, even when this annealing does not alter the grain size or cause recrystallization. The transformation on heating, as on cooling, proceeds only with changing temperature; starting with some cubic phase present, the transformation at first proceeds slowly with changing temperature; then, at a temperature above Ms, the rate becomes quite rapid but slows again near completion. The curve of hexagonal to cubic transformation shifts to higher temperatures when the alloy is carried to lower temperatures before heating. If heating is stopped while some hexagonal remains and is followed by cooling, the formation of hexagonal begins at a temperature Ms′ which lies 0° to about 18° above the normal Ms; Ms′ increases with increasing amounts of the hexagonal phase at the beginning of the cooling.

[1] C. S. Barrett and O. R. Trautz, Trans. A.I.M.E. 175, 579 (1948).

A8. The Hydrogen Permeability of Zirconium.* R. B. BERNSTEIN AND DANIEL CUBICCIOTTI, *Illinois Institute of Technology.*—The rate of permeation of hydrogen through ductile zirconium sheet was measured over the temperature range 400–900°C. Fore-pressures up to 0.5 atmos. were applied to the specimens, which were disks of 0.71 cm² exposed area, 0.13 mm thick. The back-pressure was maintained near zero. The permeabilities ranged from 10^{-5} to 10^{-1}-cc atmos. (NTP)/cm² sec. The rate of diffusion was found to decrease with time in an approximately exponential manner, with a "half-time" of about 1.5 hr. Considerable variation in the permeability of successive samples was observed. The differences were attributed in part to differences in surface contamination. At constant temperature the flow rate was found to be proportional to the square-root of the hydrogen pressure, in agreement with similar results reported for other hydrogen-metal systems. The apparent energy of activation for the permeation process, estimated from the data, appeared higher than anticipated from existing data on other metals.

* This research was carried out under the sponsorship of the ONR.

A9. Diffusion of *C* in α-Iron. CHARLES WERT, *University of Chicago.*—The diffusion coefficient, D, of C in α-iron has been measured in the neighborhood of room temperature by means of relaxation phenomena. Together with data of Stanley,[1] these measurements extend over a range of temperature from −35°C to 800°C. The range of D is from 10^{-20} cm²/sec. to 2×10^{-6} cm²/sec. The data are found to fit the equation

$$D=D_0\exp(-\Delta H/RT), \qquad (1)$$

where $D_0=0.02$ cm²/sec. and $H=20{,}100$ cal./mole. By use of a classical statistical mechanical treatment of the problem of interstitial diffusion, an expression of type shown in Eq. (1) is derived for D. Contrary to some other treatments of this problem, the present investigation shows D_0 to be independent of the absolute temperature. The present measurements tend to confirm this, but the evidence is not yet conclusive.

[1] J. Stanley, J. Inst. Metals (October, 1949).

Nuclear Physics

C1. The Isotopic Analysis of Nitrogen by Means of a Microwave Mass Spectrograph. A. L SOUTHERN, H. W. MORGAN, G. W. KEILHOLTZ AND W. V. SMITH, *Union Carbide.*—Microwave techniques have been applied to the isotopic analysis of nitrogen 14 and nitrogen 15 in ammonia. The calibrations required and precision obtained are described for the range 0.38 to 4.3 percent nitrogen 15. The microwave spectrograph is discussed in relation to the use of stable isotopes as tracer materials.

C2. Two Group Equations for the Diffusion of Neutrons in a Multiplying Medium.* E. RICHARD COHEN AND M. A. GREENFIELD, *North American Aviation, Inc.*—The diffusion of neutrons in a multiplying medium are usually approximated by replacing the slowing down process by a monoenergetic group of neutrons in which the slowing down is a mechanism which couples this group with the thermal group.[1] If one starts with the more exact "age" equation and integrates over the energy, the fast group can be defined in a way which makes maximum use of the information available. Both fission and non-fission capture of neutrons in the slowing down range can be incorporated into the theory. The net result is to give simultaneous coupled differential equations for the thermal neutron flux, nv_{th}, and the mean slowing down flux per unit energy range, nv_f. These equations are formally the same as in the usual theory, but with a redefinition of constants.

* Research carried out under contract with the AEC.
[1] H. Soodak and E. C. Campbell, "Elementary pile theory," AECD 2201, p. 35.

C3. Neutron Energy Spectra. B. L COHEN, C. E. FALK, AND S. K. KAO, *Carnegie Institute of Technology.*—Measurements were made of the energy distribution of neutrons obtained by irradiating various thick targets with 15-Mev deuterons from the University of Pittsburgh cyclotron. The low energy portion (2–12 Mev) was obtained by observing the recoil protons in photographic emulsions; the high energy

spectrum (8–18 Mev) was determined from proton recoils in a triple coincidence-anticoincidence proportional counter telescope with aluminum absorbers. The combination of these two methods gives good statistical accuracy without large corrections over the entire energy range, and mutual check in the overlapping region. All spectra could be approximated by

$$I(E)=CEe^{-E/T} \quad (1)$$

except at the extremities. As an example, for beryllium, $T=2.5$ Mev. It will be shown that (1) gives good agreement with the predictions of deuteron stripping theories over most of the range, and differs considerably from those of compound nucleus evaporation. Some deviations from (1) in the low energy region will also be discussed. This work was carried out with the assistance of ONR.

C4. Studies of Neutron Diffraction by Some Nuclei with Zero Spin. W. C. KOEHLER, E. O. WOLLAN, AND C. G. SHULL, *Oak Ridge National Laboratory.*—The accurate determination of the absolute intensity of the reflections in powder patterns presented difficulties in x-ray diffraction studies and it also presents some difficulties in corresponding neutron studies. It has been found convenient in the neutron case to normalize the observed counting rates in the patterns of samples of unknown cross section to the counting rates given by a sample for which the coherent cross section has been directly determined by transmission measurements. This can conveniently be done with powdered samples containing elements with a single isotope with zero spin and hence for which there is no isotopic or spin dependent diffuse scattering. The transmission cross section and the intensities of the powder patterns are being studied for a number of samples satisfying the above conditions and the consistency of the results obtained will be a factor in determining the over-all accuracy of coherent cross-section measurements by the crystal powder diffraction technique. Results with the oxides of Th and of the separated isotopes of Ca and Ni will be reported.

C5. Nuclear Radiations in Well Logging. CLARK GOODMAN, CHARLES W. TITTLE,* AND HENRY FAUL,† *Massachusetts Institute of Technology.*—The penetration of solid materials by neutrons and gamma-rays has been applied as an empirical index of subsurface structure and composition surrounding cased drill holes. Counters and ionization chambers have been used to detect gamma-rays from the formations. Similar probes detect gamma-rays emitted when neutrons from a portable source are captured in surrounding materials. Studies are being made under conditions that simulate field operations. Although this work is still in the initial stages, certain conclusions are appearing: (1) The possibilities and limitations of present logging techniques can be established; (2) by improvements in present operating procedures increased knowledge of subsurface conditions should result; (3) neutron flux measurements should provide additional information of practical value; (4) such measurements, when made simultaneously at several points along the axis of the drill hole in the vicinity of a porous formation, can, under favorable conditions, distinguish between oil (and/or fresh water) and salt water.

* Gulf Fellow in Physics 1944–1948, present address: North Texas State College, Denton, Texas.
† Present address: U. S. Geological Survey, Washington, D. C.

C6. Measurement of Fast Neutron Dosage to Tissue with a Proportional Counter. G. S. HURST, *Oak Ridge National Laboratory* (*Introduced by K. Z. Morgan*).—Calculations indicate that a proportional counter can be so designed that the response to fast neutrons gives an approximate measure of the radiation dosage that the neutrons would give to tissue. This implies that the counter must have an efficiency for fast neutrons that is the same function of their energy as is the reciprocal of the neutron flux required for a given dosage rate. It has been shown that, in the energy range investigated, 0.2 Mev to 10 Mev, this function can be approximated with a practical counter chamber. One such chamber has one end lined with 0.017 cm of stearin, is 3.5 cm in length, and contains a few cm (Hg) of methane. Application to neutrons of higher energy has not been investigated.

C7. Gyromagnetic Ratios of Vanadium^{51} and Manganese^{55}. WILLIAM H. CHAMBERS, ROBERT E. SHERIFF, AND DUDLEY WILLIAMS, *Ohio State University.*—Methods similar to those described in earlier reports have been used to observe nuclear magnetic resonance absorption peaks for V^{51} and Mn^{55}. The V^{51} peak was observed in a solid sample of V_2O_5. The value obtained for the gyromagnetic ratio of V^{51} is in agreement with values obtained recently in other laboratories. The Mn^{55} peak was observed with samples consisting of aqueous solutions of $Ba(MnO_4)_2$, $Ca(MnO_4)_2$, and $K(MnO_4)$. The most intense absorption peak was obtained with the $Ca(MnO_4)$ sample. Preliminary results give the following value for the ratio of the resonance frequency of Mn^{55} to the proton resonance frequency in the same field: $\nu^{55}/\nu^{1}=0.24786\pm0.00012$. Further work on the subject is in progress.

C8. Beta-Gamma-Angular Correlations. DONALD T. STEVENSON AND MARTIN DEUTSCH,* *Massachusetts Institute of Technology.*—Angular correlations between beta- and gamma-rays have been studied using a magnetic lens spectrometer to isolate beta-particles in selected energy ranges. No anisotropy was found in the decay of Na^{22}, Cs^{134}, and Co^{60}. The two first named are known to emit beta-spectra of allowed shape so that no deviation from symmetry is expected. In the case of the lower energy branch of Rb^{86} the gamma-ray has a greater probability to be emitted along the direction of the emitted beta-ray than at right angles to it. The effect is greatest near the maximum energy of the beta-spectrum, the ratio $W(180°)/W(90°)$ reaching a value of about 1.2. For beta-rays of $\frac{1}{3}$ maximum energy this ratio drops to about 1.09. These findings contradict the results of Frankel.[1] Some general considerations concerning theory and technique will be presented.

* Supported in part by the Joint Program of the ONR and the AEC. The Rb^{86} used in this investigation was supplied by the Isotopes Division, U. S. AEC.
[1] S. Frankel, Phys. Rev. **77**, 747A (1950).

C9. Scintillation Spectra of Short-Life Activities. EDWARD C. CAMPBELL AND MAX GOODRICH,* *Oak Ridge National Laboratory.*—In order to study the radiations of radioactive substances having half-lives of the order of seconds, a new method has been devised which permits a complete spectrum to be photographed in a few seconds. The method consists in displaying the pulses from an anthracene scintillation counter on an oscilloscope using a self-triggered sweep. A short time-exposure photograph gives the pulse-height spectrum of the activity being studied. By calibrating with known radiations an energy *vs.* pulse-height relation is obtained, which is linear from 0.4 to 2.5 Mev. Energy measurements are reproducible to about 2 percent. The apparatus has been installed at the fast pneumatic tube of the Oak Ridge graphite reactor in order that samples can be observed beginning 0.3 sec. after irradiation. Using this method two gamma-rays associated with a new 0.9-sec. isomeric activity in lead have been found with energies of 0.5 and 1.0 Mev. The energy of the gamma-ray associated with the 24-sec. period of Ag^{110} is 0.66 ± 0.01 Mev in good agreement with the Ag^{110} decay scheme proposed by Siegbahn.

* On leave from Louisiana State University.

C10. Gamma-Spectrum of Barium 131. E. B. DALE, E. L. ZIMMERMAN, D. G. THOMAS, AND J. D. KURBATOV, *Ohio State University.*—Radioactive barium 131, $T_{\frac{1}{2}}\simeq 12$ days, has been

examined with a thin-lens spectrometer. The 364.18-kev gamma-ray emitted by iodine 131 was used for calibration of the spectrometer. The calibration was verified with cobalt 60 and scandium 46. The activated barium was obtained from the Oak Ridge National Laboratory. It was purified and the radioactive Cs^{131} was removed. An appropriate time was allowed for disintegration of barium 133. A tin radiator was used in the region up to 130 kev and a lead radiator up to 700 kev. It was found that in disintegration of barium 131 several gamma-rays are emitted. The 496.5-kev gamma-ray is several times as intense as others. K and L photoelectron peaks gave a consistent value for this gamma-energy of 496.5 ± 4 kev. Several other less intense gamma-rays were observed with consequent greater error in energy determination. The low specific activity of the Ba^{131} limited the precision of determination of energies of these less intense gamma-rays. Further work is in progress.

[1] Lind, Brown, Muller, and DuMond, Phys. Rev. 75, 1633 (1949).

C11. An Excited State of Ta^{181} with 1.1×10^{-8}-Second Lifetime.* W. C. BARBER, *Stanford University.*—Using sources of Hf^{181} ($T=46$ days) some excited states of Ta^{181} have been investigated. Delayed coincidence measurements have been made with a system employing stilbene scintillation counters. Pulses from the counters are delayed in coaxial cable, amplified with fast amplifiers (distributed amplifiers of band width about 60 megacycles/sec.) and mixed in an electronic circuit. Curves of coincidence rate as a function of delay, taken with various sources, indicate that the resolving time of the system is about 1.3×10^{-8} second. Gamma-γ-coincidences taken with Hf^{181} as source indicate a metastable state of half-life about 1.1×10^{-8} second. Absorption in lead of the radiation following the metastable state is consistent with the interpretation that γ-rays of 470 and 340 kev follow this metastable state. Using a delayed coincidence system employing univibrators, the 22 μ-sec. level of Ta^{181} has also been investigated. Hard and soft γ-rays are found to follow this state, but no γ- or x-radiation is observed to precede it. The prompt β-(hard γ-) coincidences previously reported by the author were not observed in a second sample of Hf^{181} and were probably mostly due to an impurity in the original sample. This evidence indicates that, as first suggested by Chu and Wiedenbeck, most of the transitions from Hf^{181} lead directly to the 22 μ-sec. level of Ta^{181}.

* Assisted by the Joint Program of ONR and AEC.

C12. Steady High Magnetic Fields. MARTYN H. FOSS, *Carnegie Institute of Technology.*—With sufficient power, very high steady magnetic fields can be obtained. Consider the following dimensionless ratios characteristic of a design $h=H/(fj_0r_0)$, $p=P/(fr_0^3j_0^2\rho)$, $v=V/(fr_0^3)$. First determine h using the required field; the maximum space factor times current density; and the minimum inside radius. There is an ideal design for each h which uses the smallest power, P, for a given (sufficiently large) volume of conductor, V. A practical design can approach this efficiency. This work was carried out with the assistance of ONR and AEC.

C13. Synchro-Cyclotron Magnet.* M. H. FOSS, J. G. FOX, R. B. SUTTON AND E. CREUTZ, *Carnegie Institute of Technology.*—A synchro-cyclotron magnet designed[1] to produce 400-Mev protons at a field of about 20 kilogauss will be described. The full scale magnet has duplicated very closely the characteristics of the model. Curves will be shown which give the field shape for various absolute field strengths and at various distances from the geometrical mid-plane of the gap. The vertical distance within which magnetic focusing exists is about two inches. The probable maximum radius of the ion beam ($n=0.2$ point) is about 96 percent of the radius of the pole face at which point the field is about 96 percent of its value at the center. The radius of the pole face is 141.6 in., of the pole base 163.4 in. The total weight of the iron is 1500 tons, the copper 130 tons. The current is 20,000 amps. and the power consumption 320 kw.

* This work was carried out with the assistance of ONR and AEC.
[1] M. Foss, Tech. Report No. 1, Contract N7ONR30301.

C14. Integral Relationships Between Nuclear Masses and the Electron Mass. ENOS E. WITMER, *University of Pennsylvania.*—Recent experiments[1] show that the ratio of the proton mass to the electron mass is very close to 1836. We[2] believe that it is *exactly* 1836. This permits an accurate determination of m in mass units from H^1. Using this it is found that the mass of O^{16} is $(29155.018\pm0.080)m$. This is so close to an integer that we are justified in assuming that the nuclear mass of O^{16} is exactly $29147m$. This enables us to determine m in MU to an astounding degree of precision. We will now introduce a new unit of mass, namely $m/11$, which we shall designate *the prout*. This prout is about one-fourth of the prout previously used by the writer.[3] It appears to be true that *the masses of all nuclei, not subject to β-decay, are an integral number of prouts. Some of those subject to β-decay also follow the integral rule.* This fits in with the writer's general notion of the dominance of integers[2,3] in the nuclear domain.

[1] Hipple, Sommer, and Thomas, Phys. Rev. 76, 1877 (1949).
[2] E. E. Witmer, Abstracts L7 and SP1, Bull. Am. Phys. Soc. 25, No. 1. New York Meeting (February 2, 1950).
[3] E. E. Witmer, Proc. Nat. Acad. Sci. 32, 283 (1946).

Papers on Various Topics

E1. On the Heat of Devitrification of Aqueous Solutions. B. LUYET, *St. Louis University.*—When a droplet of a concentrated solution (we used 1.8 M sucrose) is cooled at a rate of several hundred degrees per second, it solidifies into an amorphous, transparent mass. Upon being rewarmed this mass devitrifies, becoming white and opaque (at -32°C for 1.8 M sucrose). In an attempt to estimate the heat of devitrification, we recorded photographically the warming curves of cylindrical pieces (1 mm thick, 3 mm diameter) of vitrified material in which one junction of a thermocouple, connected to a string galvanometer, was inserted, the other junction being either kept at constant temperature or inserted in a similar cylinder of water cooled and rewarmed simultaneously with that of solution. With this differential method the sensitivity of the string could be increased considerably. No change in the slope of the curves was detected during devitrification. Since the melting of the ice cylinder, which absorbed some 560 millicalories, lasted about 45 seconds (long plateau in the curve) in test experiments with ice alone, the heat of devitrification of the solution must be exceedingly little not to affect the curve. This raises the question of whether devitrification involves a crystallization of the solvent.

* Supported by Research Corporation.

E2. The Use of Three Long Narrow Coils for Neutralization of the Earth's Magnetic Field in a Beta-Ray Spectrometer. S. K. HAYNES AND J. W. WEDDING, *Vanderbilt University.*—Accurate neutralization of the earth's magnetic field over a long cylindrical region is necessary to extend the energy range of a magnetic-lens spectrometer to very low energy electrons. Three parallel rectangular coils are used.[1] The center coil has a width $2a$, a length equal to five times the width, and contains N turns. Each outer coil has a width $\sqrt{2}a$, the same length, and $N/\sqrt{2}$ turns. They are placed at a distance $a/\sqrt{2}$ on each side of the center coil. In a plane transverse to the length of the coils the radial variation of the field is given approximately by the term $H_0(r/a)^6$. This term gives variations of about plus and minus one percent separated by 30° azimuthally. With the coil current set for zero deflection for axial electrons, the rotation of the non-axial trajectories averages out these deviations so that the effective residual field is about 0.1 percent of the

earth's field. For a one meter spectrometer 10-kev electrons are deflected 0.1 millimeter.

[1] J. H. Sweer, Naval Ordnance Memorandum No. 8582.

E3. Quantum-Electrodynamics. FREDERIK J. BELINFANTE, *Purdue University.*—In manifestly covariant quantum-electrodynamics, the vacuum is a superposition $\Psi=\Pi_{\mathbf{k}}(\Sigma_{mn}c_{mn}{}^{\mathbf{k}}\chi_{mn}{}^{\mathbf{k}})$ of states $\chi_{mn}{}^{\mathbf{k}}$ with m longitudinal positive energy photons and n "scalar" negative energy photons present with wave vector $\mathbf{k}$.[1] In zero-order approximation by $c_{mn}{}^{\mathbf{k}}=c_n{}^{\mathbf{k}}\delta_{mn}$ the energies of longitudinal and scalar photons cancel. Since in this approximation $c_n{}^{\mathbf{k}}=(-)^n c_0{}^{\mathbf{k}}$, Ψ is not properly normalizable. This fact may lead to mathematical ambiguities in the calculation of the electron self-energy.[1] These ambiguities now can be avoided at least formally, if in Eqs. (33)[1] we avoid the sums over n of terms with factors c^*c by writing them as vacuum expectation-values of products of photon annihilation and creation matrices $a_{\mathbf{k}}$, $b_{\mathbf{k}}$, $a_{\mathbf{k}}{}^*$, $b_{\mathbf{k}}{}^*$ describing the transitions listed under A-I[1a]. Taking along these expectation values through the calculation, using only the commutation relations of a, a^*, b, b^*, we find for the electron self-energy the usual expression plus terms proportional to $\langle(a^*+b)(a+b^*)\rangle_0$ and $\langle(a+b^*)(a^*+b)\rangle_0$, which vanish by the Lorentz conditions Eqs. (12)–(13).[1] Thus explicit use of $c_n{}^{\mathbf{k}}=(-)^n c_0{}^{\mathbf{k}}$ and ambiguities from explicit (diverging) sums over n are avoided.

[1] F. J. Belinfante, Phys. Rev. **76**, 226 (1949). [1a] *Ibid.*, p. 229.

E4. The Meson Mass Spectrum. ALEX E. S. GREEN, *University of Cincinnati.*—Several mathematical considerations have suggested that four meson masses occur in our generalized meson theory.[1] In virtual processes only every other meson behaves like a positive energy boson. One condition needed to overcome the difficulties attendant to the negative energy bosons is that the heaviest meson carry positive energy. The experimental picture of the meson mass spectrum and the properties of mesons has fluctuated rather wildly since we made our first proposals. However very recently a crystalization of the results seems to have firmly established the existence of the μ-, π-, and τ-mesons, with the last two behaving like N.F. mesons (alternatively called Yukawa particles or positive energy bosons). Thus nature has rejected all theories which accommodate only one N.F. meson and all theories which predict an infinity of meson masses, but she has not yet been unkind to our theory when taken with the magic number four. A provocative interpretation of the experiments and the theory would suggest itself if another particle were discovered having a mass between those of the π- and τ-mesons and having the properties (no star production etc.) of the μ-meson.

[1] A. Green, Phys. Rev. **73**, 519 (1948); **75**, 1926 (1949).

E5. The Motional Capacitance of AT-Cut Quartz Resonators. KARL S. VAN DYKE, *Wesleyan University.**—Previously reported measurements on BT-cut resonators partially plated in strips had indicated that the alternating strain in the crystal is sinoidally distributed parallel to both pairs of edges for square plates whose edges are parallel to X and Z', and that the strain falls approximately to zero at both pairs of edges. Impedance measurements on square AT plates with edges similarly parallel to X and Z' indicate a distribution such that the strain falls only to 40 percent of its central value at the edges which are parallel to X. The experimental motional capacitance for the several electrode areas used are in close accord with the theoretical analysis of an accompanying paper,† which then provides a theoretical as well as a practical basis for predicting the circuit behavior of such resonators with some precision. By viewing the distribution of strain which is found experimentally as resulting from the superposition of the strains of several coupled component simple resonators the secondary roles of the constants c_{11}' and c_{55}' are apparent. These govern the mechanical impedances of two such coupled resonators which in the composite bring about the departure of the actual distribution from the uniform distribution for a plate of infinite extent with mode dependent upon c_{66}'.

* Work supported by U. S. Army Signal Corps.
† Abstract E6.

E6. The Theory Of Thickness-Shear Resonance of Piezoelectric Resonators. GARY D. GORDON, *Wesleyan University.** (*Introduced by K. S. Van Dyke*).—Ekstein** showed theoretically that in the fundamental thickness shear resonance of thin rectangular plates the distribution of strain along a direction perpendicular to the axis of shear is sinoidal. Hok† showed similarly that the approximate distribution along the parallel direction should be somewhere between uniform and sinoidal, in the form $\cos[(\pi\sigma_p z')/w]$. By minimizing Hamilton's Integral for this distribution, the parameter σ_p can be expressed in terms of secondary elastic constants of the material and of the length to width ratio of the plate. Known values of the constants, c_{11}' and c_{55}', for quartz yield numerical values for the parameter σ_p of 0.98 and 0.72 for square BT and AT-cut plates, respectively. The strain falls nearly to zero along the edges parallel to X in the BT plate but not in the AT. The motional capacitance for plates having fractional area electrodes computed on the basis of these theoretical distributions agrees excellently with experimental determinations, which are described in an accompanying paper.††

* Work supported by U. S. Army Signal Corps.
** H. Ekstein, Phys. Rev. **70**, 76 (1946).
† G. Hok, J. Acous. Soc. Am. **20**, 406–407 (1948).
†† Paper E5.

E7. The Dependence of the Piezoelectric Effect of $BaTiO_3$ Single Crystals on Temperature up to 160°C.* W. J. MERZ, *Massachusetts Institute of Technology.*—The behavior of the electromechanical coupling and of the piezoelectric resonant frequencies of $BaTiO_3$ was investigated by the resonance method from room temperature through the Curie point up to about 160°C. In analogy to the other ferroelectrics, the so-called single domain crystals, consisting of parallel and antiparallel domains, give very strong resonances at low frequencies, which shows that the crystal is rather soft in the directions of spontaneous deformation. The d_{31} and d_{33} coefficients increase to a high maximum a few degrees below the Curie point and then drop suddenly. Above the Curie point, maximum of the dielectric constant, we still have a piezoelectric response but it is smaller and decreases with increasing temperature. The resonance frequency traverses at the Curie point a very sharp minimum. The situation above the Curie point can be explained by the shift of the Ti ions under the influence of an external field as was verified by optical observation of the birefringence; the crystal becomes tetragonal. The effect of a d.c. bias field has also been investigated.

* Sponsored by the ONR, the Army Signal Corps, and the Air Force under ONR Contract.

E8. The Infra-red Properties of Diamond, Silicon, and Germanium. E. BURSTEIN AND JOHN J. OBERLY, *Crystal Branch, Naval Research Laboratory, Washington, D. C.*—The fundamental vibrations of the diamond structure which has O_h symmetry should be inactive in infra-red absorption. The absorption bands at 8 microns in the region of the fundamental vibration (1332 cm^{-1}) observed in Type I diamonds have been attributed to diamond structures having T_d symmetry.[1] It is suggested rather that these bands are due to the presence of impurities in the lattice of Type I diamonds. Both Type I and II diamonds exhibit bands at 5 microns. These obviously are combination bands resulting from the coupling between modes

of vibration. The existence of such bands is, in fact, a striking illustration of the role played by the deformation of the electron shells during vibration.[2] The infra-red absorption spectra of silicon and germanium due to lattice vibrations should resemble that of diamond. This has now been verified by absorption measurements over the range of 2 to 25 microns. Because of their relatively high dielectric constants, silicon and germanium containing donor- and acceptor-type impurities exhibit additional absorption due to free electrons and holes which are absent in diamond at room temperature.

[1] C. V. Raman, Proc. Ind. Acad. Sci. 19, 189 (1944).
[2] E. Burstein and J. J. Oberly, Proc. Ind. Acad. Sci. 28, 388 (1948).

E9. New Optical Glasses Transparent in the Infra-red up to 12μ.* R. FRERICHS, *Northwestern University.*—According to Zachariasen[1] in oxide glasses polyhedra of oxygen atoms around the cations form an extended unperiodic network of open structure. The glass-forming oxides are found under the small ions of the fourth and fifth column of the periodical table. The majority of these oxides have been observed in the glassy state, but very little is known about other glass-forming compounds. Arsenic tri-sulfide forms a perfectly clear, stable red glass which has remarkable optical properties hitherto unknown. 2.6 mm of As_2S_3 pass 45 percent radiation between the red and 8μ, and this amount decreases to 21 percent at 12μ. 0.15 mm transmit 65 percent throughout this region, indicating high reflection losses due to a high index of refraction. The index of refraction $N_{Li(red)}$ is about 2.5. The glass softens at 300°C, distills without decomposition at 500°C, and is non-hygroscopic. It can be melted in Pyrex tubes and forms binary glasses with different sulfides. An investigation of this group of sulfide glasses, which have optical properties not realized in oxide glasses, is planned.

* This work was sponsored by the U. S. Navy, Bureau of Ships.
[1] W. H. Zachariasen, J. Am. Chem. Soc. 54, 3841 (1932).

Miscellany in Electron Physics and Solid-State Physics

G1. Transit Time of Electrons in Simple Diodes as a Function of Current Density. DELBERT N. EGGENBERGER AND PAUL L. COPELAND, *Armour and Company and Illinois Institute of Technology.*—Calculations by Ivey[1] suggest that there is a universal function describing the variation of the field at the cathode of a vacuum tube as the current is increased to its saturation value. Since the cathode field is one of the most important data for the calculation of electron transit time in the case in which all electrons are assumed to leave the cathode with zero velocity, the equation given by Ivey may be used in such calculations. The solution of the plane parallel case presents no difficulties. For coaxial cylinders a Maclaurin's series is suggested for expressing the transit time in powers of the ratio of the current to the saturation current, and the leading terms of this series are found to be functions of the transit time in the absence of space charge.

[1] H. F. Ivey, Phys. Rev. 76, 554 (1949).

G2. Notes on the 1P21 Photo-Multiplier Tube When Used for Astronomical Photometry. J. H. DEWITT, JR. AND C. K. SEYFERT, *Radio Station* WSM *and Vanderbilt University.*—A description is given of the operation of the Vanderbilt University stellar photoelectric photometer attached to the DeWitt 12-inch telescope. A 1P21 photo-multiplier tube and d.c. amplifier designed by Kron are used. The chief sources of troublesome leakage currents and their remedies are outlined in some detail together with a simple method for distinguishing between cell leakage current and dark current. Reduction of dark current is accomplished through refrigeration of the leads to the tube elements using solid CO_2 cylinders instead of CO_2 snow. A simple method of cutting and using the solid CO_2 is described. A 1000-volt regulated power supply replaces the batteries usually employed to provide the accelerating voltages for the 1P21 tube. A description of the power supply and a detailed parts list for it are provided. The problems involved in placing the amplifier and recording meter outside the observatory dome (i.e., cable leakage and communications) are dealt with. Finally a light curve of the eclipsing star SV Camelopardalis obtained with the instrument described is reproduced. The probable error of a single magnitude determination with this instrument on relatively bright stars (7th mag.) is ±0.005 magnitude.

G3. Secondary Emission of Electrons at Oblique Angles of Incidence. JAMES J. BROPHY, *Illinois Institute of Technology.*—Wooldridge's theory of secondary emission[1] predicts fairly well the secondary efficiency curves for pure metals; however, the predicted emission at low energies is somewhat less than that observed. The use of an oblique angle of primary incidence serves as a more severe test of the present theory. Wooldridge's equation giving the efficiency curve has been modified for use with primary angles of incidence other than normal incidence. The predicted results are compared with experimentally determined curves for gold, silver, and platinum, and for primary angles of incidence of 0° and 45°. The agreement is considerably worse for oblique than for normal incidence. If the difference between the observed and predicted efficiency curve is plotted against primary energy, nearly the same curve is obtained for all surfaces and both angles of incidence. This is taken to suggest that a new effect is taking place at low energies. By analogy with photoelectric emission, it is suggested that a "surface secondary emission effect" exists that together with Wooldridge's "body effect" would more completely describe the phenomena of secondary emission.

[1] D. E. Wooldridge, Phys. Rev. 56, 562 (1939).

G4. Scintillation Counters as Detectors of Soft X-Rays.* JOHN P. NEISSEL AND DONALD C. MOORE, *Rensselaer Polytechnic Institute.*—The radiation from a copper-anode Coolidge tube, operating at 36 kv, was measured, using a photomultiplier tube and scintillating crystal as a detector. The equipment consisted of a photo-multiplier tube and crystal, video amplifier, discriminator, and pulse counter. Types 931A and 5819 photo-multipliers were used with crystals of stilbene, calcium tungstate, and sodium iodide (with 1 percent thallium), and with no crystal. The tubes were not cooled. The x-ray beam was limited by a 3-mm diameter aperture, and its intensity was controlled by using aluminum as an attenuator. The use of crystals with the 931A reduced the sensitivity below that obtained with the tube used alone; using the tube with no crystal, the net counting rate equalled the background rate with 1½ inches of aluminum, and this x-ray intensity required four minutes to just darken a photographic plate. The use of calcium tungstate with the 5819 reduced the sensitivity below that obtained with the tube used alone, but the sodium iodide crystal increased the sensitivity to a point where about 2½ inches of aluminum were required to reduce the counting rate to the level of the background rate; this latter intensity would require about 50 hours to just darken a photographic plate.

* Supported in part by the Rensselaer Polytechnic Institute Research Fund.

G5. The Response of the Anthracene Scintillation Counter to Monoenergetic Electrons.* JOHN I. HOPKINS,† *Oak Ridge National Laboratory.*—Using a 180-cm single-lens β-ray spectrometer to supply monoenergetic electrons, pulse height-energy studies for electrons in the 30- to 3000-kev range have been made. An extension of previously reported work[1] shows that a very definite linear relation exists between pulse height and energy for the range 125 kev to 1900 kev. The pulse height

versus energy curve shows a decreasing slope below 125 kev for an anthracene crystal 1.29±0.02 cm in thickness. If one assumes normal electron absorption in 1.55 g/cm² of anthracene one might expect a linear relation to exist up to 3100 kev. Line width studies as a function of energy have been made. The counting rate *versus* energy curves for a given electron energy follows a normal distribution curve very closely.

*This work is based on work performed for the AEC project at Oak Ridge National Laboratory.
† On leave from Vanderbilt University; J. I. Hopkins, Phys. Rev. 77, 406 (1950).

G6. Characteristics of Scintillation Counters Using Pulsed Photo-Multipliers. R. F. POST AND N. S. SHIREN, *Stanford University.*—As a part of the electron linear accelerator program* at Stanford an effort is being made to develop high speed counting equipment. Since these accelerators operate with microsecond acceleration times it is essential for many experiments that counting, coincidence, and scaling resolving times should be much less than this. A desirable additional requirement is that the equipment should record only those events occurring during the acceleration time. It has been found possible to operate photo-multiplier counters under pulsed conditions with agreeably short resolving times. When operated with d.c. at rated voltages, the amplification factor of most photo-multipliers is about 10^6. To actuate a high speed coincidence or scaling circuit, it is then usually necessary to provide additional amplifiers, which in themselves tend to decrease the counting speed. However, operation of a photo-multiplier at higher voltages can increase its amplification greatly, so that it may not be necessary to use additional amplifiers.[1] With d.c. operation, however, a limit is reached when noise from regenerative ionization effects becomes too large to be tolerated and no further advantage is gained from raising the voltage. For pulsed operation this does not seem to be the case.

* Program supported by ONR.
[1] R. E. Bell and H. E. Petch, Phys. Rev. 76, 1409 (1949).

G7. Luminescence of Color Centers in Lithium Fluoride. CLIFFORD C. KLICK, *Naval Research Laboratory.*—Color center absorption bands in alkali halides have been widely investigated. The present work was intended to determine whether after excitation these color centers return to their original condition by a radiationless process or by luminescent emission. X-rayed lithium fluoride showed luminescent emission in a band at 7000A when excited in the 4600A absorption band which is the *M* band for this material. Irradiation in the *F* band at 2500A did not show visible luminescence even at liquid helium temperatures. The 7000A emission of the *M* band was observed at liquid nitrogen and liquid helium temperatures as well as at room temperature. Even at liquid helium temperature the emission is several hundred angstroms wide and is not appreciably different from the emission at liquid nitrogen temperature. If the luminescent intensity of x-rayed lithium fluoride is measured as a function of the wave-length of exciting light, there is a major peak at 4600A and small peaks at 2300A, 2500A, and 3100A. The 2500A peak may represent the transformation of *F* center to *M* centers. Absorption peaks corresponding to the 2300A and 3100A excitation peaks were not observed in the present investigation.

G8. A Study of Color Centers Produced in Quartz by X-Rays. GUY FORMAN, *Vanderbilt University* AND *University of Kentucky.*—*Z* cut sections of natural quartz crystals were colored to saturation by *x* irradiation from a beryllium window x-ray tube. The crystal sections were decolored by heating and recolored by further *x* radiation. The same optical transmissions, at saturation, were obtained when the energy distribution of the x-ray beam was the same but were different when different voltages were applied to the x-ray tube. The heat treatment used in removing the color from quartz does not affect the value of the optical transmission when recolored by *x* radiation to saturation. It was observed that in every case the rate of coloration was greater after the section had been cleared and re-irradiated than when the color was being produced for the first time. If the heat treatment is restricted to an amount barely sufficient to remove the coloration, then the rate follows the same curve on successive irradiation cycles. If the crystal section is baked for a longer period of time than that stated above, the rate decreases and approaches that of fresh quartz. The change in rate of coloration of quartz is governed by the immediately preceding heat treatment employed in removing the color centers. No "memory" of previous heat treatments appears to be present.

G9. Cold Work and Particle Size Broadening in X-Ray Diffraction Lines. B L. AVERBACH AND B. E. WARREN, *Massachusetts Institute of Technology.*—Cold work and particle size broadening in x-ray diffraction patterns have been studied by making precision measurements of peak shapes with a Geiger-counter spectrometer. The corrected shapes are represented in terms of a Fourier cosine series and a set of amplitudes, A_n, is determined. The form of the function of A_n *vs.* n distinguishes between particle size and cold work broadening. Data for particle size broadening in MgO have been obtained. The initial slope of the A_n curves gives the mean particle size and the second derivative gives directly the particle size distribution. Cold work distortion has been observed in alpha-brass filings and this has been interpreted in terms of root mean square distortions averaged over lengths, na_3. An attempt has been made to determine a distribution function of the strains by measuring several orders of a given plane.

G10. Random-Circuit Theory of Resistance and Noise in a Composition Resistor. R. P. COLEMAN, *Franklin Institute.*—Common types of resistors are made from a mixture of finely divided conducting particles in an insulating medium. A theory based on a concept of a random electrical circuit has been developed, in which the imperfect electrical contacts between conducting particles constitute the resistance elements and the conducting particles constitute the junctions between resistance elements. An expression for terminal resistance in terms of an assumed statistical distribution of local resistance values is obtained. The derivation involves an equivalent circuit representing one local resistance together with the average effect of all the remaining local resistances. The method is also applicable to the study of related properties such as temperature coefficient of resistance. If noise generation in each local region is represented by any assumed law of e.m.f. and resistance fluctuation, the corresponding noise at the terminals is given by random-circuit theory. An expression for an upper bound to resistance-fluctuation noise is also obtained.

Semi-Conductors

I1. Semiconductivity of Polycrystalline Graphite. S MROZOWSKI, *University of Buffalo.*—The experimentally observed dependence of the resistance of polycrystalline graphite from temperature can be explained by assuming the existence of an energy gap between the filled and conduction bands. Such a graphite is an intrinsic semiconductor at room temperature. The energy gap is so small however (25×10^{-3} ev) that at higher temperature its presence becomes immaterial and the substance shows a metallic behavior. The size of the gap increases with decreasing dimensions of crystallites. The conductivity of polycrystalline graphite at low temperatures and of fine crystalline carbons (cokes) in general are due mainly to excess electrons in the conduction band, the peripheral carbon

atoms with free valences playing the role of N-centers. The complete system of resistivity curves from the low temperature cokes up to well-graphitized specimens can be understood in forms of these assumptions. The scattering of electrons due to the finite size of crystallites, lattice imperfections and so forth gives in commercial graphite a contribution to the resistivity decreasing with increase of temperature in the region of low temperature ($\sim$150°K) and tending to a constant value at higher temperatures.

I2. Electron Mobilities in Conducting Phosphors. LEE GILDART AND A. W. EWALD, *Northwestern University.*—The mobility of electrons in those semiconductors which are also phosphors can be found in a new way as follows: The crystal to be investigated is irradiated with square-wave pulses of energetic quanta (ultraviolet light or x-rays). The response of the crystal to these pulses gives (1) a conductivity rise-and-decay curve (2) a luminescence rise-and-decay curve. Analysis of these curves, which are recorded simultaneously, gives the mobility directly. Related parameters are also derivable. Measurements on a small polycrystal of cadmium sulfide gave these values: Mobility $\sim$6.0 cm²/volt sec.; density of electrons in the conduction band $\sim 10^{11}$ per cm³; lifetime of an electron in the conduction band $\sim 10^{-3}$ sec.; schubweg $\sim$25 mm.

I3. The Effect of Surface States on the Fermi Level of a Semiconductor. PAULA FEUER AND HUBERT M. JAMES, *Purdue University.*—Over a wide range of conditions, the number of electrons n per unit volume in the conduction band at temperature T is proportional to $\exp(\zeta/kT)$, where ζ is the Fermi level. For N-type semiconductors in the impurity range, ζ is usually determined by the condition $n+n'=N$, n' being the number of electrons in impurity states and N the number of impurities per unit volume. If electrons can also occupy surface states, the condition for determining ζ is $n+n'+n''(A/V)=N$, where n'' represents the number of electrons per unit area in surface states, A the area and V the volume of the sample. When the number of electrons on the surface becomes comparable with the number of conduction electrons, the surface term becomes important and the Fermi level is lowered. Calculations show that surface states can be important in samples of small N (e.g., 10^{16} impurities/cm³) at low temperatures (e.g., 20°K); n is smaller and the resistivity higher than that predicted by previous theory. This effect depends strongly on the activation energy for the electrons and is particularly large in the case of thin films, where A/V is large.

I4. A. C. Circuit for Rapid Determination of Hall Coefficients of Semiconductors.* B. R. RUSSELL, P. H. MILLER, JR., AND C. F. WAHLIG, *University of Pennsylvania.*—Direct current methods and usual alternating current methods of measuring small transverse voltages due to the Hall effect require at least two separate measurements to eliminate thermal e.m.f. or stray signals which are always present. A faster method is needed in order to make measurements upon semiconducting oxides at elevated temperatures where rapid changes in composition occur. When both the magnetic field and the current are made to alternate sinusoidally but at different frequencies, the resulting Hall voltage has two components (the sum and difference frequencies) which can be separated from one another and from stray voltages by a band pass filter. Thus the output is directly proportional to the Hall voltage and no second measurement is necessary. A test circuit based on this idea has been constructed and found to yield values of Hall coefficients which agree within experimental error ($\pm$10 percent) with conventionally determined values. Using Cu_2O samples the signal to noise ratio is about 100 to 1 at room temperatures [$R\sim 10^{-3}$ (volt-cm/amp.-gauss), $I\sim 10^{-3}\sin 2\pi 70t$ amp., $B\sim 10^{3}\sin 2\pi 60t$ gauss, $\sigma\sim 10^{-3}$ ohm^{-1} cm^{-1}] and decreases slowly to about 7 to 1 at 300°C, R having decreased by a factor of about 60.

* Work supported in part by the Bureau of Ships.

I5. Recrystallization Purification of Germanium. R. N. HALL, *General Electric Research Laboratory.*—A recrystallization technique will be described which is very effective in the removal of impurities from germanium. Chemically purified germanium dioxide is reduced in hydrogen, vacuum melted in a graphite boat, and directionally cooled so as to concentrate the impurities in the ends of the ingot. Successive recrystallizations of the central sections remove impurities to the point where the room temperature electrical conductivity is essentially intrinsic. Impurity distributions, as determined by conductivity measurements, are consistent with an analysis which predicts that an impurity be distributed in proportion to the $(k-1)$ power of the distance from the end of the ingot which cools last, where k is the ratio of the impurity solubility in the solid phase to that in the liquid phase at the melting point. Silicon and boron are found to be more soluble in the solid phase, while nearly all other impurities show a strong preference for the liquid phase. Control of impurities makes possible the preparation and study of doped samples of known composition. Preliminary results of such experiments will be presented.

I6. Fast Neutron Bombardment Effects in Germanium. J. H. CRAWFORD, JR. AND K. LARK-HOROVITZ, *O. R. N. L.*—The concentration of lattice defects produced by a given fast integrated neutron flux (nvt) in N-type germanium semiconductors was studied assuming that each defect produces one acceptor. The number of defects produced per incident neutron may be obtained from the slope of the conductivity *vs.* nvt curve. In the initial portion of the curve—concentration of electrons very large compared to that of holes—in which the mobility remains nearly constant,

$$d\sigma/d(\text{nvt}) = -ebK, \tag{1}$$

where e is the electronic charge, b is the mobility, and K is the net number of defects produced per incident neutron which is between 1 and 5 in most cases. Due to the rate of healing of defects the rate of production of defects is given by

$$dN/dt = fK' - k_2'N^2, \tag{2}$$

where k_2' is the second-order rate constant, f is the fast flux and K' is the number of defects introduced by irradiation.

I7. Germanium Semiconductor Alloys Produced by Transmutation. J. CLELAND, K. LARK-HOROVITZ, AND J. C. PIGG, *O.R.N.L.*—Germanium exposed in a nuclear reactor becomes a P-type semiconductor. This is due to (a) lattice displacement (fast neutrons) and (b) impurity centers produced by transmutations (slow neutrons). The displacement effect can be healed out by prolonged heat treatment at 450°C. The remaining increase in P-type centers is due to the difference between Ga atoms and As atoms produced by transmutation. Using absorption cross sections on separated Germanium isotopes determined by H. Pomerance (O.R.N.L.) the predicted number of excess P-type impurity centers is about 2 percent of the integrated slow flux. Comparison between Hall effect measurements before neutron irradiation, after irradiation and finally after heat treatment shows that within the limits of error (flux measurements, absorption cross section, variations in heat treatment), one current carrier is released per impurity center produced, in agreement with former theoretical considerations.[1]

[1] Lark-Horovitz, Middleton, Miller, and Coalerstein, Phys. Rev. 69, 258 (1946).

I8. Germanium $P-N$ Barriers as Counters.* C. ORMAN, H. Y. FAN, G. J. GOLDSMITH, AND K. LARK-HOROVITZ, *Purdue University.*—The high resistance of a $P-N$ barrier in germanium makes it sensitive to ionizations produced in the barrier. This makes it possible to use $P-N$ barriers as counters for nuclear radiations. McKay[1] has recently reported the use of point contact rectifiers as counters for alpha-particles and pointed out that such a device will respond effectively only to particles of high specific ionization. It has been found that $P-N$ barriers respond to alpha-particles from polonium and also to betas from RaE. From the pulse shape and the source strength it is evident that the pulses observed are produced by individual ionizing particles. The magnitude and time constant of the pulses depend upon the capacitance and the resistance of the barrier. The resistance of the barrier can be varied by varying the temperature; the barrier capacitance depends upon the dimensions of the crystal and can be controlled further to a certain extent in the case of the artificial barriers produced by nucleon bombardment.[2]

* Work supported by the Signal Corps.
[1] K. G. McKay, Phys. Rev. **76**, 1537 (1949).
[2] See K. Lark-Horovitz, *et al.*, Phys. Rev. **73**, 1256 (1948).

I9. Changes in Conductivity of Germanium Induced by Alpha-Particle Bombardment. W. H. BRATTAIN AND G. L. PEARSON, *Bell Telephone Laboratories.*—K. Lark-Horovitz *et al.*[1] found that the electrical conductivity of germanium can be changed by nucleon bombardment. The bombardment of 8 ohm cm n-type germanium by alpha-particles from polonium first removes the conducting electrons at the rate of 78 per alpha-particle. After the electrons are gone conducting holes are introduced at the initial rate of 8.6 per alpha-particle. Some of these holes disappear with time at room temperature after bombardment is stopped, leaving only 2 conducting holes per alpha-particle. This change takes place only to the depth of penetration of the particles, namely, 1.9×10^{-3} cm. The distribution of holes with depth is not uniform. The concentration rises from an initial value to a maximum at 1.4×10^{-3} cm depth and then falls to zero. The maximum is about 2.5 times the initial value and the integral under the curve is, of course, 2 holes per alpha-particle. The number of centers capable of removing electrons from the conduction band (traps or acceptors) is about 9 times larger than the net number of conducting holes produced by the bombardment.

[1] W. E. Johnson and K. Lark-Horovitz, Phys. Rev. **76**, 442 (1949).

I10. The Technique of Cutting Germanium Filaments. W. L. BOND, *Bell Telephone Laboratories.*—A germanium slab is etched to prove that it is a single crystal, then is diamond-sawed and ground on a carborundum belt grinder to required orientation with the help of x-rays. The blank thus produced is etched if required to have an undisturbed surface and cemented to a substrate (commonly glass). The cement is polyvinyl butyral, which after curing is not attacked by etchants or solvents, nor softened by heat. Intricate shapes are cut with a die which is oscillated vertically 6000 cycles per second, driven by a magnetostrictive drive. Emery charged water surrounds the tool and work during cutting. The tool while lifting pumps in water and emery and drives the emery into the germanium on the down stroke, thus pulverizing a thin layer of germanium. The tool and drive assembly are lowered slowly by turning a micrometer screw until its reading indicates that the tool has passed through the blank. This device produces very straight walls and sharp angles and gives fine detail. Similar devices are made by the Balco Research Laboratories, Newark, New Jersey.

I11. The Quantum Yield of Electron-Hole Pairs in Germanium. F. S. GOUCHER, *Bell Telephone Laboratories.*—The central portion of a long filamentary single crystal of n-type germanium is irradiated with monochromatic light of known energy, in the presence of a uniform field, E. The unilluminated ends are long in comparison with the mean range of generated holes. Under these conditions, the measured photocurrent Δi equals $NeE^2\tau_p(\mu_p+\mu_n)/V$, where N is the number of electron-hole pairs produced per second, e the magnitude of the electronic charge, τ_p the lifetime of a positive hole, μ_p and μ_n the hole and electron mobilities, respectively, and V the potential difference between the ends of the specimen. The number of quanta S absorbed per second is known from the energy, wavelength, absorption distance, and refractive index. By comparing the calculated values of N and S, the quantum yield is determined. Within the limits of experimental error, this yield is shown to equal unity.

I12. Noise in Germanium Related to Fluctuations in Hole Concentration. H. C. MONTGOMERY AND W. SHOCKLEY, *Bell Telephone Laboratories.*—Filaments of single crystal germanium carrying a d.c. current exhibit electrical noise having power per cycle bandwidth inversely proportional to frequency. Measurements at audiofrequencies in filaments of n type germanium show that the noise voltages in adjacent sections are uncorrelated when the mean life-path of holes is much shorter than the section-length, but are highly correlated when the life-path exceeds the section-length. A magnetic field produces substantial changes in noise level, which can be explained by spatial redistribution of holes in the filament under Hall effect forces with consequent variation in lifetime.[1] These results suggest that the observed noise is due to irregular variations in hole concentration in the specimen, resulting in fluctuations in conductivity and consequent modulation of the biasing current. A possible mechanism for such variation may be recombination of holes and electrons through traps and the reverse generation process; these processes for one trap may be modulated noisily by changing charges on other traps.

[1] H. Suhl and W. Shockley, Phys. Rev. **75**, 1617 (1949).

I13. The Magneto-Resistance Effect in Oriented Single Crystals of Germanium. G. L. PEARSON, *Bell Telephone Laboratories.*—The electrical conductivity in oriented single crystals of both n- and p-type germanium has been studied as a function of magnetic field strength, direction of magnetic field, and direction of electric current. Measurements were made from 10^3 to 10^5 gauss[1] at 77 and 300°K. The current flow was either along the 100 or the 110 direction and measurements were made with the magnetic field oriented in various directions. At small fields $\Delta\rho/\rho$ is proportional to H^2. The three coefficients which determine the angular dependence have been obtained. For electrons the transverse effect is the expected magnitude but there is a large longitudinal effect not given by the simple theory. For holes the longitudinal effect is very small as expected by theory, but the transverse effect is anomalously large. Theory indicates that $\Delta\rho/\rho$ is proportional to the square of the mobility. The mobility varies as T^{-1} and it is found that $\Delta\rho/\rho$ varies as T^{-3}. At high fields $\Delta\rho/\rho$ becomes linear with H. Values of ρ_H/ρ_0 as large as 3 have been observed for 10^5 gauss at 300°K and 10^4 gauss at 77°K.

[1] The measurements at high fields were made possible through the cooperation of the magnet laboratory at Massachusetts Institute of Technology.

I14. Measurements of Magnetoresistance of Germanium in very Intense Magnetic Fields. H. SUHL.—The magnetoresistance of germanium samples was measured in fields up to about 170 kilogauss. Measurements at room temperature and at 77°K were made with current and magnetic field along various crystallographic axes. Saturation of the resistance *vs.* magnetic field plot was reached in some orientations. The apparatus for producing the magnetic field consists of a bank

of condensers charged slowly to about 100 volts and discharged rapidly through two ignitron tubes in series with a small coil. The field thus produced in its interior remains above 70 percent of its peak value for about 400 μsec. A voltage proportional to the magnetic field is displayed as X deflection on an oscilloscope. This voltage is obtained from an integrating circuit fed from a probe coupled into the main coil. The X deflection is then calibrated in terms of field by means of a second probe coil of known characteristics situated within the main coil. The second probe coil is then removed and replaced by the germanium sample. This is supplied with a fixed current and the voltage drop across it (which is proportional to its resistance) is displayed as Y deflection. The oscilloscope therefore plots the resistance *vs.* magnetic field, and the trace is photographed.

I15. Growth of Germanium Single Crystals. G. K. TEAL AND J. B. LITTLE, *Bell Telephone Laboratories (To be read by title).*—The growth in the number of ideas of possible conduction mechanisms of practical value that might be realized in germanium has emphasized the importance of developing specific methods of producing germanium single crystals in which the relevant properties of the material are controlled. In the present study germanium single crystals of a variety of shapes, sizes, and electrical properties have been produced by means of a pulling technique distinguished from that of Czochralski and others in improvements necessary to produce controlled semiconducting properties. Germanium is a solid that expands markedly on solidifying and is very sensitive to factors, such as physical strain, which give rise to twinning. The method of pulling the germanium single crystal progressively from the melt at such a rate as to have a stationary interface between the solid and the liquid only slightly above the liquid surface is very well suited to the material since it avoids the constraints inherent in solidifying the germanium within inflexible walls and provides a simple planar thermal gradient in the neighborhood of the interface thereby minimizing thermally induced strains. Single crystal rods up to 8 inches in length and ¾ inch in diameter and having a high degree of crystalline lattice perfection have been produced. Measurements in these Laboratories have shown the bulk lifetimes of injected carriers in these materials to be greater than 200 microseconds.

Author Index to Papers Presented at the Oak Ridge Meeting

Anderson, P. W.—No. D4
Averbach, B. L. and B. E. Warren—No G9
Axel, Peter—No. H3
Barbar, W. C.—No. C11
Barrett, C. S. and D. F. Clifton—No. A7
Belinfante, Frederik J.—No. E3
Bell, P. R.—No. H2
Bernstein, R. B. and Daniel Cubicciotti—No. A8
Bloemberge, N.—No F4
Bond, W. L.—No. I10
Bowles, J. S.—No. A6
Brattain, W. H. and G. L. Pearson—No. I9
Brophy, James J.—No. G3
Burstein, E. and John J. Oberly—No. E8
Campbell, Edward C. and Max Goodrich—No C9
Chambers, William H., Robert E. Sheriff, and Dudley Williams—No. C7
Cleland, J., K. Lark-Horovitz, and J. C. Pigg—No. I7
Cohen, B. L., C. E. Falk, and S. K. Kao—No C3
Cohen, E. Richard and M. A. Greenfield—No. C2
Coleman, R. P.—No. G10
Crawford, J. H., Jr. and K. Lark-Horovitz—No. I6
Dale, E. B., E. L. Zimmerman, D. G. Thomas, and J. D. Kurbatov—No. C10
DeWitt, J. H., Jr. and C. K. Seyfert—No. G2
Eggenberger, Deilbert N. and Paul L. Copeland—No. G1
Feuer, Paula and Hubert M. James—No. I3
Fireman, E. L.—No. H5
Forman, Guy—No. G8
Foss, Martyn H.—No. C12
Foss, M. H., J. G. Fox, R. B. Sutton, and E. Creutz—No. C13
Frerichs, R.—No. E9
Gildhart, Lee and A. W. Ewald—No. I2
Goodman, Clark, Charles W. Tittle, and Henry Faul—No. C5
Gordon, Gary D.—No. E6
Goucher, F. S.—No. I11
Green, Alex E. S.—No. E4
Hall, R. N.—No. I5
Haynes, S. K. and J. W. Wedding—No. E2
Hopkins, John I.—No. G5
Hurst, G. S.—No. C6
Klick, Clifford C.—No. G7
Koehler, W. C., E. O. Wollan, and C. G. Shull—No. C4
Konopinski, E. J.—No. H1
Lark-Horovitz, K.—No B1
Luyet, B.—No. E1
McGowan, F. K. and S. De Benedetti—No. H4
Merz, W. J.—No. E7
Montgomery, H. C. and W. Shockley—No. I12
Mrozowski, S.—No I1
Neissel, John P. and Donald C. Moore—No. G4
Nesbitt, E. A.—No. A3
Orman, C., H. Y. Fan, G. J. Goldsmith, and K. Lark-Horovitz—No. I8
Pearson, G. L.—No. I13
Post, R. F. and N. S. Shiren—No. G6
Rasor, N. S. and W. E. Parkins—No. A5
Rhodin, T. N., Jr.—No. A1
Russell, B. R., P. H. Miller, Jr., and C. F. Wahlig—No. I4
Schulz, L. G.—No. A2
Seitz, F.—No. D2
Shockley, W.—No. B2
Shull, C. G.—No. D3
Slater, J. C.—No. F3
Smoluchowski, R.—No. A4, B3
Southern, A. L., H. W. Morgan, G. W. Keilhotlz, and W. V. Smith—No. C1
Stevenson, Donald T. and Martin Deutsch—No. C8
Suhl, H.—No. I14
Teal, G. K. and J. B. Little—No. I15
Van Dyke, Karl S.—No. E5
Von Hippel, A.—No. F2
Warren, B. E.—No. D1
Wert, Charles—No. A9
Williams, H. J.—No. F1
Witmer, Enos E.—No. C14
Zener, C.—No. B4

Minutes of the 1950 Spring Meeting of the Ohio Section at Columbus

THE Annual Business Meeting of the Ohio Section of the American Physical Society was held at the Department of Physics, Capital University in Columbus on Saturday, April 29, 1950. To try to satisfy needs of a meeting with Section F, Ohio Academy, a conflict with the Washington Meeting of The American Physical Society was endured. It was decided that such a conflict should not be scheduled again. There were few papers offered and the attendance was only 60 persons. New officers for the coming year were elected:

Donald W. Dunipace, *Libby-Owens-Ford Glass Company*, Chairman;

F. L. Berger, Sr., *Ohio Northern University*, Vice-Chairman;

Leon E. Smith, *Denison University*, Secretary-Treasurer.

The following papers were presented: "Remarks on the New Science Building," by G. C. Fromm of Capital University; "Coincident Geiger Counters Used in Absolute Measurements," by Stanley G. Fultz of Ohio State University; "Observations on the Motion of the Pulley in Melde's Experiment," by Arthur L. Lutz, Wittenberg College; "Concerning the Teaching of Reactionary Forces," by R. L. Edwards of Miami University. There was an invited lecture by Dr. John Schuler of Cincinnati University, "Construction and Operation of a Mass Spectrograph."

Leon E. Smith, *Secretary*
Denison University
Granville, Ohio